DISEASE MODELLING ON MEASLES IMMUNITY: THEORETICAL AND NUMERICAL ANALYSES

ELENA ARUFFO

A DISSERTATION SUBMITTED TO THE FACULTY OF GRADUATE STUDIES
IN PARTIAL FULFILMENT OF THE REQUIREMENTS
FOR THE DEGREE OF
DOCTOR OF PHILOSOPHY

GRADUATE PROGRAM IN MATHEMATICS AND STATISTICS
YORK UNIVERSITY
TORONTO, ONTARIO

JULY, 2020

© ELENA ARUFFO, 2020

Abstract

Although measles vaccine is considered safe and highly effective, cases continue to be reported globally, even in countries, such as Canada, where herd immunity (a form of indirect protection provided by immunized individuals) threshold is reached. Biological processes and social behaviours are fundamental factors in understanding the re-emergence of this childhood disease in highly vaccinated populations. In the past decades, the assumption that vaccine-induced immunity is life long has started to vacillate and many studies show how measles antibodies wane over time. However, the time needed to wane immunity partially, or fully, is still unknown. During this waning stage, immunity can experience a boosting process, if an encounter with the pathogen occurs. However, in absence of virus, immunity can wane until individuals return fully susceptible. In a society where mobility, travel and immigration are a daily routine, infection's stages and levels of immunity are important factors to potentially increase or reduce the spread of a virus. In particular, with the assumption that measles-induced immunity is lifelong, immigrants' immunity provides an increase of protection in the host country. On the other hand, immunity heterogeneity in a community creates pockets of individuals vulnerable to the infection, and movement of infectious cases might lead to relatively big outbreaks.

In this thesis, we investigate how waning immunity, boosting and vaccination processes, immigration and migration affect the achievement of herd immunity and the spread of the infection. We propose different compartmental models described by systems of ordinary and partial differential equations, following, and extending, the Susceptible-Exposed-Infectious-Recovered framework. We employ both deterministic and stochastic models in order to capture those factors which mostly affect the infection dynamics and immunity of individuals as well as to investigate the probability of extinction or outbreak. Since measles vaccine is given at different ages, from 12 months up to 6 years, we also employ age structured models, discrete and continuous, to capture the age groups which mostly experience waning immunity and infection. Meta-population models are also used to investigate the effect of mobility on the spread of measles infection. We derive expressions for the basic and control reproduction numbers as well as performing sensitivity analysis on the model parameters and its outcomes.

Dedication

To my wonderful and beloved family

Acknowledgements

This thesis would not have been possible without the help and support of many wonderful people I had met in the past years.

I would like to express my deepest gratitude to my supervisor, Professor Jane Heffernan, for giving me the opportunity to work with her and learn from her experience. I would like to thank her for the support and guidance she gave me throughout this journey, her patience and empathy, and all those opportunities that made my researching skills improve.

I also would like to thank my committee members Professor Neal Madras and Professor Jianhong Wu for accepting the responsibility to supervise me within these years.

I want to express my gratitude to Dr. Teslya for supporting and helping me during our collaborations.

Without my parents, Dino and Rosa, I would have never been able to start my PhD in Canada. They gave me and my family a chance to begin a new and better life. I cannot thank them enough for this. I would also like to thank them for their daily support and help taking care of my children when I was busy with work and conferences.

Many special thanks go to my children, Enrica and Emma, who, without knowing it, have given me the strength to go forward, even if with some difficulties.

My gratitude goes also to my sister, Eleonora, for her continuous moral support and wisdom and always ready to help and listen.

I am immensely grateful to my husband, Eric, for showing infinite patience, his moral support and helping in taking care of our children.

I am also grateful to my mother-in-law, Elizabeth, who helped in taking care of the children, while I was at work.

I would like to thank Rachael, Bing, Neda, Vishal, Safia, Marco, Jude and Allysa for their support and fun. A special thanks goes to Mahdis, Angie and Yohana, who became part of my family and helped me in many different ways over these years.

I would like to thank my friends Alessandra, Elena, Elisa and Dorotea for their support. They have been always there and ready to listen and encourage me throughout the past 15 years.

My gratitude also goes to Sara for pushing me to keep going and supporting me, even when she was more in need of encouragement. I would have loved sharing this achievement with her.

I am grateful to the Department of Mathematics and Statistics, York University. Professors and staff have always been kind and available to help.

Table of Contents

List of Tables

List of Figures

Chapter 1

Introduction

1.1 Measles

Measles is a highly infectious childhood respiratory disease. It is caused by the measles morbillivirus (MeV) belonging to the Paramyxoviridae family. The first symptoms of the infection are fever, cough, coryza, conjunctivitis and some white spots inside the cheeks (Koplik spots). These signs appear about 10 to 12 days since the exposure to the pathogen has occurred. The subsequent symptom, which is the most typical, is a red rash which starts on the face and neck reaching the limbs successively. This rash starts diminishing after 5 days from onset.
What makes measles a serious infection is the complications it leads to, above all, in young children (less than 5 years old) or adults aged more than 30 years. This infection can cause dehydration, otitis, pneumonia, as well as, more severe consequences such as blindness and death.

Although there is not a specific antiviral for MeV, measles is a vaccine preventable infection. In 1963, the first measles vaccine was licensed in the USA [1, 2, 3] and it was given to children aged 9 months. In the following years the trend of reported cases of measles experienced a sharp drop, with the presence of smaller peaks in the 1970s. However, in the 1980s measles cases were reported in both unvaccinated infants and among children with a single dose of vaccine, probably due to primary vaccine failure (that is, the immunity system did not respond to the inoculation)[3]. Hence, in 1989 a new immunization policy was implemented with the recommendation of giving a second dose to school-aged children [3]. This new policy led to a further reduction in measles cases. Nowadays, almost globally, the first dose is given at 12-15 months, and the second one at any time before school age [4, 5].
Worldwide vaccination campaigns have been promoted over the past decades [6, 7, 8]. The World Health Organization [6] states that in the first 18 years of the new millennium, measles vaccine prevented more than 23 million deaths globally [6] . Moreover, in 2018, 86 % of children got immunized, at least with the first dose, in the world [6].

Although the infection incidence decreased due to the implementation of vaccine policies, in the past years a visible re-emergence of measles has been registered internationally [9, 10,

11], even in countries where the percentage of vaccinated individuals is high enough to ensure herd immunity (with a vaccination coverage in the range $93\% - 95\%$ [12, 13, 14, 15, 16]) in the community (see Figure (1.1)). Herd immunity indicates an " indirect" protection that vaccinated individuals provide to vulnerables.

The cases reported in highly vaccinated societies have been calling into question what is causing this re-emergence. In these communities, including Canada, the index case has always been imported from endemic countries [17] (Figure 1.2). Hence immigration is considered as one of the factors promoting measles resurgence. However, the reason for these outbreaks can be linked to biological and social causes. For example, the possibility that vaccine-induced immunity is not lifelong can also be considered as a factor. Small groups or clusters of non-vaccinated individuals, because of vaccine denial, delay or hesitancy may also be culprit.

Indeed, different opinions are shared on measles immunity. It is widely accepted that the infection-acquired immunity is lifelong [18, 19, 20, 21], but regarding the vaccine-induced immunity not all scientists agree on this a permanent protection [21, 22, 23, 24, 25]. In the past years, different studies show that vaccine-induced immunity wanes over time, at least, within the first 20 years after the immunization [21, 22, 23, 24]. This immunity reduction is crucial from an outbreak prevention point of view. In fact, a decreased level of protection will make vaccinated individuals, again, susceptible to the pathogen and hence generate an outbreak bigger than expected. Moreover, vaccinated individuals who become infected, might transmit the infection with a force of infection different from primary cases. However, this transmission rate is still unknown.

Measles in Canada

Before the MeV immunization program started in Canada, measles outbreaks occurred every 2 to 5 years, reporting a large number of cases and deaths[17, 26]. Similar to the USA, Canada licensed the first measles vaccine in 1963, making the first dose publicly funded at the beginning of the 1970s [17, 26, 27] and reducing the cases by 99% in the following years [27] (see Figure (1.2a). Although this important drop in the total cases was observed, relatively large measles outbreaks were reported annually between 1990 and 1997 [26]. Hence, a second dose vaccine program was implemented in 1996-1997 [17, 26]. In the following year, measles was declared not endemic in Canada [17].

Despite the high vaccination coverage [28], in the past years, small outbreaks have been recorded in Canada annually [17, 29, 30]. Measles infections have mainly been reported in unvaccinated individuals or people who were not properly vaccinated and travel to endemic regions bringing the infection when returning to Canada. Between 1998 and 2013, 134 cases were imported into Canada [17] (see Figure (1.2b)), and others were registered in the following years [29, 30].

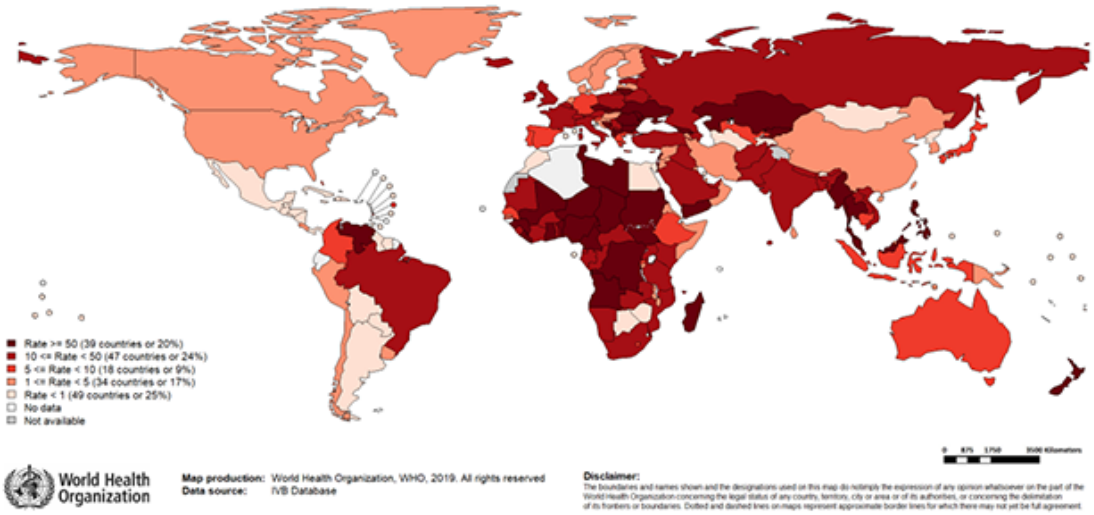

(a)

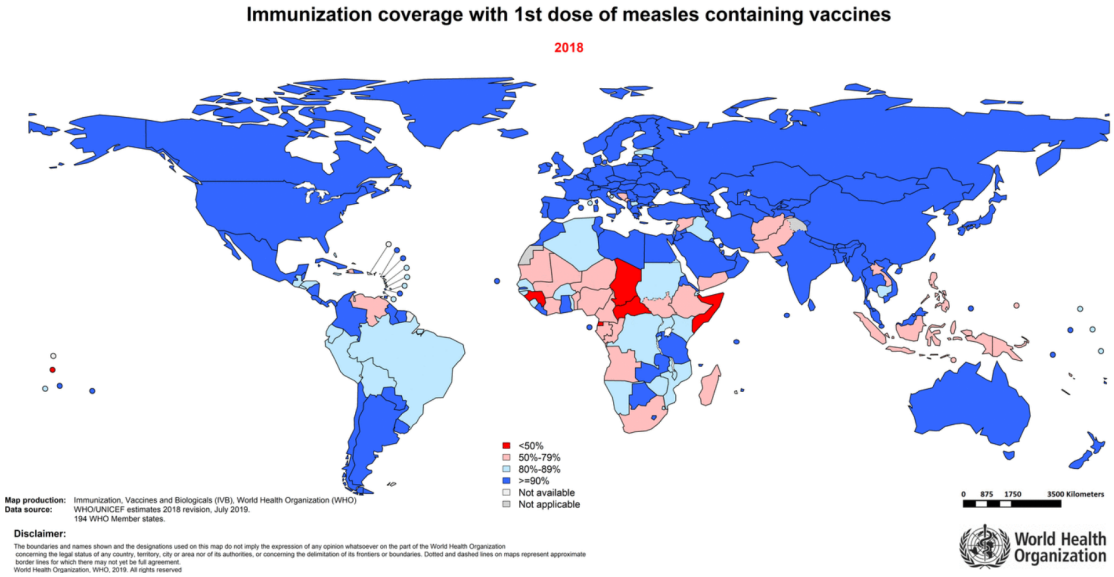

(b)

Figure 1.1: (a) Map of measles reported cases worldwide in 2019. Taken from [31] (b) Map of measles vaccine (1 dose) coverage worldwide in 2018. Taken from [31]

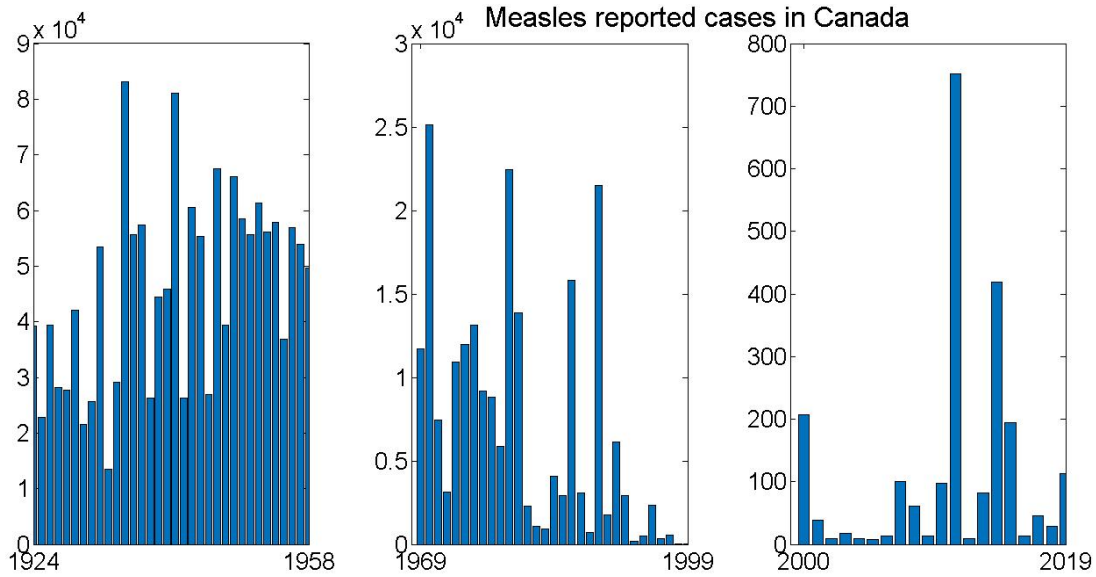

(a)

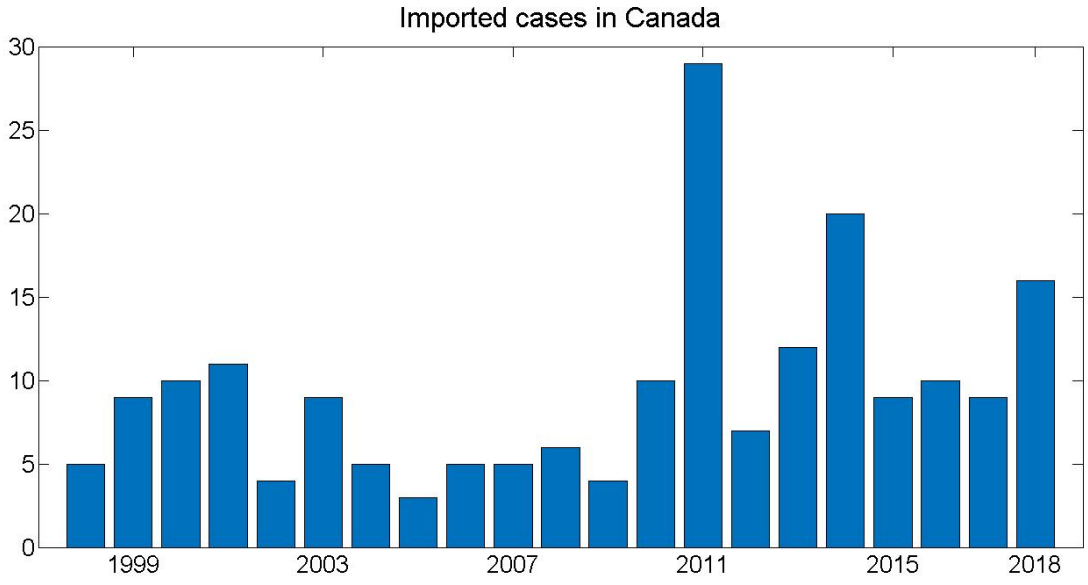

(b)

Figure 1.2: (a) Cases reported in Canada from 1924 to 2019 (1958-1968 data not available) [32] (b) Cases imported to Canada from endemic countries from 1998 to 2018 [17, 33].

1.2 Disease Modelling

The field of Disease Modelling encompasses all mathematical models of disease, including infections and non-infection diseases, and acute and chronic infections, caused by a myriad of pathogens (both micro and macroparasites). Many different mathematical methods can be used to study the change of disease prevalence over time. Herewith, we limit our discussion of mathematical models/tool that are directly related to the works of this thesis.

Susceptible Infectious Recovered (SIR)

The idea of using mathematical tools to describe epidemiological phenomena dates back to 1766, when Bernoulli [34] published the first study on smallpox mortality and the advantages that vaccination against this infection will have on the population life expectancy.
Starting in 1927 mathematical compartmental models were introduced by O. Kermack and A.G. McKendrick [35, 36, 37] in order to study the transmission of infection diseases.
One of the simplest cases of compartmental models is the *Susceptible-Infectious-Recovered (SIR)* [38, 39, 40, 41, 42] framework without demographics. This model divides the population into three different classes: individuals who are vulnerable to the infection, or susceptible (S), individuals who, after encountering the pathogen, become infectious (I), and individuals who recover from the infection and are fully immune/resistant to the pathogen (R). The transmission of the infection from an infected individual to a healthy one occurs with a given *force of infection* ($\beta I, \beta I/N$), where this term is the probability of contact between S and I individuals, and includes the rate of transmission of the disease. After a period $1/\gamma$, sick individuals recover. The transition among all these steps is defined by a system of *Ordinary Differential Equations (ODEs)*.

$$S' = -\beta SI \tag{1.1a}$$
$$I' = \beta SI - \gamma I \tag{1.1b}$$
$$R' = \gamma I \tag{1.1c}$$

Latent period

Not all diseases share the same stages leading to the infection. Some viruses, such as MeV [1, 17, 43], after entering the host, stays latent for a certain period of time (called *incubation period,* $1/\alpha$) before being able to be transmitted to other hosts. Within this period, the host does not manifest any infection symptoms and, although infected, is not infectious. This stage of the infection is fundamental to predict the outcome of an outbreak and allow public health to make a quick response to control it. The incubation period is introduced in a mathematical model by adding the following equation

$$E' = -\beta SI - \alpha E$$

between S' and I', which will become $I' = \alpha E - \gamma I$ [40, 41, 44]. In this model, it is assumed that individuals in E do not show symptoms and are not infectious, whereas I individuals are infectious and with visible infection symptoms.

Severity of symptoms

In the models shown so far, the individuals carrying the disease show symptoms while infectious. However, for some diseases, individuals might not show any sign of the symptoms or might present a very mild level of severity. For example, a previous immunization, which wanes over time, can allow individuals to be infected again after encountering a specific pathogen, but they might be sub-clinical (or asymptomatic) cases. They can also transmit and recover from the virus differently from primary infected cases. Given the difficulty in detecting the asymptomatic infectious cases, different studies have been done in trying to understand the effect that they have on the dynamics of the infection [45, 46, 47, 48, 49]. In oder to capture this phenomenon, in a disease model, the infectious compartment is divided into two sub groups: symptomatic and asymptomatic:

$$S' = -\beta SI - \hat{\beta} SA \tag{1.3a}$$
$$E' = \beta SI + \hat{\beta} SA - \alpha E \tag{1.3b}$$
$$A' = (1-q)\alpha E - \gamma_A A \tag{1.3c}$$
$$I' = q\alpha E - \gamma_I I \tag{1.3d}$$
$$R' = \gamma_A A + \gamma_I I \tag{1.3e}$$
$$\tag{1.3f}$$

where q is the probability of showing symptoms, $\hat{\beta}$ is the transmission from asymptomatic cases and γ_A and γ_I are the different recovery rates for asymptomatic and symptomatic cases, respectively.

Immunity: vaccination and waning process

It has been already discussed that some childhood diseases, such as measles, are vaccine preventable. Vaccination reduces the size of the susceptible class and, consequently, the spread of the infection. It is then possible to add a further compartment (V) to mathematical models to distinguish vaccinated individuals from the susceptibles [40, 41, 50, 51]. In particular, if we define Λ and d as the population birth and death rates, respectively, the ODEs related to the susceptible and vaccinated compartments become:

$$S' = (1-p)\Lambda - \beta SI - dS \tag{1.4a}$$
$$V' = p\Lambda - dV \tag{1.4b}$$

where p is the proportion of population with vaccine-induced immunity.

It is globally recognized that vaccination is an extraordinary practice to reduce the spread of the infection. However, if its efficacy wanes over time, individuals might become partially or fully susceptible if there is no exposure to the pathogen or any booster vaccines that help to boost immunity that has waned.

Different mathematical models incorporate waning immunity and boosting processes in a typical SIR model framework or in-host framework [49, 51, 52, 53, 54, 55, 56, 57, 58]. The simplest form is the SIRWS model:

$$S' = -\beta SI + k_1 W \tag{1.5a}$$
$$I' = \beta SI - \gamma I \tag{1.5b}$$
$$R' = \gamma I - k_2 R + \omega W \tag{1.5c}$$
$$W = k_2 R - \omega W - k_1 W \tag{1.5d}$$

where k_1 represents the waning rate at which individual in the waning stage return fully susceptible, k_2 is the waning rate from R to W and ω represents the immunity boosting process.

Meta-population models

Since the most ancient ages, humans have always been travelers. We can now reach destinations that a few years ago seemed too distant. We need to consider the movement of individuals and how movements of susceptible, exposed, infected, vaccinated, recovered, immune, etc affect disease spread. Models of population movement are called *meta-population* models [40, 41]. The idea of this spatial model is to divide the entire geographical area into n patches. Each patch will then have its own population which can move from one region to the others for various lengths of time. For example, immigration can be defined as a long-term spatial movement between countries or, in a smaller case, commuting from one area to another of the same city is a short term spatial movement. There exist two different approaches used in multi-patch models capturing the migration and the commuting behaviours: Eulerian and Lagrangian. In the first approach, the residency of the travellers is not considered and the infection depends on the patch where individuals are. The Lagrangian approach allows to keep track of the residency of individuals and the infection rate depends on the mean time spent in a specific location and its risk of transmission.

In mathematical models, the mobility among patches can be captured by introducing new rates at which individuals leave or return to their residency patch [59, 60, 61, 62, 63, 64]. Multiple studies have been done in this direction by Arino et al.[61, 62, 63, 64]. In this framework, the population of each subregion is divided into two groups: individuals who don't leave their home patch and individuals who commute. The typical notation is the following: $\mathcal{X}_{ij}$, where $\mathcal{X}$ indicates any of the compartments described in the previous paragraphs. $\mathcal{X}_{ij}$ has to be read as: individuals in $\mathcal{X}$ compartment currently in patch i that lives in patch j [41]. The dynamics of the total population can be defined as

$$N'_{ii} = \nu_{ii} - \sum_j l_{ji} N_{ii} + \sum_j r_{ji} N_{ji} - \mu_{ii} N_{ii} \tag{1.6a}$$

$$N'_{ij} = \nu_{ij} + l_{ij} N_{jj} - r_{ij} N_{ij} - \mu_{ij} N_{ij} \tag{1.6b}$$

where l_{ij} is the rate at which individuals living in j commute to i, r_{ij} is their returning rate, ν_{ij} individuals born in j currently in i. The force of infection in these models is defined by the standard incidence, i.e. the transmission in patch i is given by:

$$\beta_i S_{ii} \frac{\sum_j I_{ij}}{\sum_j N_{ij}} \tag{1.7a}$$

$$\beta_i S_{ij} \frac{\sum_j I_{ij}}{\sum_j N_{ij}} \tag{1.7b}$$

Although this approach is able to capture the movements of individuals and keep track of their residency, the estimation of the mobility rates is not always feasible. A more recent meta-population method models the migration among n regions by using *residency times* [65, 66, 67, 68]. The transmission of the infection in each patch is determined by the time individuals from different regions spend in a specific patch and the effective population which at a given time is in each region. In particular, Bichara [66, 68] and Stolerman [65] assume that individuals from patch i spend in patch j a certain proportion of time $p_{ij} \in [0, 1]$, satisfying the condition $\sum_{j=1}^{n} p_{ij} = 1, \quad \forall i = 1, 2, ..., n$. The transmission in patch i is then modelled as

$$\beta_j S_i p_{ij} \frac{\sum_{k=1}^{n} I_k p_{kj}}{\sum_{k=1}^{n} N_k p_{kj}} \tag{1.8}$$

where β_j is the patch specific transmission, $S_i p_{ij}$ indicates the susceptible individuals from patch i currently in j, $\frac{\sum_{k=1}^{n} I_k p_{kj}}{\sum_{k=1}^{n} N_k p_{kj}}$ is the proportion of infected individuals in patch j (i.e. the infected individuals in patch j from the other regions over the total population currently in patch j).

Age structured model

In a simple SIR model, and its extensions, the population is divided into groups depending on their infection status. However, a population can be classified based on the age of the individuals, who tend to have various contacts with other individuals in different age groups. Mossong et al. [69] have presented contact matrices over different age groups for a subset of European countries (see Figure (1.3)). Prem et al. [70] have presented contact matrices for all other countries of the world by extrapolating the data from [69] and projecting contact patterns for 144 countries . From the contact matrices, it is clear that individuals have most of their contacts with others belonging to the same age group. It is also visible that

children have contacts with adults, which is reasonable considering the contacts among family members.
As mentioned, the transmission of an infection depends also on the contacts that infectious individuals have with others. Hence, in a disease model with an age-structure, the contacts among people should depend on the their age group.
The easiest approach to capture the age factor in a model is to divide the population in age-dependent subgroups (e.g., children and adults) which follow similar infection dynamics [41, 71, 72]. For example, the model in Eq.(1.1) will present two susceptible, two infectious and two recovered classes, defined as $S_C, I_C, R_C, S_A, I_A, R_A$, where C denotes children and A adults. The transmission terms will depend on the contacts among these new classes and they are defined as $\beta_{CA}, \beta_{CC}, \beta_{AA}$, representing the contact between Children-Adults, Children-Children and Adults-Adults, respectively.
It may be preferable to represent age in a continuous fashion, rather than using discrete age groups. Here, we would use a system of *Partial Differential Equations (PDE)* [40, 57, 58, 69, 73, 74, 75, 42, 76]. In these models, the variables (e.g., S, I, R) are defined as functions depending on both the time (t) and age (a):

$$\frac{\partial S(a,t)}{\partial t} + \frac{\partial S(a,t)}{\partial a} = -S(t,a)\int_0^{+\infty} \beta(a,\tau) I(t,\tau) d\tau \tag{1.9a}$$

$$\frac{\partial I(a,t)}{\partial t} + \frac{\partial I(a,t)}{\partial a} = S(t,a)\int_0^{+\infty} \beta(a,\tau) I(t,\tau) d\tau - \gamma I(a,t) \tag{1.9b}$$

$$\frac{\partial R(a,t)}{\partial t} + \frac{\partial R(a,t)}{\partial a} = \gamma I(a,t) \tag{1.9c}$$

where $\beta(a,\tau)$ represents the transmission rate between an infected individual of age τ and a susceptible of age a. Hethcote provides a wide literature on this topic by using both theoretical and numerical approaches [57, 58, 74].

Stochastic models

The models described in the previous sections use a deterministic approach. They do not take into consideration the stochasticity that we experience in real life. To capture this process, we need to refer to another type of model: *stochastic models* [40, 41, 77, 78]. Allen carried out extensive studies on this topic with application to biology and epidemiology [40, 77, 79, 80, 78].

Stochastic models allow for the determination of variation in model outcomes, rather than looking at the mean behaviour that is capture by deterministic models. Stochastic models also allow for the calculation of the probability of a disease outbreak, or the extinction probability of a disease in a population given public health mitigation strategies.

In a stochastic modelling, the compartments used in the deterministic ODEs are defined as *disease states*. Individuals move from one state to another, where movements are determined by probabilities at the current time. In some models the states (e.g. S,I, R, etc..) are defined

as discrete random variables:

$$\mathcal{D}(t) \in 0, 1, 2, ..., N$$

where $\mathcal{D}$ represent any of the infection dynamic states. However, the processes can be defined over a discrete (i.e. $t \in 0, 1, 2, ...$) or continuous time (i.e., $t \in [0, +\infty)$). In the first case we define the process as *Discrete Time Markov Chain (DTMC)*, while the latter case is defined as *Continuous Time Markov Chain (CTMC)*. In this work we will employ Continuous Time Markov Chain.

When we define an epidemiological stochastic model, the infection dynamic is captured by *events* which change the population size in each state. For example, if we consider the dynamic outlined in Eq. (1.1) the events we need to define are the transmission and the recovery. The transitions among the states are defined, respectively, as follows:

$$I \to I + 1; S \to S - 1; \tag{1.10a}$$
$$I \to I - 1; R \to R + 1; \tag{1.10b}$$
$$\tag{1.10c}$$

In the scope of this thesis, we carry out numerical analyses and simulations using the *Gillespie's Direct Method* [81].

Mathematical Models of Measles Infection and/or Waning Immunity

There have been many mathematical modelling studies of measles spread in populations. There have also been some modelling studies of waning immunity, as pertaining to measles and other pathogens. Here, we provide a simple review of the literature, outlining studies that are pertinent to the current work.

Lavine et al. [56] developed an age-structured Susceptible-Infectious-Recovered-Waning-Susceptible (SIRWS) model to describe the dynamic of pertussis and investigate its re-emergence. They assumed that the absence of the pathogen does not allow immunity to be boosted, and, consequently, it wanes. On the other hand, while staying in the waning stage, if individuals are exposed to the pathogen, they boost their immunity. This work is able to capture some of the phenomena occurring in highly vaccinated communities. In particular, the age groups experiencing the infection are shifted (from younger to older) and re-emergence over time. These results are possible assuming that a low exposure to the pathogen triggers immunity boosting.

Others employed the same model framework with different applications [82, 54].

Leung et al. [54] extended the model proposed by Lavine et al. [56] by including a vaccinated compartment and different waning periods for infection-acquired or vaccine-induced immunity. Two infectious compartments are considered: one for primary infected and one for secondary cases. The level of infectiousness of both primary and secondary cases is assumed to be equal. Also, the authors assumed that, to trigger the boosting process, individuals need a lower exposure to the virus than the one needed to become primary infected. However, age

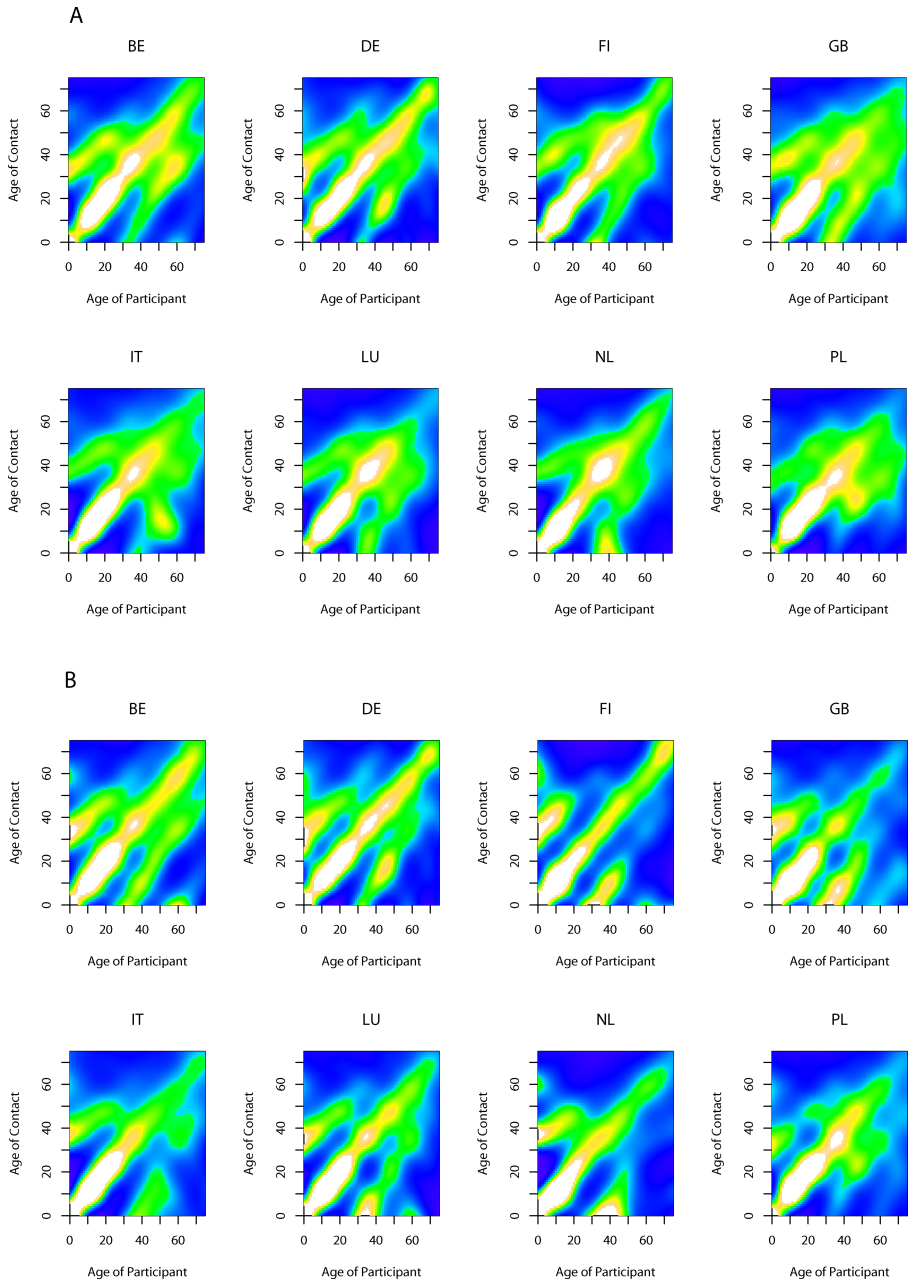

(a)

Figure 1.3: Contact matrices for different European countries (A) all reported contacts (B) physical contacts weighted by sampling weights [69]

structure is not considered. They found that different waning periods can lead to different infection dynamics, and hence it is necessary to understand them comprehensively.

Next, we introduce some of mathematical models of measles infection. The framework used to describe this childhood infection is, typically, the SEIR model, and its extensions. Several models have been used to study the effect of waning immunity at a population level. In 1999, Mosson, J. et al. [49] employed an epidemiological compartmental model considering waning processes of passive maternal immunity and vaccine-induced immunity. The population was divided between immunized and non-immunized, assuming their infectiousness is the same. Their findings suggest that, if individuals do not encounter the pathogen for a long period, their level of protection decays over time, creating a large pocket of susceptibles in the community. They also derived the expression for the control reproduction number highlighting how transmission from vaccinated cases needs more understanding.
In 2003, Mossong and Muller [75] expanded the model used in [49] including age structure. Their results show how waning periods and transmission from a vaccinated case are extremely important to define the time to the first reemergence of measles. The longer the waning periods are and the less strong the force of infection of vaccinated cases is, the more time is needed to experience the reemergence of the infection.

It has already been mentioned that we live in an era where travelling among cities or countries is extremely easy. Measles infection has been studied also considering the movement of individuals.
Mpande, L.C. et al. [83] modelled the movement of a vaccinated population by using a meta-population model on two patches. After deriving both the disease free and endemic equilibria and reproduction numbers, the results on the bifurcation analysis and incidence showed how the number of cases decreases in both patches if the vaccination coverage is increased in both regions. However, this model does not keep into consideration the residency patch of travelers.
Alexander et al. [84] formulated an $SEIR$ multi-patch model to investigate the impact that vaccination heterogeneity has on the transmission of measles in France. Theoretical and numerical approaches were used to evaluate the reproduction number and the infection dynamics. Their results show how a wide diversity in the vaccination coverage increases the transmissibility of measles leading to outbreaks.

When we investigate a disease, we cannot exclude the biological aspect of the virus. Heffernan and Keeling [45, 52] have intensely investigated, focusing on boosting and waning processes. In their first paper [45], the authors proposed in-host models describing the immune system and the cellular dynamics of MeV. They explored the relation between the basic reproduction number (which determined the transmission of infection at the population level) and the level of memory cells in the plasma after being exposed to the virus. Their findings suggest that as the memory cells in the immune system increase, the transmissibility of the infection decreases.
In their second study, Heffernan and Keeling [52] used the results obtained in their cellular-level study [45] to investigate the consequences they have on a population level. This analysis was focused on the impact that vaccination and waning immunity processes have on the

prevalence of infectious individuals. After a period of absence of endemic measles virus in a vaccinated population, the introduction of infectious individuals triggers relatively large outbreaks. The infectious cases show higher peaks as the period of waning immunity increases. For high immunization coverage, the authors were able to capture the periodical outbreaks which are visible in highly vaccinated countries. Although the authors model measles infection, their models include waning immunity from infection and don't include age structure. Also, the models have no theoretical results, and has no stochastic simulations.

Basic and Control reproduction numbers: $\mathcal{R}_0$ and $\mathcal{R}_c$

The diffusion of a disease outbreak is an event strictly related to a fundamental epidemiological factor: the *basic reproduction number*, $\mathcal{R}_0$. This quantity is defined as the average of secondary cases generated by a primary infectious individual in a totally susceptible population within its infectious period[38, 85, 86, 87, 42]. If $\mathcal{R}_0 > 1$, infectious individuals will generate more than one secondary case, which, in turn, will generate successive generations of the outbreak. On the other hand, if $\mathcal{R}_0 < 1$, the infection will die out. Anderson and May [12, 38] estimated the basic reproduction number for different childhood diseases as *rubella* $(6-7)$, *whooping cough* and *measles* $(12-18)$.
Mathematically, the reproduction number can be expressed in terms of transmission rates, population and average infection periods. For example, for Model in Eq. (1.1), $\mathcal{R}_0$ is defined as

$$\mathcal{R}_0 = \frac{\beta N}{\gamma} \tag{1.11}$$

Given the importance of this concept, different methods have been provided by scientists to derive a mathematical expression for this quantity [85, 88, 86, 89, 90, 91, 92].
Following the definition and the conditions according to which an outbreak can occur or not ($\mathcal{R}_0 \lesseqgtr 1$), the basic reproduction number is a concept directly correlated to the stability of the disease free equilibrium (DFE). Hence, a way to derive a formula for the $\mathcal{R}_0$ is to analyze the Jacobian matrix of the disease model, evaluated at the DFE. The reproduction number is obtained by the parameters which allow all the eigenvalues of the Jacobian to have negative real part [86].

Although this method is easily applicable, for complex system it does not provide a clear expression of the $\mathcal{R}_0$ that can be biologically interpreted.
Diekmann et al. [88] introduced an innovative technique, the *Next Generation Matrix method*, successively elaborated by van Den Driessche and Watmough [90]. The authors give a detailed description on how to apply this approach to compute the $\mathcal{R}_0$ in compartmental models. The central concept of the *next generation matrix* method is to capture, through matrices, the rates at which new infection appear in the infected compartment (collected in the matrix $\mathcal{F}$) and the rates of any other transition through the infected compartments (collected in the matrix $\mathcal{V}$). The reproduction number is then defined as $\mathcal{R}_0 = \rho(\mathcal{F}\mathcal{V}^{-1})$, where ρ indicates the spectral radius of $\mathcal{F}\mathcal{V}^{-1}$. The authors also proved that the reproduction number, evaluated through this method, corresponds to the critical value for the stability of the disease free equilibrium.

For models describing different infected classes and infection stages, the evaluation of the eigenvalues of $\mathcal{F}\mathcal{V}^{-1}$ might be complicated. In 2010, Diekmann et al. [89] introduced a new method based on the concept used for the *next generation matrix*. When the matrix $\mathcal{F}$ presents one or more rows equal to zero, indicating that individuals are not in that stage after the infection, it is possible to reduce the *next generation matrix* ($\mathcal{F}\mathcal{V}^{-1}$). To implement the reduction, it is necessary to introduce an *auxiliary matrix* ($\mathcal{E}$) that is able to capture only rows and column in $\mathcal{F}\mathcal{V}^{-1}$ relevant to determine the reproduction number. $\mathcal{E}$ is built by unit vectors e_i, where i are all the rows in $\mathcal{F}$ not zero. Once this matrix is generated, the *reduced next generation matrix* is evaluated as $E^T\mathcal{F}\mathcal{V}^{-1}E$. The reproduction number is the spectral radius of the reduced matrix.

As already mentioned, vaccination plays a fundamental role in the dynamics of infectious diseases, by reducing the size of the susceptible population. When control measures, as immunization, are taken into account, then the population is not fully vulnerable to the pathogen, hence it is necessary to define a new type of reproduction number: the *control reproduction number*, $\mathcal{R}_c$. If we consider a vaccine to be 100% effective and provides lifelong immunity, the expression for the $\mathcal{R}_c$ can be defined as

$$\mathcal{R}_c = (1-p)\mathcal{R}_0 \tag{1.12}$$

where p is the fraction of vaccinated individuals in a population. It is evident that if there is no vaccination policy (i.e. $p = 0$), the control reproduction number corresponds to $\mathcal{R}_0$.

Herd immunity

Herd immunity is defined as an indirect protection that vaccinated people provide to susceptible individuals and it is strictly correlated to the control reproduction number. There exists a threshold of vaccinated individuals needed to prevent the spread of the infection. If that threshold is satisfied, the control reproduction number is less than 1 and hence the infection is not sustained.
Keeping in mind that the reproduction numbers are thresholds for the occurrence of an outbreak, from Eq. (1.12) it is possible to derive the critical vaccination coverage providing $\mathcal{R}_c < 1$. By setting $\mathcal{R}_C = 1$, we can express p as

$$p_c = 1 - \frac{1}{\mathcal{R}_0} \tag{1.13}$$

Eq. (1.13) gives the minimum vaccination coverage needed to achieve *herd immunity* in a population. For example, according to Anderson and May [12] the basic reproduction number of measles lies in the interval $12 - 18$, hence, by using Eq.(1.13), roughly $92\% - 94\%$ of the population needs to be immunized in order to maintain the reproduction number less than 1. This calculation, however, requires that immunity be lifelong, and therefore, ignores the effects of waning immunity.

Sensitivity Analysis

In disease models, the parameters used are not always known and sometimes need to be be estimated. The uncertainty of these values affect the outcomes of the model, leading to their variability. Sensitivity analysis is a great approach to provide insights on which parameters are more significant to the results variability.
A tool commonly used to conduct sensitivity analysis is the *Latin hypercube sampling/Partial Rank Correlation Coefficient (LHS/PRCC)* [93, 94]. LHS is a sampling technique introduced in 1979 by McKay et al.[94]. In this method each parameter is chosen only once for the analysis and independently from each other. The parameters are sampled within a specific range and their distribution is divided into sub intervals with equal probability. This method generates a matrix whose columns are the parameters sampled and the rows correspond to the number of samples. Then, the simulations are run for each parameter set.
Following the LHS step, the PRCC analysis is performed. The PRCC provides a measure of correlation between inputs (parameters) and outputs (the model outcomes) which have a monotonic relationship. In this method, the significance of the inputs over the outputs is classified as *negative* if $PRCC < -0.5$ or as *positive* if $PRCC > 0.5$. Any PRCC value smaller, in magnitude, than 0.5 is defined as *non significant*. The closer these values are to -1, or 1, the higher is the variability. Once the correlation is established, it is ranked depending on the magnitude of the significance.

1.3 Modelling Tools

The population dynamics in our compartmental models are defined with Ordinary or Partial Differential Equations. The tool used in this work to simulate the differential equations solutions and plot them is the programming language MATLAB, developed by MathWorks [95]. This language was also used to investigate the parameters sensitivity analysis. Different versions were used: 2014b and 2016a.

To perform heavy analytical computations, we used a different programming language: Maple, developed by Maplesoft [96]. This tool is able to execute complex symbolic calculations. It was used to evaluate the systems equilibria and their stability analysis as well as derive the expressions of reproduction numbers. The version used was Maple17.

1.4 Scope of Thesis

Although many studies have been conducted over the past years on understanding the dynamics of measles and the cause of its re-emergence, some key questions are still unresolved.

In a highly vaccinated country, such as Canada, the index case of the latest outbreaks were imported from endemic countries [17, 29, 30]. These events are leading Public Health to consider immigration as a possible source of infection. On the other hand, since it is widely accepted that MeV provides life-long immunity, individuals who immigrate to a country with

a high immunization level, increase the level of protection in the local population. It is then fundamental to investigate the immunity distribution of Canadians and immigrants and determine which factors, in each sub-population, are more relevant to prevent the spread of the infection in the country.

In the past years different phenomena (as anti-vaccine movements or general mistrust in vaccination [97]) increased the vaccine hesitancy in Canada. This phenomenon leads to a reduction of immunized citizens which, consequently, creates vaccine heterogeneity across the country. In a society where home place and work place do not often coincide and individuals need to travel daily, the infection can easily be "moved" from one region to another. Indeed, infectious cases, above all if asymptomatic, can represent a real threat in areas where the vaccine coverage is low. It is crucial to investigate the potential impact that infectious individuals have on a community with low immunity in order to suggest vaccination strategies to Public Health decision makers.

Waning immunity plays an important role in the spread of the infection, and Public Health has been making different efforts in trying to understand how this process, along with vaccinated cases force of infection, impacts the re-emergence of measles [23, 24]. However, these are still open questions which need immediate answers. Public Health Ontario (PHO) has conducted different systematic reviews on measles waning immunity, published by Bolotin [23] and Hughes [24], and potential transmission from vaccinated cases, which is still under study. In collaboration with PHO we will extend these findings to a mathematical framework.

In this thesis, we use mathematical models to provide Public Health detailed answers and suggest policies to control the transmission of measles. Moreover it highlights factors, both biological and social, which need more attention and investigation from Public Health officials.

In Chapter 2, we propose an $SEIRV$ age structure model. The population is divided into subgroups according to age (Newborns-Children-Adults) and place of birth (Canadians-Foreign borns). The age groups used are based on the vaccination age recommendation. We propose a first model with two age groups: 6 months-5 years (Children) and older than 5 years (Adults). A second model considers three age groups: 6 months-1 year (Newborns), 1-5 years (Children) and older than 5 years (Adults). We derive both the basic and control reproduction number and carry out sensitivity analysis (LHS/PRCC). We find that the vaccination coverage of Canadian newborns and children is extremely significant in controlling the spread of the infection and increasing herd immunity. Similar results are visible for foreign adults. We can conclude that Public Health should focus on increasing the immunization of Canadian children.

In Chapter 3, we develop a multi-patch model considering 5 regions in the Greater Toronto Area (GTA): Toronto, Peel, York, Halton and Durham. We allow individuals to move among these patches. We describe the infection dynamic with a $SEAIRV$ framework, where the infectious stage is divided into asymptomatic and symptomatic. In terms of movement, all the classes are allowed to leave their own patch, except for the symptomatic one. We investigate how the movement of individuals who do not show the sign of the infection and different level of immunity in the patches affect the total transmissibility of measles. We found that the

highly vaccinated patches residents are able to decrease the overall transmission in their own and other regions. The asymptomatic cases are a real threat for the infection transmission, since it is very hard to control them. However, this risk can be reduced by increasing the vaccine coverage uniformly.

In Chapter 4, we develop a SII_wRVWS model with and without age structure. We assume that children receive one single dose of vaccine and they wane their immunity over time. If individuals in the waning stage encounter the pathogen, they can either boost their immunity level back to the vaccination level or become infected. However, the infectivity of vaccinated cases is still unknown. Hence, we consider two situations: in one, the secondary cases are not infectious, in the second one the vaccinated cases are as infectious as primary cases. We investigate the conditions on reproduction number, vaccine coverage, waning periods and boosting rate which can provide the achievement of herd immunity. We found that this is possible only if the vaccine-induced immunity is lifelong and for small reproduction numbers. For a shorter period of coverage, the indirect protection is never achievable. We also derive a stochastic model and investigate the probability of extinction. Similar to the herd immunity, the probability of an outbreak occurrence increases if the immunity is life long.

In Chapter 5, we explore a short term measles dynamics by using the age structure model delineated in Chapter 4. We investigate how the waning periods affect the duration, peak, time of peak occurrence and final size of a potential outbreak. We find that for a waning period shorter than life span, the outbreak lasts within 5 and 12 months. For a life long immunity, the outbreak may either stay sustained for over one year or not occur. As expected the peak increases as the reproduction number increases, in both short and long immunity period. The final size results show that if immunity wanes faster, most of the cases are visible in the age groups between 5 and 29 years. These results suggest that if the time needed to become susceptible again from a vaccinated status decreases a large vulnerable group of individuals is generated.

In Chapter 6, we extend the age-structured model described in Chapter 4 by adding a second dose of vaccine at the age group 5-9 years. Similar to the analysis in Chapter 4, we investigate how the control reproduction number changes depending on the waning periods, basic reproduction numbers and vaccine coverage. We immediately observe that the control reproduction number is, in magnitude, smaller than the one obtained with one single dose of vaccine. Also, we observe that herd immunity can be achieved only for a life-long vaccine-induced immunity.

In Chapter 7, we propose a final conclusion of our work and outline of future works.

Chapter 2

Distribution of Immunity: An Immigration Model

2.1 Introduction

This work has been conducted in collaboration with Dr. Heffernan and Dr. Teslya. I worked on developing the model, searching data, conducting theoretical and numerical analyses.

Immunity against measles virus can be gained either through the infection itself or inoculation. It is accepted that the immunity acquired by the infection is life-long [18, 19, 20, 21]. Regarding the immunization, two doses of vaccine are recommended: the first one given at 12-15 months of age and the second one given around school entry age. [4, 11]. In highly vaccinated countries, such as Canada, measles outbreaks occur every year ([33, 9]). Generally, the sources of these episodes are travel-related cases from countries where measles is endemic and the spread of the infection can be associated to different factors as waning immunity, vaccine failure or vaccine hesitancy. Although the index case of these outbreaks is imported from endemic countries, it is important to observe that individuals immigrating from these regions can be fundamental to strengthen the immunity distribution in the host countries since their immunity to the pathogen can be infection-acquired and hence life-long.

The 2016 Canadian census, provided by Statistics Canada[98, 99], shows that the rate of immigration has been having an increasing trend over the years with approximately the 50% of newcomers landing in Ontario. It is important to mention that *landed immigrants* refers to all individuals arriving in Canada as permanent resident, that is, they share some of the most fundamental duties and rights with Canadian citizens, including complete access to the health system. The same census reports that landed immigrants are from over 200 different countries (see Figure (2.1)), hence the health background of newcomers is extremely diversified. If we compare the countries of origin of immigrants with the map showing countries with endemic measles (Figure 1.1a) and the one showing the global vaccination coverage (Figure 1.1b), we observe that many immigrants are from regions that are highly vaccinated or with a high incidence of measles cases and low immunization coverage. Hence, a proportion of newcomers have encountered the pathogen and have become fully immune to the virus for life. However, a

fraction of the Canadian immigrant population have immigrated from non-endemic countries where the immunity against measles is provided by vaccination.

Over the years, several mathematical models have been employed to study the effect that immigration has on the spread of a specific infection in the local population. Many of them consider immigration as a constant incoming flow of susceptible and/or infectives [100, 36, 101, 102, 103, 73, 104]. Brauer and Van den Driessche [100] developed models following SIS and SIR frameworks in which the infected compartment is continuously replenished by immigrants. Their results suggest that an endemic equilibrium always exists and it can be reduced by reducing the continuous flow of infectives. Some studies focus on the effect of immigration and vaccination on the infection dynamics [105, 102]. In their study, Piccolo and Billings [105] developed an SIR model, and followed immigrants and local citizens through these classes. In their assumptions, immigrants present a lower level of vaccination and the transmission rates are different when contacts are within the same sub-population or between the two subgroups. The authors derived a vaccination threshold that can lead the infection to extinction or persistence. Moreover, the contact rates determine a lag time between the outbreak in the immigrant and local populations.

Despite the important results from these studies on the disease dynamics, some factors are not considered, such as age structure and different immigration rates depending on the immunological background of individuals. Our work is focused on understanding how immigrants' immunity can affect the distribution of the Canadian population immunity and protect the unvaccinated individuals from potential outbreaks.

We propose mathematical models following a Susceptible-Exposed-Infectious-Recovered ($SEIR$) framework including vaccination with discrete age structure. Moreover, since Ontario is hosting the highest number of newcomers, our model considers it as the main province of our study. The provincial population is divided into two subgroups depending on the country of origin (Canadian or Foreign-borns), to capture the various health backgrounds. However, since the vaccination policy is mainly applied to children, we divide further each sub-population into age-dependent subgroups. We propose two models: in the first one there are two age groups (0-5 years and older than 5 years), while the second one present three age groups (0-1 years, 2-5 years and older than 5 years). As we are interested in the immunity distribution within the communities, both vaccination, demographics and immigration rates are fundamental for this purpose and, hence, they need to be studied carefully. However, all these rates present are not clearly known, hence we employ the *Latin Hypercube Sampling* and *Partial Rank Correlation Coefficient* (LHS/PRCC) sensitivity analysis on the mentioned parameters to determine their uncertainty.

2.2 Model and Methods

2.2.1 Model

In this work, we consider a family of models taking into account that the Ontario population is divided into Canadian-born and immigrants sub-populations and each sub-group is divided

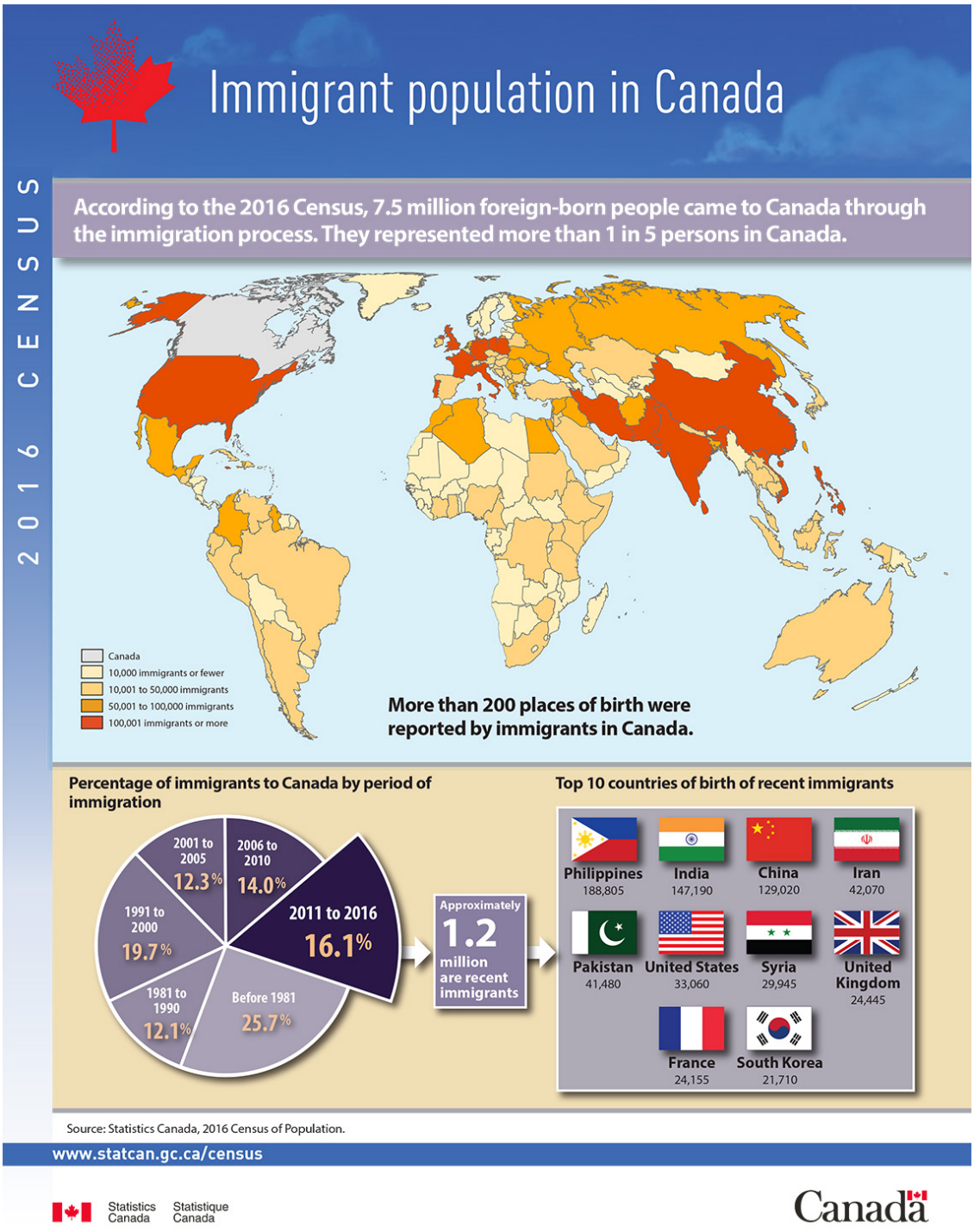

Figure 2.1: Map of countries whose citizens immigrated to Canada in the period 2011-2016. Taken from [98, 99]

based on age. All models are based on the following demographics dynamics, infection dynamics and assumptions.

Demographic

- Canadian-born: Susceptible children enter the population at rate Λ_C (birth rate). At 12 months and 6 years of age, a ν_c portion of them receives a first and second dose of vaccine, while the remaining part is still susceptible to the infection;

- Immigrants: Children enter the Canadian community at recruitment rate Λ_{IN} and Λ_{IJ}, depending on the age (newborn or juvenile). A proportion of them is considered susceptible, a fraction underwent the infection in their country of origin and then is treated as recovered with full immunity and a fraction shows vaccine-induced full immunity. Once in Ontario, vaccinated immigrant children follow the Canadian Up-To-Date (UTD) procedure and get the two-vaccine doses as recommended, at rate ν_i, as applied to Canadian juveniles. At rate Λ_{IA} immigrant adults enter Ontario. Again, a fraction did not encounter the infection during the time spent in their country of origin and so it presents susceptibility to the virus, while a proportion has obtained life-long immunity through infection or vaccination.

- Each subpopulation is divided in the following age groups: 0-1, 1-5 years and 5 + years. This division is due to the vaccination policy according to which the first dose is given at 12 through 15 months of age and the second dose 4 through 6 years of age

- We will indicate the subpopulation with the following subscripts: CN, Canadian newborns, CJ, Canadian juveniles, CA, Canadian adults, IN, immigrant newborns, IJ immigrant juveniles, IA, immigrant adults

Infection dynamics

- when susceptible individuals encounter the virus, with transition rate β_{k-l}, where $k, l = CN, CJ, CA, IN, IJ, IA$ indicating the transmission among subgroups, they become infected. Given the complexity in determining the values for the contact rates, we assume that all individuals can have contacts with homogeneous mixing and spread the infection at the same rate β.

- The latent non infectious-period lasts for 8 days ($1/\alpha = 8$ days), after which individuals become infectious and so able to transmit the infection. Their recovery period is about 7 days ($1/\gamma = 7$ days) and successively people are fully immunized and permanently moved to the R compartment.

Immunity

- Acquired from the pathogen is considered to be life long as well as the one induced by the vaccine

Figures (2.2-2.3) represent the flow diagram of the dynamics described above when two or three ages are considered, respectively.

Variables and Parameters

Table (2.1) and Table (2.2) summarize the population variables and parameters used in the mathematical models.

Parameters Evaluation

In our models, d represents the average outgoing rate. Λ_{IN}, Λ_{IJ}, Λ_{IA}, Λ_C and d are balanced so that the population is constant to keep the population constant. It has been calculated by using data available in *Statistics Canada*[106, 107]. In 2015/2016, the Ontario population was $13,448,494$ and the daily birth rate (Λ_C) was about 383.35 $people \times days^{-1}$. In the same period, $120,346$ newcomers landed in the province with a daily rate of 329.71 $people \times days^{-1}$. Since we are exploring models that include age groups, we divide the immigration rate into newborns, juveniles and adult immigration rate (Λ_{IN}, Λ_{IJ} and Λ_{AI}, respectively). In order to define the percentage of children and adults landing in Ontario, we use the data reported by Statistics Canada [107].

We assume that children in the age group 5-9 are evenly distributed and we add 1/5 of this group to the youngest group. We calculate that about $11,904$ children aged between 0 and 5 years immigrated in Ontario and this is roughly the 10% of the total immigrants. Since this age group can be divided into 5 subgroups, we assume that 2% of this 10% represents newborns $(0, 1]$ and 8% children aged $1 - 5$ years. The remaining 90% are all the immigrants aged 5 years and above. In absence of infection, the demographic dynamics is described by the equation $N' = \Lambda_C + \Lambda_{IN} + \Lambda_{IJ} + \Lambda_{IA} - dN$. Since we are assuming that the population is at the equilibrium $N^* = 13,448,494$, we solve the the previous equation in terms of d and we obtain $d \approx 0.00005302$ $people \times days^{-1}$.

2.2.2 Mathematical Model: Two Age Groups

We present here the first model describing the measles infection dynamics. As already mentioned, the Ontario population is divided into two subgroups depending on the country of origin. Each subpopulation is then divided by age: individuals whose age ranges between 0 and 5 years are considered juveniles, while the ones aged more than 5 years are defined as adults. Since the vaccine dose is given at the age of 4-6 years, all juveniles younger than that age are assumed to be completely susceptible.

We present the system of ordinary equations describing the epidemic dynamics illustrated in the main section:

$$S'_{CJ} = \Lambda_C - dS_{CJ} - \mu_J S_{CJ} - (\beta_{CJ-CJ} I_{CJ} + \beta_{CA-CJ} I_{CA} + \beta_{IJ-CJ} I_{IJ} + \beta_{IACJ} I_{IA}) S_{CJ} \tag{2.1a}$$

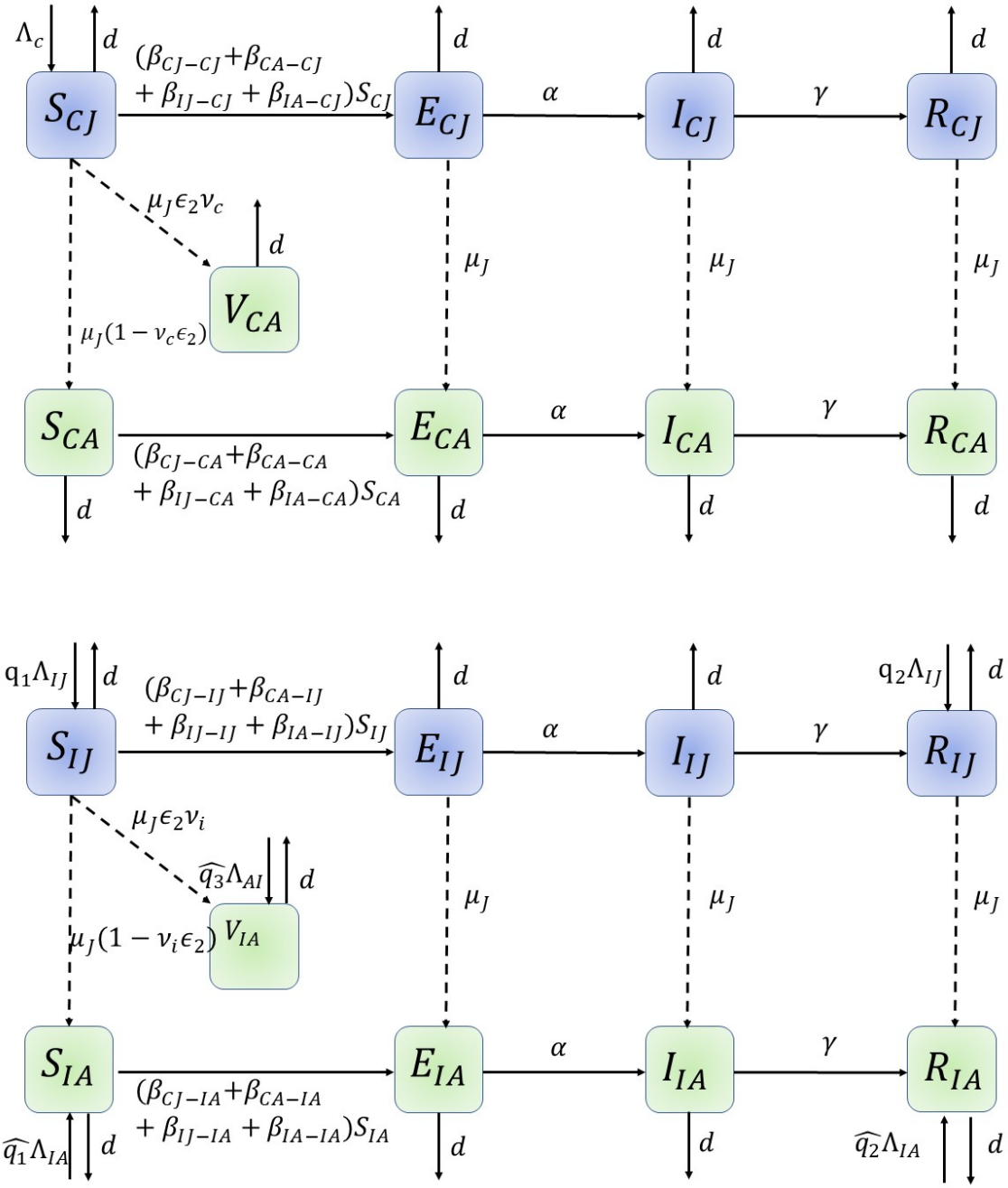

Figure 2.2: Flow diagram for Model (2.1) with two age classes, children(J), and adults (A), from immigrant (I) and Canadian populations (C). The model follows susceptible, exposed, infected, recovered and vaccinated individual in each class for each population

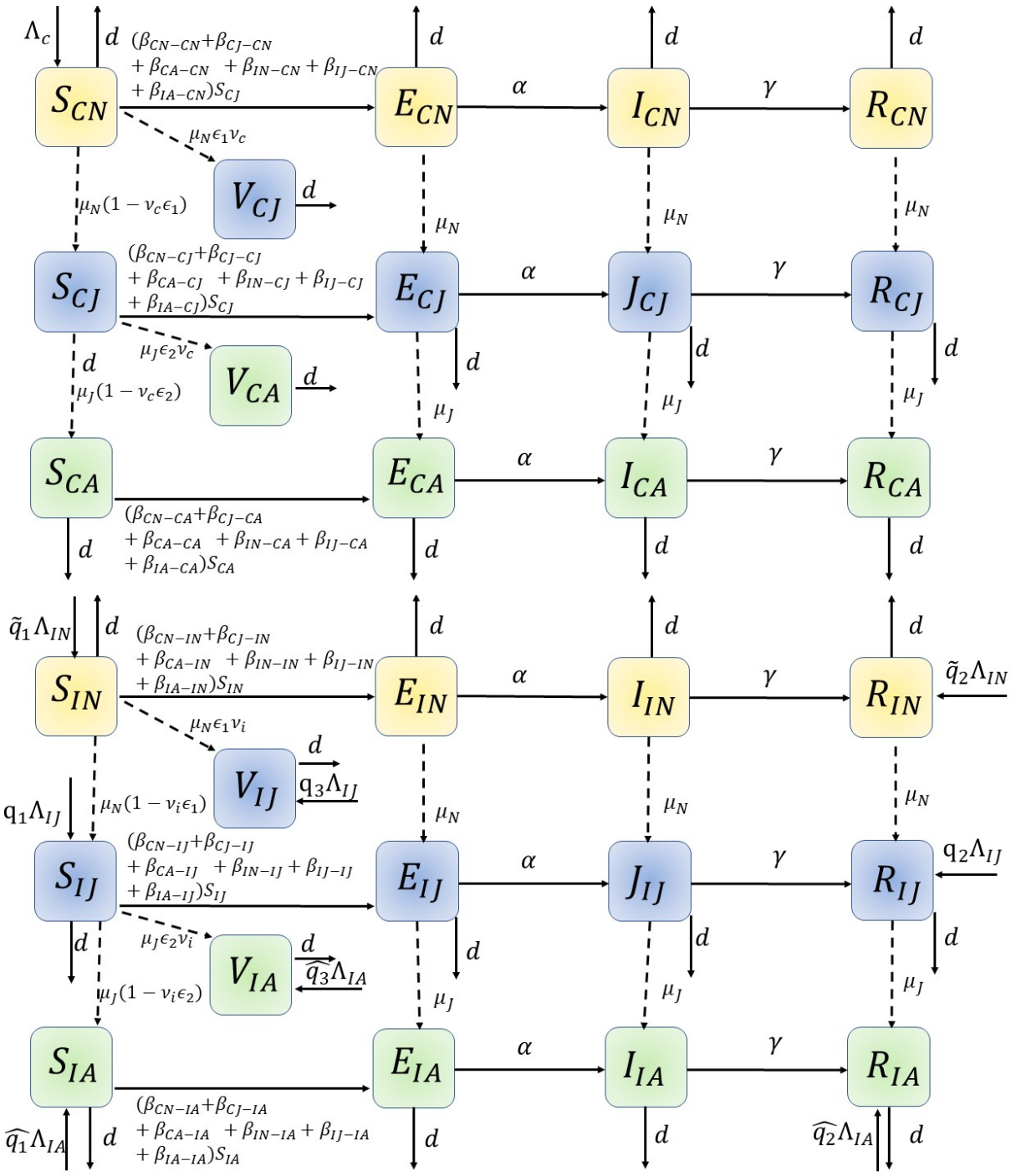

Figure 2.3: Flow diagram for Model (2.9) with three age classes, newborns (N), children(J), and adults (A), from immigrant (I) and Canadian populations (C). The model follows susceptible, exposed, infected, recovered and vaccinated individual in each class for each population

Population	**Definition**
S_k	Fraction of Canadian ($k = CN, CJ, CA$) or immigrant ($k = IN, IJ, IA$) newborns, juveniles or adults susceptible to the virus
E_k	Fraction of Canadian ($k = CN, CJ, CA$) or immigrant ($k = IN, IJ, IA$) newborns, juveniles or adults exposed to the virus
I_k	Fraction of Canadian ($k = CN, CJ, CA$) or immigrant ($k = IN, IJ, IA$) newborns, juveniles or adults infectious
R_k	Fraction of Canadian ($k = CN, CJ, CA$) or immigrant ($k = IN, IJ, IA$) newborns, juveniles or adults recovered and fully immune to the virus
V_k	Fraction of Canadian ($k = CJ, CA$) or immigrant ($k = IJ, IA$) juveniles or adults presenting life-long vaccine-induced immunity

Table 2.1: Table of variables

Parameter	Value	Definition	Ref
Λ_C	383.35 $people \times days^{-1}$	Canadian birth rate	[106]
Λ_{IN}	2% of Λ_{IJ} $people \times days^{-1}$	Newborn immigration rate	[106]
Λ_{IJ}	32.97 $people \times days^{-1}$	Children immigration rate	[106]
Λ_{IA}	296.73 $people \times days^{-1}$	Adults immigration rate	[106]
$\tilde{q}_2$	1/2	fraction of recovered immigrant newborns	assumed
$\tilde{q}_1$	1-$\tilde{q}_2$	fraction of susceptible immigrant newborns	assumed
q_2	1/2	fraction of recovered immigrant juveniles	assumed
q_3	1/2	fraction of vaccinated immigrant juveniles	assumed
q_1	1-$q_2 - q_3$	fraction of susceptible immigrant juveniles	assumed
$\hat{q}_2$	1/2	fraction of recovered immigrant adults	assumed
$\hat{q}_3$	1/2	fraction of vaccinated immigrant adults	assumed
$\hat{q}_1$	$1 - \hat{q}_2 - \hat{q}_3$	fraction of susceptible immigrant adults	assumed
d	$1/(52 \times 365)$ $people \times days^{-1}$	average outcoming rate to keep the population constant	evaluated from [106]
μ_{NB}	$1/(1 \times 365) days^{-1}$	rate of leaving the compartment where first vaccination takes place	[4]
μ_J	$1/(5 \times 365) days^{-1}$	rate of leaving the compartment where second vaccination takes place	[4]
ν_c	0.85	Canadian vaccination rate	[31]
ν_i	0.9	immigrant vaccination rate	[31],[108]
ϵ_1	0.95	first dose vaccine efficacy	[11, 109]
ϵ_2	0.99	second dose vaccine efficacy	[11, 109]
α	$1/8 days^{-1}$	average incubation period	[1]
γ	$1/7 days^{-1}$	average recovery period	[1]
β	$2.0744e-07$ $days^{-1}$	infection rate $\beta = \beta_{k-l}$, $k, l = CN, CJ, CA, IN, IJ, IA$	evaluated

Table 2.2: Table of parameters

$$
\begin{aligned}
E'_{CJ} &= (\beta_{CJ-CJ}I_{CJ} + \beta_{CA-CJ}I_{CA} + \beta_{IJ-CJ}I_{IJ} + \beta_{IA-CJ}I_{IA})S_{CJ} \\
&\quad - dE_{CJ} - \mu_J E_{CJ} - \alpha E_{CJ}
\end{aligned} \tag{2.1b}
$$

$$
I'_{CJ} = \alpha E_{CJ} - dI_{CJ} - \mu_J I_{CJ} - \gamma I_{CJ} \tag{2.1c}
$$

$$
R'_{CJ} = \gamma I_{CJ} - dR_{CJ} - \mu_J R_{CJ} \tag{2.1d}
$$

$$
\begin{aligned}
S'_{CA} &= \mu_J(1-\nu_c\epsilon_2)S_{CJ} - (\beta_{CJ-CA}I_{CJ} + \beta_{CA-CA}I_{CA} + \beta_{IJ-CA}I_{IJ} + \beta_{IA-CA}I_{IA})S_{CA} \\
&\quad - dS_{CA}
\end{aligned} \tag{2.1e}
$$

$$
\begin{aligned}
E'_{CA} &= (\beta_{CJ-CA}I_{CJ} + \beta_{CA-CA}I_{CA} + \beta_{IJ-CA}I_{IJ} + \beta_{IA-CA}I_{IA})S_{CA} - \\
&\quad - dE_{CA} + \mu_J E_{CJ} - \alpha E_{CA}
\end{aligned} \tag{2.1f}
$$

$$
I'_{CA} = \alpha E_{CA} - dI_{CA} + \mu_J I_{CJ} - \gamma I_{CA} \tag{2.1g}
$$

$$
R'_{CA} = \gamma I_{CA} - dR_{CJ} + \mu_J R_{CJ} \tag{2.1h}
$$

$$
V'_{CA} = \mu_J \nu_c \epsilon_2 S_{CJ} - dV_{CA} \tag{2.1i}
$$

$$
\begin{aligned}
S'_{IJ} &= q_1\Lambda_{JI} - (\beta_{CJ-IJ}I_{CJ} + \beta_{CA-IJ}I_{CA} + \beta_{IJ-IJ}I_{IJ} + \beta_{IA-IJ}I_{IA})S_{IJ} - \\
&\quad - dS_{IJ} - \mu_J S_{IJ}
\end{aligned} \tag{2.1j}
$$

$$
\begin{aligned}
E'_{IJ} &= (\beta_{CJ-IJ}I_{CJ} + \beta_{CA-IJ}I_{CA} + \beta_{IJ-IJ}I_{IJ} + \beta_{IA-IJ}I_{IA})S_{IJ} - \\
&\quad - dE_{IJ} - \mu_J E_{IJ} - \alpha E_{IJ}
\end{aligned} \tag{2.1k}
$$

$$
I'_{IJ} = \alpha E_{IJ} - dI_{IJ} - \mu I_{IJ} - \gamma I_{IJ} \tag{2.1l}
$$

$$
R'_{IJ} = q_2\Lambda_{JI} + \gamma I_{IJ} - dR_{IJ} - \mu_J R_{IJ} \tag{2.1m}
$$

$$
\begin{aligned}
S'_{IA} &= \hat{q}_1\Lambda_{AI} + \mu_J(1-\nu_i\epsilon_2)S_{IJ} - (\beta_{CJ-IA}I_{CJ} + \beta_{CA-IA}I_{CA} + \beta_{IJ-IA}I_{IJ} + \beta_{IA-IA}I_{IA})S_{IA} \\
&\quad - dS_{IA}
\end{aligned} \tag{2.1n}
$$

$$
\begin{aligned}
E'_{IA} &= (\beta_{CJ-IA}I_{CJ} + \beta_{CA-IA}I_{CA} + \beta_{IJ-IA}I_{IJ} + \beta_{IA-IA}I_{IA})S_{IA} - \\
&\quad - dE_{IA} + \mu_J E_{IJ} - \alpha E_{CA}
\end{aligned} \tag{2.1o}
$$

$$
I'_{IA} = \alpha E_{CJ} - dI_{IA} + \mu_J I_{IJ} - \gamma I_{IA} \tag{2.1p}
$$

$$
R'_{IA} = \hat{q}_2\Lambda_{AI} + \gamma I_{IA} - dR_{IA} + \mu_J R_{IJ} \tag{2.1q}
$$

$$
V'_{IA} = \hat{q}_3\Lambda_{AI} + \mu_J \nu_i \epsilon_2 S_{IJ} - dV_{IA} \tag{2.1r}
$$

Observe that since the total population is divided into subgroups, we define different infection rates depending on the age and country of origin. In particular, β_{k-l} indicates the infection rate between individuals in the subgroup k and the ones in l, where $k, l = CJ, CA, IJ, IA$. Also, given the high effectiveness of measles vaccine, the vaccination rates and efficacy are combined into one single parameter.

2.2.3 Results

Disease Free Equilibrium (DFE)

Now, we derive the DFE, $\mathcal{E}_0$, in absence of vaccination for Model (2.1). Here:

$$\mathcal{E}_0 = (S_{CJ_0}, 0, 0, 0, S_{CA_0}, 0, 0, 0, S_{IJ_0}, 0, 0, R_{IJ_0}, S_{IA_0}, 0, 0, R_{IA_0}) \tag{2.2}$$

where

$$S_{CJ_0} = \tfrac{\Lambda_C}{d+\mu_J} \qquad S_{CA_0} = \tfrac{\mu_J}{d} S_{CJ_0}$$

$$S_{IJ_0} = \tfrac{q_1\Lambda_{JI}}{d+\mu_J} \qquad R_{IJ_0} = \tfrac{q_2\Lambda_{JI}}{d+\mu_J} \qquad S_{IA_0} = \tfrac{\hat{q}_1\Lambda_{AI}}{d} + \tfrac{\mu_J}{d} S_{IJ_0} \qquad R_{IA_0} = \tfrac{\hat{q}_2\Lambda_{AI}}{d} + \tfrac{\mu_J}{d} R_{IJ_0}$$

When control is introduced in the population, we define the *disease free equilibrium* as

$$\tilde{\mathcal{E}}_0 = (\tilde{S}_{CJ_0}, 0, 0, 0, \tilde{S}_{CA_0}, 0, 0, 0, \tilde{V}_{CA_0}, \tilde{S}_{IJ_0}, 0, 0, \tilde{R}_{IJ_0}, \tilde{S}_{IA_0}, 0, 0, \tilde{R}_{IA_0}, \tilde{V}_{IA_0}) \tag{2.3}$$

where

$$\tilde{S}_{CJ_0} = \tfrac{\Lambda_C}{d+\mu_J} \qquad \tilde{S}_{CA_0} = \tfrac{\mu_J(1-\nu_c\epsilon_2)}{d} S_{CJ_0} \qquad \tilde{V}_{CA_0} = \tfrac{\mu_J\nu_c\epsilon_2}{d} S_{CJ_0} \qquad \tilde{S}_{IJ_0} = \tfrac{q_1\Lambda_{JI}}{d+\mu_J}$$

$$\tilde{R}_{IJ_0} = \tfrac{q_2\Lambda_{JI}}{d+\mu_J} \quad \tilde{S}_{IA_0} = \tfrac{\hat{q}_1\Lambda_{AI}}{d} + \tfrac{\mu_J(1-\nu_i\epsilon_2)}{d} S_{IJ_0} \quad \tilde{R}_{IA_0} = \tfrac{\hat{q}_2\Lambda_{AI}}{d} + \tfrac{\mu_J}{d} R_{IJ_0} \quad \tilde{V}_{IA_0} = \tfrac{\hat{q}_3\Lambda_{AI}}{d} + \tfrac{\mu_J\nu_i\epsilon_2}{d} S_{IJ_0}$$

Observe that $\tilde{\mathcal{E}}_0$ has been re-written in terms of $\mathcal{E}_0$.

Basic and Control Reproduction Numbers ($\mathcal{R}_0$ and $\mathcal{R}_c$)

An important factor to understand the dynamics of the outbreak is the *reproduction number*. Since in our model vaccination control is included, we find both the *basic* ($\mathcal{R}_0$) and *control reproduction number* ($\mathcal{R}_c$). In order to derive them, we use the well known *Next-Generation Matrix method* [88, 86, 92, 90]. We determined the matrices $\mathcal{F}$ and $\mathcal{V}$, using the E and I compartments of each sub-population, as follows:

$$\mathcal{F} = \begin{bmatrix} 0 & 0 & 0 & 0 & \beta S_{CJ_0} & \beta S_{CJ_0} & \beta S_{CJ_0} & \beta S_{CJ_0} \\ 0 & 0 & 0 & 0 & \beta S_{IJ_0} & \beta S_{IJ_0} & \beta S_{IJ_0} & \beta S_{IJ_0} \\ 0 & 0 & 0 & 0 & \beta S_{CA_0} & \beta S_{CA_0} & \beta S_{CA_0} & \beta S_{CA_0} \\ 0 & 0 & 0 & 0 & \beta S_{IA_0} & \beta S_{IA_0} & \beta S_{IA_0} & \beta S_{IA_0} \\ 0 & 0 & 0 & 0 & 0 & 0 & 0 & 0 \\ 0 & 0 & 0 & 0 & 0 & 0 & 0 & 0 \\ 0 & 0 & 0 & 0 & 0 & 0 & 0 & 0 \\ 0 & 0 & 0 & 0 & 0 & 0 & 0 & 0 \end{bmatrix} \tag{2.4}$$

$$\mathcal{V} = \begin{bmatrix} d+\mu_J+\alpha & 0 & 0 & 0 & 0 & 0 & 0 & 0 \\ 0 & d+\mu_J+\alpha & 0 & 0 & 0 & 0 & 0 & 0 \\ -\mu_J & 0 & d+\alpha & 0 & 0 & 0 & 0 & 0 \\ 0 & -\mu_J & 0 & d+\alpha & 0 & 0 & 0 & 0 \\ -\alpha & 0 & 0 & 0 & d+\mu_J+\gamma & 0 & 0 & 0 \\ 0 & -\alpha & 0 & 0 & 0 & d+\mu_J+\gamma & 0 & 0 \\ 0 & 0 & -\alpha & 0 & -\mu_J & 0 & d+\gamma & 0 \\ 0 & 0 & 0 & -\alpha & 0 & -\mu_J & 0 & d+\gamma \end{bmatrix} \tag{2.5}$$

The reproduction number is then defined by the spectral radius of $\mathcal{F}\mathcal{V}^{-1}$, i.e. $\mathcal{R}_0 = \rho(\mathcal{F}\mathcal{V}^{-1})$. All the computations related to the reproduction numbers for Model (2.1) are shown in Appendix A. The basic reproduction number for Model (2.1) is defined as:

$$\mathcal{R}_0 = \frac{\alpha\beta(S_{CJ_0} + S_{CA_0} + S_{IJ_0} + S_{IA_0})}{(d+\alpha)(d+\gamma)} \tag{2.6}$$

By following the same steps, we are able to express the control reproduction number as

$$\mathcal{R}_c = \frac{\alpha\beta}{(d+\alpha)(d+\gamma)}\left(S_{CJ_0} + S_{CA_0} + S_{IJ_0} + S_{IA_0} - \epsilon_2\frac{\mu_J}{d}\left(\nu_c S_{CJ_0} + \nu_i S_{IJ_0}\right)\right) \tag{2.7}$$

Observe that the second term in Eq.(2.7) is composed of the total susceptible population minus the proportion of individuals who is successfully immunized. Moreover, it is possible to rewrite Eq. (2.7) in terms of $\mathcal{R}_0$, i.e.

$$\mathcal{R}_c = \left(1 - \frac{\epsilon_2\frac{\mu_J}{d}\left(\nu_c S_{CJ_0} + \nu_i S_{IJ_0}\right)}{S_{CJ_0} + S_{CA_0} + S_{IJ_0} + S_{IA_0}}\right)\mathcal{R}_0 \tag{2.8}$$

Observe that both $\mathcal{R}_0$ and $\mathcal{R}_c$ and the disease free equilibria expressions show a linear correlation on the proportion of susceptible immigrant juveniles (q_1) and susceptible immigrant adults ($\hat{q}_1$). Although the basic reproduction number of measles is considered to range between 12 and 18 [12], a recent systematic review [15] provides a wider range (6- $\approx$ 200). In order to understand how the control reproduction number depends on the $\mathcal{R}_0$ and the susceptible immigration rates, we fix $\mathcal{R}_0 = 6, 8, 10, 14, 18, 20$ and vary $q_1, \hat{q}_1 \in [0, 1]$ and we investigate how $\mathcal{R}_c$ varies (Figure (2.4)). Observe that for the given set of $\mathcal{R}_0$, $\mathcal{R}_c$ assumes values in the interval $(3.4, 12.3)$.

Infected Equilibrium

The infected equilibrium cannot be found analytically. We provide some plots on the dynamics of S, E, I, R compartments in Figure (2.5a). V is not included since it is always constant. We

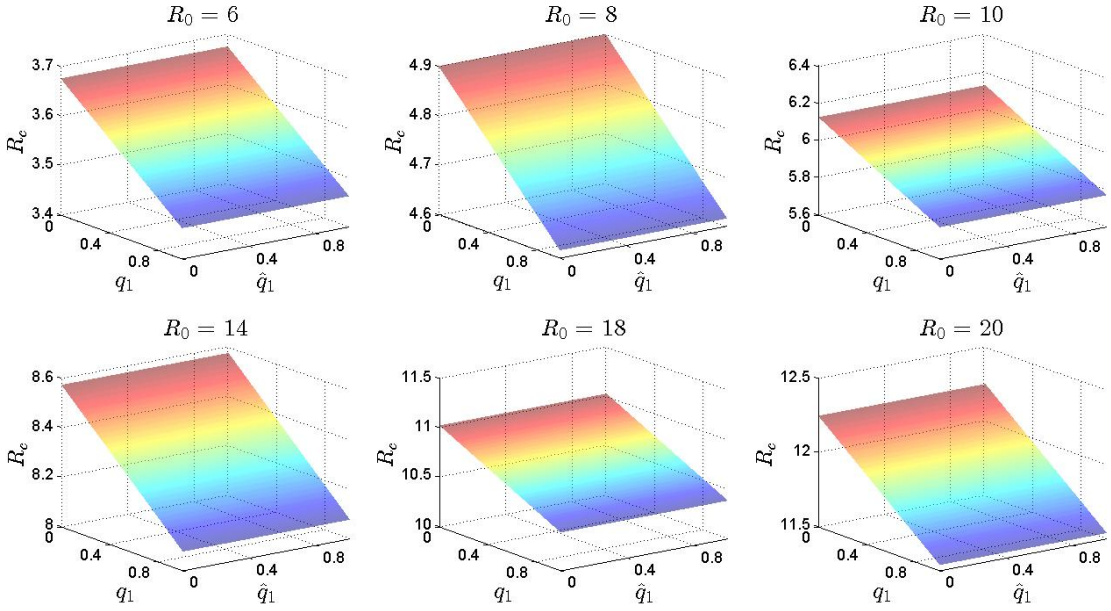

(a)

Figure 2.4: $\mathcal{R}_c$ surface plots for $q_1, \hat{q}_1 \in [0, 1]$ and $\mathcal{R}_0 = 6, 8, 10, 14, 18, 20$

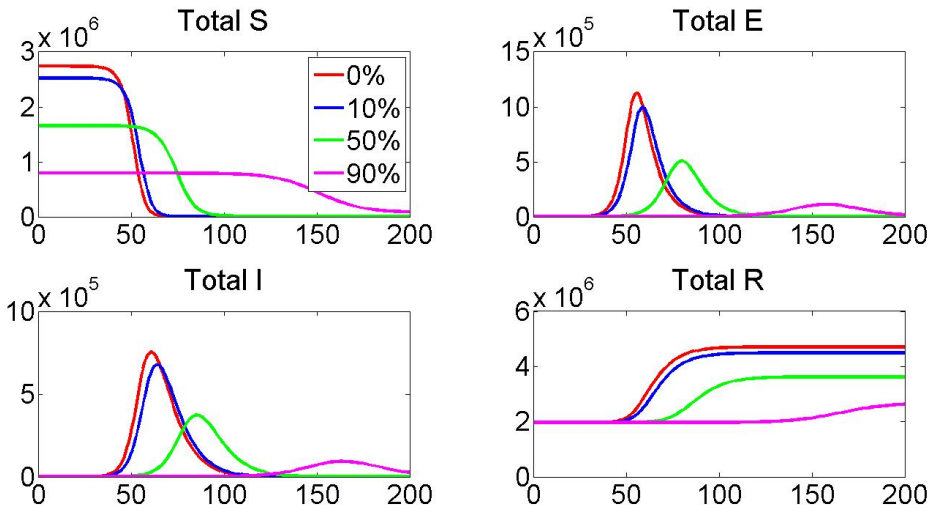

(a)

Figure 2.5: Dynamics of total S, E, I, R compartments when both ν_c and $\hat{q}_1$ were increased and reduced, respectively, by $0\%, 10\%, 50\%, 90\%$

set $\nu_c = 85\%$ and $\hat{q}_1 = 1/2$. We compare the dynamics by increasing the Canadian vaccination coverage and reducing the proportion of susceptible adult immigrants by $0\%, 10\%, 50\%, 90\%$. We observe that under these conditions the peak of the infection is smaller and sustained for longer time.

Sensitivity Analysis

Given the uncertainty of the parameters used, we carry out the *Latin Hypercube Sampling* and *Partial Rank Correlation Coefficient* (LHS/PRCC) sensitivity analysis in order to explore the effect that these values have on the model. First, we investigate the influence that the parameters related to demographics (i.e. birth, death, immigration, aging and vaccination rates) have on the population at the disease free equilibrium. Then, we focus on a single outbreak dynamics, which coincides with roughly 350 days, and we look at the impact that disease-related parameters (i.e. infection, incubation and recovery rate) and the subpopulations at the disease free equilibrium have on the magnitude of peak of infection, time at which the peak of infection occurs, time at which the epidemic end and outbreak final size.

We start with investigating the DFE. By using LHS, we generate a set of $\Omega = 20000$ samples for each parameter. Since the proportion of susceptible, recovered and vaccinated juvenile and adult immigrants depend on $q_1, q_2, \hat{q}_1, \hat{q}_2, \hat{q}_3$, we need to sample these values so that $q_1 + q_2 = 1$, $\hat{q}_1 + \hat{q}_2 + \hat{q}_3 = 1$. In particular, for immigrant juveniles we sample $q_2 \in [0, 1]$ and define $q_1 = 1 - q_2$, for immigrant adults $\hat{q}_2$ is chosen between 0 and 1, $\hat{q}_3$ is randomly picked in the interval $[0, 1 - \hat{q}_2]$ and $\hat{q}_1 = 1 - \hat{q}_2 - \hat{q}_3$. Additionally, since we assume the population to be constant, we filter the population at the disease free equilibrium to be ranged in the interval $(1.1e07, 1.5e07)$. Out of the initial Ω sampled set, the number of samples that satisfy all the mentioned conditions is roughly the 52%. Monotonicity has been analysed for all the parameters sampled.

The sensitivity analysis on the disease free equilibrium $\tilde{\mathcal{E}}_0$ is shown in Figure (2.6). Observe that the population at the equilibrium is affected mostly by outgoing and birth/incoming rates. As expected, d presents a significant negative correlation, hence if individuals leave the population at a faster rate, then the population size decreases. On the other hand, the Ontario birth rate and immigrant adults incoming rate increases the population size increases as well. Note that the incoming rate of immigrant juveniles does not show any impact on the community magnitude.

Knowing the distribution of immunity in a population is fundamental in order to predict and prevent the infection spread. Since our model assumes that life long immunity is provided by both the virus and vaccination, it is important to understand if and under which conditions herd immunity is achievable and sustained. Hence, our investigation is focused on the ratio of the R and V compartments over the susceptible class. Figure (2.7) shows the PRCC of demographics-related parameters on $(R_{IA} + R_{IJ})/S$, $(V_{CA} + V_{IA})/S$, $(R_{IA}+R_{IJ}+V_{CA}+V_{IA})/S$ where S indicates the total number of susceptible in the population (i.e. $S = S_{CJ} + S_{CA} + S_{IJ} + S_{IA}$). Figure (2.7a) shows the ratio of recovered-susceptible

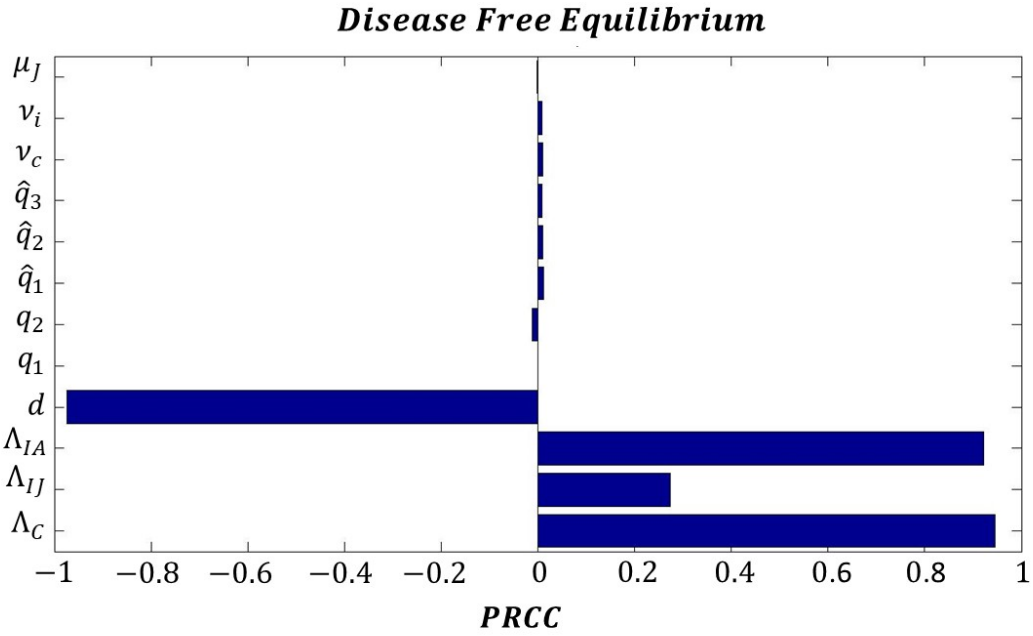

(a)

Figure 2.6: Disease free equilibrium $\tilde{\mathcal{E}}_0$

classes. Observe that the proportion of Canadians vaccinated (ν_c) and the proportion of recovered immigrant adults ($\hat{q}_2$) present a significant positive correlation on this ratio (i.e. the PRCC is greater than 0.5). On the other hand, a significant negative correlation (i.e. PRCC is less than -0.5) is shown for the proportion of susceptible immigrant adults ($\hat{q}_1$). These correlations imply that when the vaccination rate of Canadians and the recruitment rate of recovered immigrant adults increase and less susceptible adults immigrate, recovered individuals exceeds the population in the total susceptible class, making the most vulnerable groups less exposed to a possible infection. Similar PRCC is visible in Figure (2.7b) where the ratio of vaccinated and susceptible individuals is shown. The Canadian vaccination rate and the proportion of vaccinated immigrant adults present a significant positive correlation, while the fraction of susceptible adults shows a significant negative correlation. Hence, when more children in Ontario are vaccinated and more vaccinated adults are immigrating, the proportion of V becomes larger than S, suggesting that in case of outbreak, susceptible individuals will be indirectly protected by vaccinees. Figure (2.7c) describes the PRCC on the total recovered and vaccinated individuals over the total susceptible classes. Contrary to the previous cases where recovered and vaccinated immigrant adult present significant positive correlation, here the only parameter affecting the ratio positively is the Ontario vaccination rate. The more children in Ontario are protected by vaccine-induced immunity, the more the number of individuals with long life immunity exceeds the number of susceptible people. On the other hand, a significant negative correlation is visible for the proportion of susceptible immigrant adults. This suggests that as $\hat{q}_1$ decreases, less susceptibility is present in the population.

From the results of our sensitivity analysis, we show the change in the fractions R/S, $(R+V)/S$ and V/S when we vary ν_c between 50% and 95% and $\hat{q}_1 = 1/2, 1/5, 1/10, 1/20$ (Figure2.8). We observe that the change in the ratios agrees with what is shown in the sensitivity analysis. As the vaccination coverage of Canadian children increases and the proportion of susceptible decreases, the individuals in R and V increase.

Given the health background of immigrants, we can believe that most of the adults are immune to the pathogen through either infection or inoculation. It is then more essential to increase the Ontario vaccination coverage in order to increase the number of individuals presenting life long immunity. However, the possibility to offer a measles vaccine shot to newcomers, decreasing the size of possible susceptible immigrants, should be considered by Public Health officials.

Now, since we know the demographic and immigration parameters of our population, we keep them as constant and investigate the infection dynamics with a secondary sensitivity analysis. In particular, we focus on peak magnitude, peak time, end of epidemic, epidemic final size.

In this investigation, we sample S_{CJ_0},S_{CA_0}, V_{CA_0}, S_{IJ_0}, R_{IJ_0},S_{IA_0}, R_{IA_0}, V_{IA_0} by ranging them between their minimum and maximum values provided by the previous LHS. Then, we consider only the parameters giving total population size that lies in the interval $(1.1e07, 1.5e07)$. A further condition is then applied on the controlled reproduction number. We only accept samples satisfying $\mathcal{R}_c \in [3, 18]$. The initial samples are $\Omega_2 = 20000$ and the ones satisfying

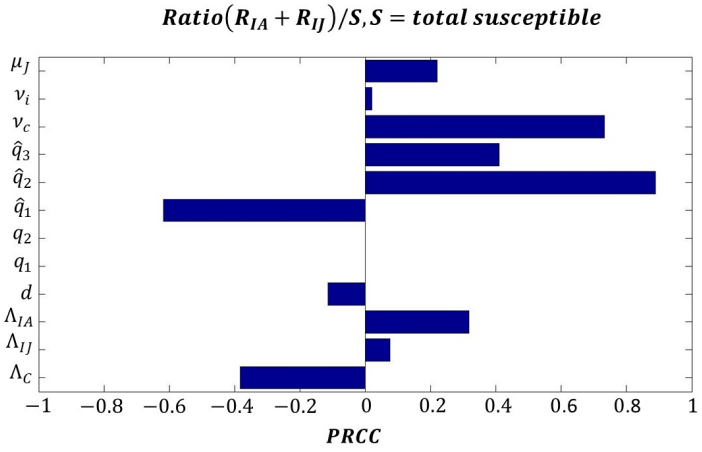

(a)

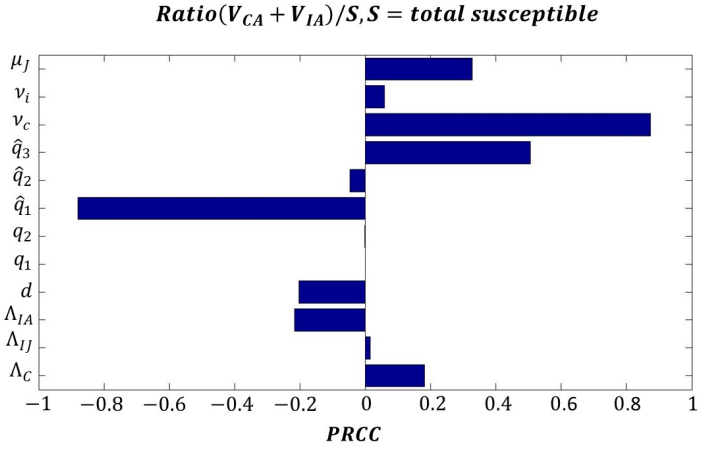

(b)

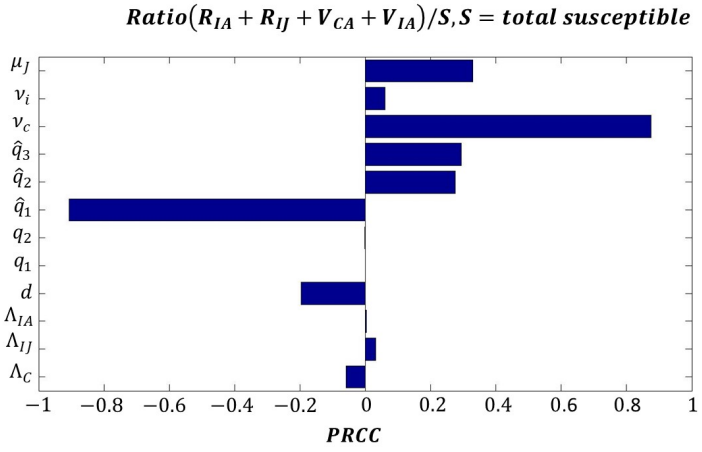

(c)

Figure 2.7: LHS/PRCC plots for the parameters μ_j, ν_i, ν_c, $\hat{q}_1$, $\hat{q}_2$, $\hat{q}_3$, q_1, q_2, d, Λ_C, Λ_{IJ} and Λ_{IA} on ratio (a) $(R_{IA}+R_{IJ})/S$ (b)$(V_{CA}+V_{IA})/S$ (c) $(R_{IA}+R_{IJ}+V_{CA}+V_{IA})/S$, where $S = S_{CJ0}+S_{CA0}+S_{IJ0}+S_{IA0}$

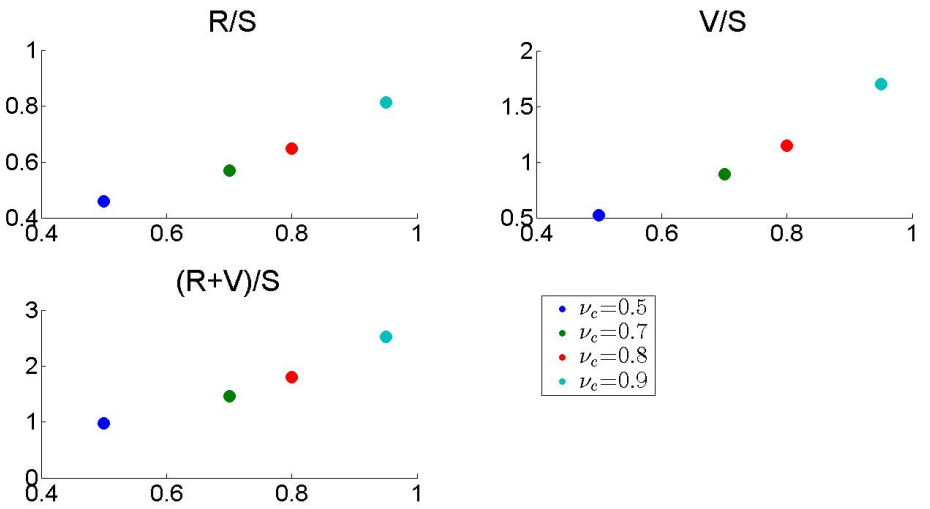

(a)

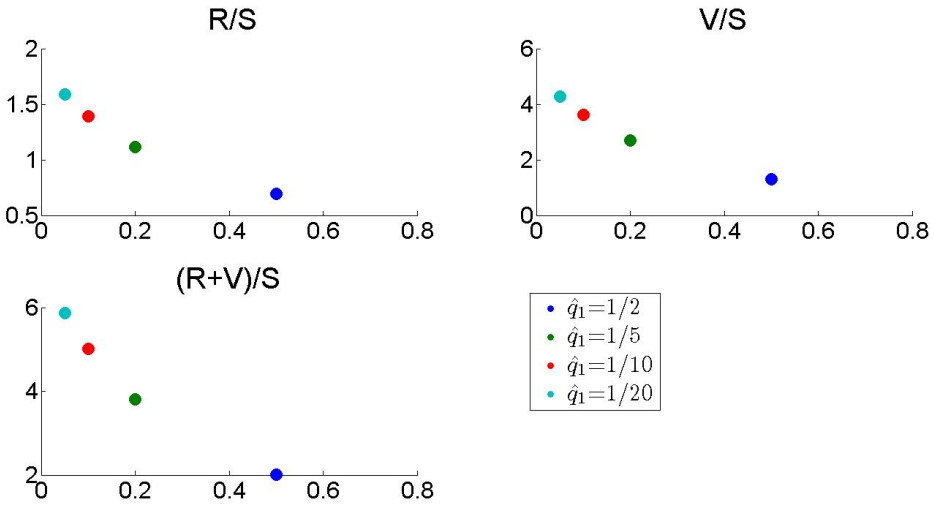

(b)

Figure 2.8: Plot of ratios of total recovered, total vaccinated, total R+V over total susceptible population, varying (a) ν_c, with $\hat{q}_1 = 1/2$ (b) $\hat{q}_1$, with $\nu_c = 0.85$

the conditions on the total population and $\mathcal{R}_c$ are roughly the 48%.

We look at the PRCC for the initial population sizes and infection-related parameters on the total population and, successively, on the single sub-populations (country of origin and age dependent).
Figure (2.9) shows that susceptible immigrant adults, susceptible Canadian children and adults and the transmission rate β present a significant positive correlation on the controlled reproduction number $\mathcal{R}_c$. This indicates that the number of secondary cases increases as these values increase. Given the health background of adult immigrants, S_{IA_0} should be small, hence the main goal is to reduce the transmission rate and the size of vulnerable Canadian children and adult through vaccination.

Observe that the population of susceptible immigrant and Canadians (both adults and juveniles) ($S_{IA_0}, S_{IJ_0}, S_{CA_0}, S_{CJ_0}$, respectively) and β present a significant positive correlation on the peak of the infection (Figure (2.10a)). This indicates that increasing the size of these subpopulations and the infection transmission, the outbreak will grow. Hence, to reduce the magnitude of the outbreak, it is important minimize the size of susceptible Canadians and newcomers. On the other hand, the time needed to reach the peak of the infection increases as the infection rate and susceptible immigrant decreases (Figure (2.10b)). It appears that the susceptible immigrant adults carry the burden of delaying the time at which the infection reaches its maximum. Figure (2.11a) shows the correlation on the time at which the epidemic ends and similarly on the time of the infection peak, S_{IA_0} shows significant negative correlation. This suggests the outbreak will develop more slowly if the immigrant adults subclass grows. After the infection completes its natural course, it is fundamental to analyze the number of people who experienced the disease in order to understand which age groups were more affected. For this purpose, we study the proportion of susceptible that did experience the infection (Figure (2.11b)). Similar to the previous analyses, the susceptible classes of immigrant and Canadian, both juveniles and adults, are the most significant. As the pool of the mentioned subclasses increases, the number of individuals experiencing the infection will increase. Observe that the parameters related to the infection show the correlation as expected.
The results on the single subpopulations are intuitive and so are shown in Appendix C.

Similar to our first results, as expected, the outbreak dynamics appears to be affected mostly by the susceptible individuals, in particular immigrants and young Canadians. However, the proportion of S_{IA_0} is relatively small, since immigrants might have acquired the immunity via vaccine or infection. Hence, Public Health should focus mainly on increasing the immunization of the youngest groups and decreasing the transmission, by implementing contact tracing and social distancing policies.

2.2.4 Mathematical Model: Three Age Groups

The model we propose now takes into consideration the recommended age for two measles vaccine doses provided by the Government of Canada [11]: first dose given at 12-15 months of age and second dose around school age. Moreover, CDC [1] asserts that two doses of vaccine

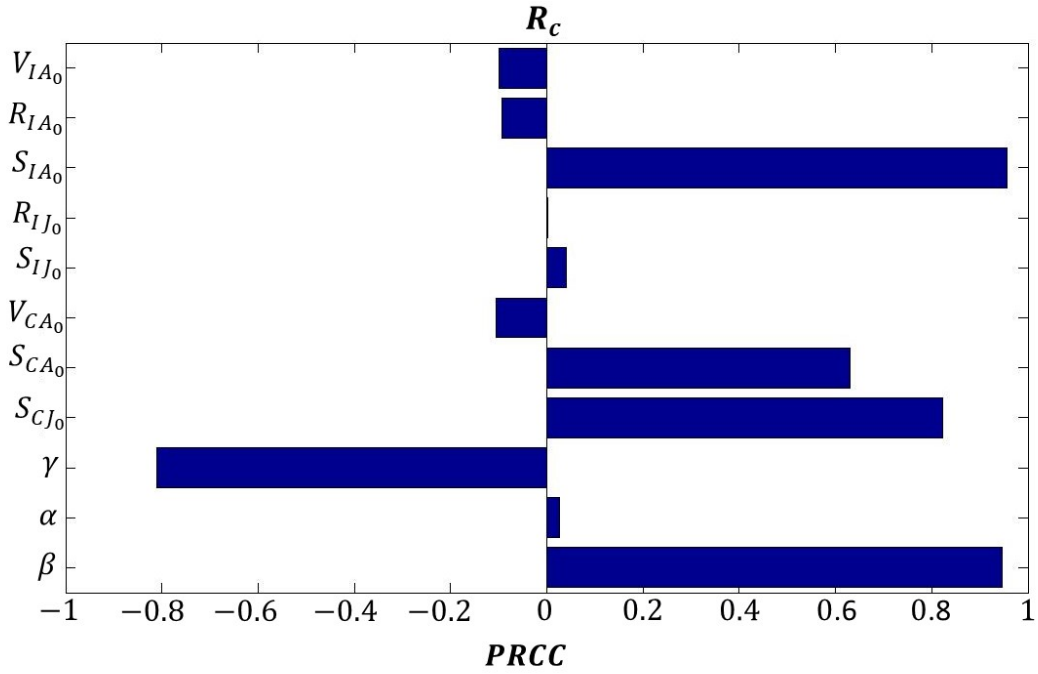

(a)

Figure 2.9: LHS/PRCC plots for the population at the disease free equilibrium and parameters γ, α, β on $\mathcal{R}_c$

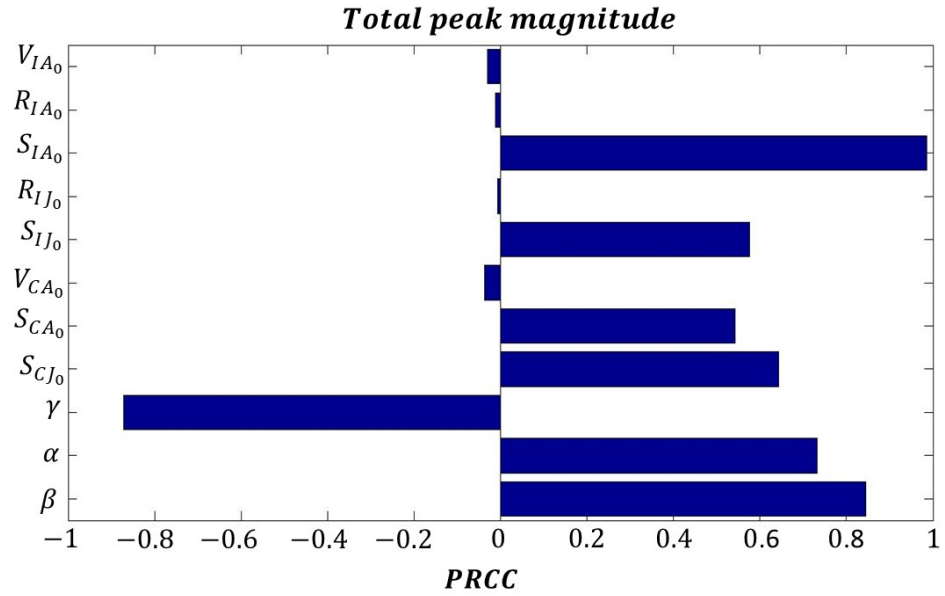

(a)

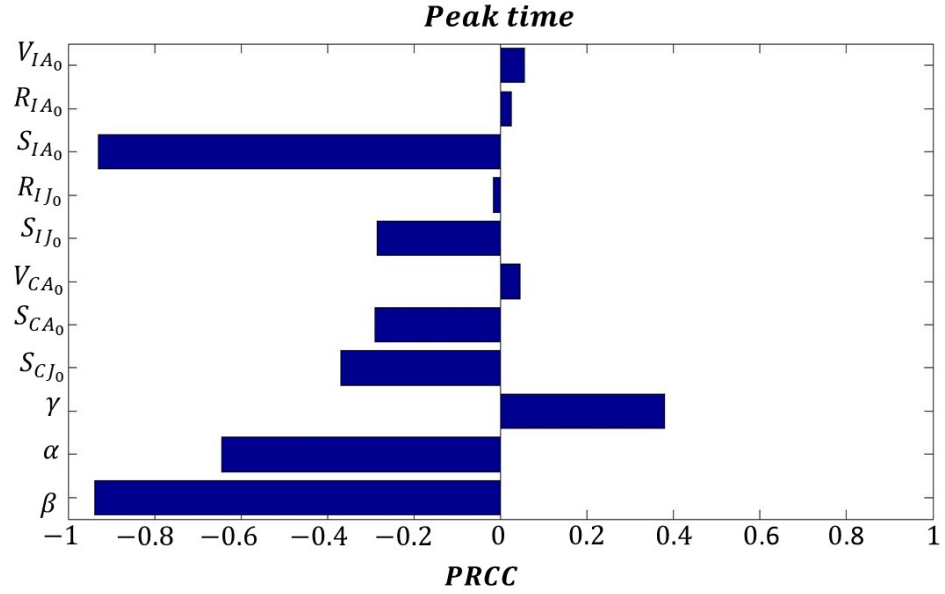

(b)

Figure 2.10: LHS/PRCC plots for the population at the disease free equilibrium and parameters γ, α, β on total population (a) peak magnitude (b) time of maximum peak

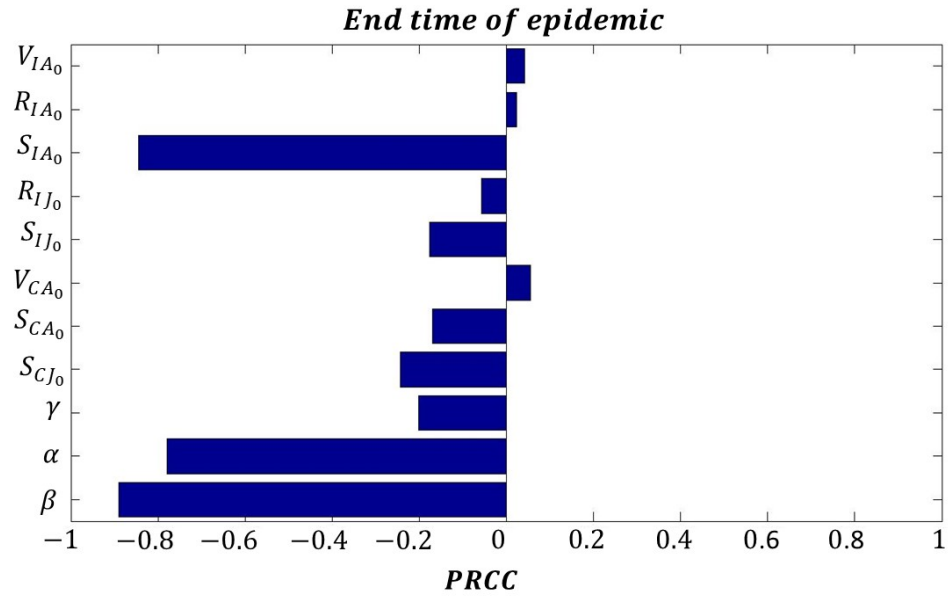

(a)

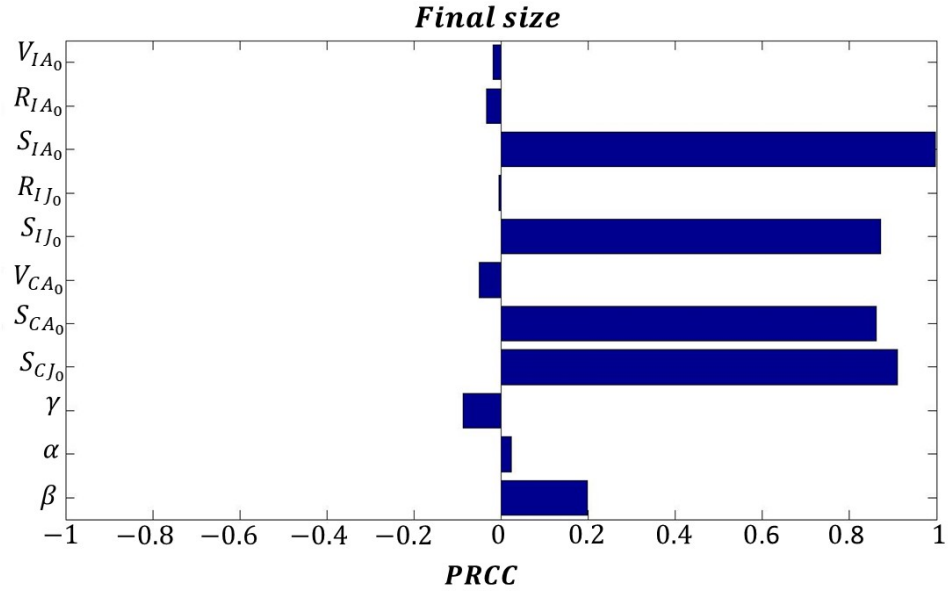

(b)

Figure 2.11: LHS/PRCC plots for the population at the disease free equilibrium and parameters γ, α, β on (a) time of end of epidemic (b) final size (number of total infected individuals)

effectiveness is about 97%, while one single dose's is around 93%. Since the two doses are given at different ages, we formulate a mathematical model that gathers this immunization schedule considering the population clustered into three groups. We modify Model (2.1) by dividing the juvenile age group into two subgroups: 0-1 year, 1-5 years. The third group corresponds to the population which is 6 years and older. These clusters are identified with subscript N (Newborn), J (Juveniles), A (Adults), respectively. We assume that newborn immigrants might have acquired the infection while in their country of origin. Hence, at the time of immigration, they might be either susceptible or recovered. For juveniles and adults coming from abroad, we assume that they might be susceptible, recovered if encountered the infection while living outside Canada, or vaccinated. Moreover, we assume that Canadian newborns aged less than 1 year are fully susceptible ignoring immunity gained from maternal antibodies. This assumption is to describe a worst-case scenario in order to get results that will best protect this vulnerable population.
The system of differential equations describing the infection dynamics is the following:

$$\begin{aligned} S'_{CN} &= \Lambda_C - dS_{CN} - \mu_{NB}S_{CN} - S_{CN}(\beta_{CN-CN}I_{CN} + \beta_{CN-CJ}I_{CJ} + \beta_{CN-CA}I_{CA}) - \\ &\quad - S_{CN}(\beta_{CN-IN}I_{IN} + \beta_{CN-IJ}I_{IJ} + \beta_{CN-IA}I_{IA}) \end{aligned} \tag{2.9a}$$

$$\begin{aligned} E'_{CN} &= -dE_{CN} - \mu_{NB}E_{CN} - \alpha E_{CN} + S_{CN}(\beta_{CN-CN}I_{CN} + \beta_{CN-CJ}I_{CJ} + \beta_{CN-CA}I_{CA}) + \\ &\quad + S_{CN}(\beta_{CN-IN}I_{IN} + \beta_{CN-IJ}I_{IJ} + \beta_{CN-IA}I_{IA}) \end{aligned} \tag{2.9b}$$

$$I'_{CN} = \alpha E_{CN} - dI_{CN} - \mu_{NB}I_{CN} - \gamma I_{CN} \tag{2.9c}$$

$$R'_{CN} = \gamma I_{CN} - dR_{CN} - \mu_{NB}R_{CN} \tag{2.9d}$$

$$\begin{aligned} S'_{CJ} &= \mu_{NB}(1-\epsilon_1\nu_c)S_{CN} - S_{CJ}(\beta_{CN-CN}I_{CN} + \beta_{CN-CJ}I_{CJ} + \beta_{CN-CA}I_{CA}) - \\ &\quad - S_{CJ}(\beta_{CN-IN}I_{IN} + \beta_{CN-IJ}I_{IJ} + \beta_{CN-IA}I_{IA}) - dS_{CJ} - \mu_J S_{CJ} \end{aligned} \tag{2.9e}$$

$$\begin{aligned} E'_{CJ} &= S_{CJ}(\beta_{CJ-CN}I_{CN} + \beta_{CJ-CJ}I_{CJ} + \beta_{CJ-CA}I_{CA}) + \\ &\quad S_{CJ}(\beta_{CJ-IN}I_{IN} + \beta_{CJ-IJ}I_{IJ} + \beta_{CJ-IA}I_{IA}) - dE_{CJ} - \mu_J E_{CJ} - \alpha E_{CJ} + \mu_{NB}E_{CN} \end{aligned} \tag{2.9f}$$

$$I'_{CJ} = \alpha E_{CJ} - dI_{CJ} - \mu_J I_{CJ} - \gamma I_{CJ} + \mu_{NB}I_{CN} \tag{2.9g}$$

$$R'_{CJ} = \gamma I_{CJ} - dR_{CJ} - \mu_J R_{CJ} + \mu_{NB}R_{CN} \tag{2.9h}$$

$$V'_{CJ} = \mu_{NB}\epsilon_1\nu_c S_{CN} - dV_{CJ} - \mu_J V_{CJ} \tag{2.9i}$$

$$\begin{aligned} S'_{CA} &= \mu_J(1-\epsilon_2\nu_c)S_{CJ} - dS_{CA} - S_{CA}(\beta_{CA-CN}I_{CN} + \beta_{CA-CJ}I_{CJ} + \beta_{CA-CA}I_{CA}) - \\ &\quad - S_{CA}(\beta_{CA-IN}I_{IN} + \beta_{CA-IJ}I_{IJ} + \beta_{CA-IA}I_{IA}) \end{aligned} \tag{2.9j}$$

$$\begin{aligned} E'_{CA} &= \mu_J E_{CJ} - \alpha E_{CA} - dE_{CA} + S_{CA}(\beta_{CA-CN}I_{CN} + \beta_{CA-CJ}I_{CJ} + \beta_{CA-CA}I_{CA}) + \\ &\quad + S_{CA}(\beta_{CA-IN}I_{IN} + \beta_{CA-IJ}I_{IJ} + \beta_{CA-IA}I_{IA}) \end{aligned} \tag{2.9k}$$

$$I'_{CA} = \alpha E_{CA} - dI_{CA} + \mu_J I_{CJ} - \gamma I_{CA} \tag{2.9l}$$

$$R'_{CA} = \gamma I_{CA} - dR_{CA} + \mu_J R_{CJ} \tag{2.9m}$$

$$V'_{CA} = \mu_J\epsilon_2\nu_c S_{CJ} - dV_{CA} + \mu_J V_{CJ} \tag{2.9n}$$

$$
\begin{aligned}
S'_{IN} &= \tilde{q}_1\Lambda_{IN} - dS_{IN} - \mu_{NB}S_{IN} - S_{IN}(\beta_{IN-CN}I_{CN} + \beta_{IN-CJ}I_{CJ} + \beta_{IN-CA}I_{CA}) - \\
&\quad - S_{IN}(\beta_{IN-IN}I_{IN} + \beta_{IN-IJ}I_{IJ} + \beta_{IN-IA}I_{IA}) && (2.9o)\\
E'_{IN} &= S_{IN}(\beta_{IN-CN}I_{CN} + \beta_{IN-CJ}I_{CJ} + \beta_{IN-CA}I_{CA}) + \\
&\quad + S_{IN}(\beta_{IN-IN}I_{IN} + \beta_{IN-IJ}I_{IJ} + \beta_{IN-IA}I_{IA}) - dE_{IN} - \mu_{NB}E_{IN} - \alpha E_{IN} && (2.9p)\\
I'_{IN} &= \alpha E_{IN} - dI_{IN} - \mu_{NB}I_{IN} - \gamma I_{IN} && (2.9q)\\
R'_{IN} &= \tilde{q}_2\Lambda_{IN} + \gamma I_{IN} - dR_{IN} - \mu_{NB}R_{IN} && (2.9r)\\
S'_{IJ} &= q_1\Lambda_{IJ} + \mu_{NB}(1-\epsilon_1\nu_i)S_{IN} - S_{IJ}(\beta_{IJ-CN}I_{CN} + \beta_{IJ-CJ}I_{CJ} + \beta_{IJ-CA}I_{CA}) - \\
&\quad - S_{IJ}(\beta_{IJ-IN}I_{IN} + \beta_{IJ-IJ}I_{IJ} + \beta_{IJ-IA}I_{IA}) - dS_{IJ} - \mu_J S_{IJ} && (2.9s)\\
E'_{IJ} &= S_{IJ}(\beta_{IJ-CN}I_{CN} + \beta_{IJ-CJ}I_{CJ} + \beta_{IJ-CA}I_{CA}) + \\
&\quad + S_{IJ}(\beta_{IJ-IN}I_{IN} + \beta_{IJ-IJ}I_{IJ} + \beta_{IJ-IA}I_{IA}) - dE_{IJ} - \mu_J E_{IJ} - \alpha E_{IJ} + \mu_{NB}E_{IN} && (2.9t)\\
I'_{IJ} &= \alpha E_{IJ} - dI_{IJ} - \mu_J I_{IJ} - \gamma I_{IJ} + \mu_{NB}I_{IN} && (2.9u)\\
R'_{IJ} &= q_2\Lambda_{IJ} + \gamma I_{IJ} - dR_{IJ} - \mu_J R_{IJ} + \mu_{NB}R_{IN} && (2.9v)\\
V'_{IJ} &= q_3\Lambda_{IJ} + \mu_{NB}\epsilon_1\nu_i S_{IN} - dV_{IJ} - \mu_J V_{IJ} && (2.9w)\\
S'_{IA} &= \hat{q}_1\Lambda_{IA} + \mu_J(1-\epsilon_2\nu_i)S_{IJ} - S_{IA}(\beta_{IA-CN}I_{CN} + \beta_{IA-CJ}I_{CJ} + \beta_{IA-CA}I_{CA}) - \\
&\quad - S_{IA}(\beta_{IA-IN}I_{IN} + \beta_{IA-IJ}I_{IJ} + \beta_{IA-IA}I_{IA}) - dS_{IA} && (2.9x)\\
E'_{IA} &= S_{IA}(\beta_{IA-CN}I_{CN} + \beta_{IA-CJ}I_{CJ} + \beta_{IA-CA}I_{CA}) + \\
&\quad + S_{IA}(\beta_{IA-IN}I_{IN} + \beta_{IA-IJ}I_{IJ} + \beta_{IA-IA}I_{IA}) + \mu_J E_{IJ} - \alpha E_{IA} - dE_{IA} && (2.9y)\\
I'_{IA} &= \alpha E_{IA} - dI_{IA} + \mu_J I_{IJ} - \gamma I_{IA} && (2.9z)\\
R'_{IA} &= \hat{q}_2\Lambda_{IA} + \gamma I_{IA} - dR_{IA} + \mu_J R_{IJ} && (2.9aa)\\
V'_{IA} &= \hat{q}_3\Lambda_{IA} + \mu_J\epsilon_2\nu_i S_{IJ} - dV_{IA} + \mu_J V_{IJ} && (2.9ab)\\
& && (2.9ac)
\end{aligned}
$$

The description of variables and parameters used in Model (2.9) are shown in Tables 2.1 and 2.2. Observe, similar to Model (2.1), for numerical simulations, we assume that individuals in different age groups mix uniformly. Moreover, the vaccination rate (ν_c,ν_i) and vaccine efficacy ($\epsilon_{1,2}$) are considered as one parameter. This is because measles vaccine is considered extremely effective, hence this efficacy will not affect much the vaccination coverage.

Disease Free Equilibrium (DFE)

Similar to Model (2.1), we investigate the DFE of Model (2.9) with or in absence of vaccination control. The disease free equilibrium with no control is defined as

$$
\bar{\bar{\mathcal{E}}}_0 = (\bar{\bar{S}}_{CN_0}, 0, 0, 0, \bar{\bar{S}}_{CJ_0}, 0, 0, 0, \bar{\bar{S}}_{CA_0}, 0, 0, 0, \bar{\bar{S}}_{IN_0}, 0, 0, \bar{\bar{R}}_{IN_0}, \bar{\bar{S}}_{IJ_0}, 0, 0, \bar{\bar{R}}_{IJ_0}, \bar{\bar{S}}_{IA_0}, 0, 0, \bar{\bar{R}}_{IA_0}) \tag{2.10}
$$

where

$$\bar{\bar{S}}_{CN_0} = \tfrac{\Lambda_C}{d+\mu_{NB}} \qquad \bar{\bar{S}}_{CJ_0} = \tfrac{\mu_{NB}}{d+\mu_J}\bar{\bar{S}}_{CN_0} \qquad \bar{\bar{S}}_{CA_0} = \tfrac{\mu_J}{d}\bar{\bar{S}}_{CJ_0}$$

$$\bar{\bar{S}}_{IN_0} = \tfrac{\tilde{q}_1\Lambda_{IN}}{d+\mu_{NB}} \qquad \bar{\bar{R}}_{IN_0} = \tfrac{\tilde{q}_2\Lambda_{IN}}{d+\mu_{NB}} \qquad \bar{\bar{S}}_{IJ_0} = \tfrac{q_1\Lambda_{IJ}}{d+\mu_J} + \tfrac{\mu_{NB}}{d+\mu_J}\bar{\bar{S}}_{IN_0} \qquad \bar{\bar{R}}_{IJ_0} = \tfrac{q_2\Lambda_{IJ}}{d+\mu_J} + \tfrac{\mu_{NB}}{d+\mu_J}\bar{\bar{R}}_{IN_0}$$

$$\bar{\bar{S}}_{IA_0} = \tfrac{\hat{q}_1\Lambda_{IA}}{d} + \tfrac{\mu_J}{d}\bar{\bar{S}}_{IJ_0} \qquad \bar{\bar{R}}_{IA_0} = \tfrac{\hat{q}_2\Lambda_{IA}}{d} + \tfrac{\mu_J}{d}\bar{\bar{R}}_{IJ_0}$$

When control is introduced in the population, the disease free equilibrium is defined as:

$$\begin{aligned}\bar{\mathcal{E}_0} = (&\bar{S}_{CN_0}, 0, 0, 0, \bar{S}_{CJ_0}, 0, 0, 0, \bar{V}_{CJ_0}, \bar{S}_{CA_0}, 0, 0, 0, \bar{V}_{CA_0},\\ &\bar{S}_{IN_0}, 0, 0, \bar{R}_{IN_0}, \bar{S}_{IJ_0}, 0, 0, \bar{R}_{IJ_0}, \bar{V}_{IJ_0}, \bar{S}_{IA_0}, 0, 0, \bar{R}_{IA_0}, \bar{V}_{IA_0})\end{aligned} \tag{2.11}$$

where

$$\bar{S}_{CN_0} = \bar{\bar{S}}_{CN_0} \qquad \bar{S}_{CJ_0} = \bar{\bar{S}}_{CJ0} - \tfrac{\mu_{NB}(\epsilon_1\nu_c)}{d+\mu_J}\bar{\bar{S}}_{CN_0} \qquad \bar{V}_{CJ_0} = \tfrac{\mu_{NB}\epsilon_1\nu_c}{d+\mu_J}\bar{\bar{S}}_{CN_0}$$

$$\bar{S}_{CA_0} = \bar{\bar{S}}_{CA0} - \tfrac{\mu_J(\epsilon_2\nu_c)}{d}\bar{\bar{S}}_{CJ_0} \qquad \bar{V}_{CA_0} = \tfrac{\mu_J\epsilon_2\nu_c}{d}\bar{\bar{S}}_{CJ_0} + \tfrac{\mu_J}{d}\bar{\bar{V}}_{CJ_0}$$

$$\bar{S}_{IN_0} = \bar{\bar{S}}_{IN_0} \qquad \bar{R}_{IN_0} = \bar{\bar{R}}_{IN_0} \qquad \bar{S}_{IJ_0} = \bar{\bar{S}}_{IJ0} - \tfrac{\mu_{NB}\epsilon_1\nu_i}{d+\mu_J}\bar{\bar{S}}_{IN0}$$

$$\bar{R}_{IJ_0} = \bar{\bar{R}}_{IJ_0} \qquad \bar{V}_{IJ_0} = \tfrac{q_3\Lambda_{IJ}}{d+\mu_J} + \tfrac{\mu_{NB}\epsilon_1\nu_i}{d+\mu_J}\bar{\bar{S}}_{IN_0}$$

$$\bar{S}_{IA_0} = \bar{\bar{S}}_{IA0} - \tfrac{\mu_J\epsilon_2\nu_i}{d}\bar{\bar{S}}_{IJ0} \qquad \bar{R}_{IA_0} = \bar{\bar{R}}_{IA_0} \qquad \bar{R}_{IA_0} = \tfrac{\hat{q}_3\Lambda_{IA}}{d} + \tfrac{\mu_J\epsilon_2\nu_i}{d}\bar{\bar{S}}_{IJ_0} + \tfrac{\mu_J}{d}\bar{\bar{V}}_{IA0}$$

Basic and Control Reproduction Numbers ($\mathcal{R}_0$ and $\mathcal{R}_c$)

We derive the expressions for both $\mathcal{R}_{02}$ and $\mathcal{R}_{c2}$ for Model (2.9). Again, the next generation matrix method is used and related computations are given in Appendix B. The basic reproductive number is defined as:

$$\mathcal{R}_{02} = \frac{\alpha\beta(\bar{\bar{S}}_{CN_0} + \bar{\bar{S}}_{CJ_0} + \bar{\bar{S}}_{CA_0} + \bar{\bar{S}}_{IN_0} + \bar{\bar{S}}_{IJ_0} + \bar{\bar{S}}_{IA_0})}{(d+\alpha)(d+\gamma)} \tag{2.12}$$

Next, we can use the disease free equilibrium with vaccination to define the controlled reproduction number $\mathcal{R}_c$ expressed as:

$$\begin{aligned}\mathcal{R}_{c2} = \frac{\alpha\beta}{(d+\alpha)(d+\gamma)}\Big[&\bar{\bar{S}}_{CN_0} + \bar{\bar{S}}_{CJ_0} + \bar{\bar{S}}_{CA_0} + \bar{\bar{S}}_{IN_0} + \bar{\bar{S}}_{IJ_0} + \bar{\bar{S}}_{IA_0} -\\ &- \left(\frac{\epsilon_1\mu_{NB}\left(\nu_c\bar{\bar{S}}_{CN0} + \nu_i\bar{\bar{S}}_{IN0}\right)}{d+\mu_J} + \frac{\epsilon_2\mu_J\left(\nu_c\bar{\bar{S}}_{CJ0} + \nu_i\bar{\bar{S}}_{IJ0}\right)}{d}\right)\Big]\end{aligned} \tag{2.13}$$

Similar to Eq. (2.8), we can rewrite the controlled reproduction number in terms of $\mathcal{R}_{02}$:

$$\mathcal{R}_{c2} = \mathcal{R}_{02}\left[1 - \frac{\frac{\epsilon_1\mu_{NB}\left(\nu_c\bar{\bar{S}}_{CN0}+\nu_i\bar{\bar{S}}_{IN0}\right)}{d+\mu_J} + \frac{\epsilon_2\mu_J\left(\nu_c\bar{\bar{S}}_{CJ0}+\nu_i\bar{\bar{S}}_{IJ0}\right)}{d}}{\bar{\bar{S}}_{CN_0} + \bar{\bar{S}}_{CJ_0} + \bar{\bar{S}}_{CA_0} + \bar{\bar{S}}_{IN_0} + \bar{\bar{S}}_{IJ_0} + \bar{\bar{S}}_{IA_0}}\right] \tag{2.14}$$

Note that the expression in the brackets indicates the proportion of population who get successfully vaccinated at 1 and 5 years. If there is no vaccine control in the population, then Eq. (2.14) reduces to the basic reproduction number $\mathcal{R}_{02}$.

Figure (2.12) represents a surface plot showing the linear relation between $\mathcal{R}_{c2}$ and the susceptible immigration incoming proportions (i.e. $\tilde{q}_1$,q_1, $\hat{q}_1$) and the basic reproduction number. The fractions related to newborns and juveniles are ranged between 0 and 1, while the adults one is set as $0, 0.1, 0.3, 0.5, 0.8, 1$ and $\mathcal{R}_{02} = 6, 14, 20$. We observe that as the proportion of adult immigrants, which is vulnerable to the infection, increases, the controlled reproduction increases, but smaller than the $\mathcal{R}_{02}$ sampled. Moreover, for $\hat{q}_1 = 0$ and $\mathcal{R}_{02} = 6$, the controlled reproduction number varies in the interval $[0.9912, 1.001]$ indicating that herd immunity in the population is achievable and the infection will not establish itself. This result accentuates how the proportion of susceptible immigrant adults can affect the immunity of the community and the spread of the infection.

Infected Equilibrium

Given the complexity of Model (2.9), the endemic equilibrium cannot be evaluated analytically. However, we provide some plots describing the infection dynamics (see Figure (2.13)). We observe that increasing the Canadian vaccination coverage and reducing the incoming rate of susceptible adult immigrants, the outbreak diminishes its size and is sustained for a longer period.

Sensitivity Analysis

Similar to the previous two-age model, we employed LHS/PRCC methodology to investigate which parameter in this new scenario affect the distribution of immunity at the DFE and the behavior of a potential outbreak. Before investigating the PRCC we confirm the monotonicity for all the parameters sampled.

The first analysis is related to the demographic dynamics including birth, death, immigration and vaccination. First, we generate 20000 values for each parameter by following the *Latin Hypercube Sampling*. To derive the the immigration rates for juveniles (q_1, q_2, q_3) and adults $(\hat{q}_1, \hat{q}_2, \hat{q}_3)$, we sample q_2 and $\hat{q}_2$ in the range $[0, 1]$, then we randomly pick q_3 and $\hat{q}_3$ in $[0, 1 - q_2]$ and $[0, 1 - \hat{q}_2]$, respectively. Hence, we define $q_1 = 1 - q_2 - q_3$ and $\hat{q}_1 = 1 - \hat{q}_2 - \hat{q}_3$. Next, we determine the total population for each set of values generated by LHS and we filter it in order to bound the total population between $1.1e07$ and $1.5e07$. After applying this condition, the samples used for the PRCC analysis are around 52% of the original samples.

Similar to the model with two ages, the PRCC on the DFE of System (2.9) (Figure (2.14)) presents significant positive correlation of the parameters related to Canadian birth rate and

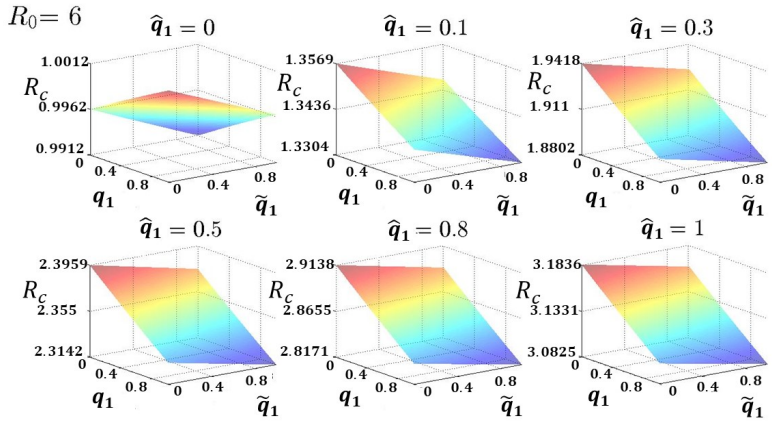

(a)

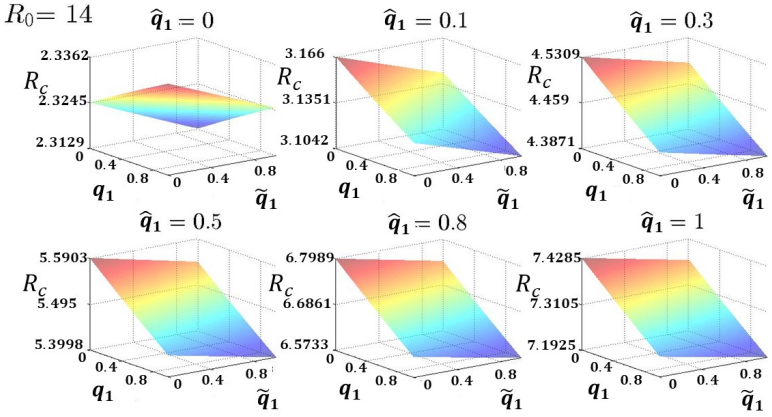

(b)

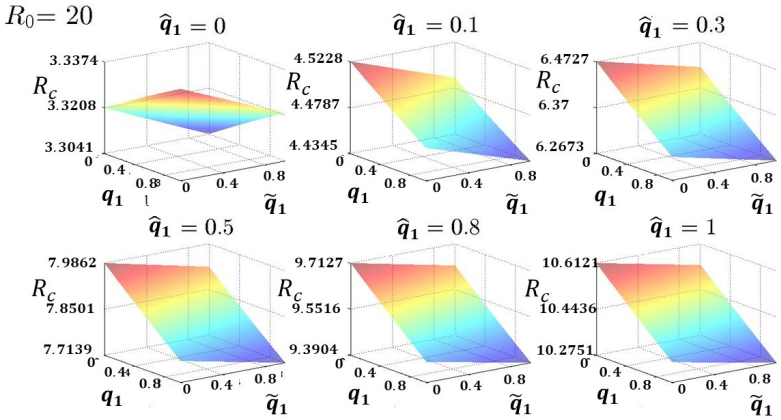

(c)

Figure 2.12: Surface plot of $\mathcal{R}_{c2}$ for q_1, $\tilde{q}_1 \in [0,1]$, $\hat{q}_1 = 0$, 0.1, 0.3, 0.5, 0.8, 1 and (a)$\mathcal{R}_{02} = 6$ (b)$\mathcal{R}_{02} = 14$ (c)$\mathcal{R}_{02} = 20$

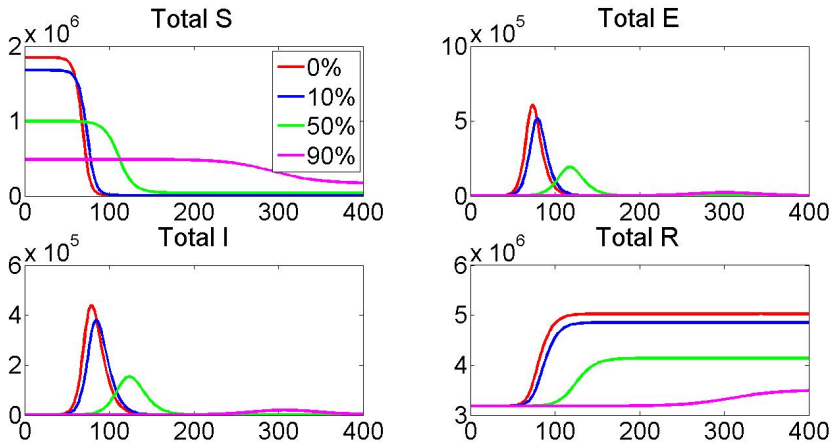

(a)

Figure 2.13: Dynamics of total S, E, I, R compartments when both ν_c and $\hat{q}_1$ were, respectively, increased and reduced by 0%, 10%, 50%, 90%

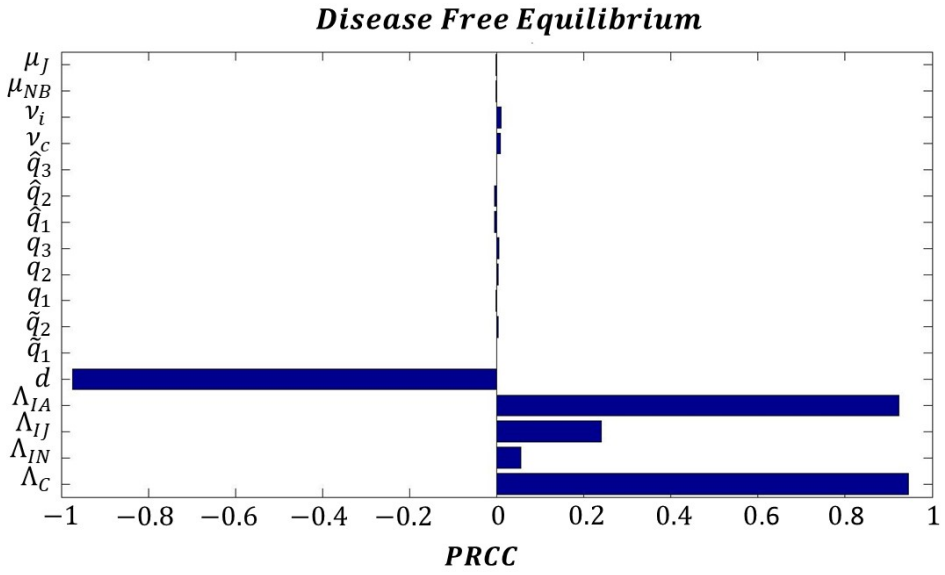

(a)

Figure 2.14: LHS/PRCC plots for the population at the disease free equilibrium and parameters γ, α, β on Rc

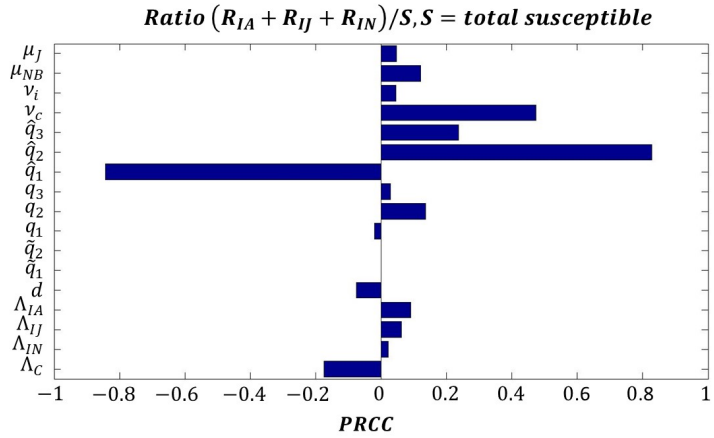

(a)

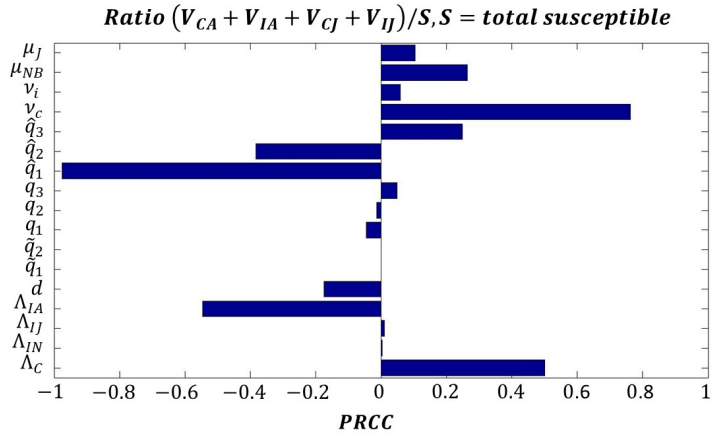

(b)

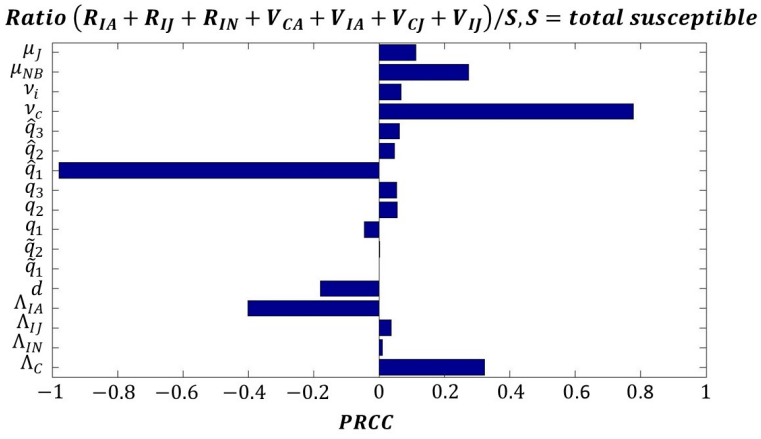

(c)

Figure 2.15: LHS/PRCC plots for the parameters μ_j, μ_{NB}, ν_i, ν_c, $\hat{q}_1$, $\hat{q}_2$, $\hat{q}_3$, q_1, q_2, q_3, $\tilde{q}_1$, $\tilde{q}_2$, d, Λ_C, Λ_{IJ} and Λ_{IA} on ratio (a) $(R_{IA} + R_{IJ} + R_{IN})/S$ (b)$(V_{CA} + V_{IA} + V_{CJ} + V_{IJ})/S$ (c) $(R_{IA} + R_{IJ} + R_{IN} + V_{CA} + V_{IA} + V_{CA} + V_{IA} + V_{CJ} + V_{IJ})/S$, where $S = S_{CN0} + S_{CJ0} + S_{CA0} + S_{IN0} + S_{IJ0} + S_{IA0}$

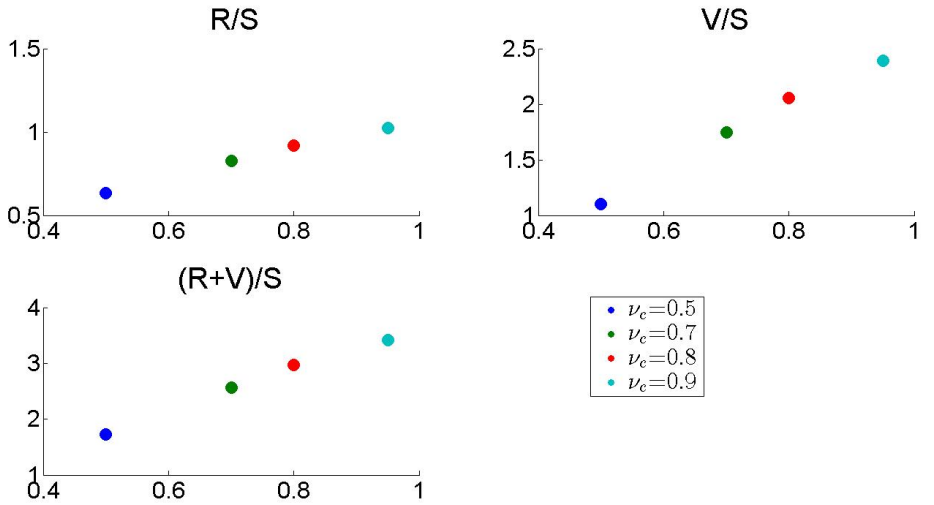

(a)

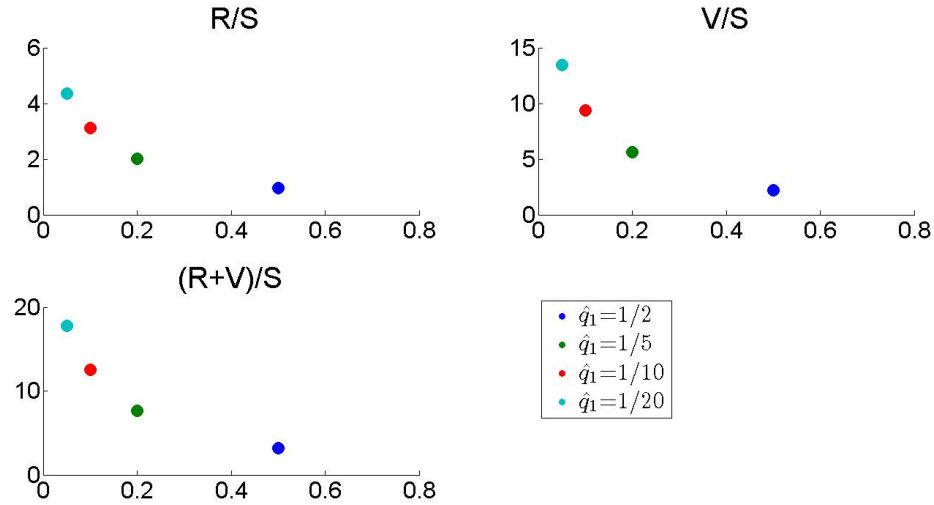

(b)

Figure 2.16: Plot of ratios of total recovered, total vaccinated, total R+V over total susceptible population, varying (a) ν_c, with $\hat{q}_1 = 1/2$ (b) $\hat{q}_1$, with $\nu_c = 0.85$

immigrant adults incoming rate.

We investigated the ratio between the total recovered, vaccinated, and the sum of these two classes over the total susceptible population. Figure (2.15a) describes the ratio of newborn, juvenile and adult recovered immigrants over the sum of all susceptible subclasses. We observe that in order to ensure a larger indirect protection to susceptibles by individuals with life-long infection-acquired immunity, the proportion of susceptible adults immigrating should be reduced and the Canadian vaccination rate should be increased. This can be deduced by the negative and positive correlation that $\hat{q}_1$ and ν_c show, respectively. Similarly, when we examine the ratio of vaccinated individuals over susceptibles, we observe that the most significant parameters providing high level of protection in the population are, as before, the Canadian vaccination rate, showing positive correlation, and proportion of susceptible adult immigrants, showing significant negative correlation. In particular, the protection provided by vaccine-induced immunity increases as ν_c increases and $\hat{q}_1$ decreases (Figure (2.15b)). Identical results are shown in Figure (2.15c) where the ratio of recovered and vaccinated over the susceptible class is analyzed. Again, the parameters most significant to reduce the number of individuals who are more vulnerable to the infection are ν_c, significantly positive correlated, and $\hat{q}_1$, significantly negative correlated.
Figure (2.16) shows how the ratios R/S, $(R+V)/S$, V/S increases as the Canadian vaccination coverage increases and the proportion of susceptible immigrant adult decreases. This confirms the results provided by LHS/PRCC analysis.
We deduce that to increase the protection of population against the measles virus, it is fundamental to focus in increasing vaccination rate among Canadians and limit the number of susceptible adult immigrants which can be done by offering newcomers the opportunity to get a measles vaccine shot.

Next, we apply the LHS/PRCC methods to investigate the behavior of a single outbreak. Similar to Model (2.1), we generate 20000 sampled values of population size at the disease free equilibrium ($\bar{\mathcal{E}}_0$) and infection-related parameters(α, β, γ) by using the *LHS* and then we filter the samples in order to obtain the parameters providing the population size at the disease free equilibrium to be in the range $(1.1e07, 1.5e07)$ and the reproduction number ranged in $[3, 11]$ according to the intervals provided in Figure (2.12). After this, the sampled set is narrowed to roughly 50% of the original values and we evaluate the PRCC on $\mathcal{R}_{c2}$, the magnitude of infectious individuals, time at which the peak of the infection occurs, when the outbreak ends and the total final size.
As expected, the PRCC plot on the controlled reproduction number (Figure (2.17)) shows that increasing the proportion of susceptible adults and infection rate, the reproduction number increases as well.
Figure (2.18a), representing the PRCC plots for the parameters on the magnitude of infectious individual at the peak of the infection, shows significant positive correlation of S_{IA_0}, S_{CA_0} and S_{CN_0} and β. Hence, the number of individuals experiencing the infection increases as susceptible immigrant and Canadian adults and Canadian newborns increase as well as the infection rate. Observe that the correlation of S_{IA_0} is much stronger than the one reported

by S_{CA_0} and S_{CN_0}. On the other hand, the susceptible immigrant adults and the infection rate show a negative correlation on the time at which the infection reaches its peak and its end (Figures (2.18b) and (2.19a)). In other words, the infection will spread more slowly by reducing susceptible adult immigrants and this is possible if the susceptible classes receive vaccination. Similar to Model (2.1), we define final size as the number of individual that encounter the infection through all the outbreak and this is shown in Figure (2.19b). We observe that the parameters affecting the size of the infection are S_{IA_0}, S_{CA_0} and S_{CN_0}, present a significant positive correlation. Hence, as the number of susceptible adults and Canadian newborns increase, bigger the size of the outbreak will be.

It is evident how the susceptible adults class, in both subpopulations and Canadian newborns, is fundamental to determine the outbreak direction and this last analysis confirms the results in Figure (2.15) which suggest to reduce the size of susceptible adults and Canadian newborns.

2.3 Conclusion

In a highly vaccinated country, such as Canada, measles outbreaks are associated to imported cases through immigration and travel. Here, we investigate the immigration of immunity in order to determine the actual immunity distribution in the Canadian population.

We develop a model keeping into account the Ontario population divided into two groups: Canada-borns and foreign-borns. Moreover, we include a further division vaccination age-dependent in order to understand better which age groups are the ones most affected by a potential oubreak and which ones have the highest impact on the distribution of immunity in the population. We formulate two models: in the first one the age groups are $0-5$ years and 6 years and older; in the second one the age groups are $0-12$ months, $1-5$ years, 6 years and older. This division is based on the recommended doses of measles vaccine. Sensitivity analysis is conducted to comprehend the effect that birth, death, vaccination and immigration rates have on the population immunity and what is the effect of the single subgroup population on a potential outbreak.

In the model with two age groups, the PRCC plots show that in order to guarantee an indirect protection to susceptible individuals provided by the immunized compartments R and V, it is decisive to keep a high level of vaccination coverage among Canadian children and reduce the number of susceptible immigrant adults. In case of a measles outbreak, all the susceptible groups have impact on the size of the epidemic and final size of it. However, the adult immigrants, who are vulnerable to the infection, are the ones who, mostly, affect the length of the outbreak.

When an extra age group is considered to best represent the vaccination routine, the results are similar to the first model. Herd immunity is achievable as the size of individuals with life-long immunity is bigger than the susceptible one. This is possible if the vaccination coverage of Canadian children increases and the proportion of susceptible immigrant adults decreases. The size of a potential outbreak is mostly affected by susceptible adults (both Canadian-born and foreign-born) and Canadians aged 0-12 months. Similar to the model with

two age groups, the duration of the outbreak is mainly influenced by the size of susceptible immigrant adults.

Our results suggest that in order to increase the level of immunity in Ontario, it is necessary to increase the local vaccination uptake and decrease the susceptible adult newcomers. To achieve the latter case, public health can offer a vaccine boost shot to all the newcomers who do not provide a proof of immunity.

Even if our models keep into account different ages at which the vaccine shots are given, it is assumed that the vaccine-induced immunity is life-long. According to new studies [23, 24, 25], measles immunity provided by vaccination may wane over time and this will lead to an increase of susceptibility in the population. The process of waning immunity can be included in this study in order to understand how the dynamics of immunity and infection will be affected by it. Moreover, our model assumes that the mixing is uniform among all the age groups. Hence, in order to capture the different contacts that individuals in the society have, it will be necessary to include a contact matrix.

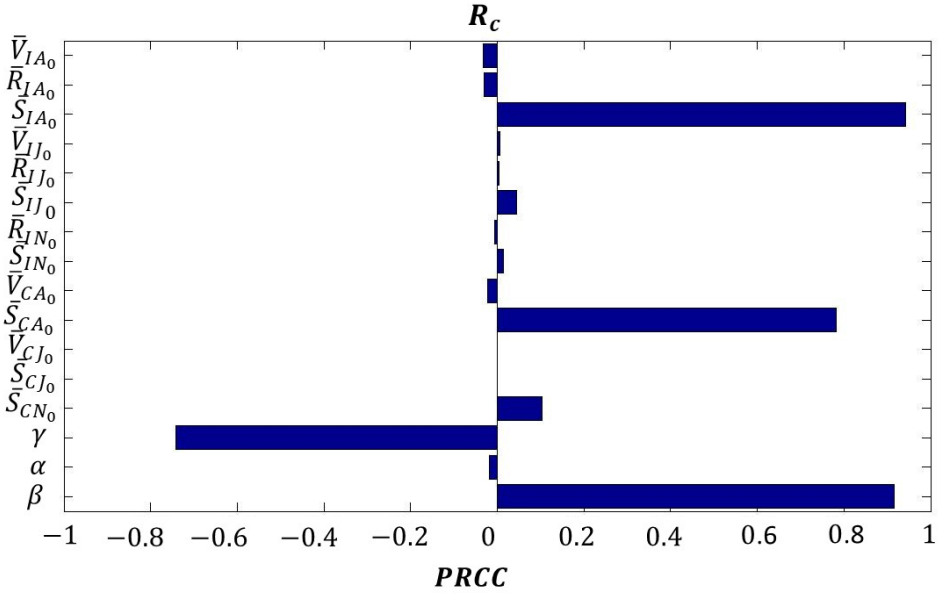

(a)

Figure 2.17: LHS/PRCC plots for the population at the disease free equilibrium and parameters γ, α, β on Rc

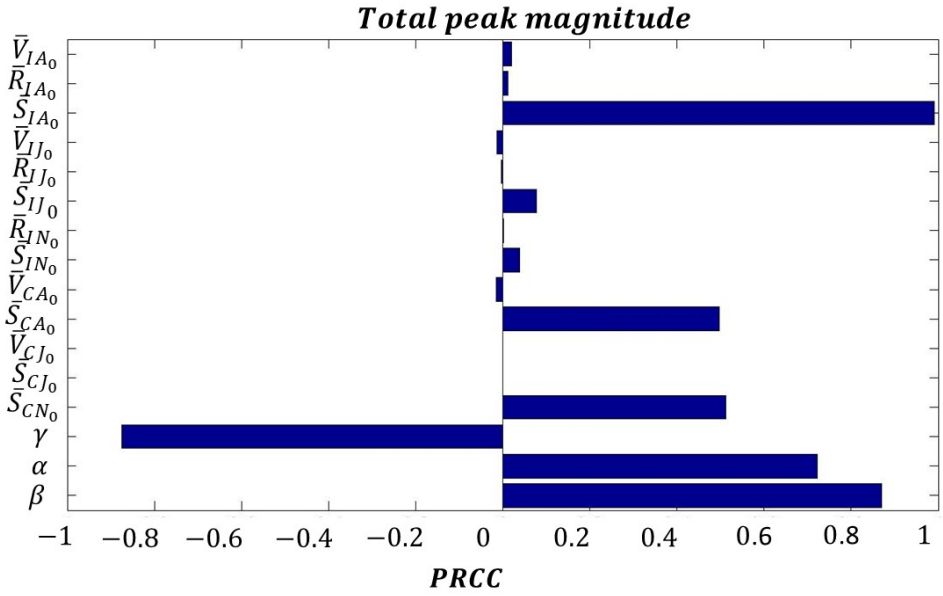

(a)

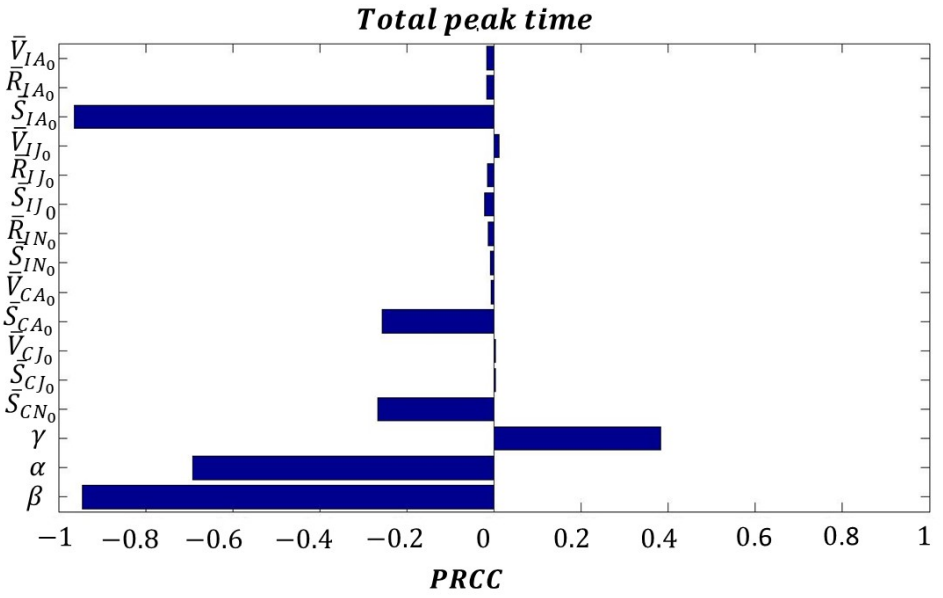

(b)

Figure 2.18: LHS/PRCC plots for the population at the disease free equilibrium and parameters γ, α, β on total population (a) peak magnitude (b) time of maximum peak

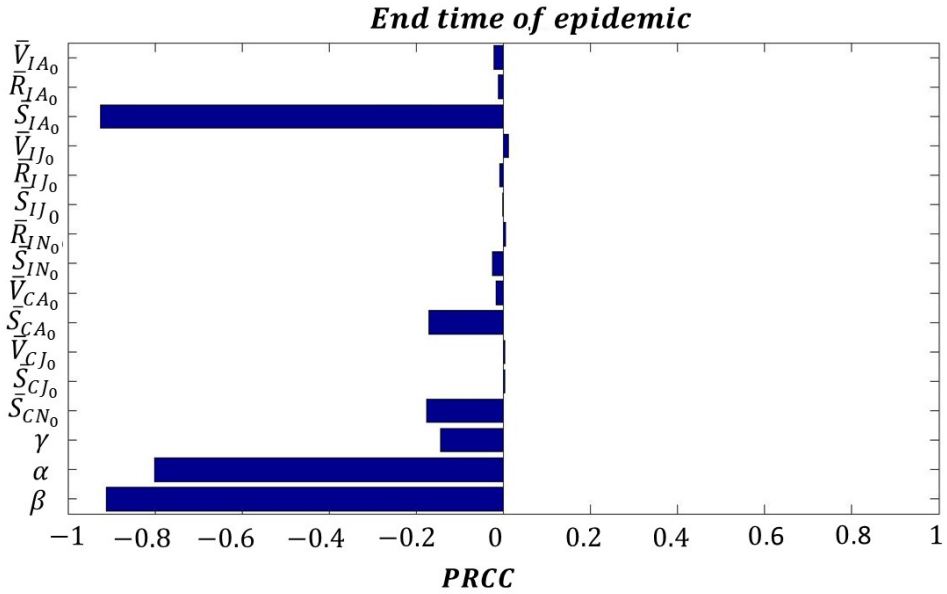

(a)

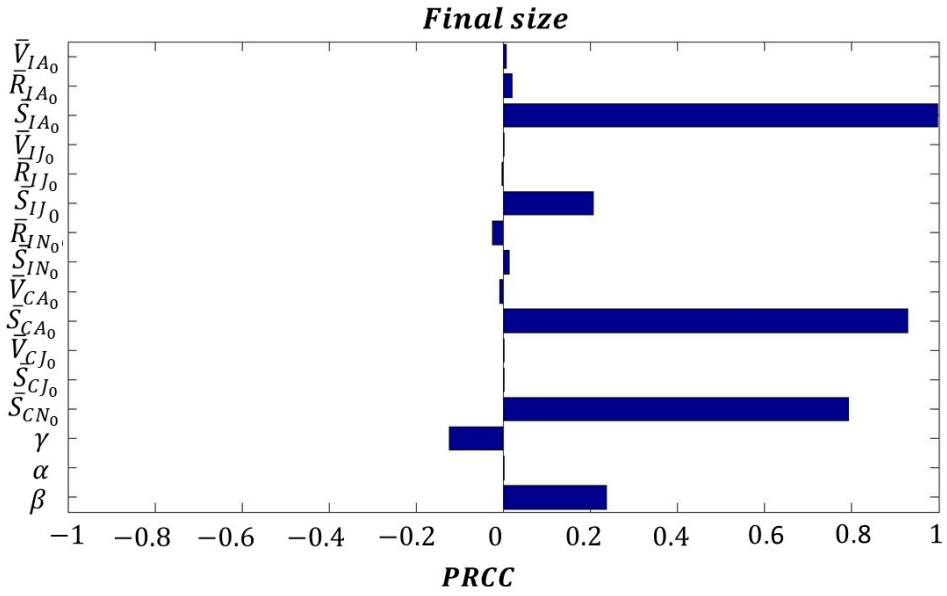

(b)

Figure 2.19: LHS/PRCC plots for the population at the disease free equilibrium and parameters γ, α, β on total population (a) time of end of epidemic (b) final size (number of total infected individuals)

Chapter 3

Impact of Vaccination Heterogeneity on the Greater Toronto Area

3.1 Introduction

With the rapid growth of big cities nowadays, many workers need to commute from their house to the workplace daily. In 2016, Canada implemented a population census [110] where details on location of residence and workplace were asked. The Canadian commuting flow had been recorded in data tables [111], where it is possible to select a census region as place of residence or work and get data on commuters from/to that region to/from other areas. For example, more than 400000 people commute to Toronto for work from neighboring regions (as York, Peel, Halton and Durham).

It is important to highlight that if commuters are sick, the pathogen travels with them. Hence, if one or more regions present a specific disease outbreak, the movement among them and the time spent in the workplace areas can increase the total risk of infection in the entire city [112, 113, 114, 115]. It also important to distinguish the difference between long term and short term travels. Long travels indicate a permanent movement towards a different area. Short term travels can be for a relatively long period of time (migration) or daily (commuting/residency). When a group of individuals migrate towards a new place, they remain there for a relatively long time, becoming, in that time-frame, part of the hosting population. On the other hand, when traveling or commuting, the period of time spent in a region different from the residency area is very short, hence the proportion of individuals leaving and returning home is the same.

Meta-population models are the most common spatial models. Sattenspiel and Dietz [59] proposed a multi-patch SIR model in which the population was divided into residents and commuters. Individuals were assumed to move among patches by following mobility rates (leaving-returning rates). The number of contacts and probability of transmission generating new infected were rescaled by dividing them by the total population actually present in the patch. The same approach has been used by Arino et al. [64, 61, 62, 63] who have made an extensive use of multi-patch models in oder to simulate and understand

the transmission of the infection among different communities. In particular, the authors used general frameworks, as SEIR or SI, where travel rates among different patches were included. The authors were able to derive mathematical expressions of the basic reproduction number both patch specific and total, identify the patch more responsible in sustaining the infection among all the regions and the effect that the mobility rates have on the transmission. Alexander et al. [84] include vaccination heterogeneity in a multi-patch $SEIR$ model. They found that the transmission of measles, in French regions, will decrease by increasing the vaccination coverage.

Although these models give important results on the infection transmission and spread, the mobility rates need to be available or estimated by traveling data. Unfortunately, the availability of these data is not always feasible. However, we can model the mobility process in absence of data. Many methods capture the migration rates by using the proportion of population commuting or time spent in different patches by commuters [68, 66, 67, 116, 65]. Stolerman et al [65] use a SIR-network model to describe Dengue fever dynamics among regions in Brazil. The mobility is described by a matrix defining the proportion of commuters from one region to another. The authors assumed that each patch presents its specific infection rate. The equations are all normalized by the total effective population, which include residents and commuters from other patches. Similar approach has been used by Bichara et al [68, 66]. In these papers the authors capture the mobility among patches with a residence time matrix whose entries are the proportions of time that commuters spend in each patch. The frameworks used are SIS, SIR and $SEIRS$. Similar to Stolerman, the risk of infection depends on the patch, but the transmission depends on the time that commuters and residents spend in a specific patch. This approach has also been used by Chang et al. [116] in a more recent paper. With game theory modelling, the authors include vaccination in an SIR framework. In this paper the mobility is analysed to understand its effects on the vaccination strategies.

All these works findings outline how transmission, spread and vaccine intervention depend on the mobility among individuals. However, asymptomatic infectious cases were not considered nor the effect that, combined with vaccination heterogeneity, they have on measles transmission. Since we are focusing on measles, we employ a $Susceptible - Exposed - Asymptomatic - Infectious - Recovered - Vaccinated$ ($SEAIRV$) model, using the Lagrangian approach and dividing the infectious compartment into symptomatic and asymptomatic. Our investigation is over a short period of time, hence demographics are not included and the population is assumed to be at a disease free equilibrium with vaccination. In our models we consider residency patches and individuals move towards a different patch within 24 hours. Following Bichara et al. [68, 66], we capture the mobility by using the time spent by individuals in each patch. We consider n patches for a general formulation of the model, but we will investigate two cases: $n = 2, 3$. The patches considered belong to the Greater Toronto Area (Toronto, Peel, York, Halton and Durham regions) and have been chosen after examining the commuting data tables provided by Statistics Canada [111]. These regions are the closest geographically and with the highest number of commuters. We derive the expression for the patch specific reproduction number and the total reproduction number

($\mathcal{R}_c$). We investigate the effect that the residence times, probability of showing symptoms and immunity levels have on the $\mathcal{R}_c$ and sensitivity analysis on a potential outbreak is then studied. These analyses are carried out considering each patch either highly susceptible (S is the 90% of the total population) or highly vaccinated (V is the 90% of the total population).

3.2 Model and Methods

3.2.1 Model

In this project, we describe measles infection by using a multi-patch approach and a *Susceptible-Exposed-Asymptomatic-Infected-Recovered-Vaccinated* ($SEAIRV$) model framework to describe the infection dynamic. We adopt the residency patch time model, as used by Stolerman [65] and Bichara [66]. The movement between patches is indirectly captured by identifying the proportion of time that individuals in each compartment spend in different patches (i.e. s_{ij}, e_{ij}, a_{ij}, $\tilde{p}_{ij}$, r_{ij},v_{ij} are the proportion of times that susceptible, exposed, asymptomatic, symptomatic, recovered and vaccinated individuals from patch i spend in patch j). This hypothesis introduces the definition of *current population* in a patch at a specific time t. In fact, if we define the total population of patch i as $N_i = S_i + E_i + A_i + I_i + R_i + V_i$, then $s_{ij}S_i + e_{ij}E_i + a_{ij}A_i + \tilde{p}_{ij}I_i + r_{ij}R_i + v_{ij}V_i$ is the population from patch i that spends time in patch j. From here, we can define the total *current population* of patch j as $N_j = \sum_{i=1}^{n} s_{ij}S_i + e_{ij}E_i + a_{ij}A_i + \tilde{p}_{ij}I_i + r_{ij}R_i + v_{ij}V_i$.

The transmission of infection is modeled by the following term:

$$\sum_{j=1}^{n} \beta_j S_i s_{ij} \frac{\sum_{k=1}^{n}(A_k\eta_k a_{kj} + I_k\tilde{p}_{kj})}{\sum_{k=1}^{n}(S_k s_{kj} + E_k e_{kj} + A_k a_{kj} + I_k\tilde{p}_{kj} + R_k r_{kj} + V_k v_{kj})}$$

It is assumed that transmission of infection in patch i is possible through the transmission risk β_i, which we assume to be specific for each patch. We also assume that the infection depends on the size of the patch given all movement probabilities. Moreover, we assume two infectious classes (A and I), where the asymptomatic class is less infectious than the symptomatic. This reduction in infectiousness is given by $0 < \eta_k < 1$. After infection, we assume that exposed individuals can show symptoms with probability b and move to I, and with probability $1 - b$ move to A. We also assume recovery rates are γ, γ_1 for I and A, respectively.

Hence, we summarize how the infection occurs: the susceptible individuals from patch i encounter the asymptomatic or symptomatic cases from any patch and become exposed; after a latent period α, the individuals can become asymptomatic or symptomatic with probability $1 - b$ or b, respectively; the infectious period is then followed by a recovery stage and individuals remain there, assuming that the immunity provided by the infection is life long. Since we are not including the demographics, the effect of vaccination is counted in the initial conditions of the compartments S and V. The infection dynamics in patch i is represented in the flow diagram in Figure 3.1.

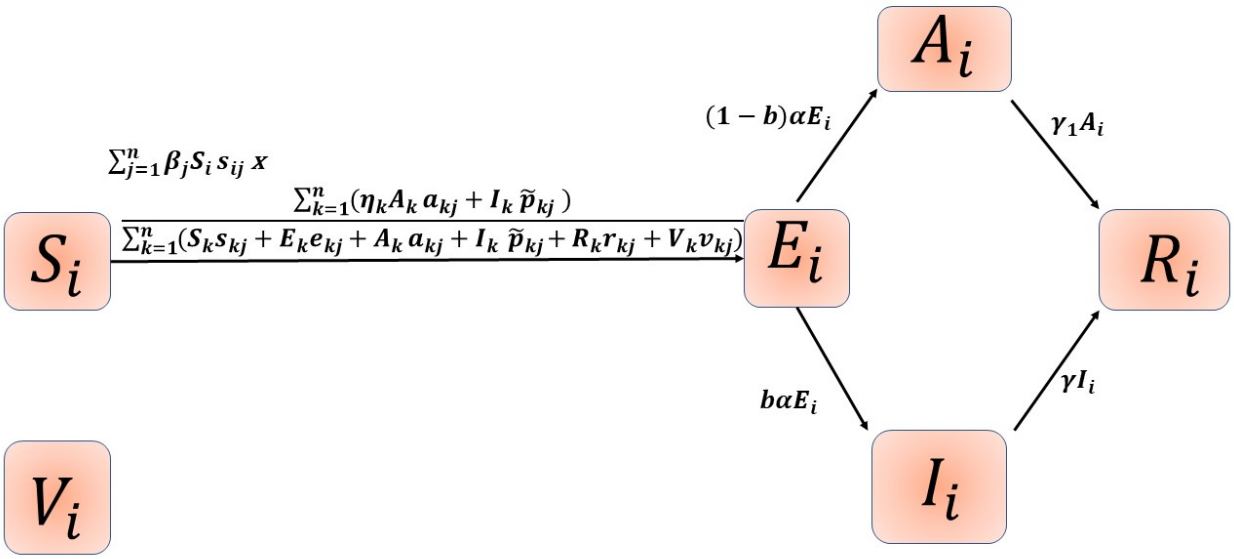

Figure 3.1: Flow diagram for Model (3.1) in patch i

The following system of ODEs describe the infection dynamics explained above:

$$S_i' = -\sum_{j=1}^{n} \beta_j S_i s_{ij} \frac{\sum_{k=1}^{n}(A_k \eta_k a_{kj} + I_k \tilde{p}_{kj})}{\sum_{k=1}^{n}(S_k s_{kj} + E_k e_{kj} + A_k a_{kj} + I_k \tilde{p}_{kj} + R_k r_{kj} + V_k v_{kj})} \tag{3.1a}$$

$$E_i' = \sum_{j=1}^{n} \beta_j S_i s_{ij} \frac{\sum_{k=1}^{n}(A_k \eta_k a_{kj} + I_k \tilde{p}_{kj})}{\sum_{k=1}^{n}(S_k s_{kj} + E_k e_{kj} + A_k a_{kj} + I_k \tilde{p}_{kj} + R_k r_{kj} + V_k v_{kj})} \tag{3.1b}$$

$$-\alpha E_i \tag{3.1c}$$

$$A_i' = (1-b)\alpha E_i - \gamma_1 A_i \tag{3.1d}$$

$$I_i' = b\alpha E_i - \gamma I_i \tag{3.1e}$$

$$R_i' = \gamma_1 A_i + \gamma I_i \tag{3.1f}$$

$$V_i' = 0 \tag{3.1g}$$

where $i, k, j = 1, ..., n$ are the patches. Model (3.1) initial conditions, at the disease free equilibrium, are $\mathcal{E}_{i0} = (S_{i0}, 0, 0, 0, 0, V_{i0})$.
The description of the variables and parameters present in Model (3.1) are shown in Table 3.1 and Table 3.2, respectively.

List of variables	
Variables	**Definition**
S_i, $i, j = 1, 2, 3$	Susceptible population currently in patch j from patch i
E_i, $i = 1, 2, 3$	Exposed population currently in patch j from patch i
A_i, $i = 1, 2, 3$	Asymptomatic population currently in patch j from patch i
I_i, $i = 1, 2, 3$	Symptomatic population currently in patch j from patch i
R_{ij}, $i = 1, 2, 3$	Recovered population currently in patch j from patch i
V_i, $i = 1, 2, 3$	Vaccinated population currently in patch j from patch i

Table 3.1: List of variables used in Model (3.1)

List of parameters			
Parameters	**Value**	**Interval of sampling**	**Definition**
$\mathcal{R}_{0i}$, $i = 1, 2, 3$	1.8, 16	$1.2 - 18$	reproduction number in patch i
b	0.05, 0.1, 0.3, 0.7, 0.9	$0.001 - 1$	probability of showing symptoms
η	0.5	$0.001 - 1$	reduced infectivity of asymptomatic cases
s_i, $i = 1, 2, 3$	$0 - 1$	$0.001 - 1$	proportion of susceptible in patch i
$s_{i,j}$, $e_{i,j}$, $a_{i,j}$, $r_{i,j}$, $v_{i,j}$, $i, j = 1, 2, 3$	$0 - 1$	$0.001 - 1$	proportion of time spent by patch i S, E, A, R, and V residents in patch j (assumed to be equal $p_{i,j}$)
$\tilde{p}_{i,j}$, $i, j = 1, 2, 3$	$\tilde{p}_{i,i} = 1; \tilde{p}_{i,j} = 0$	-	proportion of time spent by patch i I residents in patch j
α	$1/8\ days^{-1}$	–	latent rate
γ	$1/7\ days^{-1}$	–	recovery rate from infected cases
γ_1	$1/7\ days^{-1}$	–	recovery rate from asymptomatic cases
β_j, $j = 1, 2, 3$	estimated	–	transmission risk in patch j

Table 3.2: List of parameters used in Model (3.1). The third column indicates the interval chosen to sample values for the LHS/PRCC sensitivity analysis

Observe that in absence of infection, the population in each patch is constant and the total population $N_i = S_i + V_i$.

Control Reproduction Number $\mathcal{R}_c$

In order to investigate the infection dynamics in each patch i, we determine the control reproduction number $\mathcal{R}_{c_i}$ using the *Next Generation Matrix* method [88, 86, 90, 92], where $\mathcal{R}_{c_i}$ is given by the spectral radius of $\mathcal{F}(-\mathcal{V}^{-1})$ where $\mathcal{F}$ and $-\mathcal{V}$ are matrices defined by:

$$\mathcal{F} = \begin{bmatrix} 0 & \beta_i S_{i0} s_{ii} \frac{\eta_i a_{ii}}{S_i s_{ii} + V_i v_{ii}} & \beta_i S_i s_{ii} \frac{\tilde{p}_{ii}}{S_i s_{ii} + V_i v_{ii}} \\ 0 & 0 & 0 \\ 0 & 0 & 0 \end{bmatrix} \tag{3.2}$$

$$-\mathcal{V} = \begin{bmatrix} \alpha & 0 & 0 \\ -(1-b)\alpha & \gamma_1 & 0 \\ -b\alpha & 0 & \gamma \end{bmatrix} \tag{3.3}$$

The reproduction number is expressed as:

$$\mathcal{R}_{ci} = \rho(\mathcal{F}(-\mathcal{V}^{-1})) = \frac{\beta_i S_{i0} s_{ii}}{S_{i0} s_{ii} + V_i v_{ii}} \left(\frac{b\tilde{p}_{ii}}{\gamma} + \frac{(1-b)\eta_i a_{ii}}{\gamma_1} \right) \tag{3.4}$$

Observe that Eq.(3.4) is given by the sum of two terms: the first one is related to the new infected cases generated by individuals whose symptoms are visible, the second one represents the new infected cases generated by asymptomatic individuals. Moreover, we observe that the control reproduction number Eq. (3.4) depends on the proportion of time spent in patch i by its own population, $s_{ii}, v_{ii}, \tilde{p}_{ii}, a_{ii}$.

Model Parameterization

In the next sections, we analyze two different scenarios, considering 2 or 3 patches. In both cases, we derive the total reproduction number and carry out numerical investigations and sensitivity analysis. In the first analysis, we show the relationship between the proportion of residence times and the total control reproduction number when the patches present different levels of immunity in S and V at the time the pathogen is introduced into the population. That is, different proportions of vaccinated and susceptible individuals in each patch are considered as initial conditions. In particular, we compare how the control reproduction number changes if patches are highly susceptible (90% of the population is vulnerable to the pathogen) or highly vaccinated (90% of individuals present immunity against the infection). Moreover, for our analysis we compare different probabilities of symptom manifestation (i.e. $b = 0.05, 0.1, 0.3, 0.7, 0.9$) in order to understand the impact that asymptomatic cases might have on the spread of the infection. Since commuters can live close or far from the workplace, we examine two scenarios: in the first one the patches are relatively geographically close, but patch 1 is considered as the main patch whose resident are not moving, spending all their time in it, while residents in patch 2 or 3 spend some of their time in patch 1; in the second scenario the patches are geographically close and the residents in both areas commute between them.

Given the difference in the immunity background in each patch, we consider that they can be either *high risk* (i.e. 90% of population is susceptible) or *low risk* (i.e. 90% of population is highly vaccinated). The force of the infection in the *high risk* patch is given when $\mathcal{R}_{c_i} \approx 16$, while if the population is highly vaccinated then $\mathcal{R}_{c_i} \approx 1.8$. These two values have been evaluated by using the *herd immunity* relation $\mathcal{R}_c = (1-p)\mathcal{R}_0$, where p is the proportion of vaccinated individuals in a population. Recall that the basic reproduction number for measles is considered to be 18. Hence, when $p = 0.9$, then $\mathcal{R}_c = 0.1 \times \mathcal{R}_0$. On the other hand, when $p = 0.1$, then $\mathcal{R}_c = 0.9 \times \mathcal{R}_0$. These values are reasonable since a higher vaccination coverage reduces the infection transmission. We end the numerical analysis with a sensitivity analysis of all the model parameters.

In order to investigate a realistic scenario, we use information on Ontario commuters provided by Statistics Canada [111] from the 2016 Canadian census data tables to determine which zones in Ontario would reflect our assumptions on the patches. According to the census, most Toronto residents work in Toronto and a small portion of them work in adjacent regions as York or Peel or more distant regions as Halton or Durham. On the other hand, the residents of all the other mentioned regions commute to Toronto to work. It is essential to highlight that these regions present different population sizes, reported in Table 3.3. Since Toronto is the main destination of many commuters, we define Toronto as patch 1, while the other patches are defined depending on the scenario studied.

For the numerical simulations, we assume that susceptible, exposed, asymptomatic, recovered and vaccinated individuals have the same proportion of residence times ($i.e, s_{ij} = e_{ij} = a_{ij} = r_{ij} = v_{ij} = p_{ij}$), while symptomatic cases are not allowed to leave their own residence patch (i.e.$\tilde{p}_{ii} = 1, \tilde{p}_{ij} = 0$ for $i \neq j$).

Population size in 2016 [110]	
Region	**size**
Toronto	$2,731,571$
Peel	$1,381,739$
York	$1,109,909$
Durham	$645,862$
Halton	$548,435$

Table 3.3: Population size of Toronto, Peel, York, Durham and Halton regions in 2016

Sensitivity Analysis

After investigating the total reproduction number dependency on the residency times, we perform sensitivity analysis on the other model parameters. We focus on the amount of infected asymptomatic and symptomatic cases within an outbreak as well as the time needed to reach the peak of the infection and the time at which at least 100 individuals were in the I compartment. This information allows us to understand which factors affect mostly the beginning of an outbreak and its development. In order to perform this analysis, we use the known method *Latin Hypercube Sampling* (LHS) / *Partial Rank Correlation Coefficient* (PRCC)[94, 93]. We assume that the population at the beginning of the outbreak is divided into susceptible or vaccinated at different proportions: s_i and v_i, where $v_i = 1 - s_i$. Similar to the study on the total reproduction number, we investigate the sensitivity analysis by setting two scenarios: in the first one, patch 1 residents do not move, while the others do; in the second one residents of all the patches are moving. We analyze the model output after seeding one infected in either I_1 or I_2 and compare if the sensitivity analysis shows any difference. By using LHS, we generate 50000 samples for each parameter varying them in a specific interval (see Table 3.2). After generating the samples, we verified that the parameters and the model outputs of interest showed a monotonic relationship and, consequently, evaluated the PRCC .

3.2.2 Two-patch Model

Control Reproduction Number $\mathcal{R}_c$

In this section, we carry out some analytical computations to derive a clear expression of the total reproduction number when two patches are considered. By using the *Next Generation Matrix Method* [88, 86, 90, 92], we can derive the control reproduction number for the general system (3.1) when n=2. The matrix describing the infection transmission, $\mathcal{F}$, evaluated at the disease free equilibrium, is defined as:

$$\mathcal{F} = \begin{bmatrix} 0 & S_{1_0}\sum_{j=1}^{2}\frac{\beta_j s_{1j} a_{1j}\eta_1}{\sum_{k=1}^{2}(S_k s_{kj}+V_k v_{kj})} & S_{1_0}\sum_{j=1}^{2}\frac{\beta_j s_{1j}\tilde{p}_{1j}}{\sum_{k=1}^{2}(S_k s_{kj}+V_k v_{kj})} & 0 & S_{1_0}\sum_{j=1}^{2}\frac{\beta_j s_{1j} a_{2j}\eta_2}{\sum_{k=1}^{2}(S_k s_{kj}+V_k v_{kj})} & S_{1_0}\sum_{j=1}^{2}\frac{\beta_j s_{1j}\tilde{p}_{2j}}{\sum_{k=1}^{2}(S_k s_{kj}+V_k v_{kj})} \\ 0 & 0 & 0 & 0 & 0 & 0 \\ 0 & 0 & 0 & 0 & 0 & 0 \\ 0 & S_{2_0}\sum_{j=1}^{2}\frac{\beta_j s_{2j} a_{1j}\eta_1}{\sum_{k=1}^{2}(S_k s_{kj}+V_k v_{kj})} & S_{2_0}\sum_{j=1}^{2}\frac{\beta_j s_{2j}\tilde{p}_{1j}}{\sum_{k=1}^{2}(S_k s_{kj}+V_k v_{kj})} & 0 & S_{2_0}\sum_{j=1}^{2}\frac{\beta_j s_{2j} a_{2j}\eta_2}{\sum_{k=1}^{2}(S_k s_{kj}+V_k v_{kj})} & S_{2_0}\sum_{j=1}^{2}\frac{\beta_j s_{2j}\tilde{p}_{2j}}{\sum_{k=1}^{2}(S_k s_{kj}+V_k v_{kj})} \\ 0 & 0 & 0 & 0 & 0 & 0 \\ 0 & 0 & 0 & 0 & 0 & 0 \end{bmatrix} \tag{3.5}$$

The matrix $\mathcal{V}$ is defined as:

$$\mathcal{V} = \begin{bmatrix} -\alpha & 0 & 0 & 0 & 0 & 0 \\ \alpha(1-b) & -\gamma_1 & 0 & 0 & 0 & 0 \\ \alpha b & 0 & -\gamma & 0 & 0 & 0 \\ 0 & 0 & 0 & -\alpha & 0 & 0 \\ 0 & 0 & 0 & \alpha(1-b) & -\gamma_1 & 0 \\ 0 & 0 & 0 & \alpha b & 0 & -\gamma \end{bmatrix} \tag{3.6}$$

The reproduction number is given by the spectral radius of the matrix $\Theta = \mathcal{F}(-\mathcal{V})^{-1}$, defined as:

$$\Theta = \begin{bmatrix} \Psi + \Xi & \frac{\Psi}{1-b} & \frac{\Xi}{b} & \Delta + \Gamma & \frac{\Delta}{1-b} & \frac{\Gamma}{b} \\ 0 & 0 & 0 & 0 & 0 & 0 \\ 0 & 0 & 0 & 0 & 0 & 0 \\ \Psi' + \Xi' & \frac{\Psi'}{1-b} & \frac{\Xi'}{b} & \Delta' + \Gamma' & \frac{\Delta'}{1-b} & \frac{\Gamma'}{b} \\ 0 & 0 & 0 & 0 & 0 & 0 \\ 0 & 0 & 0 & 0 & 0 & 0 \end{bmatrix} \tag{3.7}$$

where:

$$\Psi = S_{1_0} \sum_{j=1}^{2} \frac{\beta_j s_{1j} a_{1j} \eta_1}{\sum_{k=1}^{2} (S_k s_{kj} + V_k v_{kj})} \frac{1-b}{\gamma_1} \tag{3.8a}$$

$$\Xi = S_{1_0} \sum_{j=1}^{2} \frac{\beta_j s_{1j} \tilde{p}_{1j}}{\sum_{k=1}^{2} (S_k s_{kj} + V_k v_{kj})} \frac{b}{\gamma} \tag{3.8b}$$

$$\Delta = S_{1_0} \sum_{j=1}^{2} \frac{\beta_j s_{1j} a_{2j} \eta_2}{\sum_{k=1}^{2} (S_k s_{kj} + V_k v_{kj})} \frac{1-b}{\gamma_1} \tag{3.8c}$$

$$\Gamma = S_{1_0} \sum_{j=1}^{2} \frac{\beta_j s_{1j} \tilde{p}_{2j}}{\sum_{k=1}^{2} (S_k s_{kj} + V_k v_{kj})} \frac{b}{\gamma} \tag{3.8d}$$

$$\Psi' = S_{2_0} \sum_{j=1}^{2} \frac{\beta_j s_{2j} a_{1j} \eta_1}{\sum_{k=1}^{2} (S_k s_{kj} + V_k v_{kj})} \frac{1-b}{\gamma_1} \tag{3.8e}$$

$$\Xi' = S_{2_0} \sum_{j=1}^{2} \frac{\beta_j s_{2j} \tilde{p}_{1j}}{\sum_{k=1}^{2} (S_k s_{kj} + V_k v_{kj})} \frac{b}{\gamma} \tag{3.8f}$$

$$\Delta' = S_{2_0} \sum_{j=1}^{2} \frac{\beta_j s_{2j} a_{2j} \eta_2}{\sum_{k=1}^{2} (S_k s_{kj} + V_k v_{kj})} \frac{1-b}{\gamma_1} \tag{3.8g}$$

$$\Gamma' = S_{2_0} \sum_{j=1}^{2} \frac{\beta_j s_{2j} \tilde{p}_{2j}}{\sum_{k=1}^{2} (S_k s_{kj} + V_k v_{kj})} \frac{b}{\gamma} \tag{3.8h}$$

Observe that the entries of the Next Generation Matrix (3.7) defined in Eq.(3.8) represent the *type reproduction numbers* as follows:

$$\Psi = \mathcal{R}_{cA_1A_1,1} + \mathcal{R}_{cA_1A_1,2} \tag{3.9a}$$

$$\Xi = \mathcal{R}_{cI_1I_1,1} + \mathcal{R}_{cI_1I_1,2} \tag{3.9b}$$

$$\Delta = \mathcal{R}_{cA_2A_1,1} + \mathcal{R}_{cA_2A_1,2} \tag{3.9c}$$

$$\Gamma = \mathcal{R}_{cI_2I_1,1} + \mathcal{R}_{cI_2I_1,2} \tag{3.9d}$$

$$\Psi' = \mathcal{R}_{cA_1A_2,1} + \mathcal{R}_{cA_1A_2,2} \tag{3.9e}$$

$$\Xi' = \mathcal{R}_{cI_1I_2,1} + \mathcal{R}_{cI_1I_2,2} \tag{3.9f}$$
$$\Delta' = \mathcal{R}_{cA_2A_2,1} + \mathcal{R}_{cA_2A_2,2} \tag{3.9g}$$
$$\Gamma' = \mathcal{R}_{cI_2I_2,1} + \mathcal{R}_{cI_2I_2,2} \tag{3.9h}$$

The meaning of the type reproduction numbers is given below:

- $\Psi = \mathcal{R}_{cA_1A_1,1} + \mathcal{R}_{cA_1A_1,2}$: patch 1 asymptomatic resident generated by patch 1 asymptomatic in patch 1 and patch 2
- $\Xi = \mathcal{R}_{cI_1I_1,1} + \mathcal{R}_{cI_1I_1,2}$: patch 1 symptomatic resident generated by patch 1 symptomatic in patch 1 and patch 2
- $\Delta = \mathcal{R}_{cA_2A_1,1} + \mathcal{R}_{cA_2A_1,2}$: patch 1 asymptomatic resident generated by patch 2 asymptomatic in patch 1 and patch 2
- $\Gamma = \mathcal{R}_{cA_2A_1,1} + \mathcal{R}_{cA_2A_1,2}$: patch 1 symptomatic resident generated by patch 2 symptomatic in patch 1 and patch 2
- $\Psi' = \mathcal{R}_{cA_1A_2,1} + \mathcal{R}_{cA_1A_2,2}$: patch 2 asymptomatic resident generated by patch 1 symptomatic in patch 1 and patch 2
- $\Xi' = \mathcal{R}_{cI_1I_2,1} + \mathcal{R}_{cI_1I_2,2}$: patch 2 symptomatic resident generated by patch 1 symptomatic in patch 1 and patch 2
- $\Delta' = \mathcal{R}_{cA_2A_2,1} + \mathcal{R}_{cA_2A_2,2}$: patch 2 asymptomatic resident generated by patch 2 asymptomatic in patch 1 and patch 2
- $\Gamma' = \mathcal{R}_{cI_2I_2,1} + \mathcal{R}_{cI_2I_2,2}$: patch 2 symptomatic resident generated by patch 2 symptomatic in patch 1 and patch 2

Hence, we can rewrite Θ as

$$\Theta = \begin{bmatrix} \mathcal{R}_{cA_1A_1,1} + \mathcal{R}_{cA_1A_1,2} + \\ + \mathcal{R}_{cI_1I_1,1} + \mathcal{R}_{cI_1I_1,2} & \frac{\mathcal{R}_{cA_1A_1,1}}{1-b} + \\ + \frac{\mathcal{R}_{cA_1A_1,2}}{b} & \frac{\mathcal{R}_{cI_1I_1,1}}{b} + \\ + \frac{\mathcal{R}_{cI_1I_1,2}}{b} & \mathcal{R}_{cA_2A_1,1} + \mathcal{R}_{cA_2A_1,2} + \\ + \mathcal{R}_{cI_2I_1,1} + \mathcal{R}_{cI_2I_1,2} & \frac{\mathcal{R}_{cA_2A_1,1}}{1-b} + \\ + \frac{\mathcal{R}_{cA_2A_1,2}}{1-b} & \frac{\mathcal{R}_{cI_2I_1,1}}{b} + \\ + \frac{\mathcal{R}_{cI_2I_1,2}}{b} \\ 0 & 0 & 0 & 0 & 0 & 0 \\ 0 & 0 & 0 & 0 & 0 & 0 \\ \mathcal{R}_{cA_1A_2,1} + \mathcal{R}_{cA_1A_2,2} + \\ + \mathcal{R}_{cI_1I_2,1} + \mathcal{R}_{cI_1I_2,2} & \frac{\mathcal{R}_{cA_1A_2,1}}{1-b} + \\ + \frac{\mathcal{R}_{cA_1A_2,2}}{1-b} & \frac{\mathcal{R}_{cI_1I_2,1}}{b} + \\ + \frac{\mathcal{R}_{cI_1I_2,2}}{b} & \mathcal{R}_{cA_2A_2,1} + \mathcal{R}_{cA_2A_2,2} + \\ + \mathcal{R}_{cI_2I_2,1} + \mathcal{R}_{cI_2I_2,2} & \frac{\mathcal{R}_{cA_2A_2,1}}{1-b} + \\ + \frac{\mathcal{R}_{cA_2A_2,2}}{1-b} & \frac{\mathcal{R}_{cI_2I_2,1}}{b} + \\ + \frac{\mathcal{R}_{cI_2I_2,2}}{b} \\ 0 & 0 & 0 & 0 & 0 & 0 \\ 0 & 0 & 0 & 0 & 0 & 0 \end{bmatrix} \tag{3.10}$$

As mentioned, the reproduction number of System (3.1) for n=2 is defined by the dominant eigenvalue of the matrix Θ. The eigenvalues (λ) of System (3.1) are:

$$\lambda = \begin{bmatrix} 0 \\ 0 \\ 0 \\ 0 \\ \frac{1}{2}\begin{pmatrix}\mathcal{R}_{cA_1A_1,1}+\mathcal{R}_{cA_1A_1,2}+\mathcal{R}_{cI_1I_1,1}+\mathcal{R}_{cI_1I_1,2}+\\ \mathcal{R}_{cA_2A_2,1}+\mathcal{R}_{cA_2A_2,2}+\mathcal{R}_{cI_2I_2,1}+\mathcal{R}_{cI_2I_2,2}\end{pmatrix}+ \\ +\frac{1}{2}\sqrt{\begin{bmatrix}\mathcal{R}_{cA_2A_2,1}+\mathcal{R}_{cA_2A_2,2}+\mathcal{R}_{cI_2I_2,1}+\mathcal{R}_{cI_2I_2,2}-\\ -\mathcal{R}_{cA_1A_1,1}-\mathcal{R}_{cA_1A_1,2}-\mathcal{R}_{cI_1I_1,1}-\mathcal{R}_{cI_1I_1,2}\end{bmatrix}^2+4\begin{pmatrix}\mathcal{R}_{cA_1A_2,1}+\mathcal{R}_{cA_1A_2,2}+\\ +\mathcal{R}_{cI_1I_2,1}+\mathcal{R}_{cI_1I_2,2}\end{pmatrix}\begin{pmatrix}\mathcal{R}_{cA_2A_1,1}+\mathcal{R}_{cA_2A_1,2}+\\ +\mathcal{R}_{cI_2I_1,1}+\mathcal{R}_{cI_2I_1,2}\end{pmatrix}} \\ \frac{1}{2}\begin{pmatrix}\mathcal{R}_{cA_1A_1,1}+\mathcal{R}_{cA_1A_1,2}+\mathcal{R}_{cI_1I_1,1}+\mathcal{R}_{cI_1I_1,2}+\\ \mathcal{R}_{cA_2A_2,1}+\mathcal{R}_{cA_2A_2,2}+\mathcal{R}_{cI_2I_2,1}+\mathcal{R}_{cI_2I_2,2}\end{pmatrix}- \\ -\frac{1}{2}\sqrt{\begin{bmatrix}\mathcal{R}_{cA_2A_2,1}+\mathcal{R}_{cA_2A_2,2}+\mathcal{R}_{cI_2I_2,1}+\mathcal{R}_{cI_2I_2,2}-\\ -\mathcal{R}_{cA_1A_1,1}-\mathcal{R}_{cA_1A_1,2}-\mathcal{R}_{cI_1I_1,1}-\mathcal{R}_{cI_1I_1,2}\end{bmatrix}^2+4\begin{pmatrix}\mathcal{R}_{cA_1A_2,1}+\mathcal{R}_{cA_1A_2,2}+\\ +\mathcal{R}_{cI_1I_2,1}+\mathcal{R}_{cI_1I_2,2}\end{pmatrix}\begin{pmatrix}\mathcal{R}_{cA_2A_1,1}+\mathcal{R}_{cA_2A_1,2}+\\ +\mathcal{R}_{cI_2I_1,1}+\mathcal{R}_{cI_2I_1,2}\end{pmatrix}} \end{bmatrix} \tag{3.11}$$

Observe that the terms under the square root are always positive, hence the dominant eigenvalue is the fifth element of vector λ, i.e.

$$\mathcal{R}_c = \frac{1}{2}\begin{pmatrix}\mathcal{R}_{cA_1A_1,1}+\mathcal{R}_{cA_1A_1,2}+\mathcal{R}_{cI_1I_1,1}+\mathcal{R}_{cI_1I_1,2}+\\ \mathcal{R}_{cA_2A_2,1}+\mathcal{R}_{cA_2A_2,2}+\mathcal{R}_{cI_2I_2,1}+\mathcal{R}_{cI_2I_2,2}\end{pmatrix}+ \\ +\frac{1}{2}\sqrt{\begin{bmatrix}\mathcal{R}_{cA_2A_2,1}+\mathcal{R}_{cA_2A_2,2}+\mathcal{R}_{cI_2I_2,1}+\mathcal{R}_{cI_2I_2,2}-\\ -\mathcal{R}_{cA_1A_1,1}-\mathcal{R}_{cA_1A_1,2}-\mathcal{R}_{cI_1I_1,1}-\mathcal{R}_{cI_1I_1,2}\end{bmatrix}^2+4\begin{pmatrix}\mathcal{R}_{cA_1A_2,1}+\mathcal{R}_{cA_1A_2,2}+\\ +\mathcal{R}_{cI_1I_2,1}+\mathcal{R}_{cI_1I_2,2}\end{pmatrix}\begin{pmatrix}\mathcal{R}_{cA_2A_1,1}+\mathcal{R}_{cA_2A_1,2}+\\ +\mathcal{R}_{cI_2I_1,1}+\mathcal{R}_{cI_2I_1,2}\end{pmatrix}} \tag{3.12}$$

It is possible to derive the reproduction number by reducing the matrix (3.10) to a new one with a smaller dimension (2×2). Diekmann et al [89] provide a detailed description on how to construct the next generation matrix and reduce it by eliminating the unnecessary terms in the transmission matrix $\mathcal{F}$. By following the steps in Diekmann [89], we use an auxiliary matrix E_{aux} defined as:

$$E_{aux} = \begin{bmatrix} 1 & 0 \\ 0 & 0 \\ 0 & 0 \\ 0 & 1 \\ 0 & 0 \\ 0 & 0 \end{bmatrix} \tag{3.13}$$

The reduced next generation matrix is then given by: $E_{aux}^T \mathcal{F}(-\mathcal{V}^{-1})E_{aux}$. After evaluating this multiplication, the matrix (3.10) is reduced to a new next generation matrix ($\mathcal{M}$) with dimension $2x2$:

$$\mathcal{M} = \begin{bmatrix} \mathcal{R}_{cA_1A_1,1}+\mathcal{R}_{cA_1A_1,2}+\mathcal{R}_{cI_1I_1,1}+\mathcal{R}_{cI_1I_1,2} & \mathcal{R}_{cA_2A_1,1}+\mathcal{R}_{cA_2A_1,2}+\mathcal{R}_{cI_2I_1,1}+\mathcal{R}_{cI_2I_1,2} \\ \mathcal{R}_{cA_1A_2,1}+\mathcal{R}_{cA_1A_2,2}+\mathcal{R}_{cI_1I_2,1}+\mathcal{R}_{cI_1I_2,2} & \mathcal{R}_{cA_2A_2,1}+\mathcal{R}_{cA_2A_2,2}+\mathcal{R}_{cI_2I_2,1}+\mathcal{R}_{cI_2I_2,2} \end{bmatrix} \tag{3.14}$$

Since the reduced matrix $\mathcal{M}$ has dimensions $2x2$ its spectral radius, and hence the reproduction number, can be expressed in terms of its trace and determinant, as follows:

$$\mathcal{R}_c = \frac{1}{2}Tr(\mathcal{M}) + \frac{1}{2}\sqrt{Tr(\mathcal{M})^2 - 4Det(\mathcal{M})} \tag{3.15}$$

where:

$$Tr(\mathcal{M}) = \mathcal{R}_{cA_1A_1,1} + \mathcal{R}_{cA_1A_1,2} + \mathcal{R}_{cA_2A_2,1} + \mathcal{R}_{cA_2A_2,2} + \mathcal{R}_{cI_1I_1,1} + \mathcal{R}_{cI_1I_1,2} + \mathcal{R}_{cI_2I_2,1} + \mathcal{R}_{cI_2I_2,2} \tag{3.16}$$

$$\begin{aligned} Det(\mathcal{M}) = &\{[(\mathcal{R}_{cA_1A_1,1} + \mathcal{R}_{cA_1A_1,2}) + (\mathcal{R}_{cI_1I_1,1} + \mathcal{R}_{cI_1I_1,2})] \times \\ &[(\mathcal{R}_{cA_2A_2,1} + \mathcal{R}_{cA_2A_2,2}) + (\mathcal{R}_{cI_2I_2,1} + \mathcal{R}_{cI_2I_2,2})]\} - \\ &\{[(\mathcal{R}_{cA_2A_1,1} + \mathcal{R}_{cA_2A_1,2}) + (\mathcal{R}_{cI_2I_1,1} + \mathcal{R}_{cI_2I_1,2})] \times \\ &[(\mathcal{R}_{cA_1A_2,1} + \mathcal{R}_{cA_1A_2,2}) + \mathcal{R}_{cI_1I_2,1} + \mathcal{R}_{cI_1I_2,2}] \end{aligned} \tag{3.17}$$

Observe that the expression provided in Eq. (3.12) and in Eq. (3.15) are equivalent.
Using R_c given in Eq. (3.15), we now derive conditions that provide a reproduction number $\mathcal{R}_c < 1$. For simplicity of notation, we define the entries of the matrix $\mathcal{M} = (\mathcal{A} \quad \mathcal{B}; \mathcal{C} \quad \mathcal{D})$. Since the reproduction number is defined as the spectral radius of the matrix $\mathcal{M}$, the square root present in the Eq.(3.15) must be positive. This is possible if the determinant of $\mathcal{M}$ is negative or $Det(\mathcal{M}) < \frac{Tr(\mathcal{M})^2}{4} \iff \mathcal{AD} - \mathcal{BC} < \frac{(\mathcal{A}+\mathcal{D})^2}{4}$. After algebraic computations, the condition providing the total reproduction number to be less than 1 can be rewritten as:

$$\sqrt{(\mathcal{A}+\mathcal{D})^2 - 4(\mathcal{AD} - \mathcal{BC})} < 2 - (\mathcal{A}+\mathcal{D}) \tag{3.18}$$

Observe that the terms on the right hand side of the inequality might assume either positive or negative sign. Both cases are analysed.

- **Case 1:** $(\mathcal{AD} - \mathcal{BC}) < 0$ **and** $0 < \mathcal{A} + \mathcal{D} < 2$
  Under these conditions both terms in the inequality (3.18) are positive and after raising them to the power of two, we obtain the inequality

  $$\mathcal{AD} - \mathcal{BC} > \mathcal{A} + \mathcal{D} - 1 \tag{3.19}$$

  Observe that the term $(\mathcal{AD} - \mathcal{BC})$ is always negative, hence for the inequality to hold it is necessary that the term $\mathcal{A} + \mathcal{D} - 1$ is negative as well. This provides the following further condition: $0 < \mathcal{A} + \mathcal{D} < 1$.

- **Case 2:** $(\mathcal{AD} - \mathcal{BC}) < 0$ **and** $\mathcal{A} + \mathcal{D} > 2$
  The term on the right hand side of the inequality (3.18) is negative, hence before raising its both terms to the power of two, it is necessary to reverse the inequality sign. After rearranging the elements in (3.18), we obtain the following condition:

  $$\mathcal{AD} - \mathcal{BC} < \mathcal{A} + \mathcal{D} - 1 \tag{3.20}$$

- **Case 3:** $(\mathcal{AD} - \mathcal{BC}) > 0$, $\mathcal{AD} - \mathcal{BC} < \frac{(\mathcal{A}+\mathcal{D})^2}{4}$ **and** $0 < \mathcal{A} + \mathcal{D} < 2$
  Similar to Case 1, the inequality (3.18) can be rewritten as

  $$\mathcal{AD} - \mathcal{BC} > \mathcal{A} + \mathcal{D} - 1 \tag{3.21}$$

  Under the given assumptions, the inequality (3.21) is verified if $\mathcal{A}+\mathcal{D}-1 < \mathcal{AD}-\mathcal{BC} < \frac{(\mathcal{A}+\mathcal{D})^2}{4}$.

- **Case 4:** $(\mathcal{AD} - \mathcal{BC}) > 0$, $\mathcal{AD} - \mathcal{BC} < \frac{(\mathcal{A}+\mathcal{D})^2}{4}$ **and** $\mathcal{A} + \mathcal{D} > 2$
  In order to analyze Case 4, we follow the same steps done in Case 2. After algebraic computations, the inequality (3.18) expression becomes

$$\mathcal{AD} - \mathcal{BC} < \mathcal{A} + \mathcal{D} - 1 \tag{3.22}$$

  This inequality holds if $\mathcal{AD} - \mathcal{BC} < \frac{(\mathcal{A}+\mathcal{D})^2}{4}$

Table 3.4 summarizes the previous investigation.

$\boldsymbol{\mathcal{R}_c = \frac{1}{2}(\mathcal{A}+\mathcal{D}) + \frac{1}{2}\sqrt{(\mathcal{A}+\mathcal{D})^2 - 4(\mathcal{AD}-\mathcal{BC})} < 1}$		
	$\boldsymbol{\mathcal{AD} - \mathcal{BC} < 0}$	$\boldsymbol{\mathcal{AD} - \mathcal{BC} > 0}$
$\boldsymbol{\mathcal{A} + \mathcal{D} < 2}$	$\mathcal{AD} - \mathcal{BC} > \mathcal{A} + \mathcal{D} - 1$ and $0 < \mathcal{A} + \mathcal{D} < 1$	$\mathcal{A} + \mathcal{D} - 1 < \mathcal{AD} - \mathcal{BC} < \frac{(\mathcal{A}+\mathcal{D})^2}{4}$
$\boldsymbol{\mathcal{A} + \mathcal{D} > 2}$	$\mathcal{AD} - \mathcal{BC} < \mathcal{A} + \mathcal{D} - 1$	$\mathcal{AD} - \mathcal{BC} < \frac{(\mathcal{A}+\mathcal{D})^2}{4}$

Table 3.4: Conditions on trace and determinant of the next generation matrix $\mathcal{M}$ (3.14)

Numerical Results

Control Reproduction Number ($\mathcal{R}_c$)

In this section we show the numerical investigation on the relationship between residency times and total reproduction number $\mathcal{R}_c$. Based on the data reported in the 2016 Canadian Census [110], a large size of Halton residents commute to Toronto to work, but not the opposite. However, Toronto residents do commute towards York region daily, and vice versa. Hence, we assume that Halton is the patch whose residents move to Toronto, while York is the second patch in the scenario where Toronto residents move as well. Since our interest is to investigate the sustainability of the infection when the patches present different immunity background, we consider that extreme proportions of vaccinated individuals to be 10% or 90% of the population. The infectiousness of the virus is defined depending on the immunity background of the patch. If highly susceptible, the specific patch $\mathcal{R}_c = 16$, otherwise $\mathcal{R}_c = 1.8$.

$V_{1_0} = 10\%, V_{2_0} = 10\%$

Here, we report the results when both patches present only the 10% of the total population vaccinated.

When Toronto is the region whose residents are not moving (Figure 3.2), we observe that the total control reproduction number slightly decreases as the probability of showing symptoms increases. This is easily interpretable since less asymptomatic cases from Halton will move, and hence, reducing the spread of the infection in Toronto. Moreover, it is visible how the total $\mathcal{R}_c$ shows a decreasing trend as patch 2 residents spend more time in Toronto, with a lower infectivity. Also, it is important to look at the extreme cases: when $p_{22} = 0$ (i.e. Halton residents spend all their time in Toronto), the total reproduction number corresponds to the one present in patch 1; when $p_{22} = 1$ (i.e. isolation) the total reproduction number correspond to the maximum of the two specific $\mathcal{R}_c$, which is the one in Halton.

Now we consider the scenario in which the residents of both patches commute (Figure 3.3). As mentioned, we consider the two census region Toronto and York, as patch 1 and patch 2, respectively. Since patch 1 residents can spend time in patch 2 and vice versa, we investigate the relationship between the total control reproduction number and the residency times p_{11} and p_{22}.
Similar to the previous scenario, we observe that there are increased reductions of the total control reproduction number when the probability of showing symptoms increases and the combination of p_{11} and p_{22} values becomes larger. When the patches are isolated $p_{11} = p_{22} = 1$, the total reproduction number is the maximum of the two specific $\mathcal{R}_{c_{1,2}}$. If Toronto residents do not leave their patch, we observe the same trend visible in Figure (3.2): the total reproduction number decreases as Halton residents spend most of their time in Toronto. Moreover, note that as $p_{11} = 1$ and $p_{22} = 0$ $\mathcal{R}_c$ gradually increases and its maximum value will be close, but smaller, to $\mathcal{R}_{c_2}$. While, as $p_{11} = 0$ and $p_{22} = 0$ the total reproduction number is smaller that the highest specific $\mathcal{R}_{c_{1,2}}$, but close to that value.

In this section we provide results in the scenario where both patches are highly susceptible. We observe that the control policy of not allowing symptomatic cases to travel, decreases the overall transmission of the infection. Moreover, we observe that in case of isolation, the total reproduction number takes the maximum of the two specific $\mathcal{R}_{ci}$, $i = 1, 2$. However, when both patches residents are moving, there is a reduction in the total infectivity. In particular, the maximum reduction is obtained when all individuals spend all their time in the patch with a smaller reproduction number.
Our results show that the total transmission does not change significantly, hence, to reduce it globally, Public Health should focus in decreasing the susceptibility in the patches.

$V_{1_0} = 10\%, V_{2_0} = 90\%$

In this section, we investigate the total reproduction number when the population of the biggest patch (Toronto) is highly susceptible (with $\mathcal{R}_{c_1} \approx 16$), while the vaccinated individuals in the second patch are the 90% of the total population (with $\mathcal{R}_{c_2} \approx 1.8$). In particular, we are interested in understanding if the patch greatly immunized can reduce the infection in

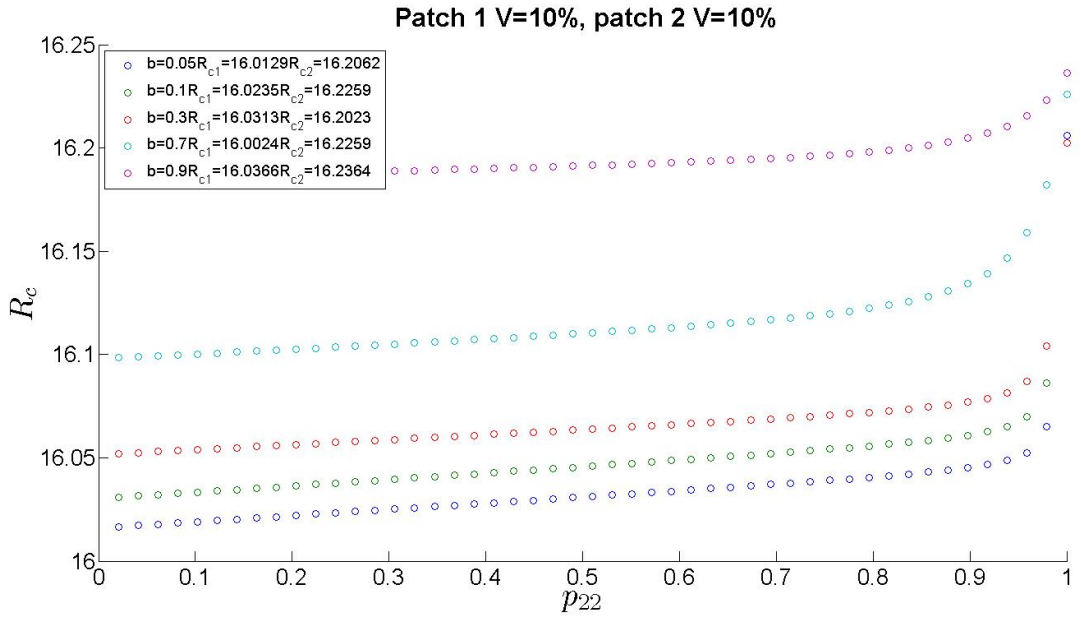

Figure 3.2: Toronto-Halton (Halton moving): relationship between the total reproduction number and residency time p_{21} when only patch 2 (Halton) residents are moving $V_{1_0} = 10\%$, $V_{2_0} = 10\%$,$R_{c_{1,2}} \approx 16$ and $b = 0.05, 0.1, 0.3, 0.7, 0.9$

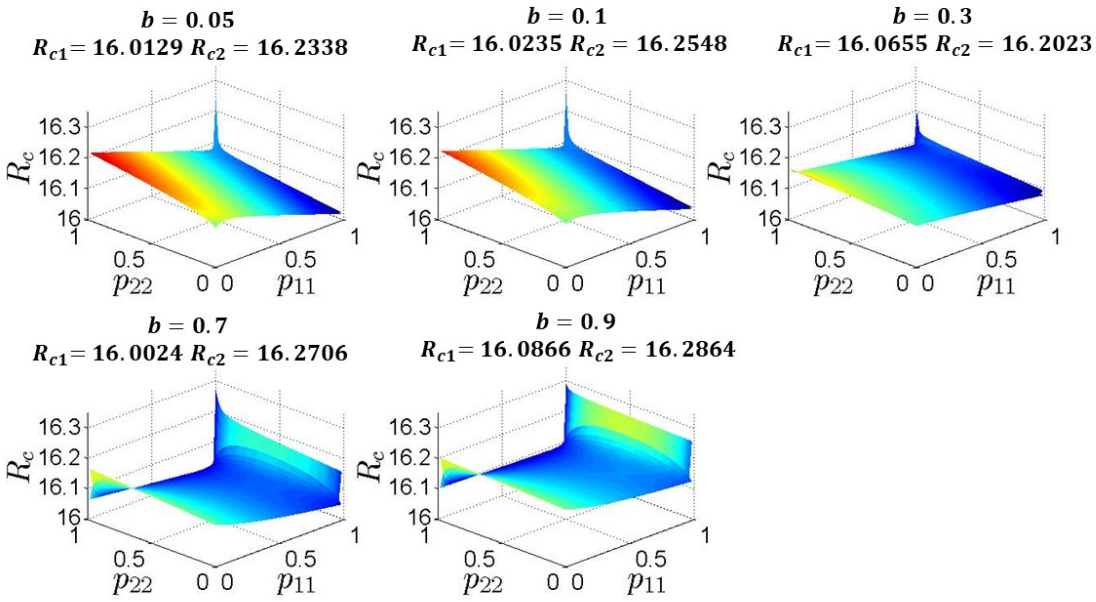

Figure 3.3: Toronto-York (all moving): relationship between the total reproduction number and residency time p_{11}, p_{22} when both patches residents are moving, $V_{1_0} = 10\%$, $V_{2_0} = 10\%$,$R_{c_{1,2}} \approx 16$ and (a) $b = 0.05$ (b) $b = 0.1$ (c) $b = 0.3$ (d) $b = 0.7$ (e) $b = 0.9$.

both patches. Similar to the analysis conducted in Section 3.2.2, we compare two scenarios: the first one, when only patch 2 residents commute to patch 1 (Figure 3.4); the second one when the residents of both patches commute (Figure 3.5).

When only the low risk patch residents are moving (Figure 3.4), we note that in case of isolation ($p_{22} = 1$) the total reproduction number is equal to the one present in the high risk patch (i.e. $\mathcal{R}_c \approx 16$). As Halton residents spend most of their time in Toronto ($p_{22} < 1$), we can observe that the presence of highly vaccinated individuals in an almost completely vulnerable population decreases the total transmission by roughly 15%. We also observe that the probability of showing symptoms does not have a significant impact on the total $\mathcal{R}_c$, especially when $p_{22} > 0.5$. This is expected since not many infected will move from a highly vaccinated patch to spread the infection.

A different scenario is visible when the high risk patch residents travel to another patch (Figure 3.5). We observe that for all the sampled b, when $p_{11} = 1$ the trend of the total reproduction number corresponds to the one seen in Figure 3.4. However, contrary to the previous case, here we observe that the probability of manifesting symptoms is an important factor on the change in the total $\mathcal{R}_c$. In particular, we observe that as b increases (hence, less infectious people are traveling), the reduction of the total reproduction number is extremely significant (from ≈ 16 to ≈ 5). The maximum reduction is provided when $b > 0.3$ and Toronto residents spend more than 80% of their time in the highly vaccinated patch. On the other hand, we observe that for $b < 0.3$, the reduction in the total reproduction number is minimal.

This analysis results suggest that if the biggest of the two patches is highly vaccinated, no policy on both communities' isolation should be implemented in case of outbreak. However, decreasing the vaccine heterogeneity will provide a total reduction on the transmission.

$\boldsymbol{V_{1_0} = 90\%, V_{2_0} = 10\%}$

We are now considering the scenario in which the patch with the largest population (Toronto, patch 1) is the region highly vaccinated (90%), while patch 2 (Halton or York region) population is mostly vulnerable to the infection.

Similar to all the previous cases, we start our analysis setting Toronto as the non-commuting patch (Figure 3.6). Immediately we observe that if the probability of showing symptoms increases, reducing then the mobility of asymptomatic cases, the total reproduction number increases reaching the infectivity level present in the high risk patch. Moreover, if the patches are not interacting, the total reproduction number assumes the value of the highest specific $\mathcal{R}_{c_{1,2}}$ (i.e., $\mathcal{R}_c \approx 16$ for $p_{22} = 1$). However, if the high risk patch residents spend more time in the highly vaccinated region, then the total $\mathcal{R}_c$ decreases. This reduction can be up to 70% (for extreme case $b = 0.05$ and $p_{22} = 0$). These findings suggest that the movement of asymptomatic cases towards a highly vaccinated patch results in a decreasing trend of the total infectivity.

Figure 3.7 shows the $\mathcal{R}_c$ surface when both patches residents commute. We observe that under this condition, the maximum reduction of the total reproduction number is provided

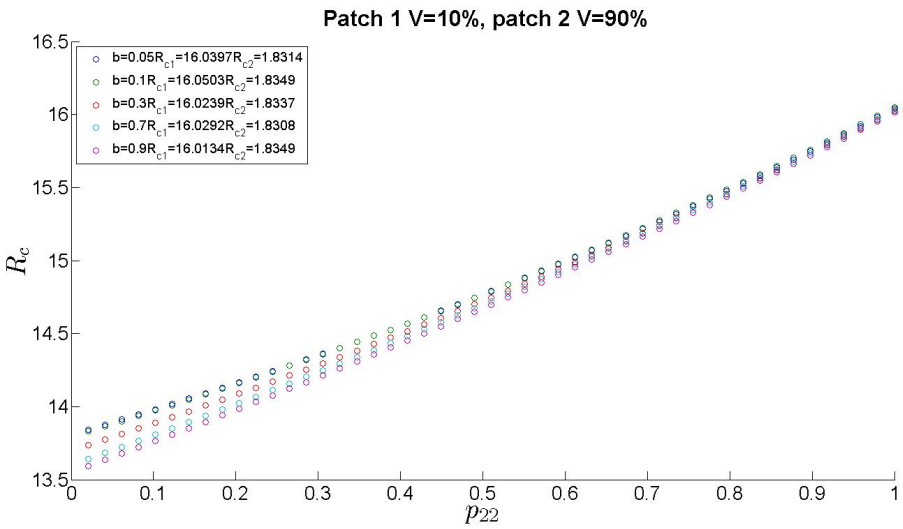

Figure 3.4: Relationship between the total reproduction number and residency time p_{21} when only patch 2 residents are moving $V_{1_0} = 10\%$, $V_{2_0} = 90\%$, $R_{c_1} \approx 16$, $R_{c_2} \approx 1.8$ and $b = 0.05, 0.1, 0.3, 0.7, 0.9$

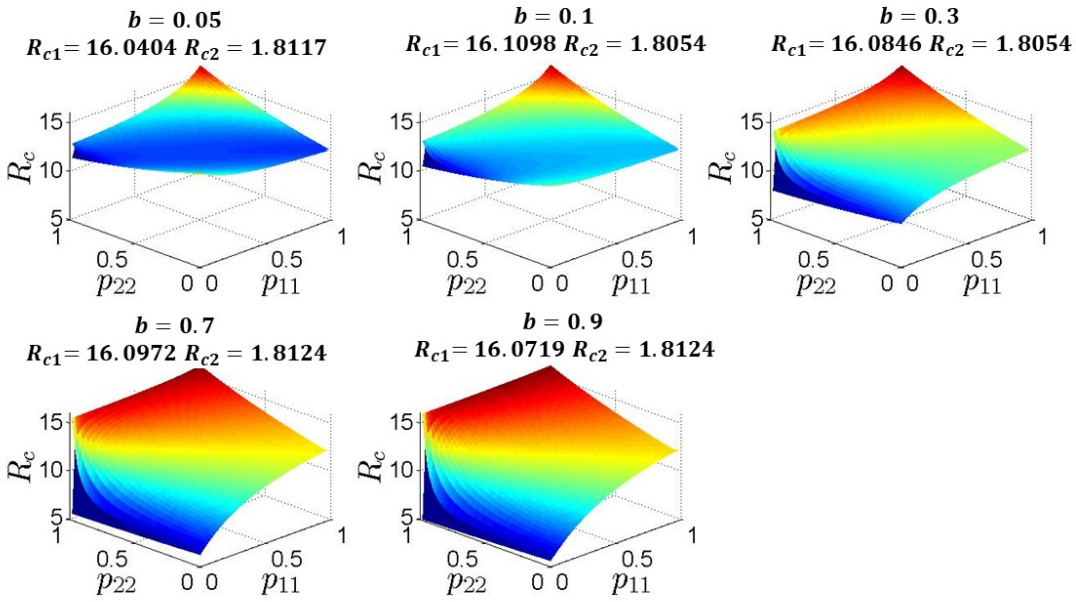

Figure 3.5: Toronto-York (all moving): relationship between the total reproduction number and residency time p_{11}, p_{22} when both patches residents are moving, $V_{1_0} = 10\%$, $V_{2_0} = 90\%$,$R_{c_1} \approx 16$, $R_{c_2} \approx 1.8$ and (a) $b = 0.05$ (b) $b = 0.1$ (c) $b = 0.3$ (d) $b = 0.7$ (e) $b = 0.9$.

when $b > 0.3$. This reduction is also given if the vaccinated Toronto residents spend most of their time in the vulnerable patch. This suggests that even if asymptomatic cases are not many, the immunized individuals from Toronto reduce the overall $\mathcal{R}_c$. Moreover, if we look at the case when $p_{11}, p_{22} \approx 0$ (indicating that Toronto residents are mostly in York, and vice versa), we observe that for small b, the total reproduction number assumes values close to $\mathcal{R}_{c_2}$. This indicates that when more asymptomatic cases travel towards a susceptible region, the infection will keep spreading. However, as b increases, reducing the proportion of infected individuals travelling, the movement of vaccinated individual results in a reduction of the infectivity.

$\boldsymbol{V_{1_0} = 90\%, V_{2_0} = 90\%}$

In this last section, we report the scenario in which both patches have a highly vaccinated population.

In Figure 3.8 (Toronto residents are not leaving their patch) we observe that the total reproduction number increases as Halton residents spend most of their time in their own region. At the extreme case $p_{22} = 1$, $\mathcal{R}_c$ assumes the value of the highest specific reproduction number (which is $\mathcal{R}_{c_2}$). Moreover, as the probability of showing the signs of the infection increases, the reproduction number reduction becomes smaller. Since both patches are highly vaccinated and low risk, the change in the total reproduction number is minimal.

When both patches residents commute (Figure 3.9), we observe that, similar to the previous scenario, the reduction in the total reproduction number is not significant. The highest values of the total $\mathcal{R}_c$ are given in case of isolation and when Toronto residents spend all their time in York region.

The results provided in this section indicate that if both patches are highly vaccinated, the movement of infected cases do not increase the overall infectivity visibly. On the other hand, the immunity brought in the workplace region does not decrease the spread of the infection.

Infection Dynamics

We show some examples of infection dynamics when the probability of showing symptoms b, reproduction numbers are varied: $1.8, 9, 16$ (Figures (3.10)-(3.11)). We see how increasing b the size of asymptomatic cases decreases, while the symptomatic increases. Moreover, as the transmission decreases we observe how the dynamic of the infection is delayed and the peak becomes smaller. These results are visible when only Halton residents are moving (3.10) or both patches (Toronto and York) are moving (Figure 3.11).

Sensitivity Analysis

In this section we will present the results on the uncertainty of the parameters of the model on its outputs. After seeding the infection in the two different patches, we observe that the PRCC plots on the sum of all the asymptomatic and symptomatic cases is similar in both

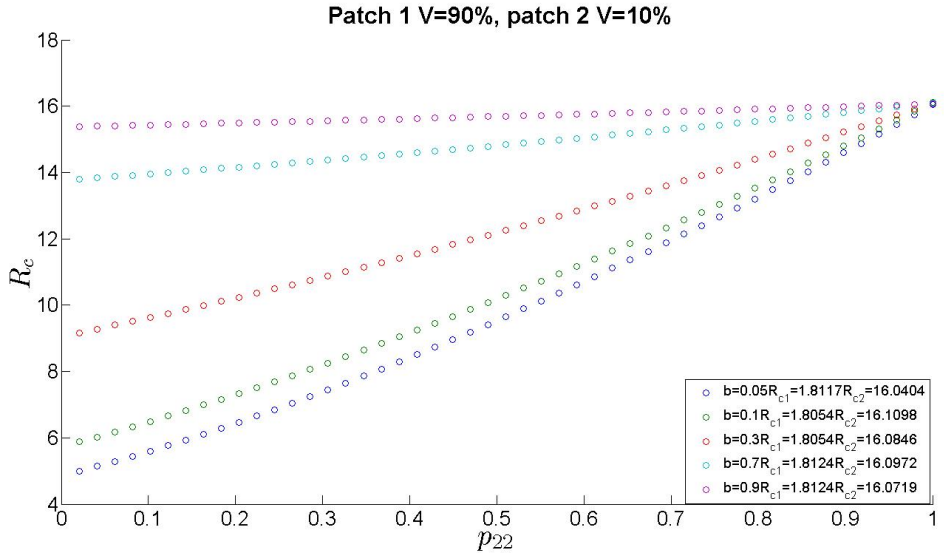

Figure 3.6: Relationship between the total reproduction number and residency time p_{21} when only patch 2 residents are moving $V_{1_0} = 90\%$, $V_{2_0} = 10\%$, $R_{c_1} \approx 1.8$, $R_{c_2} \approx 16$ and $b = 0.05, 0.1, 0.3, 0.7, 0.9$

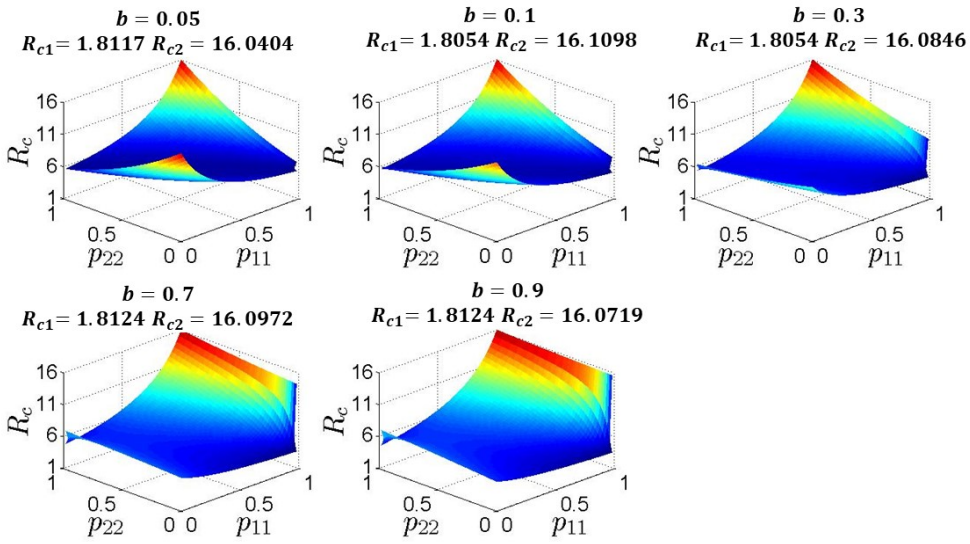

Figure 3.7: Relationship between the total reproduction number and residency time p_{11}, p_{22} when both patches residents are moving, $V_{1_0} = 90\%$, $V_{2_0} = 10\%$,$R_{c_1} \approx 1.8$, $R_{c_2} \approx 16$ and (a) $b = 0.05$ (b) $b = 0.1$ (c) $b = 0.3$ (d) $b = 0.7$ (e) $b = 0.9$.

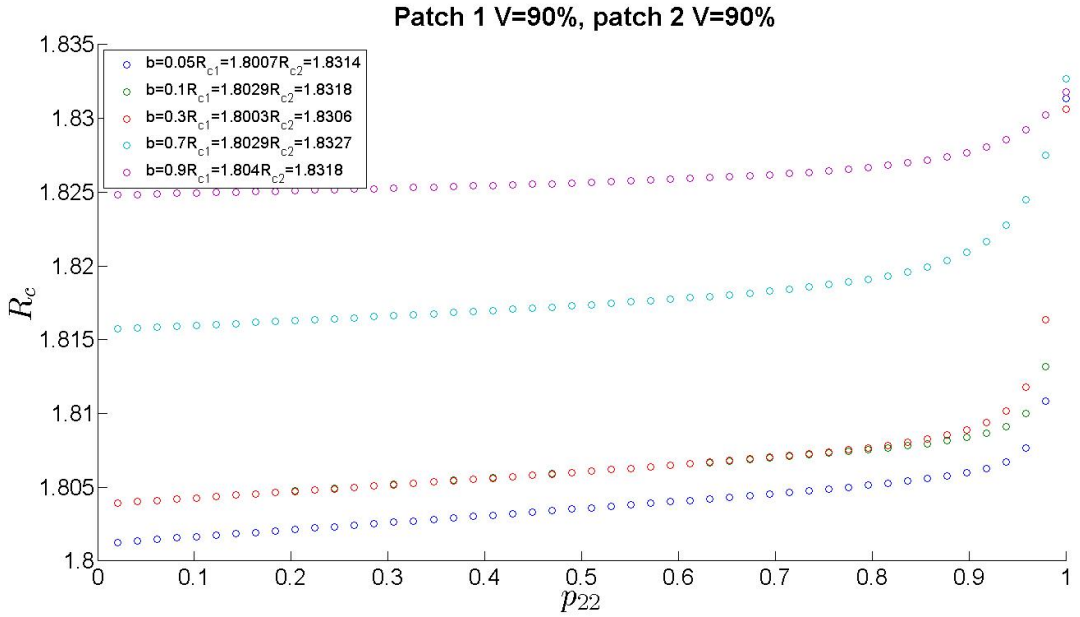

Figure 3.8: Relationship between the total reproduction number and residency times p_{12} when only patch 2 residents are moving $V_{1_0} = 90\%$, $V_{2_0} = 90\%$, $R_{c_{1,2}} = \approx 1.8$ and (a) $b = 0.05$ (b) $b = 0.1$ (c) $b = 0.3$ (d) $b = 0.7$

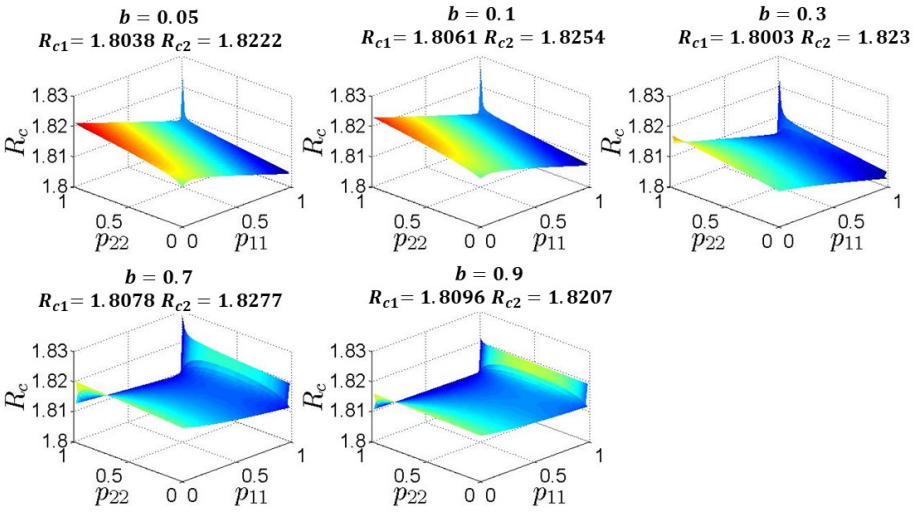

Figure 3.9: Relationship between the total reproduction number and residency times p_{12} and p_{21} when only patch 2 residents are moving $V_{1_0} = 90\%$, $V_{2_0} = 90\%$, $R_{c_{1,2}} = \approx 1.8$ and (a) $b = 0.05$ (b) $b = 0.1$ (c) $b = 0.3$ (d) $b = 0.7$

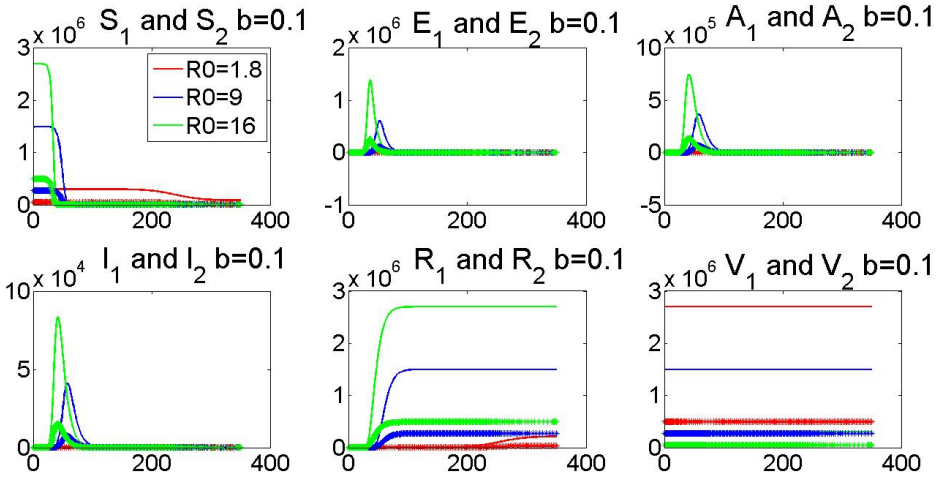

(a)

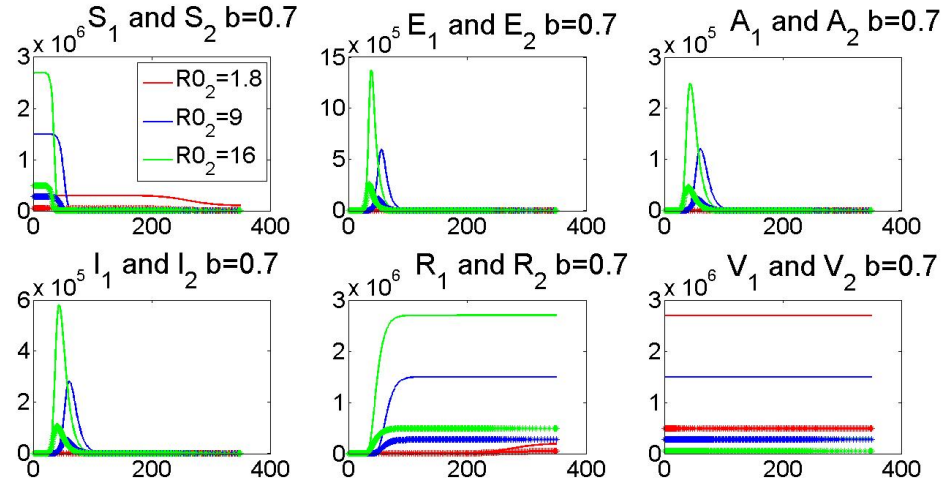

(b)

Figure 3.10: Toronto (solid line) and Halton (starred line)dynamics of $S_{1,2}$, $E_{1,2}$, $I_{a_{1,2}}$, $I_{s_{1,2}}$, $R_{1,2}$, $V_{1,2}$ for $b = 0.1$, 0.7

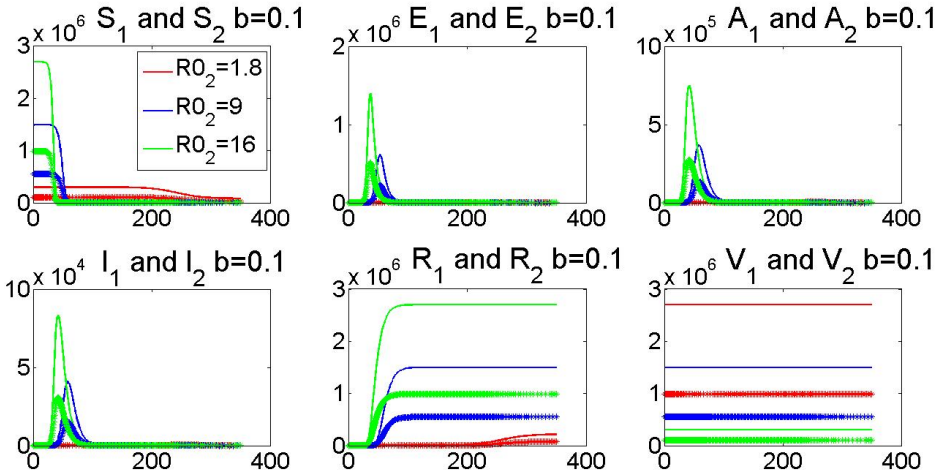

(a)

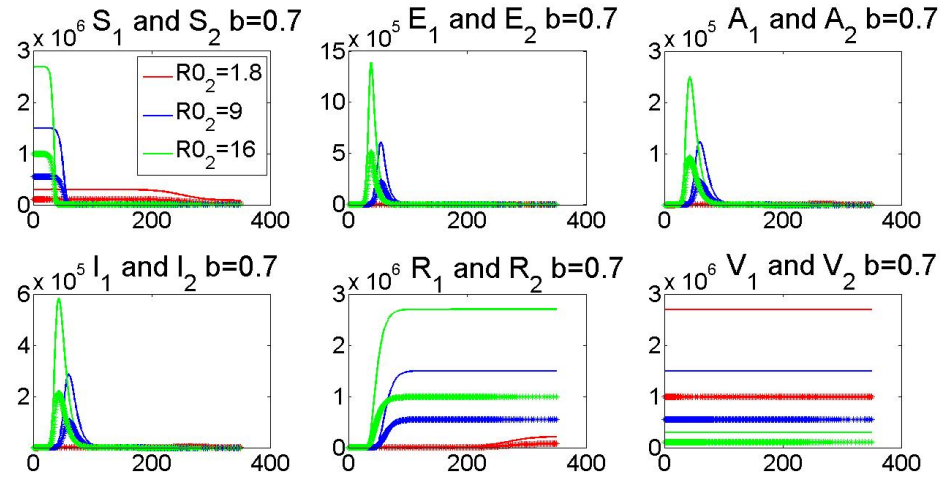

(b)

Figure 3.11: Toronto (solid line) and York (starred line) dynamics of $S_{1,2}$, $E_{1,2}$, $I_{a_{1,2}}$, $I_{s_{1,2}}$, $R_{1,2}$, $V_{1,2}$ for $b = 0.1$, 0.7

cases, hence we are presenting only one case. On the other hand, the time at which the first 100 symptomatic cases and the peak of A and I occur present different PRCC plots and they are all discussed. Observe that we consider only the first cases of I because this is the compartment where the infection is seeded.

Toronto-Halton

We start with showing the case considering the patches Toronto-Halton. Figure 3.12 shows the correlation between the parameters and the total asymptomatic (Figures (3.12a), (3.12b), (3.12c)) and symptomatic (Figures (3.12d), (3.12e) cases, (3.12f)) in each individual patch and globally. The significant positive correlation between the transmission in the single patch and the total number of asymptomatic cases indicates that as the transmission increases, the asymptomatic cases increase as well. Moreover, in both patches the probability of showing symptoms present a significant negative correlation, indicating a reduction of the asymptotic cases as b increases. The significant positive correlation of $\mathcal{R}_{01}$ on the total cases indicates that patch 1 is responsible for majority of the cases. In relation to symptomatic cases, we can see that for patch 1, $\mathcal{R}_{01}$, b and s_1 are all significantly positively correlated to the increase of I_1 (Figure (3.12d)). Similar results are visible for I_2. In the global case, we observe that both s_1 and s_2 and $\mathcal{R}_{01}$ are significantly positively correlated to the symptomatic cases, indicating that mainly patch 1 is responsible for the infection spread. This can be explained since the size of Toronto is much bigger than Halton's, hence the spread of the infection is higher.

The next results shown correspond to the scenario when Toronto is the patch seeded with the infection. When Halton is the first infected patch, the correlations are intuitive and very similar to the scenario described for Toronto. They are shown in Appendix E.
We start looking at the time at which A and I reach their peak. When Toronto is the first patch to be infected, then the time at which A_1 or I_1 reaches its maximum decreases as the infectivity of the patch increases. Indeed, the less infectious the patch is, the more time is needed to reach the peak of the infection. When we look at the time needed to reach the peak of the infection in patch 2, if we start the infection in Toronto, the achievement of the peak of A and I is delayed if both reproduction numbers $\mathcal{R}_{01}$ and $\mathcal{R}_{02}$ increase (Figures (3.13b), (3.14b)). However, we also observe that the peak is reached faster if s_1 increases (Figure (3.13b) and (3.14b)). When we investigate the PRCC on the time to reach the maximum A and I globally, if Toronto presents the first symptomatic case, we find again that the parameters related to patch 1 are the ones more significant and their correlation reflects the scenario for the individual A_1 and I_1 (Figures (3.13c) and 3.14c)). The last analysis on the uncertainty of the parameters is on the time at which the first 100 symptomatic cases occurs (Figure 3.15).
We observe that $\mathcal{R}_{01}$ and b are the only parameters which show a significant negative correlation on the first 100 cases in patch 1 (Figure 3.15a)). This indicates the at the beginning of the outbreak, if the level of infectivity in patch 1 and the probability of showing symptoms increase then it takes a longer time to reach 100 symptomatic cases. When we

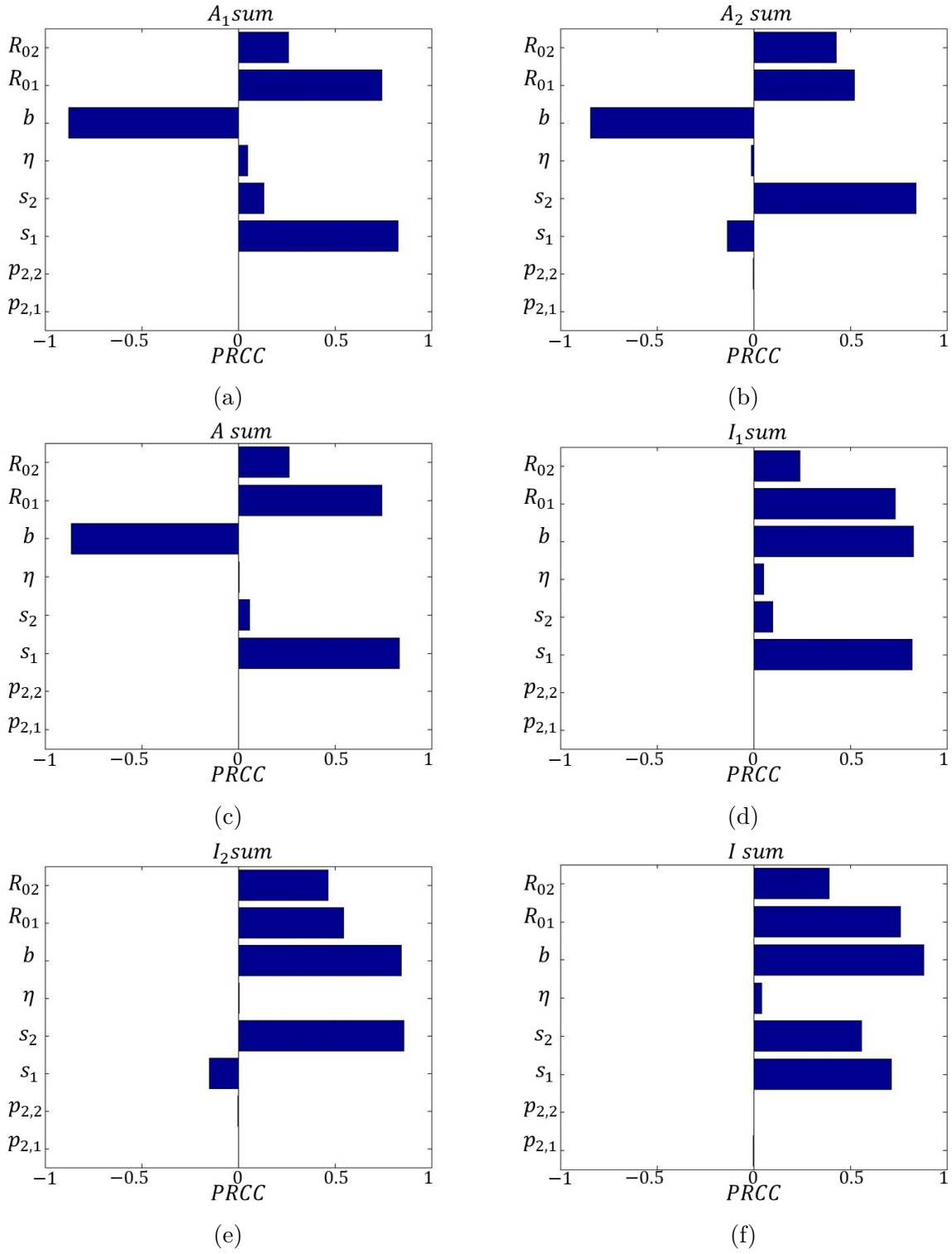

Figure 3.12: Toronto-Halton (Halton moving): PRCC plots on the sum of all the asymptomatic and symptomatic cases over the outbreak

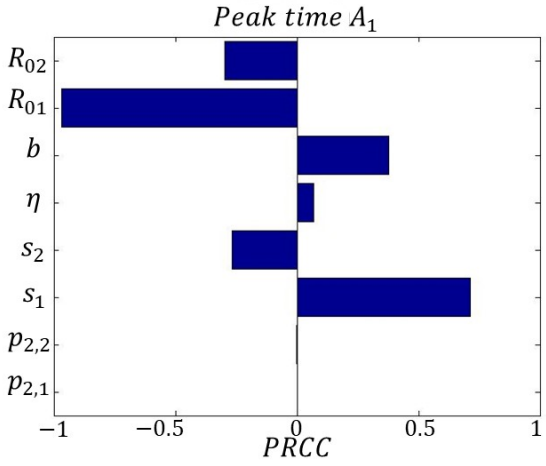

(a)

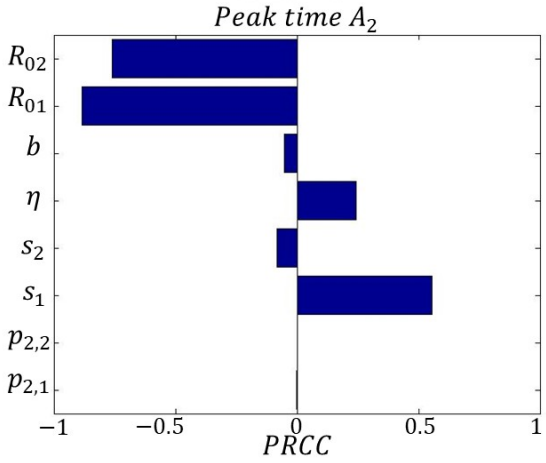

(b)

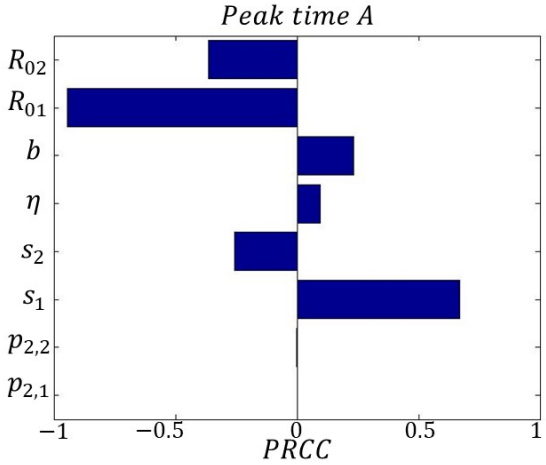

(c)

Figure 3.13: Toronto-Halton (Halton moving): PRCC plots on the time at which the asymptomatic cases reach the peak when the infection is seeded in patch 1

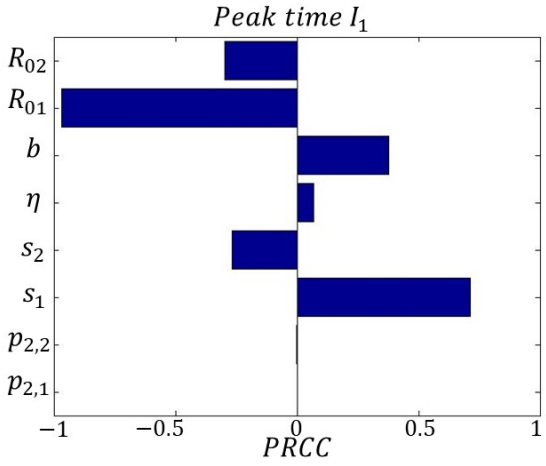

(a)

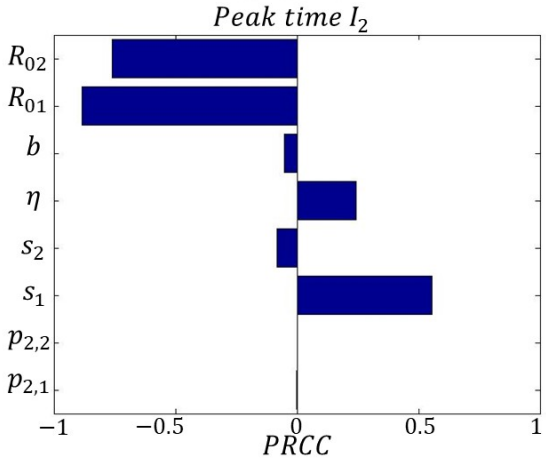

(b)

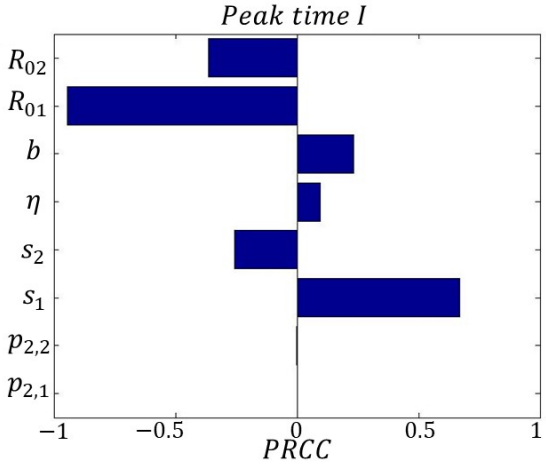

(c)

Figure 3.14: Toronto-Halton (Halton moving): PRCC plots on the time at which the symptomatic cases reach the peak when the infection is seeded in patch 1

look at the first cases in patch 2 and Toronto primary infected (Figure 3.15b)), then we observe that the time needed to reach the first cases in I_2 is delayed if the number of patch 1 susceptible increase. A significant negative correlation is shown for $\mathcal{R}_{01}$, $\mathcal{R}_{02}$, b and s_2. This indicates that if the infectivity of both patches , the probability of showing symptoms and proportion of susceptibles in patch 2 increases, then there is a delay in reaching 100 symptomatic cases in patch 2. Finally, to have at least 100 symptomatic globally, we observe that the more susceptible are present in patch 1 and less infectious patch 1 is, the longer will take to reach 100 cases (Figure 3.15c)).

Toronto-York

Now, we investigate the regions Toronto and York, assuming that the residents of both areas commute.
Similar to Toronto-Halton, we observe that the region where we start the infection does not affect much the total asymptomatic and symptomatic cases (Figure (3.16)). However, for the analysis on the peak time of the infectious compartments and time for the first 100 infectious cases, we only show the scenario with Toronto as first infected. The results for York are similar and intuitive and are shown in Appendix E.
As expected, the probability of showing symptoms shows a significant positive and negative correlation on the total symptomatic and asymptomatic cases, respectively Figure (3.16). Moreover, the transmission in Toronto, as well as the fraction of susceptible individuals, increases the number of cases ($\mathcal{R}_{01}$ shows a significant positive correlation). This indicates that, during the entire outbreak, the transmission in Toronto is responsible for the spread.
The time needed to reach the maximum number of asymptomatic (Figure (3.17)) and symptomatic (Figure (3.18)) cases is negatively significantly affected by the reproduction number in Toronto. While, $\mathcal{R}_{02}$ is slightly negatively significant. This indicates that the transmission in patch 1 and 2, if high, accelerate the achievement of the peak of cases. This result is different from the case Toronto-Halton, since Toronto and York have a similar population size and hence both transmission affect the dynamic of the infection. Similar correlations are visible when we investigate the time needed to reach at least 100 cases (Figure (3.19)).

3.2.3 Three-patch Model

Since Toronto is surrounded by many different regions, we are now extending our model by including three patches, by using $n = 3$ in system 3.1. Similar to the two patches case, we investigate the change of the total reproduction number by comparing the following scenarios: in the first one, Toronto (patch 1) residents are not moving, while Halton (patch 2) and Durham (patch 3) residents commute to Toronto, but not between them since they are geographically far; in the second one, Toronto, York (path 2) and Peel (patch 3) residents travel among all the patches. We start our analysis by finding the total reproduction number of the system. Again, we will use the next generation matrix method as before. The matrix

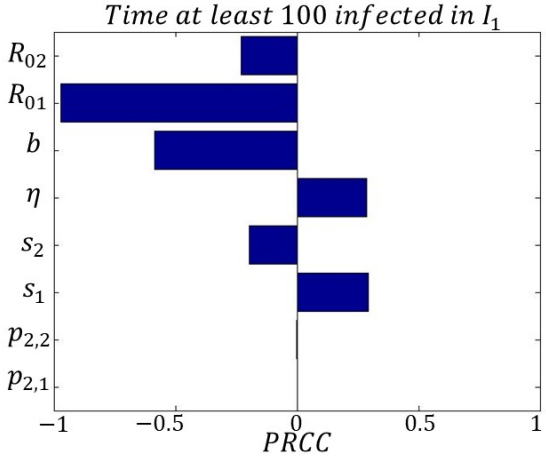

(a)

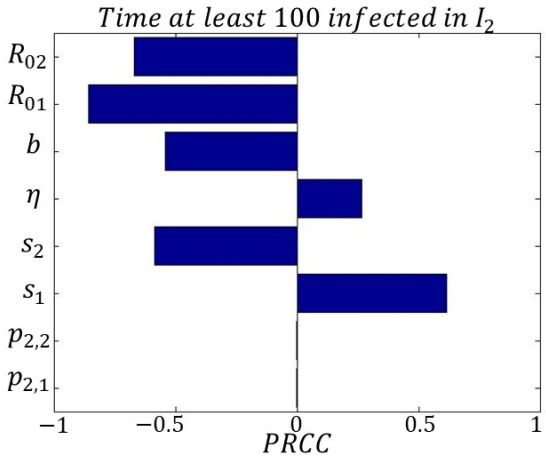

(b)

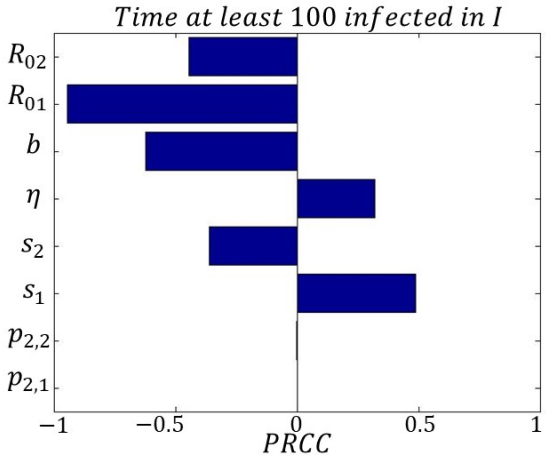

(c)

Figure 3.15: Toronto-Halton (Halton moving): PRCC plots on the time at which the first 100 symptomatic cases occur when the infection is seeded in patch 1

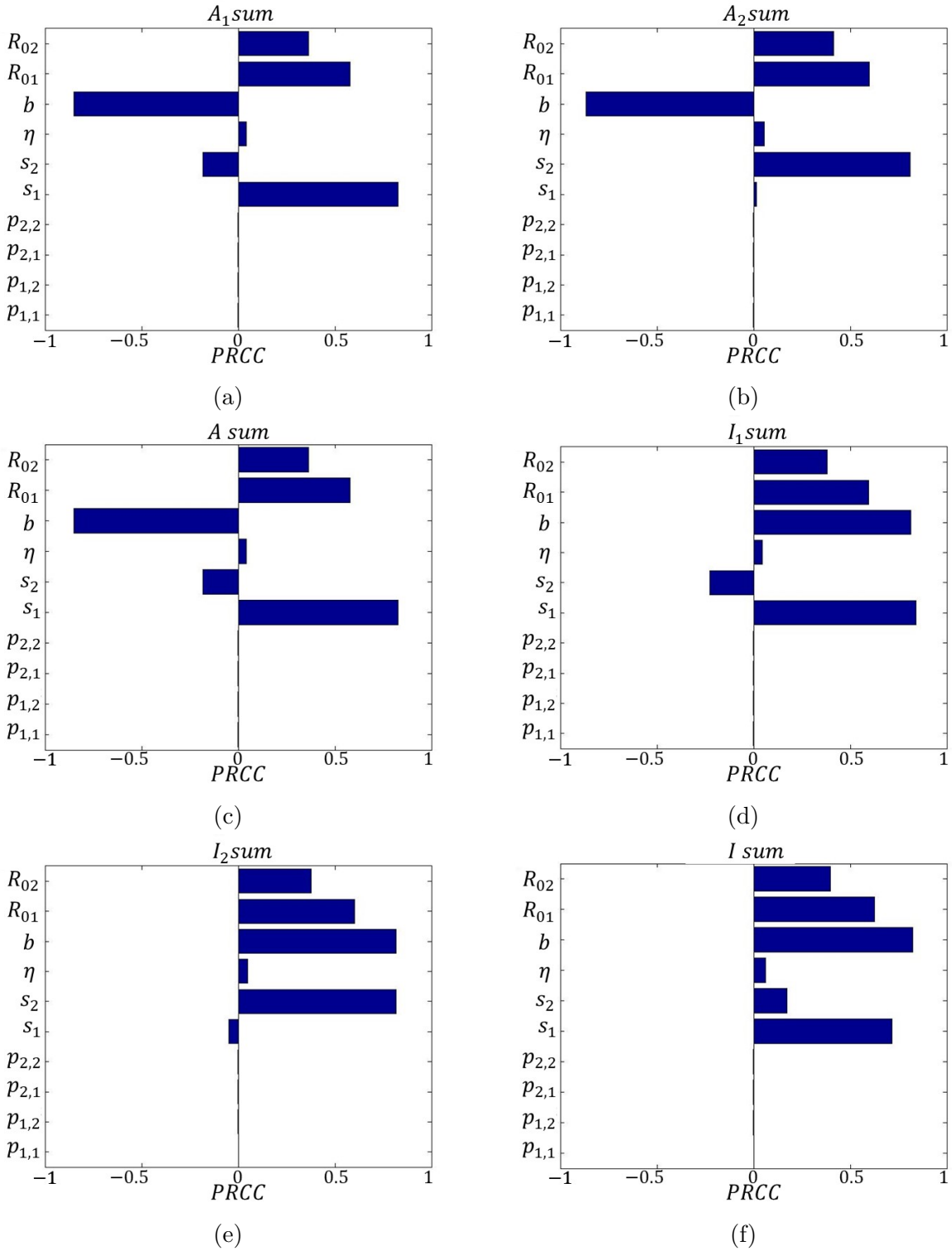

Figure 3.16: Toronto-York (all moving): PRCC plots on the sum of all the asymptomatic and symptomatic cases over the outbreak when all residents are moving

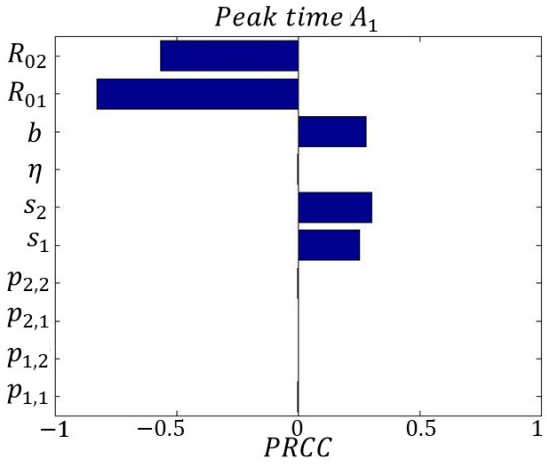

(a)

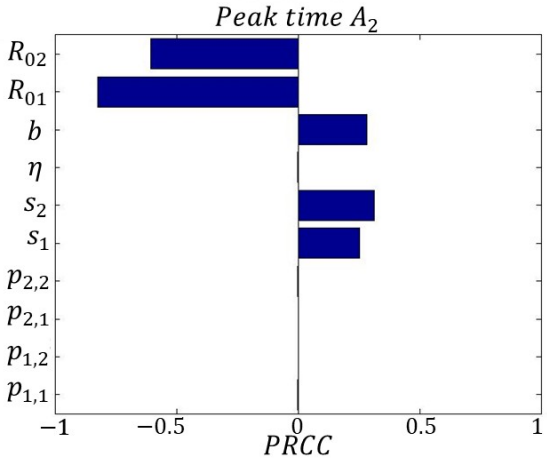

(b)

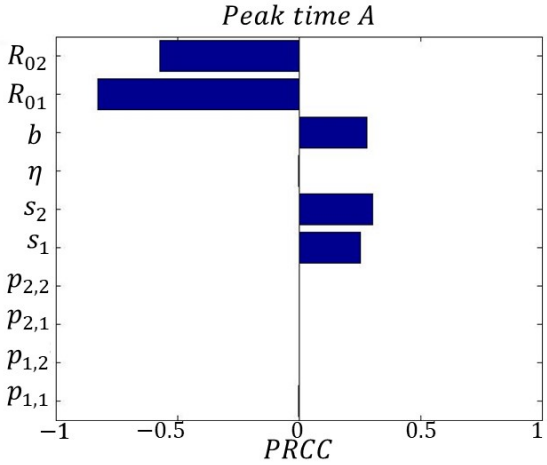

(c)

Figure 3.17: Toronto-York (all moving): PRCC plots on the time at which the asymptomatic cases reach the peak when the infection is seeded in patch 1 and when all residents are moving

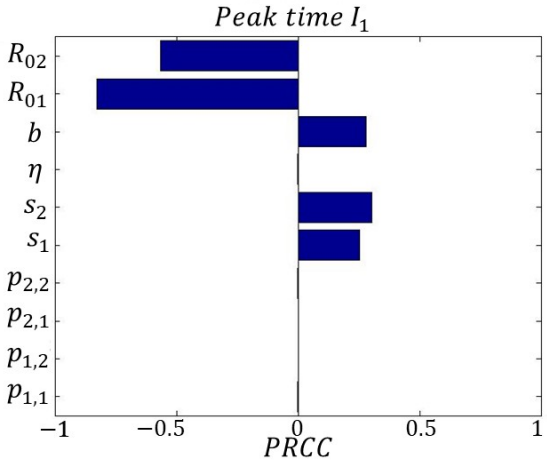

(a)

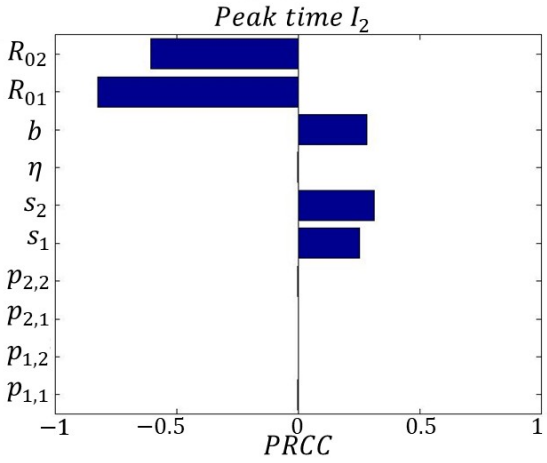

(b)

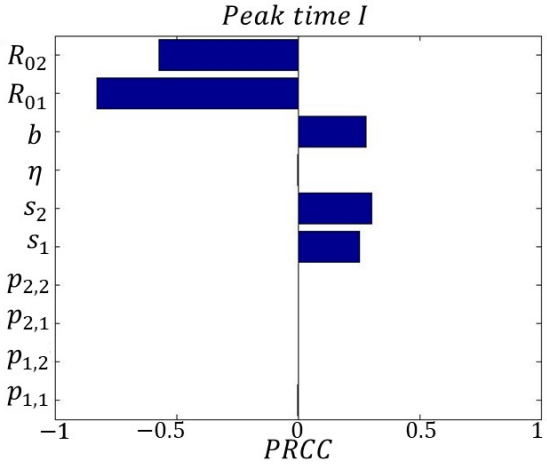

(c)

Figure 3.18: Toronto-York (all moving): PRCC plots on the time at which the symptomatic cases reach the peak when the infection is seeded in patch 1 and when all residents are moving

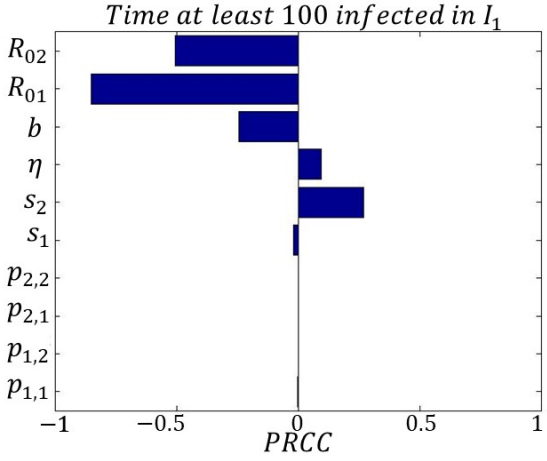

(a)

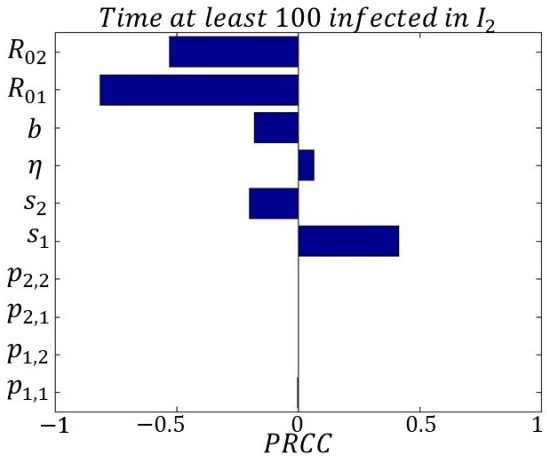

(b)

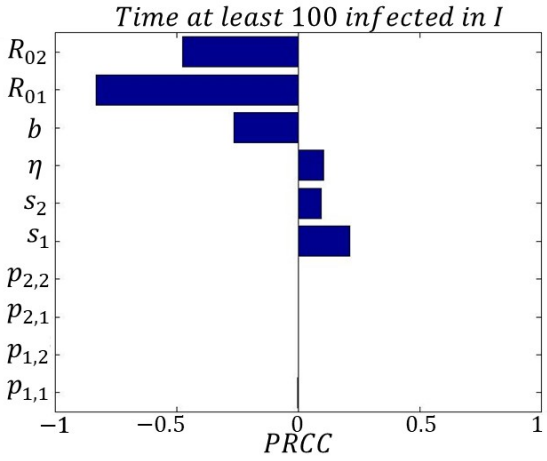

(c)

Figure 3.19: Toronto-York (all moving): PRCC plots on the time at which the first 100 symptomatic cases occur when the infection is seeded in patch 1 and when all residents are moving

describing the infection transmission, $\mathcal{F}$, evaluated at the disease free equilibrium, is defined as:

$$\mathcal{F}_3 = \begin{bmatrix} 0 & 0 & 0 & 0 & S_{1_0}\sum_{j=1}^{3}\frac{\beta_j s_{1j} a_{1j}\eta_1}{\sum_{k=1}^{3}\left(S_k s_{kj}+V_k v_{kj}\right)} & S_{1_0}\sum_{j=1}^{3}\frac{\beta_j s_{1j} a_{2j}\eta_2}{\sum_{k=1}^{3}\left(S_k s_{kj}+V_k v_{kj}\right)} & S_{1_0}\sum_{j=1}^{3}\frac{\beta_j s_{1j}\tilde{p}_{1j}}{\sum_{k=1}^{3}\left(S_k s_{kj}+V_k v_{kj}\right)} & S_{1_0}\sum_{j=1}^{3}\frac{\beta_j s_{1j}\tilde{p}_{2j}}{\sum_{k=1}^{3}\left(S_k s_{kj}+V_k v_{kj}\right)} \\ 0 & 0 & 0 & 0 & S_{2_0}\sum_{j=1}^{3}\frac{\beta_j s_{2j} a_{1j}\eta_1}{\sum_{k=1}^{3}\left(S_k s_{kj}+V_k v_{kj}\right)} & S_{2_0}\sum_{j=1}^{3}\frac{\beta_j s_{2j} a_{2j}\eta_2}{\sum_{k=1}^{3}\left(S_k s_{kj}+V_k v_{kj}\right)} & S_{2_0}\sum_{j=1}^{3}\frac{\beta_j s_{2j}\tilde{p}_{1j}}{\sum_{k=1}^{3}\left(S_k s_{kj}+V_k v_{kj}\right)} & S_{2_0}\sum_{j=1}^{3}\frac{\beta_j s_{2j}\tilde{p}_{2j}}{\sum_{k=1}^{3}\left(S_k s_{kj}+V_k v_{kj}\right)} \\ 0 & 0 & 0 & 0 & S_{3_0}\sum_{j=1}^{3}\frac{\beta_j s_{3j} a_{1j}\eta_1}{\sum_{k=1}^{3}\left(S_k s_{kj}+V_k v_{kj}\right)} & S_{3_0}\sum_{j=1}^{3}\frac{\beta_j s_{2j} a_{3j}\eta_2}{\sum_{k=1}^{3}\left(S_k s_{kj}+V_k v_{kj}\right)} & S_{3_0}\sum_{j=1}^{3}\frac{\beta_j s_{3j}\tilde{p}_{1j}}{\sum_{k=1}^{3}\left(S_k s_{kj}+V_k v_{kj}\right)} & S_{3_0}\sum_{j=1}^{3}\frac{\beta_j s_{3j}\tilde{p}_{2j}}{\sum_{k=1}^{3}\left(S_k s_{kj}+V_k v_{kj}\right)} \\ 0 & 0 & 0 & 0 & 0 & 0 & 0 & 0 \\ 0 & 0 & 0 & 0 & 0 & 0 & 0 & 0 \\ 0 & 0 & 0 & 0 & 0 & 0 & 0 & 0 \\ 0 & 0 & 0 & 0 & 0 & 0 & 0 & 0 \\ 0 & 0 & 0 & 0 & 0 & 0 & 0 & 0 \\ 0 & 0 & 0 & 0 & 0 & 0 & 0 & 0 \end{bmatrix} \tag{3.23}$$

The matrix $-\mathcal{V}_3$ is defined as:

$$-\mathcal{V}_3 = \begin{bmatrix} \alpha & 0 & 0 & 0 & 0 & 0 & 0 & 0 & 0 \\ 0 & \alpha & 0 & 0 & 0 & 0 & 0 & 0 & 0 \\ 0 & 0 & \alpha & 0 & 0 & 0 & 0 & 0 & 0 \\ -\alpha(1-b) & 0 & \gamma_1 & 0 & 0 & 0 & 0 & 0 & 0 \\ 0 & -\alpha(1-b) & 0 & \gamma_1 & 0 & 0 & 0 & 0 & 0 \\ -\alpha b & 0 & 0 & 0 & \gamma & 0 & 0 & 0 & 0 \\ 0 & -\alpha b & 0 & 0 & 0 & \gamma & 0 & 0 & 0 \\ 0 & -\alpha b & 0 & 0 & 0 & \gamma & 0 & 0 & 0 \\ 0 & -\alpha b & 0 & 0 & 0 & 0 & 0 & 0 & \gamma \end{bmatrix} \tag{3.24}$$

Similar to the two-patch case, it is not easy to analyze the total control reproduction number by the product $\mathcal{F}_3(-\mathcal{V}_3^{-1})$. Hence, we employ the same technique used for the simpler case introduced by Diekmann [89]. We need to define a new auxiliary matrix E_{aux_3} defined as:

$$E_{aux}^T = \begin{bmatrix} 1 & 0 & 0 & 0 & 0 & 0 & 0 & 0 & 0 \\ 0 & 1 & 0 & 0 & 0 & 0 & 0 & 0 & 0 \\ 0 & 0 & 1 & 0 & 0 & 0 & 0 & 0 & 0 \end{bmatrix}^T \tag{3.25}$$

After multiplying $E_{aux_3}^T \mathcal{F}_3(-\mathcal{V}_3^{-1})E_{aux_3}$, we obtain a matrix with 3×3 dimension defined as:

$$\mathcal{M}_3 = \begin{bmatrix} S_{1_0}\sum_{j=1}^{3}\frac{\beta_j s_{1j} a_{1j}\eta_1}{\sum_{k=1}^{3}\left(S_k s_{kj}+V_k v_{kj}\right)}\frac{1-b}{\gamma_1} & S_{1_0}\sum_{j=1}^{3}\frac{\beta_j s_{1j} a_{2j}\eta_2}{\sum_{k=1}^{3}\left(S_k s_{kj}+V_k v_{kj}\right)}\frac{1-b}{\gamma_1} & S_{1_0}\sum_{j=1}^{3}\frac{\beta_j s_{1j} a_{3j}\eta_2}{\sum_{k=1}^{3}\left(S_k s_{kj}+V_k v_{kj}\right)}\frac{1-b}{\gamma_1} \\ +S_{1_0}\sum_{j=1}^{3}\frac{\beta_j s_{1j}\tilde{p}_{1j}}{\sum_{k=1}^{3}\left(S_k s_{kj}+V_k v_{kj}\right)}\frac{b}{\gamma} & +S_{1_0}\sum_{j=1}^{3}\frac{\beta_j s_{1j}\tilde{p}_{2j}}{\sum_{k=1}^{3}\left(S_k s_{kj}+V_k v_{kj}\right)}\frac{b}{\gamma} & +S_{1_0}\sum_{j=1}^{3}\frac{\beta_j s_{1j}\tilde{p}_{3j}}{\sum_{k=1}^{3}\left(S_k s_{kj}+V_k v_{kj}\right)}\frac{b}{\gamma} \\ S_{2_0}\sum_{j=1}^{3}\frac{\beta_j s_{2j} a_{1j}\eta_1}{\sum_{k=1}^{3}\left(S_k s_{kj}+V_k v_{kj}\right)}\frac{1-b}{\gamma_1} & S_{2_0}\sum_{j=1}^{3}\frac{\beta_j s_{2j} a_{2j}\eta_2}{\sum_{k=1}^{3}\left(S_k s_{kj}+V_k v_{kj}\right)}\frac{1-b}{\gamma_1} & S_{2_0}\sum_{j=1}^{3}\frac{\beta_j s_{2j} a_{3j}\eta_2}{\sum_{k=1}^{3}\left(S_k s_{kj}+V_k v_{kj}\right)}\frac{1-b}{\gamma_1} \\ +S_{2_0}\sum_{j=1}^{3}\frac{\beta_j s_{2j}\tilde{p}_{1j}}{\sum_{k=1}^{3}\left(S_k s_{kj}+V_k v_{kj}\right)}\frac{b}{\gamma} & +S_{2_0}\sum_{j=1}^{3}\frac{\beta_j s_{2j}\tilde{p}_{2j}}{\sum_{k=1}^{3}\left(S_k s_{kj}+V_k v_{kj}\right)}\frac{b}{\gamma} & +S_{2_0}\sum_{j=1}^{3}\frac{\beta_j s_{2j}\tilde{p}_{3j}}{\sum_{k=1}^{3}\left(S_k s_{kj}+V_k v_{kj}\right)}\frac{b}{\gamma} \\ S_{3_0}\sum_{j=1}^{3}\frac{\beta_j s_{2j} a_{1j}\eta_1}{\sum_{k=1}^{3}\left(S_k s_{kj}+V_k v_{kj}\right)}\frac{1-b}{\gamma_1} & S_{3_0}\sum_{j=1}^{3}\frac{\beta_j s_{2j} a_{2j}\eta_2}{\sum_{k=1}^{3}\left(S_k s_{kj}+V_k v_{kj}\right)}\frac{1-b}{\gamma_1} & S_{3_0}\sum_{j=1}^{3}\frac{\beta_j s_{2j} a_{3j}\eta_2}{\sum_{k=1}^{3}\left(S_k s_{kj}+V_k v_{kj}\right)}\frac{1-b}{\gamma_1} \\ +S_{2_0}\sum_{j=1}^{3}\frac{\beta_j s_{2j}\tilde{p}_{1j}}{\sum_{k=1}^{3}\left(S_k s_{kj}+V_k v_{kj}\right)}\frac{b}{\gamma} & +S_{2_0}\sum_{j=1}^{3}\frac{\beta_j s_{2j}\tilde{p}_{2j}}{\sum_{k=1}^{3}\left(S_k s_{kj}+V_k v_{kj}\right)}\frac{b}{\gamma} & +S_{3_0}\sum_{j=1}^{3}\frac{\beta_j s_{2j}\tilde{p}_{3j}}{\sum_{k=1}^{3}\left(S_k s_{kj}+V_k v_{kj}\right)}\frac{b}{\gamma} \end{bmatrix} \tag{3.26}$$

Although the new matrix is smaller than the original one, it is still hard to compute the spectral radius and derive an analytic expression for R_c. Hence, for this case, the total control reproduction number is evaluated only numerically.

Numerical Results

When three patches are all commuting (Toronto-York-Peel), $\mathcal{R}_c$ is investigated for fixed values of p_{11}, when $p_{11} = 0, 0.3, 0.5, 0.8$. Recall that the extreme case $p_{11} = 1$ corresponds to the scenario in which Toronto residents are not moving. Moreover, we assume that p_{12} is never 0, while p_{13} can be either 0 or another constant.

$\boldsymbol{V_{1_0} = 10\%, V_{2_0} = 10\%, V_{3_0} = 10\%}$

Similar to the case involving only two patches, we start our investigation by analyzing the case in which all the patches are highly susceptible. Figure 3.20 describes the results when the census regions Toronto-Halton-Durham (where Toronto residents are not moving) are considered. Figures 3.21-3.22-3.23-3.24 show the results for the patches Toronto-York-Peel.

When Toronto residents are not moving (Figure 3.20), we observe that the total reproduction number is slightly changing varying from approximately 16 to roughly 16.2. The reduction becomes almost insignificant for high values of b. However, we note that when Durham region (patch 3) residents are staying in their own patch ($p_{33} = 1$), independently of the time that Halton region residents spend in Toronto, the total reproduction number assumes the value of the highest specific $\mathcal{R}_{c_3}$. This suggests that when two patches are isolated, and one of the two is the region with highest risk of transmission, then this patch will lead the sustainability of the infection. Hence, the reduction in the reproduction number occurs if patch 3 residents commute to other patches.

Figure 3.21 to Figure 3.24 show the total reproduction number for $p_{11} \neq 1$, with movements between Toronto, York, and Peel regions. The top panel shows the scenario in which $p_{12}, p_{13} \neq 0$, while the bottom plots represent the case $p_{12} = 1 - p_{11}$ and $p_{13} = 0$. We immediately observe that when Toronto residents are not commuting to Peel region (i.e. $p_{13} = 0$), the trend of the total reproduction number reflects the one shown in Figure 3.20. These results indicate that in order to reduce the total transmission, Toronto residents should not commute to the patch with highest transmissibility and patch 3 residents should spend more time in the patches with lower reproduction number.

A different result is visible when Toronto residents move to Peel region (top panels) as well as to York. Under this scenario, the change in the trend of the reproduction number is more significant (roughly 15 to 16.3). However, as the probability of showing symptoms increases, this gap in the reduction becomes almost imperceptible. Moreover, in this scenario, contrary to the previous ones, we observe that the maximum magnitude of the reproduction number is provided when Durham residents spend most of their time in the other patches.

From the results of this section, we conclude that if two of the three patches are not commuting, independently of the time that the third patch residents spend in the two, the total transmission is governed by the highest patch specific reproduction number. This may

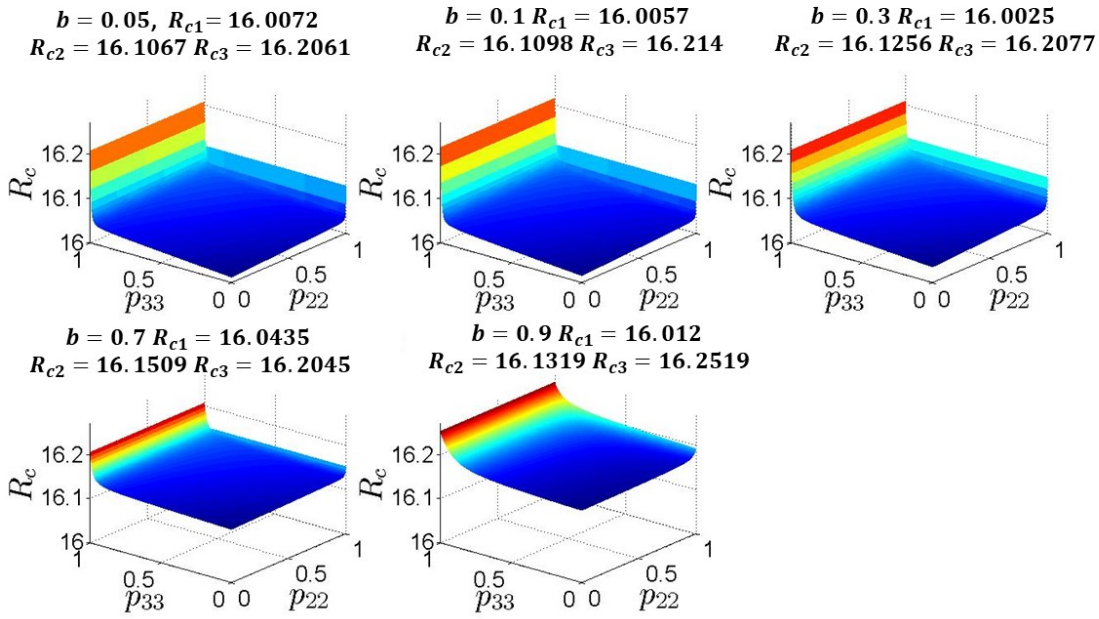

Figure 3.20: Toronto-Halton-Durham (Halton-Durham moving): relationship between the total reproduction number and residency times p_{22} and p_{33} when only patch 2 and 3 residents are moving $V_{1_0} = 10\%$, $V_{2_0} = 10\%$,$V_{3_0} = 10\%$, $R_{c_{1,2,3}} \approx 16$ and (a) $b = 0.05$ (b) $b = 0.1$ (c) $b = 0.3$ (d) $b = 0.7$ (e) $b = 0.9$

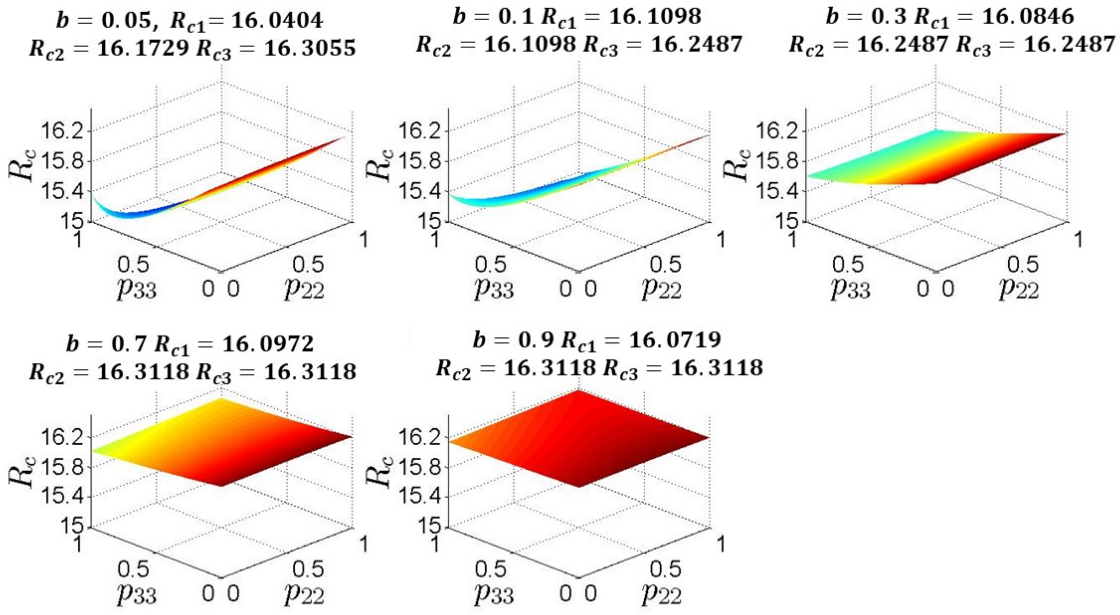

(a)

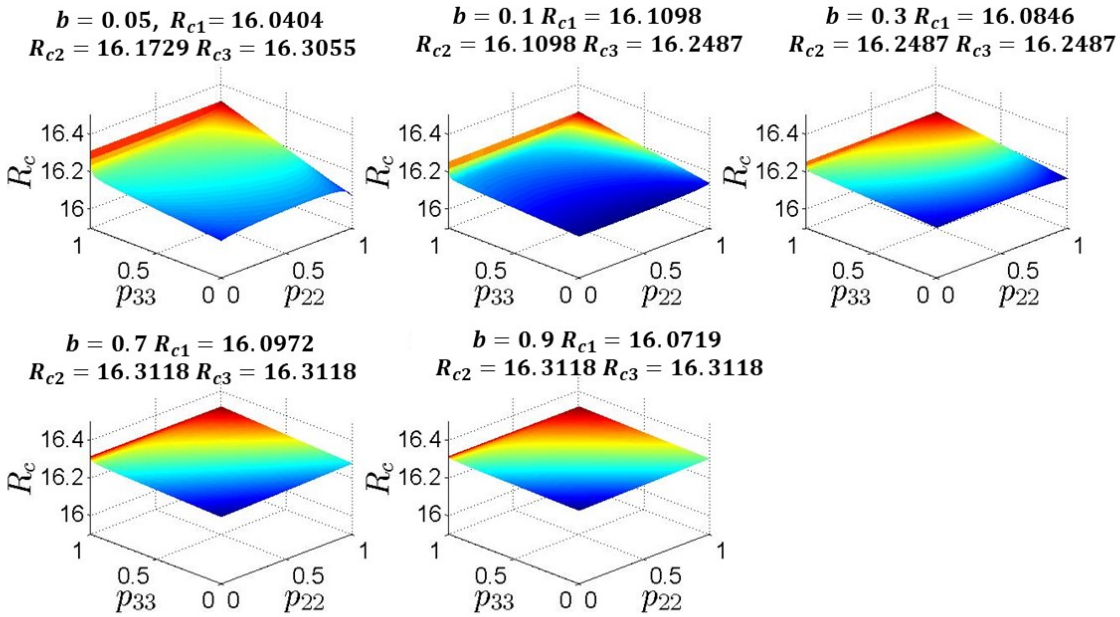

(b)

Figure 3.21: Toronto-York-Peel (all moving): relationship between the total reproduction number and residency times p_{22} and p_{33}. $V_{1_0} = 10\%$, $V_{2_0} = 10\%$,$V_{3_0} = 10\%$, $R_{c_{1,2,3}} \approx 16$, $b = 0.05$, 0.1, 0.3, 0.7, 0.9 when (a) $p_{11} = 0$, $p_{12} = 0.5$, $p_{13} = 0.5$ (b) $p_{11} = 0$, $p_{12} = 1$, $p_{13} = 0$

lead Public Health to consider, in case of outbreak, a reduction in the transmission and increasing the vaccination coverage in these pockets with more susceptible individuals.

$V_{1_0} = 10\%, V_{2_0} = 90\%, V_{3_0} = 90\%$

Next, we investigate the scenario in which Toronto's population is highly susceptible, while the other 2 patches residents are almost completely immune to the infection.

We start our analysis with the assumption that $p_{11} = 1$ (Figure 3.25). It is clearly visible that the reduction of the total transmission is not affected by the decrease of asymptomatic cases. In fact, the range in which $\mathcal{R}_c$ lies is roughly $11.47 - 16.04$ for all b. We also observe that in case of isolation (i.e. $p_{22} = p_{33} = 1$) the total $\mathcal{R}_c$ assumes the value of $\mathcal{R}_{c_1}$, which is the highest among the three. On the other hand, the highest reduction is visible when both Halton and Durham residents spend most of their time outside their own region (i.e. $p_{22} = p_{33} = 0$). This result is expected since patch 2 and 3 are highly vaccinated, hence their movement prevent the spread of the infection. When we look at the patches Toronto-York-Peel (Figures 3.26, 3.27, 3.28, 3.29), we observe that the total $\mathcal{R}_c$ presents a trend similar to Figure 3.25 for $p_{11} \geq 0.5$, while for $p_{11} \leq 0.3$, the results obtained are different. In particular, when $p_{11} = 0$ and Toronto population spends half time in patch 2 and half time in patch 3 (top panel in Figure 3.26), for $b = 0.05, 0.1$, the total reproduction number reaches its maximum reduction when the other two patches are isolated. Under the same conditions, the maximum magnitude of the reproduction number is obtained when York and Peel region residents do not spend time in their own region. This result can be explained by the fact that a highly susceptible population stays in the low risk patches, increasing the transmission. On the other hand, if $b \geq 0.3$, the total reproduction number is roughly 5, showing a reduction of approximately 70% from the highest $\mathcal{R}_{c_1}$. The bottom panel in Figure 3.26 shows the scenario in which Toronto residents spend all their time in patch 2. In this situation, we observe that for $b \leq 0.1$, the magnitude of $\mathcal{R}_c$ is slightly reduced, varying its values between 14 and 12. The highest values are assumed when York residents spend all their time outside their patch, independently of the time spent in patch 3 by its own residents. For $b \geq 0.3$, the total reproduction number decreases from roughly 9 to 2. The smallest values are visible if York residents do not leave their patch and Peel residents spend time there as well. This is due to the fact that more vaccinated individuals reduce the transmission of the infection.
If two of the three patches are highly vaccinated, our findings show that the movement of susceptible individuals towards the less vulnerable patches decreases the transmission. In case the susceptible patch is not moving, then the reduction is achievable if the highly vaccinated populations spend their time in this patch.

$V_{1_0} = 90\%, V_{2_0} = 10\%, V_{3_0} = 10\%$

We are here showing the results obtained by setting Toronto population to be highly vaccinated, while Halton - Durham or York - Peel to be mostly susceptible.

Contrary to the scenario with $V_{1_0} = 10\%$, $V_{2_0} = 90\%$, $V_{1_0} = 90\%$ shown in Figure 3.25, when Toronto is the patch less vulnerable and its residents are not commuters, the reduction

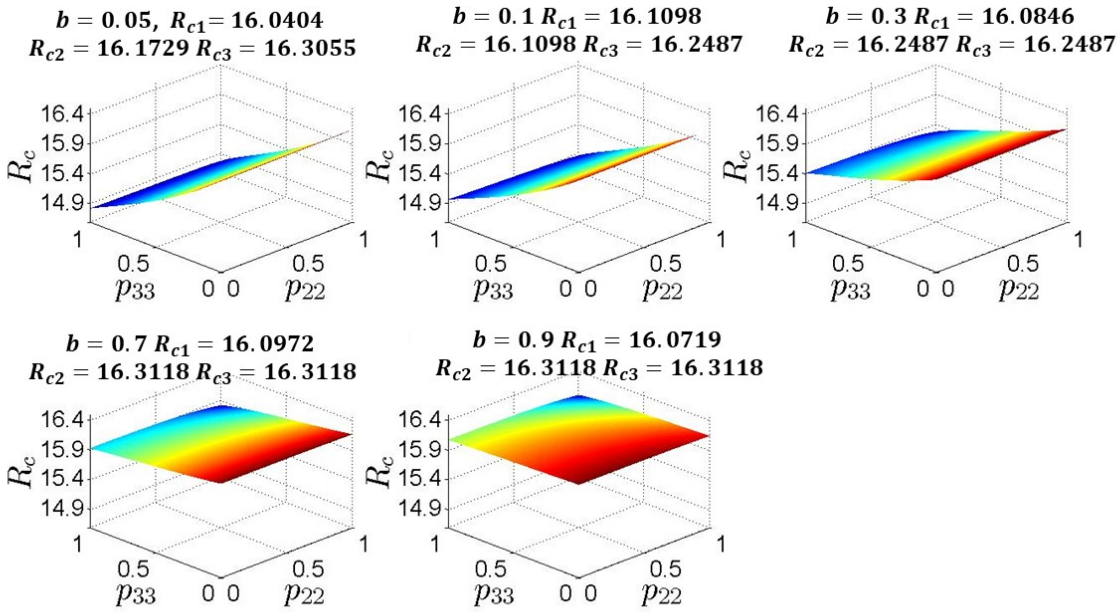

(a)

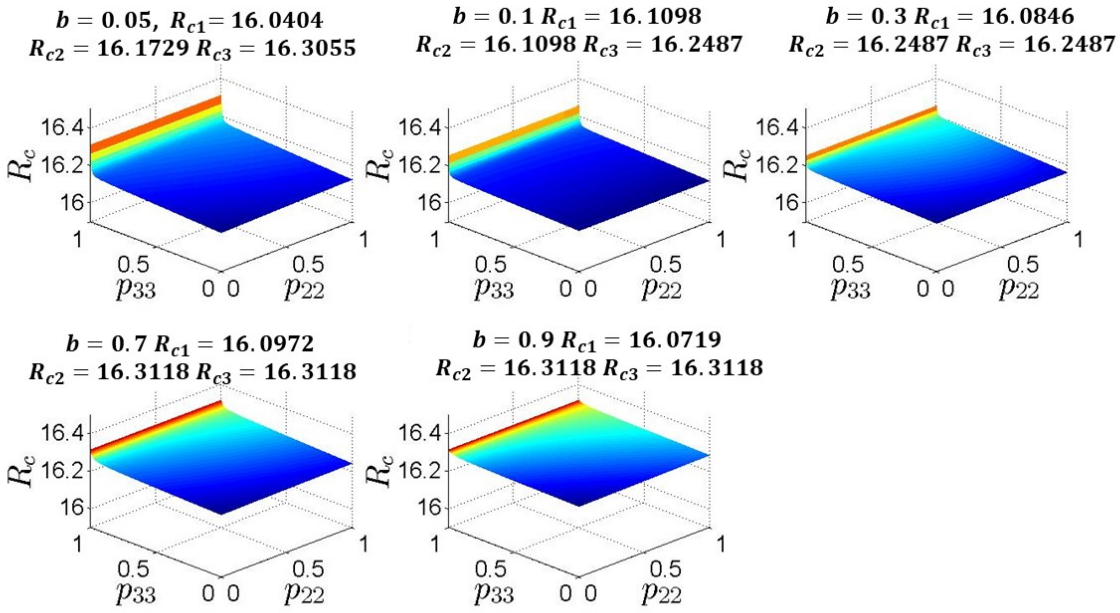

(b)

Figure 3.22: Toronto-York-Peel (all moving): relationship between the total reproduction number and residency times p_{22} and p_{33}. $V_{1_0} = 10\%$, $V_{2_0} = 10\%$,$V_{3_0} = 10\%$, $R_{c_{1,2,3}} \approx 16$, $b = 0.05$, 0.1, 0.3, 0.7, 0.9 when (a) $p_{11} = 0.3$, $p_{12} = 0.4$, $p_{13} = 0.3$ (b) $p_{11} = 0.3$, $p_{12} = 0.7$, $p_{13} = 0$

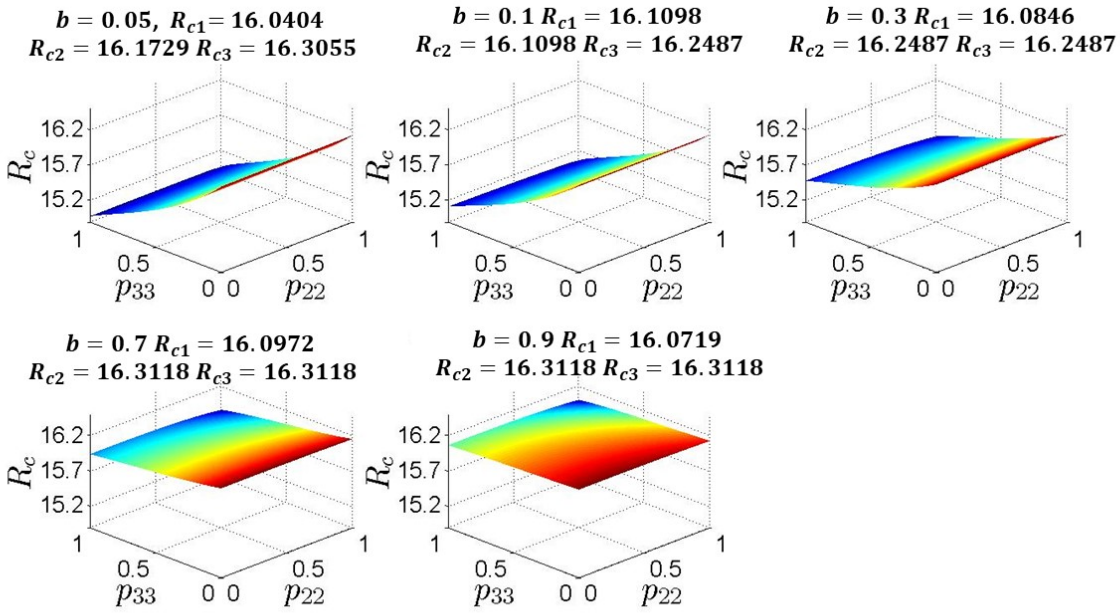

(a)

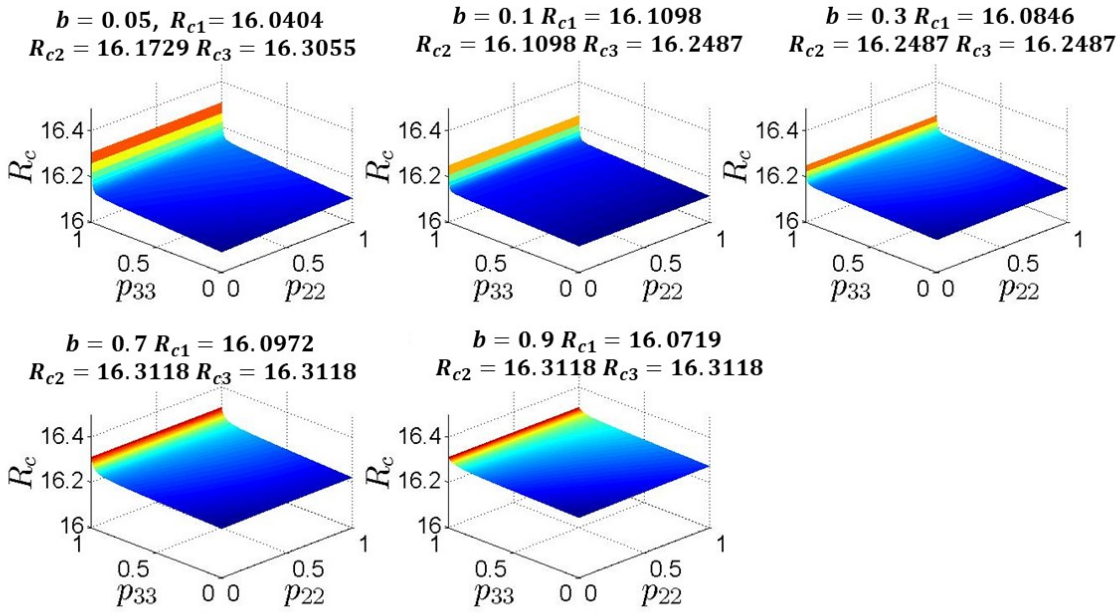

(b)

Figure 3.23: Toronto-York-Peel (all moving): relationship between the total reproduction number and residency times p_{22} and p_{33}. $V_{1_0} = 10\%$, $V_{2_0} = 10\%$,$V_{3_0} = 10\%$, $R_{c_{1,2,3}} \approx 16$, $b = 0.05$, 0.1, 0.3, 0.7, 0.9 when (a) $p_{11} = 0.5$, $p_{12} = 0.3$, $p_{13} = 0.2$ (b) $p_{11} = 0.5$, $p_{12} = 0.5$, $p_{13} = 0$

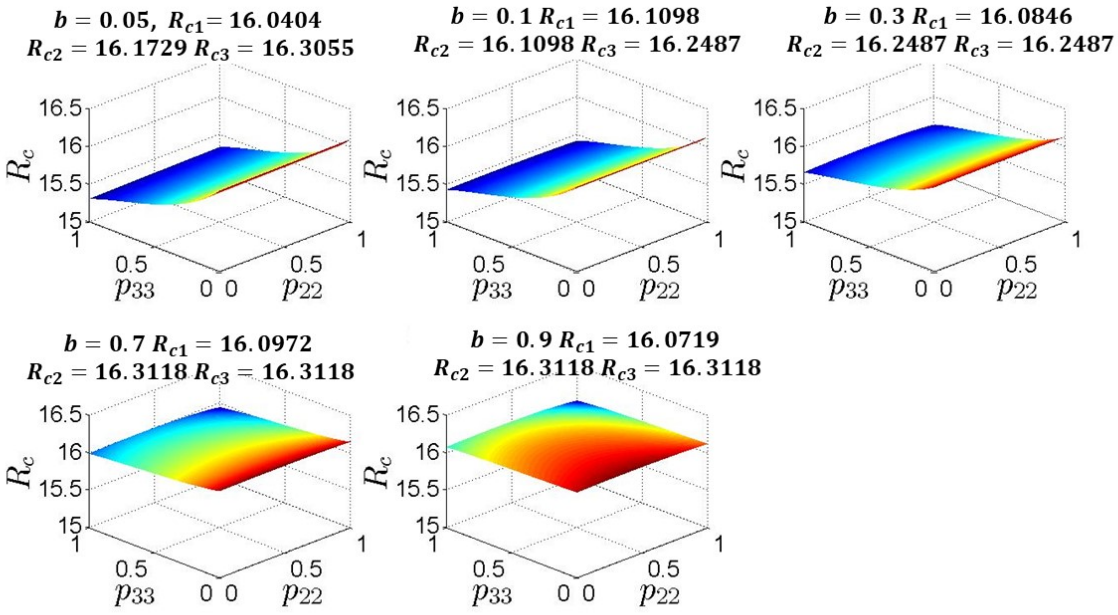

(a)

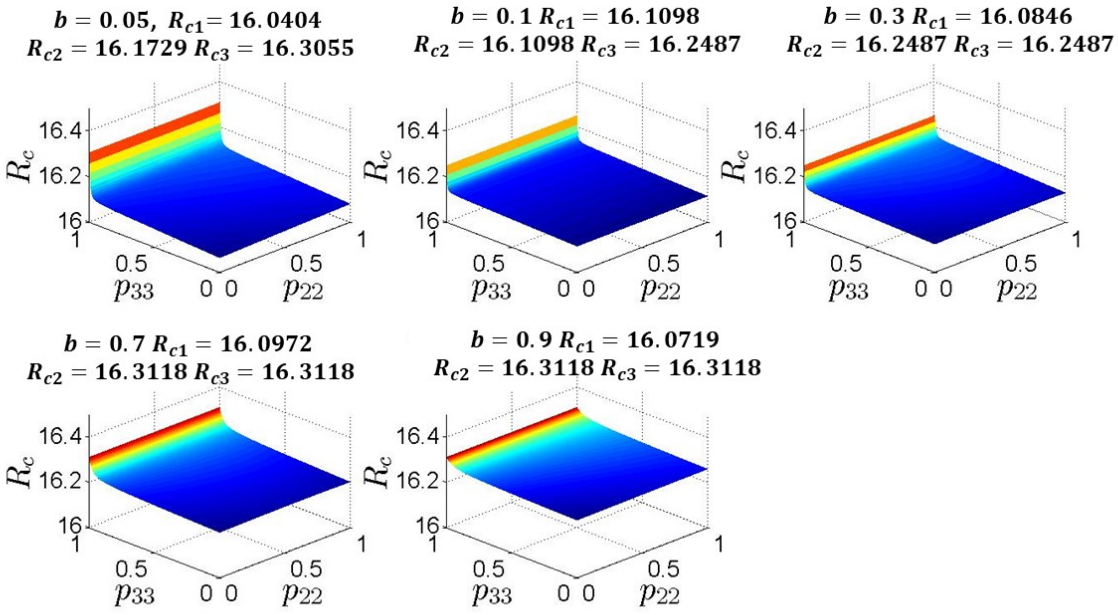

(b)

Figure 3.24: Toronto-York-Peel (all moving): relationship between the total reproduction number and residency times p_{22} and p_{33}. $V_{1_0} = 10\%$, $V_{2_0} = 10\%$,$V_{3_0} = 10\%$, $R_{c_{1,2,3}} \approx 16$, $b = 0.05$, 0.1, 0.3, 0.7, 0.9 when (a) $p_{11} = 0.8$, $p_{12} = 0.1$, $p_{13} = 0.1$ (b) $p_{11} = 0.8$, $p_{12} = 0.2$, $p_{13} = 0$

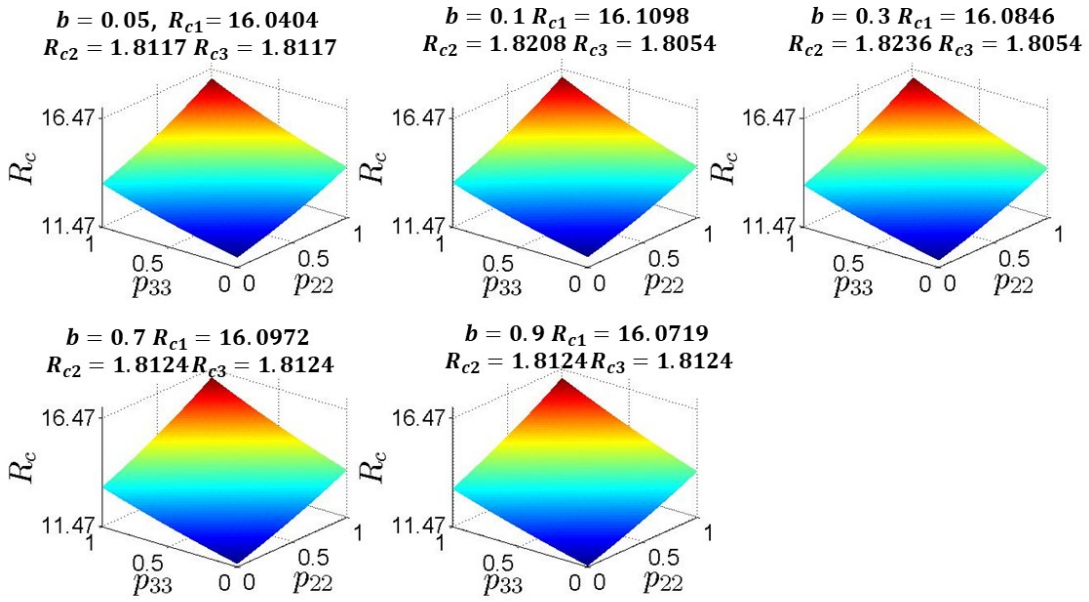

Figure 3.25: Toronto-Halton-Durham (Halton-Durham moving): relationship between the total reproduction number and residency times p_{22} and p_{33} when only patch 2 and 3 residents are moving $V_{1_0} = 10\%$, $V_{2_0} = 90\%$,$V_{3_0} = 90\%$, $R_{c_1} \approx 16$, $R_{c_{2,3}} \approx 1.8$ and (a) $b = 0.05$ (b) $b = 0.1$ (c) $b = 0.3$ (d) $b = 0.7$ (e) $b = 0.9$

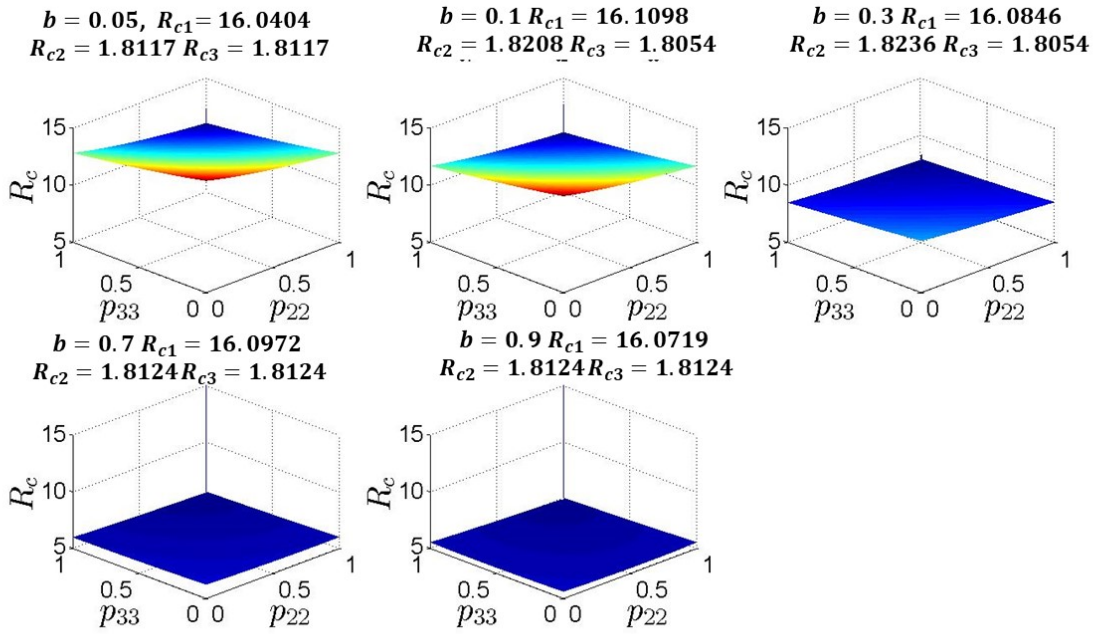

(a)

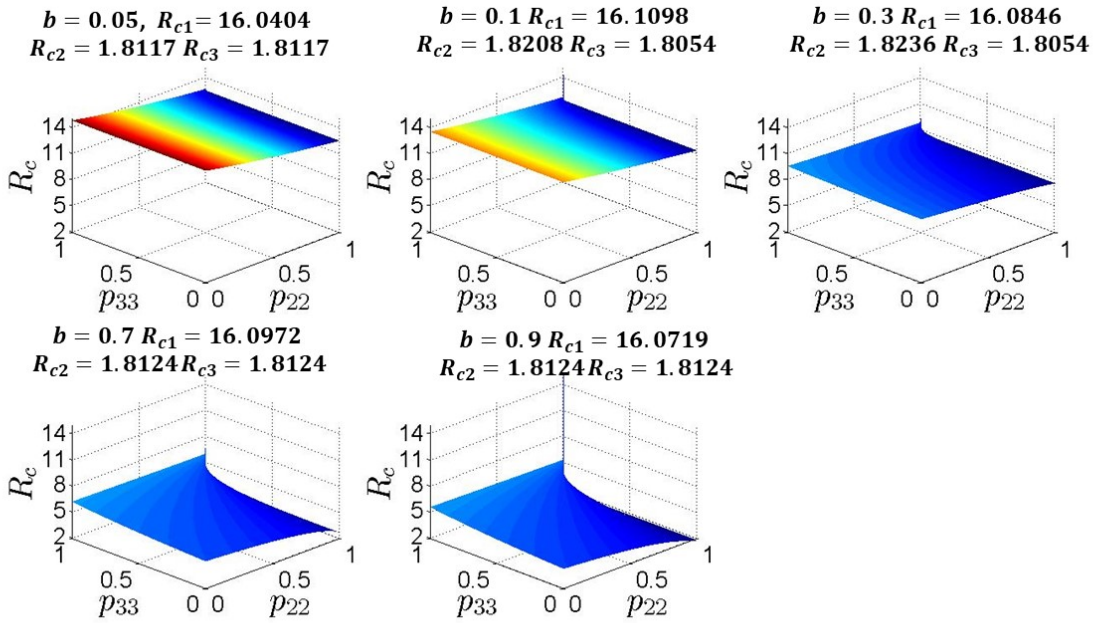

(b)

Figure 3.26: Toronto-York-Peel (all moving): relationship between the total reproduction number and residency times p_{22} and p_{33}. $V_{1_0} = 10\%$, $V_{2_0} = 90\%$,$V_{3_0} = 90\%$, $R_{c_1} \approx 16$, $R_{c_{2,3}} \approx 1.8$, $b = 0.05$, 0.1, 0.3, 0.7, 0.9 when (a) $p_{11} = 0$, $p_{12} = 0.5$, $p_{13} = 0.5$ (b) $p_{11} = 0$, $p_{12} = 1$, $p_{13} = 0$

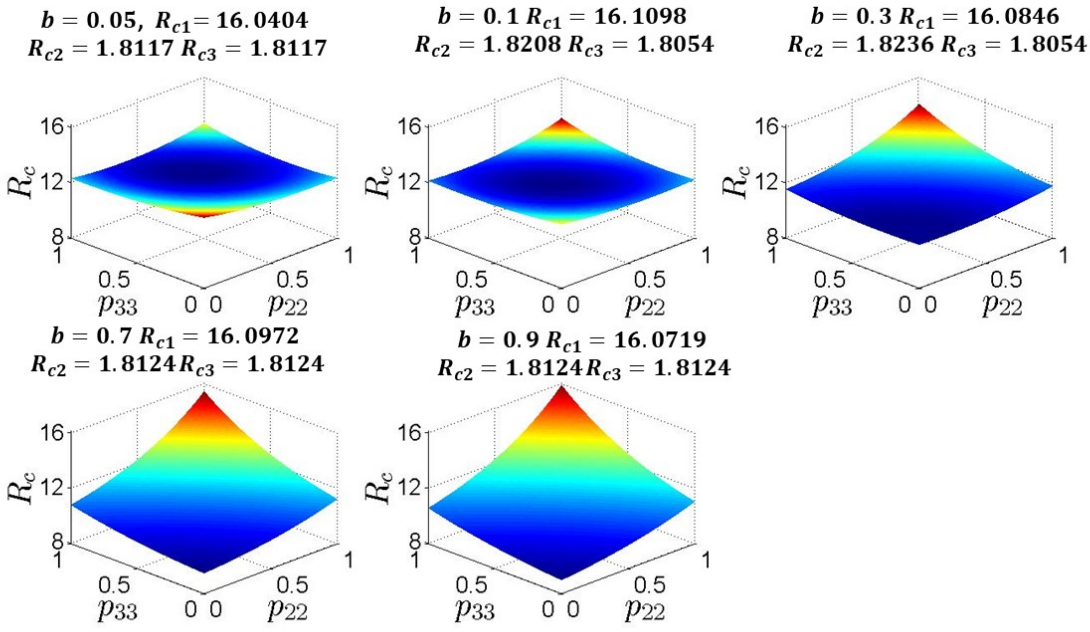

(a)

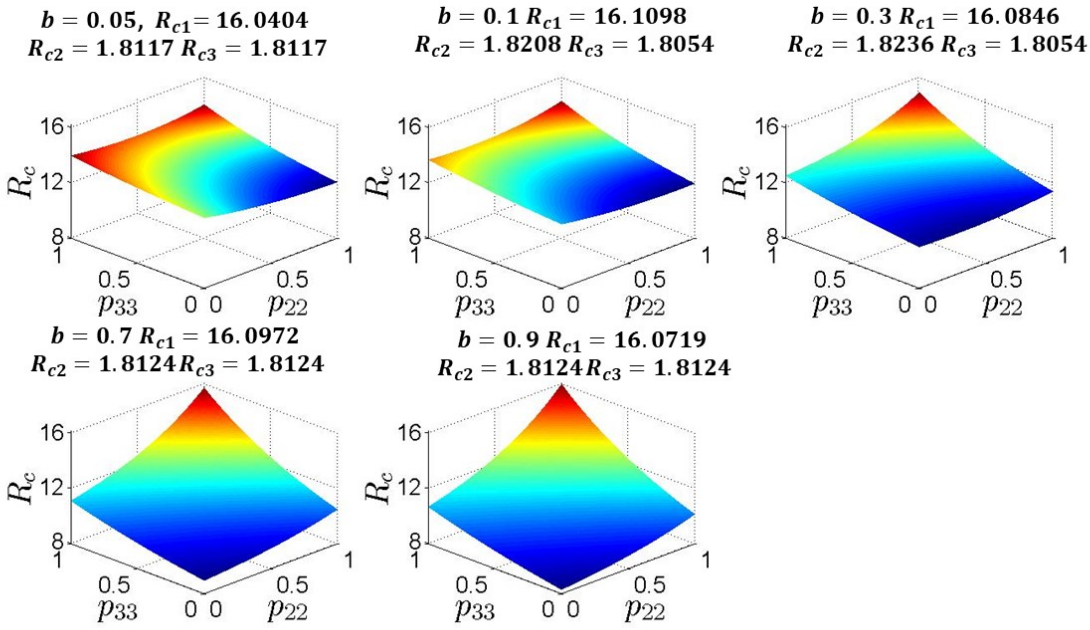

(b)

Figure 3.27: Toronto-York-Peel (all moving): relationship between the total reproduction number and residency times p_{22} and p_{33}. $V_{1_0} = 10\%$, $V_{2_0} = 90\%$,$V_{3_0} = 90\%$, $R_{c_1} \approx 16$, $R_{c_{2,3}} \approx 1.8$, $b = 0.05$, 0.1, 0.3, 0.7, 0.9 when (a) $p_{11} = 0.3$, $p_{12} = 0.4$, $p_{13} = 0.3$ (b) $p_{11} = 0.3$, $p_{12} = 0.7$, $p_{13} = 0$

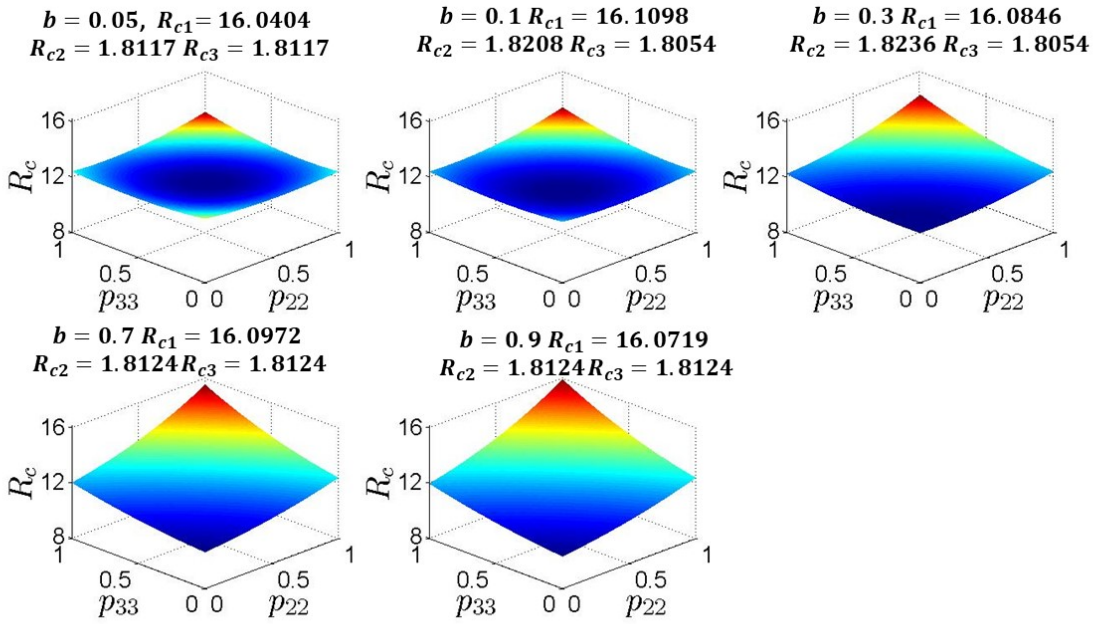

(a)

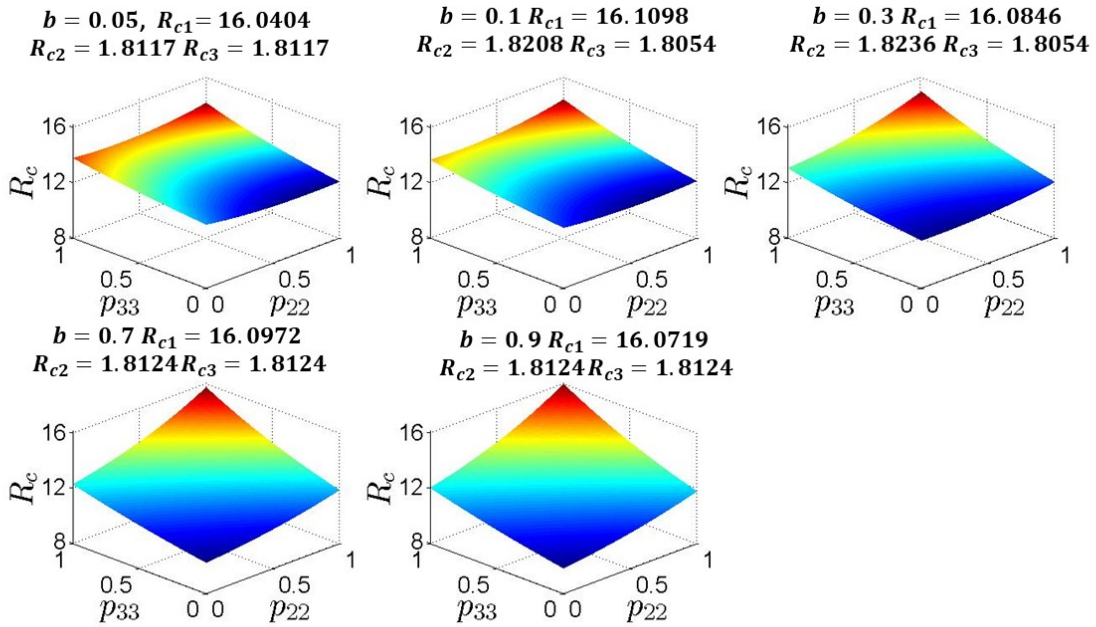

(b)

Figure 3.28: Toronto-York-Peel (all moving): relationship between the total reproduction number and residency times p_{22} and p_{33}. $V_{1_0} = 10\%$, $V_{2_0} = 90\%$,$V_{3_0} = 90\%$, $R_{c_1} \approx 16$, $R_{c_{2,3}} \approx 1.8$, $b = 0.05$, 0.1, 0.3, 0.7, 0.9 when (a) $p_{11} = 0.5$, $p_{12} = 0.3$, $p_{13} = 0.2$ (b) $p_{11} = 0.5$, $p_{12} = 0.5$, $p_{13} = 0$

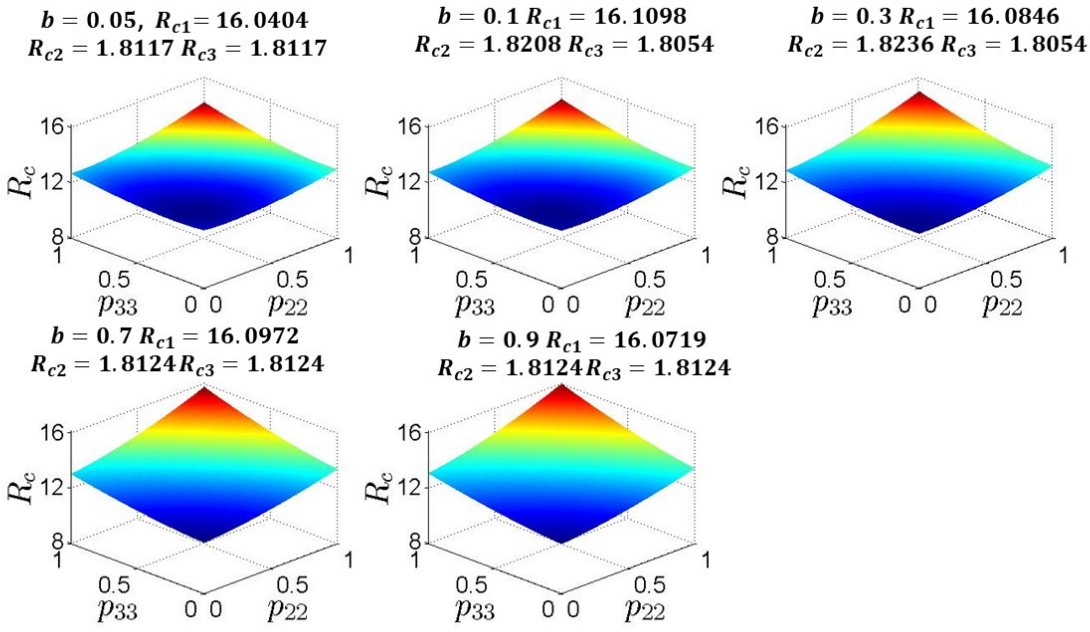

(a)

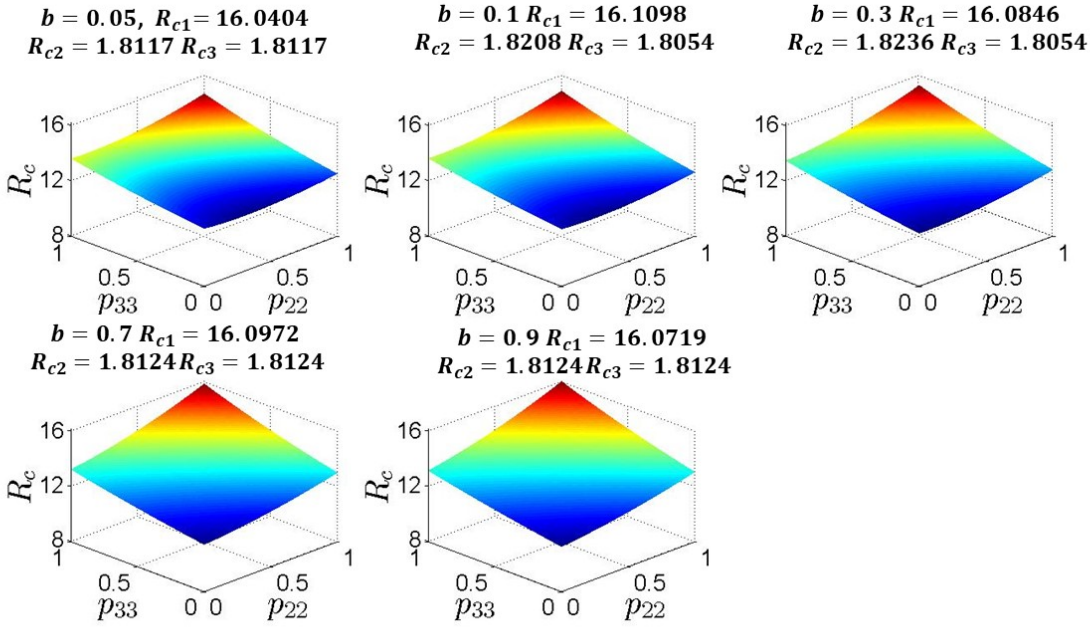

(b)

Figure 3.29: Toronto-York-Peel (all moving): relationship between the total reproduction number and residency times p_{22} and p_{33}. $V_{1_0} = 10\%$, $V_{2_0} = 90\%$,$V_{3_0} = 90\%$, $R_{c_1} \approx 16$, $R_{c_{2,3}} \approx 1.8$, $b = 0.05$, 0.1, 0.3, 0.7, 0.9 when (a) $p_{11} = 0.8$, $p_{12} = 0.1$, $p_{13} = 0.1$ (b) $p_{11} = 0.8$, $p_{12} = 0.2$, $p_{13} = 0$

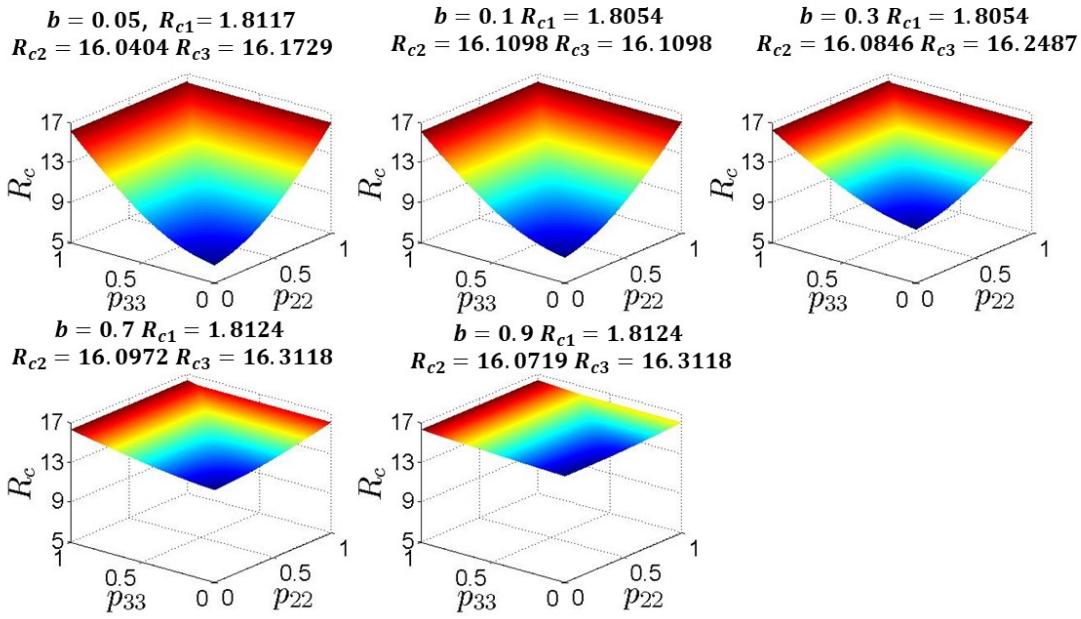

Figure 3.30: Toronto-Halton-Durham (Halton-Durham moving): relationship between the total reproduction number and residency times p_{22} and p_{33} when only patch 2 and 3 residents are moving $V_{1_0} = 90\%$, $V_{2_0} = 10\%$,$V_{3_0} = 10\%$, $R_{c_1} \approx 1.8$, $R_{c_{2,3}} \approx 16$ and (a) $b = 0.05$ (b) $b = 0.1$ (c) $b = 0.3$ (d) $b = 0.7$ (e) $b = 0.9$

in the total reproduction number is more visible. In particular, if the probability of showing symptoms is less than 0.7, the total $\mathcal{R}_c$ has a maximum magnitude of roughly 16, which corresponds to the highest value of the specific $\mathcal{R}_{c_{2,3}}$, but it drops to a minimum of roughly 5. The highest value is assumed when either both patch 2 and 3 are isolated or just one of them. The maximum reduction is possible when both Halton and Durham residents spend most of their time in Toronto. This is reasonable due to the fact that in this scenario Halton and Durham are not considered connecting patches, hence they only move to Toronto which is highly vaccinated, and so at a lower risk of transmission. When the possibility of showing signs of the infection becomes larger (above 70%), then reduction in the total $\mathcal{R}_c$ is minimal. This is to be related to the minimal movement of symptomatic cases. In fact, the lowest value of the reproduction number is obtained when $p_{22} = p_{33} \approx 0$.

When all the patches are geographically close and the commuters are moving among them (Figures 3.31, 3.32, 3.33, 3.34), we observe a different trend depending on the values assumed by b and p_{13}. Figure 3.31 shows the change in the total reproduction number when Toronto residents spend either half of their time in patch 2 or 3 (top panel) or they are only in York (bottom panel). In the first case, the transmission decreases as the probability of showing symptoms increases. For small b, $\mathcal{R}_c \approx 14.5$ either both York and Peel residents spend most of their time outside their patch or either of the two is isolated. This is due to the fact that many asymptomatic case travel and sustain the transmission in the other regions. On the other hand, the maximum reduction is visible when both patches are isolated. This is because the highly vaccinated individuals from Toronto provide a decrease in the transmission. As b increases, the total $\mathcal{R}_c$ reduces further. When Toronto commuters move only towards York region, the trend is very similar to the case in which Toronto residents are not moving and, in magnitude, it is higher than the case with $p_{13} = 0.5$.

When $p_{11} = 0.3$, we assume that $p_{12} = 0.4$ and p_{13} or $p_{12} = 0.7$ and $p_{13} = 0$, top and bottom panel, respectively, in Figure 3.32. In the first scenario, we immediately observe that the reproduction number values lie in the interval $(4.5, 7)$. If compared with the case $p_{11} = 0$, these values are definitely smaller. In fact, Toronto commuters decrease the transmission in patch 2 and 3, but at the same time they keep a lower transmission in their own patch. The transmission increases if York and Peel residents spend most of their time outside their patch, and their susceptibility and asymptomatic cases are significant to spread the infection. As b increases the pattern looks like the one shown in Figure 3.25. For $p11 \geq 0.5$ and $p_{13} \neq 0$, we observe the same trend seen in Figure 3.25 and the total $\mathcal{R}_c$ varies from approximately 3.5 to 8. Hence, under this condition the transmission is highly reduced if compared to the specific $\mathcal{R}_{c_{2,3}}$ Differently, if $p_{12} = 0.5, 0.2$ and $p_{13} = 0$, we observe that the total reproduction number drops from 15.5 to roughly 3.5. We also note that the highest transmission is possible when patch 3 is isolated. This is reasonable since they do not move towards a highly vaccinated patch and immune individuals do not commute there reducing their transmission. On the other hand, the minimum transmission is obtained when patch 3 commuters spend most of their time in the other patches. As the probability of showing symptoms increases, the reduction in the total transmission decreases. This is due to the fact that more symptomatic cases remain in highly vulnerable patches sustaining the high transmission.

Our findings show that if only one of the three patches is highly vaccinated, its commuters can provide a reduction in the total transmission. In case they are not leaving their patch, the total reproduction number is decreased if the commuters from high susceptible regions spend most of their time in Toronto.

$V_{1_0} = 90\%, V_{2_0} = 90\%, V_{3_0} = 90\%$

In this last section, we are showing the results when all the patches are almost completely vaccinated. The shape of the surfaces describing $\mathcal{R}_c$ is very similar to the ones seen for $V_{1,2,3_0} = 10\%$ in 3.2.3. The total reproduction number varies in the interval $(1.8 - 1.85)$, hence the commuters do not affect the transmission drastically (Figures (3.35)-(3.36)-(3.37)-(3.38)-(3.39)).

Infection Dynamic

Here, we present some plots describing the infection dynamics for the patches Toronto-Halton-Durham (Figure (3.40)) and for Toronto-York-Peel (Figure (3.41)). We observe that in both cases the probability of showing symptoms affect mostly the cases is A, if small, and in I, if large. Moreover, the smaller the transmission is, the smaller the peak of the infection is and longer the outbreak is.

Sensitivity Analysis

We end our numerical analysis section by showing sensitivity analysis of the model parameters on the model outputs. The first results are on the patches Toronto-Halton-Durham and then we focus on the regions Toronto-York-Peel. The infection is seeded either in patch 1 or patch 2. Given the similar and intuitive results, the case of patch 2 primarily infected is shown in Appendix F.
Similar to the previous PRCC plots, the output we focus on are the sum of all the infectious cases, the time needed to reach the peak of A and I and the time needed to reach the first 100 symptomatic cases.

Toronto-Halton-Durham

Figure 3.43 and Figure 3.42 show the PRCC on the sum of A and of I, respectively. We observe that the number of asymptomatic cases in each patch are extremely affected by the probability of showing symptoms (negative correlation) and the proportion of susceptibles in each patch (positive correlation). Indeed, a growth of susceptible will increase the infected cases. Moreover, the infectivity of patch 1 is positively affecting the total number of asymptomatic cases in all patches, even if with less effect in patch 2 and 3 (Figures (3.42a), (3.42b) and (3.42c)). When we look at the global cases of A, then the individuals vulnerable to the infection from patch 1 are responsible for the increase of the cases as well as $\mathcal{R}_{01}$ (Figures (3.42d)). This indicates how patch 1, which is the one with the biggest size, is

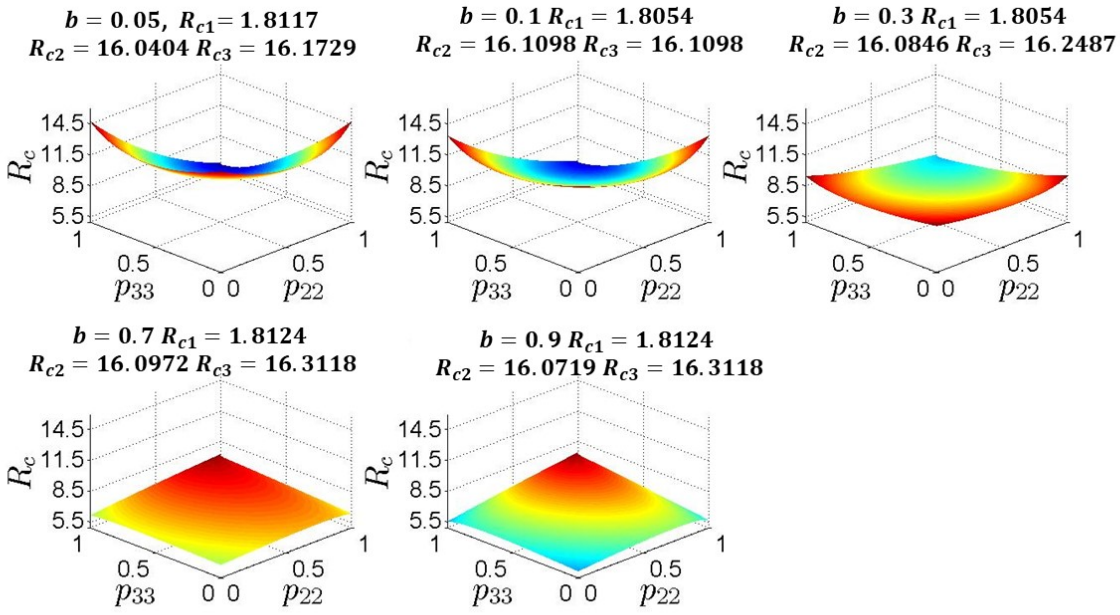

(a)

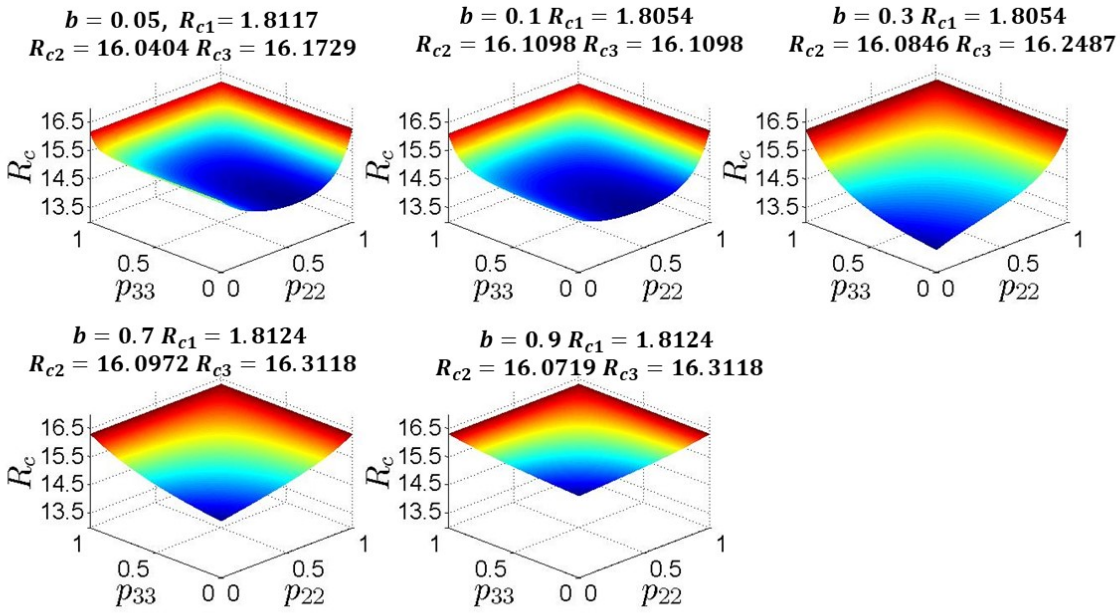

(b)

Figure 3.31: Toronto-York-Peel (all moving): relationship between the total reproduction number and residency times p_{22} and p_{33}. $V_{1_0} = 90\%$, $V_{2_0} = 10\%$,$V_{3_0} = 10\%$, $R_{c_1} \approx 1.8$, $R_{c_{2,3}} \approx 16$, $b = 0.05$, 0.1, 0.3, 0.7, 0.9 when (a) $p_{11} = 0$, $p_{12} = 0.5$, $p_{13} = 0.5$ (b) $p_{11} = 0$, $p_{12} = 1$, $p_{13} = 0$

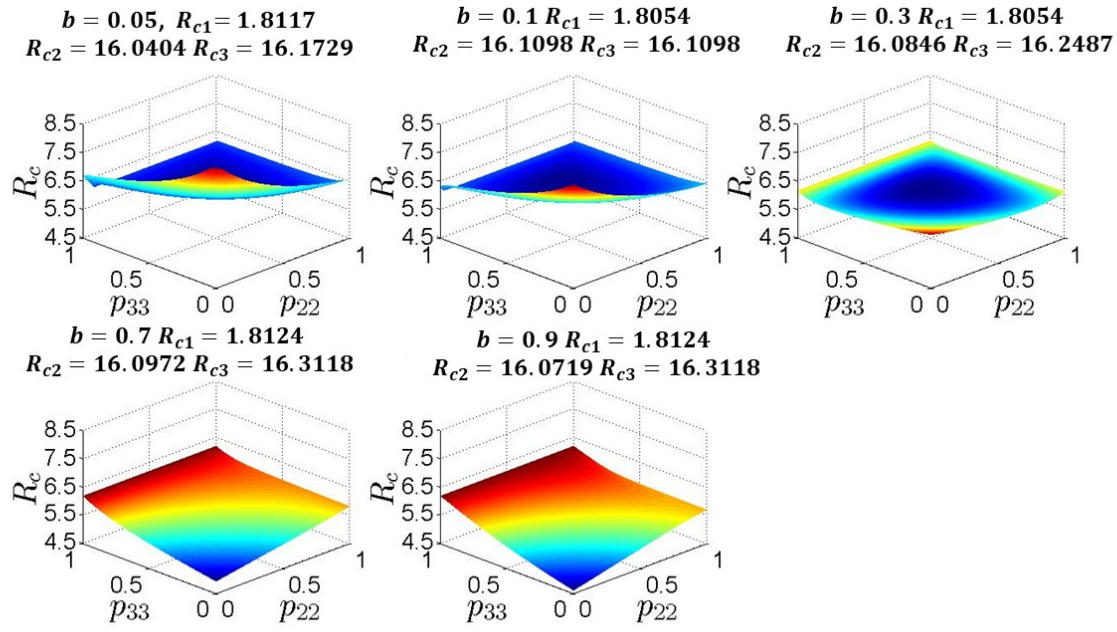

(a)

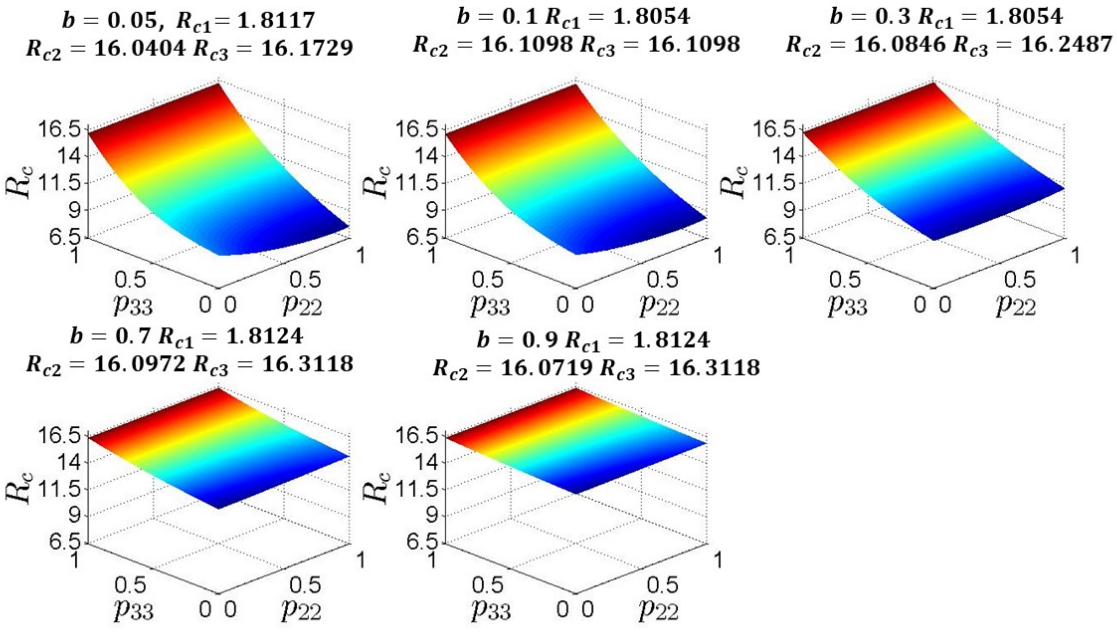

(b)

Figure 3.32: Toronto-York-Peel (all moving): relationship between the total reproduction number and residency times p_{22} and p_{33}. $V_{1_0} = 10\%$, $V_{1_0} = 90\%$, $V_{2_0} = 10\%$,$V_{3_0} = 10\%$, $R_{c_1} \approx 1.8$, $R_{c_{2,3}} \approx 16$, $b = 0.05$, 0.1, 0.3, 0.7, 0.9 when (a) $p_{11} = 0.3$, $p_{12} = 0.4$, $p_{13} = 0.3$ (b) $p_{11} = 0.3$, $p_{12} = 0.7$, $p_{13} = 0$

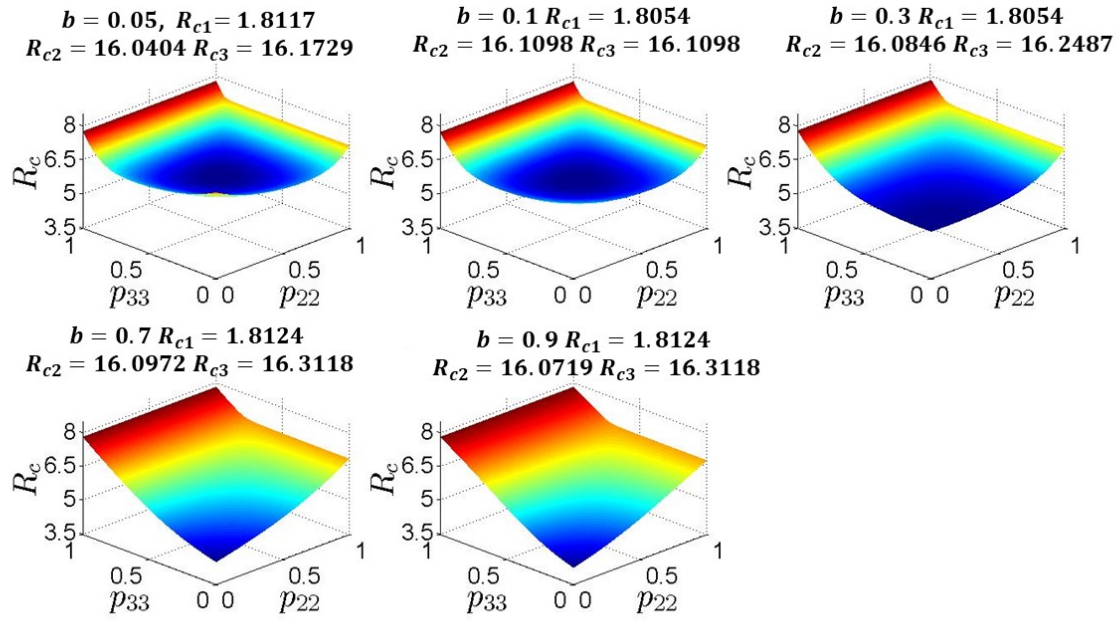

(a)

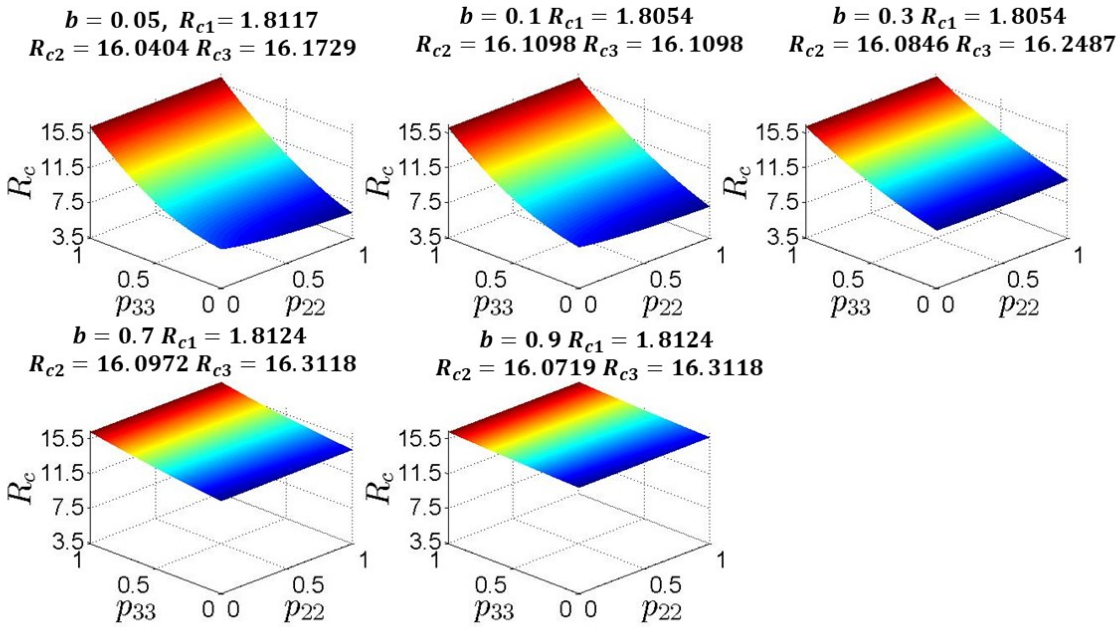

(b)

Figure 3.33: Toronto-York-Peel (all moving): relationship between the total reproduction number and residency times p_{22} and p_{33}. $V_{1_0} = 90\%$, $V_{2_0} = 10\%$,$V_{3_0} = 10\%$, $R_{c_1} \approx 1.8$, $R_{c_{2,3}} \approx 16$, $b = 0.05$, 0.1, 0.3, 0.7, 0.9 when (a) $p_{11} = 0.5$, $p_{12} = 0.3$, $p_{13} = 0.2$ (b) $p_{11} = 0.5$, $p_{12} = 0.5$, $p_{13} = 0$

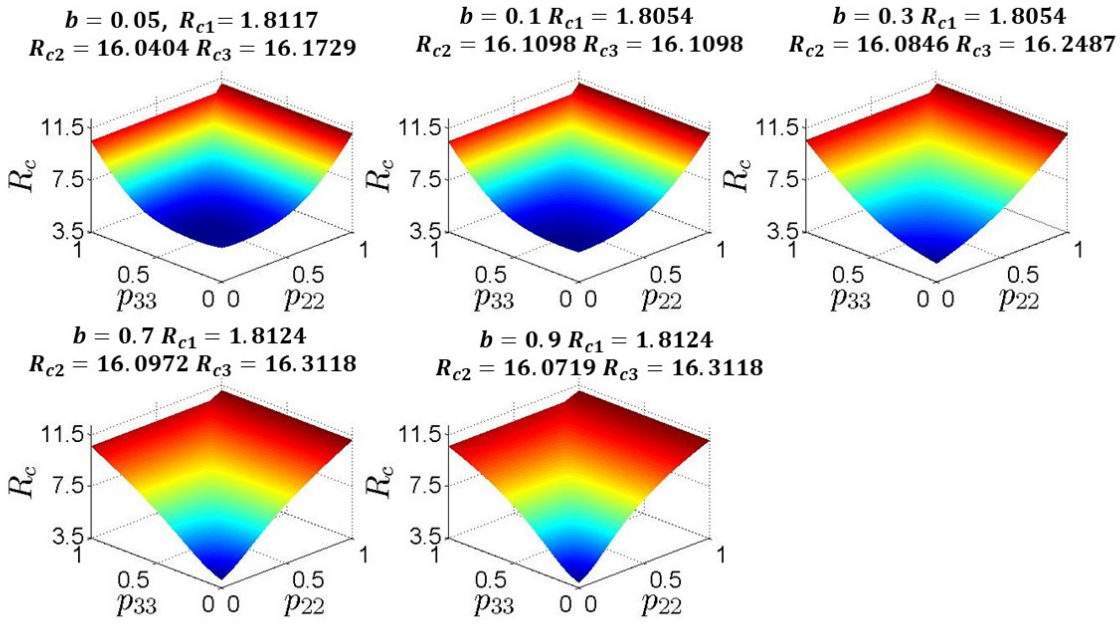

(a)

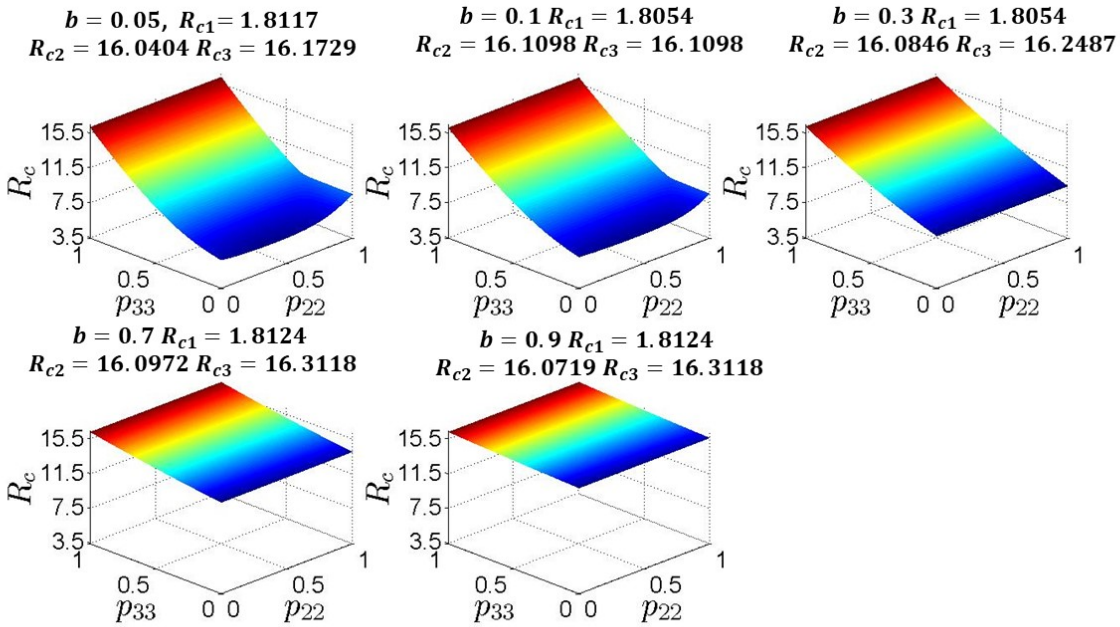

(b)

Figure 3.34: Toronto-York-Peel (all moving): relationship between the total reproduction number and residency times p_{22} and p_{33}. $V_{1_0} = 90\%$, $V_{2_0} = 10\%$,$V_{3_0} = 10\%$, $R_{c_1} \approx 1.8$, $R_{c_{2,3}} \approx 16$, $b = 0.05, 0.1, 0.3, 0.7, 0.9$ when (a) $p_{11} = 0.8$, $p_{12} = 0.1$, $p_{13} = 0.1$ (b) $p_{11} = 0.8$, $p_{12} = 0.2$, $p_{13} = 0$

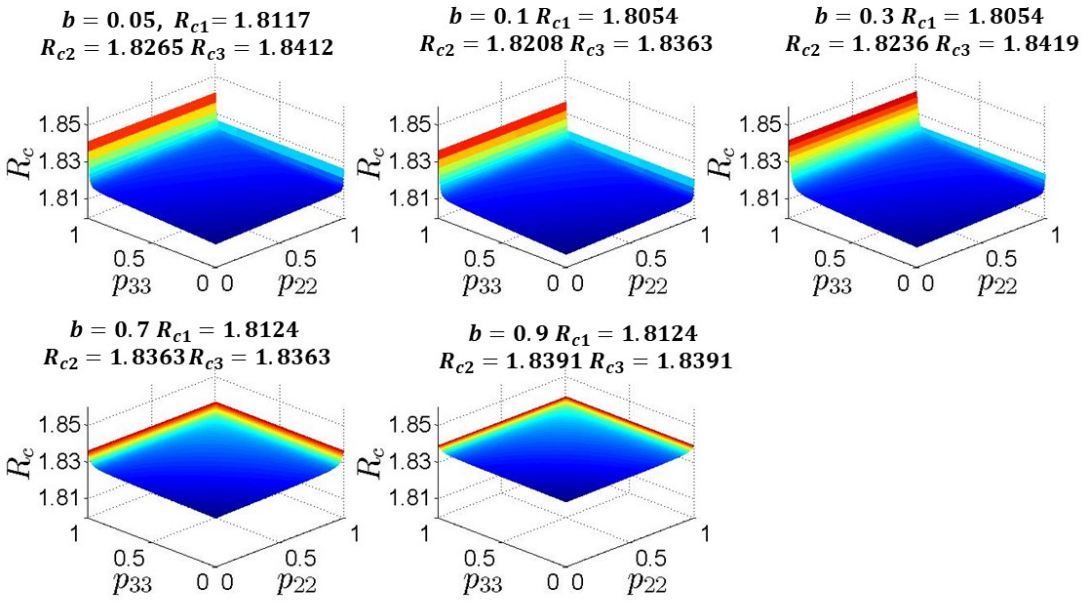

Figure 3.35: Toronto-York-Peel (all moving): relationship between the total reproduction number and residency times p_{22} and p_{33} when only patch 2 and 3 residents are moving $V_{1_0} = 90\%$, $V_{2_0} = 90\%$,$V_{3_0} = 90\%$, $R_{c_{1,2,3}} \approx 1.8$ and (a) $b = 0.05$ (b) $b = 0.1$ (c) $b = 0.3$ (d) $b = 0.7$ (e) $b = 0.9$

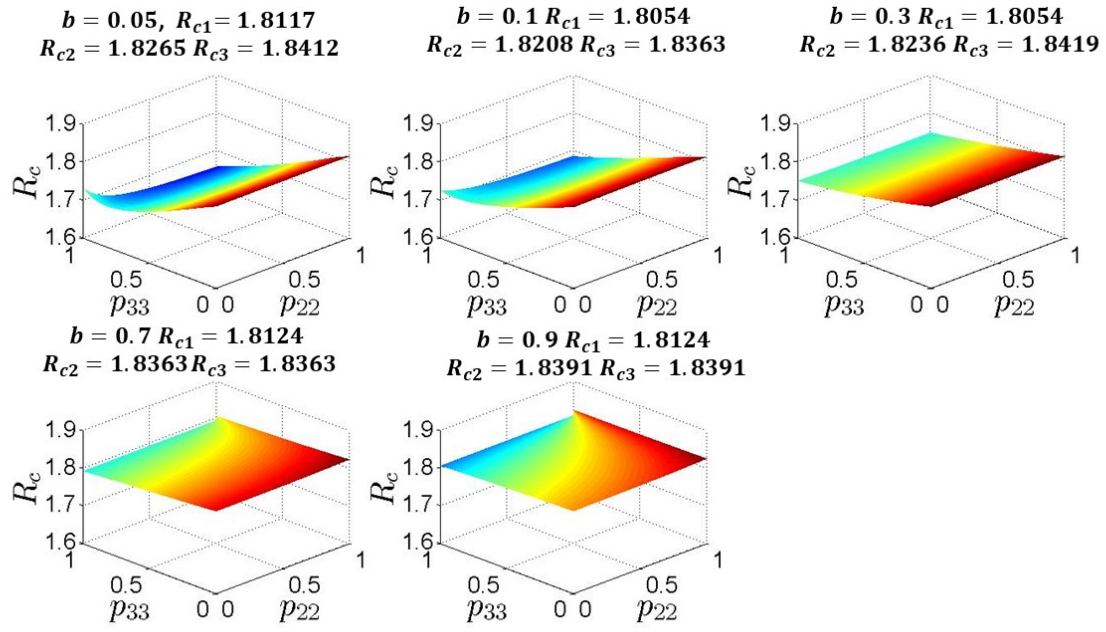

(a)

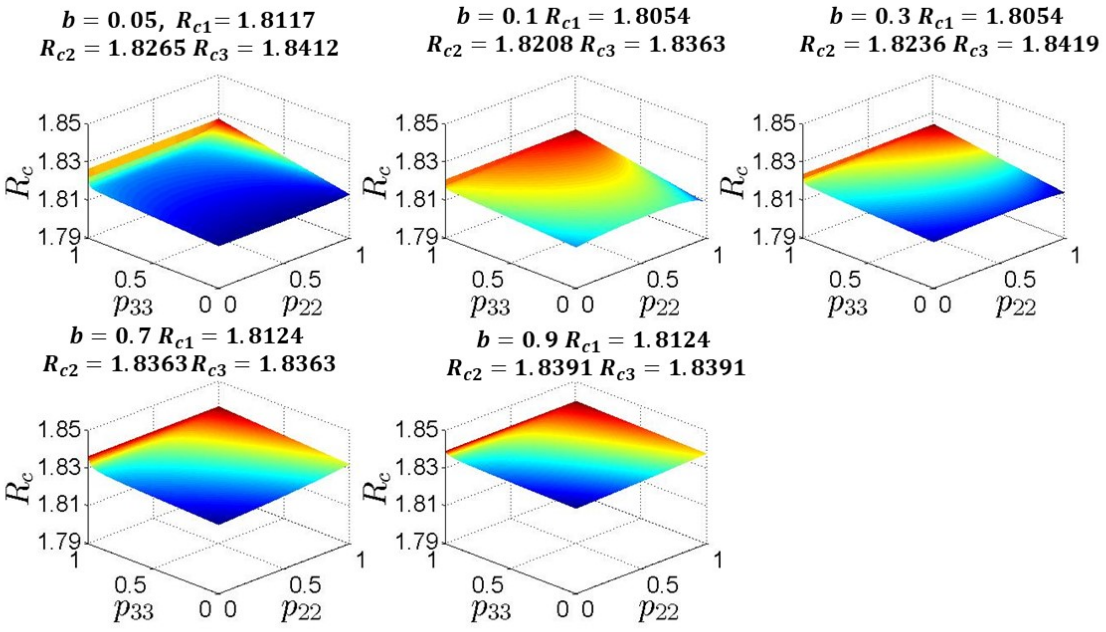

(b)

Figure 3.36: Toronto-York-Peel (all moving): relationship between the total reproduction number and residency times p_{22} and p_{33}.$V_{1_0} = 90\%$, $V_{2_0} = 90\%$,$V_{3_0} = 90\%$, $R_{c_{1,2,3}} \approx 1.8$, $b = 0.05$, 0.1, 0.3, 0.7, 0.9 when (a) $p_{11} = 0$, $p_{12} = 0.5$, $p_{13} = 0.5$ (b) $p_{11} = 0$, $p_{12} = 1$, $p_{13} = 0$

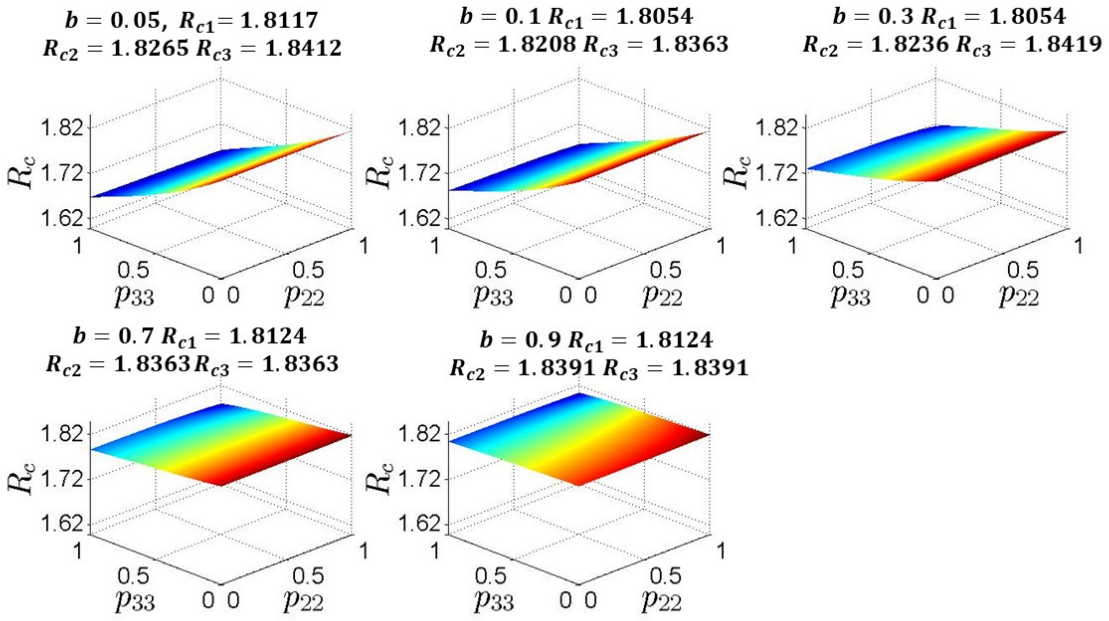

(a)

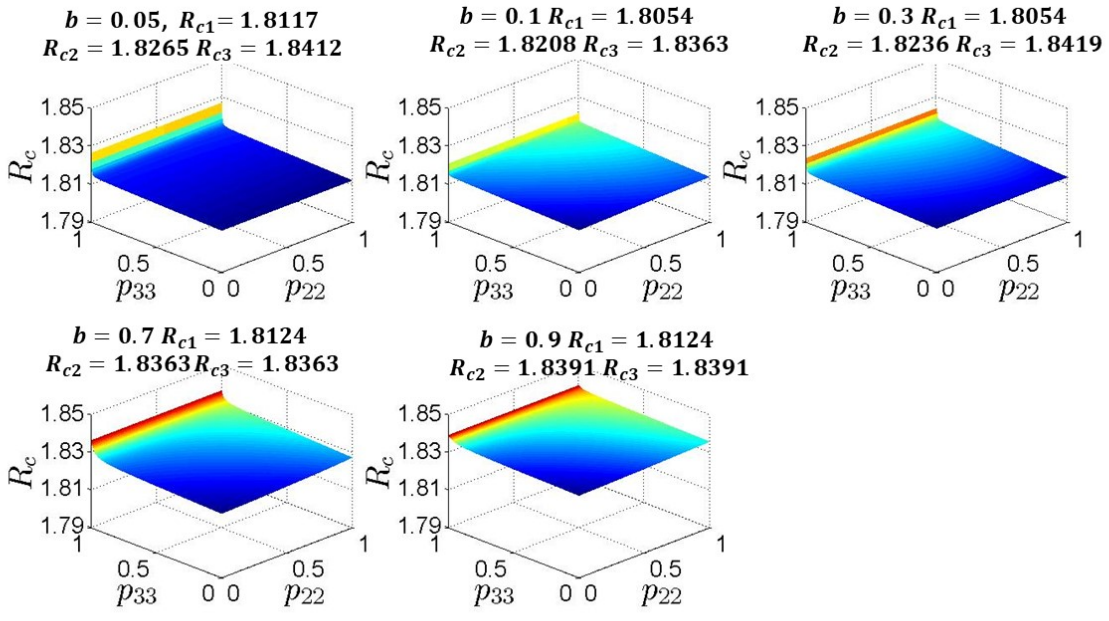

(b)

Figure 3.37: Toronto-York-Peel (all moving): relationship between the total reproduction number and residency times p_{22} and p_{33}.$V_{1_0} = 90\%$, $V_{2_0} = 90\%$,$V_{3_0} = 90\%$, $R_{c_{1,2,3}} \approx 1.8$, $b = 0.05$, 0.1, 0.3, 0.7, 0.9 when (a) $p_{11} = 0.3$, $p_{12} = 0.4$, $p_{13} = 0.3$ (b) $p_{11} = 0.3$, $p_{12} = 0.7$, $p_{13} = 0$

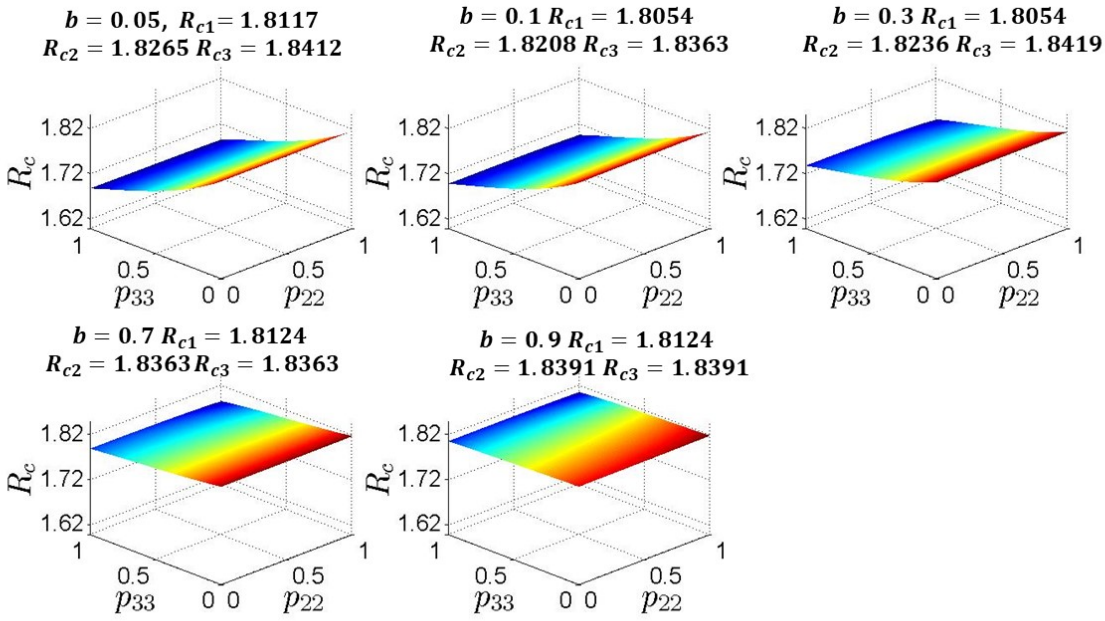

(a)

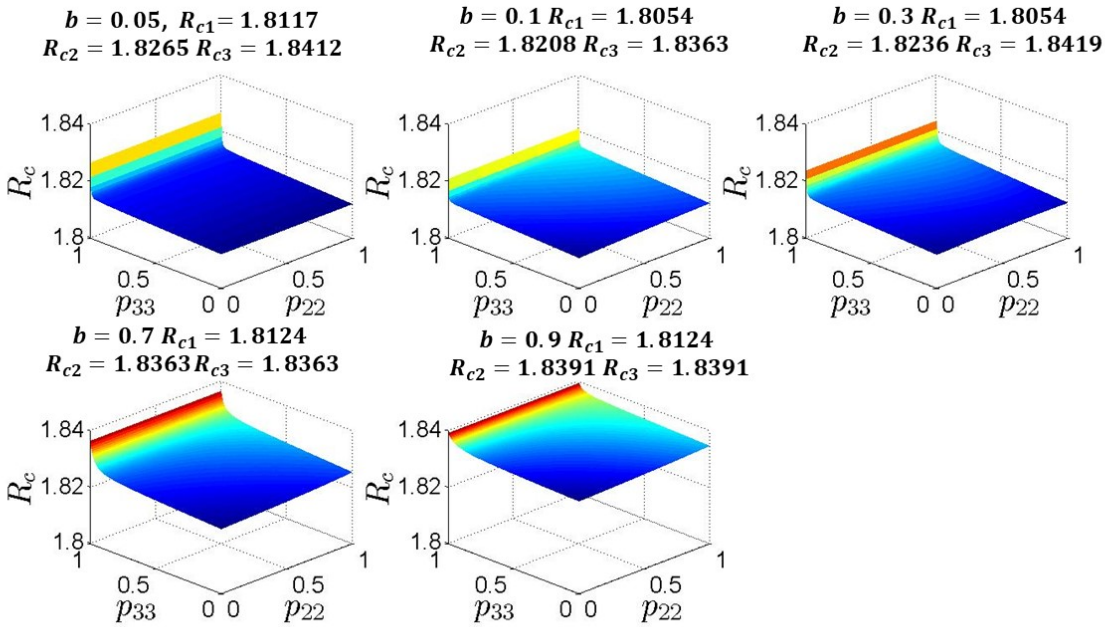

(b)

Figure 3.38: Toronto-York-Peel (all moving): relationship between the total reproduction number and residency times p_{22} and p_{33}. $V_{1_0} = 90\%$, $V_{2_0} = 90\%$,$V_{3_0} = 90\%$, $R_{c_{1,2,3}} \approx 1.8$, $b = 0.05$, 0.1, 0.3, 0.7, 0.9 when (a) $p_{11} = 0.5$, $p_{12} = 0.3$, $p_{13} = 0.2$ (b) $p_{11} = 0.5$, $p_{12} = 0.5$, $p_{13} = 0$

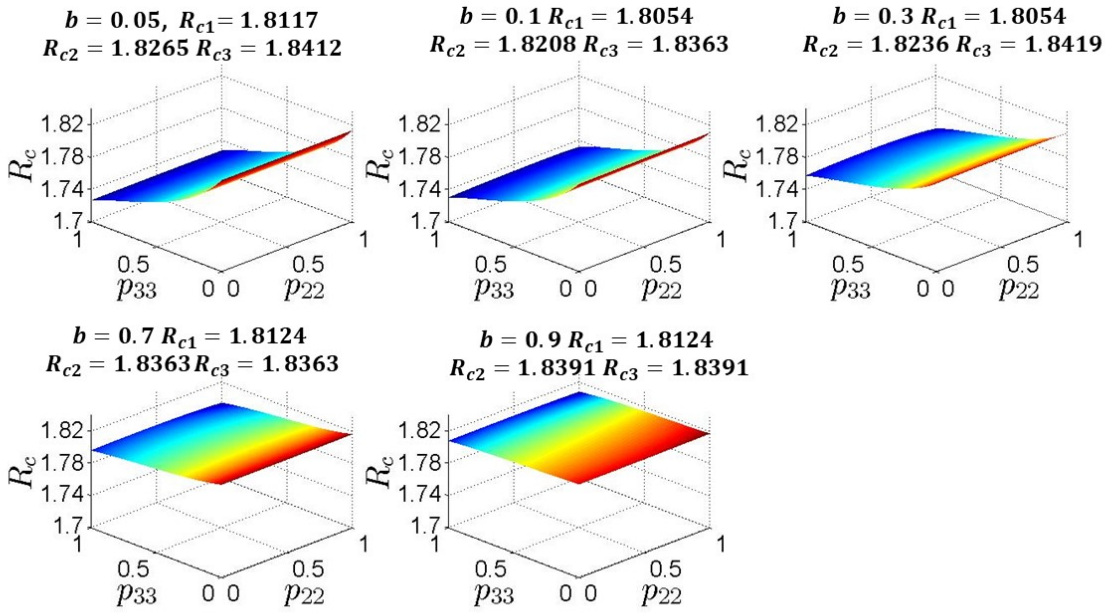

(a)

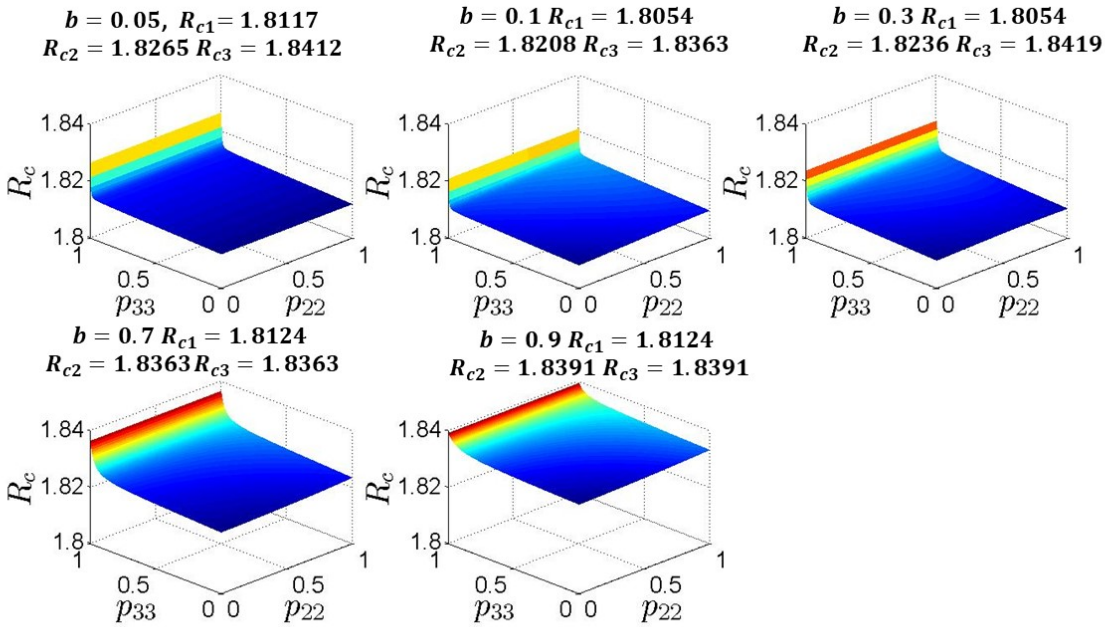

(b)

Figure 3.39: Toronto-York-Peel (all moving): relationship between the total reproduction number and residency times p_{22} and p_{33}. $V_{1_0} = 90\%$, $V_{2_0} = 90\%$,$V_{3_0} = 90\%$, $R_{c_{1,2,3}} \approx 1.8$, $b = 0.05$, 0.1, 0.3, 0.7, 0.9 when (a) $p_{11} = 0.8$, $p_{12} = 0.1$, $p_{13} = 0.1$ (b) $p_{11} = 0.8$, $p_{12} = 0.2$, $p_{13} = 0$

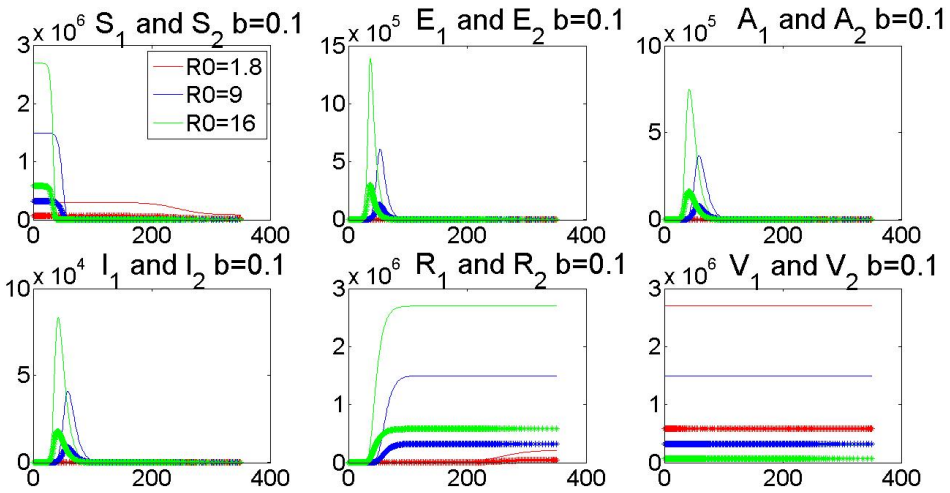

(a)

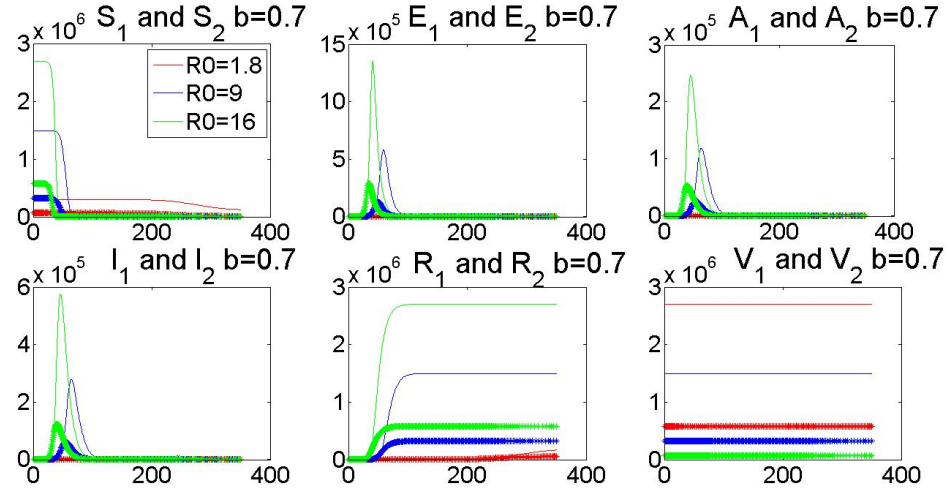

(b)

Figure 3.40: Toronto (solid line) and Halton (starred line) dynamics of $S_{1,2}$, $E_{1,2}$, $I_{a_{1,2}}$, $I_{s_{1,2}}$, $R_{1,2}$, $V_{1,2}$ for $b = 0.1, 0.7$

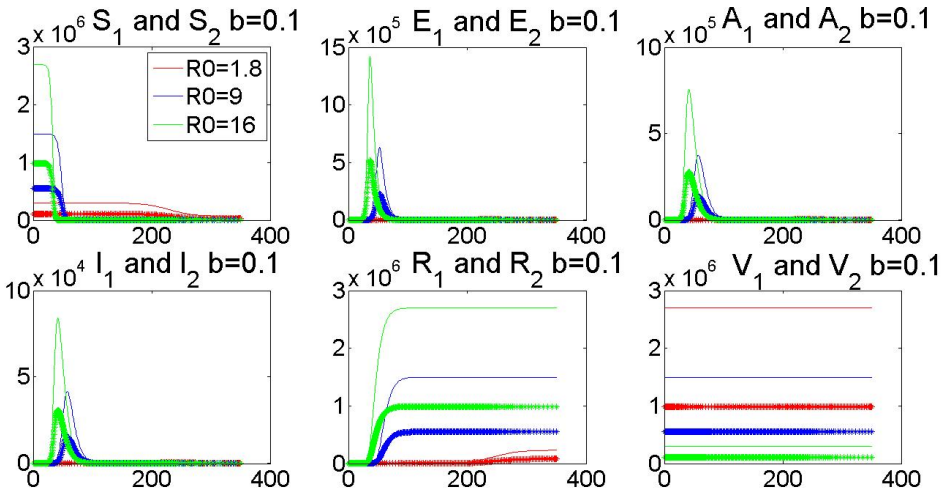

(a)

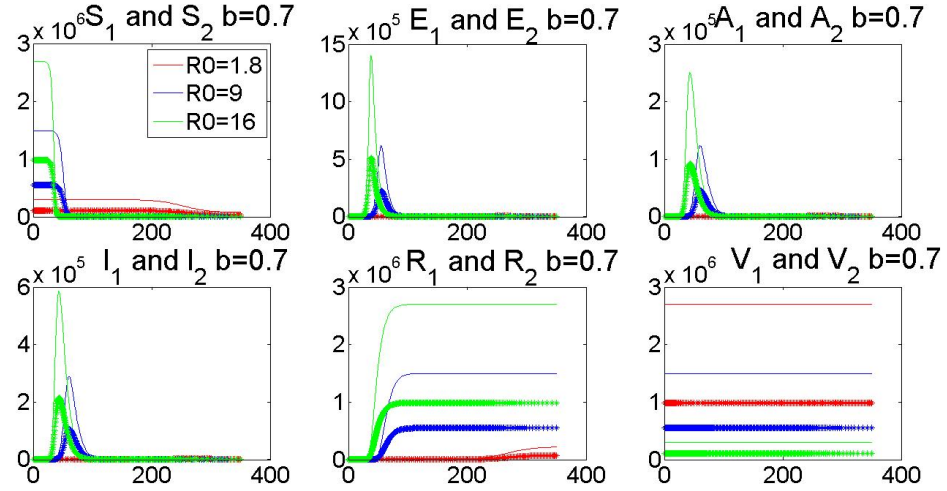

(b)

Figure 3.41: Toronto (solid line) and York (starred line) dynamics of $S_{1,2}$, $E_{1,2}$,$I_{a_{1,2}}$, $I_{s_{1,2}}$, $R_{1,2}$, $V_{1,2}$ for $b = 0.1, 0.7$

responsible for the increase of the cases. Similar results are visible for the cases in the I compartment. However, in this scenario b shows a positive correlation on the symptomatic cases growth (Figures (3.43a), (3.43b), (3.43c) and (3.43d)).

Next, we investigate the uncertainty of the parameters on the time at which A and I reach their maximum value. We observe that when Toronto is infected at the beginning of the outbreak for all the patches, it takes longer for the asymptomatic cases to reach their peak if the infectivity of patch 1 increases (significant negative correlation) and s_1 increases (significant positive correlation). Hence, the proportion of susceptible people in patch 1 affects the delay of the spread in all the other patches. However, the correlation of $\mathcal{R}_{c_1}$ is predominant. Moreover, for patch 2 and 3, even their specific reproduction number shows a negative correlation (Figures (3.44a), (3.44a) and (3.44a). The global peak time of asymptomatic cases is mainly affected by the infectivity in patch 1 (negatively) and s_1 (positively) (Figures (3.44d)). This confirms that globally patch 1 is responsible for the delay of the infection.

Figure 3.45 shows the PRCC plots on the peak time of the symptomatic compartment. It is visible that, when Toronto is seeded first with the infection, as the proportion of susceptible individuals from patch 1 increases and the infectivity in patch 1 decreases, the time needed to reach the peak of I in all the patches is longer (Figures (3.45a), (3.45b), (3.45c)). Similar results are visible for the global case (Figure 3.45d). However, the achievment of the maximum symptomatic cases is delayed in patch 1 as $\mathcal{R}_{02}$ increases and in patch 2 as $\mathcal{R}_{03}$ increases.

The last analysis for the case Toronto-Halton-Durham is shown in Figures (3.46a), (3.46b), (3.46c), (3.46d) and it describes the PRCC plots on the time needed to reach the first 100 symptomatic cases.

We observe that in all patches and globally, the infectivity in patch 1 shows a negative correlation, while s_1 is positively correlated. However, the probability of showing symptoms has a negative effect in patch 1, 2 and globally and positive in patch 3. This indicates that if less infectious people are allowed to leave their own patch (i.e. b is high), patch 1 and 2 reach the first cases quickly, but not in patch 3, where it takes longer. Moreover, an increment of susceptible in patch 2 and patch 3 results in delaying the growth of the infection in patch 1 and 2, respectively .

Toronto-York-Peel

Next, we consider the patches Toronto-York-Peel, where all the residents commute from one patch to another.
Again, we start with the investigation on the sum of all the infected cases (Figure (3.47)-(3.48). It is visible how in all the patches, and for both the total A and I, the number of cases increases as the susceptible proportion of each single patch increases, while globally the susceptibles from patch 1 are the ones more significant to raise the infected individuals. Moreover, as expected, b is positively correlated to the cases in I and negatively correlated to the cases in A. In all the situations, the infectivity of patch 1 is slightly positively significant to develop the growth of the infection.

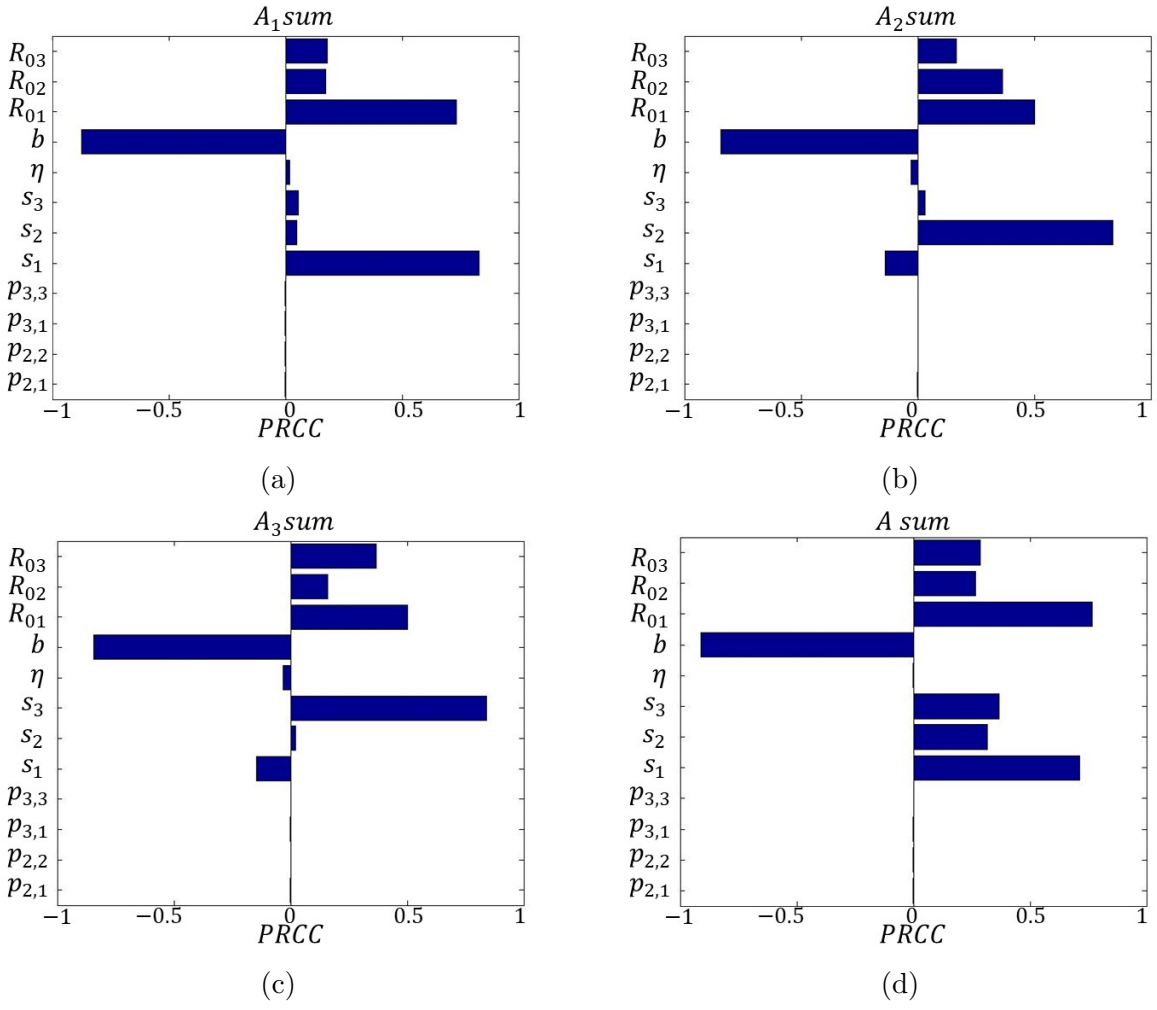

Figure 3.42: Toronto-Halton-Durham (Halton-Durham moving): PRCC plots on the sum of all the asymptomatic cases over the outbreak

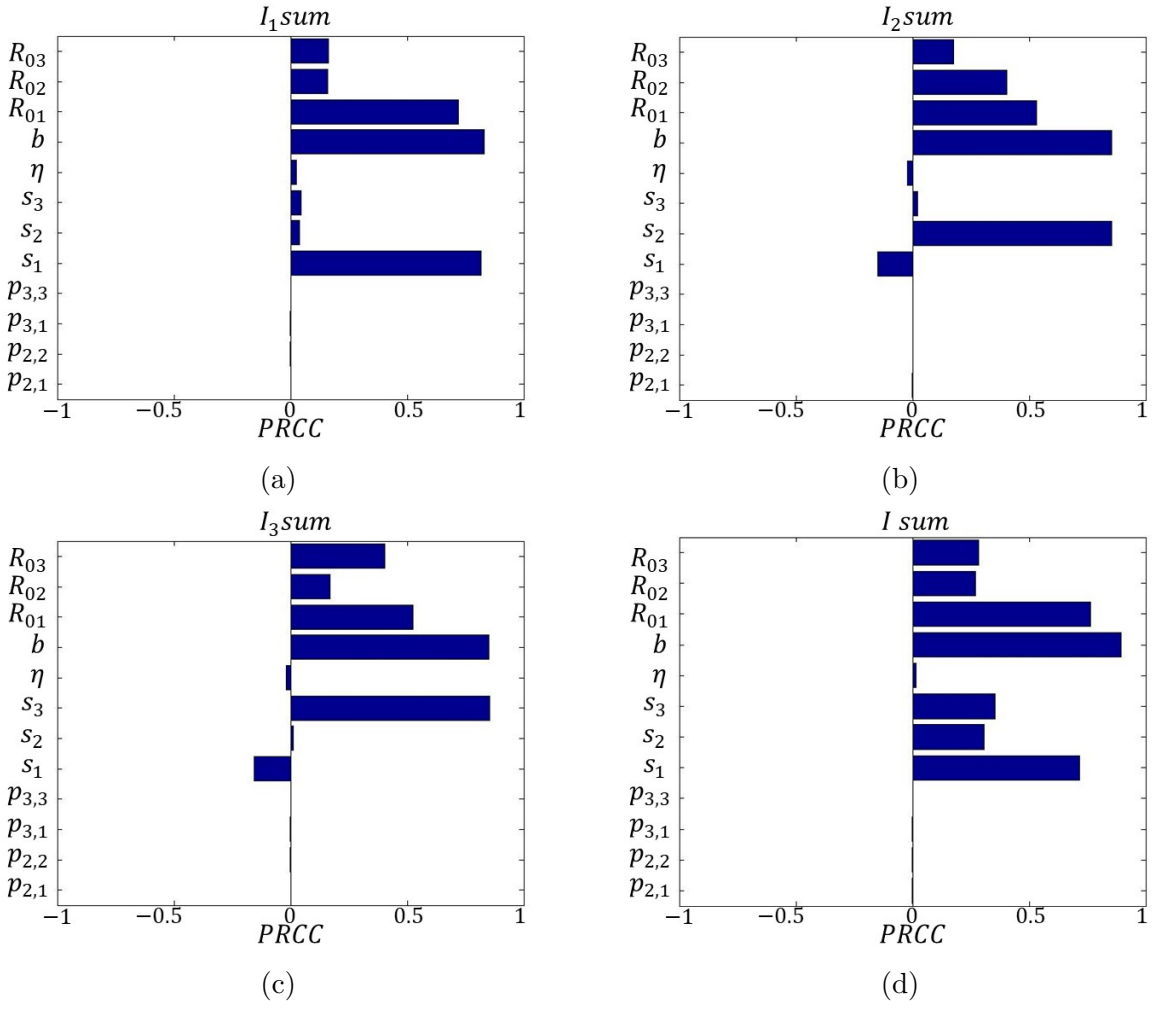

Figure 3.43: Toronto-Halton-Durham (Halton-Durham moving): PRCC plots on the sum of all the symptomatic cases over the outbreak

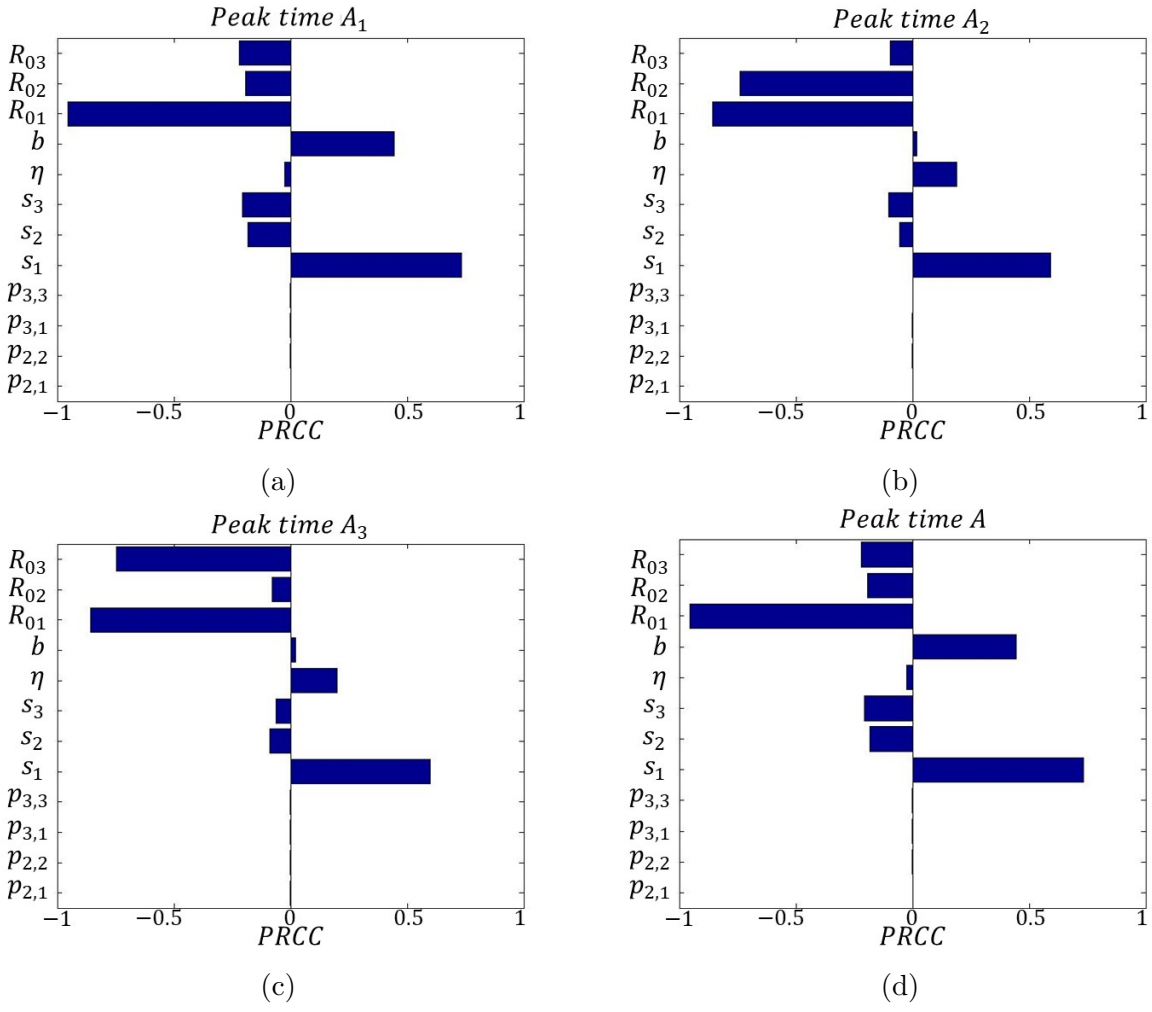

Figure 3.44: Toronto-Halton-Durham (Halton-Durham moving): PRCC plots on the time at which the asymptomatic cases reach the peak when the infection is seeded in patch 1

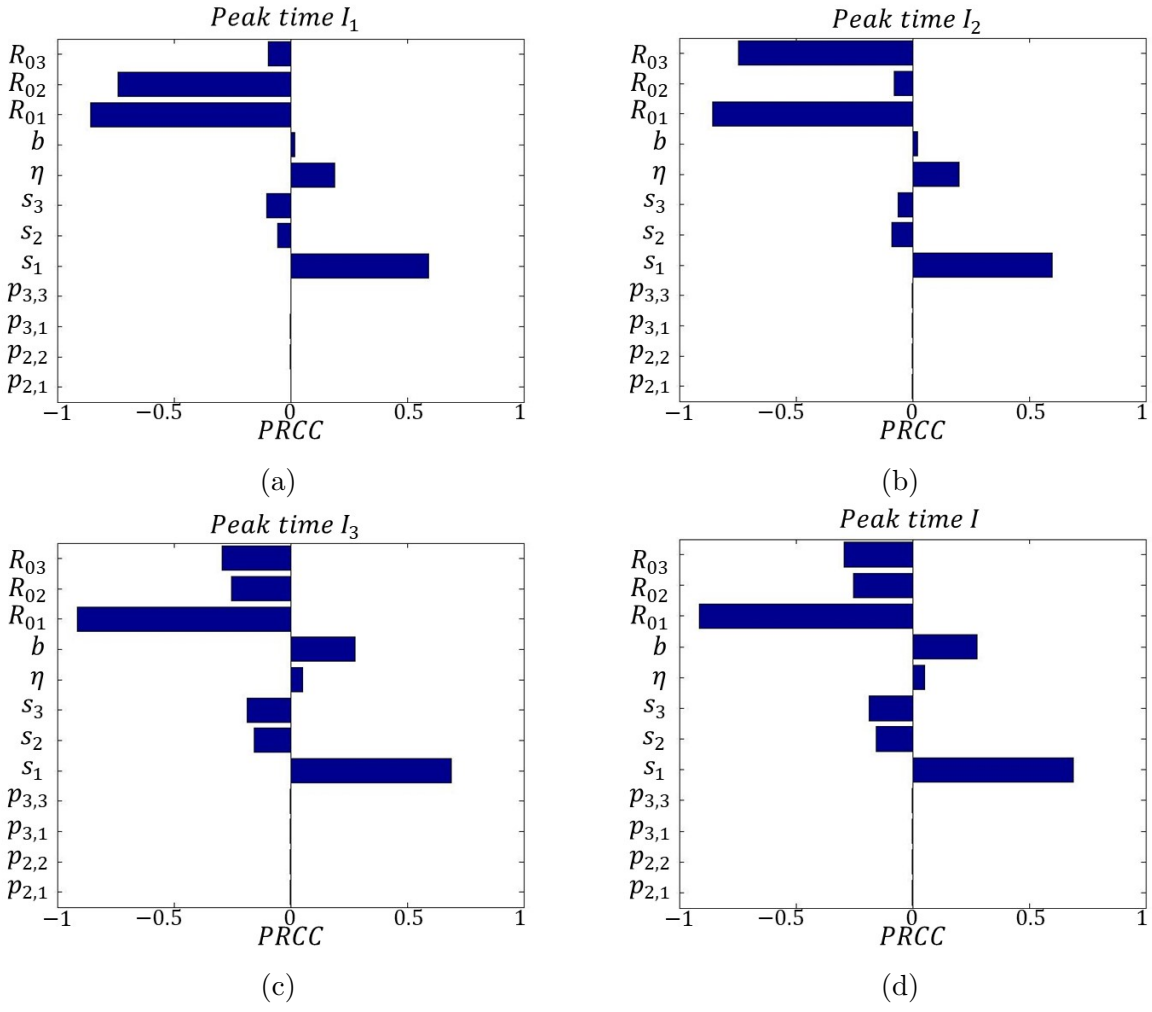

Figure 3.45: Toronto-Halton-Durham (Halton-Durham moving): PRCC plots on the time at which the asymptomatic cases reach the peak when the infection is seeded in patch 1

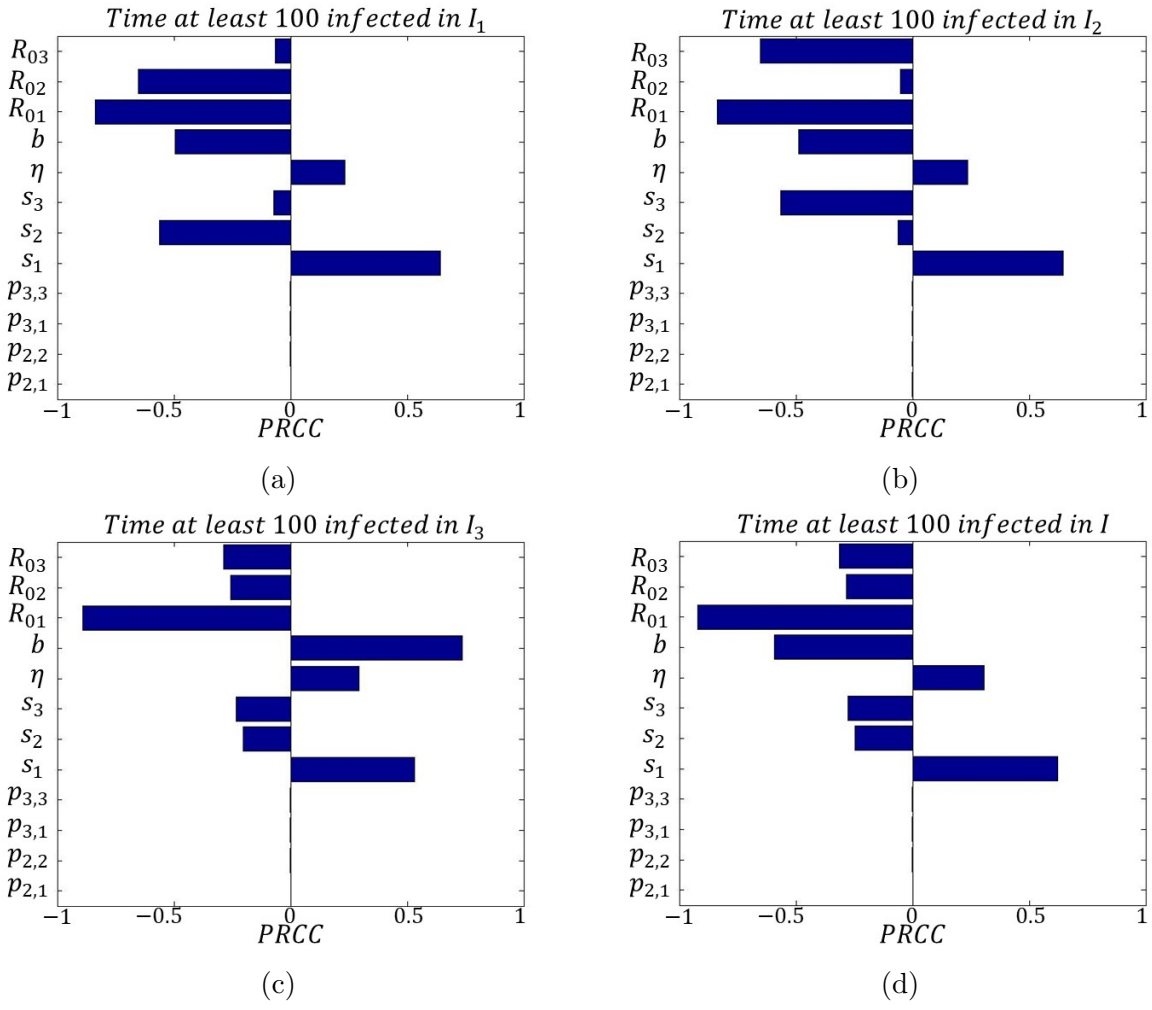

Figure 3.46: Toronto-Halton-Durham (Halton-Durham moving): PRCC plots on the time at which the first 100 symptomatic cases occur when the infection is seeded in patch 1

In Figure 3.49, we can see the PRCC plots on the time at which the asymptomatic cases reach their peak. We observe that in all patches and globally the only parameter showing a strong correlation is $\mathcal{R}_{01}$. In particular, the reproduction number of patch 1 delays the spread of the infection as it decreases. Nevertheless, only in patch 3, $\mathcal{R}_{03}$ shows a slightly negative correlation. Next, we investigate the time needed to reach the peak of I (Figure 3.50). Similar to A, as the infectivity in patch 1 decreases, it takes longer to achieve the maximum value of I in each patch and globally. Moreover, in patch 2, a slight correlation between the peak time and $\mathcal{R}_{03}$ is noticeable. This result is visible when either Toronto or York is firstly infected.

Lastly, we look at the PRCC on when the first 100 symptomatic cases occur (Figure 3.51). The top two rows indicate the case when the infection starts in Toronto. We observe that in all patches and globally, the infectivity of patch 1 is the parameter showing a strong significant negative correlation, indicating that the infection spreads slower as $\mathcal{R}_{01}$ decreases.

3.3 Conclusion

In our study we employ a multi patch model with n patches to investigate the effect that residence times as well as asymptomatic cases have on the transmission and sustainability of the infection in specific patches which can be highly susceptible or immunized to the pathogen. We chose five census regions in Ontario which are geographically relatively close: Toronto, York, Peel, Halton and Durham. Our investigation is mainly focused on two cases for $n = 2, 3$. In each case, we compare two scenarios: when Toronto residents are not commuting to other regions and when they do.

When two patches are considered, we are able to derive a mathematical expression for the total reproduction number $\mathcal{R}_c$. We observe that when both patches present the same immunity background (both are either highly vaccinated or susceptible), the total transmission is not significantly affected by the asymptomatic cases nor the residence times. On the other hand, when the immunization coverage is different, then we observe that the overall reproduction number is reduced if either the highly susceptible commuters spend most of their time in the patch with low risk of transmission or the residents of almost fully immunized patched spend their time in the vulnerable patch. In case of isolation, then the total transmission is driven by the highest patch specific reproduction number.

Similar results are found in the case with $n = 3$. In this scenario the reproduction number cannot be derived analytically, but numerically. When more than two patches are involved, again we observe that the reduction in the total reproduction number is achieved when susceptible commuters leave the high risk patches towards the low risk ones, or the vaccinated residents spend most of their time in the vulnerable patch to decrease the transmission.

We conclude our investigation with sensitivity analysis of the model parameters on the total cases of asymptomatic and symptomatic cases as well as the time at which these compartments reach the first 100 cases and the peak. We observe that the patch specific reproduction numbers $\mathcal{R}_{c_{1,2,3}}$ present a significant positive correlation with the number of infected cases, but as the transmission decrease, they delay the time needed to reach the

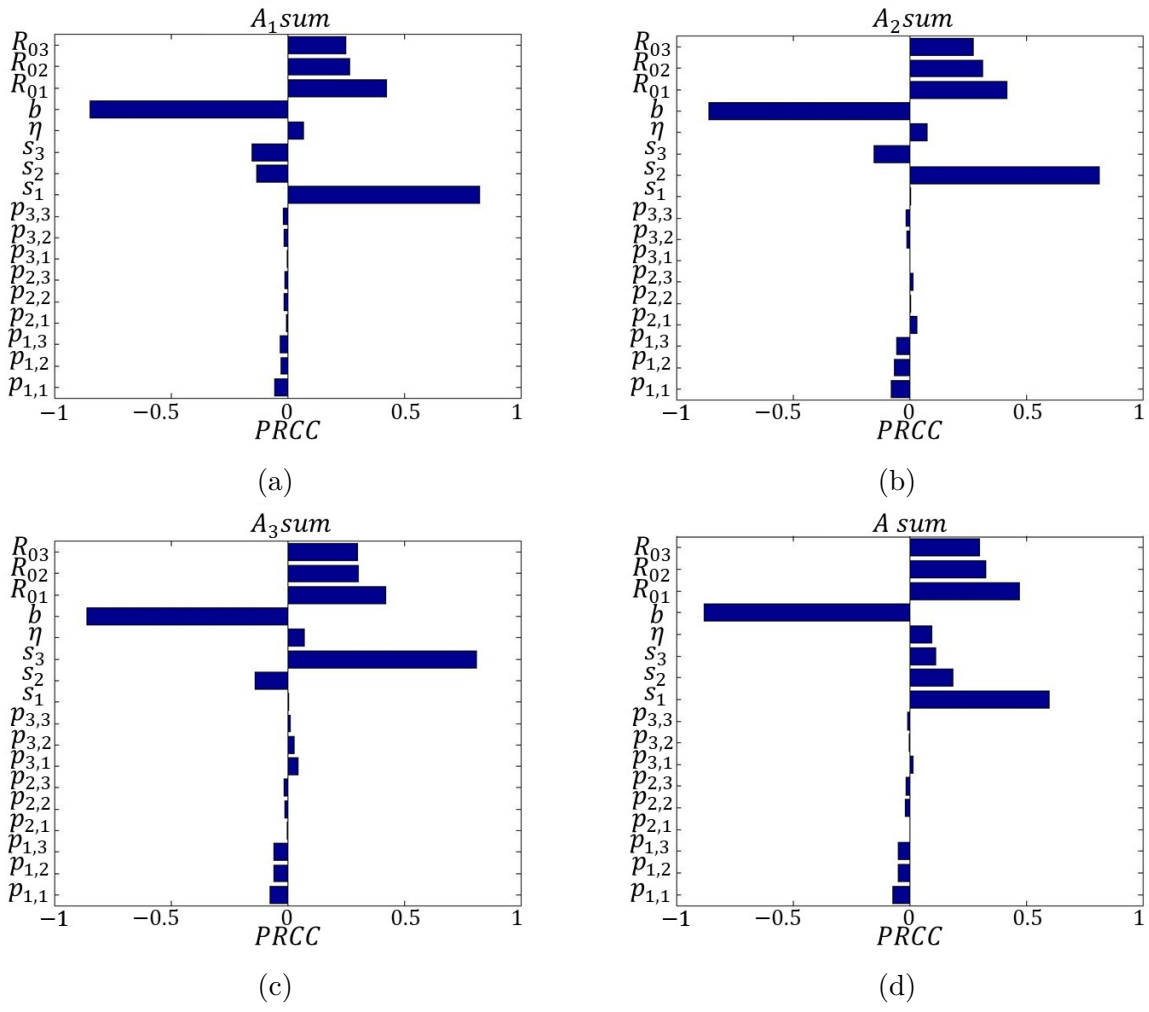

Figure 3.47: Toronto-York-Peel (all moving): PRCC plots on the sum of all the asymptomatic cases over the outbreak

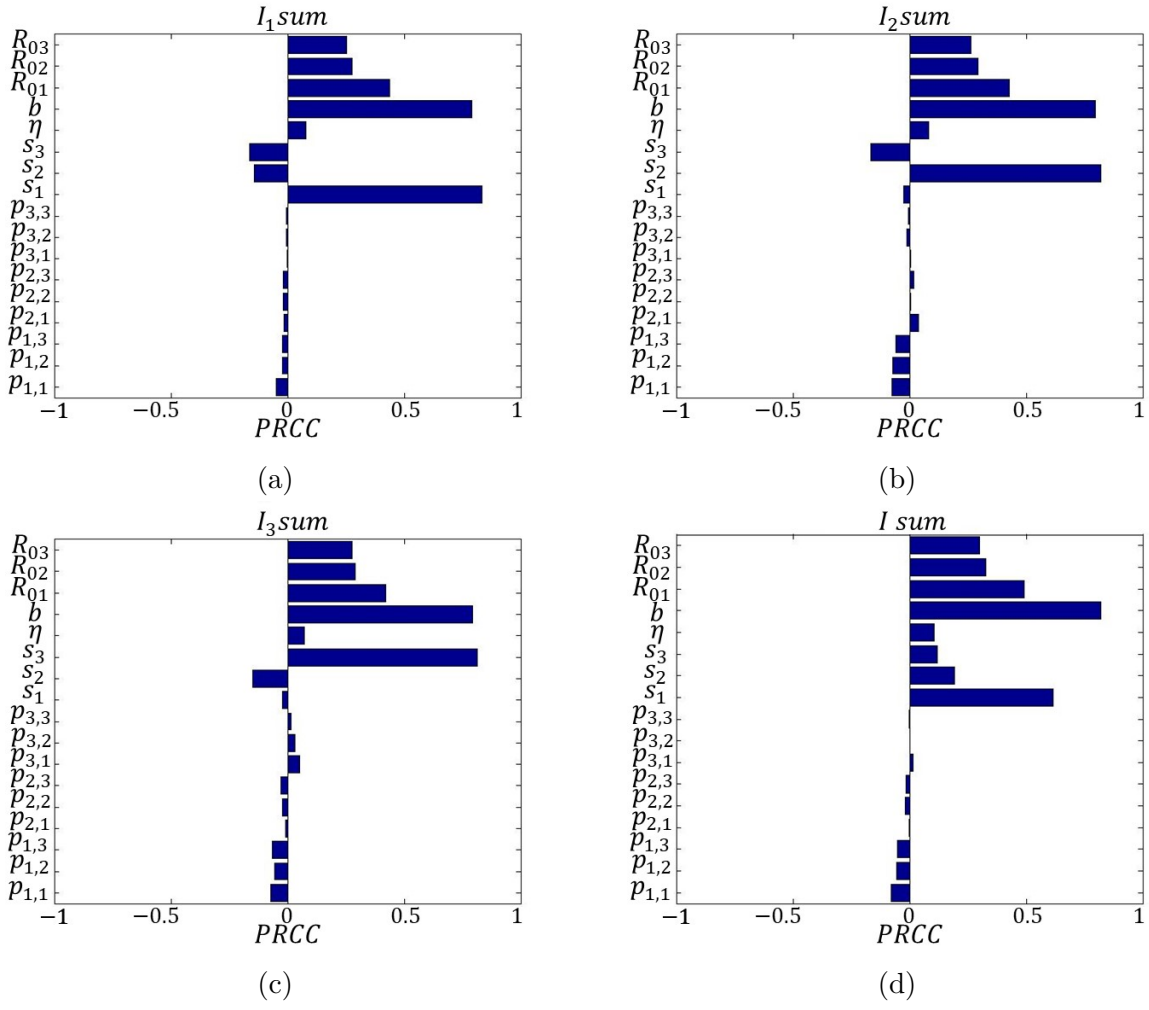

Figure 3.48: Toronto-York-Peel (all moving): PRCC plots on the sum of all the symptomatic cases over the outbreak

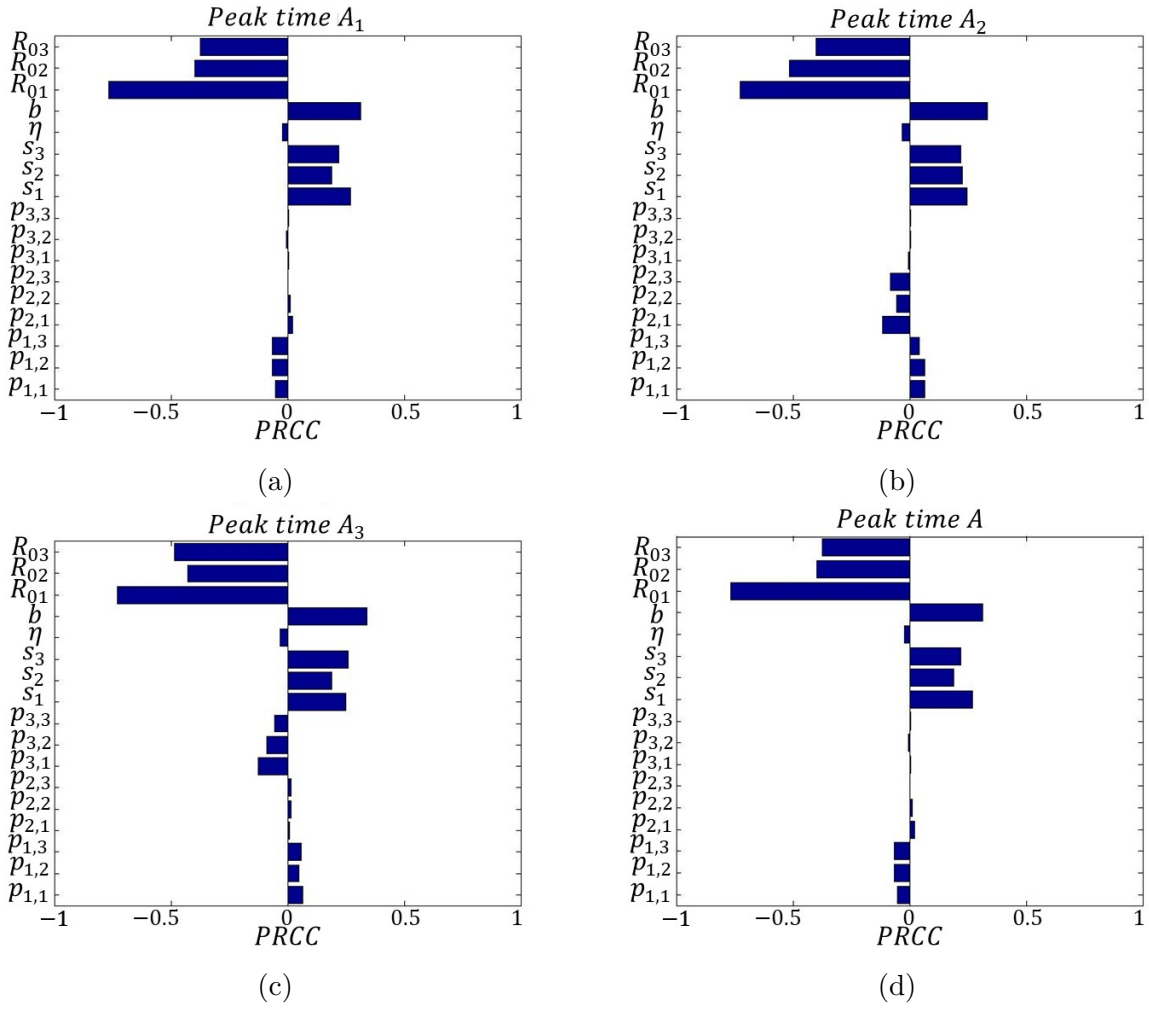

Figure 3.49: Toronto-York-Peel (all moving): PRCC plots on the time at which the asymptomatic cases reach the peak when the infection is seeded in patch 1

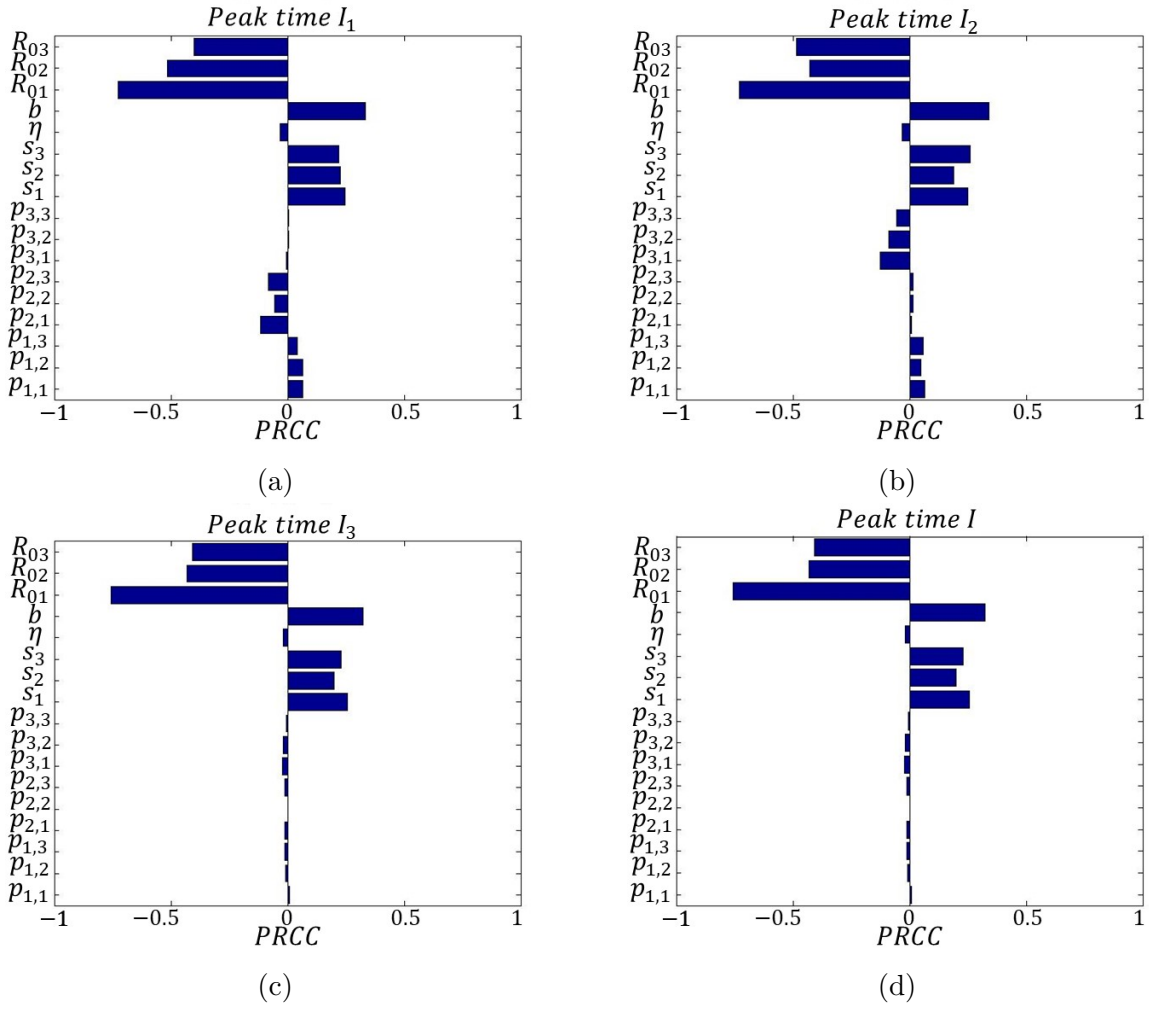

Figure 3.50: Toronto-York-Peel (all moving): PRCC plots on the time at which the asymptomatic cases reach the peak when the infection is seeded in patch 1

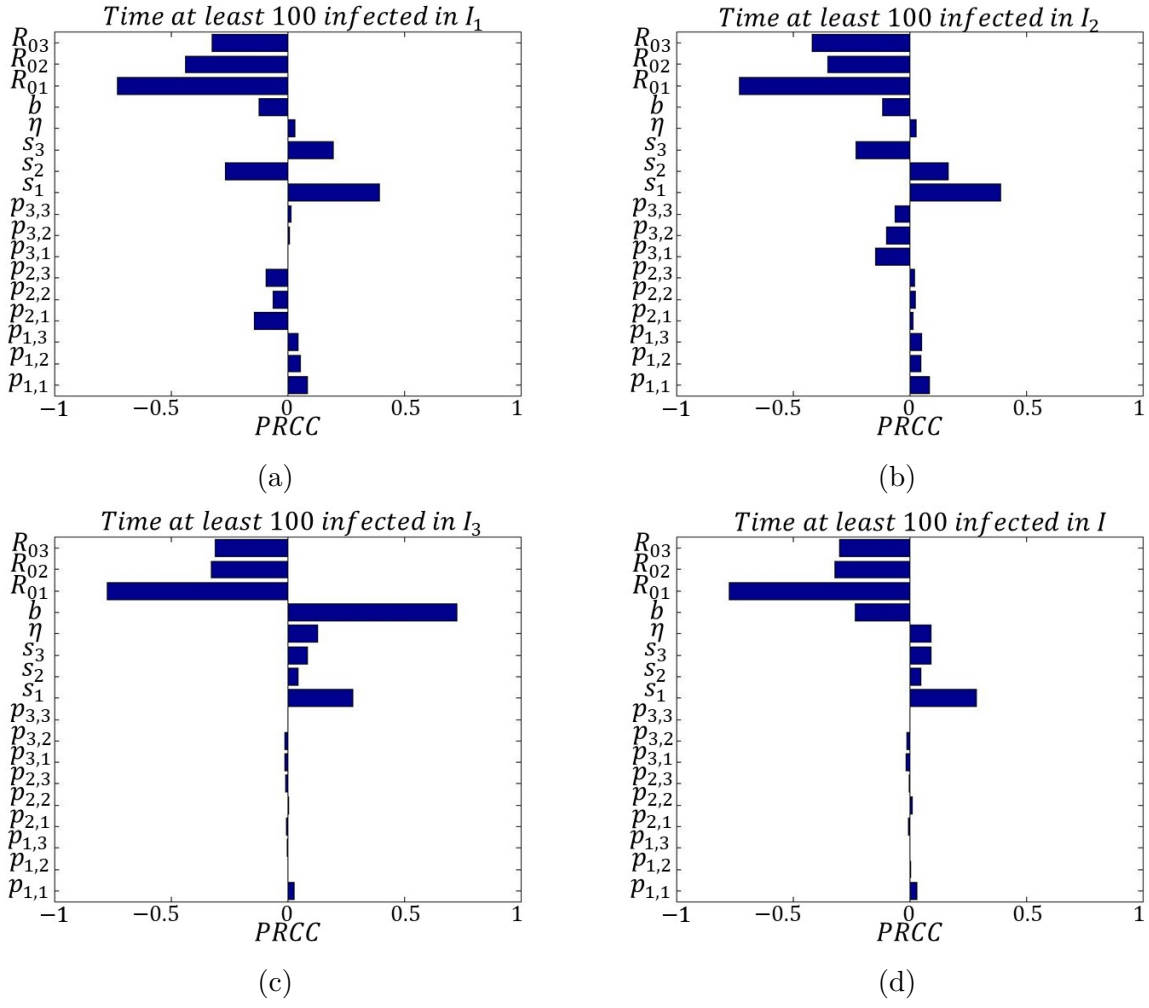

Figure 3.51: Toronto-York-Peel (all moving): PRCC plots on the time at which the first 100 symptomatic cases occur when the infection is seeded in patch 1

peak and the first 100 cases. Moreover, as the proportion of susceptible residents increases, the number of cases increases as well.

Our findings show how reducing the heterogeneity of vaccination is important to reduce the transmission of the infection. The main goal for Public Health is to reduce the susceptible pockets present in the country and cities by improving and increasing the vaccination coverage.

Our model is only looking at the residence times that all residents spend in their own or other patches. A further extension can be assumed that not all the residents are commuters and introduce age structure in order to investigate the age class that is responsible to change the total transmission among all the patches. Moreover, if children age class is included, it might be useful to consider seasonality to catch the reduced commuting towards schools in the summer and winter breaks.

Chapter 4

Waning Immunity: Herd Immunity and Infection Dynamics

4.1 Introduction

This work has been conducted in collaboration with Dr. Heffernan, Dr. Teslya, Dr. Crowcroft and Dr. Bolotin. I have collaborated in defining the models, theoretical and numerical analyses. Parameters estimation, Figure 4.3a and Figure 4.6 were made by Dr. Teslya.

In this work, we consider that immunity developed against the MeV through vaccination might not be life-long, and wanes over time. We assume that individuals with waning immunity can show a mild infection (defined as secondary infection), but it is still unsure what the level of their infectiousness is. The phenomenon of waning immunity and the force of infection of vaccinated cases is currently a subject of study in Public Health. In particular, departments in Public Health Ontario have been conducting systematic review to investigate reported waning immunity and transmission from vaccinated cases [23, 24]. We investigate different scenarios comparing different level of force of infection of vaccinated cases. This topic is particularly important for Public Health, since it can help in managing any future outbreak.

Different mathematical models have studied the waning process of measles vaccine. Heffernan and Keeling [45] proposed an in-host model taking into consideration the immunity system and cellular dynamics trying to understand how different levels of immune memorycells can affect the trend of the infection when the body is exposed to the virus. A fundamental result is on the basic reproduction number and how it is correlated to the level of memory cells in the plasma. They found that, as the memory cells increase, the transmission from any individual previously immunized is less than the one from a fully susceptible individual experiencing the infection for the first time.

In a second paper, Heffernan and Keeling [52] formulated a population-level model applying to it the immunological findings showed in [45]. Again, they investigated the interactions among vaccination, waning immunity process and infection dynamic. Their results show that when immunity wanes over a long period, as an outbreak occurs, this can generate a higher

number of cases than the scenario provided by a shorter waning period. Also, in a highly vaccinated population if the waning period is fairly short, the infection outbreaks are visible and are mainly characterized by asymptomatic cases and showing a biannual period as the outbreaks occurring in highly vaccinated countries.

In 1999, Mossong, et al. [49] explored the infectiousness of sub clinical cases when individuals wane their vaccine-induced immunity. They found that if the infection is absent from the population for a relatively long period, the level of protection decreases and hence measles elimination is not achievable.

The transmission from vaccinated cases has been studied as well. Rota, et al. [117] reported in 2011 cases of measles in two fully vaccinated physicians. Their symptoms did not indicate a measles primary infection, hence, neglecting the possibility of transmission they continued working and visiting patients. Nevertheless, no cases were reported among the contacts. However, Rosen, et al. [118] reported measles transmission from a vaccinated case. The individuals gained measles immunity through two doses of vaccine. He showed symptoms compatible with the infection. Several contacts have been confirmed and some of them developed the infection as secondary cases. Tertiary cases were not reported.

Since in the past years measles cases have been present in different age groups, it is important to investigate the relation between vaccination, waning immunity and age structures. Hethcote, et al [74],[57], [58] developed different studies on age-structure epidemiological models on pertussis transmission in which both vaccination-induced and infection-induced immunity wane over time. They employed $SIRV$ model framework including waning immunity and different infection levels (from high to low). The population is divided into groups age-dependent, from newborns to 85 and over years of age. The findings in [57], show that if a booster vaccination shot is given to the population every 10 years, the age groups counting more infected are the ones related to adulthood. In [58], Hethcote, et al shows that shifting the second booster shot from 18 months of age to 15-27 years the infection incidence is reduced over all the age groups. Mossong [75] proposed an extension of his model in [49] including age structure. They studied the impact that waning periods and transmission from a vaccinated case have on the time to the first re-emergence of measles. Their results suggest that if the force of infection of vaccinated individuals is low and vaccine-induced immunity wane over a long period, more time is required to experience measles re-emergence.

Susceptible-Infected-Recovered-Waning- Susceptible (SIRWS) framework models have been developed to study the re-emergence of pertussis [56, 82, 54]. Lavine et al. [56] applied an age-structured SIRWS model to investigate the pertussis re-emergence and the effect of boosting process. The immunity is assumed to wane over time and, after exposure to the pathogen, the boosting process is triggered. Their model was able to capture the infection re-emergence occurring in highly vaccinated countries as well as the shift in the age group of the cases. Moreover, these results were achieved under the assumption that a low exposure to the pathogen triggers immunity boosting. Others studies on pertussis have been done employing this framework [82, 54]. Leung et al. [54] extended the model in [56] by including a vaccinated compartment and assuming that vaccine-acquired and infection-induced immunity wane at different rates. Moreover, the authors consider one infection compartment for primary

infected and one for secondary cases with the same level of infectiousness. Similar to Lavine et al [56], the boosting process is triggered with a lower exposure to the virus than the one needed to become primary infected. Age structure is not considered. They found that the different waning periods can lead to different infection dynamics, and hence it is necessary to understand them deeply. Although the $SIRWS$ describes waning immunity process, it is not applicable here, since we only consider waning immunity from vaccination.

We present a mathematical model following the SII_WRVWS framework, taking into account both waning of vaccine-induced immunity, vaccination routine and boosting process, which occurs after being exposed to the virus. After encountering the pathogen, individuals are assumed to either increase their immunity level or become infected/infectious. We differentiate the classes I (defined as primary cases) and I_W (defined as secondary cases) to investigate the best and worst case scenarios of transmission from infecteds that had some immunity at the time of infection. In particular, since the force of infection of vaccinated cases is still unknown, we consider the following cases: one, the secondary infection (I_W) will make individuals as infectious as the primary infection (I) (defined as worst case scenario), the other one assumes that secondary infectious individuals will not be able to transmit the virus (defined as best case scenario). Since measles cases are reported in different age groups and vaccine doses are given at different ages, we extend the model by including age structure as well. We investigate how waning and boosting processes affect the achievement of herd immunity, by evaluating both the *basic* and *control reproduction number* ($\mathcal{R}_0$ and $\mathcal{R}_C$, respectively). Moreover, we detect the age groups that mostly experience the infection in case of outbreak. The distribution obtained by the age structure gives an insight on which age groups are more susceptible to any new infection and which are fully immunized. Also, we developed Continous Time Markov Chain (CTMC) stocahstic model with and without age structure to investigate the probability of outbreak. These results can benefit public health decisions in case of outbreaks as well as highlight how measles immunity waning periods and vaccinated cases' infectiousness need a deeper understanding.

4.2 Model and Methods

4.2.1 Model

The model that we present follows the *Susceptible-Infectious-Recovered-Vaccinated-Waning* framework with some extensions. Given the different levels of immunity in the population, we assume that the infectious individuals are divided into primary and secondary cases. The first category refers to the people who are totally susceptible to the pathogen and become infectious for the first time, while the second one indicates the individuals who are vaccinated but undergo the waning immunity process, which makes them vulnerable to the infection. It is important to recall that the infection force of vaccinated cases is not established yet. Recent systematic reviews has been conducted by a *Public Health Ontario* team to investigate any documented transmission from vaccinees cases ad waning immunity [23, 24]. Hence, we investigate two different scenarios: when the secondary cases are as infectious as the primary

cases and when the secondary cases are not infectious. To differentiate these possibilities, in our model, we introduce a parameter G, which can assume value 1 or 0, depending on the infection force of the vaccinated cases (fully infectious or not, respectively).

We assume that individuals enter the susceptible class at 12 months of age, when the first dose of measles vaccine is given [119, 17]. Moreover, the population is assumed to be at the equilibrium $N = \lambda/d$, where λ is the birth rate and d the death rate, so the model has been scaled in order to have each compartment as a fraction of the total population N.

The dynamics is described as follows. Susceptible individuals are introduced into the population and a fraction p of it is vaccinated. When susceptible individuals encounter an infectious individual, with transition rate $\beta S(I + GI_W)$, the former will become infectious as well. After the recovery period ($1/\gamma$, if primary case, $1/\gamma_w$, if secondary case), individuals move to the recovered class R where they acquire life-long immunity. On the other hand, vaccine-induced immunity can wane over time and with rate k_1 individuals will move from class V to the waning compartment W. People in W will boost their immunity or become infectious once they encounter the virus, with rate $\nu\beta(I + GI_W)W$. Once the boosting process happens, a portion $1 - q$ of individuals will be moved to the V compartment, while a proportion q will either move to the compartment I, becoming mildly infectious, or move to the compartment I_W, where individuals are not able to transmit the infection and move to R after a recovery period. Figure 4.1 represents the flow diagram of the above mentioned dynamics. The following Table 4.1 and Table4.2 give a description of the parameters and variables used in the model, respectively. Observe that, hereafter, the immunity is considered to be life-long if the waning periods are 100 years or longer.

We begin our investigations by analysing a general SII_WRVW model framework, which we will extend by including age structure.

4.2.2 Model with No Age Atructure: Deterministic

The ordinary differential equations (ODE) describing the infection dynamics are given by the following system :

$$\begin{aligned}
S' =& d(1-p) - \beta S(I + GI_W) + k_2 W - dS \\
I' =& \beta S(I + GI_W) - \gamma I - dI \\
I'_W =& \nu(1-q)\beta(I + GI_W)W - \gamma_W I_W - dI_W \\
R' =& \gamma I + \gamma_W I_W - dR \\
V' =& dp - dV - k_1 V + q\nu\beta(I + GI_W)W \\
W' =& k_1 V - \nu(1-q)\beta(I + GI_W)W - k_2 W - dW
\end{aligned} \tag{4.1}$$

Parameter	**Definition**	**Value [Ref]**
λ	Birth rate	people $\times$ year^{-1}
p	Fraction of newborns effective vaccination (obtained vaccine and gained a level of neutralizing immunity)	[0.91,0.93,0.96]
d	Natural death rate	0.012 year^{-1} [120]
β	Infection rate	[34.691-312.22] (people $\times$year)$^{-1}$ [15]
γ	Recovery rate.	52/2 year^{-1} [6]
γ_w	Recovery rate, from I_W to R.	52/2 year^{-1} [6]
ν	Boosting proportionality constant	1
q	Fraction of those boosted that move to V. $(1-q)$ experience mild infection and are boosted to R (via I_W)	[0,1]
k_1	Waning rate from V to W	[1/300,1] year^{-1}
k_2	Waning rate from W to S	[1/300,1/25] year^{-1}
G	quantity defining the infection force of secondary cases	0,1
a_i	Age group $i = 1, ..., 19$ $a_1 = [0.5, 1)$, $a_2 = [1, 5)$, $a_3 = [5, 10)$, ... , $a_{18} = [80, 85)$, $a_{19} = [85, \infty)$	assumed
$c_i \approx \frac{1}{a_i - a_{i+1}}$	Aging rate at which individuals leave the age compartment i	evaluated $c_0 = 1$ and $c_n = 0$
$\beta_{i,j}$	Infection rate at which a person in j age interval infects an individual in i age interval	evaluated [69]
μ_i	Death rate of age group i	[121]

Table 4.1: Parameters for Model (4.1) (above dashed line) and for Models (4.8 and 4.10)(below dashed line)

Variable	Definition
S	Density of fully susceptible population
I	Density of primary infected population
I_W	Density of secondary infected population
R	Density of recovered population that is characterized by the life-long immunity
V	Density of individuals characterized by immunity comparable to that obtained immediately after vaccination.
W	Density of the population in the immunity waning stage.
S_i	Density of fully susceptible population in age group i
I_i	Density of primary infected population in age group i
I_{W_i}	Density of secondary infected population i
R_i	Density of recovered population that is characterized by the life-long immunity in age group i
V_i	Density of individuals characterized by immunity comparable to that obtained immediately after vaccination. in age group i
W_i	Density of the population in the immunity waning stage.

Table 4.2: Variables for Model (4.1) (above dashed line) and for Models (4.8 and 4.10) (below dashed line)

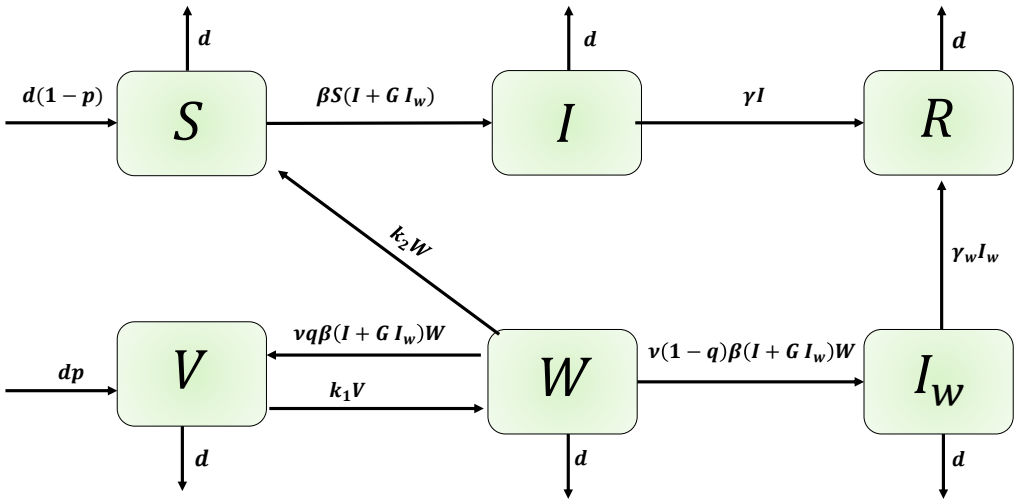

Figure 4.1: Flow diagram showing the structure of dynamics described by system (4.1).

Basic and Control Reproduction Number ($\mathcal{R}_0$ and $\mathcal{R}_c$)

We can derive the disease-free equilibrium with vaccination and it is defined as $E_0 = (S_0, 0, 0, V_0, W_0)$, where

$$\begin{aligned} S_0 =& 1 - p + \frac{pk_1k_2}{(d+k_1)(d+k_2)} \\ V_0 =& \frac{dp}{d+k_1} \\ W_0 =& \frac{dpk_1}{(d+k_1)(d+k_2)} \end{aligned} \tag{4.2}$$

Results

In order to understand the infectivity of the disease, by using the *Next-Generation Matrix method* [88, 86, 90, 92] we derive both the basic and control reproduction numbers for Model 4.1, defining them as $\mathcal{R}_0$ and $\mathcal{R}_c$ respectively. When the secondary cases are as infectious as the primary ones ($G = 1$), the expression for the reproduction number will be:

$$\mathcal{R}_0 = \frac{\beta}{(\gamma + d)} \tag{4.3}$$

while, when $G = 0$, $\mathcal{R}_0$ is obtained by replacing γ with γ_w in 4.3.

The expressions for the control reproduction numbers are the following:

$$\mathcal{R}_c = \mathcal{R}_0 \left[(1-p) + p\frac{k_1k_2}{(d+k_1)(d+k_2)} + Gp\frac{(1-q)\nu k_1 d}{(d+k_1)(d+k_2)} \right] \tag{4.4}$$

Observe that Eq.4.4 presents different terms in the square brackets: the first two indicate the new infections derived from susceptible individuals, while individuals waning immunity regulate the third component. Moreover, note that the factor $(1-q)\nu$ can affect 4.4 differently depending on its value. If a large number of individuals gets boosted to V, the third term in the expression will go to zero. However, if $(1-q)\nu >> k_2$, then the term dominating the reproduction number will be the third term of the expression. Note that when $G = 0$, waning individuals cannot transmit the infection, hence the term related to these infections in 4.4 will not be present. Moreover, if the waning rates k_1 and k_2 are close to zero, hence the immunity is life-long, then 4.4 can be expressed as $\mathcal{R}_c \approx (1-p)\mathcal{R}_0$, which is the expression of the control reproduction number in absence of waning immunity.

When an infection control protocol, as vaccination, is introduced in a population it is important to take into account what is the sufficient proportion of vaccinated individual needed to obtain herd immunity. The reproduction number expression can determine this critical threshold. By setting $\mathcal{R}_c = 1$, it is possible to solve the equation in terms of the proportion p_c.

We will use expression for R_c to obtain vaccination uptake threshold necessary to obtain herd immunity. To achieve that we set $\mathcal{R}_c = 1$ and let $p = p_c$, and solve for p_c:

$$p_c = \left(1 - \frac{1}{\mathcal{R}_0}\right) \frac{(d + k_1)(d + k_2)}{d(d + k_1 + k_2 - Gk_1\nu(1 - q))} \tag{4.5}$$

Note that when $k_1 = k_2 = 0$, Eq. 4.5 simplifies to $p_c = 1 - 1/\mathcal{R}_0$, which is the the critical vaccination threshold, given lifelong immunity.

Since the vaccination coverage assumes values between 0 and 1, we rearrange Eq. 4.5 in order to obtain a condition on the basic reproduction number providing a $p_c \in [0, 1]$.

$$\mathcal{R}_0 < \frac{(d + k_1)(d + k_2)}{k_1k_2 + Gdk_1\nu(1 - q)} \tag{4.6}$$

We use expressions obtained for $\mathcal{R}_c$ and p_c to investigate the region in the parametric space $\mathcal{R}_0 - k_1 - k_2$ where herd immunity due to vaccination is possible (Figure 4.2), by considering the scenarios in which $0\%, 1\%, 20\%, 80\%$ and 100% of individuals experiencing a mild infection are infectious, and so able to transmit the infection, and life expectancy is chosen to be 82 years.

Figure (4.2a) shows the relationship between p_c and $\mathcal{R}_0 \in (1, 18]$, waning rates sampled over the intervals $[1/100, 1]$ (top-row plots) and $[1/300, 1]$ (bottom-row plots), and $\nu(1 - q) = 0, 0.01, 0.2, 0.8, 1$. We start considering $k_1, k_2 \in [1/100, 1]$. We observe that, when all individuals at the waning stage are boosted to V, the vaccination coverage needed to reach herd immunity above 95%, if $\mathcal{R}_0 \approx 5$ and both k_1 and k_2 are extremely small. However, if the basic reproduction number is slightly above 1, herd immunity can be achieved with a lower vaccination coverage ($\approx 40\%$), but long waning periods. We also observe that, as $\nu(1 - q)$ increases, we are able to determine the vaccination threshold coverage only for $\mathcal{R}_0 < 4$ and small waning rates. Moreover, as the proportion of vaccinated infectious cases increases, k_1 is the waning rates that affect p_c. When the waning periods are considered to be 300 years each (bottom-row plots in Figure (4.2a)), we observe the same pattern as the previous case. However, it is possible to indicated the vaccination threshold needed to achieve herd immunity for larger $\mathcal{R}_0$ and for $\nu(1 - q) = 0$. This is visible only when k_1 and k_2 are very small. If $\nu(1 - q)$ increases, reaching herd immunity will be possible only for higher vaccination coverages, smaller reproduction number and small waning rates. We also observe that, for $\nu(1 - q) \leq 0.2$, p_c has a symmetric relationship with k_1 and k_2. However, as the number of secondary cases increases, this relationship is not visible and k_1 becomes more significant to herd immunity achievement, than k_2. Figure (4.2b) captures the combinations of k_1 and k_2 on the threshold condition for the basic reproductive number, given by the right-hand side of Eq.(4.6), providing a $p_c \in [0, 1]$. We observe that the condition $p_c < 1$ holds only when the immunity wanes completely within 200 years or longer (top-row plots) and the reproductive number is below 5. On the other hand, when the waning periods are 300 years each, then $\mathcal{R}_0$ can assume values up to 15. In both scenarios, the critical value of the reproductive number decreases as the proportion of infectious secondary cases increases, $1 - q$.

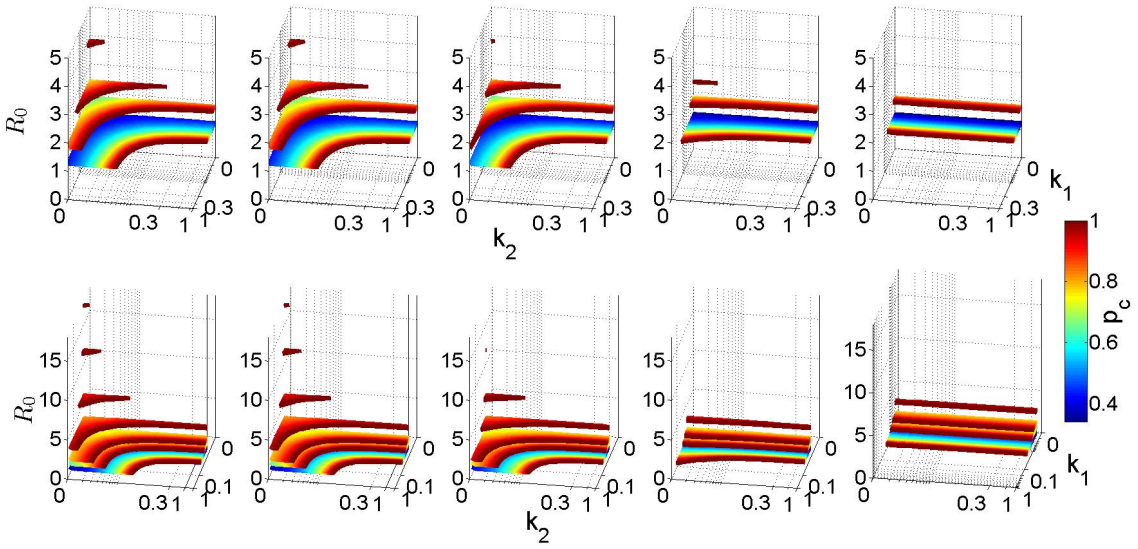

(a)

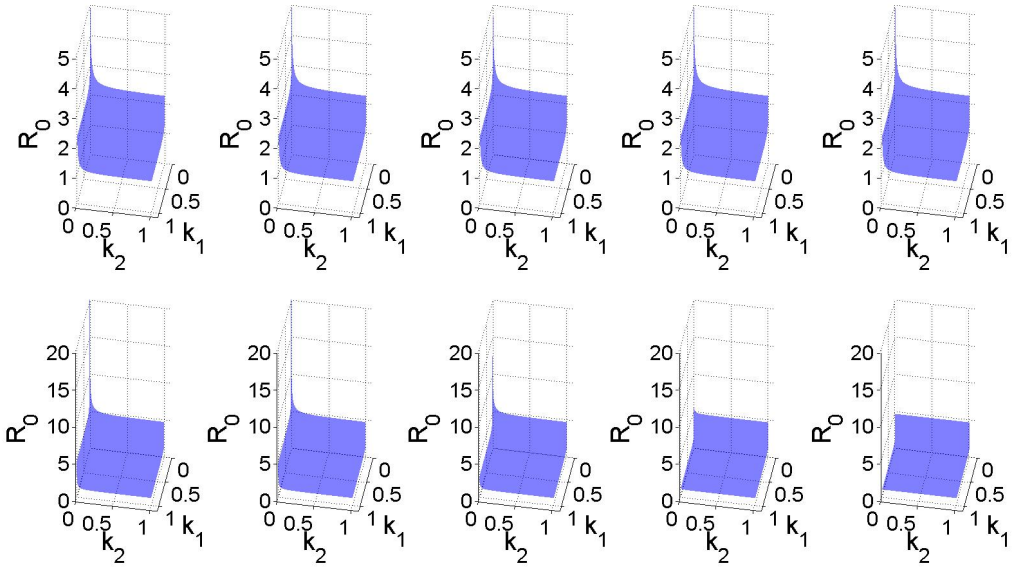

(b)

Figure 4.2: Threshold conditions necessary to obtain herd immunity. Upper rows: $k_1, k_2 \in [1/100, 1]$ and bottom rows: $k_1, k_2 \in [1/300, 1]$ and $\mathcal{R}_0$ given $\nu(1-q) = (0, 0.01, 0.2, 0.8, 1)$ and $d = 1/82$ years^{-1} on (a) threshold condition for vaccination rate p, given different sets of waning periods, ratio of secondary infections and basic reproductive number (b) threshold condition on $\mathcal{R}_0$ necessary to obtain herd immunity as specified by Eq. (4.6). k_1 and k_2 are shown in log-scale.

	Waning periods and vaccination threshold for herd immunity feasibility			
	$\boldsymbol{\nu(1-q)=0.01}$ $\boldsymbol{k_1=k_2=k}$		$\boldsymbol{\nu(1-q)=0.25}$ and $\boldsymbol{k_1 \neq k_2}$ $\boldsymbol{1/k_2=33.3}$ years	
	$\boldsymbol{\mathcal{R}_0=2}$	$\boldsymbol{\mathcal{R}_0=15}$	$\boldsymbol{\mathcal{R}_0=2}$	$\boldsymbol{\mathcal{R}_0=15}$
p	$\boldsymbol{1/k}$ years	$\boldsymbol{1/k}$years	$\boldsymbol{1/k_1}$ years	$\boldsymbol{1/k_1}$ years
0.9	41.7	-	62.5	-
0.92	40	-	58.8	-
0.94	38.5	1000	55.5	9090
0.96	37	416.7	52.6	2222
0.98	35.7	303	50	1265
1	34.5	238	47.6	909

Table 4.3: Vaccination rate $p \in [0.9, 1]$ and waning periods are shown for different $\nu(1-q)$ and basic reproduction number values. When the proportion of "waning" individuals becoming infectious is small, k_1 and k_2 have a symmetric relationship, hence they can be combined and set as $k_1 = k_2 = k$. On the other hand, when that proportion gets bigger, the waning rates do not satisfy the symmetric relationship and $1/k_2$ is fixed as 33.3 years and $1/k_1$ is found and shown on the table.

Our next analysis will keep into account that $p \in [0.9, 1]$ and we investigate the waning periods needed to reach herd immunity. Since the waning rates show different relationships depending on the values of $(1-q)\nu$, we study the cases when $\nu(1-q) = 0.01$ with $k_1 = k_2$ and when $\nu(1-q) = 0.25$ with $k_1 \neq k_2$. We focus our analysis on the waning rate k_1 to investigate which waning period allows herd immunity to be achievable when vaccination coverage is above 90%. Figure (4.3b) shows that, for $\nu(1-q) = 0.25$ and relatively long waning period to become susceptible again, herd immunity can be achieved by a wide range of k_1 and $\mathcal{R}_0$. On the other hand, when $\nu(1-q)$ is fairly small, the interval of of k_1 and $\mathcal{R}_0$ values making the indirect protection possible is smaller (Figure 4.3a). Table 4.3 summarizes the results presented in Figure 4.3 by showing the waning periods necessary to obtain herd immunity when $\mathcal{R}_0 = 2, 15$.

4.2.3 Model with No Age Structure: Stochastic

The deterministic approach of Model 4.1 gives fundamental information on the necessary conditions to obtain full protection against the pathogen in the population. However, it does not provide any details on the probability that, under these conditions, an outbreak can occur. To answer this question, we develop a stochastic model and we investigate the probability of extinction, defined as 0 new cases, and the probability of an outbreak with at least 10 or 150 cumulative cases. We simulate only the transitions related to the infection, by seeding one infectious individual in a population at the DFE with vaccination. We compare the results for different vaccination coverage $p = 0.91, 0.93, 0.96$, $q = 0.2, 0.8$ and, for the waning rates, we consider the following cases:

$$(k_1, k_2) = \{(1/300, 1/300), (1/30, 1/30), (1/50, 1/5), (1/5, 1/50), (1, 1/25)\} \tag{4.7}$$

The cases for k_1 and k_2 were chosen in consultation with Public Health Ontario. Here, we report the results for the life long immunity assumption and $k_1 = k_2$. The other cases, similar to the scenario with 30 years as waning rates, are shown in Appendix H.

Case $k_1 = k_2 = 1/300$

Here, we consider immunity to be life long. We immediately observe that for small reproduction numbers and $G = 0$, the probability of having an outbreak with 10 cases (Figure (4.4a))is extremely small if compared to the probability of extinction. On the other hand, if secondary cases are infectious, we observe how the probability of having 0 cases is still higher than the chance of getting an outbreak, but the difference between the two is not as evident as $G = 0$. Opposite scenario for large reproduction numbers, where the probability of extinction is extremely low and an outbreak will occur with high probability.

Similar results are visible in Figure (4.4b), where the cumulative cases of the outbreak are 150. We observe that for $\mathcal{R}_0 = 6$, $G = 0$ and $q = 0.2, 0.8$ the probability of having a big outbreak is 0. For $G = 1$, this probability can reach 0.34 for $q = 0.2$, but it becomes 0 as q increases. Again, for large reproduction numbers, the probablity of extinction is smaller than the outbreak probability.

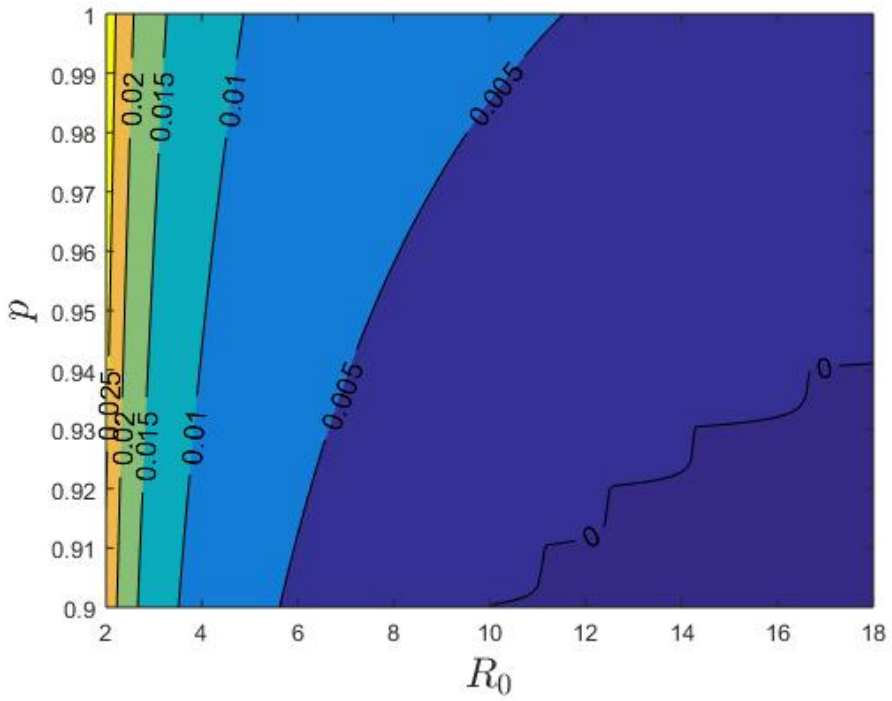

(a)

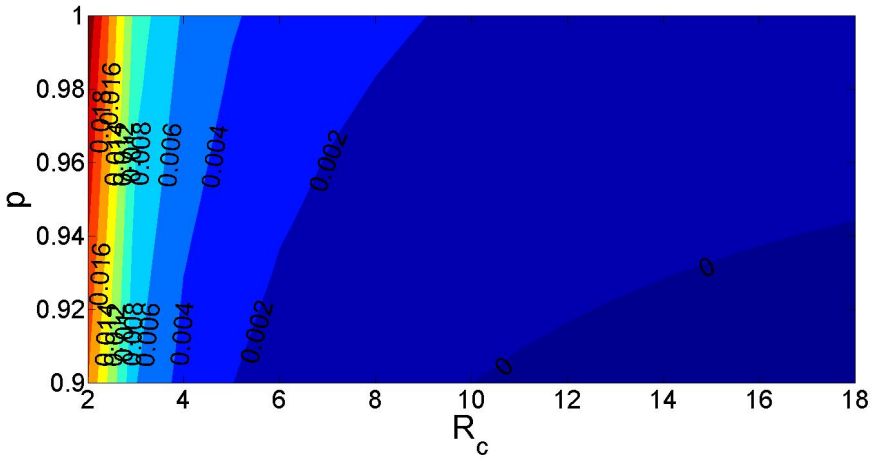

(b)

Figure 4.3: Waning rate k_1 required to obtain herd immunity given $p = [0.9, 1]$, and specific values of k_2, $\mathcal{R}_0$, and $\nu(1-q)$. Level curves (black lines) give the waning rate k_1 that allows herd immunity to be achieved. (a) $\nu(1-q) = 0.01$, $k_1 = k_2 = k$ (b) $\nu(1-q) = 0.25$, $k_2 = 0.03$.

G=0														
				R0=6						R0=18				
		q=0.2			q=0.8			q=0.2				q=0.8		
cases		p=0.91	p=0.93	p=0.96	p=0.91	p=0.93	p=0.96	p=0.91	p=0.93	p=0.96		p=0.91	p=0.93	p=0.96
0		0.41	0.41	0.44	0.50	0.54	0.59	0.18	0.17	0.20		0.27	0.30	0.31
1		0.18	0.18	0.20	0.15	0.17	0.17	0.09	0.09	0.11		0.07	0.09	0.11
2		0.09	0.09	0.11	0.08	0.07	0.08	0.05	0.05	0.08		0.04	0.04	0.06
3		0.05	0.06	0.06	0.04	0.05	0.04	0.03	0.03	0.05		0.02	0.02	0.04
4		0.03	0.04	0.04	0.03	0.02	0.03	0.02	0.03	0.03		0.01	0.02	0.03
5		0.02	0.03	0.03	0.03	0.03	0.01	0.01	0.02	0.02		0.01	0.01	0.01
6		0.02	0.02	0.02	0.02	0.02	0.02	0.01	0.01	0.02		0.01	0.00	0.01
7		0.02	0.02	0.02	0.01	0.01	0.01	0.01	0.01	0.01		0.00	0.01	0.01
8		0.01	0.01	0.01	0.01	0.01	0.01	0.00	0.01	0.01		0.00	0.00	0.01
9		0.02	0.01	0.01	0.01	0.01	0.01	0.00	0.01	0.01		0.00	0.00	0.00
10		0.15	0.13	0.07	0.12	0.07	0.03	0.59	0.57	0.46		0.58	0.50	0.40
G=1														
				R0=6						R0=18				
		q=0.2			q=0.8			q=0.2				q=0.8		
cases		p=0.91	p=0.93	p=0.96	p=0.91	p=0.93	p=0.96	p=0.91	p=0.93	p=0.96		p=0.91	p=0.93	p=0.96
0		0.41	0.39	0.43	0.49	0.53	0.57	0.18	0.20	0.19		0.26	0.29	0.31
1		0.08	0.10	0.11	0.13	0.14	0.15	0.03	0.03	0.04		0.05	0.06	0.07
2		0.05	0.04	0.05	0.07	0.06	0.07	0.01	0.01	0.01		0.02	0.02	0.03
3		0.02	0.03	0.03	0.04	0.04	0.05	0.00	0.00	0.00		0.01	0.01	0.02
4		0.02	0.02	0.03	0.03	0.03	0.02	0.00	0.00	0.00		0.01	0.01	0.01
5		0.01	0.01	0.02	0.02	0.02	0.02	0.00	0.00	0.00		0.00	0.00	0.01
6		0.01	0.01	0.01	0.02	0.02	0.02	0.00	0.00	0.00		0.00	0.00	0.00
7		0.00	0.01	0.01	0.01	0.02	0.01	0.00	0.00	0.00		0.00	0.00	0.00
8		0.01	0.01	0.01	0.01	0.01	0.01	0.00	0.00	0.00		0.00	0.00	0.00
9		0.00	0.00	0.01	0.01	0.01	0.01	0.00	0.00	0.00		0.00	0.00	0.00
10		0.39	0.37	0.29	0.17	0.13	0.06	0.78	0.75	0.75		0.66	0.61	0.54

(a)

G=0														
				R0=6						R0=18				
		q=0.2			q=0.8			q=0.2				q=0.8		
cases		p=0.91	p=0.93	p=0.96	p=0.91	p=0.93	p=0.96	p=0.91	p=0.93	p=0.96		p=0.91	p=0.93	p=0.96
0		0.40	0.42	0.44	0.50	0.54	0.58	0.19	0.18	0.22		0.25	0.27	0.34
1-5		0.37	0.39	0.28	0.33	0.34	0.17	0.20	0.22	0.29		0.15	0.18	0.23
5-10		0.08	0.07	0.11	0.07	0.06	0.13	0.03	0.04	0.07		0.02	0.02	0.04
10-30		0.09	0.09	0.13	0.06	0.05	0.10	0.02	0.03	0.06		0.00	0.01	0.03
30-50		0.03	0.02	0.03	0.02	0.01	0.02	0.00	0.01	0.02		0.00	0.00	0.01
50-70		0.01	0.01	0.01	0.01	0.00	0.01	0.00	0.00	0.00		0.00	0.00	0.00
70-90		0.01	0.00	0.00	0.00	0.00	0.00	0.00	0.00	0.00		0.00	0.00	0.00
90-110		0.01	0.00	0.00	0.00	0.00	0.00	0.00	0.00	0.00		0.00	0.00	0.00
110-130		0.00	0.00	0.00	0.00	0.00	0.00	0.00	0.00	0.00		0.00	0.00	0.00
130-150		0.00	0.00	0.00	0.00	0.00	0.00	0.00	0.00	0.00		0.00	0.00	0.00
150		0.00	0.00	0.00	0.00	0.00	0.00	0.57	0.52	0.34		0.57	0.51	0.34
G=1														
				R0=6						R0=18				
		q=0.2			q=0.8			q=0.2				q=0.8		
cases		p=0.91	p=0.93	p=0.96	p=0.91	p=0.93	p=0.96	p=0.91	p=0.93	p=0.96		p=0.91	p=0.93	p=0.96
0		0.41	0.40	0.44	0.51	0.54	0.58	0.19	0.19	0.21		0.26	0.28	0.31
1-5		0.20	0.21	0.23	0.28	0.29	0.28	0.03	0.04	0.05		0.08	0.11	0.14
5-10		0.03	0.04	0.04	0.06	0.06	0.05	0.00	0.00	0.00		0.00	0.01	0.02
10-30		0.02	0.03	0.05	0.06	0.06	0.06	0.00	0.00	0.00		0.00	0.00	0.00
30-50		0.00	0.00	0.01	0.03	0.02	0.01	0.00	0.00	0.00		0.00	0.00	0.00
50-70		0.00	0.00	0.01	0.02	0.01	0.00	0.00	0.00	0.00		0.00	0.00	0.00
70-90		0.00	0.00	0.01	0.01	0.00	0.00	0.00	0.00	0.00		0.00	0.00	0.00
90-110		0.00	0.00	0.01	0.01	0.01	0.00	0.00	0.00	0.00		0.00	0.00	0.00
110-130		0.00	0.00	0.00	0.01	0.00	0.00	0.00	0.00	0.00		0.00	0.00	0.00
130-150		0.00	0.00	0.00	0.00	0.00	0.00	0.00	0.00	0.00		0.00	0.00	0.00
150		0.34	0.31	0.20	0.02	0.00	0.00	0.78	0.76	0.73		0.66	0.61	0.53

(b)

Figure 4.4: Probability of having extinction, 10 (a) or 150 (b) cases when $G = 0, 1$ for $p = 0.91, 0.93, 0.96$, $q = 0.2, 0.8$ $\mathcal{R}_0 = 6, 18$ and $k_1 = k_2 = 1/300$

Over all, the probability of extinction increase as the vaccination rate and the proportion of waning individuals boosted to V increases.

Case $k_1 = k_2 = 1/30$

Here, the immunity is shorter than life span and the period needed to become fully susceptible is 60 years. A different scenario from the life long immunity is visible. The probability of having an outbreak, with 10 or 150 cumulative cases can occur with very high probability for both small and large reproduction number (Figures (4.5a)- (4.5b). Also, we observe that the probability of extinction increases as the vaccination coverage increases, if we consider the secondary cases not infectious and if $q = 0.8$.

4.2.4 Model with Age Structure: Deterministic

Although Model 4.1 provides meaningful results and insights about the conditions needed to achieve herd immunity and probability of an outbreak, it does not consider any population nor contact structure. The model that we present now incorporates both population and contact structures including age structure as well as vaccination, boosting and waning immunity processes and it follows the same framework used in Model 4.1. The new model will then be based on age structure and the contact rate β will be dependent on the age of both infectious (a) and susceptible (u) individuals, i.e. $\beta(a, u)$. In order to include the mentioned structures and the infection dynamics, we develop a partial-differential equations (PDEs) system. The PDEs system analogous to Model 4.1 is given by:

$$\begin{aligned}\frac{\partial S(t,a)}{\partial t} + \frac{\partial S(t,a)}{\partial a} =& -\mu(a)S(t,a) - S(t,a)\int_0^\infty \beta(a,u)\left[I(t,u) + GI_W(t,u)\right]\,\mathrm{d}u + \\ &+ k_2 W(t,a)\end{aligned} \tag{4.8a}$$

$$\frac{\partial I(t,a)}{\partial t} + \frac{\partial I(t,a)}{\partial a} = S(t,a)\int_0^\infty \beta(a,u)\left[I(t,u) + GI_W(t,u)\right]\,\mathrm{d}u - \mu(a)I(t,a) - \gamma_1 I(t,a) \tag{4.8b}$$

$$\begin{aligned}\frac{\partial I_W(t,a)}{\partial t} + \frac{\partial I_W(t,a)}{\partial a} =& \nu(1-q)W(t,a)\int_0^\infty \beta(a,u)\left(I(t,u) + GI_W(t,u)\right)\,\mathrm{d}u - \\ &- \mu(a)I_W(t,a) - \gamma_2 I(t,a)\end{aligned} \tag{4.8c}$$

$$\frac{\partial R(t,a)}{\partial t} + \frac{\partial R(t,a)}{\partial a} = \gamma_1 I(t,a) + \gamma_2 I_W(t,a) - \mu(a)R(t,a) \tag{4.8d}$$

$$\begin{aligned}\frac{\partial V(t,a)}{\partial t} + \frac{\partial V(t,a)}{\partial a} =& q\nu W(t,a)\int_0^\infty \beta(a,u)\left(I(t,u) + GI_W(t,u)\right)\,\mathrm{d}u \\ &- \mu(a)V(t,a) - k_1 V(t,a)\end{aligned} \tag{4.8e}$$

G=0															
				R0=6							R0=18				
		q=0.2				q=0.8				q=0.2				q=0.8	
cases		p=0.91	p=0.93	p=0.96		p=0.91	p=0.93	p=0.96		p=0.91	p=0.93	p=0.96		p=0.91	p=0.93	p=0.96
0		0.20	0.19	0.20		0.20	0.22	0.22		0.06	0.08	0.07		0.08	0.08	0.10
1		0.05	0.05	0.06		0.04	0.05	0.05		0.02	0.01	0.02		0.01	0.02	0.01
2		0.02	0.02	0.02		0.02	0.02	0.01		0.00	0.01	0.01		0.00	0.00	0.00
3		0.01	0.01	0.01		0.01	0.01	0.01		0.00	0.00	0.00		0.00	0.00	0.00
4		0.00	0.00	0.01		0.00	0.01	0.00		0.00	0.00	0.00		0.00	0.00	0.00
5		0.00	0.00	0.00		0.00	0.00	0.00		0.00	0.00	0.00		0.00	0.00	0.00
6		0.00	0.00	0.00		0.00	0.00	0.00		0.00	0.00	0.00		0.00	0.00	0.00
7		0.00	0.00	0.00		0.00	0.00	0.00		0.00	0.00	0.00		0.00	0.00	0.00
8		0.00	0.00	0.00		0.00	0.00	0.00		0.00	0.00	0.00		0.00	0.00	0.00
9		0.00	0.00	0.00		0.00	0.00	0.00		0.00	0.00	0.00		0.00	0.00	0.00
10		0.72	0.71	0.70		0.71	0.71	0.69		0.92	0.90	0.90		0.91	0.90	0.89
G=1															
				R0=6							R0=18				
		q=0.2				q=0.8				q=0.2				q=0.8	
cases		p=0.91	p=0.93	p=0.96		p=0.91	p=0.93	p=0.96		p=0.91	p=0.93	p=0.96		p=0.91	p=0.93	p=0.96
0		0.19	0.19	0.19		0.21	0.21	0.23		0.07	0.07	0.08		0.08	0.08	0.09
1		0.03	0.03	0.03		0.03	0.04	0.04		0.00	0.01	0.01		0.01	0.01	0.01
2		0.01	0.02	0.01		0.01	0.01	0.01		0.00	0.00	0.00		0.00	0.00	0.00
3		0.00	0.01	0.00		0.01	0.01	0.00		0.00	0.00	0.00		0.00	0.00	0.00
4		0.00	0.00	0.00		0.00	0.00	0.00		0.00	0.00	0.00		0.00	0.00	0.00
5		0.00	0.00	0.00		0.00	0.00	0.00		0.00	0.00	0.00		0.00	0.00	0.00
6		0.00	0.00	0.00		0.00	0.00	0.00		0.00	0.00	0.00		0.00	0.00	0.00
7		0.00	0.00	0.00		0.00	0.00	0.00		0.00	0.00	0.00		0.00	0.00	0.00
8		0.00	0.00	0.00		0.00	0.00	0.00		0.00	0.00	0.00		0.00	0.00	0.00
9		0.00	0.00	0.00		0.00	0.00	0.00		0.00	0.00	0.00		0.00	0.00	0.00
10		0.77	0.76	0.76		0.73	0.73	0.70		0.93	0.93	0.92		0.91	0.91	0.90

(a)

G=0															
				R0=6							R0=18				
		q=0.2				q=0.8				q=0.2				q=0.8	
cases		p=0.91	p=0.93	p=0.96		p=0.91	p=0.93	p=0.96		p=0.91	p=0.93	p=0.96		p=0.91	p=0.93	p=0.96
0		0.18	0.18	0.19		0.22	0.21	0.23		0.07	0.06	0.07		0.08	0.08	0.09
1-5		0.09	0.11	0.10		0.07	0.08	0.08		0.02	0.03	0.03		0.01	0.02	0.01
5-10		0.01	0.01	0.01		0.00	0.00	0.00		0.00	0.00	0.00		0.00	0.00	0.00
10-30		0.00	0.00	0.00		0.00	0.00	0.00		0.00	0.00	0.00		0.00	0.00	0.00
30-50		0.00	0.00	0.00		0.00	0.00	0.00		0.00	0.00	0.00		0.00	0.00	0.00
50-70		0.00	0.00	0.00		0.00	0.00	0.00		0.00	0.00	0.00		0.00	0.00	0.00
70-90		0.00	0.00	0.00		0.00	0.00	0.00		0.00	0.00	0.00		0.00	0.00	0.00
90-110		0.00	0.00	0.00		0.00	0.00	0.00		0.00	0.00	0.00		0.00	0.00	0.00
110-130		0.00	0.00	0.00		0.00	0.00	0.00		0.00	0.00	0.00		0.00	0.00	0.00
130-150		0.00	0.00	0.00		0.00	0.00	0.00		0.00	0.00	0.00		0.00	0.00	0.00
150		0.73	0.70	0.71		0.71	0.70	0.69		0.90	0.91	0.91		0.91	0.91	0.90
G=1															
				R0=6							R0=18				
		q=0.2				q=0.8				q=0.2				q=0.8	
cases		p=0.91	p=0.93	p=0.96		p=0.91	p=0.93	p=0.96		p=0.91	p=0.93	p=0.96		p=0.91	p=0.93	p=0.96
0		0.18	0.19	0.19		0.21	0.22	0.22		0.07	0.07	0.08		0.08	0.08	0.09
1-5		0.05	0.05	0.05		0.06	0.05	0.06		0.01	0.01	0.01		0.01	0.01	0.01
5-10		0.00	0.00	0.00		0.00	0.00	0.00		0.00	0.00	0.00		0.00	0.00	0.00
10-30		0.00	0.00	0.00		0.00	0.00	0.00		0.00	0.00	0.00		0.00	0.00	0.00
30-50		0.00	0.00	0.00		0.00	0.00	0.00		0.00	0.00	0.00		0.00	0.00	0.00
50-70		0.00	0.00	0.00		0.00	0.00	0.00		0.00	0.00	0.00		0.00	0.00	0.00
70-90		0.00	0.00	0.00		0.00	0.00	0.00		0.00	0.00	0.00		0.00	0.00	0.00
90-110		0.00	0.00	0.00		0.00	0.00	0.00		0.00	0.00	0.00		0.00	0.00	0.00
110-130		0.00	0.00	0.00		0.00	0.00	0.00		0.00	0.00	0.00		0.00	0.00	0.00
130-150		0.00	0.00	0.00		0.00	0.00	0.00		0.00	0.00	0.00		0.00	0.00	0.00
150		0.77	0.77	0.76		0.73	0.73	0.72		0.92	0.92	0.91		0.91	0.91	0.91

(b)

Figure 4.5: Probability of having extinction, 10 (a) or 150 (b) cases when $G = 0, 1$ for $p = 0.91, 0.93, 0.96$, $q = 0.2, 0.8$ $\mathcal{R}_0 = 6, 18$ and and $k_1 = k_2 = 1/30$

$$\frac{\partial W(t,a)}{\partial t} + \frac{\partial W(t,a)}{\partial a} = k_1 V(t,a) - \mu(a) W(t,a) - k_2 W(t,a) - \\ - q\nu W(t,a) \int_0^\infty \beta(a,u) \left(I(t,u) + G I_W(t,u) \right) \, \mathrm{d}u \tag{4.8f}$$

with:

$$\begin{aligned} S(t,0) &= d(1-p) \\ V(t,0) &= dp \\ I(t,0) &= I_W(t,0) = R(t,0) = W(t,0) = 0 \end{aligned}$$

and some age distribution of the population at the initial time $t = 0$. Similar to the model with no age structure, we assume that the population is set at steady equilibrium age distribution and the total population, defined as $N = S + I + R + V + W$, is determined by the following equation:

$$\frac{\partial N}{\partial t} + \frac{\partial N}{\partial a} = -\mu(a) N(t,a)$$

with $N(t,0) = d$ and $\int_0^\infty N(t,a)\,\mathrm{d}a = 1$, for all t.

In order to obtain a system of ODEs, we discretize the system 4.8 by following Hethcote et al. [74]. We first divide the age interval $[0,\infty)$ into n small subintervals: $[a_{i-1}, a_i]$, for $i = 1 \ldots n$ with $a_n = \infty$. The population is then divided into groups depending on the subintervals, and each compartment is defined as

$$X_i = \int_{a_{i-1}}^{a_i} X(t,a)\,\mathrm{d}a$$

where X can be defined as S, I, I_W, R, V and W or N. Observe that the infection rate previously defined as $\beta(u,a)$, will be now referred as $\beta_{i,j}$, indicating the rate at which a person in j age interval infects an individual in i age interval. Moreover, the death rate is now age-dependent and it will be represented by μ_i. Since our model keeps account of the vaccination process, we assume that only one shot is given to children when they turn 12 months old.
The system of ODEs is given by:

$$\frac{\mathrm{d}S_1}{\mathrm{d}t} = d - (\mu_1 + c_1) S_1 - S_1 \sum_{j=1}^{n} \beta_{1,j} (I_j + G I_{W_j}) \tag{4.10a}$$

$$\frac{\mathrm{d}S_2}{\mathrm{d}t} = (1-p) c_1 S_1 - (\mu_2 + c_2) S_2 - S_2 \sum_{j=1}^{n} \beta_{2,j} (I_j + G I_{W_j}) + k_2 W_2 \tag{4.10b}$$

$$\frac{\mathrm{d}S_i}{\mathrm{d}t} = c_{i-1} S_{i-1} - (\mu_i + c_i) S_i - S_i \sum_{j=1}^{n} \beta_{i,j} (I_j + G I_{W_j}) + k_2 W_i \ , \ i = 3 \ldots n-1 \tag{4.10c}$$

$$\frac{\mathrm{d}S_n}{\mathrm{d}t} = c_{n-1}S_{n-1} - \mu_n S_n - S_n \sum_{j=1}^{n} \beta_{n,j}(I_j + GI_{W_j}) + k_2 W_n \tag{4.10d}$$

$$\frac{\mathrm{d}I_1}{\mathrm{d}t} = -(\mu_1 + c_1)I_1 + S_1 \sum_{j=1}^{n} \beta_{1,j}(I_j + GI_{W_j}) - \gamma_1 I_1 \tag{4.10e}$$

$$\frac{\mathrm{d}I_2}{\mathrm{d}t} = c_1 I_1 - (\mu_2 + c_2)I_2 + S_2 \sum_{j=1}^{n} \beta_{2,j}(I_j + GI_{W_j}) - \gamma_1 I_2 \tag{4.10f}$$

$$\frac{\mathrm{d}I_i}{\mathrm{d}t} = c_{i-1}I_{i-1} - (\mu_i + c_i)I_i + S_i \sum_{j=1}^{n} \beta_{i,j}(I_j + GI_{W_j}) - \gamma_1 I_i \ , \ i = 3 \dots n-1 \tag{4.10g}$$

$$\frac{\mathrm{d}I_n}{\mathrm{d}t} = c_{n-1}I_{n-1} - \mu_n I_n + S_n \sum_{j=1}^{n} \beta_{n,j}(I_j + GI_{W_j}) - \gamma_1 I_n \tag{4.10h}$$

$$\frac{\mathrm{d}I_{W_1}}{\mathrm{d}t} = 0 \tag{4.10i}$$

$$\frac{\mathrm{d}I_{W_2}}{\mathrm{d}t} = -(c_2 + \mu_2)I_{W_2} + \nu(1-q)W_2 \sum_{j=1}^{n} \beta_{2,j}(I_j + GI_{W_j}) - \gamma_2 I_{W_2} \tag{4.10j}$$

$$\frac{\mathrm{d}I_{W_i}}{\mathrm{d}t} = c_{i-1}I_{W_{i-1}} - (c_i + \mu_i)I_{W_i} + \nu(1-q)W_i \sum_{j=1}^{n} \beta_{i,j}(I_j + GI_{W_j}) - \gamma_2 I_{W_i} \ , \ i = 3 \dots n-1 \tag{4.10k}$$

$$\frac{\mathrm{d}I_{W_n}}{\mathrm{d}t} = c_{n-1}I_{W_{n-1}} - \mu_n I_{W_n} + \nu(1-q)W_n \sum_{j=1}^{n} \beta_{n,j}(I_j + GI_{W_j}) - \gamma_2 I_{W_n} \tag{4.10l}$$

$$\frac{\mathrm{d}R_1}{\mathrm{d}t} = -(\mu_1 + c_1)R_1 + \gamma_1 I_1 \tag{4.10m}$$

$$\frac{\mathrm{d}R_2}{\mathrm{d}t} = c_1 R_1 - (\mu_2 + c_2)R_2 + \gamma_1 I_1 + \gamma_2 I_{W_2} \tag{4.10n}$$

$$\frac{\mathrm{d}R_i}{\mathrm{d}t} = c_{i-1}R_{i-1} - (\mu_i + c_i)R_i + \gamma_1 I_i + \gamma_2 I_{W_i} \ , \ i = 3 \dots n-1 \tag{4.10o}$$

$$\frac{\mathrm{d}R_n}{\mathrm{d}t} = c_{n-1}R_{n-1} - \mu_n R_n + \gamma_1 I_n + \gamma_2 I_{W_n} \tag{4.10p}$$

$$\frac{\mathrm{d}V_1}{\mathrm{d}t} = 0 \tag{4.10q}$$

$$\frac{\mathrm{d}V_2}{\mathrm{d}t} = pc_1 S_1 - (\mu_2 + c_2 + k_1)V_2 + q\nu W_2 \sum_{j=1}^{n} \beta_{2,j}(I_j + GI_{W_j}) \tag{4.10r}$$

$$\frac{\mathrm{d}V_i}{\mathrm{d}t} = c_{i-1}V_{i-1} - (\mu_i + c_i + k_1)V_i + q\nu W_i \sum_{j=1}^{n} \beta_{i,j}(I_j + GI_{W_j}) \ , \ i = 3 \dots n-1 \tag{4.10s}$$

$$\frac{\mathrm{d}V_n}{\mathrm{d}t} = c_{n-1}V_{n-1} - (\mu_n + k_1)V_n + q\nu W_n \sum_{j=1}^{n} \beta_{n,j}(I_j + GI_{W_j}) \tag{4.10t}$$

$$\frac{\mathrm{d}W_1}{\mathrm{d}t} = 0 \tag{4.10u}$$

$$\frac{\mathrm{d}W_2}{\mathrm{d}t} = k_1 V_2 - (\mu_2 + k_2 + c_2)W_2 - \nu W_2 \sum_{j=1}^{n} \beta_{2,j}(I_j + GI_{W_j}) \tag{4.10v}$$

$$\frac{\mathrm{d}W_i}{\mathrm{d}t} = c_{i-1}W_{i-1} + k_1 V_i - (\mu_i + k_2 + c_i)W_i - \nu W_i \sum_{j=1}^{n} \beta_{i,j}(I_j + GI_{W_j}),\ i = 3 \ldots n-1 \tag{4.10w}$$

$$\frac{\mathrm{d}W_n}{\mathrm{d}t} = c_{n-1}W_{i-1} + k_1 V_n - (\mu_n + k_2)W_n - \nu W_n \sum_{j=1}^{n} \beta_{n,j}(I_j + GI_{W_j}) \tag{4.10x}$$

Here, the value c_i represents the rate at which individuals leave the age compartment i (i.e. aging rate). Assuming that the total population is at the steady state, we define c_i as follows:

$$c_i = \frac{\mu_i}{exp\left[\mu_i(a_i - a_{i+1})\right] - 1}\ ,\ i = 1 \ldots n\ . \tag{4.11}$$

where $c_0 = 1$ and $c_n = 0$. Since the death rates for some of the age groups are 0, we approximate c_i, using Taylor expansion, as follows:

$$c_i \approx \frac{1}{a_i - a_{i+1}}\ .$$

The demographics dynamic of each group is given by:

$$N_1 = d - (\mu_1 + c_1)N_1 \tag{4.12a}$$

$$N_2 = c_1 N_1 - (\mu_2 + c_2)N_2 \tag{4.12b}$$

$$\vdots \tag{4.12c}$$

$$N_n = c_{n-1}N_{n-1} - \mu_n N_n \tag{4.12d}$$

The total population dynamic is obtained by adding up the equations in (4.12) and it is given by:

$$\frac{\mathrm{d}N}{\mathrm{d}t} = d - N\frac{\sum_{i=1}^{n}\mu_i N_i}{N} \tag{4.13}$$

Given the ODEs in System 4.10, we derive the disease-free equilibrium in absence of vaccination as $I_i = I_{W_i} = R_i = V_i = W_i = 0$ and

$$S_i = d\frac{\prod_{j=1}^{i} c_{j-1}}{\prod_{j=1}^{i}\mu_j + c_j}\ ,\ \text{for } i = 1 \ldots n\ . \tag{4.14}$$

Parameters

For Model 4.10, we consider 19 age groups defined in the following intervals:

$$a_1 = [0.5, 1)\ ,\ a_2 = [1, 5)\ ,\ a_3 = [5, 10),\ \ldots\ ,\ a_{18} = [80, 85)\ ,\ a_{19} = [85, \infty)\ .$$

These age groups are used to estimate parameters as aging rates c_i, death rates μ_i and contact rates $\beta_{i,j}$. In order to evaluate the mentioned parameters, we consult data provided by WHO [121] and Mossong et al. [69], given in Appendix G. The death rates are approximated by using data given by [121] related to males, shown in Figure G.1. Observe that our youngest age group is $a_1 = [0.5, 1)$, while in the WHO [121] table, the first age group includes all children aged less than 1 year old, we, hence, assume that the death rate for the age group $a_1 = [0.5, 1)$ is 0.0025. We estimated the average death rate (d) of the population to be 0.0128. This approximation was obtained by adding all the groups of the disease-free equilibrium (in Eq. (4.14)), substituting the estimate of the aging rate c_i, setting the sum equal to 1 and solved the equation for d.

Since an age-structured model is employed, it is necessary to identify the age-specific contact rates. In order to approximate the values of $\beta_{i,j}$, we used the contact matrices provided by Mossong et al. [69]. Specifically, we used the matrix for The Netherlands (G.1), since their demographics structure is similar to the Canadian one. However, the data reported in this matrix does not provide any contact structure for age group $[0.5, 1)$ and age groups older than 70 years. Hence, it was necessary to make some assumptions. By dividing the age interval 0-4 years into smaller interval of 6 months each, children in the age group $6 - 12$ months produce $1/10$ of the total contacts occurring in the original interval. Children in the age group $[1, 4)$ are responsible for $8/10$ of the contacts. For the elderly groups, since individuals aged more than 70 years are divided into four sub-groups, the interval $[70, +\infty)$ is divided into 4, and their contact rates are given according to the male population size of each sub-group.

The average infection period of measles is considered to be two weeks, then, we set the recovery rates $\gamma = \gamma_1 = \gamma_2 = 52/2$ years^{-1}. The proportion of vaccinated individuals, p, is assumed to be sampled in the interval $[0, 1]$. The waning rates, k_1 and k_2, are taken in the interval $(0, 1]$. We assume that all individuals are encountering the pathogen and that the fraction of boosted people, q, (to V or R) is taken in the interval $[0, 1]$.

Results

Disease Free Equilibrium (DFE)

Similar to Model 4.1, we derive the control reproduction numbers for the age-structured models. The disease-free equilibrium with vaccination for Model 4.8 is given by:

$$S_1 = \frac{d}{\mu_1 + c_1} \tag{4.15a}$$

$$V_1 = 0 \tag{4.15b}$$

$$V_2 = \frac{pc_1}{\mu_2 + c_2 + k_1} S_1 \tag{4.15c}$$

$$V_i = \frac{c_{i-1}}{\mu_i + c_i + k_1} V_{i-1} \ , \ i = 3, \ldots, n-1 \tag{4.15d}$$

$$V_n = \frac{c_{n-1}}{\mu_n + k_1} V_{n-1} \tag{4.15e}$$

$$W_1 = 0 \tag{4.15f}$$

$$W_2 = \frac{k_1}{\mu_2 + c_2 + k_2} V_2 \tag{4.15g}$$

$$W_i = \frac{c_{i-1}}{\mu_i + c_i + k_2} W_{i-1} + \frac{k_1}{\mu_i + c_i + k_2} V_i \ , \ 3 = 1, \ldots, n-1 \tag{4.15h}$$

$$W_n = \frac{c_{n-1}}{\mu_n + k_2} W_{n-1} + \frac{k_1}{\mu_n + k_2} Vn \tag{4.15i}$$

$$S_2 = \frac{(1-p)c_1}{\mu_2 + c_2} S_1 + \frac{k_2}{\mu_2 + c_2} W_2 \tag{4.15j}$$

$$S_i = \frac{c_{i-1}}{\mu_i + c_i} S_{i-1} + \frac{k_2}{\mu_i + c_i} W_i \ , \ i = 3, \ldots, n-1 \tag{4.15k}$$

$$S_n = \frac{c_{n-1}}{\mu_n} S_{n-1} + \frac{k_2}{\mu_n} W_n \tag{4.15l}$$

Basic and Control Reproduction Numbers ($\mathcal{R}_0$ and $\mathcal{R}_c$)

The expression for the control reproduction number is found by using the *next-generation matrix method* [88]. We define the matrix F as follows:

$$F^1_{i,j} = \beta_{i,j} \left[S_i + \nu(1-q) W_i \right]$$

$$F^2_{i,j} = \beta_{i,j} S_i$$

for system (4.10), for $G = 1$ and $G = 0$, respectively. Observe that S_i and W_i represent the terms of susceptible and individuals in the waning stage at the disease free equilibrium. The matrix V is defined as follows:

$$\begin{aligned} \mathcal{V}_{i,i-1} = & \quad -c_{i-1} \\ \mathcal{V}_{i,i} = & \quad \mu_i + c_i + \gamma \end{aligned}$$

and

$$\begin{aligned} \mathcal{V}_{1,1} = & \quad \mu_1 + c_1 + \gamma \\ \mathcal{V}_{19,18} = & \quad -c_{18} \\ \mathcal{V}_{19,19} = & \quad \mu_{19} + \gamma \end{aligned}$$

for $1 < i < 19$. In both $F^{1,2}$ and $\mathcal{V}$ all the remaining entries are zero. Similar to Eq. (4.4), $\mathcal{R}_c$ is given by the spectral radius of $F^1\mathcal{V}^{-1}$ and $F^2\mathcal{V}^{-1}$.

We investigate the achievement of herd immunity (i.e. $\mathcal{R}_c < 1$) in relation to waning rates, boosting, vaccination coverage and $\mathcal{R}_0$. For our analyses, we fix the waning rates as defined in Eq. 4.7. Observe that the blue and red surfaces, in Figure (4.6) and Figure (4.7), represent the threshold $\mathcal{R}_c = 1$ when $G = 1$ and $G = 0$, respectively. For $G = 1$, we explore only the case for the smallest basic reproduction number,$\mathcal{R}_0 = 6$ (Figure (4.6)). This

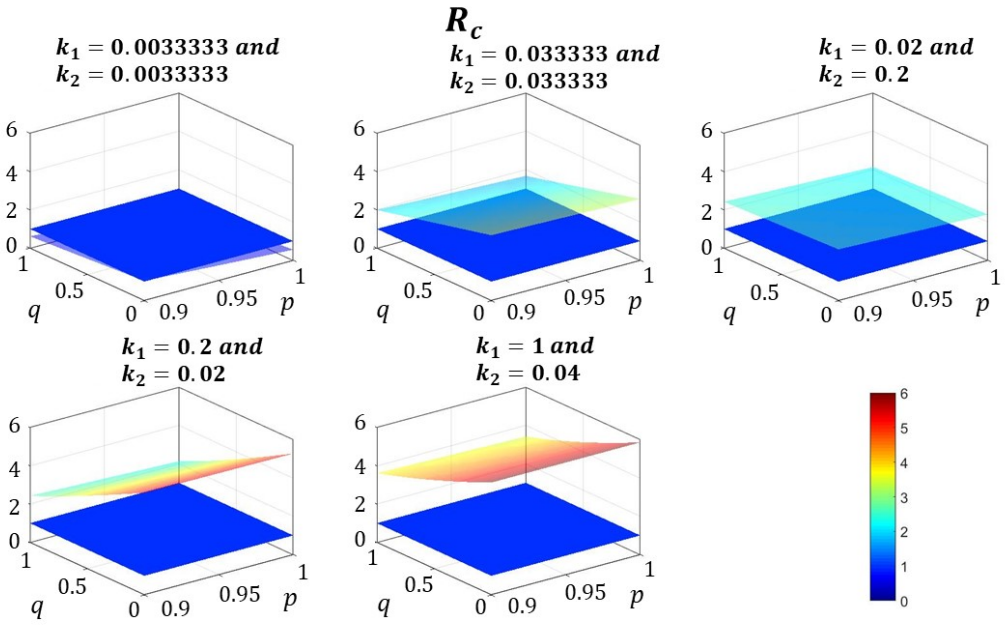

Figure 4.6: Surface plots of control reproductive number for $G = 1, \mathcal{R}_0 = 6$ in the single-dose framework for Model (4.10). The blue surface indicates the threshold $\mathcal{R}_c = 1$.

is because numerical investigations show that higher values do not provide any condition making herd immunity achievable, and they are not reported. We sample $q, p \in [0, 1]$ and we explore when herd immunity is achievable. Figure 4.6 shows that when immunity is life long ($k_1 = k_2 = 1/300$) herd immunity is achievable for a wide interval of p and q. However, as the waning rates increase, $\mathcal{R}_c$ appears to always obtain values greater than 1 and, hence, the indirect protection is no longer achievable. Moreover, note that $\mathcal{R}_c$ presents a significant sensitivity to the waning rate k_1 (from V to W). In fact, the slope of the surface increases visibly as k_1 increases. The number of new infected generated when $G = 0$ (Figure (4.7)) does not depend on the individuals who become infectious after the exposure to the virus. Hence, we study $\mathcal{R}_c$ in relation to different basic reproduction numbers ($\mathcal{R}_0 \in [6, 20]$) and p by fixing the waning rates as before. Figure 4.7 shows that herd immunity is achievable only when the immunity is life-long (Fig 4.7a). In particular, $\mathcal{R}_c$ is always less than 1 for fairly small $\mathcal{R}_0$ (6-8), while for $\mathcal{R}_0 > 14$ herd immunity is achievable when the vaccination coverage exceed 94%. Similar to the previous case, the indirect protection is not obtainable when the waning periods become shorter. Moreover, the figure shows the sensitivity of k_1 on the control reproduction number.

Numerical Results

The next investigation will be on the immunity distribution of the population. We first show the age distribution related to system (4.10) (Figure 4.8). Observe that the distribution presents a decreasing trend, starting at age group 5-9 years, which stops at the last age group which corresponds to all the individuals aged 85+. Next, we study the immunity distribution at the disease free equilibrium with vaccination, which is the same for both cases $G = 0, 1$, when the waning periods are set as Eq.(4.7) and the probability rate p is set as 0.91,0.93 and 0.96 (Figure 4.9). Observe that the distribution is presented as a fraction of the respective age interval.

It is visible how the distribution of susceptible individuals shows an increasing trend over the years and its ratio becomes more evident as the waning period to return to S compartment (k_2) increases. This result shows that the elderly are more at risk of infection in case of an outbreak than the youngest age groups. Moreover, as expected the susceptible tendency decreases as the vaccination coverage increases. Observe that individuals in W show a different pattern:1. when immunity is life long (top-row plot of Figure 4.9) the youngest age groups do not show any proportion in the waning compartment, while elderly groups show a small percentage of individual waning their immunity; 2. when the waning period is shorter than the life span (last three rows plots of Figure 4.9), we observe that the distribution of W is even for $k_1 = 1/50, k_2 = 1/5$ case, even if it is slightly more evident among young age groups. In all the other cases the individuals in the waning stage are clustered in the youngest age groups (1-4 to 30-34 years).

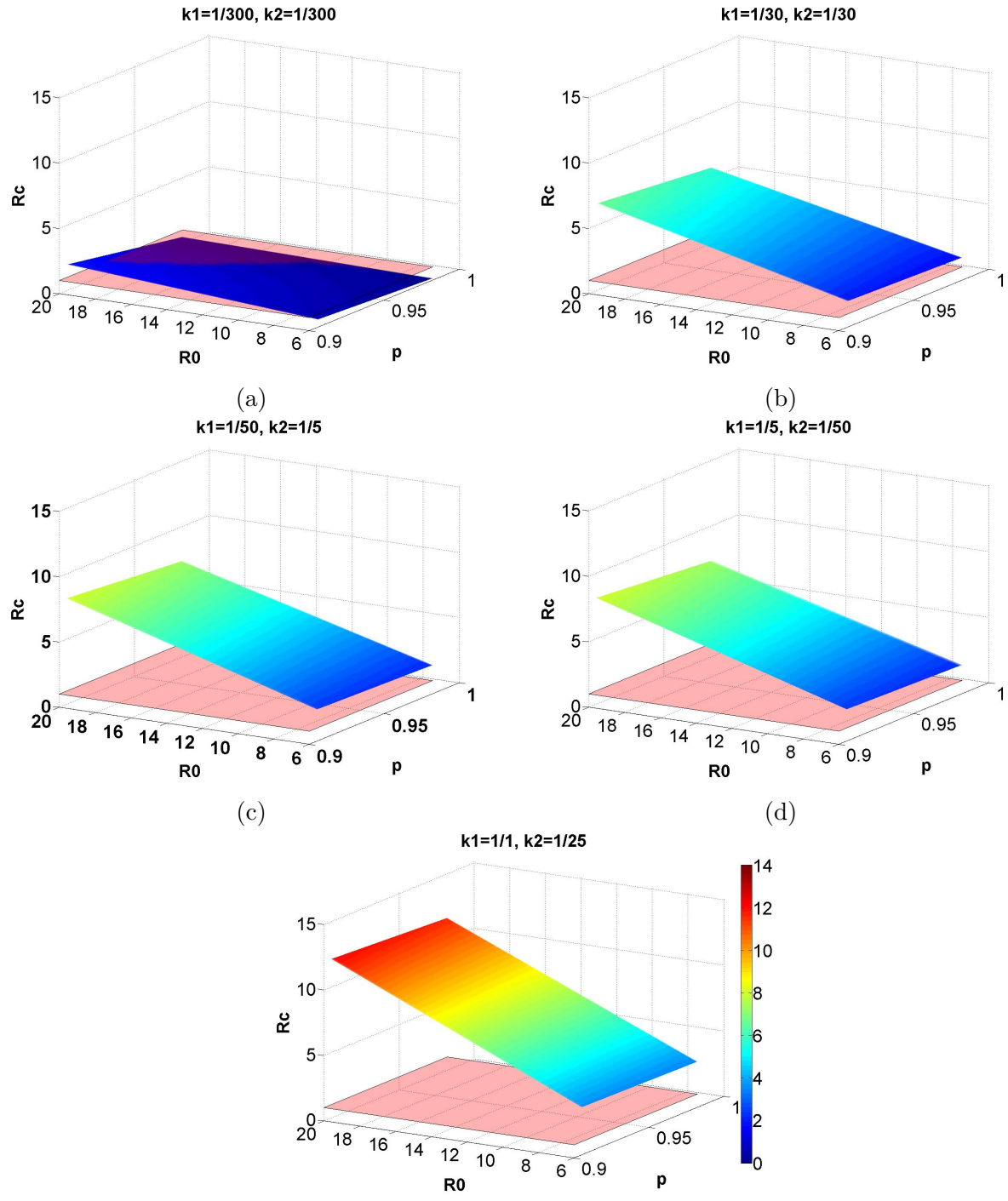

Figure 4.7: Surface plots of control reproductive number for $G = 0$ in the single-dose framework for Model (4.10). The red surface indicates the threshold $\mathcal{R}_c = 1$.

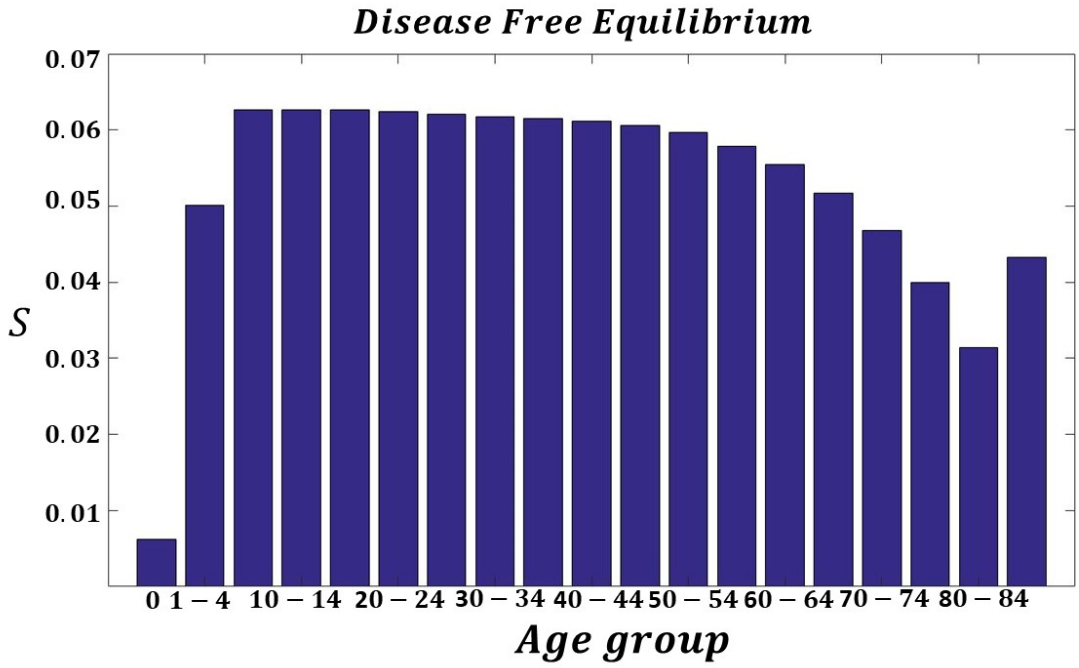

Figure 4.8: Age distribution of the population

Endemic Equilibrium

Now, we examine the immunity distribution at the endemic equilibrium for different p and $\mathcal{R}_0$. We assume all individuals encounter the pathogen and then their immunity is boosted. The fraction q is set as $0.2, 0.8$ and $p = 0.91, 0.93, 0.96$. The waning rates will be chosen according to Eq.(4.7). We study the distribution of the population by looking at the individuals in S, R, V, W and, separately, at the infected individuals that can encounter primary infection (I) and secondary infection (I_W).
We consider the following cases:

Case $k_1 = k_2 = 1/300$

This section describes the life-long immunity scenario (i.e. the total waning period to become fully susceptible is 600 years). Figures (4.6) and (4.7) show that herd immunity is achievable for small $\mathcal{R}_0$. When the basic reproduction number assumes values ≥ 12, the case describing non-infectious secondary cases ($G = 0$) appears to be more likely to present herd immunity (bottom-row plots in Figures 4.10a-4.10b and 4.12a-4.12b). When secondary cases are as infectious as primary ones, herd immunity is no more feasible for $\mathcal{R}_0 \geq 18$ (top-row plots in Figures 4.10a-4.10b and 4.12a-4.12b). Note that individuals in the waning stage are mostly distributed among the elderly age groups and their ratio is drastically smaller if compared to the vaccinated one. Furthermore, we observe that when infection persists, the distribution of infected individuals is bi-modal showing the highest peak at age group 5-9 years and a second peak, at age group 34-39 years. These peaks become less visible as the vaccination coverage increases (Figures 4.11a and 4.13a). As expected, as q increases, this distribution is more affected by individuals encountering the primary infection.

Case $k_1 = k_2 = 1/30$

In this section we assume that the total waning period is 60 years, which is shorter that the average lifespan (82 years). Contrary to the life-long immunity case, in this scenario herd immunity is never achievable (even when $\mathcal{R}_0$ assumes small values). Observe that even if the ratio of susceptible becomes less visible as $\mathcal{R}_0$ increases (Figures 4.14a-4.14b and 4.16a-4.16b), it appears to be more prevalent when secondary cases are not infectious (bottom-row plots). Moreover, observe that the ratios of W and S present a sharp drop at the age group 25-29 years due to the waning immunity process. After this age group, we also observe that vaccination ratios are slowly increasing and this is due to the contribution of individuals with waning immunity. Similar to the previously observed pattern, the infected curve shows a bimodal trend with peaks visible at age group 5-9 years and 30-35 years. This second peak reflects the sudden decrease observed in S and W compartments. Note that for $\mathcal{R}_0 = 12$ as the proportion of vaccinated individuals increases and secondary cases decreases, the magnitude of the first peak decreases becoming smaller than the one at age group 30-35 years (Figures 4.15a-4.15b). For larger $\mathcal{R}_0 \geq 18$, when secondary cases are able to transmit the infection, the first peak at age group 5-9 years is sustained for different vaccination rates

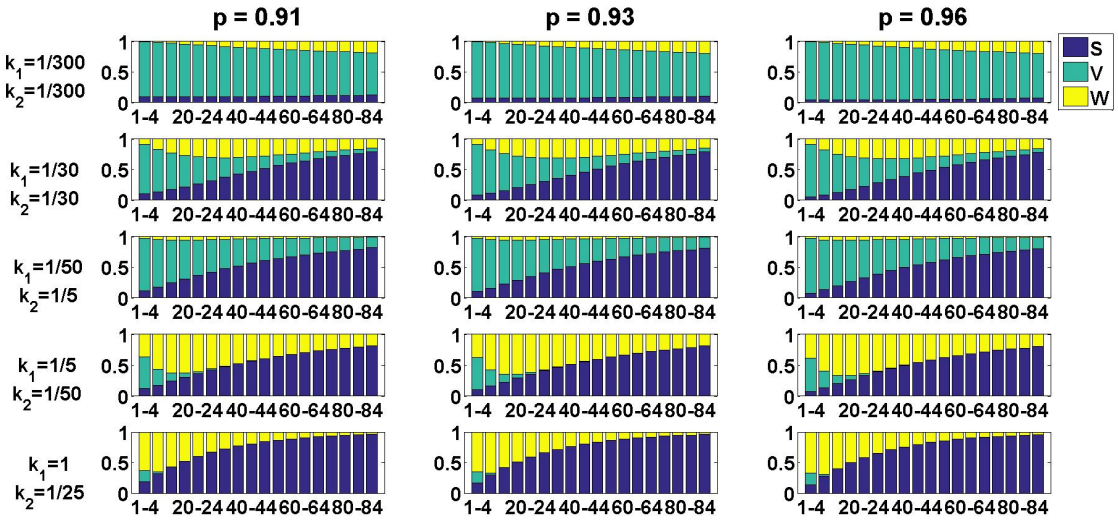

Figure 4.9: Distribution of susceptible, vaccinated and waning compartments at the disease-free equilibrium with vaccination.

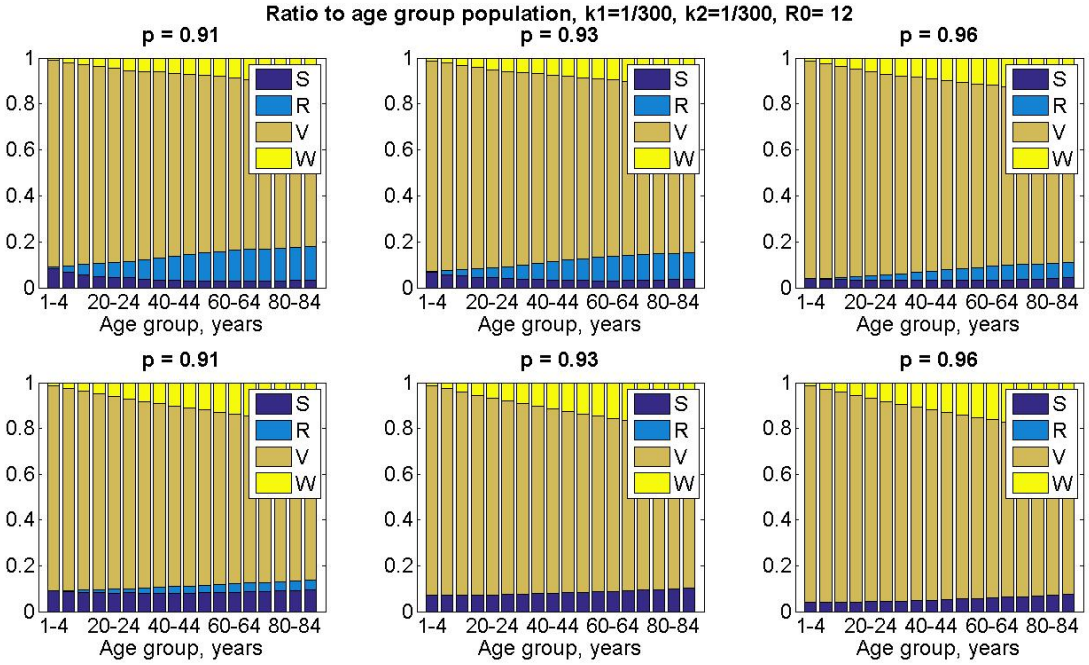

(a)

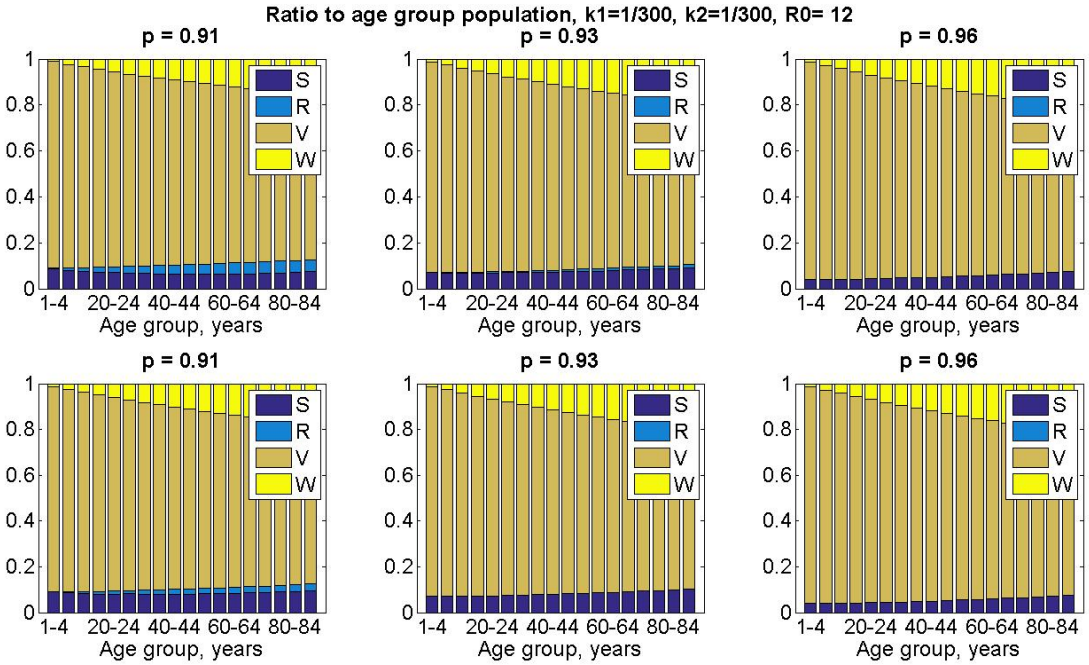

(b)

Figure 4.10: Distribution of (a-b) susceptible, recovered, vaccinated and waning compartments for $R_0 = 12$ and $q = 0.2, 0.8$, respectively. The top-row plots describe the scenario when $G = 1$, while bottom-row plots describe the scenario when $G = 0$

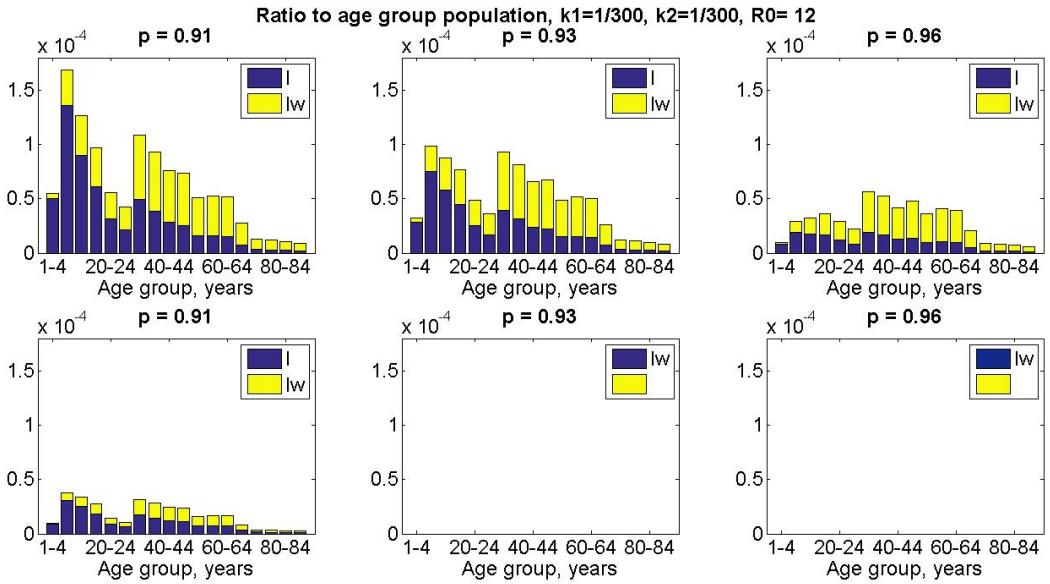

(a)

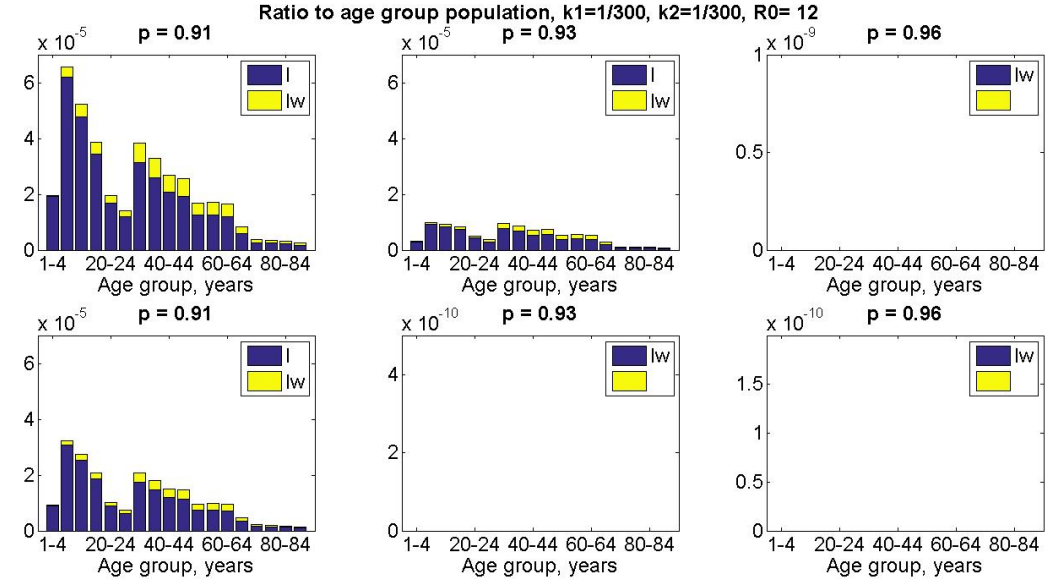

(b)

Figure 4.11: Distribution of (a-b) infected compartments for $R_0 = 12$ and $q = 0.2, 0.8$, respectively. The top-row plots describe the scenario when $G = 1$, while bottom-row plots describe the scenario when $G = 0$

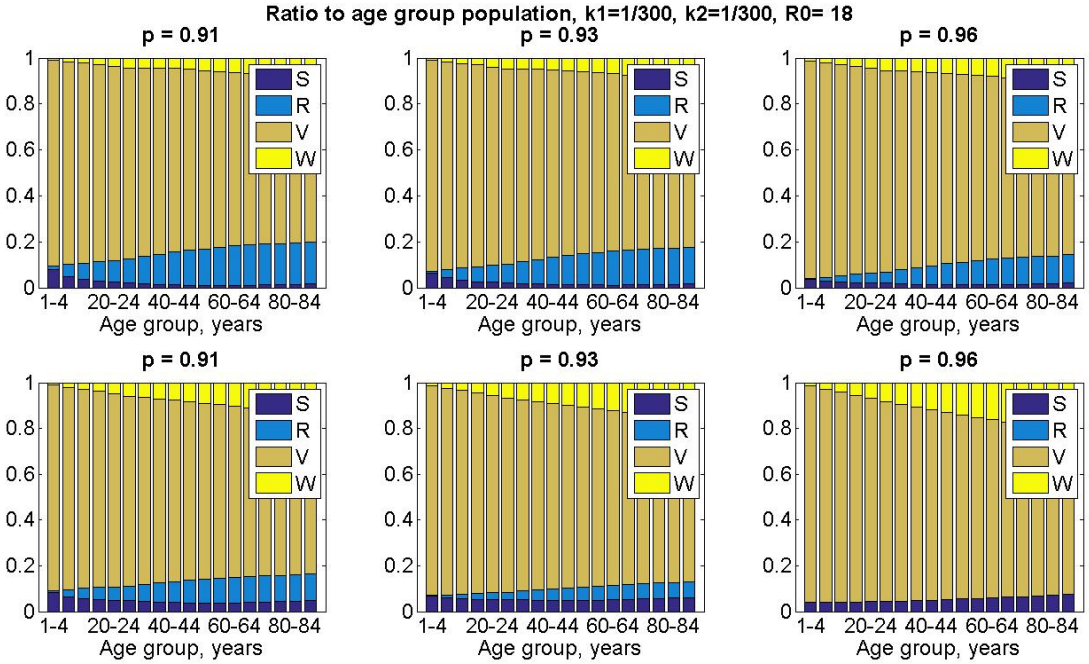

(a)

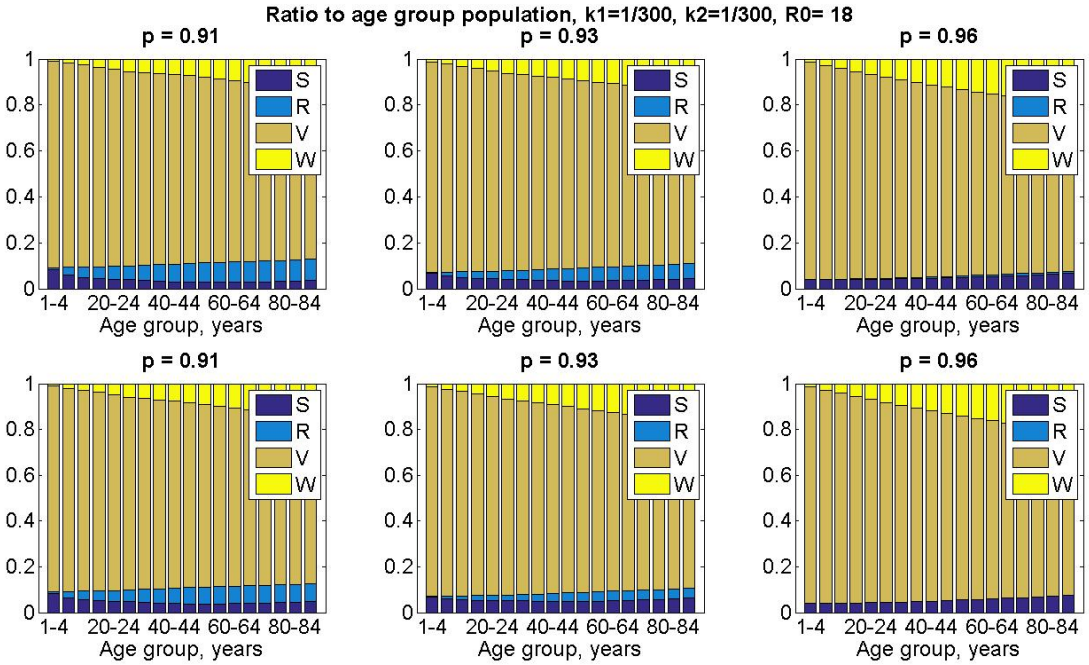

(b)

Figure 4.12: Distribution of susceptible, recovered, vaccinated and waning compartments for $R_0 = 18$ and $q = 0.2, 0.8$,(a)-(b) respectively. The top-row plots describe the scenario when $G = 1$, while bottom-row plots describe the scenario when $G = 0$

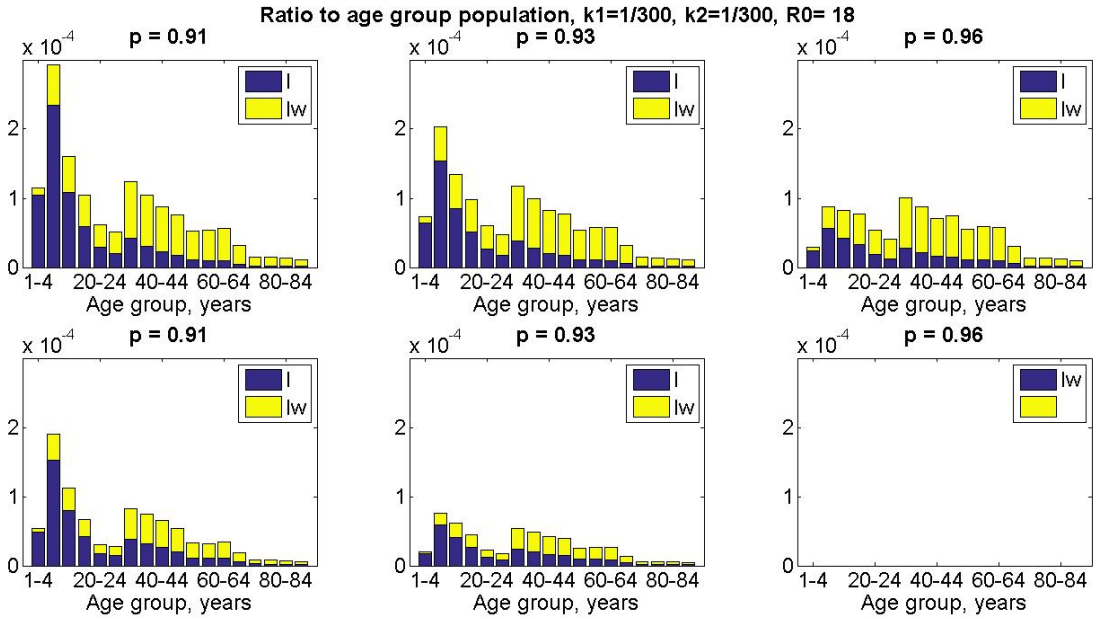

(a)

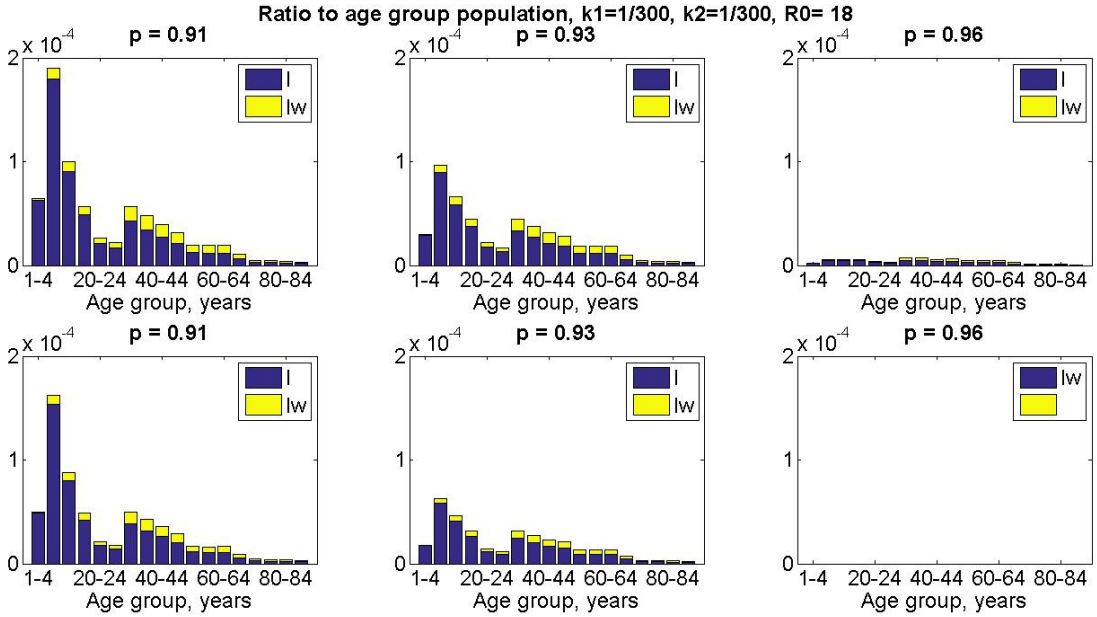

(b)

Figure 4.13: Distribution of infected compartments for $R_0 = 18$ and $q = 0.2$,0.8, (a)-(b) respectively. The top-row plots describe the scenario when $G = 1$, while bottom-row plots describe the scenario when $G = 0$

and q. On the other hand, when transmission is not possible from "waning" individuals, the first peak decreases and becomes smaller than the peak at age group 39-34 years for $p \geq 96$ (Figures 4.17a-4.17b).

Case $k_1 = 1/50$ and $k_2 = 1/5$

In this scenario the total waning period is 55 years, which is similar to the case presented in section with $k_1 = k_2 = 1/30$. However, here, the waning period to return to fully susceptible is smaller than the one to go to W compartment. We observe that the distribution of recovered individuals is much lower than the one observed in the previous case (see, for example, Figures 4.22a and 4.18a). Note that contrary to all the previous analyses, the distribution of individuals in the waning immunity stage is extremely low, showing a slight predominance among the youngest groups. This pattern is present when secondary cases are as infectious as primary infected and when they are not infectious at all (top and bottom-row plots in Figures 4.18a-4.18b and 4.20a-4.20b, respectively). We observe again the sharp drop in S and W at the same loci (25-29 years) present in all the previous cases. The distribution of susceptible individuals shows an increasing trend with respect to the age and it becomes more visible when the only people who can transmit the infection are the ones who experience the infection for the first time as well as when relatively small $\mathcal{R}_0$ are considered. The bimodal curve already shown in all the previous cases is still visible here. For $\mathcal{R}_0 < 12$, we observe that the first peak is located among the age groups 5 through 19 years, when the vaccination rate increases then the peak is shifted at age group 15-19 years. For larger $\mathcal{R}_0$, the bimodal curve is still visible with peaks at 5-9 years and 30-34 years age groups, but as p and q increase, the magnitude of the first peak becomes smaller and is slightly shifted to the right 1 or 2 age groups (Figures 4.19a-4.19b). For $\mathcal{R}_0 \geq 18$, the age groups presenting the highest peaks of infected are still the ones corresponding to 5-9 years and 30-34 years. Contrary to smaller values of $\mathcal{R}_0$, as the vaccination rate and q increase, the first peak becomes smaller but not shifted (Figures 4.21a-4.21b). This pattern is similar for both cases $G = 0, 1$. This scenario shows that the population present a high number of individuals in V compartment above all among the youngest age groups. Since $k_1 = 1/50$, all these children will wane their immunity and become susceptible when they will be adults and this might lead to big outbreak in case an infectious case enter the population.

Case $k_1 = 1/5$ and $k_2 = 1/50$

In this scenario, the total waning period corresponds to the one considered in the previous case 4.2.4, but the waning period needed to transit from V to W is shorter than the one needed to become fully susceptible. We observe that the ratio of recovered individuals is largely wide, indicating that a substantial portion of the population experienced the infection. A reduction in the number of recovered individuals is visible as the number of infectious secondary cases decreases (Figures 4.22b and 4.24b). Observe that, when the infection can be transmitted also by individuals in the waning stage and small q, almost all individuals belonging to age group 40-44 and older underwent the infection and hence fully immunized

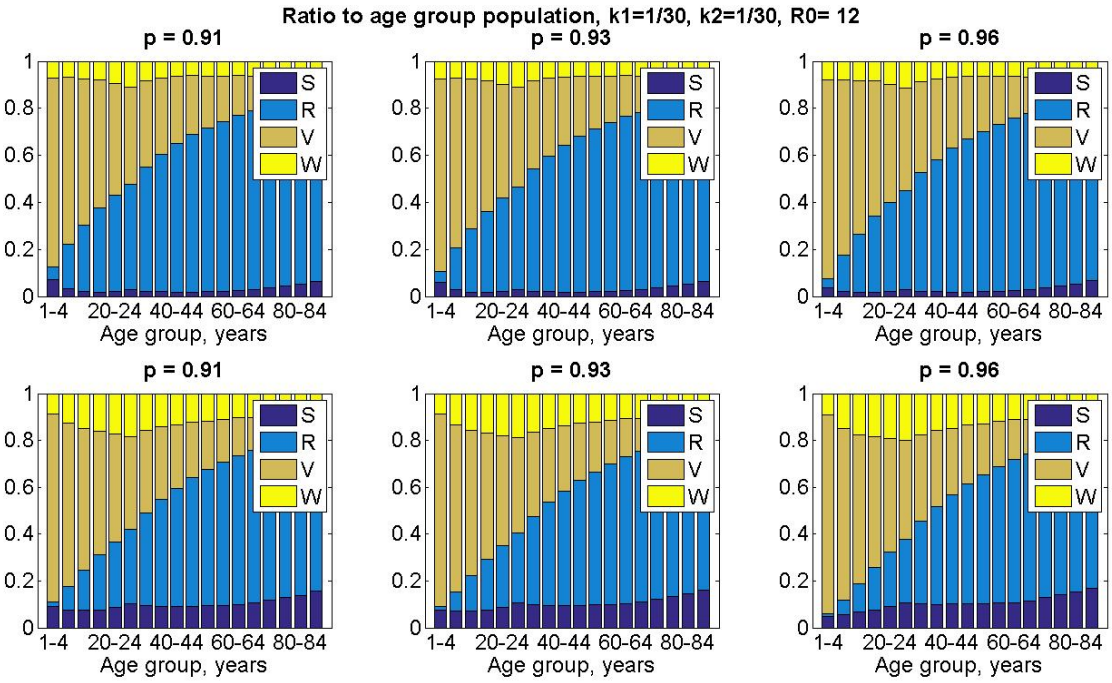

(a)

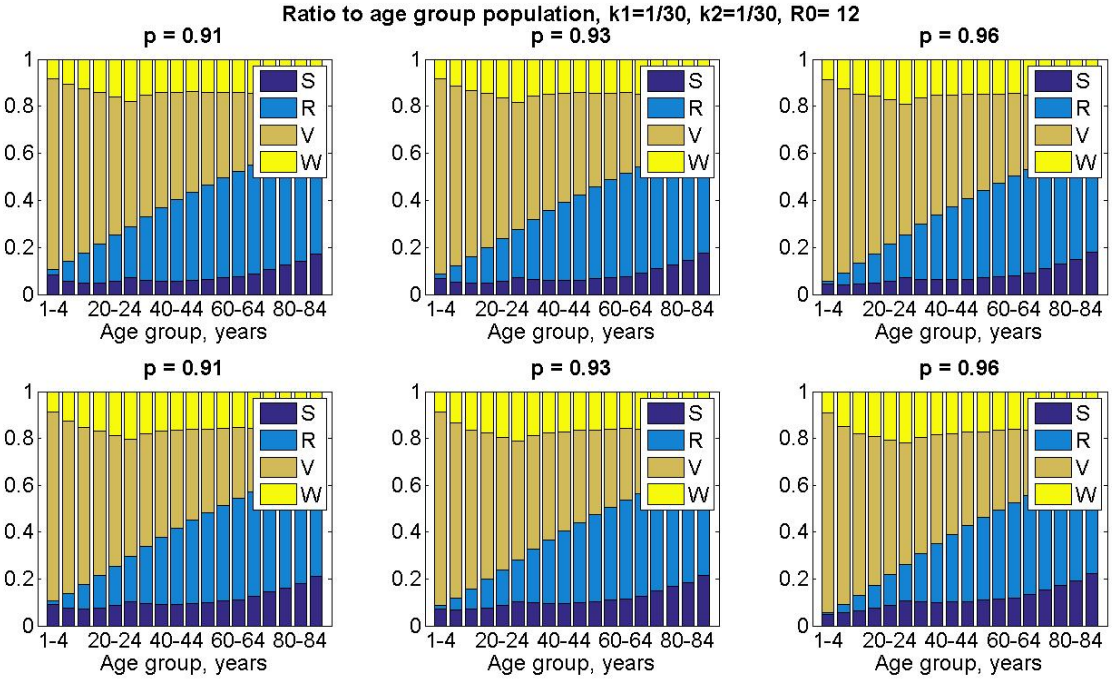

(b)

Figure 4.14: Distribution of susceptible, recovered, vaccinated and waning compartments for $R_0 = 12$ and $q = 0.2$,0.8, (a)-(b) respectively. The top-row plots describe the scenario when $G = 1$, while bottom-row plots describe the scenario when $G = 0$

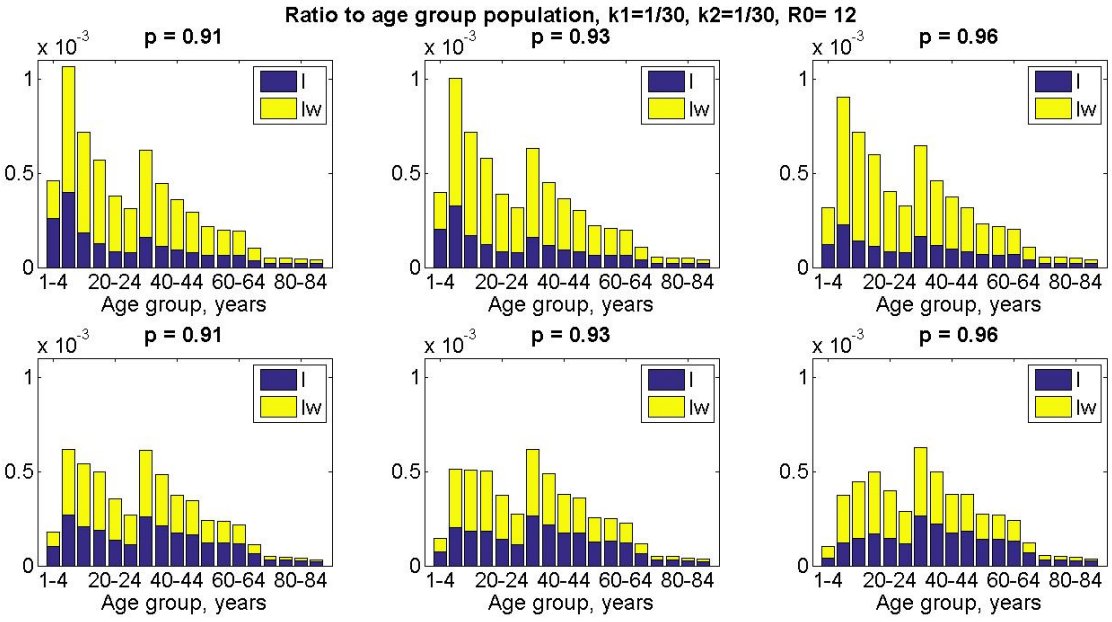

(a)

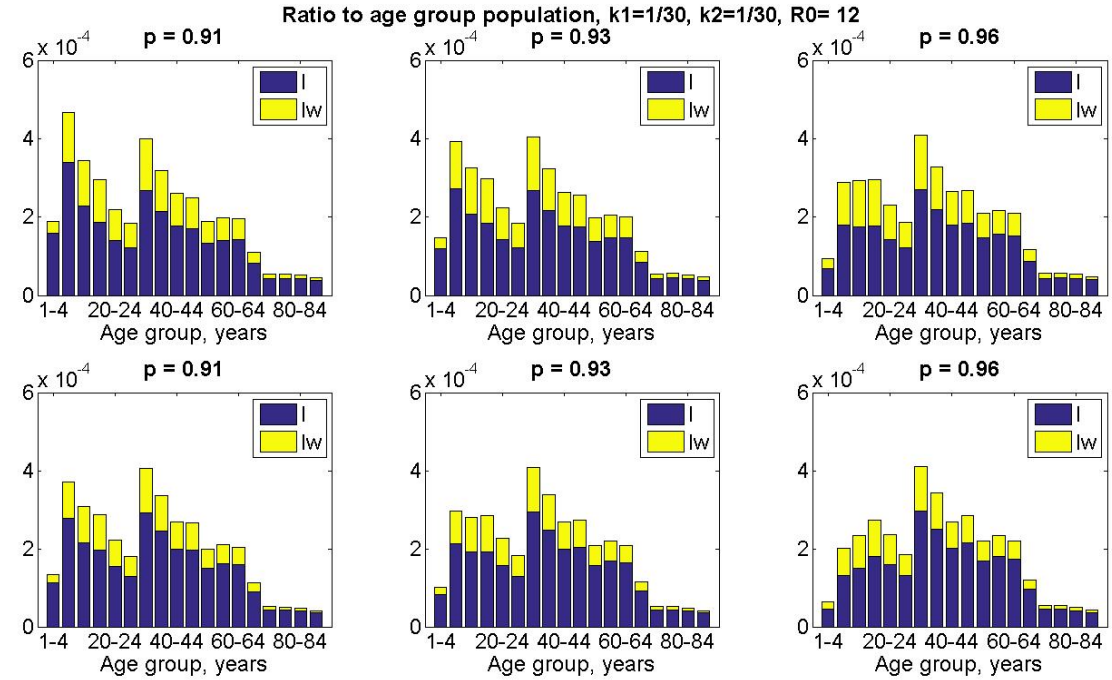

(b)

Figure 4.15: Distribution of infected compartments for $R_0 = 12$ and $q = 0.2$,0.8, (a)-(b) respectively. The top-row plots describe the scenario when $G = 1$, while bottom-row plots describe the scenario when $G = 0$

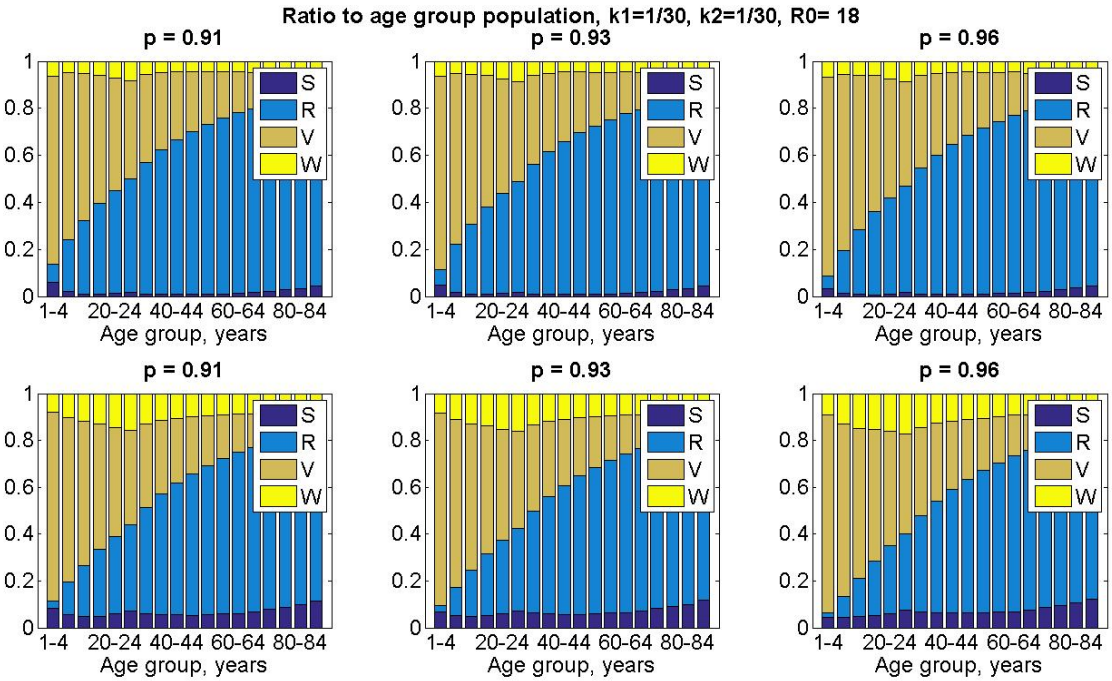

(a)

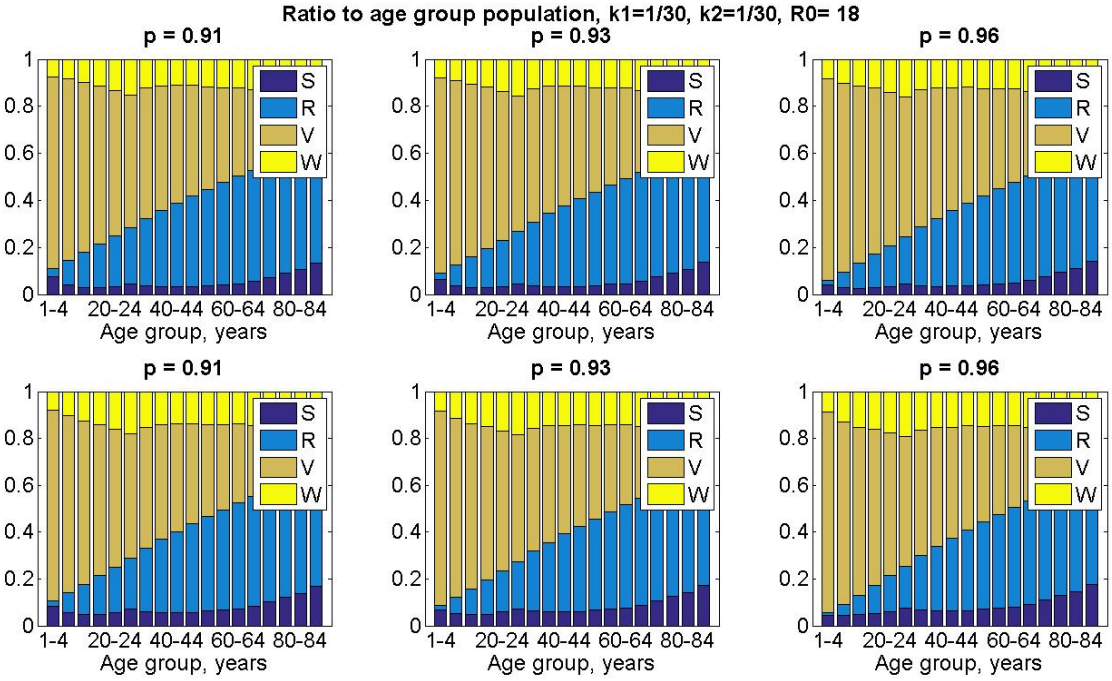

(b)

Figure 4.16: Distribution of susceptible, recovered, vaccinated and waning compartments for $R_0 = 18$ and $q = 0.2$,0.8, (a)-(b) respectively. The top-row plots describe the scenario when $G = 1$, while bottom-row plots describe the scenario when $G = 0$

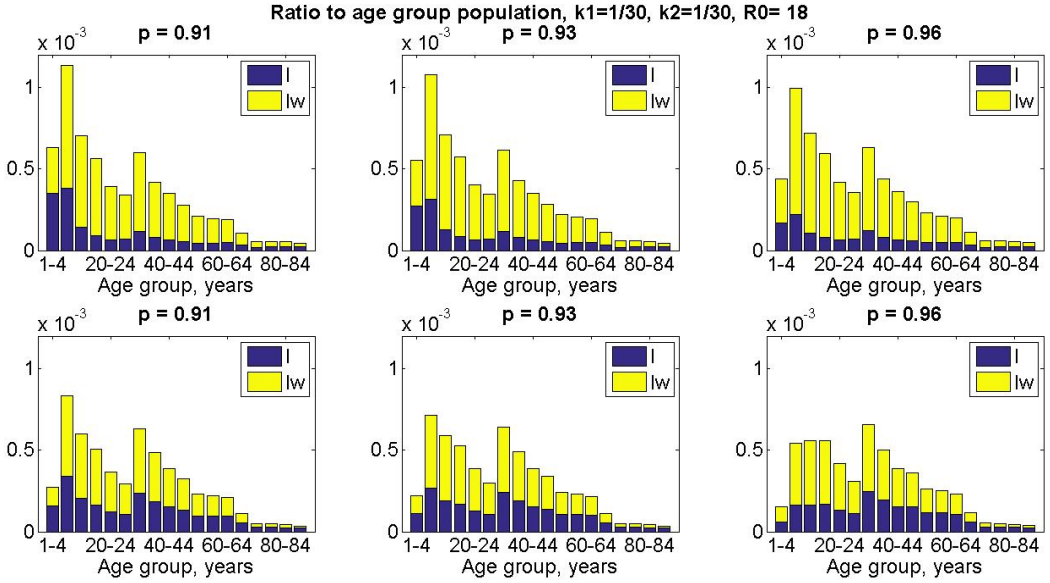

(a)

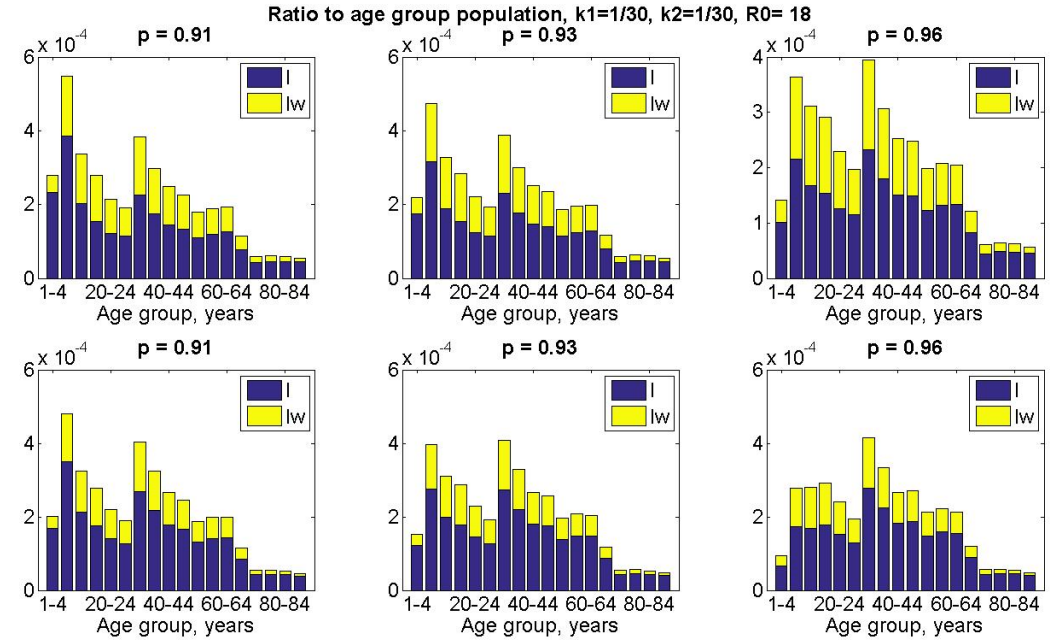

(b)

Figure 4.17: Distribution of infected compartments for $R_0 = 18$ and $q = 0.2$,0.8, (a)-(b) respectively. The top-row plots describe the scenario when $G = 1$, while bottom-row plots describe the scenario when $G = 0$

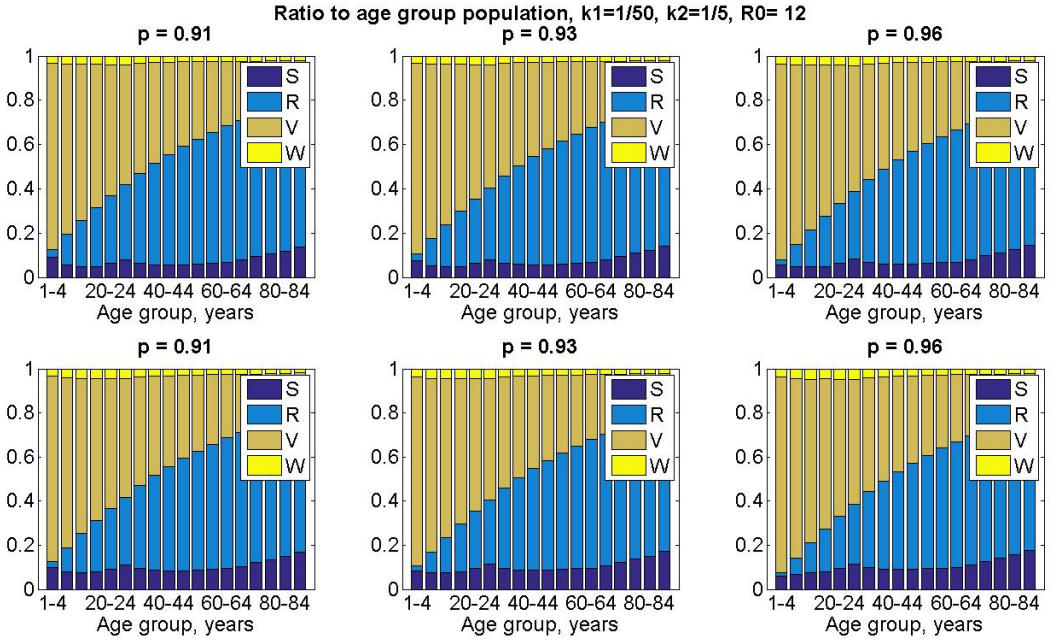

(a)

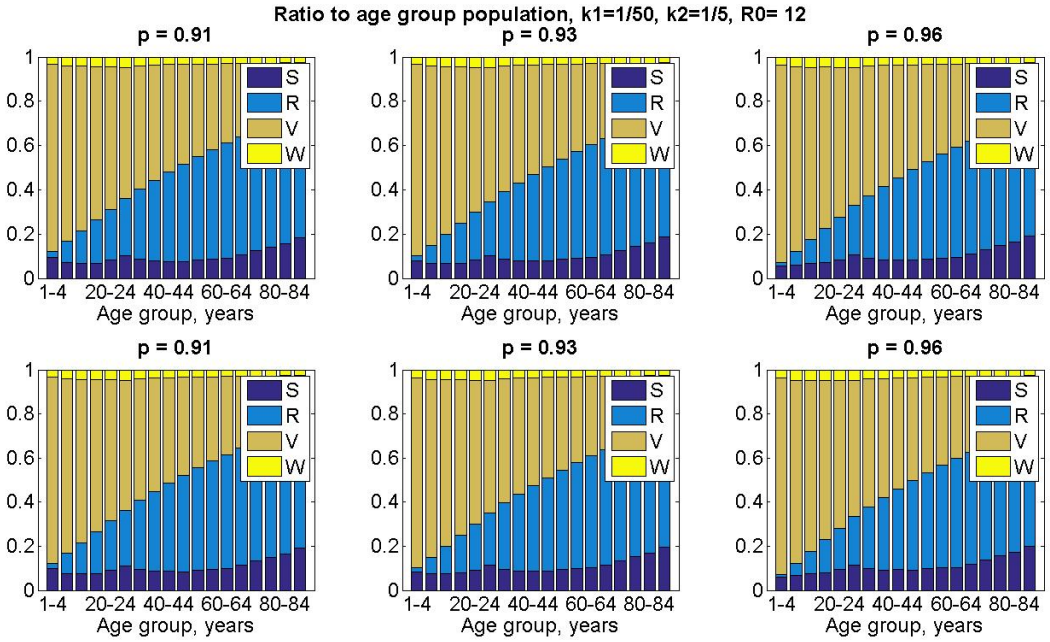

(b)

Figure 4.18: Distribution of susceptible, recovered, vaccinated and waning for $R_0 = 12$ and $q = 0.2$,0.8, (a)-(b) respectively. The top-row plots describe the scenario when $G = 1$, while bottom-row plots describe the scenario when $G = 0$

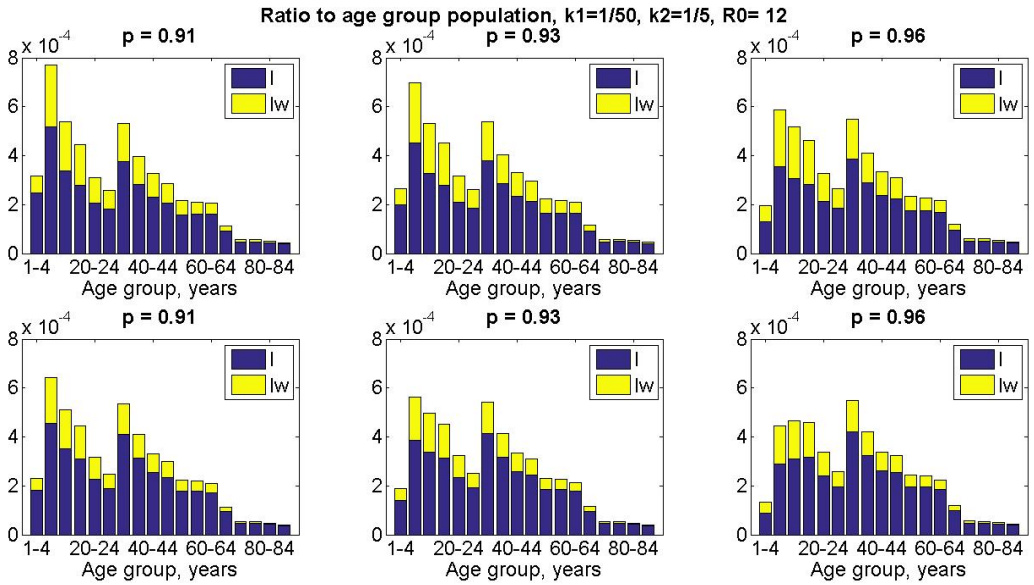

(a)

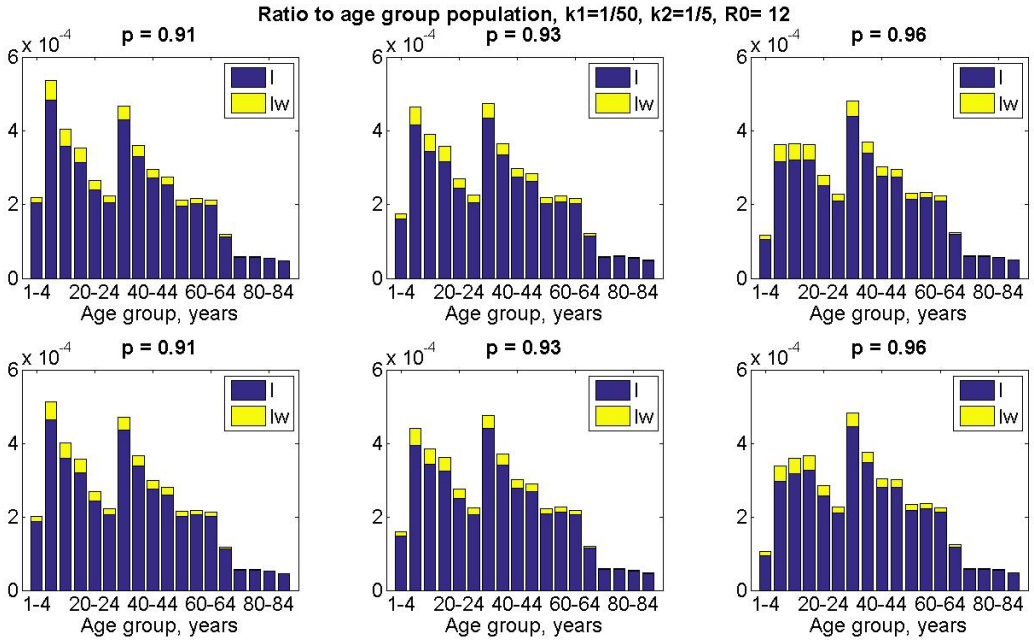

(b)

Figure 4.19: Distribution of infected compartments for $R_0 = 12$ and $q = 0.2$,0.8, (a)-(b) respectively. The top-row plots describe the scenario when $G = 1$, while bottom-row plots describe the scenario when $G = 0$

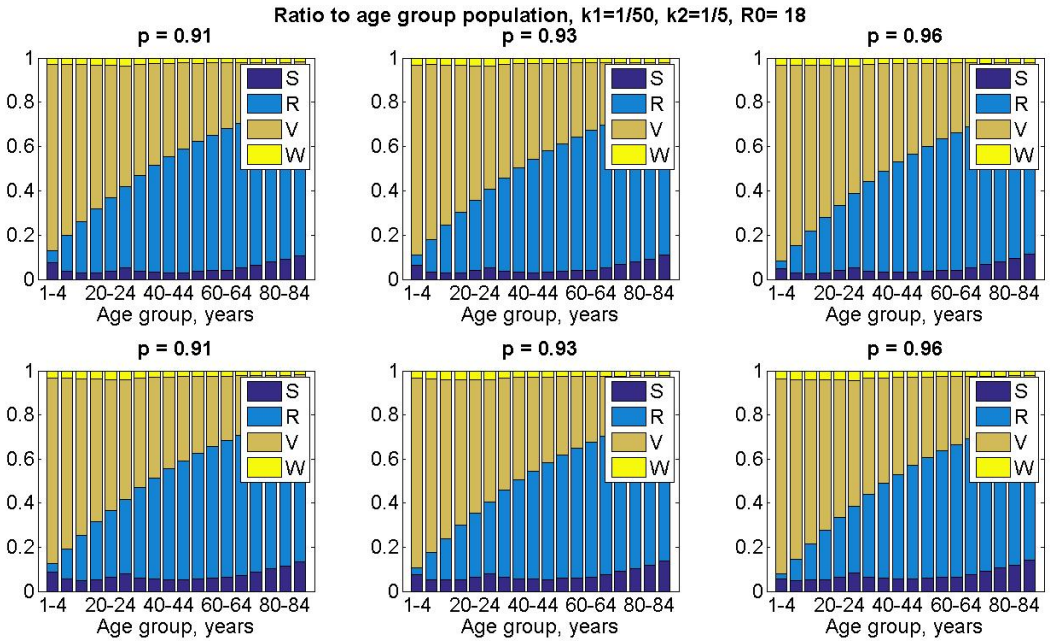

(a)

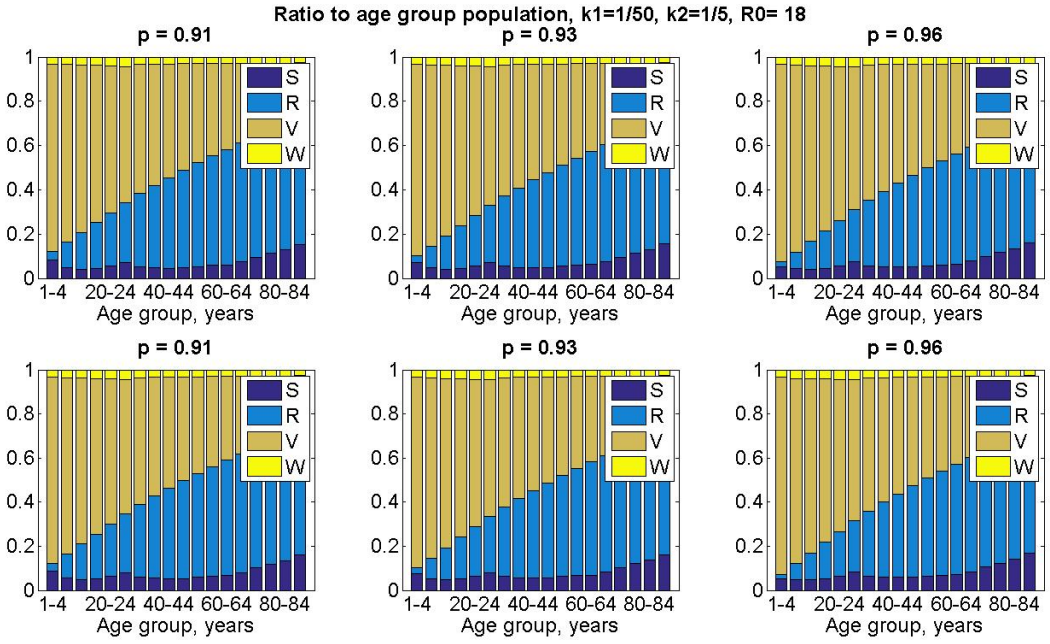

(b)

Figure 4.20: Distribution of susceptible, recovered, vaccinated and waning for $R_0 = 18$ and $q = 0.2$,0.8, (a)-(b) respectively. The top-row plots describe the scenario when $G = 1$, while bottom-row plots describe the scenario when $G = 0$

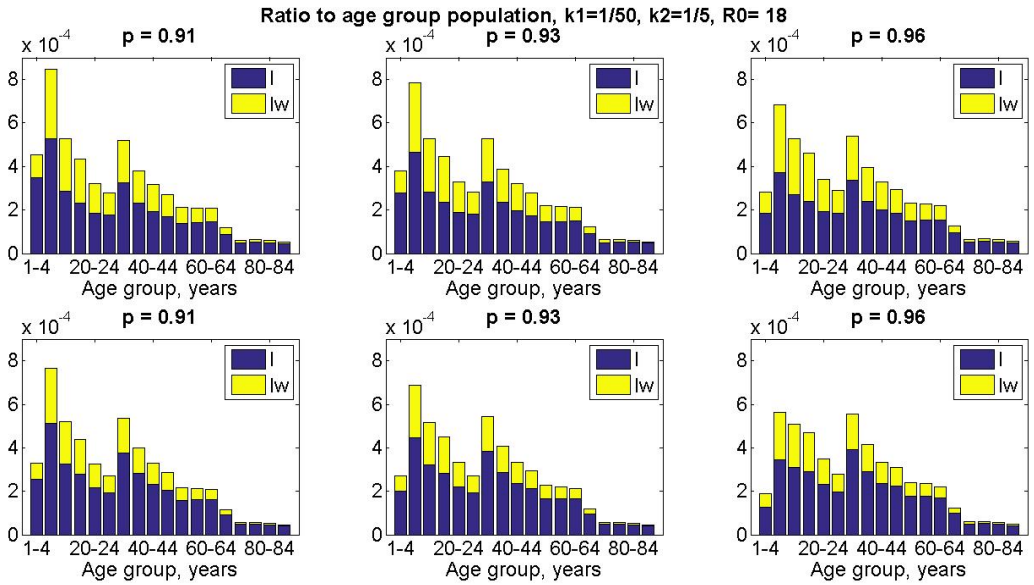

(a)

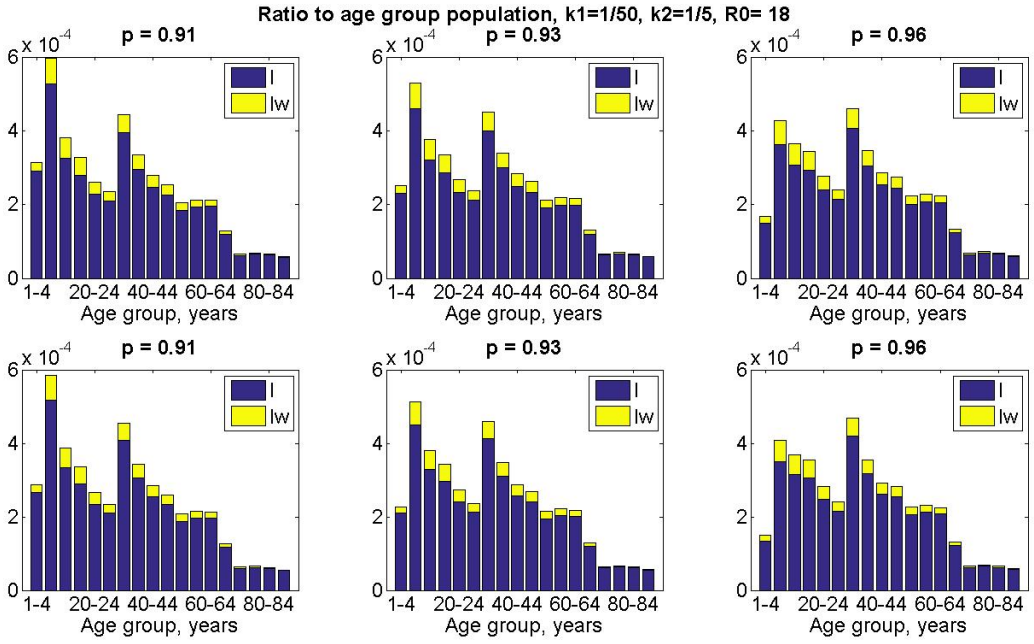

(b)

Figure 4.21: Distribution of infected compartments for $R_0 = 18$ and $q = 0.2$,0.8, (a)-(b) respectively. The top-row plots describe the scenario when $G = 1$, while bottom-row plots describe the scenario when $G = 0$

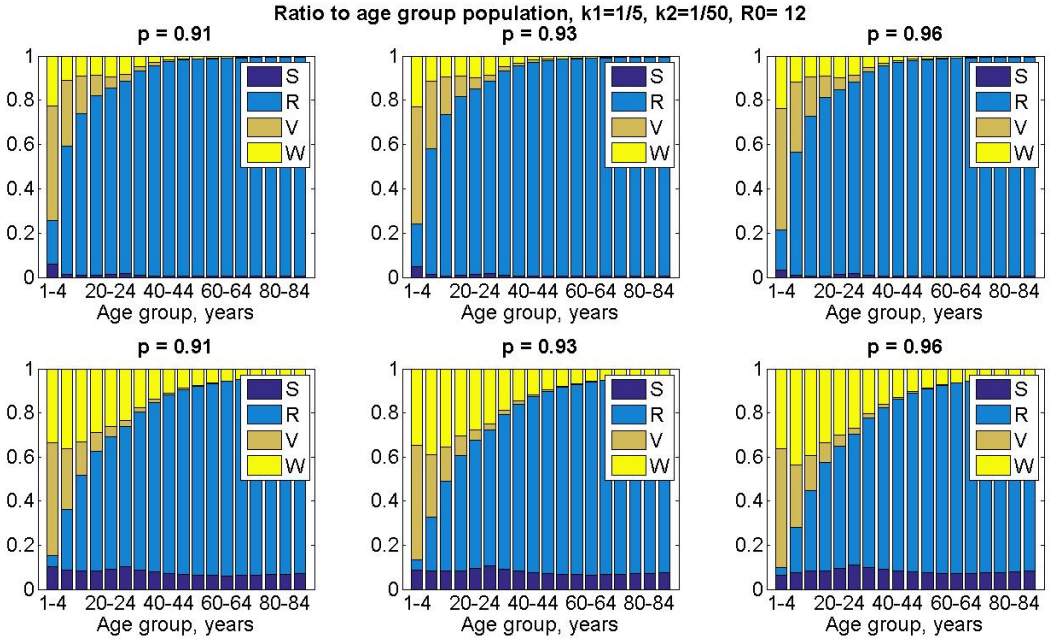

(a)

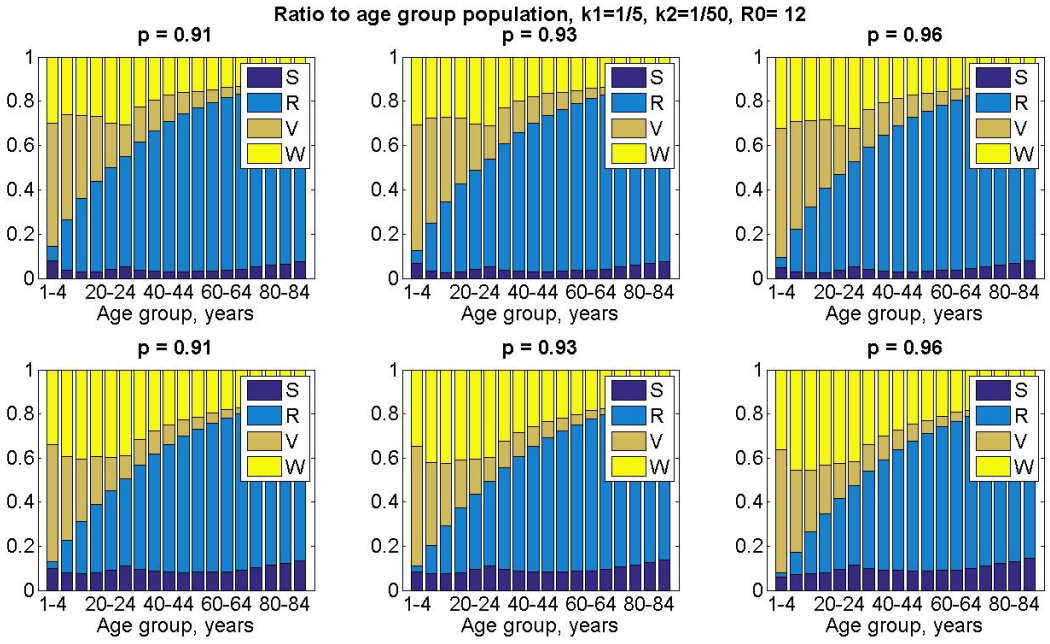

(b)

Figure 4.22: Distribution of susceptible, recovered, vaccinated and waning for $R_0 = 12$ and $q = 0.2$,0.8, (a)-(b) respectively. The top-row plots describe the scenario when $G = 1$, while bottom-row plots describe the scenario when $G = 0$

for life (top-row plots in Figures (4.22a and 4.24a)). The distribution of V and W appears to be more prevalent over the youngest age groups. However, the distribution of individuals in W is significantly more dominant than the one in V. As observed in 4.2.4, a sharp drop in the ratios of susceptible and waning individuals is visible at age group 25-29 years and it becomes more prevalent when secondary cases are not infectious (bottom-row plots in Figures (4.22b and 4.24b)). The distribution of infected individuals presents a bimodal curve as already observed in the previous cases. The highest peak is the most visible and occurs at age group 5-9 years, while the second one, drastically smaller, at age group 30-35, reflecting the drop in S and W compartments (Figures 4.23a-4.23b and 4.25a-4.25b).

Case $k_1 = 1$ and $k_2 = 1/25$

We conclude our numerical results by studying the scenario with short waning period to W and longer period to return to S. Similar to all the cases where immunity is not life-long, herd immunity is not achievable.

We observe that for both small and large $\mathcal{R}_0$, most of the population experience the infection and the recovered compartments present distribution similar to $k_1 = 1/5$ and $k_2 = 1/50$ (for example Figures 4.22a and 4.26a). For $q = 0.2$, when individuals in the waning stage transmit the infection, it appears that all people aged 40-44 years and older experience the infection and became recovered (top-row plots in Figures (4.26a) and (4.28a)). On the other hand, for $q = 0.2$, when only primary infectious cases are able to transmit the infection, the threshold age group after which the totality of individuals undergo the outbreak is the one corresponding to 60-64 years (bottom-row plots in Figures (4.26a) and (4.28a)). Observe that, as q increases, and so less individuals in W become secondary cases, the ratio of recovered individuals decreases (see Figures (4.26b) and (4.28b)). The distribution of vaccinated people is almost non-existent and this behaviour becomes more evident for all age groups 55-59 and above which, however, show a large proportion of recovered. As the basic reproduction number increases, susceptible distribution becomes less visible. However, these ratios show a peak at age group 25-29 years, similar to all the previous scenarios. This gap becomes more prevalent when $G = 0$ (bottom rows in Figures 4.26band 4.28b). The waning distribution is concentrated among the youngest age groups and this makes these individuals susceptible to a possible outbreak. Again, the infected distribution show a bimodal curve. Observe that, when $G = 1$ and $q = 0.2$, the highest and most dominant peaks are located at 1-4 and 5-9 years age group, while the second is shown at 30-34 years age group and it is significantly smaller than the previous two (top-row plots of Figure (4.27a) and (4.29a)). Observe that for $\mathcal{R}_0 = 12$, the peaks at the youngest ages have same magnitude, while for $\mathcal{R}_0$ the age group showing more infected is the one corresponding to 1-4 years. As q increases, the peak at the youngest age group reduces and the dominant peak belong to age group 5-9 years. Moreover, as $\mathcal{R}_0$ and p increase the second peak becomes less visible (top-row plots of Figure (4.27b) and (4.29b)). On the other hand, when individuals in W do not become infectious after encountering the pathogen, the 5-9 years age group is the most affected by the infection independently of proportion of individuals boosting immunity and reproduction

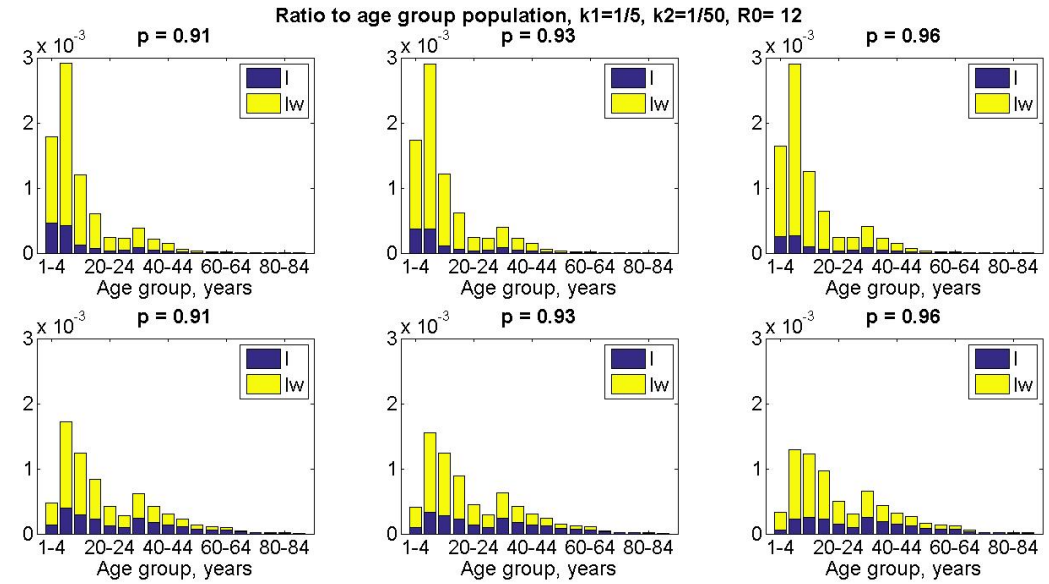

(a)

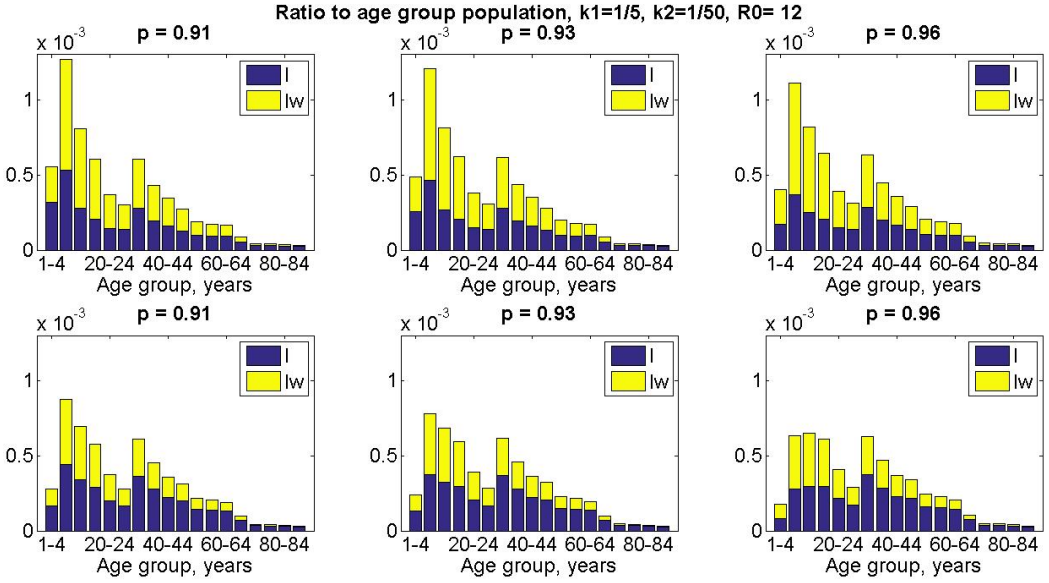

(b)

Figure 4.23: Distribution of infected compartments for $R_0 = 12$ and $q = 0.2$,0.8, (a)-(b) respectively. The top-row plots describe the scenario when $G = 1$, while bottom-row plots describe the scenario when $G = 0$

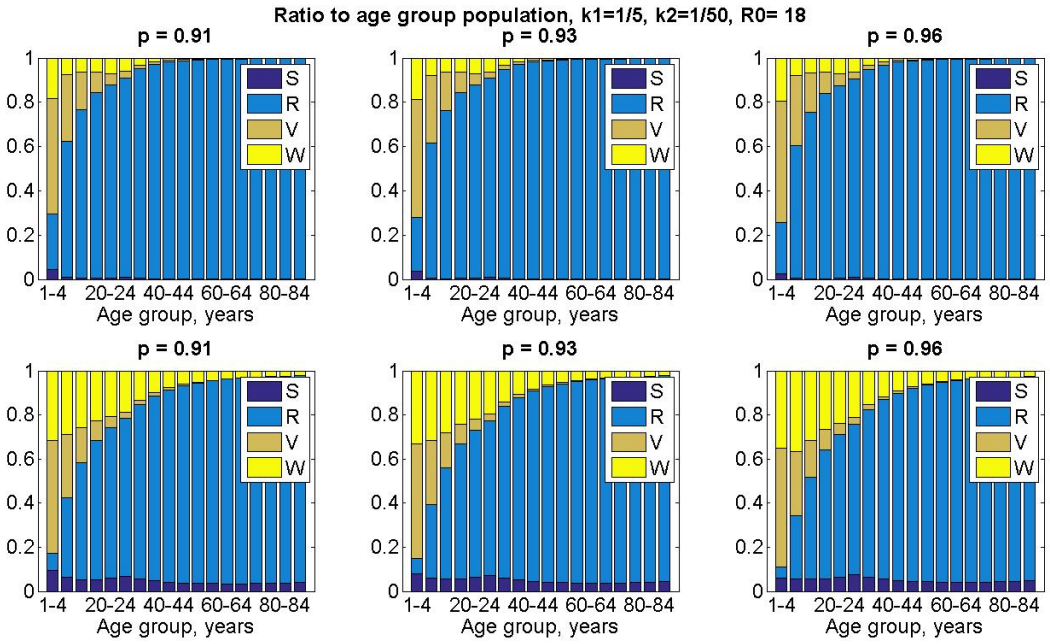

(a)

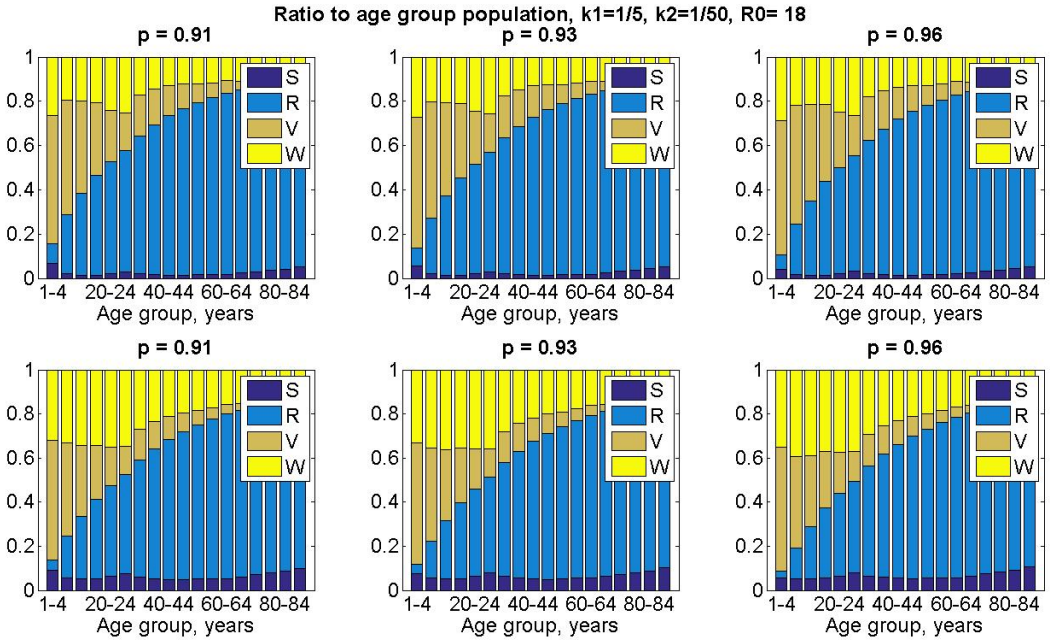

(b)

Figure 4.24: Distribution of susceptible, recovered, vaccinated and waning for $R_0 = 18$ and $q = 0.2$,0.8, (a)-(b) respectively. The top-row plots describe the scenario when $G = 1$, while bottom-row plots describe the scenario when $G = 0$

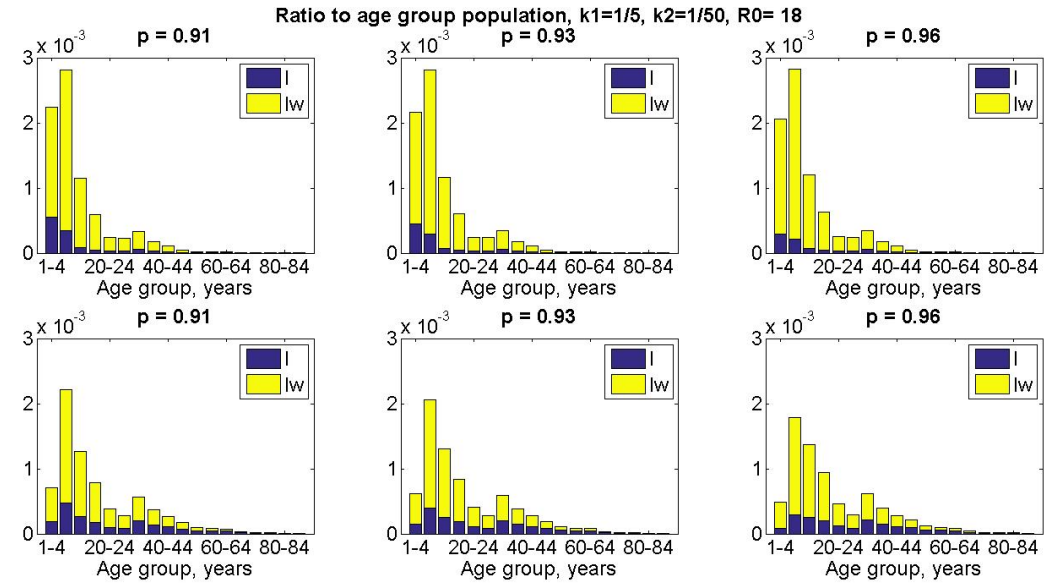

(a)

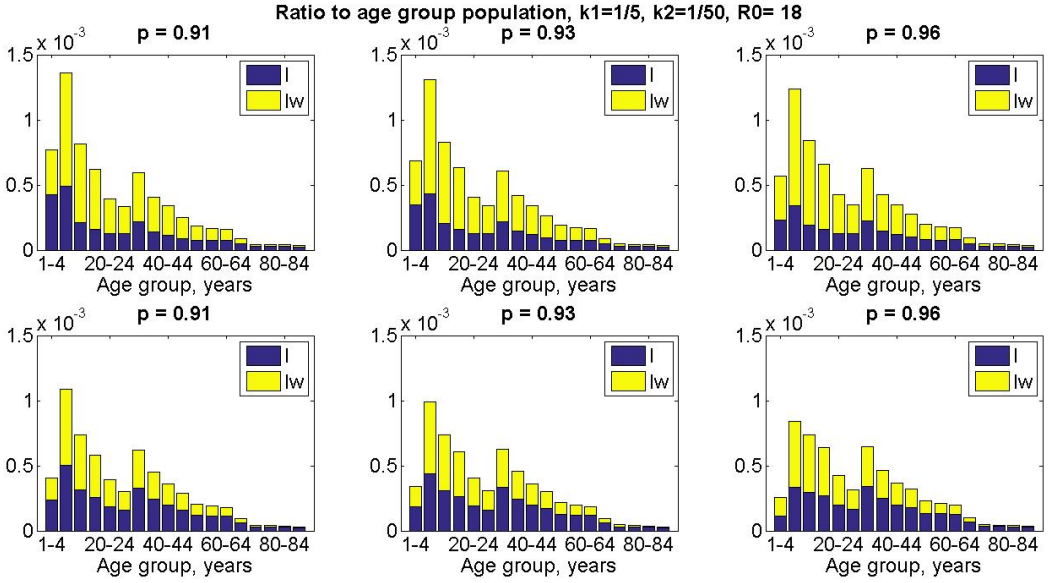

(b)

Figure 4.25: Distribution of infected compartments for $R_0 = 18$ and $q = 0.2$,0.8, (a)-(b) respectively. The top-row plots describe the scenario when $G = 1$, while bottom-row plots describe the scenario when $G = 0$

number (bottom-row plots of Figure (4.27b) and (4.29b)). If immunity wanes at rates $k_1 = 1$ and $k_2 = 1/25$, we conclude that pockets of individuals in the youngest age groups are waning their immunity suggesting a future susceptibility in these classes. Moreover, under these conditions if all the "waning" cases are infectious it is important to control the children aged between 1 and 9 years, while if these cases are not infectious, only children belonging to age group 5-9 need to be monitored to control the infection spread.

4.2.5 Model with Age Structure: Stochastic

Similar to the model without age structure, we investigate the probability of extinction and outbreak with 10 or 150 cumulative cases for Model 4.10. The infection was seeded the age group 5-9 years in a population at the DFE with vaccination. The age group was decided by the distribution of I and I_w shown in the previous section. We compare different vaccination coverages $p = 0.91, 0.93, 0.96$, $q = 0.2, 0.8$, reproduction numbers ($\mathcal{R}_0 = 6, 18$) and waning periods (as in 4.7). We present the results for $k_1 = k_2 = 1/300$ and $k_1 = k_2 = 1/30$ on the probability of extinction, having at least 10 or 150 cumulative cases. The plots regarding the other waning periods are provided in Appendix I.

Case $k_1 = k_2 = 1/300$

Our investigation of the stochastic model starts with the lifelong immunity scenario. Figure (4.30a) shows that the probability of having 0 new cases is higher for small reproduction number, while for $\mathcal{R}_0 = 18$ an outbreak with at least 10 cases can occur with up to 67% of possibility ($G = 1$, $q = 0.3$ and $p = 0.91$). Overall, we observe that the probability of extinction increases if the secondary cases are not infectious, the vaccination coverage increases and if most of the "waning" individuals is boosted to V.
Similar results are visible when we consider an outbreak with at least 150 cases (Figure (4.30b)). However, for small reproduction numbers, we observe how this large outbreak never occurs for $G = 0$, and for $G = 1$ it is possible only for $q = 0.2$. For larger $\mathcal{R}_0$, 150 cases can occur with a slightly lower probability than 10 cases. We also observe that the probability of having between 70 and 150 (non included) cases is extremely low.

Case $k_1 = k_2 = 1/30$

We now consider a case with short waning periods ($k_1 = k_2 = 1/30$). We immediately observe that the probability of having an outbreak with 10 (Figure (4.31a)) or 150 (Figure (4.31b)) cases is higher than the probability of extinction. This is visible for both small and large reproduction numbers. As expected, as the vaccination coverage increases and more individuals are boosted to V, the probability of extinction increases. Moreover this probability also increases when the secondary cases are not infectious. Similar to the lifelong immunity case, we observe that the probability of having cases in the range $70 - 149$ is low.

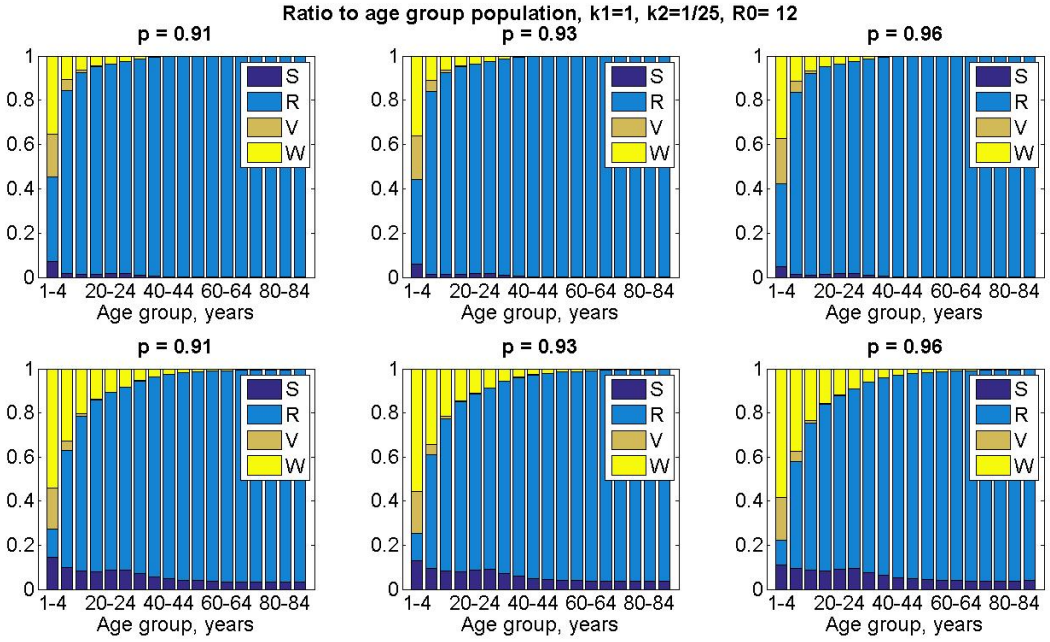

(a)

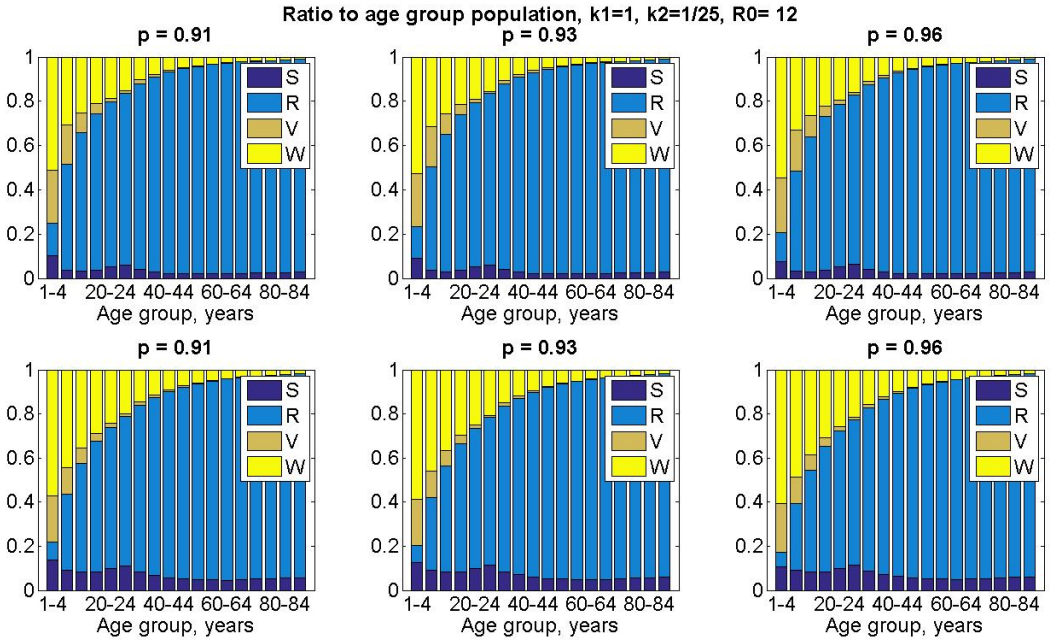

(b)

Figure 4.26: Distribution of susceptible, recovered, vaccinated and waning for $R_0 = 12$ and $q = 0.2$,0.8, (a)-(b) respectively. The top-row plots describe the scenario when $G = 1$, while bottom-row plots describe the scenario when $G = 0$

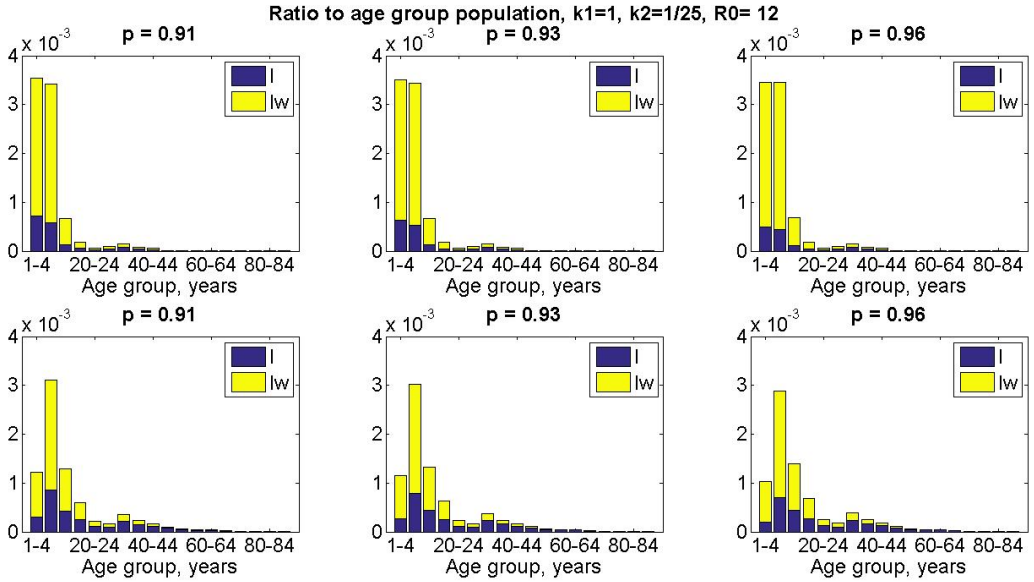

(a)

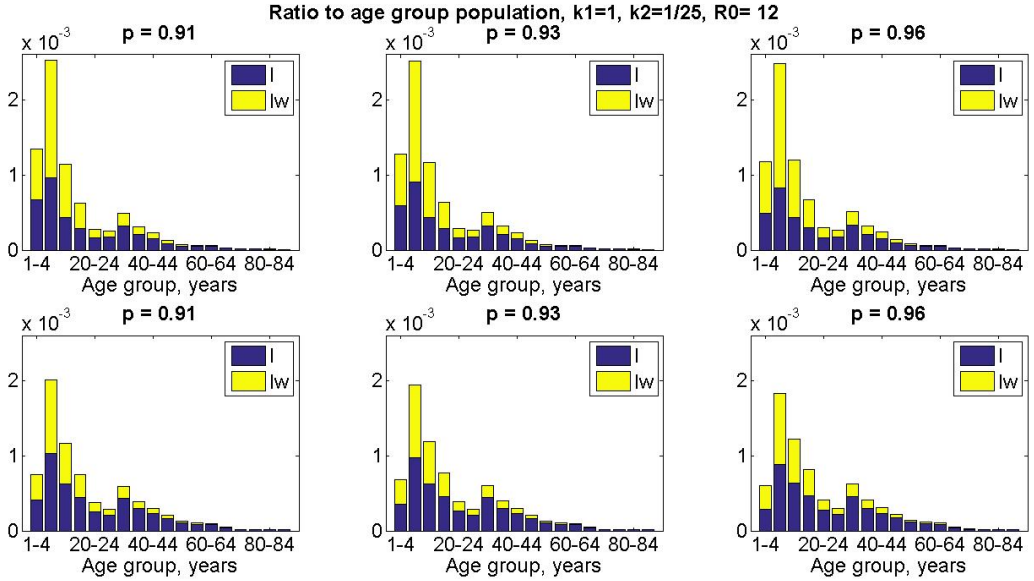

(b)

Figure 4.27: Distribution of infected compartments for $R_0 = 12$ and $q = 0.2$,0.8, (a)-(b) respectively. The top-row plots describe the scenario when $G = 1$, while bottom-row plots describe the scenario when $G = 0$

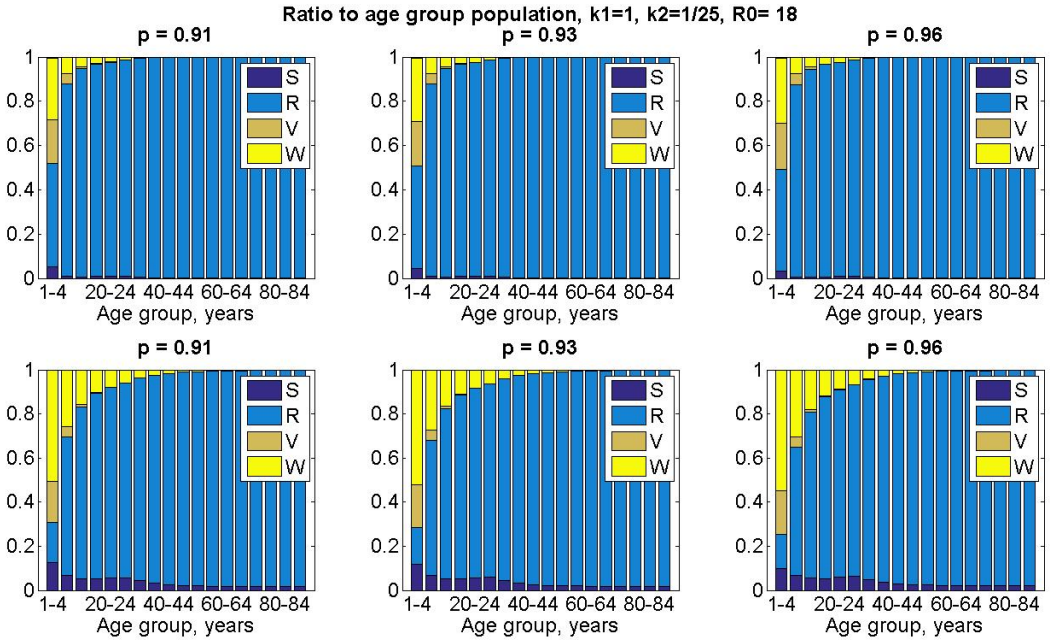

(a)

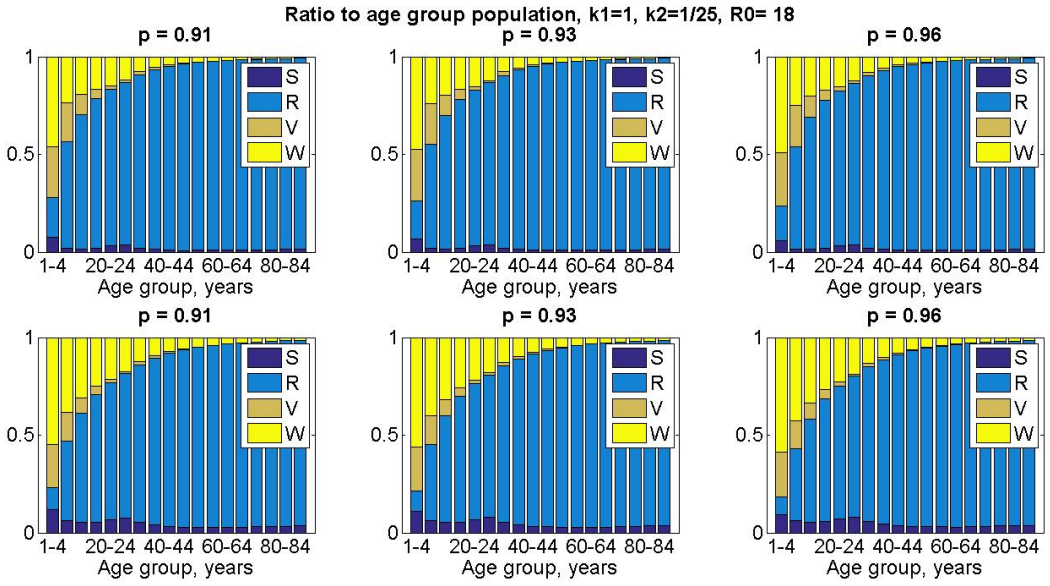

(b)

Figure 4.28: Distribution of susceptible, recovered, vaccinated and waning for $R_0 = 18$ and $q = 0.2$,0.8, (a)-(b) respectively. The top-row plots describe the scenario when $G = 1$, while bottom-row plots describe the scenario when $G = 0$

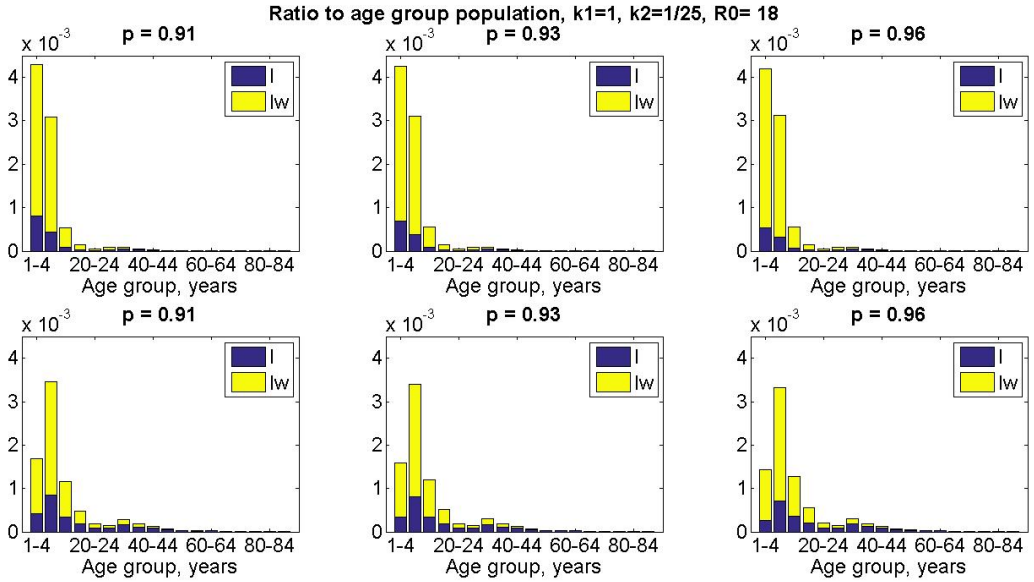

(a)

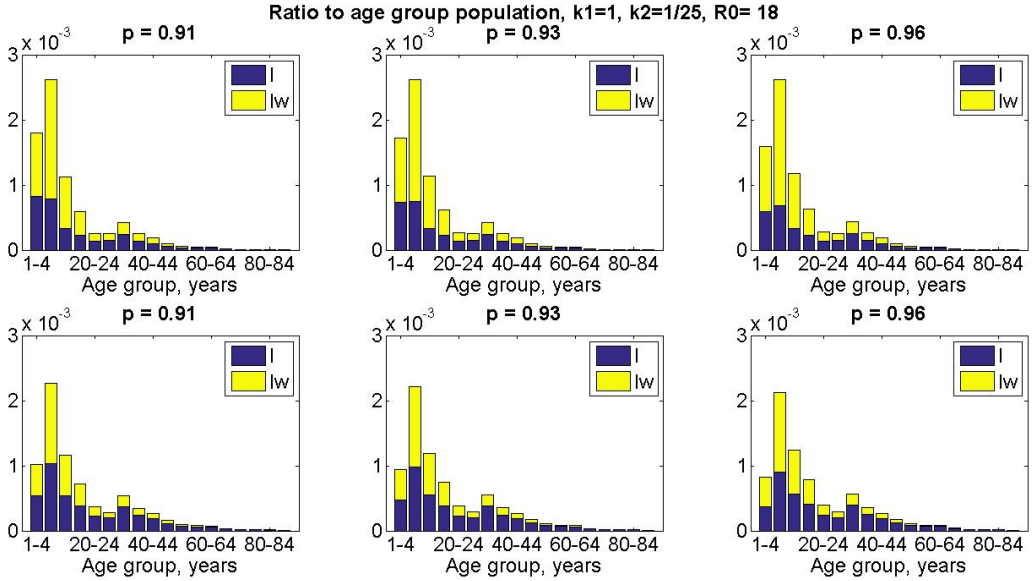

(b)

Figure 4.29: Distribution of infected compartments for $R_0 = 18$ and $q = 0.2$,0.8, (a)-(b) respectively. The top-row plots describe the scenario when $G = 1$, while bottom-row plots describe the scenario when $G = 0$

G=0														
				R0=6						R0=18				
		q=0.2			q=0.8			q=0.2				q=0.8		
cases		p=0.91	p=0.93	p=0.96	p=0.91	p=0.93	p=0.96	p=0.91	p=0.93	p=0.96		p=0.91	p=0.93	p=0.96
0		0.45	0.48	0.55	0.51	0.54	0.68	0.24	0.28	0.34		0.29	0.32	0.43
1		0.15	0.17	0.19	0.16	0.16	0.17	0.09	0.10	0.15		0.09	0.10	0.14
2		0.08	0.09	0.10	0.08	0.09	0.08	0.04	0.07	0.08		0.04	0.05	0.07
3		0.06	0.06	0.04	0.04	0.05	0.03	0.03	0.03	0.06		0.03	0.04	0.05
4		0.04	0.05	0.04	0.04	0.04	0.02	0.02	0.03	0.04		0.02	0.03	0.04
5		0.03	0.03	0.02	0.03	0.03	0.01	0.01	0.02	0.03		0.01	0.02	0.03
6		0.02	0.02	0.02	0.02	0.02	0.00	0.01	0.01	0.03		0.01	0.01	0.03
7		0.02	0.02	0.01	0.02	0.02	0.00	0.01	0.02	0.02		0.01	0.01	0.02
8		0.02	0.01	0.01	0.02	0.01	0.00	0.01	0.01	0.02		0.01	0.01	0.02
9		0.02	0.01	0.01	0.01	0.01	0.01	0.01	0.01	0.01		0.01	0.01	0.01
10		0.11	0.07	0.02	0.10	0.04	0.01	0.53	0.43	0.22		0.50	0.41	0.18
G=1														
				R0=6						R0=18				
		q=0.2			q=0.8			q=0.2				q=0.8		
cases		p=0.91	p=0.93	p=0.96	p=0.91	p=0.93	p=0.96	p=0.91	p=0.93	p=0.96		p=0.91	p=0.93	p=0.96
0		0.47	0.49	0.56	0.51	0.55	0.66	0.25	0.27	0.34		0.28	0.36	0.42
1		0.11	0.12	0.14	0.15	0.15	0.17	0.05	0.05	0.07		0.06	0.07	0.13
2		0.06	0.05	0.07	0.08	0.08	0.06	0.01	0.02	0.04		0.03	0.04	0.06
3		0.03	0.04	0.05	0.04	0.05	0.03	0.01	0.01	0.02		0.02	0.03	0.04
4		0.03	0.04	0.03	0.04	0.04	0.02	0.01	0.01	0.02		0.01	0.02	0.03
5		0.02	0.02	0.02	0.02	0.02	0.02	0.01	0.01	0.01		0.01	0.02	0.03
6		0.01	0.02	0.02	0.01	0.02	0.01	0.00	0.00	0.01		0.01	0.01	0.01
7		0.01	0.02	0.02	0.02	0.02	0.01	0.00	0.00	0.00		0.00	0.00	0.01
8		0.01	0.01	0.01	0.01	0.01	0.01	0.00	0.00	0.01		0.00	0.01	0.02
9		0.01	0.01	0.01	0.01	0.01	0.01	0.00	0.00	0.00		0.00	0.01	0.01
10		0.24	0.19	0.09	0.12	0.06	0.01	0.67	0.63	0.50		0.59	0.45	0.25

(a)

G=0														
				R0=6						R0=18				
		q=0.2			q=0.8			q=0.2				q=0.8		
cases		p=0.91	p=0.93	p=0.96	p=0.91	p=0.93	p=0.96	p=0.91	p=0.93	p=0.96		p=0.91	p=0.93	p=0.96
0		0.45	0.48	0.55	0.52	0.57	0.66	0.22	0.26	0.31		0.27	0.33	0.44
1-5		0.29	0.27	0.00	0.30	0.24	0.00	0.20	0.24	0.36		0.17	0.22	0.31
5-10		0.08	0.06	0.19	0.06	0.11	0.18	0.03	0.06	0.10		0.02	0.05	0.08
10-30		0.13	0.13	0.18	0.09	0.06	0.10	0.04	0.08	0.12		0.02	0.05	0.09
30-50		0.04	0.03	0.05	0.02	0.01	0.04	0.01	0.02	0.04		0.01	0.02	0.03
50-70		0.01	0.01	0.01	0.01	0.00	0.01	0.00	0.01	0.02		0.00	0.01	0.02
70-90		0.00	0.01	0.00	0.00	0.00	0.00	0.00	0.00	0.01		0.00	0.00	0.01
90-110		0.00	0.00	0.00	0.00	0.00	0.01	0.00	0.00	0.01		0.00	0.01	0.01
110-130		0.00	0.00	0.00	0.00	0.00	0.00	0.00	0.00	0.01		0.00	0.00	0.00
130-150		0.00	0.00	0.00	0.00	0.00	0.00	0.00	0.00	0.01		0.00	0.00	0.00
150		0.00	0.00	0.00	0.00	0.00	0.00	0.49	0.32	0.01		0.51	0.31	0.00
G=1														
				R0=6						R0=18				
		q=0.2			q=0.8			q=0.2				q=0.8		
cases		p=0.91	p=0.93	p=0.96	p=0.91	p=0.93	p=0.96	p=0.91	p=0.93	p=0.96		p=0.91	p=0.93	p=0.96
0		0.44	0.48	0.57	0.52	0.57	0.66	0.26	0.26	0.31		0.30	0.31	0.44
1-5		0.28	0.28	0.30	0.28	0.16	0.00	0.09	0.11	0.17		0.14	0.19	0.25
5-10		0.05	0.05	0.05	0.07	0.06	0.16	0.01	0.01	0.02		0.02	0.03	0.07
10-30		0.07	0.08	0.06	0.09	0.14	0.10	0.00	0.00	0.01		0.01	0.02	0.08
30-50		0.03	0.04	0.02	0.02	0.03	0.05	0.00	0.00	0.00		0.00	0.00	0.02
50-70		0.02	0.02	0.00	0.01	0.01	0.01	0.00	0.00	0.00		0.00	0.00	0.02
70-90		0.01	0.01	0.00	0.00	0.01	0.00	0.00	0.00	0.00		0.00	0.00	0.01
90-110		0.01	0.01	0.00	0.00	0.00	0.00	0.00	0.00	0.00		0.00	0.00	0.01
110-130		0.01	0.01	0.00	0.00	0.00	0.00	0.00	0.00	0.00		0.00	0.00	0.01
130-150		0.01	0.01	0.00	0.00	0.00	0.00	0.00	0.00	0.00		0.00	0.00	0.01
150		0.06	0.01	0.00	0.00	0.00	0.00	0.65	0.62	0.49		0.54	0.44	0.07

(b)

Figure 4.30: Probability of having extinction, (a) 10 or (b) 150 cases when $G = 0$ (top-row table) and $G = 1$ (bottom-row table) for $p = 0.91$, 0.93, 0.96, $q = 0.2$,0.8, $\mathcal{R}_0 = 6, 18$ and $k_1 = k_2 = 1/300$

G=0

	R0=6						R0=18					
	q=0.2			q=0.8			q=0.2			q=0.8		
cases	p=0.91	p=0.93	p=0.96	p=0.91	p=0.93	p=0.96	p=0.91	p=0.93	p=0.96	p=0.91	p=0.93	p=0.96
0	0.22	0.22	0.23	0.31	0.32	0.33	0.08	0.10	0.11	0.13	0.16	0.16
1	0.10	0.11	0.12	0.09	0.09	0.10	0.04	0.06	0.06	0.02	0.03	0.04
2	0.03	0.05	0.08	0.03	0.03	0.03	0.02	0.02	0.03	0.01	0.01	0.01
3	0.02	0.03	0.03	0.01	0.02	0.02	0.01	0.01	0.01	0.01	0.01	0.01
4	0.02	0.02	0.02	0.01	0.02	0.02	0.01	0.01	0.01	0.00	0.00	0.00
5	0.02	0.02	0.02	0.01	0.01	0.01	0.01	0.01	0.01	0.00	0.00	0.00
6	0.01	0.01	0.01	0.01	0.01	0.02	0.00	0.00	0.00	0.00	0.00	0.00
7	0.01	0.01	0.01	0.01	0.01	0.00	0.00	0.00	0.00	0.00	0.00	0.00
8	0.01	0.01	0.01	0.00	0.00	0.01	0.00	0.01	0.00	0.00	0.00	0.00
9	0.01	0.00	0.00	0.01	0.00	0.01	0.00	0.00	0.00	0.00	0.00	0.00
10	0.55	0.52	0.47	0.52	0.50	0.45	0.83	0.78	0.77	0.83	0.79	0.78

G=1

	R0=6						R0=18					
	q=0.2			q=0.8			q=0.2			q=0.8		
cases	p=0.91	p=0.93	p=0.96	p=0.91	p=0.93	p=0.96	p=0.91	p=0.93	p=0.96	p=0.91	p=0.93	p=0.96
0	0.22	0.23	0.24	0.30	0.32	0.33	0.10	0.09	0.11	0.14	0.15	0.16
1	0.03	0.04	0.05	0.06	0.07	0.07	0.01	0.01	0.01	0.01	0.01	0.01
2	0.01	0.02	0.03	0.02	0.03	0.02	0.00	0.00	0.00	0.00	0.01	0.01
3	0.00	0.02	0.02	0.02	0.01	0.01	0.00	0.00	0.00	0.00	0.00	0.00
4	0.00	0.01	0.01	0.01	0.01	0.01	0.00	0.00	0.00	0.00	0.00	0.00
5	0.01	0.00	0.00	0.01	0.01	0.01	0.00	0.00	0.00	0.00	0.00	0.00
6	0.01	0.00	0.00	0.01	0.00	0.01	0.00	0.00	0.00	0.00	0.00	0.00
7	0.01	0.00	0.00	0.00	0.01	0.01	0.00	0.00	0.00	0.00	0.00	0.00
8	0.00	0.00	0.00	0.01	0.00	0.01	0.00	0.00	0.00	0.00	0.00	0.00
9	0.00	0.00	0.00	0.0	0.00	0.01	0.00	0.00	0.00	0.00	0.00	0.00
10	0.71	0.69	0.67	0.57	0.57	0.52	0.89	0.89	0.88	0.85	0.83	0.82

(a)

G=0

	R0=6						R0=18					
	q=0.2			q=0.8			q=0.2			q=0.8		
cases	p=0.91	p=0.93	p=0.96	p=0.91	p=0.93	p=0.96	p=0.91	p=0.93	p=0.96	p=0.91	p=0.93	p=0.96
0	0.31	0.33	0.33	0.39	0.39	0.41	0.14	0.15	0.18	0.16	0.16	0.20
1-5	0.10	0.11	0.15	0.09	0.10	0.10	0.04	0.05	0.06	0.02	0.02	0.02
5-10	0.03	0.03	0.03	0.01	0.01	0.01	0.00	0.00	0.00	0.00	0.00	0.00
10-30	0.02	0.02	0.02	0.00	0.00	0.00	0.00	0.00	0.00	0.00	0.00	0.00
30-50	0.01	0.01	0.00	0.00	0.00	0.00	0.00	0.00	0.00	0.00	0.00	0.00
50-70	0.01	0.00	0.00	0.00	0.00	0.00	0.00	0.00	0.00	0.00	0.00	0.00
70-90	0.00	0.00	0.00	0.00	0.00	0.00	0.00	0.00	0.00	0.00	0.00	0.00
90-110	0.00	0.00	0.00	0.00	0.00	0.00	0.00	0.00	0.00	0.00	0.00	0.00
110-130	0.00	0.00	0.00	0.00	0.00	0.00	0.00	0.00	0.00	0.00	0.00	0.00
130 150	0.00	0.00	0.00	0.00	0.00	0.00	0.00	0.00	0.00	0.00	0.00	0.00
150	0.52	0.50	0.46	0.50	0.48	0.46	0.82	0.80	0.76	0.81	0.80	0.76

G=1

	R0=6						R0=18					
	q=0.2			q=0.8			q=0.2			q=0.8		
cases	p=0.91	p=0.93	p=0.96	p=0.91	p=0.93	p=0.96	p=0.91	p=0.93	p=0.96	p=0.91	p=0.93	p=0.96
0	0.26	0.26	0.3	0.37	0.38	0.40	0.10	0.11	0.13	0.14	0.17	0.18
1-5	0.03	0.03	0.03	0.04	0.05	0.05	0.00	0.00	0.00	0.00	0.00	0.00
5-10	0.00	0.00	0.00	0.00	0.00	0.00	0.00	0.00	0.00	0.00	0.00	0.00
10-30	0.00	0.00	0.00	0.00	0.00	0.00	0.00	0.00	0.00	0.00	0.00	0.00
30-50	0.00	0.00	0.00	0.00	0.00	0.00	0.00	0.00	0.00	0.00	0.00	0.00
50-70	0.00	0.00	0.00	0.00	0.00	0.00	0.00	0.00	0.00	0.00	0.00	0.00
70-90	0.00	0.00	0.00	0.00	0.00	0.00	0.00	0.00	0.00	0.00	0.00	0.00
90-110	0.00	0.00	0.00	0.00	0.00	0.00	0.00	0.00	0.00	0.00	0.00	0.00
110-130	0.00	0.00	0.00	0.00	0.00	0.00	0.00	0.00	0.00	0.00	0.00	0.00
130 150	0.00	0.00	0.00	0.00	0.00	0.00	0.00	0.00	0.00	0.00	0.00	0.00
150	0.71	0.70	0.67	0.57	0.55	0.53	0.90	0.89	0.87	0.85	0.82	0.81

(b)

Figure 4.31: Probability of having extinction, (a) 10 or (b) 150 cases when $G = 0$ (top-row table) and $G = 1$ (bottom-row table) for $p = 0.91$, 0.93, 0.96, $q = 0.2$,0.8, $\mathcal{R}_0 = 6, 18$ and $k_1 = k_2 = 1/30$

4.3 Conclusion

For the model with no age structure, we were able to give a complete and analytical expression for the basic and control reproduction numbers as well as the vaccination threshold needed to achieve herd immunity. All the results obtained from the study of Model (4.1) provide fundamental conditions on waning rates, basic reproduction numbers and fraction of individual with boosted immunity needed to achieve herd immunity. In fact, the exposure of individuals waning their immunity to the infection, will boost their immunity either to the level obtained after the first shot of vaccine, or to a life-long immunity and this increasing of immunity level can benefit the entire population by protecting the unvaccinated individuals from catching the virus. However, part of this boosting process can lead to new infectious individuals affecting the susceptible class and increasing the outbreak cases. It is then more significant increasing the period that a vaccine needs to wane so that the protection will last longer. Moreover, the stochastic model provides information on the probability of extinction. Our results show how if the vaccine-included immunity is life long, the probability of getting an outbreak is possible only for large reproduction numbers. On the other hand, for an immunity which is shorter than the life span, an outbreak is always possible.

Although these results give important information on herd immunity, the age structured model gives more detailed insights into immunity distribution and indirect protection. We find that when a single dose of vaccine is given at 12 months of age, herd immunity is achievable only for life long immunity and only for small $\mathcal{R}_0$. Moreover, we note that the infected compartments always show a bimodal curve with a first peak at age group 5 to 19 years, depending on the waning rates, and a second peak at age group 30-34. Depending on the fraction q of individuals boosting their immunity to V or I (for the case $G = 1$) or I_W (for case $G = 0$) and the vaccination rate p, we observe that the peaks change in magnitude and the peaks located among the youngest age groups shift by 1 or 2 age groups. Moreover, we note that as q increases, the symptomatic cases become more prevalent than the asymptomatic cases in the distribution of the infected compartments. Even for this model, we investigated the probability of extinction. We found that when the immunity is lifelong the probability of having an outbreak is very small. On the other hand, with waning periods shorter than the life span, we can observe the presence of an outbreak. Moreover, comparing these results with the ones in the section describing the model without age structure, we observe how the introduction of an age structure reduces the probability of outbreak. This suggests that age dependent contacts and population structure are fundamental factors to control the infection spread.

In this chapter we investigated the infection dynamic at the endemic equilibrium. However, vaccination, waning and boosting processes might affect, differently, a single outbreak. Moreover, the age structure model assumes only one vaccine dose is given, but the recommendations consider a second dose. The next two chapter are focused on the analysis of single outbreak of Model (4.10), and the herd immunity investigation when a double dose of vaccine is provided.

Chapter 5

Waning Immunity: Single Outbreak

5.1 Introduction

This work has been conducted in collaboration with Dr. Heffernan, Dr. Teslya, Dr. Crowcroft and Dr. Bolotin. I have collaborated in conducting numerical analyses.

In the previous chapter, we investigated the distribution of population at the endemic equilibrium. The stochastic simulations, shown in the previous section, provided information on the conditions under which it is possible to experience an outbreak. Now, we investigate the impact that waning and boosting processes and vaccination coverage have on the infection dynamics within a short term and how this can provide some insights into the response that public health should have in case of a potential outbreak. Here, we focus our study on a single outbreak period corresponding to roughly 1 year. We analyse final size, peak of infection, the time at which the peak occurs and the time at which the epidemic ends. We present here the analysis for Model (4.10) for $G = 0, 1$.

5.2 Results

$G = 1$

We immediately observe that when immunity is not life-long (see Figure (5.1)), the outbreaks occur over 5-12 months. On the other hand, when the period of immunity is longer than life span, different scenarios are presented: the outbreak can occur with a high peak of infected individuals and ending within one year, can be sustained for a period longer than one year or can be extremely small (Figure 5.2). When the outbreak does not end within 12 months, then it will be defined as unrealistic and not considered in the analysis.

Figure (5.3-5.4-5.5) and (5.6,5.7,5.8) refer to cases when vaccine-induced immunity is shorter than the life span and when immunity is life long, respectively. Figure (5.3a) represents the final size of S, defined as the total loss of individuals in the susceptible compartment within the outbreak. We observe that for individuals belonging to age groups 0.5 to 64 years, both large and small $\mathcal{R}_0$ present the same pattern and level of loss. However, for older age

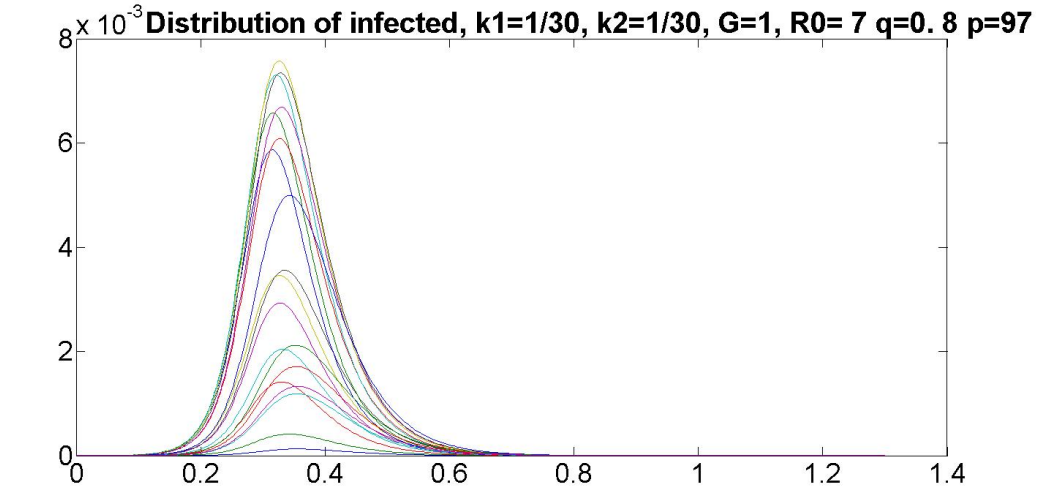

(a)

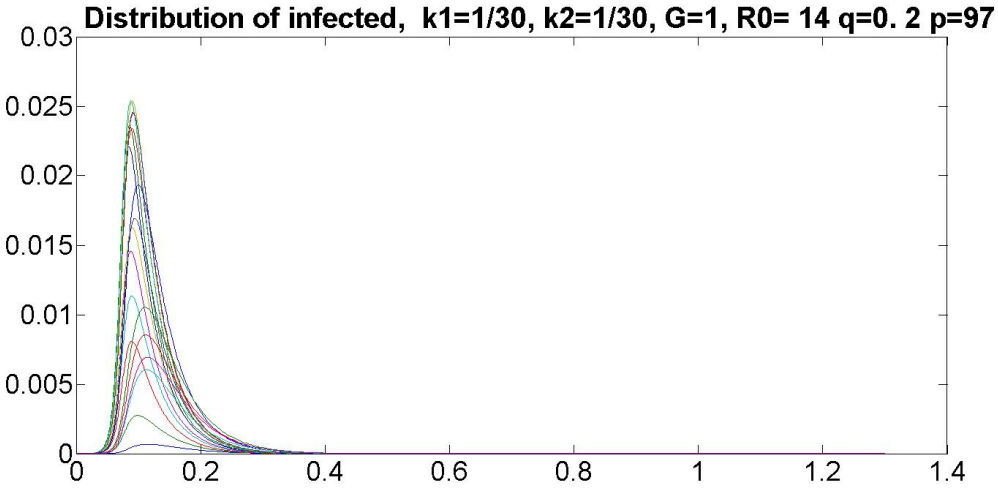

(b)

Figure 5.1: Proportion of infected individuals for $k_1 = k_2 = 1/30$, $p = 0.96$, $G = 1$ (a) $\mathcal{R}_0 = 7$, $q = 0.8$ (b) $\mathcal{R}_0 = 14$, $q = 0.2$

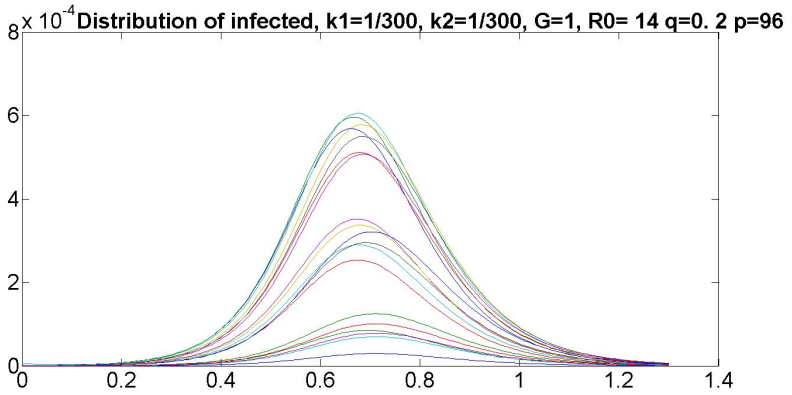

(a)

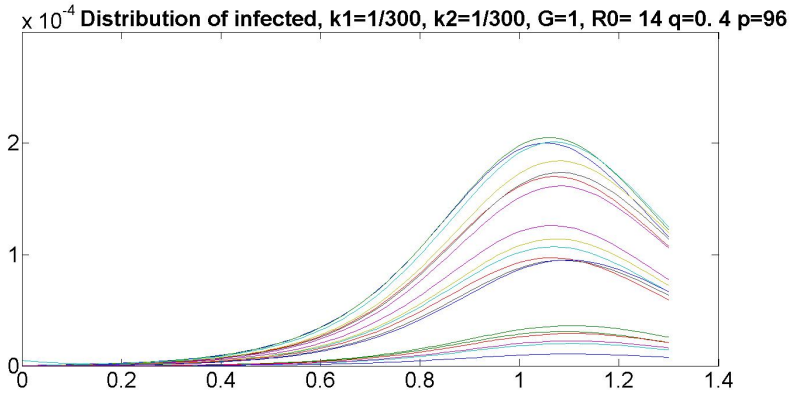

(b)

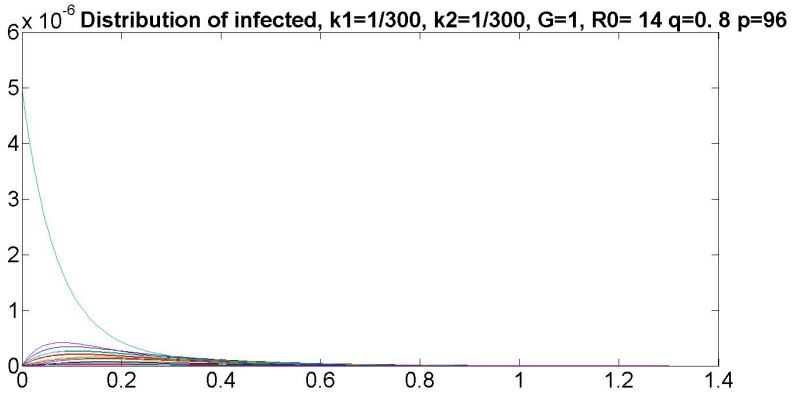

(c)

Figure 5.2: Proportion of infected individuals for $\mathcal{R}_0 = 14$, $k_1 = k_2 = 1/300$, $p = 0.96$, $G = 1$ (a) $q = 0.2$ (b) $q = 0.4$ (c) $q = 0.8$

groups, it is visible that for large reproductive numbers the loss in the susceptible individuals is higher than the one obtained for small $\mathcal{R}_0$. This suggests that for small reproductive numbers a more significant number of elderly will remain susceptible and this might lead to a bigger outbreak in case the infection is introduced in the population. A similar pattern, even if less evident, is shown in Figure (5.3b), representing the loss of individuals in the waning stage. In Figure (5.4a) we observe that as q increases, the maximum number of infected individuals decreases. Moreover, in the case $k_1 = 1/5$ and $k_2 = 1/50$ and the case $k_1 = 1$ and $k_2 = 1/25$, the age groups presenting highest peaks are the ones ranged between 5-9 and 20-24 years and in age groups 30-34 to 60-64 years. We observe that as the vaccination coverage and the number of secondary cases able to transmit the infection increase, the time needed to reach the peak of infection increases. Also, this peak is reached faster when the reproductive number assumes larger values (Figure (5.4b)). Same pattern is shown in Figure (5.5a) representing the time at which the epidemic ends. We observe that the age groups sustaining the infection for a longer period are 25-29 and 65-69 years. Figure (5.6), corresponding to $k_1 = k_2 = 1/300$, presents different outcomes. Importantly, due to unrealistic scenarios, cases with $\mathcal{R}_0 = 8, q = 0.2, p = 0.91$ and $\mathcal{R}_0 = 18, q = 0.8, p = 0.96$ are not reported. The figures related to the final size of S and W (Figures (5.6a) and (5.6b)) show that all the age groups do not present any loss for small $\mathcal{R}_0$. On the other hand, for large $\mathcal{R}_0$ the age groups presenting the highest loss of susceptible are 5-9 to 15-19 years and 30-34 to 60-64 years. Moreover, a higher vaccination coverage and number of asymptomatic cases provide a reduction in the spread of the infection and consequently a minor loss in S and W. Since for small $\mathcal{R}_0$ the infection does not result in big outbreak, the peak of infection is close to 0 and it occurs within the first month. For large reproductive numbers, a lower vaccination coverage produces bigger outbreaks and more time is needed to reach its peak (Figure 5.7a). Observe that the time needed to reach the peak of infection increases as the reproduction number and number of transmitters increase (Figure 5.7b). If the number of vaccinated individuals increases, then the spread of the infection becomes slower. In Figure (5.8a) we observe that as the number of secondary cases decreases, the time needed for the epidemic to end increases. Moreover, for small $\mathcal{R}_0$ and low vaccine coverage the outbreak needs more time to reach its end.

$G = 0$

Here, we investigate the scenario in which secondary cases are not able to transmit the infection. Similar to the previous analysis, we observe that for waning periods shorter than life span, the outbreak starts and ends within 12 months (Figure (5.9)). When the immunity lasts for life, we observe that for large reproduction numbers, as the vaccination coverage increases the outbreak can either end within the year, or being sustained for a longer time-frame or being almost insignificant (Figure (5.10)).

We immediately observe the scenario of single outbreak shown in this section is similar to the one presented in the case when secondary cases are as infectious as primary cases ($G = 1$). The distribution of the susceptible final size (Figure (5.11a)) suggests that for small

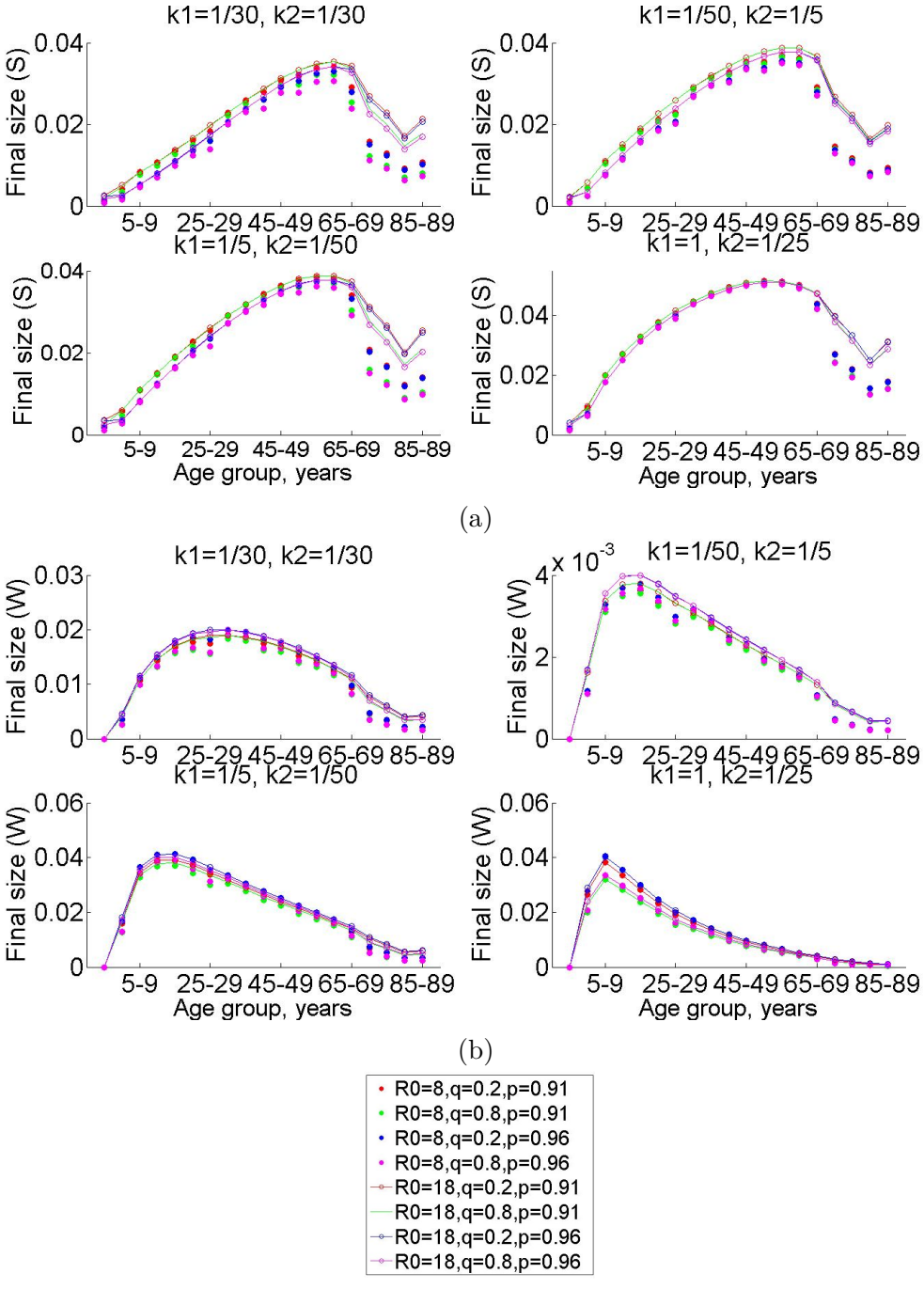

Figure 5.3: Distribution of (a) susceptible final size (b) waning final size for $\mathcal{R}_0 = 8$, 18, $q = 0.2$, 0.8 and $p = 0.91$, 0.96 and $G = 1$; (c) Legend

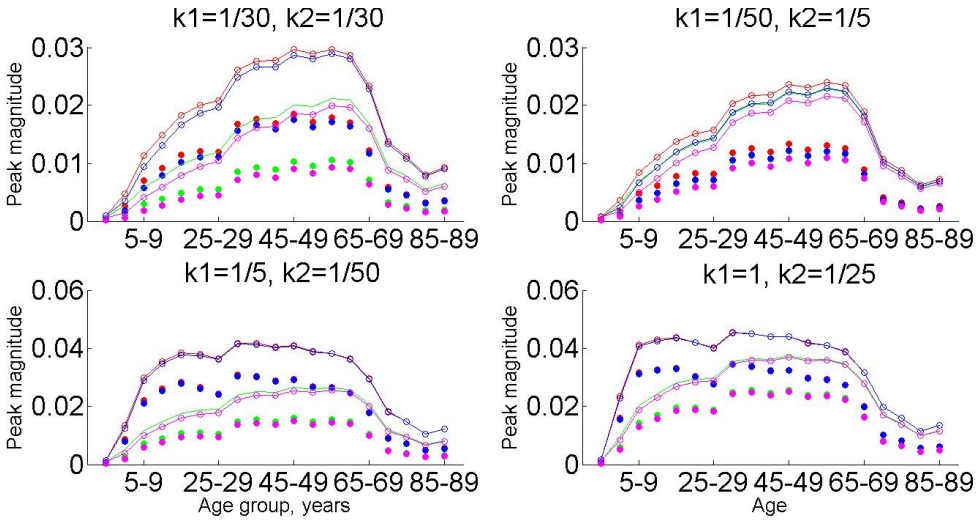

(a)

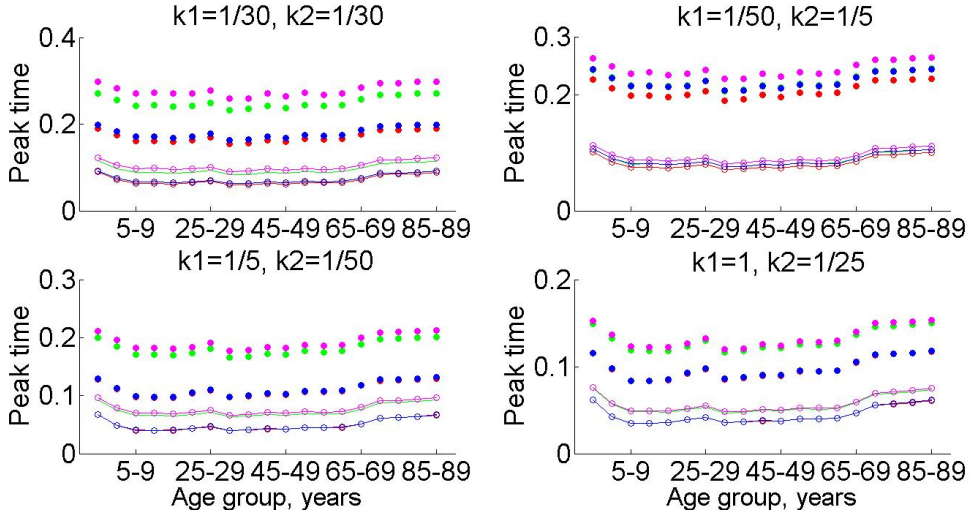

(b)

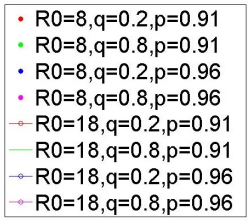

(c)

Figure 5.4: Distribution of (a) infected peak magnitude (b) time of infection peak for $\mathcal{R}_0 = 8$, 18, $q = 0.2$, 0.8 and $p = 0.91$, 0.96 and $G = 1$

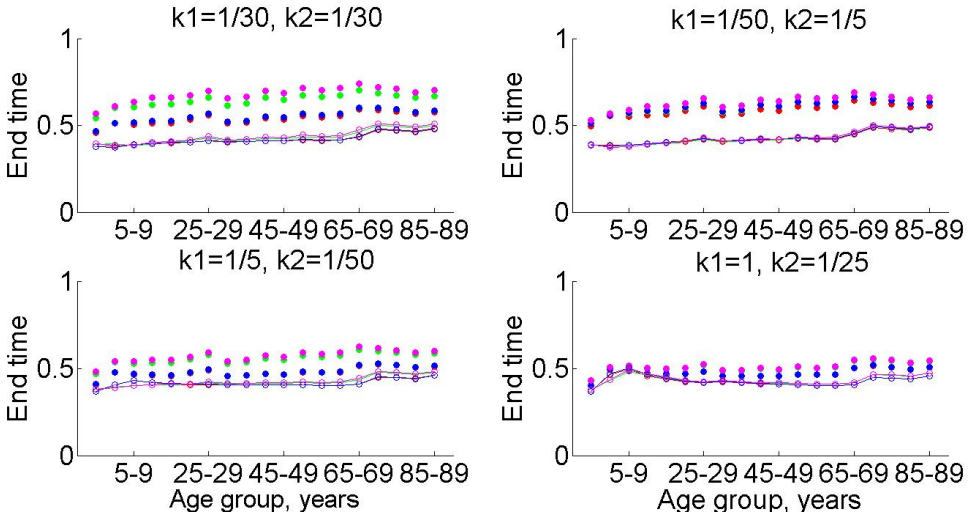

(a)

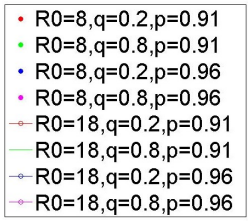

(b)

Figure 5.5: Distribution of (a) end of epidemic time for $\mathcal{R}_0 = 8$, 18, $q = 0.2$, 0.8 and $p = 0.91$, 0.96 and $G = 1$

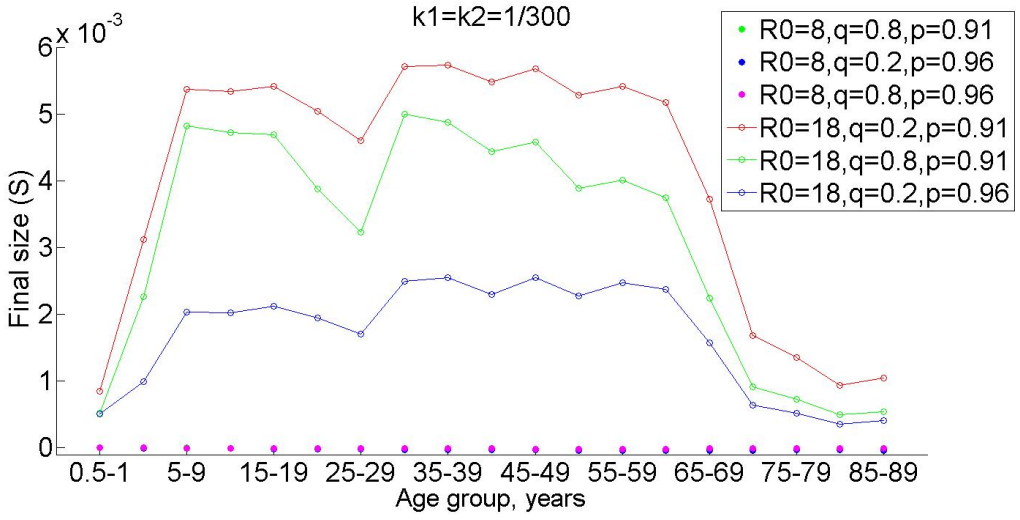

(a)

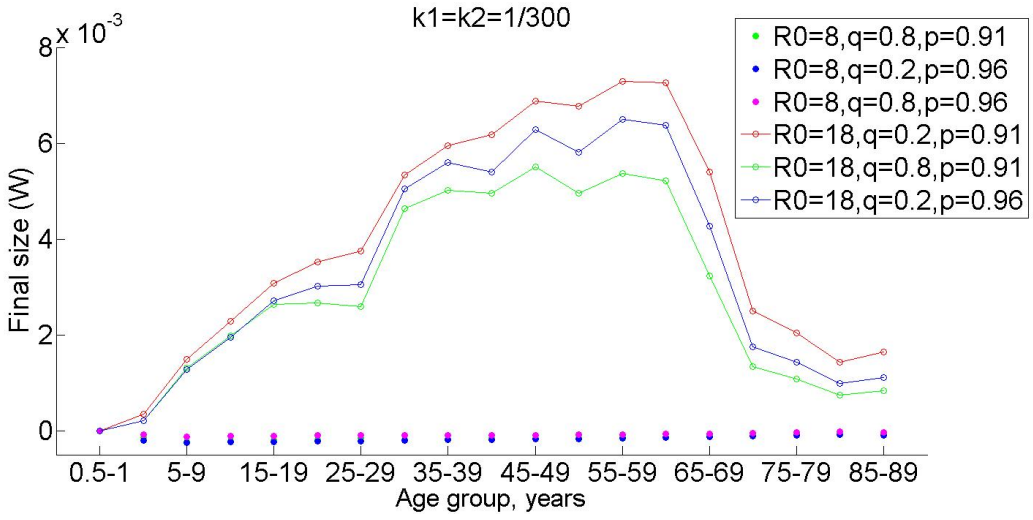

(b)

Figure 5.6: Distribution of (a) susceptible final size (b) waning final size for $\mathcal{R}_0 = 8$, 18, $q = 0.2$, 0.8 and $p = 0.91$, 0.96 and $G = 1$. Observe that the missing cases correspond to unrealistic scenarios

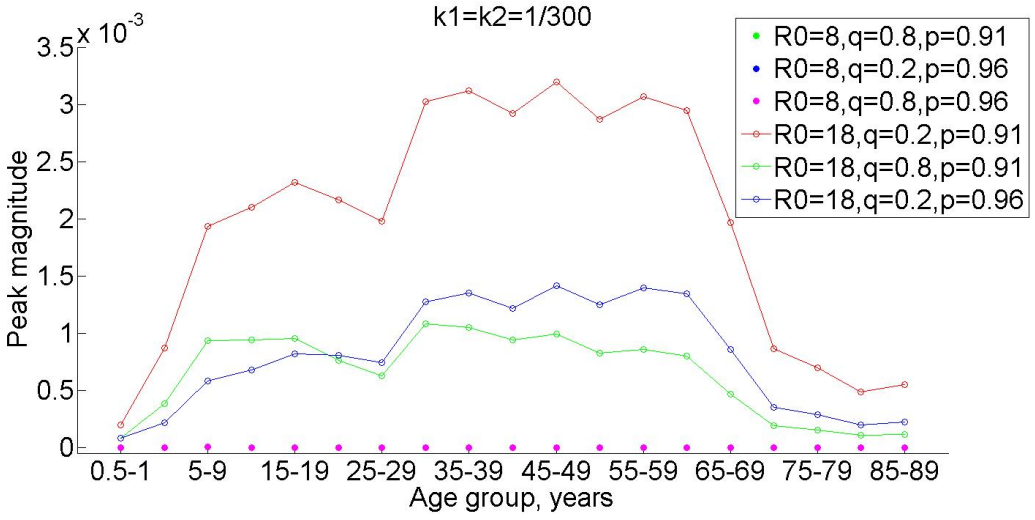

(a)

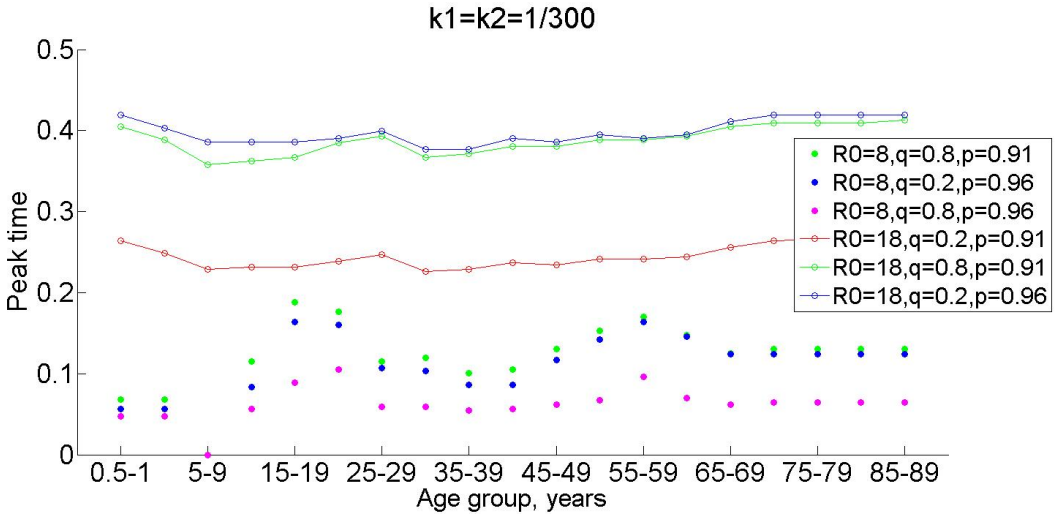

(b)

Figure 5.7: Distribution of (a) infected peak magnitude (b) time of infection peak for $\mathcal{R}_0 = 8$, 18, $q = 0.2$, 0.8 and $p = 0.91$, 0.96 and $G = 1$. Observe that the missing cases correspond to unrealistic scenarios

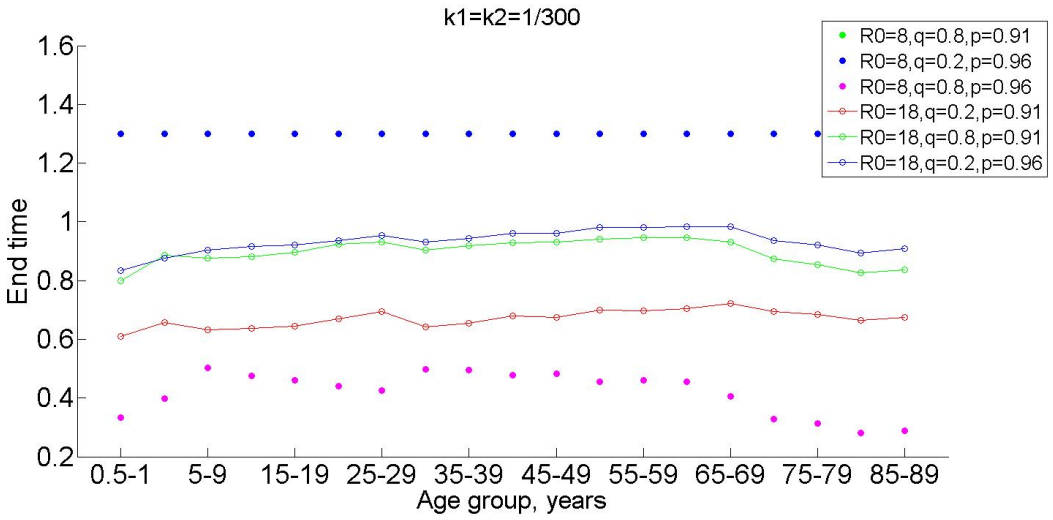

(a)

Figure 5.8: Distribution of (a) end of epidemic time for $\mathcal{R}_0 = 8$, 18, $q = 0.2$, 0.8 and $p = 0.91$, 0.96 and $G = 1$. Observe that the missing cases correspond to unrealistic scenarios

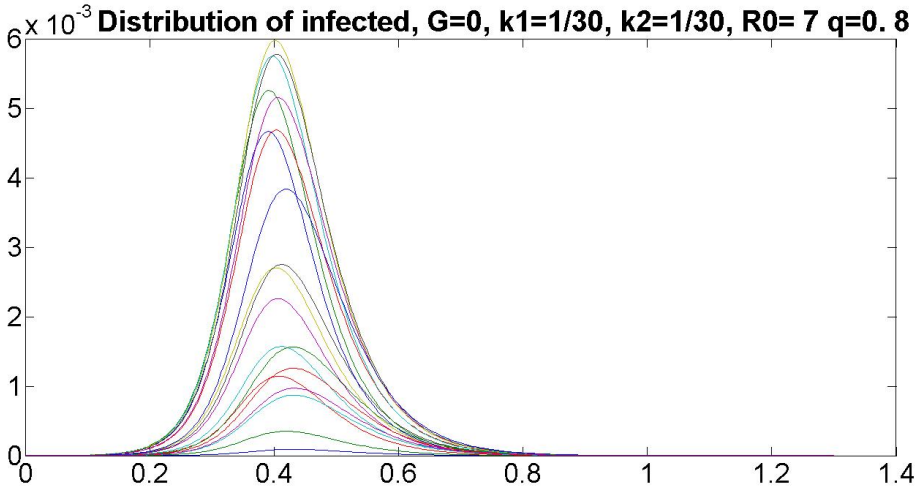

(a)

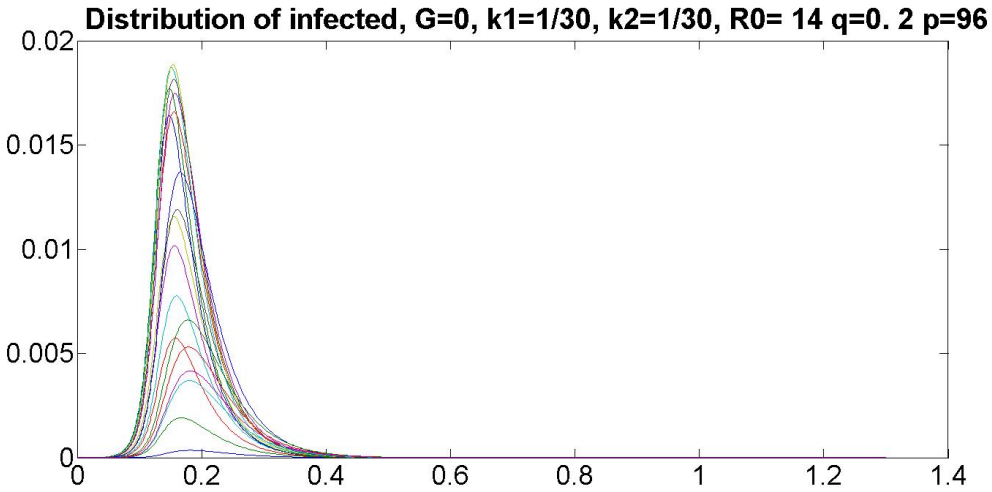

(b)

Figure 5.9: Infected individuals for $k_1 = k_2 = 1/300$, $G = 0$ (a) $\mathcal{R}_0 = 7$, $q = 0.8$ (b) $\mathcal{R}_0 = 14$, $q = 0.2$

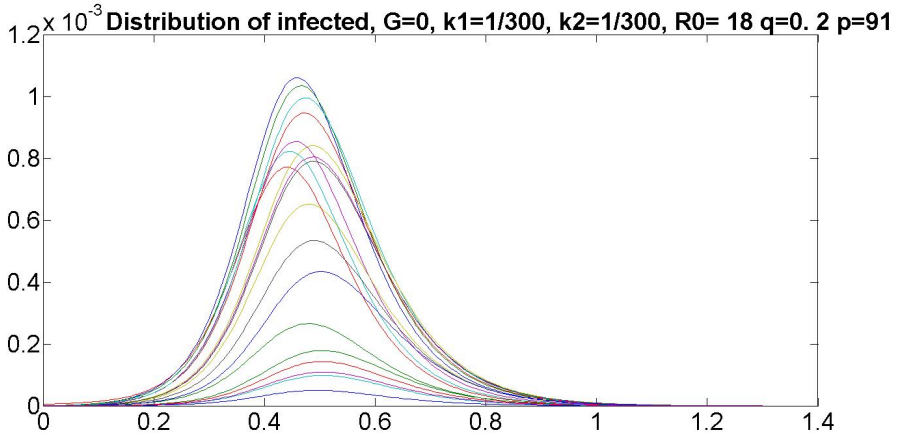

(a)

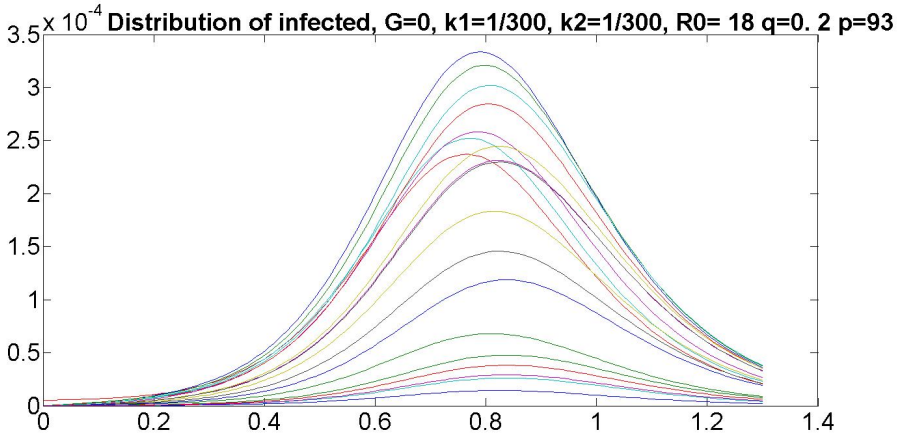

(b)

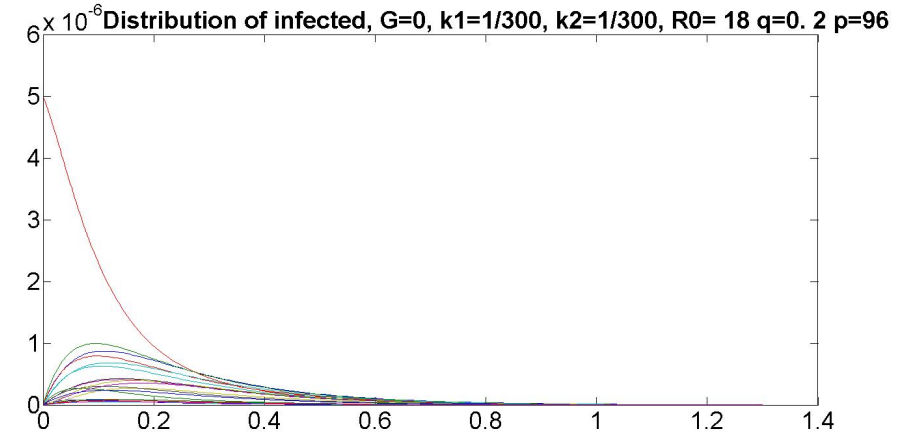

(c)

Figure 5.10: Infected individuals for $\mathcal{R}_0 = 18$, $k_1 = k_2 = 1/300$, $q = 0.2$, $G = 0$ (a) $p = 0.91$ (b) $p = 0.93$ (c) $p = 0.96$

$\mathcal{R}_0$, less individuals in the elderly age groups experience the infection when compared to the the same age groups for larger reproduction numbers. This indicates that in case of a second outbreak this proportion of population is at higher risk of infection. Similar to the model for $G = 1$, the magnitude of the peak of the infection decreases as the reproduction number value decreases and the vaccination rate increases (Figure 5.12a). Moreover, contrary to the previous analysis, the time needed to reach the maximum spread of the infection increases as the reproduction number decreases and the vaccination rate increases. (Figure 5.12b). Observe that when the proportion of secondary cases whose immunity is boosted to V increases (i.e., q increases), the infection is sustained for a shorter period. Moreover, the bigger the reproduction number is, the shorter the outbreak will be (Figure 5.13a).
Next, we investigate the life-long immunity scenario. Figure (5.14a) shows that for small $\mathcal{R}_0$ and $\mathcal{R}_0 = 18$ with $p = 0.96$ the susceptible subpopulation does not present any loss, suggesting a very small outbreak occurring. Same pattern is shown among the individuals in the waning stage. As a result of it, Figure (5.15a) shows that the outbreak is sustained affecting the population only for $\mathcal{R}_0 = 18$ and $p = 0.91$. Under the same conditions, the infection needs a longer period to achieve its maximum peak (Figure 5.15a). Moreover, the bigger the $\mathcal{R}_0$ is and the larger the proportion of vaccinated individuals is, the longer the outbreak will be (Figure 5.16a).

5.3 Conclusions

The analysis on a single outbreak reveals that if the immunity is shorter than the life span, the outbreak elapses within 5-12 months from its beginning. On the other hand, if the immunity is life-long, the outbreak can never occur, occur without ending within 12 months, or occur and ending within one year. The final size of both S and W present the same pattern. For large reproduction number, the elderly age classes (aged more than 65 years) "loss" in the susceptible and waning compartments is higher. This suggests that for small reproduction numbers, a significant proportion of elderly remain vulnerable to a possible second wave of the infection. These results indicates that Public Health should focus on protecting individuals in these age categories. We also found that the infectious cases decrease as the proportion of individuals in the waning stage getting boosted to V increases. When the waning period to become fully susceptible is long (e.g. $25 - 50$ years), we observed that the age groups with highest infected reported are within $5 - 24$ years and $60 - 64$. Moreover, the time at which the peak occurs is longer for small reproduction numbers and higher vaccination coverage. The results for the life-long immunity show that the S and W final size is not significant for small $\mathcal{R}_0$. While, for large reproduction numbers, the age groups $5 - 19$ years and $30 - 64$ years show the highest loss of S and W. For small $\mathcal{R}_0$, the outbreak is extremely small and it occurs within the first month of outbreak. When the reproduction number is bigger, a higher vaccination coverage reduces the spread and the time needed to reach the peak. We conclude our analysis stating that, according to our results, children, young adults and elderly need to be the main concern to Public Health in order to protect these individuals and prevent outbreaks. Moreover, the transmission from vaccinated case, as well as waning periods, needs

a deeper understanding, since it can affect the dynamic of the infection.

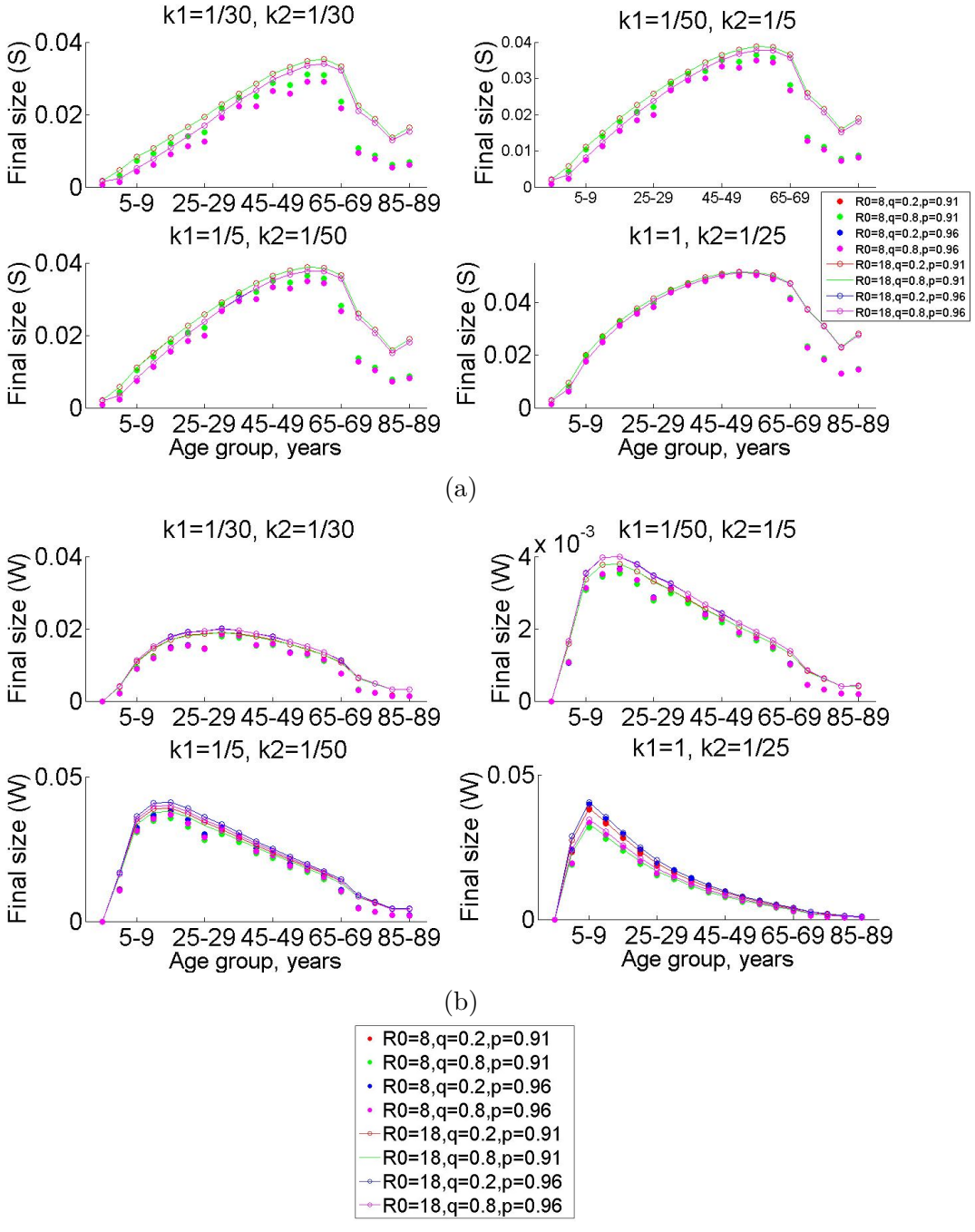

(a)

(b)

(c)

Figure 5.11: Distribution of (a) susceptible final size (b) waning final size for $\mathcal{R}_0 = 8$, 18, $q = 0.2$, 0.8 and $p = 0.91, 0.96$ and $G = 0$.

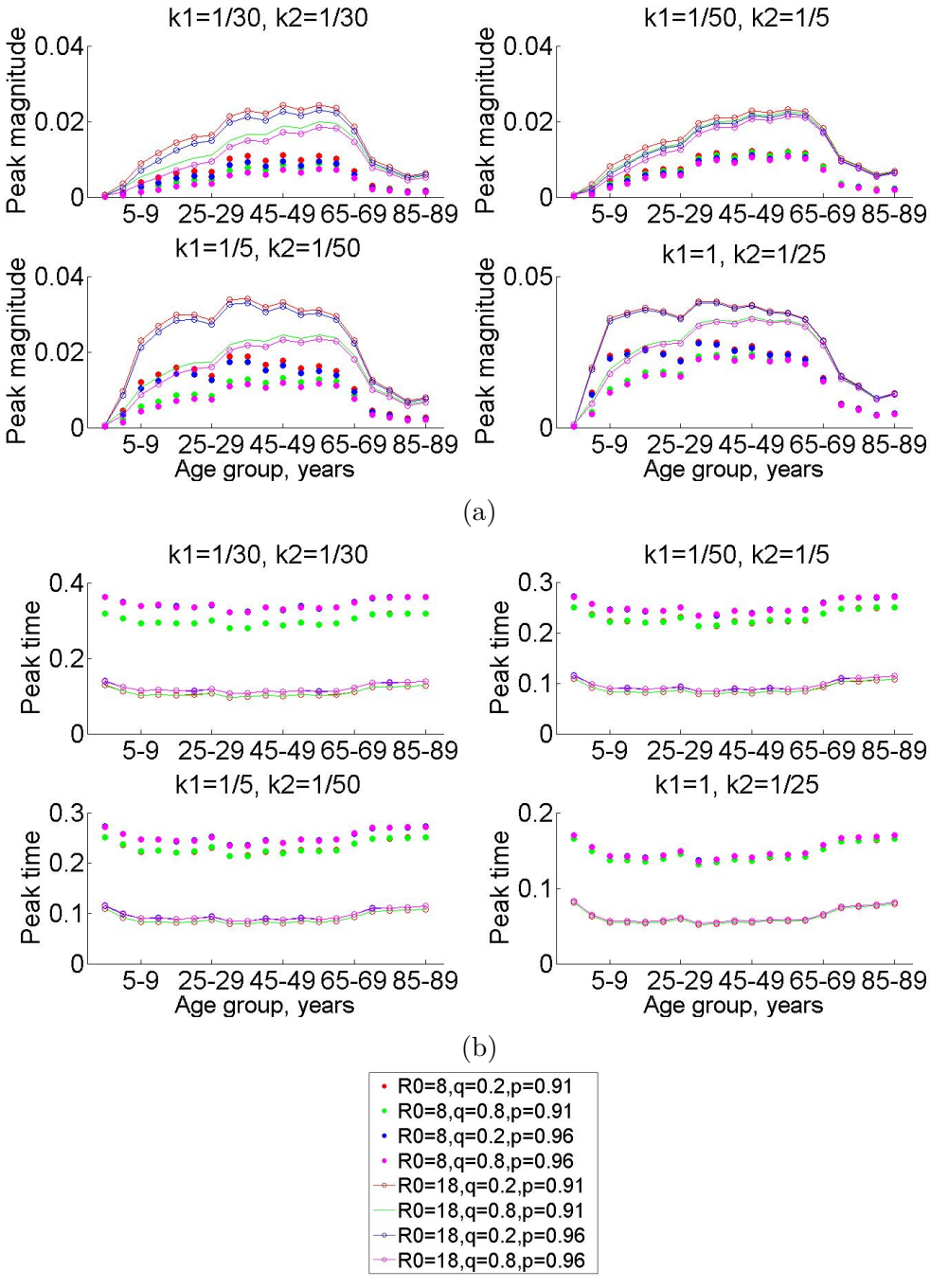

Figure 5.12: Distribution of (a) infected peak magnitude (b) time of infection peak for $\mathcal{R}_0 = 8$, 18, $q = 0.2$, 0.8 and $p = 0.91$, 0.96 and $G = 0$.

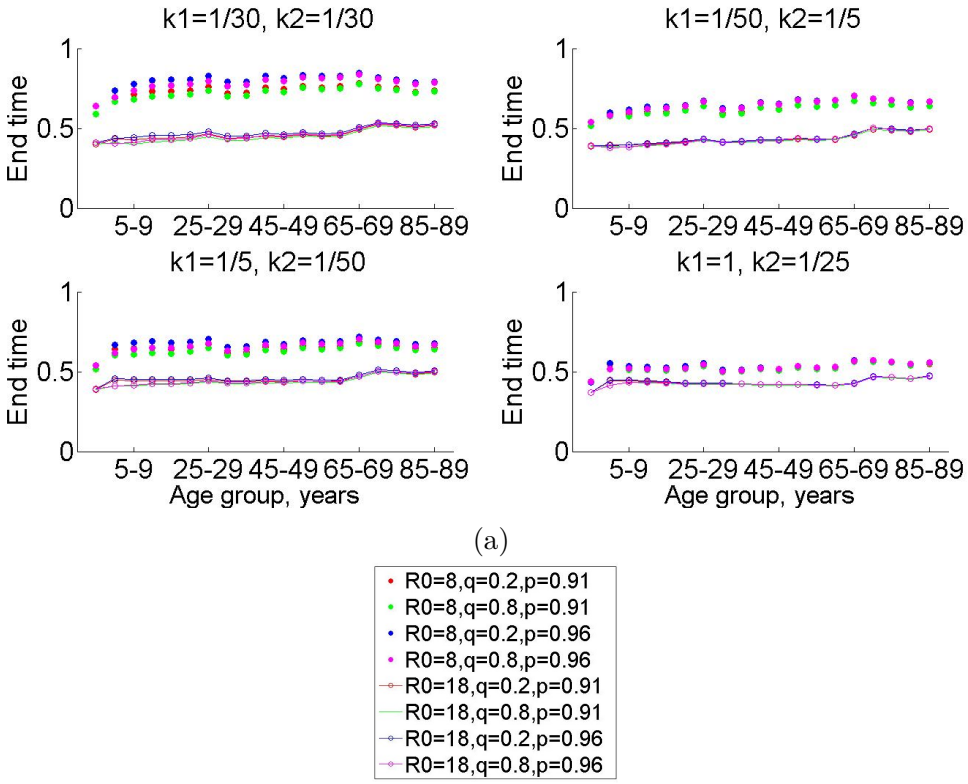

(a)

(b)

Figure 5.13: Distribution of end of epidemic time for $\mathcal{R}_0 = 8$, 18, $q = 0.2$, 0.8 and $p = 0.91$, 0.96 and $G = 0$.

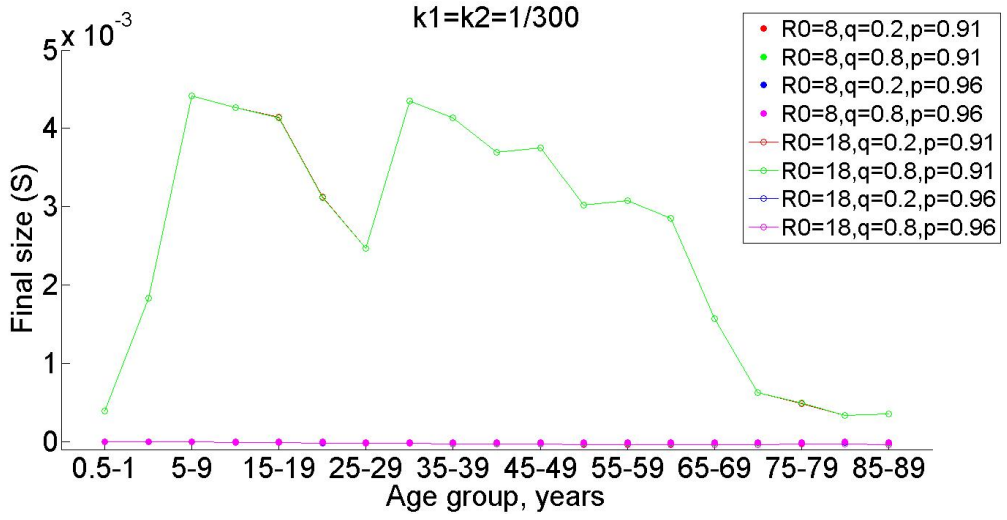

(a)

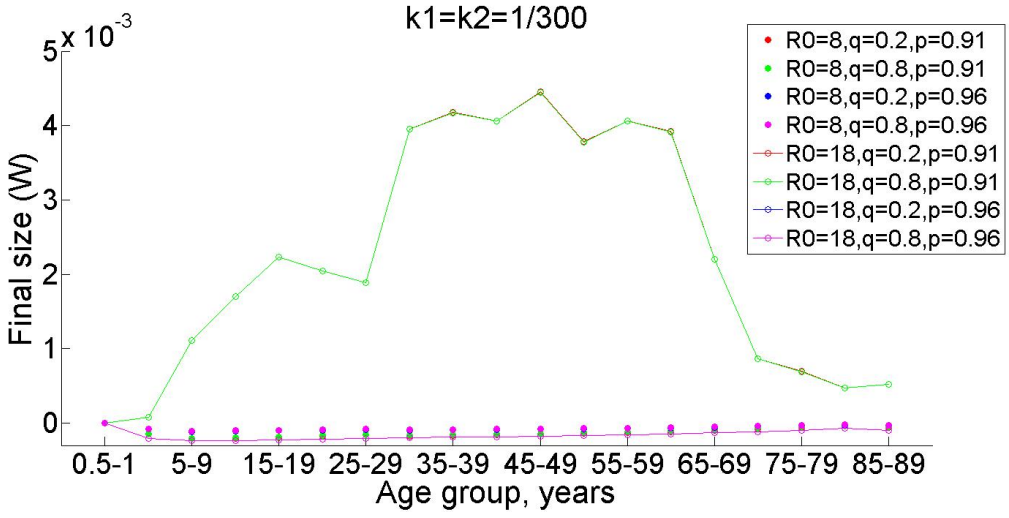

(b)

Figure 5.14: Distribution of (a) susceptible final size (b) waning final size for $\mathcal{R}_0 = 8$, 18, $q = 0.2$, 0.8 and $p = 0.91$, 0.96 and $G = 0$. Observe that the missing cases correspond to unrealistic scenarios

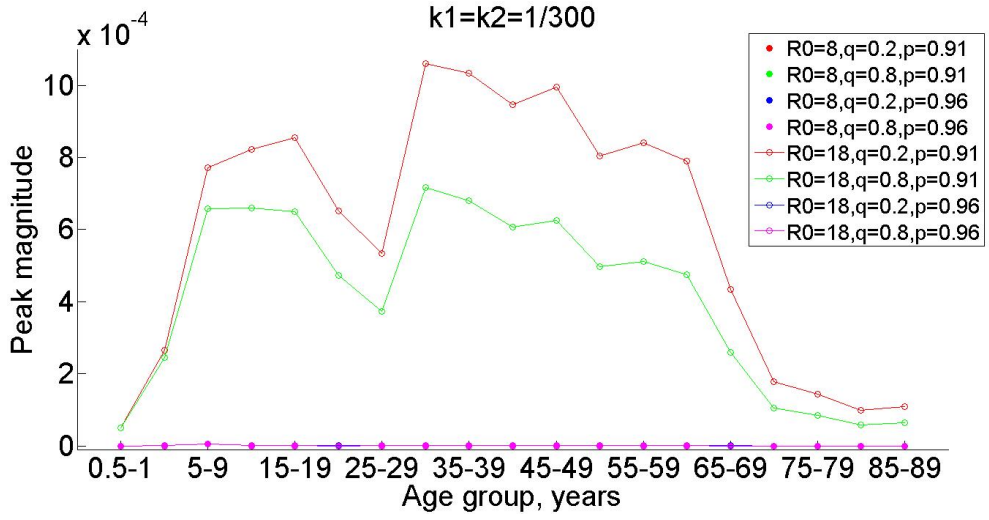

(a)

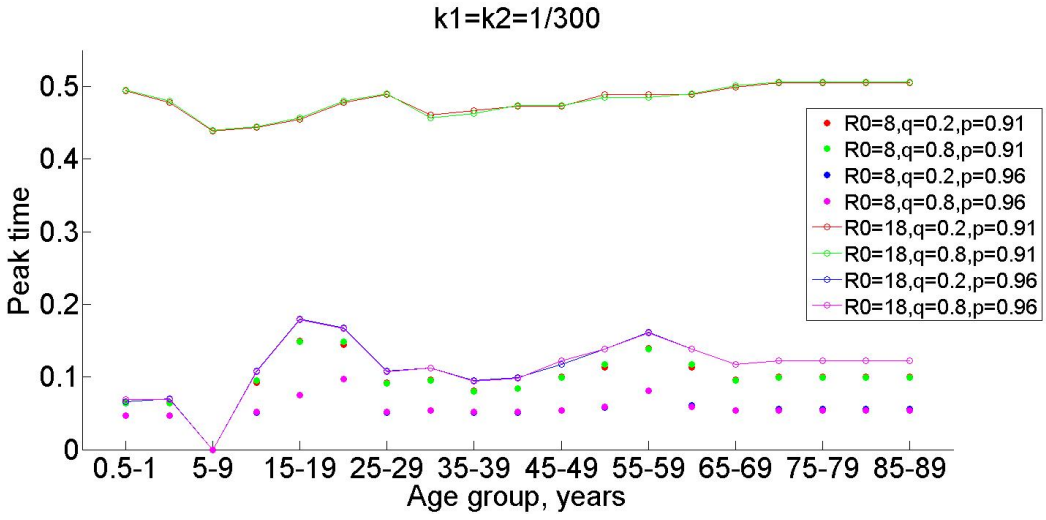

(b)

Figure 5.15: Distribution of (a) infected peak magnitude (b) time of infection peak for $\mathcal{R}_0 = 8$, 18, $q = 0.2$, 0.8 and $p = 0.91$, 0.96 and $G = 0$. Observe that the missing cases correspond to unrealistic scenarios

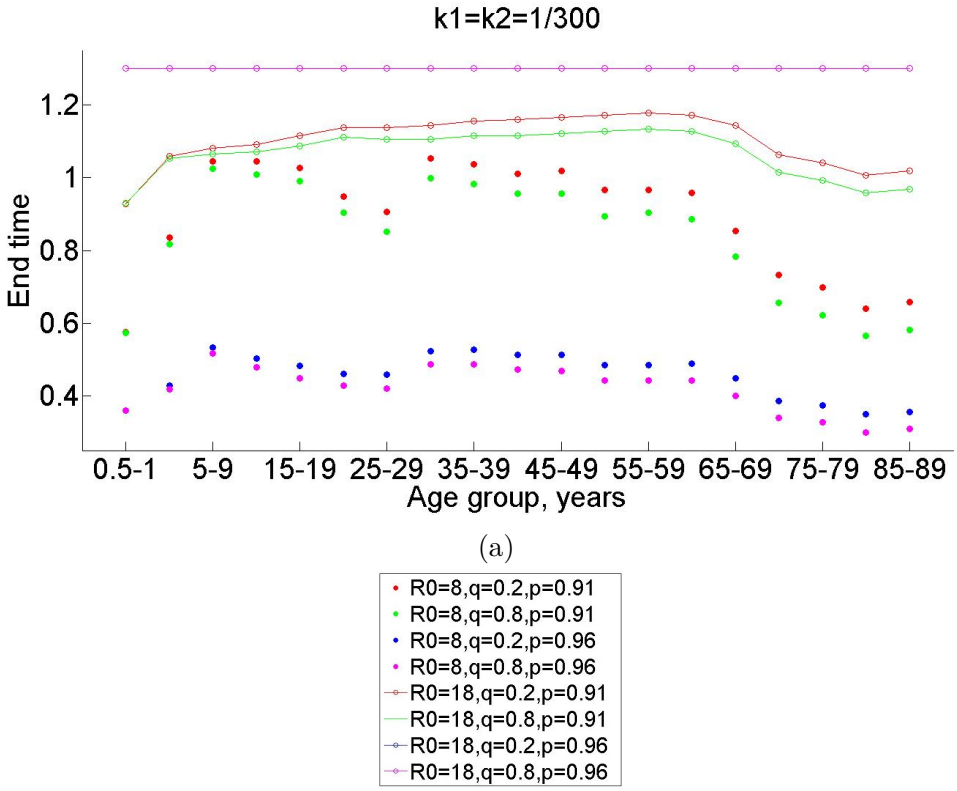

Figure 5.16: Distribution of end of epidemic time for $\mathcal{R}_0 = 8$, 18, $q = 0.2$, 0.8 and $p = 0.91$, 0.96 and $G = 0$. Observe that the missing cases correspond to unrealistic scenarios

Chapter 6

Waning Immunity: Two Vaccine Doses

6.1 Introduction

This work has been conducted in collaboration with Dr. Heffernan, Dr. Teslya, Dr. Crowcroft and Dr. Bolotin. I have collaborated in conducting theoretical and numerical analyses. Figure 6.2 was generated by Dr. Teslya.

According to the vaccination routine recommended [119, 11], a second dose of measles vaccine should be given to children aged between 18 months and school age. This program has been introduced to provide immunization coverage to these children who experience primary vaccine failure (i.e., their immune system does not produce antibodies after the first dose of vaccine). We extend Model (4.10) by including a second vaccine shot to children before turning 5. We investigate the control reproduction number in relation to waning periods, $\mathcal{R}_0$ and vaccination coverage as well as the distribution of immunity among the age groups defined in System (4.10) at the DFE.

6.2 Model and Methods

6.2.1 Model

To introduce a second vaccination dose at 5 years, we modify the equations regarding susceptible and vaccinated compartments of this age group (S_3 and V_3) as follows:

$$S_3' = (1-p)c_2S_2 - (\mu_3 + c_3)S_3 - S_3\sum_{j=1}^{n}\beta_{3,j}I_j + k_2W_3 \tag{6.1a}$$

$$V_3' = pc_2S_2 + c_2V_2 - (\mu_3 + c_3 + k_1)V_3 + q\nu W_3\sum_{j=1}^{n}\beta_{3,j}I_j \tag{6.1b}$$

Disease Free Equilibrium (DFE)

We start looking at the DFE for this model varying the waning rates according to Eq(4.7) and $p = 0.91, 0.93, 0.96$ (Figure(6.1)).

Observe that, as expected, as the vaccination rate increases, the susceptible distribution decreases. Although the vaccinated distribution increases as p increases, in some scenarios this distribution is drastically low (case $k_1 = 1, k_2 = 1/25$ in Figure 6.1). Moreover, when immunity is life-long (top panel in Figure 6.1) the distribution of W shows an increasing trend by age. On the other hand, when the immunity period is shorter than the life span, the distribution of W is more prevalent among the youngest age groups, even when this distribution is very small (case $k_1 = 1/50, k_2 = 1/5$ in Figure 6.1). These results indicate that in case of an outbreak, the youngest age groups are the ones who will experience either an immunity boosting or a mild infection.

Control Reproduction Number $\mathcal{R}_c$

Similar to system (4.10), we derive the $\mathcal{R}_c$ for system 6.1. We start by finding the DFE with vaccination. The expression is the same as the one-single dose, except for the following components:

$$V_3 = \frac{pc_2}{\mu_3 + c_3 + k_1} S_2 + \frac{c_2}{\mu_3 + c_3 + k_1} V_2 \tag{6.2a}$$

$$W_3 = \frac{c_2}{c_3 + \mu_3 + k_2} W_2 + \frac{k_1}{\mu_3 + c_3 + k_2} V_3 \tag{6.2b}$$

$$S_3 = \frac{(1-p)c_2}{\mu_3 + c_3} S_2 + \frac{k_2}{\mu_3 + c_3} W_3 \tag{6.2c}$$

We use the *next-generation matrix method* again where matrices $\mathcal{F}$ and $\mathcal{V}$ used for the calculation of $\mathcal{R}_c$ remain the same as the single dose. We investigate the control reproduction number numerically. Similar to the single dose scenario, the blue and red surfaces in Figure (6.2) and Figure (6.3) represent the threshold $\mathcal{R}_c = 1$ when $G = 1$ and $G = 0$, respectively.

Figure (6.2) shows the control reproduction number for Model (6.1) when $G = 1$. Similar to the single dose scenario, these results are for $\mathcal{R}_0 = 6$. We observe that the herd immunity is possible for a wide interval of q and p only in the case that vaccine-induced immunity is lifelong. This indicates that regardless of the fraction of infectious secondary cases and the low level of vaccination coverage, if immunity is longer than the life span, herd immunity is always achievable. On the other hand, a short immunity never makes the indirect protection possible. However, we observe that the control reproduction number in the scenario with double shot is lower than the one seen in the single dose case. For $G = 0$, we note that, contrary to the single dose, in the scenario of life-long immunity, herd immunity is always achievable, independently on the $\mathcal{R}_0$ and p (Figure 6.3a). Similar to the single dose, Figure (6.3) shows that the control reproduction number is sensitive to k_1. Similar to the case with $G = 1$, although herd immunity cannot be achieved for waning period shorter than life span,

we observe that the values of the $\mathcal{R}_c$ obtained in the double-shot scenario are lower than the ones shown in Figure 4.7.

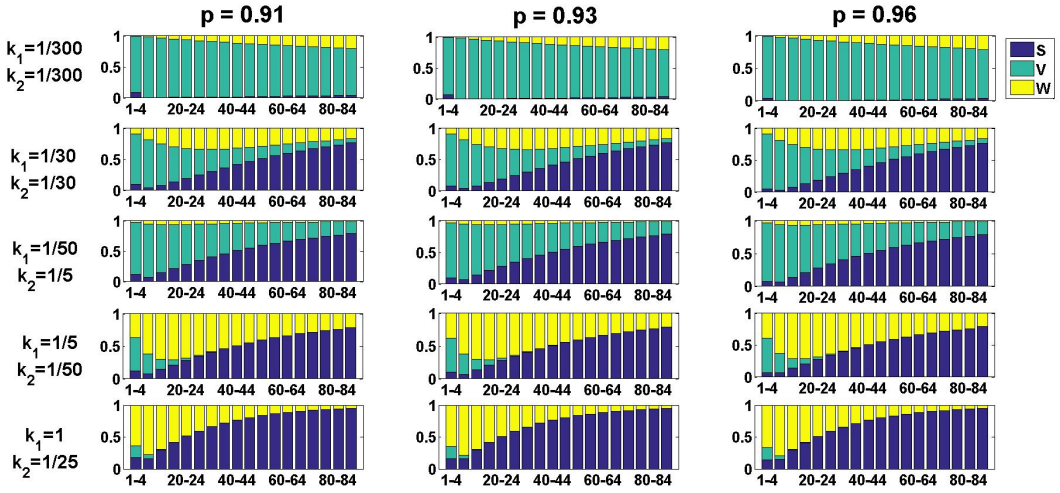

(a)

Figure 6.1: Distribution of susceptible, vaccinated and waning compartments for system (6.1) at the disease-free equilibrium.

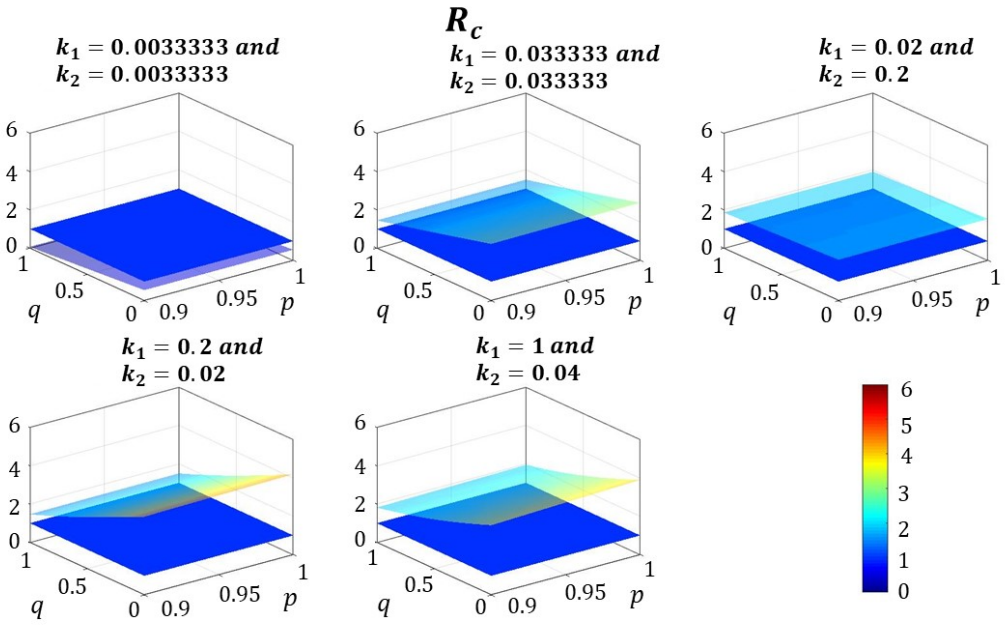

Figure 6.2: Surface plots of control reproductive number for $G = 1, \mathcal{R}_0 = 6$ in the two-dose framework for Model (6.1). The blue surfaces indicates the threshold $\mathcal{R}_c = 1$.

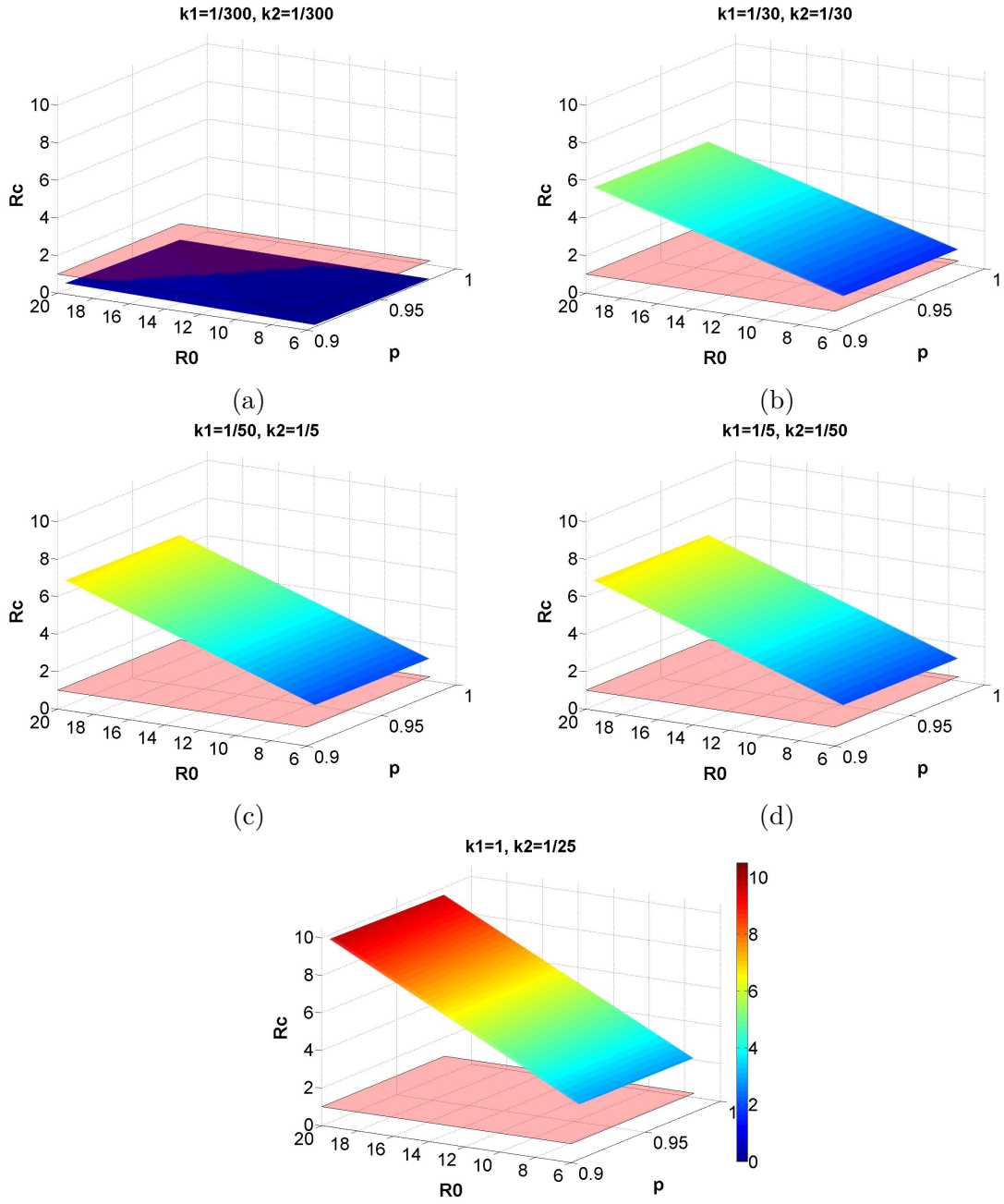

Figure 6.3: Surface plots of control reproductive number for $G = 0$ in the two-dose framework for Model (6.1). The red surfaces indicates the threshold $\mathcal{R}_c = 1$.

6.3 Conclusions

A further analysis on the age structure model has been carried out by including a second vaccination shot at age 5 years in Model (4.8). We observe that with a lifelong immunity, in both cases $G = 0$ and $G = 1$ herd immunity is always achievable for both small and large $\mathcal{R}_0$, independently, from the fraction of individuals obtaining the vaccine and the infectious secondary cases. However, as the waning period is less than the life span, achieving herd immunity will be impossible. We also note that the control reproduction number in the double-dose scenario shows a lower magnitude than the one in the single dose case.

Chapter 7

Conclusions

In this thesis we developed a series of compartmental models, both deterministic and stochastic, highlighting factors that might cause the re-emergence of measles in a highly vaccinated country as Canada. We investigated the *control reproduction number*, the dynamics of measles outbreak and the age groups mostly affected by the infection. Since the cause of these reoccurring episodes of measles might be attributed to immigration from an endemic country, the increasing vaccine hesitancy, waning immunity over time or all of them combined, we started our investigation from a large scale (population divided into Canadians and immigrants) to a smaller scale (distribution of immunity in a single population).

The $SEIR$ model with vaccination, employed to investigate if immigration is indeed affecting the spread of MeV or, instead, increasing the level of immunity in Canada, show how the recovery classes of immigrants (both children and adults) increases the level of indirect protection in the country. This suggests that individuals coming from endemic countries are bringing with them a life long immunity, acquired by the infection, which can help the local community to reduce the spread of the virus. Similarly, if vaccinated, immigrants boost the level of immunity in Canada.
However, some immigrants are from countries where vaccination is not available and they are still susceptible when landing in Canada. Our results suggest that the proportion of vulnerable immigrant adults and the vaccination coverage among Canadians are the main factors in achieving herd immunity in the country. Hence, it is crucial to reduce the susceptible class of adult immigrants and Canadian children. A reduction in the vulnerable class of immigrant adults can be obtained by offering newcomers a free measles vaccine shot upon arrival. However, the main goal of Public Health should increase, and maintain high, the vaccination coverage among local children.

After the previous general analysis, we focused on the effect that mobility and vaccine heterogeneity have on the transmission and spread of the infection in the Greater Toronto Area (GTA) (Toronto-York-Peel-Halton-Durham regions). We employ an $SEAIR$ model with vaccination where the mobility among all the patches is captured by the time that individuals spend in their home or work place patch. Given the importance of asymptomatic cases in spreading the infection, above all when they are allowed to travel, we divided the

infectious compartment into asymptomatic (A) and symptomatic (I). We investigated the total reproduction number by changing the vaccination coverage in each patch (from highly susceptible to highly vaccinated) and the proportion of asymptomatic cases. Our results suggest how if the patches share the same immunity distribution, there is no change in the total reproduction number. On the other hand, when a big disparity in the vaccination coverage is visible, the movement of vaccinated individuals towards a vulnerable patch or the movement of susceptibles towards a highly immunized region, decreases the overall reproduction number as well as diminishing the proportion of asymptomatic travellers. Our sensitivity analysis shows that the transmission of the infection in each patch and the proportion of asymptomatic cases, which both need to be reduced, are extremely significant in the dynamics of the outbreak. Our results suggest how a difference in the vaccination coverage among regions which are highly connected might still lead to the diffusion of the outbreak. Hence, it is evident how Public Health needs to increase the immunity distribution uniformly across the country.

In all the previous analyses, it was assumed that vaccination provides a life long immunity. However, different studies show this might not happen. Hence, we concluded our study by investigating the impact that basic reproduction number, waning periods and vaccination (1 dose) have on herd immunity achievement and infection dynamics. We developed an SII_wRVW model capturing both boosting and waning immunity processes. Given the unknown level of transmissibility from a vaccinated case, we considered two scenarios: in the first one, vaccinated cases are not infectious; in the second one, they are as infectious as primary cases. We also extended this model with an age structure investigating the immunity of different age groups and the ones more affected by a possible outbreak. The model without age structure suggests that herd immunity is achievable if the immunity is lifelong and the vaccination coverage is extremely high. For large $\mathcal{R}_0$, a much higher vaccine coverage is necessary to obtain herd immunity. When age is introduced, we observed that the indirect protection is possible only for small reproduction number and high vaccination coverage. If immunity is not life-long herd immunity is never achievable. Moreover, the age structured model shows that infection has two peaks: one among young children and one among age groups $20-24$ years and $60-64$ years. This suggests that these individuals are the ones more affected in case of an outbreak. It is then important to focus on reducing the susceptible individuals in these age groups. The analysis on a single outbreak underlines the same results. Although the deterministic models provide useful information, the stochastic analyses suggest that in case vaccine-induced immunity is not life long, there is still a high probability that an outbreak will occur. On the other hand, the results with the assumption that immunity given by vaccination never wanes, show that the probability of extinction is much higher than having an outbreak. Since the immunization recommendation requires a second dose of vaccine, we extended further our age structure model including an additional dose at age of 5 years. The results on the $\mathcal{R}_c$ show that the control reproduction number is less than the one evaluated for the single dose case, but if vaccine-induced immunity is shorter than life span, herd immunity is never achievable. This suggests that we might need, depending on the waning periods, which need to be investigated, extra vaccine shots to be given to the population.

This thesis highlights the importance of vaccination coverage in Canada and that the waning process need further investigation in order to detect the real waning periods. This information is extremely crucial to understand and target the age groups that mostly need supplementary measles vaccine dose.

The presented work can be extended modifying some assumptions done.
Since we defined the distribution of immigrants and Canadians by age groups, it is necessary to distinguish the contact rates that individuals have based on country of origin and age. A further extension, strictly related to contacts, might be seasonality. This work assumed a life long immunity provided by vaccination, but waning immunity can also be considered, above all for immigrants coming from highly vaccinated countries. Moreover, global stability of the DFE can be investigate when $\mathcal{R}_0 < 1$.
Our multi-patch model does not consider the population structure of the regions investigated. It might be interesting varying the proportion of each patch's residents leaving their region. Also, age structure can be implemented, considering that only teenagers and adults might be the only commuters. Seasonality can also be implemented.
The work on waning immunity with two doses of vaccine can be extended with a further analysis of the endemic equilibrium as well as considering a stochastic model.

Bibliography

[1] CDC. *Centers for Disease Control and Prevention*. Accessed: 2018-08-14. URL: https://www.cdc.gov/vaccines/pubs/pinkbook/downloads/meas.pdf.

[2] J. L. Goodson and J. F. Seward. "Measles 50 Years After Use of Measles Vaccine". In: *Infect Dis Clin N Am* 29 (2015), pp. 725–743.

[3] CDC. *Centers for Disease Control and Prevention*. Accessed: 2018-08-14. URL: https://www.cdc.gov/measles/about/history.html.

[4] CDC. *Centers for Disease Control and Prevention*. Accessed: 2018-08-14. URL: https://www.cdc.gov/measles/vaccination.html.

[5] European Centre for Disease Prevention and Control (ECDC). Accessed: 2020-04. URL: https://vaccine-schedule.ecdc.europa.eu/Scheduler/ByDisease?SelectedDiseaseId=8&SelectedCountryIdByDisease=-1.

[6] WHO. Accessed: 2018-08-14. URL: http://www.who.int/news-room/fact-sheets/detail/measles.

[7] World Health Organization (WHO) Africa. Accessed: 2020-06. URL: https://www.afro.who.int/news/who-and-partners-launch-emergency-vaccination-campaign-help-contain-worlds-largest-measles.

[8] United Nations (UN). Accessed: 2020-06. URL: https://news.un.org/en/tags/measles-vaccination-campaign.

[9] World Health Organization (WHO). Accessed: 2019-09-19. URL: https://www.who.int/immunization/newsroom/new-measles-data-august-2019/en/.

[10] European Centre for Disease Prevention and Control (ECDC). Accessed: 2020-04. URL: https://www.ecdc.europa.eu/en/publications-data/measles-annual-epidemiological-report-2019.

[11] Government of Canada. Accessed: 2020-04. URL: https://www.canada.ca/en/public-health/services/publications/healthy-living/canadian-immunization-guide-part-4-active-vaccines/page-12-measles-vaccine.html.

[12] R.M. Anderson and R.M. May. "Directly transmitted infections diseases: control by vaccination." In: *Science* 215 (1982), pp. 1053–1060.

[13] D. J. Nokes and R.M. Anderson. "The use of mathematical models in the epidemiological study of infectious diseases and in the design of mass immunization programmes." In: *Epidemiol Infect.* 101 (1988), pp. 1–20.

[14] M. Doherty et al. "Vaccine impact: Benefits for human health". In: *Vaccine* 34 (2016), pp. 6707 –6714.

[15] F.M. Guerra et al. "The basic reproduction number (R) of measles: a systematic review." In: *The Lancet. Infectious diseases* 17 (2017), e420–e428.

[16] P.E.M. Fine. "Herd Immunity: History, Theory, Practice". In: *Epidemiologic Reviews* 15 (1993), pp. 265 –302.

[17] Government of Canada. Accessed: 2020-04. URL: https://www.canada.ca/en/public-health/services/diseases/measles/health-professionals-measles.html.

[18] F. G. Blake and J. D. Jr. Trask. "Studies on measles III. Acquired immunity following experimental measles." In: *J Exp Med.* 33 (1921), pp. 621–626.

[19] D. Naniche. *Human Immunology of Measles Virus Infection*. Vol. 330. Springer, Berlin, Heidelberg. Griffin D.E., Oldstone M.B.A., 2009. ISBN: 9783540706168.

[20] D. E. Griffin. "The Immune Response in Measles: Virus Control, Clearance and Protective Immunity." In: *Viruses* 8 (2016), p. 282.

[21] B. Christenson and M. Bottiger. "Measles antibody comparison of long-term vaccination titers, early vaccination titers and naturally acquired-immunity to and booster effects on the measles virus". In: *Vaccine* 12 (1994), pp. 129 –133.

[22] I. Davidkin et al. "Persistence of Measles, Mumps, and Rubella Antibodies in an MMR-Vaccinated Cohort: A 20-Year Follow-Up". In: *The Journal of Infectious Diseases* 197 (2008), pp. 950–956.

[23] S. Bolotin, S.L. Hughes, and M.R. et al. Faulkner. "Waning of measles immunity derived from previous infection or vaccination in elimination settings A systematic review. Unpublished". In: ().

[24] S. L. Hughes et al. "The effect of time since measles vaccination and age at first dose on measles vaccine effectiveness. A systematic review". In: *Vaccine* 38 (2020), pp. 460 –469.

[25] M. H. Arguelles et al. "Measles Virus-Specific Antibody Levels in Individuals in Argentina Who Received a One-Dose Vaccine". In: *J Clin Microbiol* 44 (2006), pp. 2733 –2738.

[26] K. King et al. "Measles Elimination in Canada". In: *The Journal of Infectious Diseases* 189 (2004), pp. 236–242.

[27] Government of Canada. Accessed: 2020-04. URL: https://www.canada.ca/en/public-health/services/diseases/measles/measles-in-canada.html#a1.

[28] Government of Canada. Accessed: 2020-04. URL: https://www.canada.ca/en/public-health/services/publications/healthy-living/2015-vaccine-uptake-canadian-children-survey.html.

[29] Government of Canada. Accessed: 2020-04. URL: https://www.canada.ca/en/public-health/services/publications/diseases-conditions/measles-surveillance-canada-2016.html#a41.

[30] Government of Canada. Accessed: 2020-04. URL: https://www.canada.ca/en/public-health/services/publications/diseases-conditions/measles-surveillance-canada-2017.html#a3.3.

[31] WHO/UNICEF. Accessed: 2018-08-14. URL: https://www.who.int/immunization/monitoring_surveillance/data/en/.

[32] Government of Canada. *Reported cases from 1924 to 2017 in Canada - Notifiable diseases on-line*. URL: https://dsol-smed.phac-aspc.gc.ca/dsol-smed/ndis/charts.php?c=pl.

[33] Government of Canada. Accessed: 2019-09-19. URL: https://www.canada.ca/en/public-health/services/diseases/measles/surveillance-measles/measles-rubella-weekly-monitoring-reports.html.

[34] D. Bernouilli. "Essai d une nouvelle analyse de la mortalite causee par la petite verole". In: *Mem Math Phy Acad Roy Sci Paris* (1766).

[35] O. Kermack and A.G. McKendrick. "A contribution to the mathematical theory of epidemics". In: *Proc. R. Soc. Lond. A* 115 (1927), pp. 700–721.

[36] W. O. Kermack and A. G. McKendrick. "Contributions to the mathematical theory ofepidemics, part II." In: *Proc. Roy. Soc. London* 138 (1932), pp. 55–83.

[37] O. Kermack and A.G. McKendrick. "A contribution to the mathematical theory of epidemics. III." In: *Proc. R. Soc. Lond. A* 141 (1933), pp. 94–122.

[38] R.M. Anderson and R.M. May. *Infectious Diseases of Humans.* Oxford University Press, Oxford., 1991.

[39] J.D. Murray. *Mathematical Biology: I: An Introduction. Third Edition.* Vol. 17. Springer, Berlin, Heidelberg. New York: Springer., 2002. ISBN: 0387952233.

[40] F. Brauer, P. Van Den Driessche, and J. Wu. *Mathematical Epidemiology.* Vol. 1945. Springer-Verlag Berlin Heidelberg. Springer., 2008. ISBN: 978-3-540-78910-9.

[41] M. Keeling and P. Rohani. *Modelling Infectious Diseases in Humans and Animals.* Princeton University Press. ISBN: 978-0-691-11617-4.

[42] W.H Hethcote. "The mathematics of infectious diseases". In: *SIAM* 42 (2000), pp. 599 –653.

[43] J. Lessler et al. "Incubation periods of acute respiratory viral infections: a systematic review". In: *Lancet Infect Dis* 9 (2009), pp. 291–300.

[44] L. Sattenspiel. “Modeling the Spread of Infectious Disease in Human Populations”. In: *YEARBOOK OF PHYSICAL ANTHROPOLOGY* 33 (1990), pp. 245–276.

[45] J.M. Heffernan and Keeling M.J. “An in-host model of acute infection: measles as a case study.” In: *Theoretical Population Biology* 73 (2008), pp. 134–147.

[46] J.T. Kemper. “The effects of asymptomatic attacks on the spread of infectious disease: A deterministic model”. In: *Bulletin of Mathematical Biology* 40 (1978), pp. 707–718.

[47] M. De la Sen et al. “On a New Epidemic Model with Asymptomatic and Dead-Infective Subpopulations with Feedback Controls Useful for Ebola Disease”. In: *Hindawi Discrete Dynamics in Nature and Society* 2017 (2017), p. 22.

[48] K.L Cooke. “Models for endemic infections with asymptomatic cases. I. One group”. In: *Mathematical Modelling* 3 (1982), pp. 1–15.

[49] J. Mossong et al. “Modeling the Impact of Subclinical Measles Transmission in VaccinatedPopulations with Waning Immunity”. In: *American Journal of Epidemiology* 150 (1999), pp. 1238–1249.

[50] A. Scherer and A. McLean. “Mathematical models of vaccination”. In: *British Medical Bulletin* 62 (2002), pp. 187 –199.

[51] M. Ehrhardt, J. Gasper, and S. Kilianova. “SIR-Based MathematicalModeling of Infectious Disease with vaccination and Waning Immunity”. In: *Journal of Computational Science* 37 ().

[52] J.M. Heffernan and Keeling M.J. “Implications of vaccination and waning immunity.” In: *Proceedings. Biological sciences / The Royal Society* 276 (2009), pp. 2071–2080.

[53] M.V. Barbarossa and G. Rost. “Mathematical models for vaccination, waning immunity and immune system boosting: a general framework”. In: *Populations and Evolution (q-bio.PE)* arXiv:1501.03451 (2015), p. 18.

[54] T. Leung et al. “Infection-acquired versus vaccine-acquired immunity in an SIRWS model”. In: *Infect Dis Model.* 3 (2018), pp. 118–135.

[55] K. Glass and B.T. Grenfell. “Antibody Dynamics in Childhood Diseases: Waning and Boosting of Immunity and the Impact of Vaccination”. In: *Journal of Theoretical Biology* 221 (2003), pp. 121–131.

[56] J. S. Lavine, A.A. King, and O. N. Bjornstad. “Natural immune boosting in pertussis dynamics and the potential for long-term vaccine failure”. In: *Proc Natl Acad Sci U S A* 108 (2011), pp. 7259 –7264.

[57] W.H. Hethcote. “Simulations of pertussis epidemiology in theUnited States: effects of adult booster vaccinations”. In: *Mathematical Biosciences* 158 (1999), pp. 4–73.

[58] W.H. Hethcote, P. Horby, and P. Mcintyre. “Using computer simulations to compare pertussis vaccination strategies in Australia”. In: *Vaccine* 22 (2004), pp. 2181–2191.

[59] L. Sattenspiel and K. Dietz. “A structured epidemic model incorporating geographic mobility among regions”. In: *Math. Biosci.* 128 (1995), pp. 71–91.

[60] A. Lloyd and R.M May. “Spatial Heterogeneity in Epidemic Models”. In: *Journal of Theoretical Biology* 179 (1996), pp. 1–11.

[61] J. Arino and P. Van den Driessche. “The Basic Reproduction Number in a Multi-city Compartmental Epidemic Model”. In: *LNCIS* 294 (2003), pp. 135–142.

[62] J. Arino and P. Van den Driessche. “A multi-city epidemic model”. In: *Mathematical Population Studies* 10 (2003), pp. 175–193.

[63] J. Arino et al. “A multi-species epidemic model with spatial dynamics”. In: *Mathematical Medicine and Biology* 22 (2005), pp. 129–142.

[64] J. Arino and S. Portet. “Epidemiological implications of mobility between a large urban centre and smaller satellite cities”. In: *J. Math. Biol.* 71 (2015), pp. 1243–1265.

[65] L. M. Stolerman, D. Coombs, and S. Boatto. “SIR-Network Model and Its Application to Dengue Fever”. In: *SIAM J. APPL. MATH.* 75 (2015), pp. 2581–2609.

[66] D. Bichara et al. “SIS and SIR epidemic models under virtual dispersal”. In: *Bull Math Biol.* 77 (2015), pp. 2004–2034.

[67] C. Castillo-Chavez, D. Bichara, and B.R. Morin. “Perspectives on the role of mobility, behavior, andtime scales in the spread of diseases”. In: *PNAS* 113 (2016), pp. 14582–14588.

[68] D. Bichara and A. Iggidr. “Multi-Patch and Multi-Group Epidemic Models: A New Framework”. In: *Journal of Mathematical Biology* 77 (2017).

[69] J. Mossong et al. “Social contacts and mixing patterns relevant to the spread of infectious diseases”. In: *PLoS Medicine* (2008).

[70] K. Prem, A.R. Cook, and M. Jit. “Projecting social contact matrices in 152 countries using contact surveys and demographic data”. In: *PLoS Comput Biol* 13(9) ().

[71] I.M. Pongsumpun P. Tang. “Transmission of dengue hemorrhagic fever in an age structured population”. In: *Mathematical and Computer Modelling* 37 (2003), pp. 949 –961.

[72] F. B. Agusto et al. “Mathematical Model of Three Age-Structured Transmission Dynamics of Chikungunya Virus”. In: *Computational and Mathematical Methods in Medicine* 2016 (2016), p. 31.

[73] M. Iannelli and P. Manfredi. “Demographic Change and Immigration in Age-structured Epidemic Model”. In: *Mathematical Population Studies* 14 (2007), pp. 169–191.

[74] W.H Hethcote. “An age-structured model for pertussis transmission”. In: *Mathematical Biosciences* 145 (1997), pp. 89–136.

[75] J. Mossong and C.P. Muller. “Modelling measles re-emergence as a result of waning of immunity in vaccinated populations”. In: *Vaccine* 21 (2003), pp. 4597 –4603.

[76] M. Iannelli and F. Milner. *The Basic Approach to Age-Structured Population Dynamics*. Springer Netherlands, 2017. ISBN: 978-94-024-1145-4.

[77] L. J. S. Allen. *An Introduction to Stochastic Processes with Applications to Biology, Second Edition*. CRC Press, 2010. ISBN: 978-1-4398-1882-4.

[78] L. J. S. Allen. *Stochastic Population and Epidemic Models*. Springer, 2015. ISBN: 978-3-319-21553-2.

[79] L. J. S. Allen and G.E. Jr. Lahodny. "Extinction thresholds in deterministic and stochastic epidemic models". In: *Journal of Biological Dynamics* 6 (2013), pp. 590–611.

[80] L. J. S. Allen and P. van den Driessche. "Relations between deterministic and stochastic thresholds for disease extinction in continuous- and discrete-time infectious disease models." In: *Mathematical Biosciences* 243 (2013), pp. 99–108.

[81] D. T. Gillespie. "Exact Stochastic Simulation of Coupled Chemical Reactions". In: *The Journal of Physical Chemestry* 81 (1977), pp. 2340 –2361.

[82] M. P. DAFILIS et al. "THE INFLUENCE OF INCREASING LIFE EXPECTANCY ON THE DYNAMICS OF SIRS SYSTEMS WITH IMMUNE BOOSTING". In: *The ANZIAM Journal* 54 (2012), pp. 50–63.

[83] L.C. Mpande, D. Kajunguri, and E.A. Mpolya. "Modeling and Stability Analysis for Measles Metapopulation Model with Vaccination". In: *Applied and Computational Mathematics* 179 (2015), pp. 431 –444.

[84] E. Alexander et al. "The Effects of Regional Vaccination Heterogeneity on Measles Outbreaks with France as a Case Study". In: *arXiv:1408.0695v1 [q-bio.PE]* (July 2014).

[85] K. Dietz. "The estimation of the basic reproduction number for infectious diseases." In: *Statistical Methods in Medical Research* 2 (1993), pp. 23–41.

[86] J.M. Heffernan, R.J. Smith?, and L.M. Wahl. "Perspectives on the basic reproductive ratio". In: *J.R.Soc. Interface* 2 (2005), pp. 281–293.

[87] J.A.P. Heesterbeek. "A brief history of R0 and a recipe for its calculation." In: *Acta Biotheoretica* 50 (2002), pp. 189–204.

[88] O. Diekmann, J.A. Heesterbeek, and J.A. Metz. "On the definition and the computation of the basic reproduction ratio R0 in models for infectious diseases in heterogeneous populations." In: *J. Math. Biol* 4 (1990), pp. 365–382.

[89] O. Diekmann, J.A.P. Heesterbeek, and M.G. Roberts. "The construction of next-generation matrices for compartmental epidemic models". In: *J R Soc Interface* 7 (2010), pp. 873–885.

[90] P. van den Driessche and J. Watmough. "Reproduction numbers and sub-threshold endemic equilibria for compartmental models of disease transmission". In: *Mathematical Biosciences* 180 (2002), pp. 29–48.

[91] P. van den Driessche. "Reproduction numbers of infectious disease models". In: *Infectious Disease Modelling* 2 (2017), pp. 288–303.

[92] M.G. Roberts. "The pluses and minuses of R0." In: *J.R.Soc. Interface* 4 (2007), pp. 949–961.

[93] S. Marino et al. "A Methodology For Performing Global Uncertainty And Sensitivity Analysis In Systems Biology". In: *J Theor Biol* 7 (2008), pp. 178 –196.

[94] M.D. Mckay, R.J. Beckman, and W.J. Conover. "Comparison of 3 Methods for Selecting Values of Input Variables in the Analysis of Output from a Computer Code". In: *Technometrics* 21 (1979), pp. 239 –245.

[95] MathWorks. Accessed: 2020-04. URL: https://www.mathworks.com/products/matlab.html.

[96] Maplesoft. Accessed: 2020-04. URL: https://www.maplesoft.com/.

[97] E. Dube et al. "Understanding Vaccine Hesitancy in Canada: Results of a Consultation Study by the Canadian Immunization Research Network". In: *PLoS One* 11 (2016), e0156118.

[98] Statistics Canada-Canadian Census 2016. Accessed: 2018-08-14. URL: https://www150.statcan.gc.ca/n1/pub/11-627-m/11-627-m2017028-eng.htm.

[99] Statistics Canada. Accessed: 2019-09-11. URL: https://www12.statcan.gc.ca/census-recensement/2016/as-sa/fogs-spg/Facts-can-eng.cfm?Lang=Eng&GK=CAN&GC=01&TOPIC=7.

[100] F. Brauer and P. Van den Driessche. "Models for transmission of disease with immigration of infectives". In: *Mathematical Biosciences* 171 (2001), pp. 143–154.

[101] R. Naresh, A. Tripathi, and D. Sharma. "Modelling and analysis of the spread of AIDS epidemic with immigration of HIV infectives". In: *Mathematical and Computer Modelling* 138 (2009), pp. 880–892.

[102] E. Shim. "A note on epidemic models with infective immigrants and vaccination". In: *Mathematical bioscences and engineering* 3 (2006), pp. 557–566.

[103] P. Widyaningsih, D. R. S. Saputro, and A. W. Nugroho. "Susceptible exposed infected recovery (SEIR) model with immigration: Equilibria points and its application". In: *AIP Conference Proceedings 2014, 020165 (2018)* ().

[104] Z. Juan, L. Jianquan, and M. Zhien. "Global dynamics of an SEIR epidemic model with immigration of different compartments". In: *Mathematical and Computer Modelling* 26B (2006), pp. 551–567.

[105] C. Piccolo III and L. Billings. "The effect of vaccinations in an immigrant model". In: *Mathematical and Computer Modelling* 42 (2005), pp. 291–299.

[106] Statistics Canada. Accessed: 2018-08-14. URL: https://www12.statcan.gc.ca/census-recensement/2016/dp-pd/index-eng.cfm.

[107] Statistics Canada. Accessed: 2018-08-14. URL: https://www150.statcan.gc.ca/t1/tbl1/en/tv.action?pid=1710001401&pickMembers[0]=1.7&pickMembers[1]=2.1&pickMembers[2]=3.1.

[108] A. Guttmann et al. “Immunization Coverage Among Young Children of Urban Immigrant Mothers: Findings from a Universal Health Care System”. In: *Ambul Pediatr.* 8 (2008), pp. 205–209.

[109] A. Pillsbury and H. Quinn. “An assessment of measles vaccine effectiveness, Australia, 2006 - 2012.” In: *Western Pacific Surveillance and Response Journal* 6(3) ().

[110] Statistics Canada. Accessed: 2019-12. URL: https://www12.statcan.gc.ca/census-recensement/2016/dp-pd/prof/index.cfm?Lang=E&TABID=1.

[111] Statistics Canada. Accessed: 2019-12. URL: https://www12.statcan.gc.ca/census-recensement/2016/dp-pd/dt-td/Rp-eng.cfm?TABID=2&LANG=E&APATH=3&DETAIL=0&DIM=0&FL=A&FREE=0&GC=0&GK=0&GRP=1&PID=113344&PRID=10&PTYPE=109445&S=0&SHOWALL=0&SUB=0&Temporal=2017&THEME=125&VID=0&VNAMEE=&VNAMEF=/.

[112] Public heath Ontario (PHO). URL: https://www.publichealthontario.ca/en/diseases-and-conditions/infectious-diseases/vaccine-preventable-diseases/measles/important-measles-information.

[113] World Health Organization (WHO). URL: https://www.who.int/csr/disease/ebola/maps-2014/en/.

[114] World Health Organization (WHO). URL: https://www.who.int/csr/disease/swineflu/h1n1_maps_may/en/.

[115] World Health Organization (WHO). URL: http://www.who.int/csr/sars/map2003_05_26.gif.

[116] L.S. Chang, M. Piraveenan, and M. Prokopenko. “The Effects of Imitation Dynamics on Vaccination Behaviours in SIR-Network Model”. In: *Int J Environ Res Public Health* 16 (2019).

[117] Rota J.S. et al. “Two Case Studies of Modified Measles in Vaccinated Physicians Exposed to Primary Measles Cases: High Risk of Infection But Low Risk of Transmission”. In: *The Journal of Infectious Diseases* 204 (2011), S559–S563.

[118] J.B. Rosen et al. “Outbreak of Measles Among Persons With Prior Evidence of Immunity, New York City, 2011”. In: *Clinical Infectious Diseases* 58 (2014), pp. 1205–1210.

[119] CDC. *Centers for Disease Control and Prevention*. Accessed: 2018-08-14. URL: https://www.cdc.gov/vaccines/vpd/mmr/public/index.html.

[120] WHO. *WHO: Canada*. Accessed: 2018-08-14. URL: http://www.who.int/countries/can/en/.

[121] WHO. *GHO: By category : Life tables by country - Canada*. Accessed: 2018-08-14. URL: http://apps.who.int/gho/data/?theme=main&vid=60290.

Appendix A

Next Generation Matrix, Jacobian Matrix and Eigenvalues for Model (2.1)

In this section we report the mathematical computations needed to derive the expression for both the basic and controlled reproduction numbers $\mathcal{R}_0$ and $\mathcal{R}_c$. We start with the definition of the matrix $\mathcal{F}$ representing the rates at which individuals in each subpopulation become infected:

$$\mathcal{F} = \begin{bmatrix} 0 & 0 & 0 & 0 & \beta S_{CJ_0} & \beta S_{CJ_0} & \beta S_{CJ_0} & \beta S_{CJ_0} \\ 0 & 0 & 0 & 0 & \beta S_{IJ_0} & \beta S_{IJ_0} & \beta S_{IJ_0} & \beta S_{IJ_0} \\ 0 & 0 & 0 & 0 & \beta S_{CA_0} & \beta S_{CA_0} & \beta S_{CA_0} & \beta S_{CA_0} \\ 0 & 0 & 0 & 0 & \beta S_{IA_0} & \beta S_{IA_0} & \beta S_{IA_0} & \beta S_{IA_0} \\ 0 & 0 & 0 & 0 & 0 & 0 & 0 & 0 \\ 0 & 0 & 0 & 0 & 0 & 0 & 0 & 0 \\ 0 & 0 & 0 & 0 & 0 & 0 & 0 & 0 \\ 0 & 0 & 0 & 0 & 0 & 0 & 0 & 0 \end{bmatrix} \tag{A.1}$$

Next, we define $\mathcal{V}$, representing the matrix of all rates at which infected leaves the infected compartments.

$$\mathcal{V} = \begin{bmatrix} d+\mu_J+\alpha & 0 & 0 & 0 & 0 & 0 & 0 & 0 \\ 0 & d+\mu_J+\alpha & 0 & 0 & 0 & 0 & 0 & 0 \\ -\mu_J & 0 & d+\alpha & 0 & 0 & 0 & 0 & 0 \\ 0 & -\mu_J & 0 & d+\alpha & 0 & 0 & 0 & 0 \\ -\alpha & 0 & 0 & 0 & d+\mu_J+\gamma & 0 & 0 & 0 \\ 0 & -\alpha & 0 & 0 & 0 & d+\mu_J+\gamma & 0 & 0 \\ 0 & 0 & -\alpha & 0 & -\mu_J & 0 & d+\gamma & 0 \\ 0 & 0 & 0 & -\alpha & 0 & -\mu_J & 0 & d+\gamma \end{bmatrix} \tag{A.2}$$

After finding $\mathcal{V}^{-1}$ and multiplying it by $\mathcal{F}$, we evaluate the eigenvalues, λ, of the resulting matrix $(\mathcal{F}\mathcal{V}^{-1})$:

$$\lambda = \begin{bmatrix} 0 \\ 0 \\ 0 \\ 0 \\ 0 \\ 0 \\ 0 \\ \frac{\alpha\beta(S_{CJ_0}+S_{CA_0}+S_{IJ_0}+S_{IA_0})}{(d+\alpha)(d+\gamma)} \end{bmatrix} \tag{A.3}$$

The $\mathcal{R}_0$ is given by the spectral radius of $\mathcal{F}\mathcal{V}^{-1}$, hence we define: $\mathcal{R}_0 = \frac{\alpha\beta(S_{CJ_0}+S_{CA_0}+S_{IJ_0}+S_{IA_0})}{(d+\alpha)(d+\gamma)}$. Observe that the control reproduction number is defined as $\mathcal{R}_0$, but the susceptibles at the disease free equilibrium are considered to be the ones obtained when control is introduced in the population.

The basic reproduction number can give some insights into the stability analysis of the disease free equilibrium. In order to determine the conditions under which $\mathcal{E}_0$ is stable, we derive the Jacobian matrix of Model (2.1) and evaluate it at the disease free equilibrium. The Jacobian matrix is defined as $\mathcal{J}_0$:

$$
\begin{bmatrix}
-d-\mu_J & 0 & -\beta S_{CJ_0} & 0 & 0 & 0 & -\beta S_{CJ_0} & 0 & 0 & 0 & -\beta S_{CJ_0} & 0 & 0 & 0 & -\beta S_{CJ_0} & 0 \\
0 & -d-\alpha-\mu_J & \beta S_{CJ_0} & 0 & 0 & 0 & \beta S_{CJ_0} & 0 & 0 & 0 & \beta S_{CJ_0} & 0 & 0 & 0 & \beta S_{CJ_0} & 0 \\
0 & \alpha & -d-\gamma-\mu_J & 0 & 0 & 0 & 0 & 0 & 0 & 0 & 0 & 0 & 0 & 0 & 0 & 0 \\
0 & 0 & \gamma & d-\mu_J & 0 & 0 & 0 & 0 & 0 & 0 & 0 & 0 & 0 & 0 & 0 & 0 \\
\mu_J & 0 & -\beta S_{CA_0} & 0 & -d & 0 & -\beta S_{CA_0} & 0 & 0 & 0 & -\beta S_{CA_0} & 0 & 0 & 0 & -\beta S_{CA_0} & 0 \\
0 & \mu_J & \beta S_{CA_0} & 0 & & -d-\alpha & \beta S_{CA_0} & 0 & 0 & 0 & \beta S_{CA_0} & 0 & 0 & 0 & \beta S_{CA_0} & 0 \\
0 & 0 & \mu_J & 0 & 0 & \alpha & -d-\gamma & 0 & 0 & 0 & 0 & 0 & 0 & 0 & 0 & 0 \\
0 & 0 & 0 & \mu_J & 0 & 0 & \gamma & -d & 0 & 0 & 0 & 0 & 0 & 0 & 0 & 0 \\
0 & 0 & -\beta S_{IJ_0} & 0 & 0 & 0 & -\beta S_{IJ_0} & 0 & -d-\mu_J & 0 & -\beta S_{IJ_0} & 0 & 0 & 0 & -\beta S_{IJ_0} & 0 \\
0 & 0 & \beta S_{IJ_0} & 0 & 0 & 0 & \beta S_{IJ_0} & 0 & 0 & -d-\alpha-\mu_J & \beta S_{IJ_0} & 0 & 0 & 0 & \beta S_{IJ_0} & 0 \\
0 & 0 & 0 & 0 & 0 & 0 & 0 & 0 & 0 & \alpha & -d-\gamma-\mu_J & 0 & 0 & 0 & 0 & 0 \\
0 & 0 & 0 & 0 & 0 & 0 & 0 & 0 & 0 & 0 & \gamma & -d-\mu_J & 0 & 0 & 0 & 0 \\
0 & 0 & -\beta S_{IA_0} & 0 & 0 & 0 & -\beta S_{IA_0} & 0 & \mu_J & 0 & -\beta S_{IA_0} & 0 & -d & 0 & -\beta S_{IA_0} & 0 \\
0 & 0 & \beta S_{IA_0} & 0 & 0 & 0 & \beta S_{IA_0} & 0 & \mu_J & \beta S_{IA_0} & 0 & 0 & -d-\alpha & \beta S_{IA_0} & 0 & \\
0 & 0 & 0 & 0 & 0 & 0 & 0 & 0 & 0 & 0 & \mu_J & 0 & 0 & \alpha & -d-\gamma & 0 \\
0 & 0 & 0 & 0 & 0 & 0 & 0 & 0 & 0 & 0 & 0 & \mu_J & 0 & 0 & \gamma & -d
\end{bmatrix}
$$

The stability analysis of the disease free equilibrium is determined by the eigenvalues of $\mathcal{J}_0$:

if all the eigenvalues present negative real part, then $\mathcal{E}_0$ is stable. We evaluate the eigenvalues set of $\mathcal{J}_0$ obtaining:

$$\lambda_{\mathcal{J}_0} = \begin{bmatrix} -d-\alpha \\ -d-\gamma \\ -\frac{1}{2}\alpha - d - \frac{1}{2}\gamma + \frac{1}{2}\sqrt{4\alpha\beta S_{CJ_0} + 4\alpha\beta S_{CA_0} + 4\alpha\beta S_{IJ_0} + 4\alpha\beta S_{IA_0} + \alpha^2 - 2\alpha\gamma + \gamma^2} \\ -\frac{1}{2}\alpha - d - \frac{1}{2}\gamma - \frac{1}{2}\sqrt{4\alpha\beta S_{CJ_0} + 4\alpha\beta S_{CA_0} + 4\alpha\beta S_{CIJ_0} + 4\alpha\beta S_{IA_0} + \alpha^2 - 2\alpha\gamma + \gamma^2} \\ -d-\alpha-\mu_J \\ -d-\gamma-\mu_J \\ -d-\alpha-\mu_J \\ -d-\mu_J \\ -d-\mu_J \\ -d-\mu_J \\ -d-\mu_J \\ -d-\mu_J \\ -d \\ -d \\ -d \\ -d \end{bmatrix} \tag{A.4}$$

Observe that, since all the parameters are positive, the eigenvalues present negative real part. However, the third and fourth eigenvalues require further investigations. Note that the term under the square root is always positive and hence these eigenvalues will only be real. Hence, we can establish that the fourth eigenvalue is always negative, while the third one might present positive real part. In order to have this eigenvalue with negative real part, it is necessary to satisfy the following condition:

$$\frac{1}{2}\alpha + d + \frac{1}{2}\gamma > \frac{1}{2}\sqrt{4\alpha\beta S_{CJ_0} + 4\alpha\beta S_{CA_0} + 4\alpha\beta S_{CIJ_0} + 4\alpha\beta S_{IA_0} + \alpha^2 - 2\alpha\gamma + \gamma^2} \tag{A.5}$$

After rearranging Eq.(A.5), the condition needed to obtain negative real part of the eigenvalue becomes:

$$(d+\alpha)(d+\gamma) > \alpha\beta(S_{CJ_0} + S_{CA_0} + S_{IJ_0} + S_{IA_0})$$

By dividing both sides by $(d+\alpha)(d+\gamma)$, the condition providing $\mathcal{E}_0$ stability is:

$$\frac{\alpha\beta(S_{CJ_0} + S_{CA_0} + S_{IJ_0} + S_{IA_0})}{(d+\alpha)(d+\gamma)} < 1 \tag{A.6}$$

Note, as defined in Eq. (2.6), the term on the left hand side is the expression of the basic reproduction number $\mathcal{R}_0$.

Appendix B

Jacobian Matrix and Eigenvalues for Model (2.9)

In this appendix we provide the computations from which we derive the basic and controlled reproduction numbers $\mathcal{R}_{02}$ and $\mathcal{R}_{c2}$. Similar to the previous appendix, in order to apply the Next Generation Matrix method, we define the matrix $\mathcal{F}$ representing the rates at which individuals in each subpopulation become infected and evaluate it at the DFE:

$$\mathcal{F} = \begin{bmatrix} 0 & 0 & 0 & 0 & 0 & 0 & \beta\bar{\bar{S}}_{CN_0} & \beta\bar{\bar{S}}_{CN_0} & \beta\bar{\bar{S}}_{CN_0} & \beta\bar{\bar{S}}_{CN_0} & \beta\bar{\bar{S}}_{CN_0} & \beta\bar{\bar{S}}_{CN_0} \\ 0 & 0 & 0 & 0 & 0 & 0 & \beta\bar{\bar{S}}_{CJ_0} & \beta\bar{\bar{S}}_{CJ_0} & \beta\bar{\bar{S}}_{CJ_0} & \beta\bar{\bar{S}}_{CJ_0} & \beta\bar{\bar{S}}_{CJ_0} & \beta\bar{\bar{S}}_{CJ_0} \\ 0 & 0 & 0 & 0 & 0 & 0 & \beta\bar{\bar{S}}_{CA_0} & \beta\bar{\bar{S}}_{CA_0} & \beta\bar{\bar{S}}_{CA_0} & \beta\bar{\bar{S}}_{CA_0} & \beta\bar{\bar{S}}_{CA_0} & \beta\bar{\bar{S}}_{CA_0} \\ 0 & 0 & 0 & 0 & 0 & 0 & \beta\bar{\bar{S}}_{IN_0} & \beta\bar{\bar{S}}_{IN_0} & \beta\bar{\bar{S}}_{IN_0} & \beta\bar{\bar{S}}_{IN_0} & \beta\bar{\bar{S}}_{IN_0} & \beta\bar{\bar{S}}_{IJ_0} \\ 0 & 0 & 0 & 0 & 0 & 0 & \beta\bar{\bar{S}}_{IJ_0} & \beta\bar{\bar{S}}_{IJ_0} & \beta\bar{\bar{S}}_{IJ_0} & \beta\bar{\bar{S}}_{IJ_0} & \beta\bar{\bar{S}}_{IJ_0} & \beta\bar{S}_{IJ_0} \\ 0 & 0 & 0 & 0 & 0 & 0 & \beta\bar{\bar{S}}_{IA_0} & \beta\bar{\bar{S}}_{IA_0} & \beta\bar{\bar{S}}_{IA_0} & \beta\bar{\bar{S}}_{IA_0} & \beta\bar{\bar{S}}_{IA_0} & \beta\bar{\bar{S}}_{IA_0} \\ 0 & 0 & 0 & 0 & 0 & 0 & 0 & 0 & 0 & 0 & 0 & 0 \\ 0 & 0 & 0 & 0 & 0 & 0 & 0 & 0 & 0 & 0 & 0 & 0 \\ 0 & 0 & 0 & 0 & 0 & 0 & 0 & 0 & 0 & 0 & 0 & 0 \\ 0 & 0 & 0 & 0 & 0 & 0 & 0 & 0 & 0 & 0 & 0 & \end{bmatrix} \tag{B.1}$$

Next, we define the matrix of all rates at which infected individuals leave the infected compartments:

$$\mathcal{V} = \begin{bmatrix} d+\mu_{NB}+\alpha & 0 & 0 & 0 & 0 & 0 & 0 & 0 & 0 & 0 & 0 & 0 \\ \mu_{NB} & d+\mu_J+\alpha & 0 & 0 & 0 & 0 & 0 & 0 & 0 & 0 & 0 & 0 \\ 0 & -\mu_J & d+\alpha & 0 & 0 & 0 & 0 & 0 & 0 & 0 & 0 & 0 \\ 0 & 0 & 0 & 0 & d+\mu_{NB}+\alpha & 0 & 0 & 0 & 0 & 0 & 0 & 0 \\ 0 & 0 & 0 & -\mu_{NB} & d+\mu_J+\alpha & 0 & 0 & 0 & 0 & 0 & 0 & 0 \\ 0 & 0 & 0 & 0 & -\mu_J & d+\alpha & 0 & 0 & 0 & 0 & 0 & 0 \\ -\alpha & 0 & 0 & 0 & 0 & 0 & d+\mu_{NB}+\gamma & 0 & 0 & 0 & 0 & 0 \\ 0 & -\alpha & 0 & 0 & 0 & 0 & -\mu_{NB} & d+\mu_J\gamma & 0 & 0 & 0 & 0 \\ 0 & 0 & -\alpha & 0 & 0 & 0 & 0 & -\mu_J & d+\gamma & 0 & 0 & 0 \\ 0 & 0 & 0 & -\alpha & 0 & 0 & 0 & 0 & d+\mu_{NB}+\gamma & 0 & 0 & \\ 0 & 0 & 0 & 0 & -\alpha & 0 & 0 & 0 & -\mu_{NB} & d+\mu_J+\gamma & 0 & \\ 0 & 0 & 0 & 0 & 0 & -\alpha & 0 & 0 & 0 & 0 & -\mu_J & d+\gamma \end{bmatrix} \tag{B.2}$$

The next steps are the evaluation of $\mathcal{V}^{-1}$ and the multiplication of the two matrices $\mathcal{F}$ and $\mathcal{V}^{-1}$. The reproduction number is given by the spectral radius of $\mathcal{F}\mathcal{V}^{-1}$, hence we evaluate the eigenvalues, called λ_2:

$$\lambda_2 = \begin{bmatrix} 0 \\ 0 \\ 0 \\ 0 \\ 0 \\ 0 \\ 0 \\ 0 \\ 0 \\ 0 \\ 0 \\ \frac{\alpha\beta(\bar{\bar{S}}_{CN_0}+\bar{\bar{S}}_{CJ_0}+\bar{\bar{S}}_{CA_0}+\bar{\bar{S}}_{IN_0}+\bar{\bar{S}}_{IJ_0}+\bar{\bar{S}}_{IA_0})}{(d+\alpha)(d+\gamma)} \end{bmatrix} \tag{B.3}$$

Hence, we define $\mathcal{R}_{02}$:

$$\mathcal{R}_{02} = \frac{\alpha\beta(\bar{\bar{S}}_{CN_0}+\bar{\bar{S}}_{CJ_0}+\bar{\bar{S}}_{CA_0}+\bar{\bar{S}}_{IN_0}+\bar{\bar{S}}_{IJ_0}+\bar{\bar{S}}_{IA_0})}{(d+\alpha)(d+\gamma)}$$

By following the same steps and the disease free equilibrium with control, we are able to derive the expression for the $\mathcal{R}_{c2}$, given by Eq. (2.13).

Next, we will investigate the conditions under which $\bar{\bar{\mathcal{E}}}_0$ is stable, we derive the Jacobian matrix of Model (2.9) and evaluate it at the disease free equilibrium. The Jacobian matrix is

defined as: $\mathcal{J}_0 =$

$$
\begin{bmatrix}
-d-\mu_{NB} & 0 & -\beta\bar{\bar{S}}_{CN_0} & 0 & 0 & 0 & -\beta\bar{\bar{S}}_{CN_0} & 0 & 0 & 0 & 0 & -\beta\bar{\bar{S}}_{CN_0} & 0 & 0 & 0 & 0 & -\beta\bar{\bar{S}}_{CN_0} & 0 \\
0 & -d-\alpha-\mu_{NB} & \beta\bar{\bar{S}}_{CN_0} & 0 & 0 & 0 & \beta\bar{\bar{S}}_{CN_0} & 0 & 0 & 0 & 0 & \beta\bar{\bar{S}}_{CN_0} & 0 & 0 & 0 & 0 & \beta\bar{\bar{S}}_{CN_0} & 0 \\
0 & \alpha & -d-\gamma-\mu_{NB} & 0 & 0 & 0 & 0 & 0 & 0 & 0 & 0 & 0 & 0 & 0 & 0 & 0 & 0 & 0 \\
0 & 0 & \gamma & -d-\mu_J & 0 & 0 & 0 & 0 & 0 & 0 & 0 & 0 & 0 & 0 & 0 & 0 & 0 & 0 \\
\mu_{NB} & 0 & -\beta\bar{\bar{S}}_{CJ_0} & 0 & -d-\mu_J & 0 & -\beta\bar{\bar{S}}_{CJ_0} & 0 & 0 & 0 & 0 & -\beta\bar{\bar{S}}_{CJ_0} & 0 & 0 & 0 & 0 & -\beta\bar{\bar{S}}_{CJ_0} & 0 \\
0 & \mu_{NB} & \beta\bar{\bar{S}}_{CJ_0} & 0 & -d-\alpha-\mu_J & 0 & \beta\bar{\bar{S}}_{CJ_0} & 0 & 0 & 0 & 0 & \beta\bar{\bar{S}}_{CJ_0} & 0 & 0 & 0 & 0 & \beta\bar{\bar{S}}_{CJ_0} & 0 \\
0 & 0 & \mu_{NB} & 0 & 0 & \alpha & -d-\gamma-\mu_J & 0 & 0 & 0 & 0 & 0 & 0 & 0 & 0 & 0 & 0 & 0 \\
0 & 0 & 0 & \mu_{NB} & 0 & 0 & \gamma & -d-\mu_J & 0 & 0 & 0 & 0 & 0 & 0 & 0 & 0 & 0 & 0 \\
0 & 0 & -\beta\bar{\bar{S}}_{CA_0} & 0 & \mu_J & 0 & -\beta\bar{\bar{S}}_{CA_0} & 0 & -d & 0 & -\beta\bar{\bar{S}}_{CA_0} & 0 & 0 & -\beta\bar{\bar{S}}_{CA_0} & 0 & 0 & 0 & -\beta\bar{\bar{S}}_{CA_0} & 0 \\
0 & 0 & \beta\bar{\bar{S}}_{CA_0} & 0 & 0 & \mu_J & \beta\bar{\bar{S}}_{CA_0} & 0 & -d & 0 & \beta\bar{\bar{S}}_{CA_0} & 0 & 0 & \beta\bar{\bar{S}}_{CA_0} & 0 & 0 & 0 & \beta\bar{\bar{S}}_{CA_0} & 0 \\
0 & 0 & 0 & 0 & 0 & 0 & \mu_J & 0 & \alpha & -d-\gamma & 0 & 0 & 0 & 0 & 0 & 0 & 0 & 0 \\
0 & 0 & 0 & 0 & 0 & 0 & 0 & \mu_J & 0 & 0 & \gamma & -d & 0 & 0 & 0 & 0 & 0 & 0 \\
0 & 0 & -\beta\bar{\bar{S}}_{IN_0} & 0 & 0 & 0 & -\beta\bar{\bar{S}}_{IN_0} & 0 & 0 & 0 & -\beta\bar{\bar{S}}_{IN_0} & 0 & 0 & -\beta\bar{\bar{S}}_{IN_0} & 0 & 0 & 0 & -\beta\bar{\bar{S}}_{IN_0} & 0 \\
0 & 0 & \beta\bar{\bar{S}}_{IN_0} & 0 & 0 & 0 & \beta\bar{\bar{S}}_{IN_0} & 0 & 0 & 0 & \beta\bar{\bar{S}}_{IN_0} & 0 & 0 & \beta\bar{\bar{S}}_{IN_0} & 0 & 0 & 0 & \beta\bar{\bar{S}}_{IN_0} & 0 \\
0 & 0 & 0 & 0 & 0 & 0 & 0 & 0 & 0 & 0 & 0 & 0 & 0 & 0 & 0 & 0 & 0 & 0 \\
0 & 0 & 0 & 0 & 0 & 0 & 0 & 0 & 0 & 0 & 0 & 0 & 0 & 0 & 0 & 0 & 0 & 0 \\
0 & 0 & -\beta\bar{\bar{S}}_{IJ_0} & 0 & 0 & 0 & -\beta\bar{\bar{S}}_{IJ_0} & 0 & 0 & 0 & -\beta\bar{\bar{S}}_{IJ_0} & 0 & 0 & -\beta\bar{\bar{S}}_{IJ_0} & 0 & 0 & 0 & -\beta\bar{\bar{S}}_{IJ_0} & 0 \\
0 & 0 & \beta\bar{\bar{S}}_{IJ_0} & 0 & 0 & 0 & \beta\bar{\bar{S}}_{IJ_0} & 0 & 0 & 0 & \beta\bar{\bar{S}}_{IJ_0} & 0 & 0 & \beta\bar{\bar{S}}_{IJ_0} & 0 & 0 & 0 & \beta\bar{\bar{S}}_{IJ_0} & 0 \\
0 & 0 & 0 & 0 & 0 & 0 & 0 & 0 & 0 & 0 & 0 & 0 & 0 & 0 & 0 & 0 & 0 & 0 \\
0 & 0 & 0 & 0 & 0 & 0 & 0 & 0 & 0 & 0 & 0 & 0 & 0 & 0 & 0 & 0 & 0 & 0 \\
0 & 0 & -\beta\bar{\bar{S}}_{IA_0} & 0 & 0 & 0 & -\beta\bar{\bar{S}}_{IA_0} & 0 & 0 & 0 & -\beta\bar{\bar{S}}_{IA_0} & 0 & 0 & -\beta\bar{\bar{S}}_{IA_0} & 0 & 0 & 0 & -\beta\bar{\bar{S}}_{IA_0} & 0 \\
0 & 0 & \beta\bar{\bar{S}}_{IA_0} & 0 & 0 & 0 & \beta\bar{\bar{S}}_{IA_0} & 0 & 0 & 0 & \beta\bar{\bar{S}}_{IA_0} & 0 & 0 & \beta\bar{\bar{S}}_{IA_0} & 0 & 0 & -d-\alpha & -\beta\bar{\bar{S}}_{IA_0} & 0 \\
0 & 0 & 0 & 0 & 0 & 0 & 0 & 0 & 0 & 0 & 0 & 0 & 0 & 0 & 0 & \alpha & \gamma & -d \\
0 & 0 & 0 & 0 & 0 & 0 & 0 & 0 & 0 & 0 & 0 & 0 & 0 & 0 & 0 & 0 & -d-\gamma & 0
\end{bmatrix}
$$

The stability analysis of the disease free equilibrium is determined by the eigenvalues of $\mathcal{J}_0$: if all the eigenvalues presents negative real part, then $\mathcal{E}_0$ is stable. We evaluate the eigenvalues set of $\mathcal{J}_0$ obtaining:

$$\lambda_{2\mathcal{J}_0} = \begin{bmatrix} -d-\alpha \\ -d-\gamma \\ -\frac{1}{2}\alpha - d - \frac{1}{2}\gamma + \frac{1}{2}\sqrt{4\alpha\beta\bar{\bar{S}}_{CN_0} + 4\alpha\beta\bar{\bar{S}}_{IN_0} + 4\alpha\beta\bar{\bar{S}}_{CJ_0} + 4\alpha\beta\bar{\bar{S}}_{IJ_0} + 4\alpha\beta\bar{\bar{S}}_{IA_0} + 4\alpha\beta\bar{\bar{S}}_{CA_0} + \alpha^2 - 2\alpha\gamma + \gamma^2} \\ -\frac{1}{2}\alpha - d - \frac{1}{2}\gamma - \frac{1}{2}\sqrt{4\alpha\beta\bar{\bar{S}}_{CN_0} + 4\alpha\beta\bar{\bar{S}}_{IN_0} + 4\alpha\beta\bar{\bar{S}}_{CJ_0} + 4\alpha\beta\bar{\bar{S}}_{IJ_0} + 4\alpha\beta\bar{\bar{S}}_{IA_0} + 4\alpha\beta\bar{\bar{S}}_{CA_0} + \alpha^2 - 2\alpha\gamma + \gamma^2} \\ -d-\alpha-\mu_{NB} \\ -d-\alpha-\mu_{NB} \\ -d-\alpha-\mu_J \\ -d-\alpha-\mu_J \\ -d-\gamma-\mu_{NB} \\ -d-\gamma-\mu_{NB} \\ -d-\gamma-\mu_J \\ -d-\gamma-\mu_J \\ -d-\mu_{NB} \\ -d-\mu_{NB} \\ -d-\mu_J \\ -d-\mu_J \\ -d-\mu_J \\ -d-\mu_J \\ -d-\mu_J \\ -d-\mu_J \\ -d \\ -d \\ -d \\ -d \end{bmatrix} \tag{B.4}$$

Observe that all the eigenvalues present negative real part. However, similar to the eigenvalues shown in Appendix A, the third and fourth eigenvalues need to be analyzed. Since the terms under the square root are always positive, we can state that the eigenvalues will only be real, but the positivity and negativity must be investigated. We can easily observe that the fourth eigenvalue is always negative, while the third one might present positive real part if the root is bigger than the preceding terms. In order to have a negative eigenvalue, we need to examine the conditions satisfying the condition:

$$\frac{1}{2}\alpha + d + \frac{1}{2}\gamma > \frac{1}{2}\sqrt{4\alpha\beta\bar{\bar{S}}_{CN_0} + 4\alpha\beta\bar{\bar{S}}_{IN_0} + 4\alpha\beta\bar{\bar{S}}_{CJ_0} + 4\alpha\beta\bar{\bar{S}}_{IJ_0} + 4\alpha\beta\bar{\bar{S}}_{IA_0} + 4\alpha\beta\bar{\bar{S}}_{CA_0} + \alpha^2 - 2\alpha\gamma + \gamma^2} \tag{B.5}$$

By rearranging Eq.(B.5), we obtain the following condition to satisfy:

$$(d+\alpha)(d+\gamma) > \alpha\beta(\bar{\bar{S}}_{CN_0} + \bar{\bar{S}}_{CJ_0} + \bar{\bar{S}}_{CA_0} + \bar{\bar{S}}_{IN_0} + \bar{\bar{S}}_{IJ_0} + \bar{\bar{S}}_{IA_0})$$

By dividing both sides by $(d+\alpha)(d+\gamma)$, the condition providing $\bar{\bar{\mathcal{E}}}_0$ to be asymptotically stable is:

$$\frac{\alpha\beta(\bar{\bar{S}}_{CN_0} + \bar{\bar{S}}_{CJ_0} + \bar{\bar{S}}_{CA_0} + \bar{\bar{S}}_{IN_0} + \bar{\bar{S}}_{IJ_0} + \bar{\bar{S}}_{IA_0})}{(d+\alpha)(d+\gamma)} < 1 \tag{B.6}$$

Observe that as defined in Eq. (2.12), the term on the left hand side is the expression of the basic reproduction number $\mathcal{R}_0$. Again, the same procedure will provide the expression for $\mathcal{R}_{c2}$.

Appendix C

LHS/PRCC for Model (2.1): Single Outbreak

Here we present the PRCC plots on the single subpopulation when a possible outbreak will occur. Figures (C.1-C.2) represents the PRCC plots for the subpopulation of Canadian juveniles. We observe that the maximum peak of infectious children (Figure (C.1a)) increases as the number susceptible Canadian juveniles and the susceptible immigrant adult increase. This is due to the fact that they might spread the infection more than others. As expected, a significant positive correlation is given even by the infection rate β. Similar to the case in which we consider the total population, we observe that susceptible immigrant adults delay the end of the epidemic even in this subgroup (Figure C.2a). However, we observe that the number of susceptible experiencing the infection within the total infection increases as the number of susceptible Canadian children increases (Figure (C.2b)).

We observe that the same significant correlations seen for the Canadian children subgroup are visible when we investigate the subpopulation of Canadian adults (Figures (C.3)-(C.4)) and immigrant juveniles (Figures (C.5)-(C.6)). However, in these cases the susceptible class of Canadian adults and immigrant juveniles are more significant in the infection dynamic of their own subgroup. We can still observe how the immigrant adults play an important role in the spread of the infection (Figure (C.2a)).

In Figures (C.7)-(C.8) we observe that the number of infected in the immigrant adults subgroup increases as S_{IA_0} increases. As observed in the previous analyses, the susceptible immigrant adults are responsible for delaying the end of the outbreak (Figure (C.2a)).

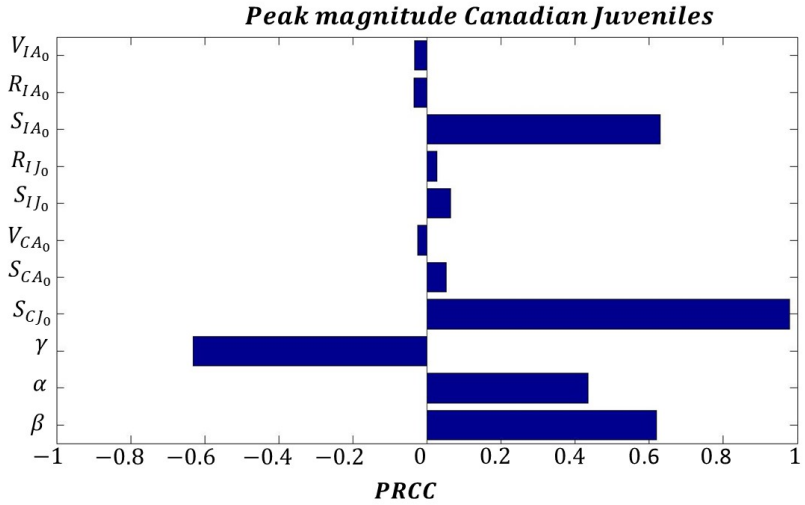

(a)

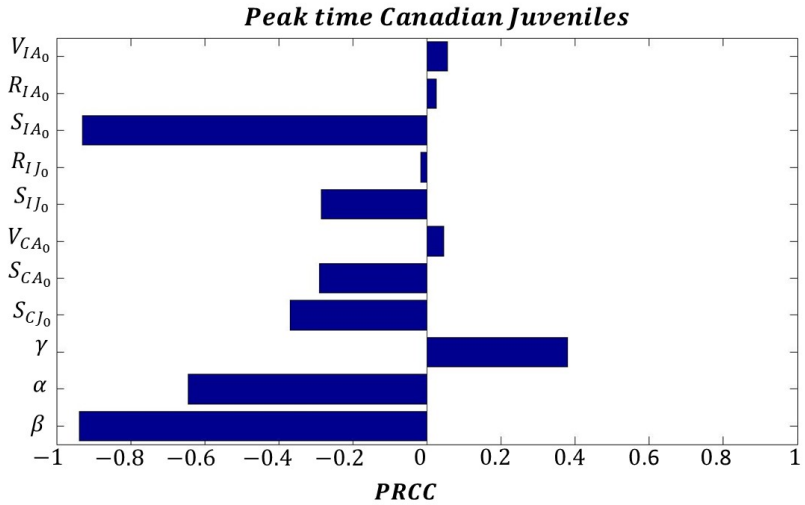

(b)

Figure C.1: LHS/PRCC plots for the population at the disease free equilibrium and parameters γ, α, β on Canadian juveniles population (a) peak magnitude (b) time of maximum peak

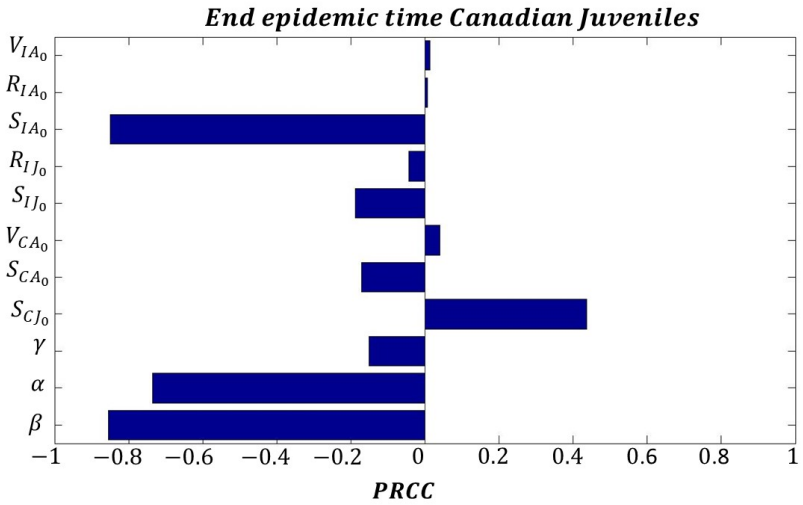

(a)

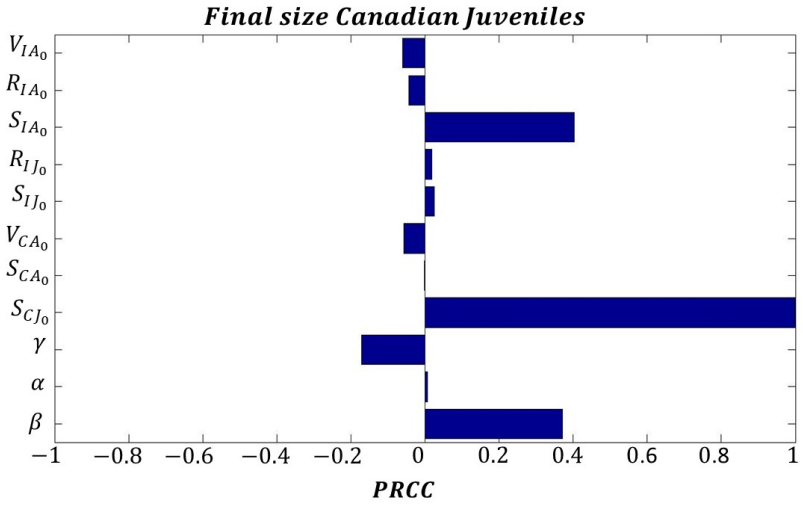

(b)

Figure C.2: LHS/PRCC plots for the population at the disease free equilibrium and parameters γ, α, β on Canadian juveniles population (a) time of end of epidemic (b) final size (number of total infected individuals)

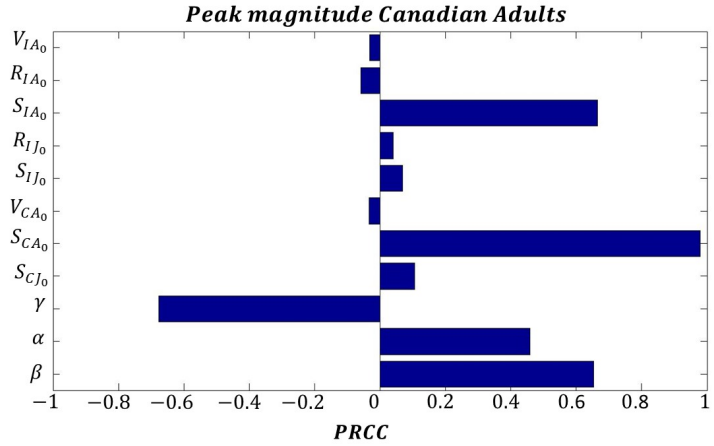

(a)

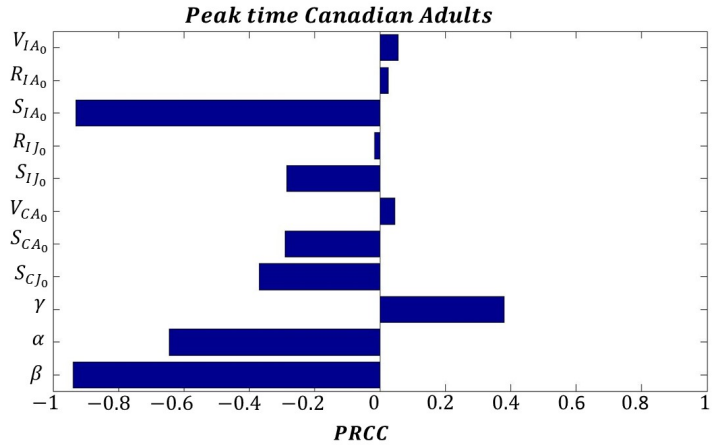

(b)

Figure C.3: LHS/PRCC plots for the population at the disease free equilibrium and parameters γ, α, β on Canadian adults (a) time of end of epidemic (b) final size (number of total infected individuals)

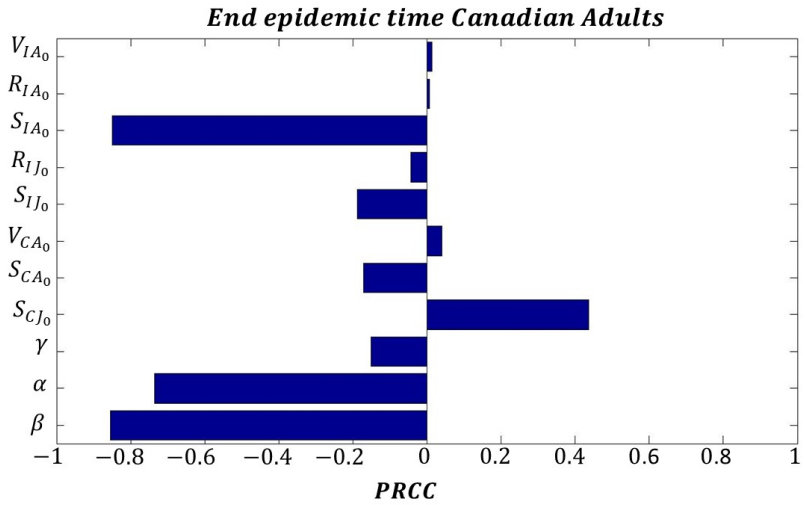

(a)

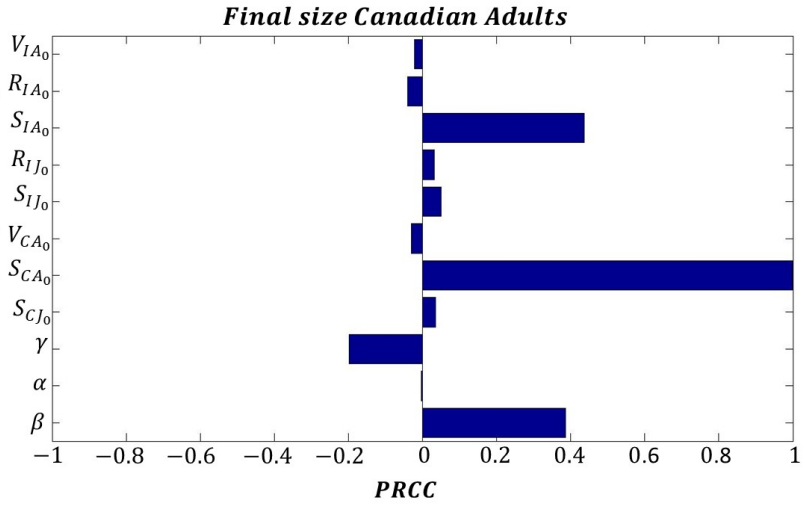

(b)

Figure C.4: LHS/PRCC plots for the population at the disease free equilibrium and parameters γ, α, β on Canadian adults (a) time of end of epidemic (b) final size (number of total infected individuals)

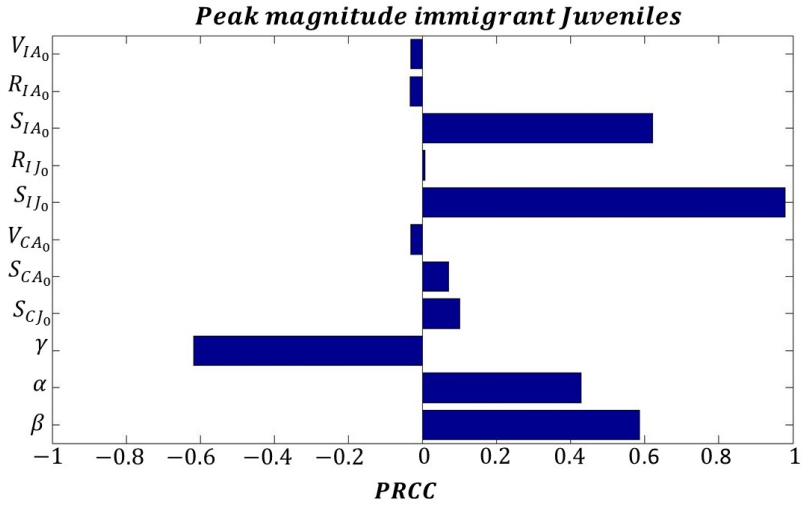

(a)

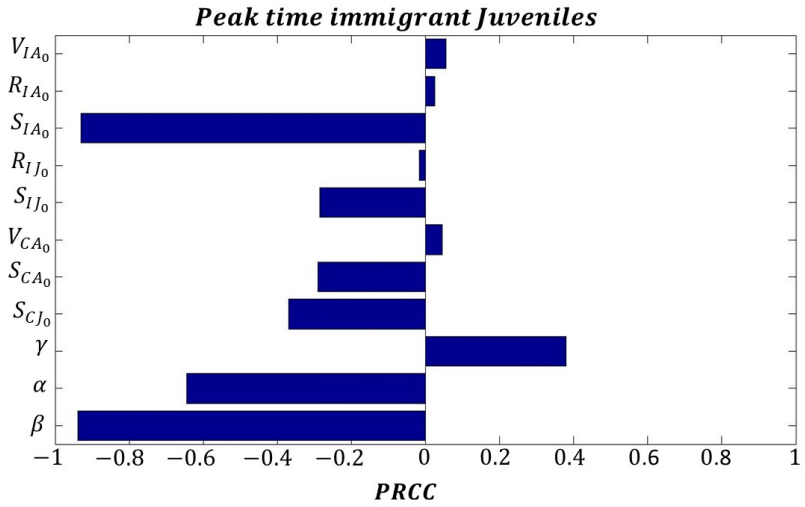

(b)

Figure C.5: LHS/PRCC plots for the population at the disease free equilibrium and parameters γ, α, β on immigrant juveniles (a) peak magnitude (b) time of maximum peak

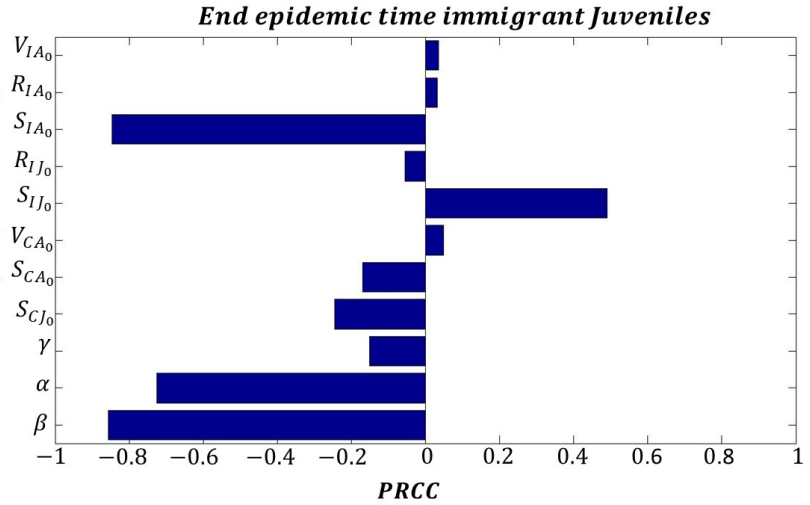

(a)

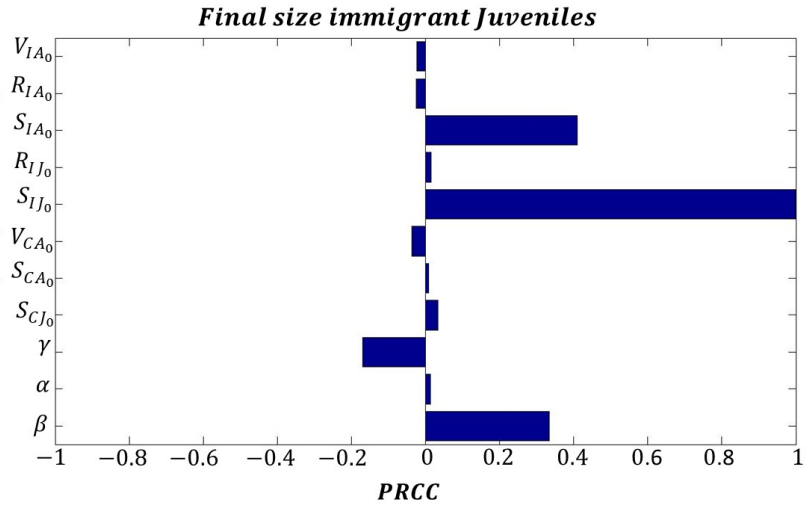

(b)

Figure C.6: LHS/PRCC plots for the population at the disease free equilibrium and parameters γ, α, β on immigrant juveniles (a) time of end of epidemic (b) final size (number of total infected individuals)

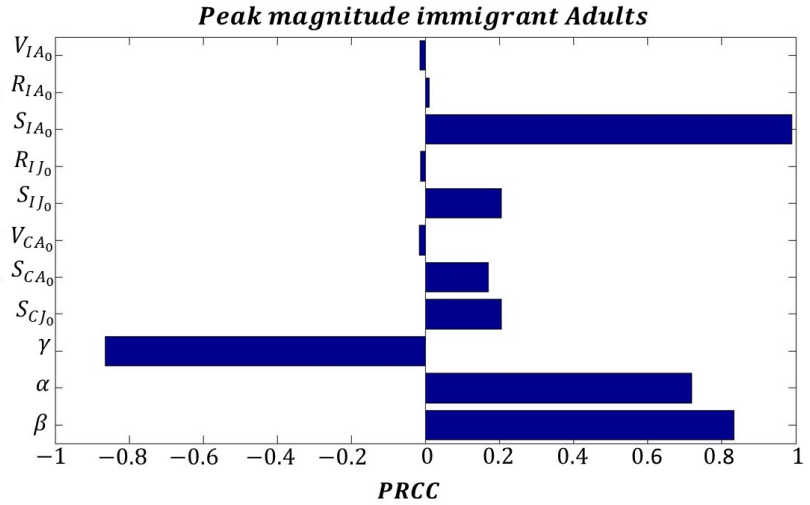

(a)

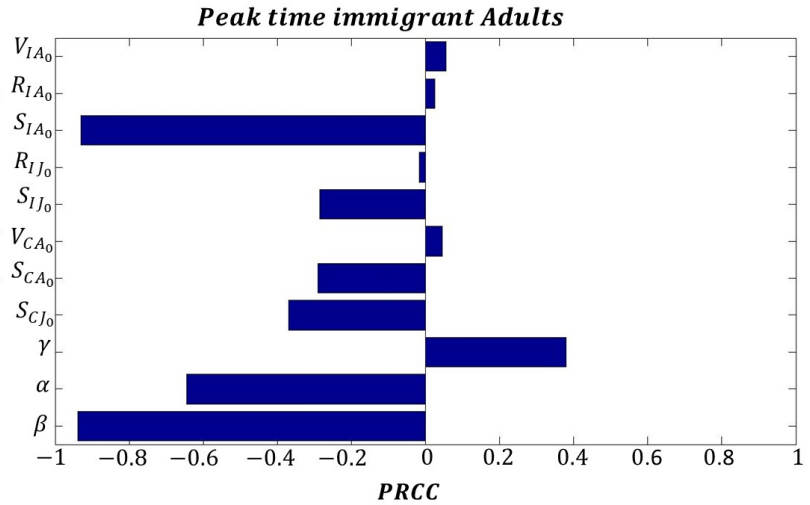

(b)

Figure C.7: LHS/PRCC plots for the population at the disease free equilibrium and parameters γ, α, β on immigrant adults (a) peak magnitude (b) time of maximum peak

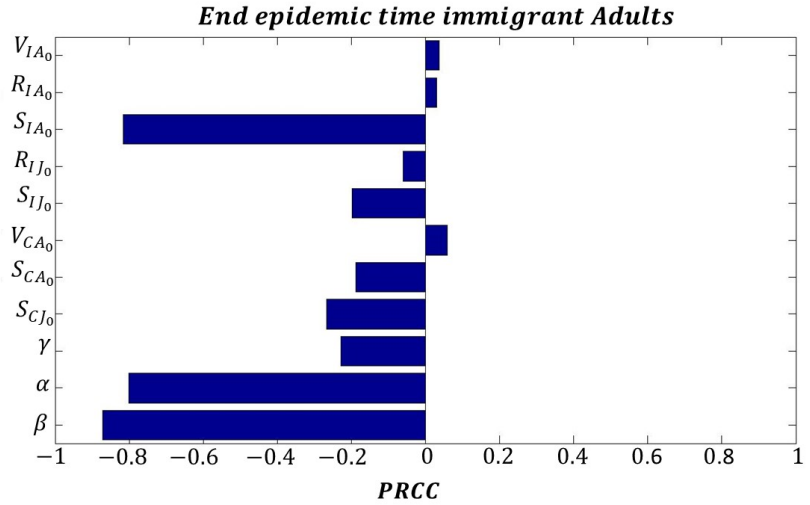

(a)

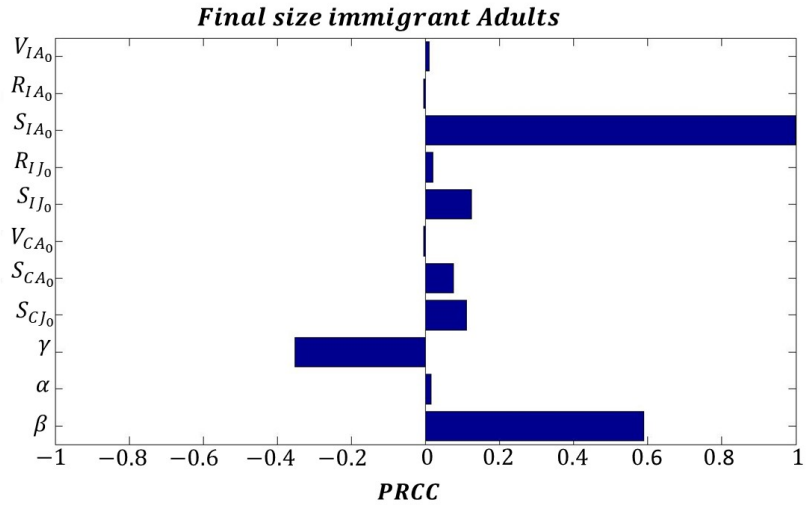

(b)

Figure C.8: LHS/PRCC plots for the population at the disease free equilibrium and parameters γ, α, β on immigrant adults (a) time of end of epidemic (b) final size (number of total infected individuals)

Appendix D

LHS/PRCC for Model (2.9): Single Outbreak

We present here the PRCC plots on the single outbreak outputs for each subpopulation when three age groups are considered. Figures (D.1-D.2) show the PRCC plots on the Canadian newborns subgroup. We observe, similar to the case with only two age classes, that the peak of the infectious individuals in this group and the total cases increase as the number of susceptible children aged between 0 and 12 months and susceptible immigrant adults and infection rate increase (Figures (D.1a) and (D.2b)). Also, the end of the epidemic is delayed as S_{IA_0} increases (Figure (D.2a)).

When we look at the Canadian children aged between 1 and 5 years, we observe again that the susceptible immigrant adults increase the maximum number of the infectious cases and the final size of this subclass (Figures (D.3a) and (D.4b)). Moreover, the same susceptible individuals contribute to extend the final stages of the infection, making the outbreak sustained for a longer period (Figure (D.4a)).

Similar significant correlations are visible in the subgroup of the Canadian adults in Figures (D.5)-(D.6). However, we observe that the peak magnitude and the final size of the infectious compartment increase as the proportion of susceptible Canadian adults increases.

The immigrant subclasses (Figures (D.7)-(D.8), (D.9)-(D.10) and (D.11)-(D.12)) present the same correlation: the maximum peak of the outbreak and the total number of infected cases(Figures (D.7a)(D.9a)(D.11a) and Figures (D.8b)(D.10b)(D.12b), respectively) increase as the number of susceptible immigrants of the analyzed subgroup increase and immigrant adults increase. In each subclass, the susceptible immigrant adults present a negative correlation with the time at which that subpopulation reaches the end of the epidemic. This result indicates that susceptible adults not born in Canada are the ones delaying the end of the epidemic.

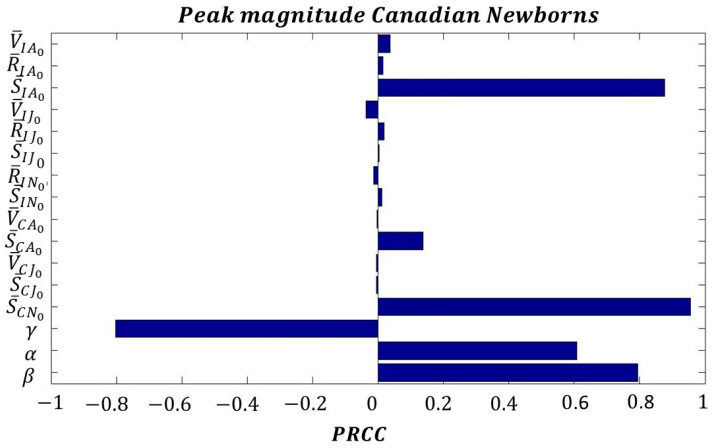

(a)

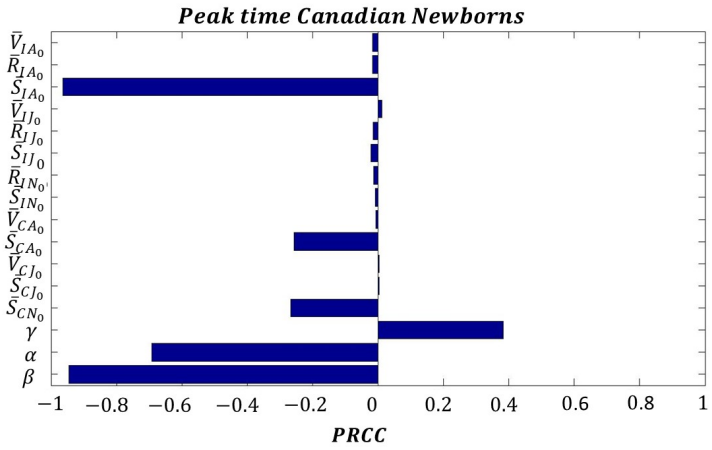

(b)

Figure D.1: LHS/PRCC plots for the population at the disease free equilibrium and parameters γ, α, β on Canadian newborns (a) peak magnitude (b) time of maximum peak

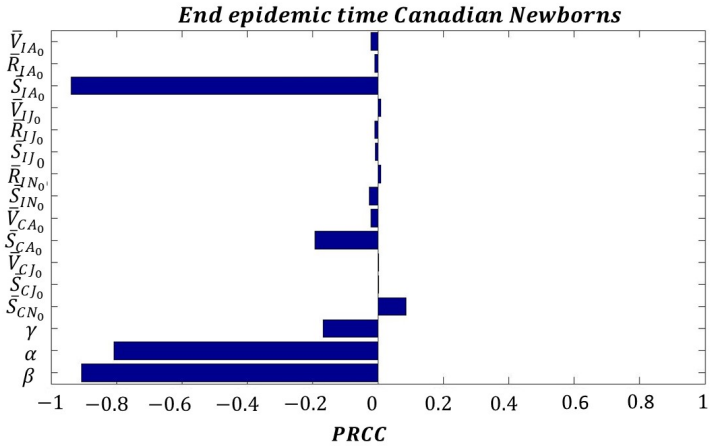

(a)

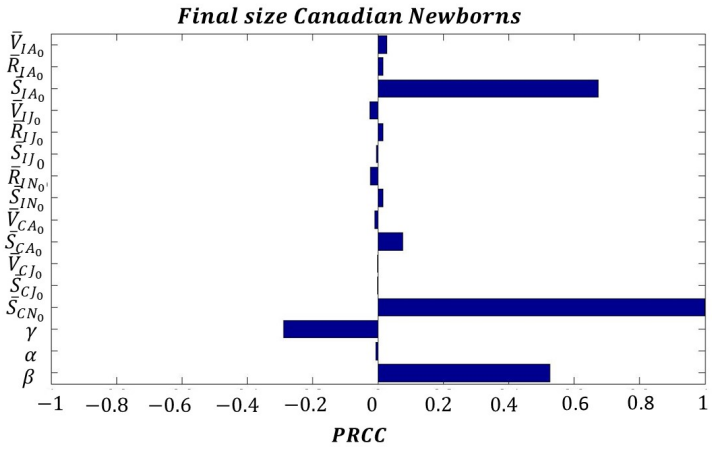

(b)

Figure D.2: LHS/PRCC plots for the population at the disease free equilibrium and parameters γ, α, β on Canadian newborns (a) time of end of epidemic (b) final size (number of total infected individuals)

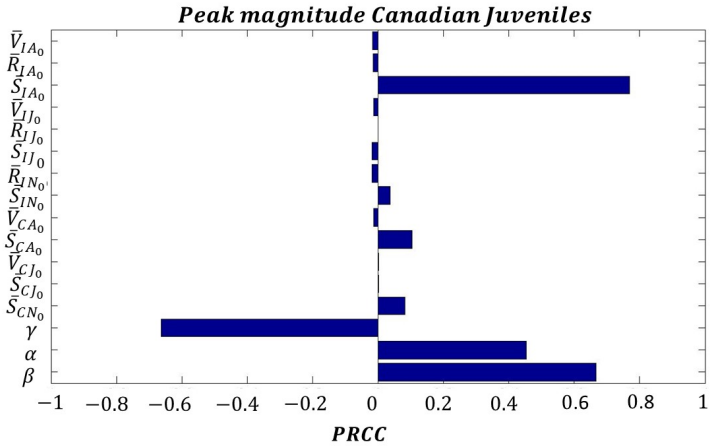

(a)

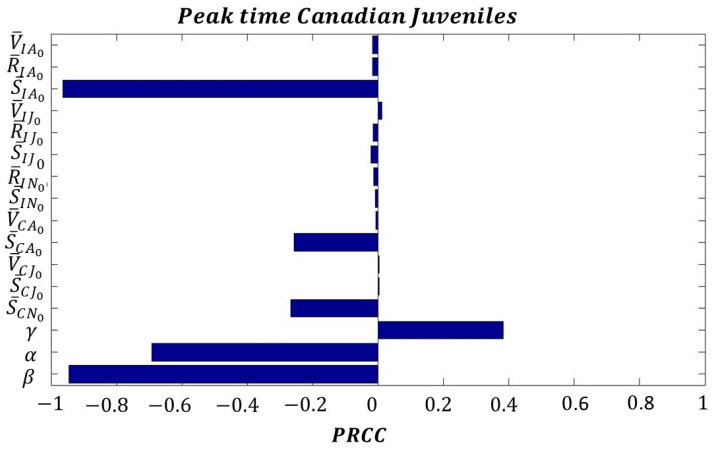

(b)

Figure D.3: LHS/PRCC plots for the population at the disease free equilibrium and parameters γ, α, β on Canadian juveniles (a) peak magnitude (b) time of maximum peak

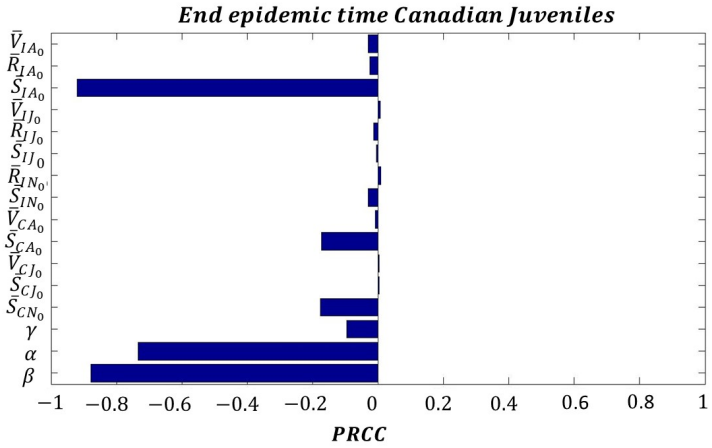

(a)

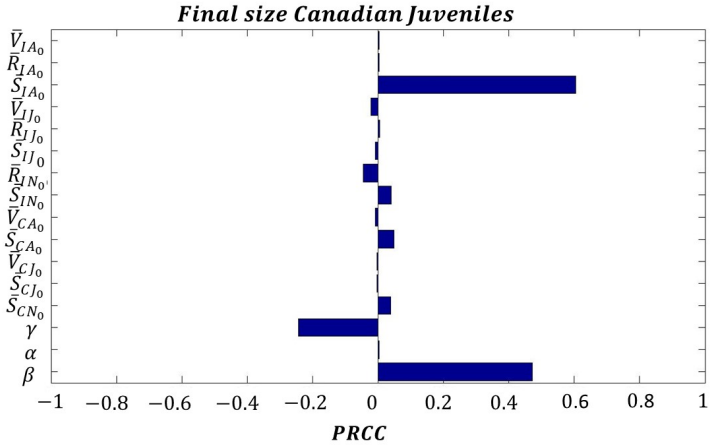

(b)

Figure D.4: LHS/PRCC plots for the population at the disease free equilibrium and parameters γ, α, β on Canadian juveniles (a) time of end of epidemic (b) final size (number of total infected individuals)

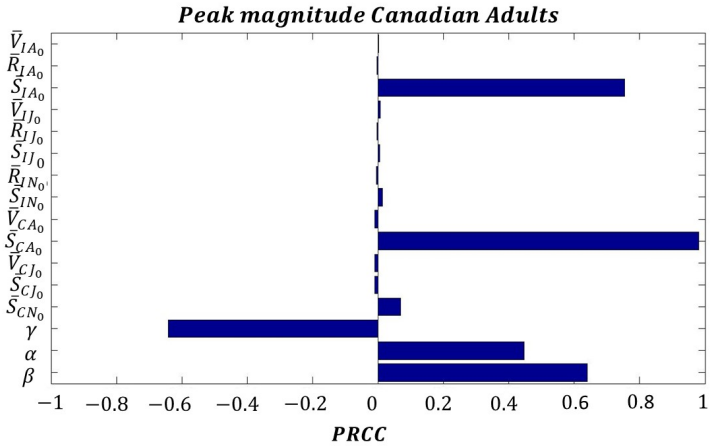

(a)

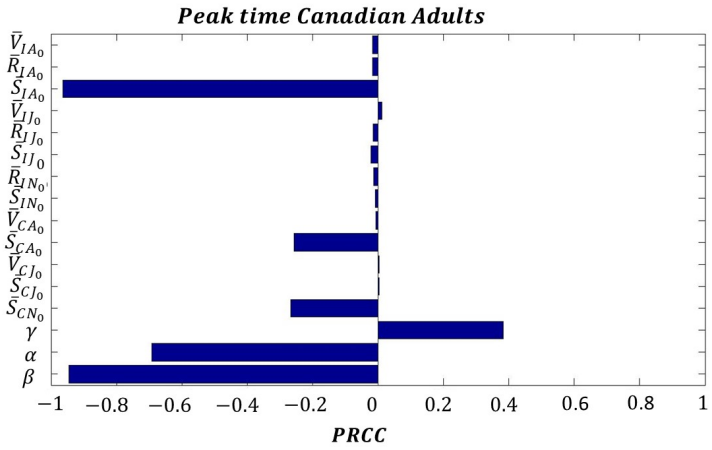

(b)

Figure D.5: LHS/PRCC plots for the population at the disease free equilibrium and parameters γ, α, β on Canadian adults (a) peak magnitude (b) time of maximum peak

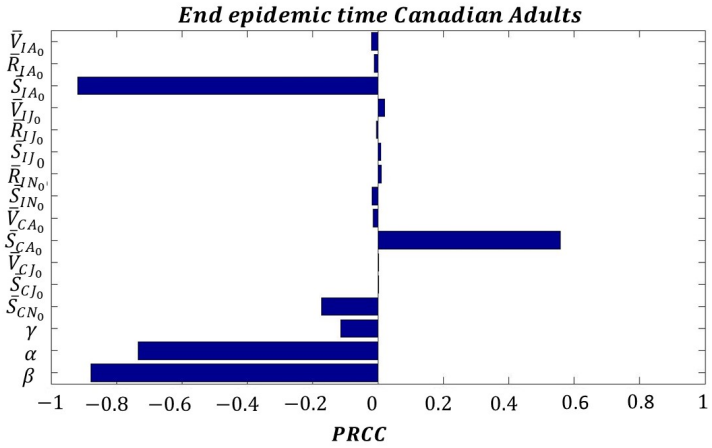

(a)

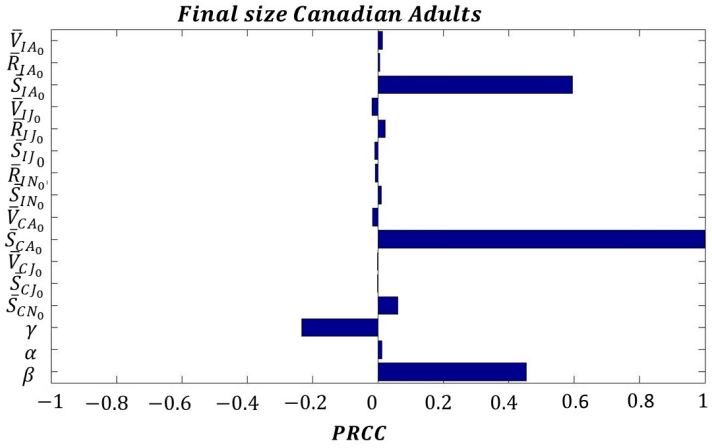

(b)

Figure D.6: LHS/PRCC plots for the population at the disease free equilibrium and parameters γ, α, β on Canadian adults (a) time of end of epidemic (b) final size (number of total infected individuals)

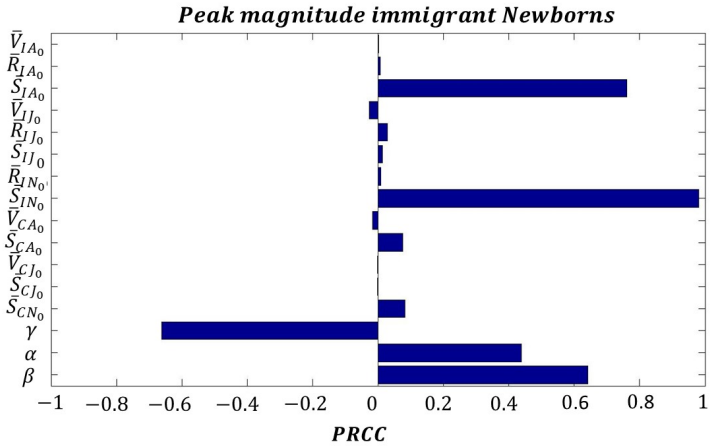

(a)

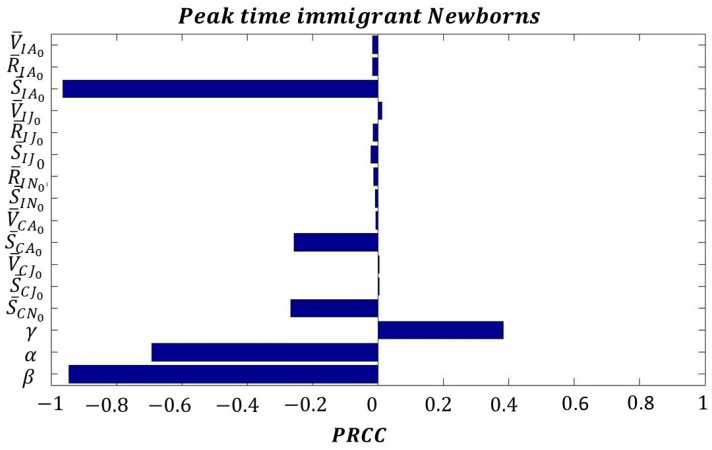

(b)

Figure D.7: LHS/PRCC plots for the population at the disease free equilibrium and parameters γ, α, β on immigrant newborns (a) peak magnitude (b) time of maximum peak

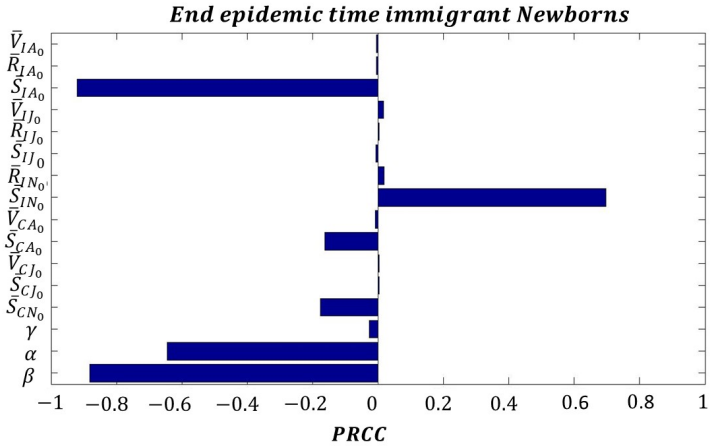

(a)

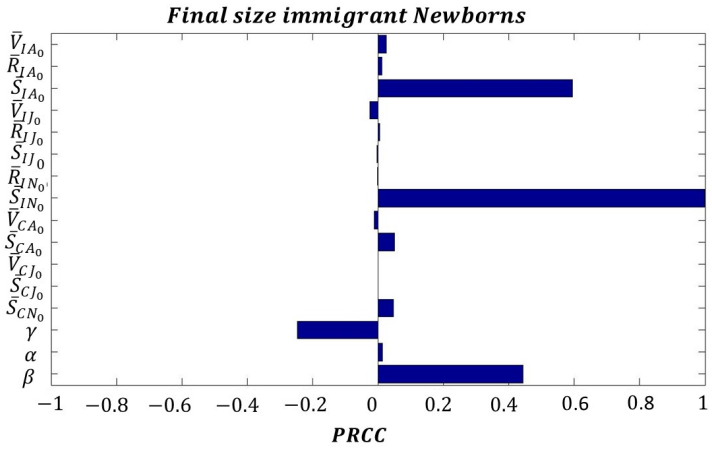

(b)

Figure D.8: LHS/PRCC plots for the population at the disease free equilibrium and parameters γ, α, β on immigrant newborns (a) time of end of epidemic (b) final size (number of total infected individuals)

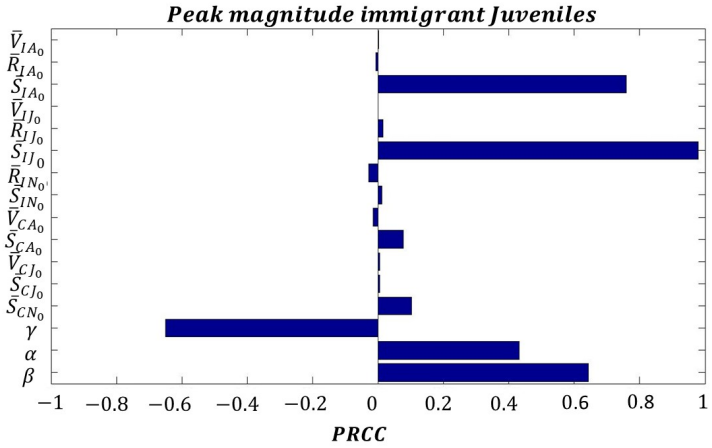

(a)

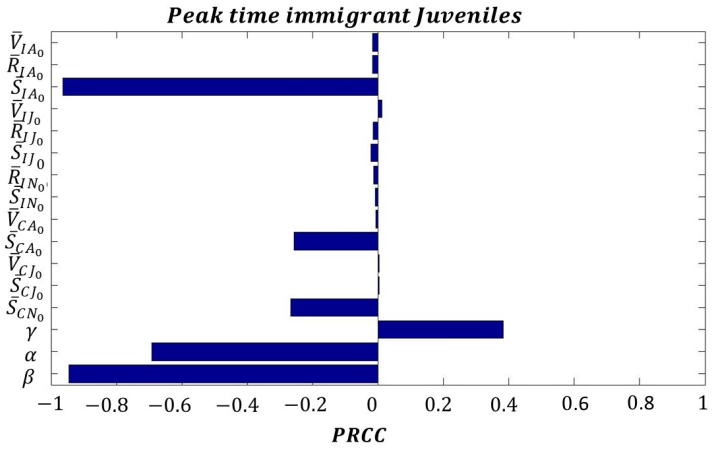

(b)

Figure D.9: LHS/PRCC plots for the population at the disease free equilibrium and parameters γ, α, β on immigrants juveniles (a) peak magnitude (b) time of maximum peak

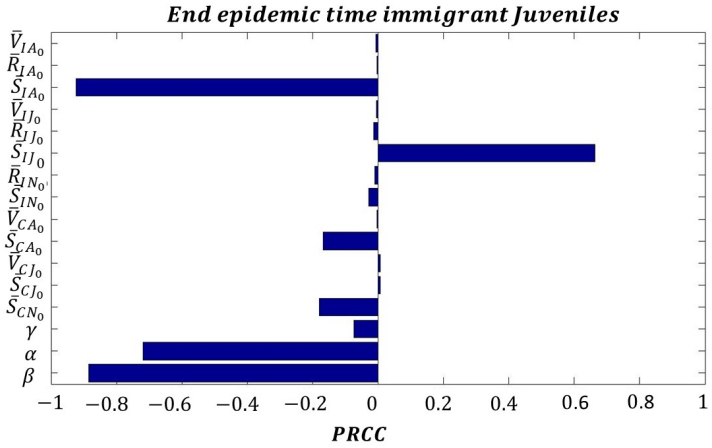

(a)

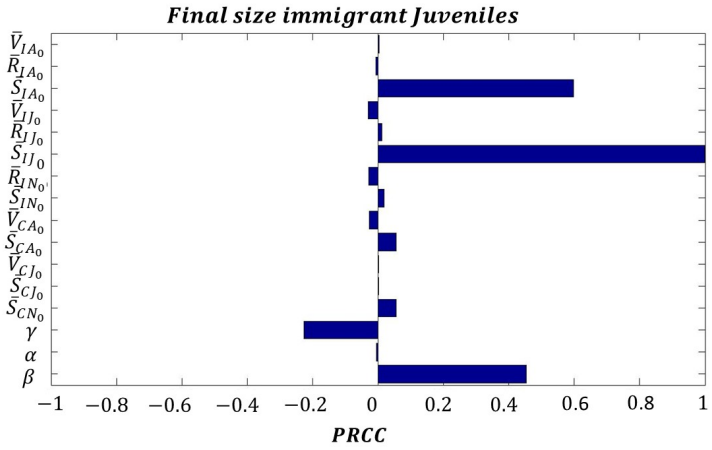

(b)

Figure D.10: LHS/PRCC plots for the population at the disease free equilibrium and parameters γ, α, β on immigrants juveniles time of maximum peak (a) time of end of epidemic (b) final size (number of total infected individuals)

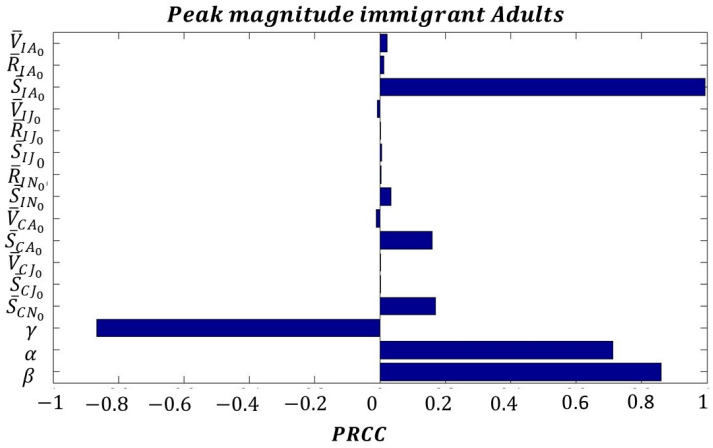

(a)

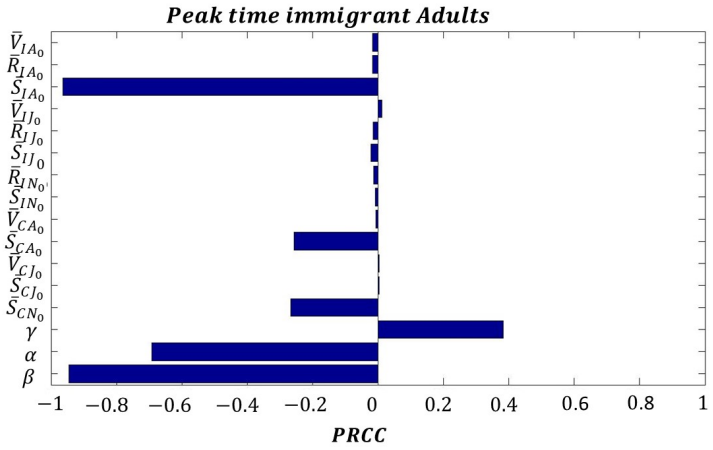

(b)

Figure D.11: LHS/PRCC plots for the population at the disease free equilibrium and parameters γ, α, β on immigrant adults (a) peak magnitude (b) time of maximum peak

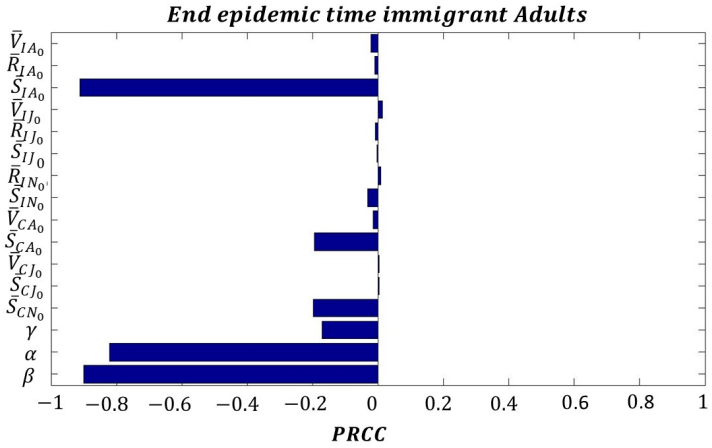

(a)

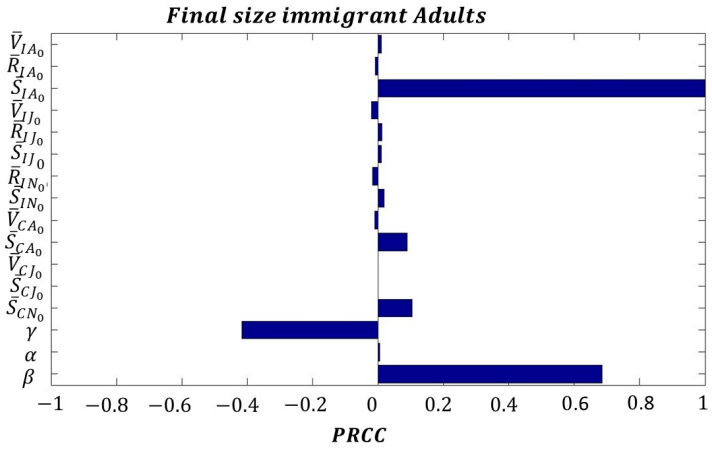

(b)

Figure D.12: LHS/PRCC plots for the population at the disease free equilibrium and parameters γ, α, β on immigrant adults (a) time of end of epidemic (b) final size (number of total infected individuals)

Appendix E

LHS/PRCC for System (3.1) when $n = 2$

We present here the LHS/PRCC analysis when the second patch is seeded with infection. When Halton is the first infected patch, to reach the peak of A_1 and I_1, we observe that besides $\mathcal{R}_{01}$ and s_1 (already explained in the main text), more time is needed if the probability of showing symptoms increases, while it is less as the infectivity in patch 2 increases (Figure (E.1a) and (E.1c)). The significant positive correlation of b is due to the fact that patch 1 is infected by commuters from patch 2, hence if more people in Halton are symptomatic, they remain in their patch, and the infection will spread slowly in Toronto. When we investigate the peak of the infectious cases in patch 2 (A_2, I_2), patch 1 parameters are significant. However, in this case a significant negative correlation is also presented on $\mathcal{R}_{02}$.
For the total peak time, the correlations of $\mathcal{R}_{0_{1,2}}$ and s_1 are similar to the ones shown in the single patch 1 (Figures (E.1c) and (E.1c)). This result confirms that patch 1 is the one that globally is more responsible for the spread.
At the beginning of the outbreak (first 100 days), when Halton is the first infected patch, both $\mathcal{R}_{02}$ and $\mathcal{R}_{01}$ show a significant negative correlation (Figure E.3a)) when we look at the single patches or both of them together. However, the time needed to reach the first 100 cases in patch 1 is delayed as s_2 increases.

When both pacthes are moving, and York is the first infected patch, the infectivity in both patches shows a significant negative correlation on the time needed to reach the peak of both A and I in both patches or globally. Contrary to the case when Toronto residents are not moving, here the probability of showing symptoms is not significant (Figures (E.4-E.5)). The time needed to reach the first 100 I cases in patch 1, 2 and globally, is delayed by the infectivity in each patch (significant negative correlation). An increase of susceptible individuals in patch 2 will delay this time in patch 1 and globally (Figure (E.6c)).

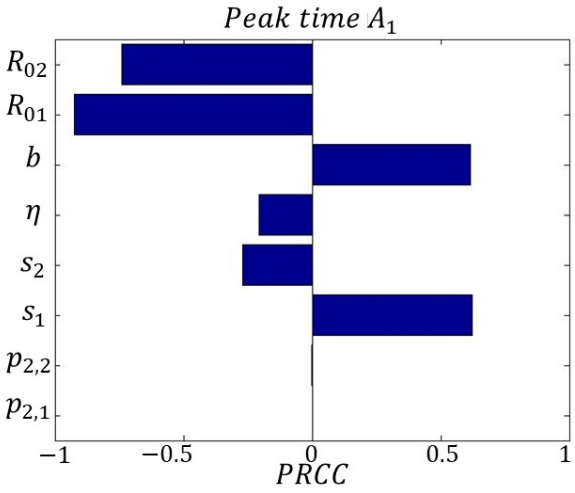

(a)

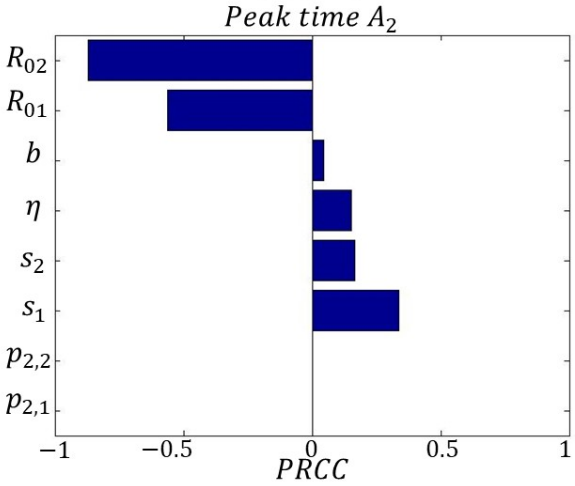

(b)

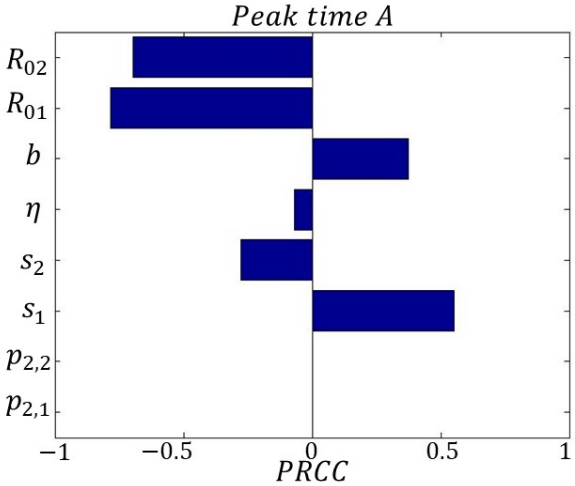

(c)

Figure E.1: Toronto-Halton (Halton infected): PRCC plots on the time at which the asymptomatic cases reach the peak when the infection is seeded in patch 2

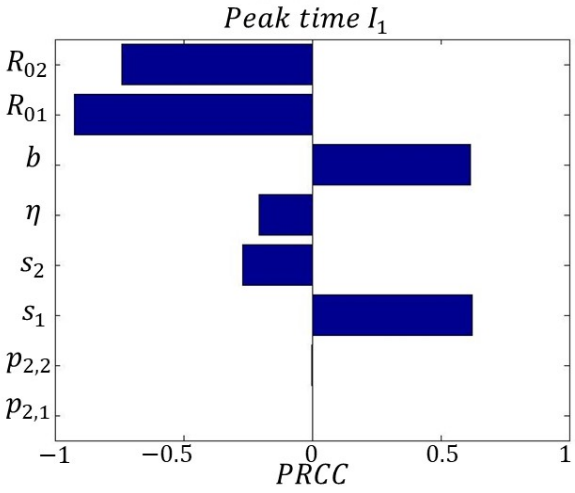

(a)

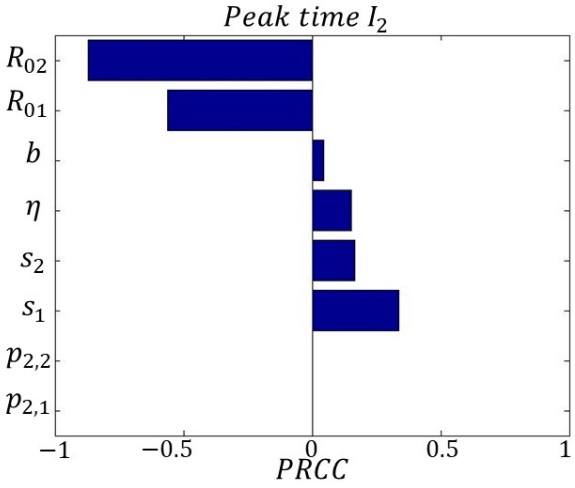

(b)

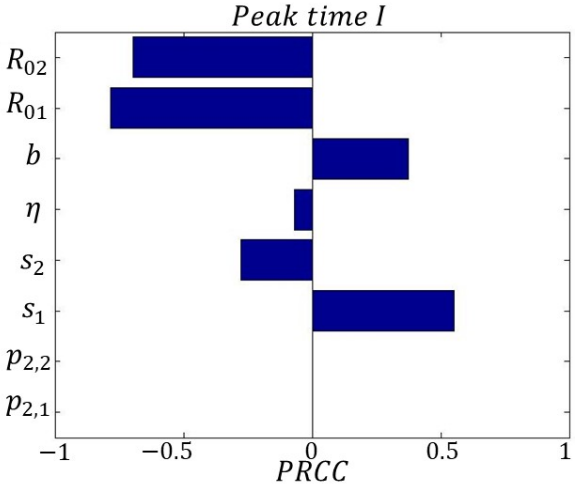

(c)

Figure E.2: Toronto-Halton (Halton infected): PRCC plots on the time at which the symptomatic cases reach the peak when the infection is seeded in patch 2

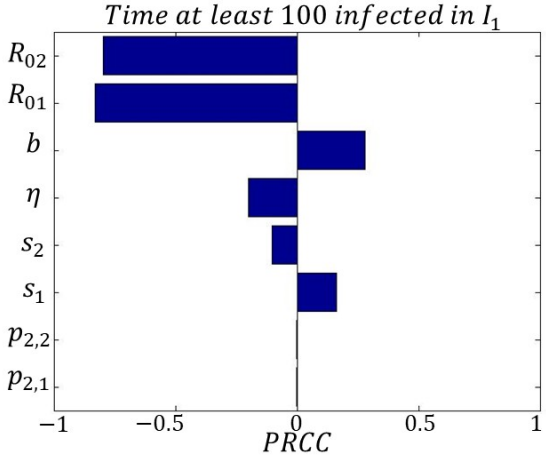

(a)

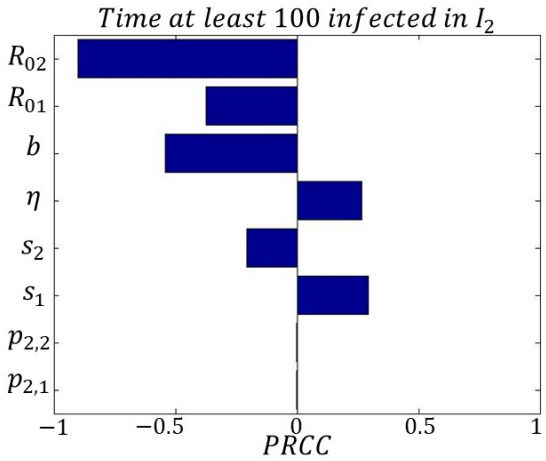

(b)

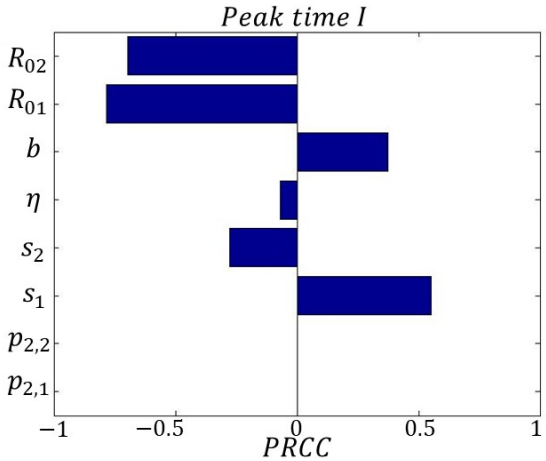

(c)

Figure E.3: Toronto-Halton (Halton infected):PRCC plots on the time at which the first 100 symptomatic cases occur when the infection is seeded in patch 2

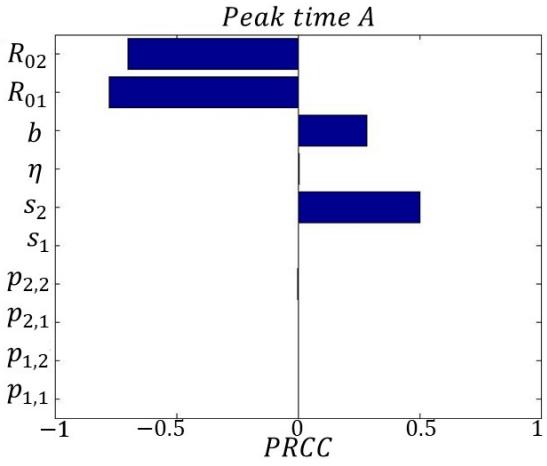

(a)

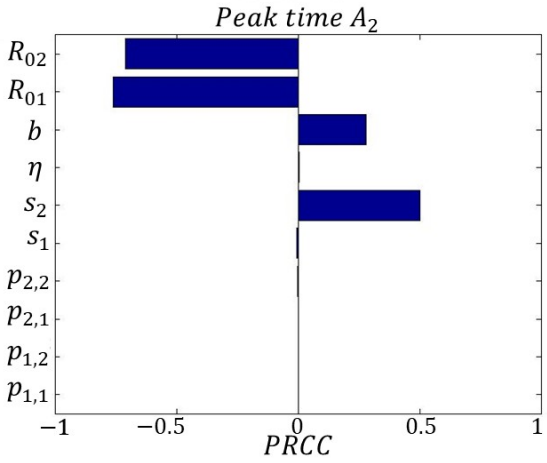

(b)

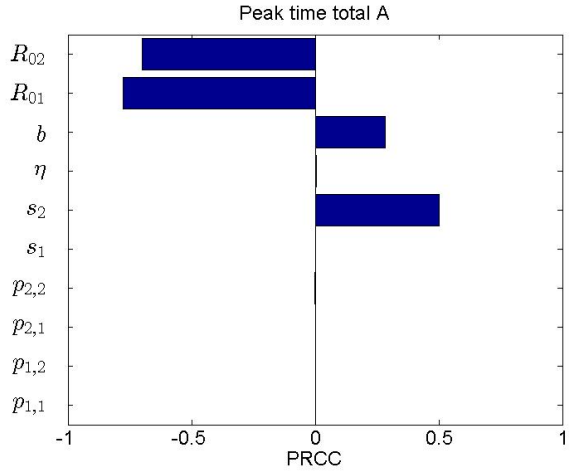

(c)

Figure E.4: Toronto-York (York infected): PRCC plots on the time at which the asymptomatic cases reach the peak when the infection is seeded in patch 2 and when all residents are moving

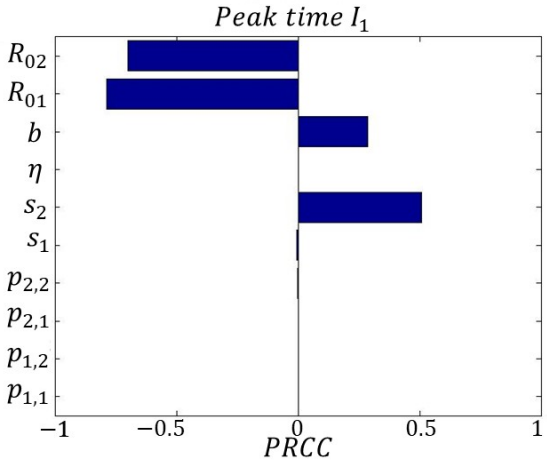

(a)

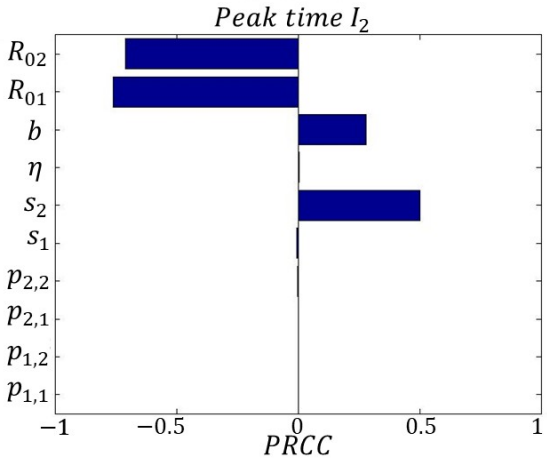

(b)

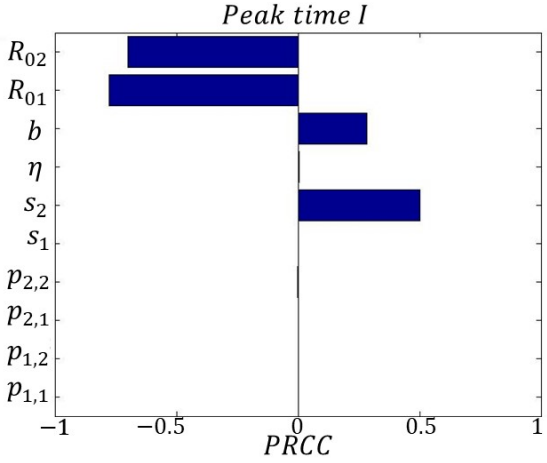

(c)

Figure E.5: Toronto-York (York infected): PRCC plots on the time at which the symptomatic cases reach the peak when the infection is seeded in patch 2 and when all residents are moving

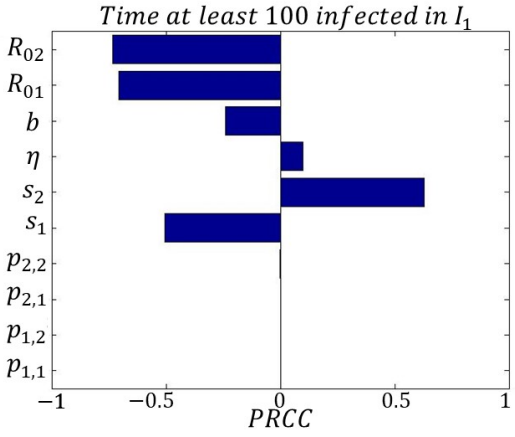

(a)

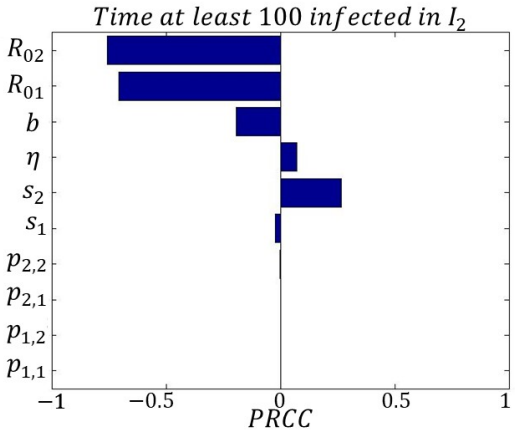

(b)

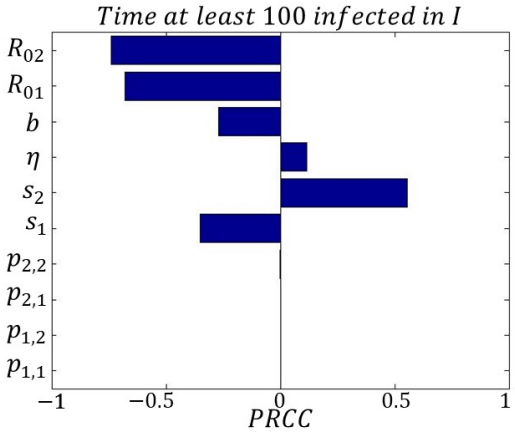

(c)

Figure E.6: Toronto-York (York infected): PRCC plots on the time at which the first 100 symptomatic cases occur when the infection is seeded in patch 2 and when all residents are moving

Appendix F

LHS/PRCC for System (3.1) when $n = 3$

Here, we show the PRCC plots on the infection dynamics when three patches are investigated. We start with the scenario where only Halton and Durham residents can move. The infection is seeded in patch 2 (Halton) . We can see that the infectivity in patch 2 increases the time to reach the peak of A in all the patches (Figure (F.1)). However, $\mathcal{R}_{01}$ and s_1 are significant, negatively and positively, respectively, in patch 1 and 3 (Figures (F.1a), (F.1b), (F.1c)). Hence, patch 2 infectivity affects the time of peak A, but simultaneously infectivity and susceptible class in patch 1 are still playing an important role. The crucial effect that $\mathcal{R}_{02}$, $\mathcal{R}_{01}$ and s_1 have on the peak of A is visible in the global analysis as well (Figures (F.1d)). When we investigate the beginning of the outbreak, when patch 2 is the first region to be infected, then the results for patch 1,2 and 3 on the achievement of the first cases in I are similar to the case with Toronto as first infected patch, but the time to reach at least 100 cases is also delayed as the infectivity in patch 2 increases(Figures (F.3a), (F.3b), (F.3c)). In the global case, the first cases occur faster if $\mathcal{R}_{02}$, $\mathcal{R}_{01}$ and b decrease (Figure (F.3d)).

Next, we analyze the scenario in which all the patches are moving (Toronto-York- Peel) and York is firstly infected. Similar results are visible in the plots in the bottom two rows of Figure F.1, representing the scenario in which patch 2 has the first infected individual. However, in this scenario the infectivity of patch 2 shows a strong negative correlation and a bit more significant than $\mathcal{R}_{01}$. Similar to A, as the infectivity in patch 1 decreases, it takes longer to achieve the maximum value of I in each patch and globally (Figure (F.2)). Moreover, in patch 2, a slight correlation between the peak time and $\mathcal{R}_{03}$ is noticeable. This result is visible when either Toronto or York is firstly infected. However, the initial infected in patch 2, makes the correlation between the output and $\mathcal{R}_{02}$ stronger. In fact, patch 2 infectivity delays the moment at which the peak of the infection occurs. Next, we investigate the beginning of the outbreak. Figure F.6 shows that an increase of $\mathcal{R}_{01}$ results in a delay in reaching the first 100 cases in I. Moreover, in patch 2 and globally, $\mathcal{R}_{02}$ and the proportion of s_2 show a significant negative and positive correlation, respectively. Hence, globally the susceptible in the second patch can increase the spread of infection.

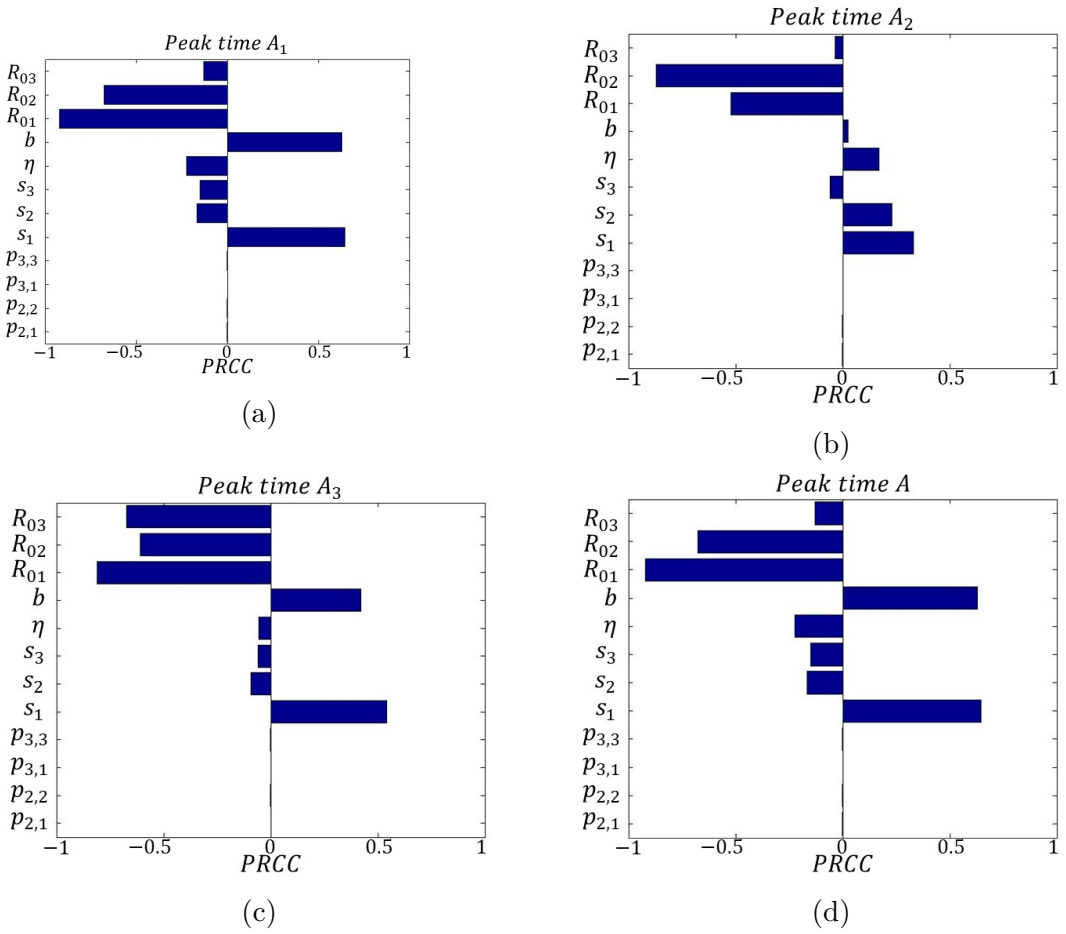

Figure F.1: Toronto-Halton-Durham (Halton infected):PRCC plots on the time at which the asymptomatic cases reach the peak when the infection is seeded in patch 2

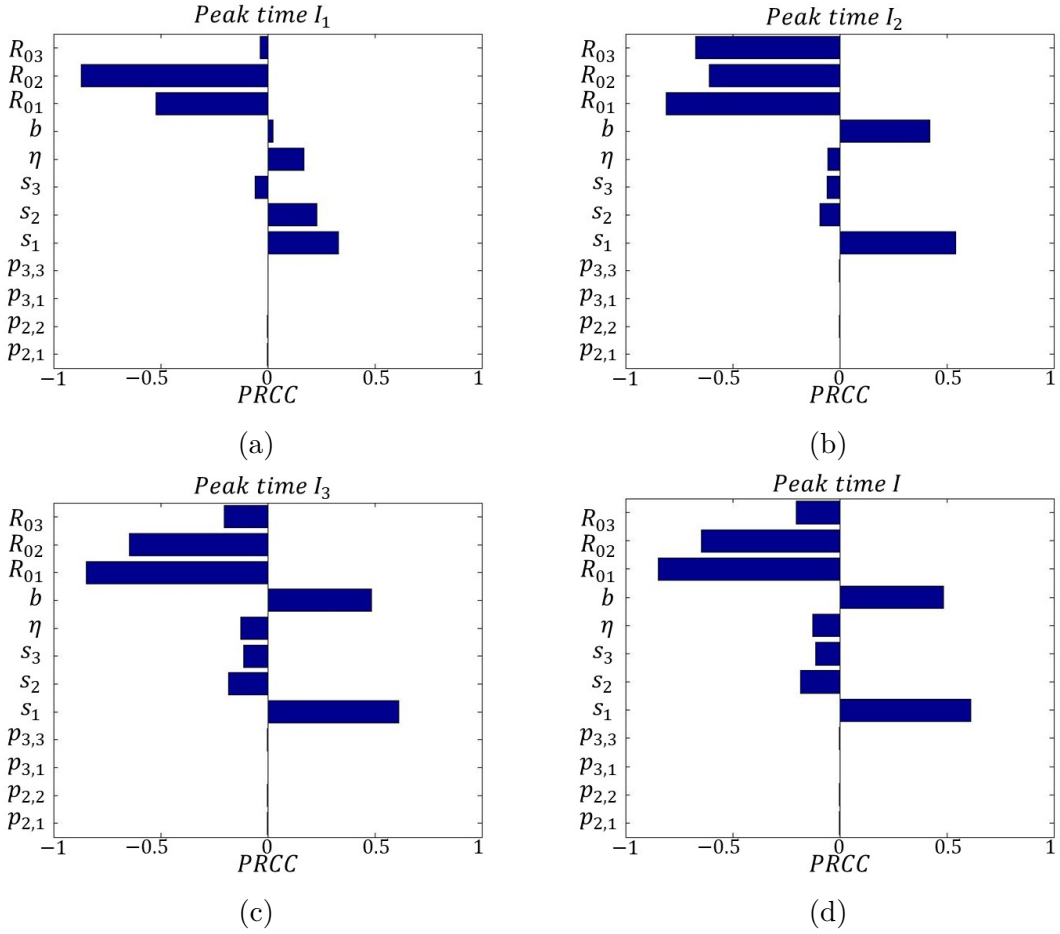

Figure F.2: Toronto-Halton-Durham (Halton infected):PRCC plots on the time at which the asymptomatic cases reach the peak when the infection is seeded in patch 2

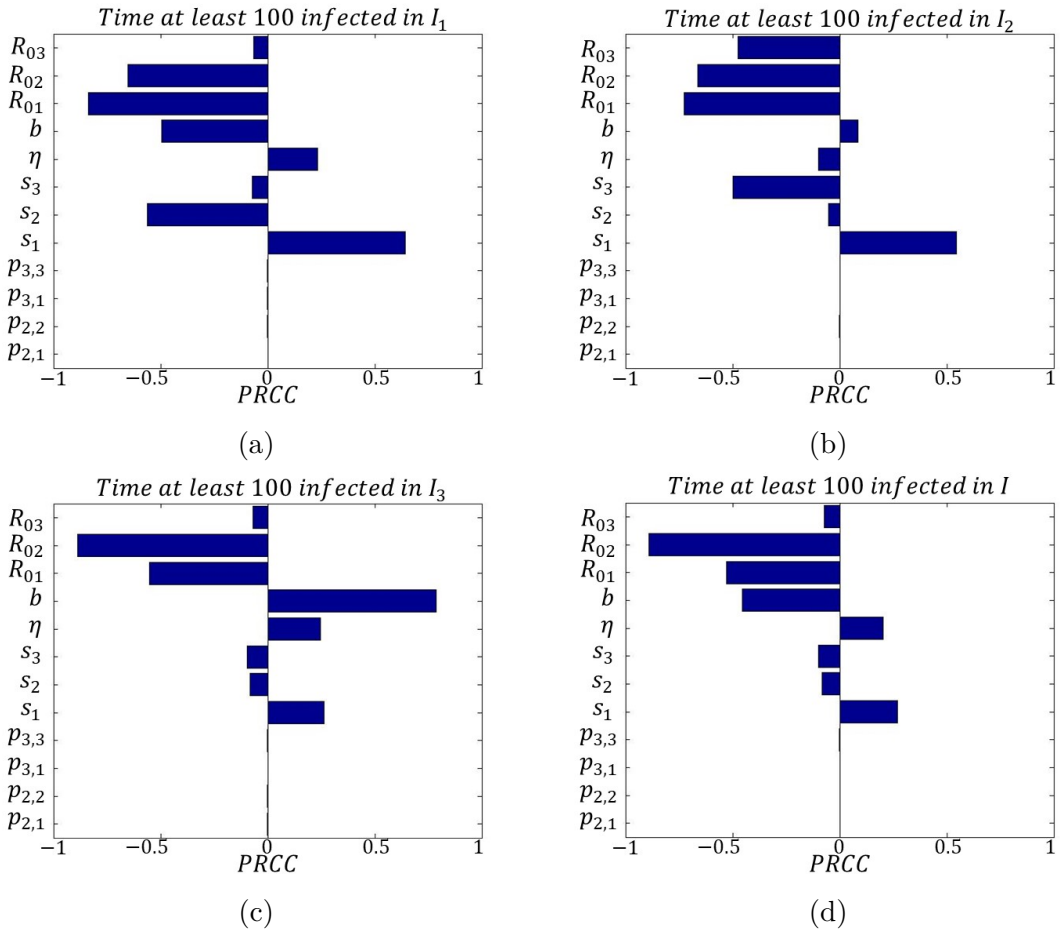

Figure F.3: Toronto-Halton-Durham (Halton infected): PRCC plots on the time at which the first 100 symptomatic cases occur when the infection is seeded in patch 2

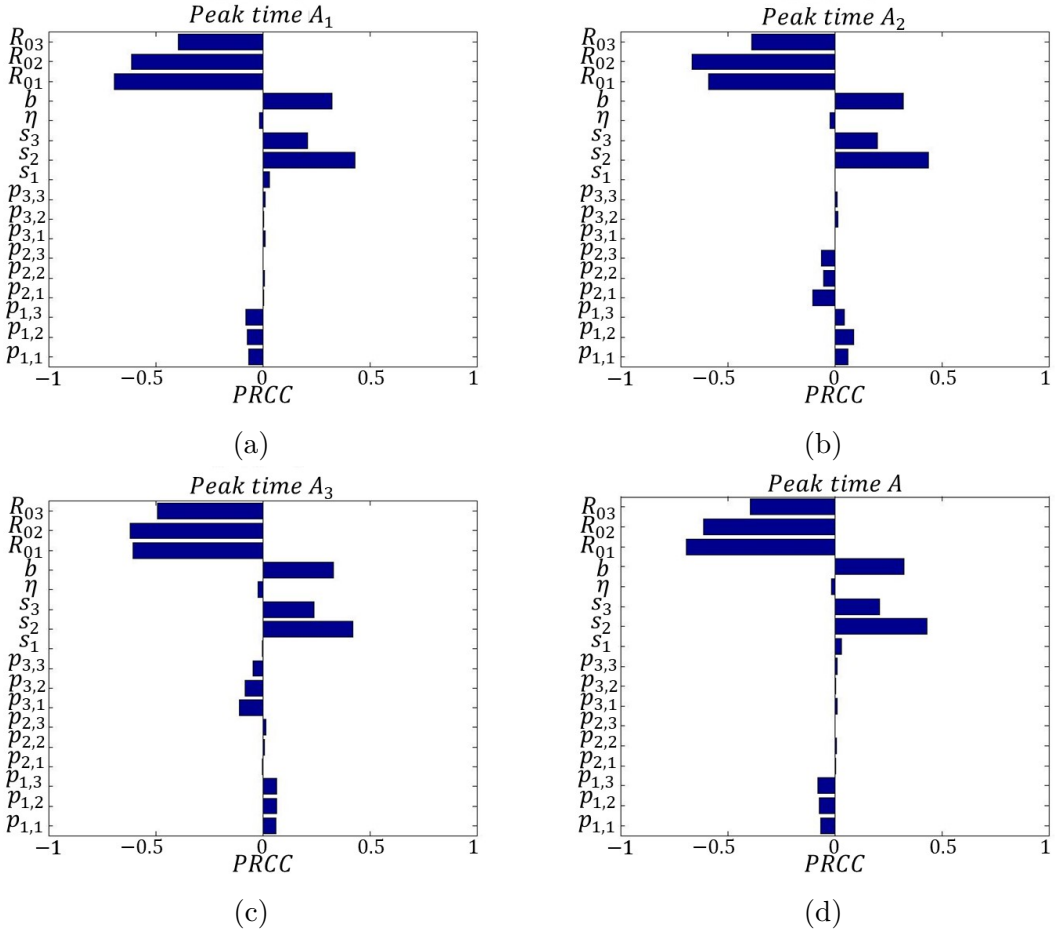

Figure F.4: Toronto-York-Peel (York infected): PRCC plots on the time at which the asymptomatic cases reach the peak when the infection is seeded in patch 2

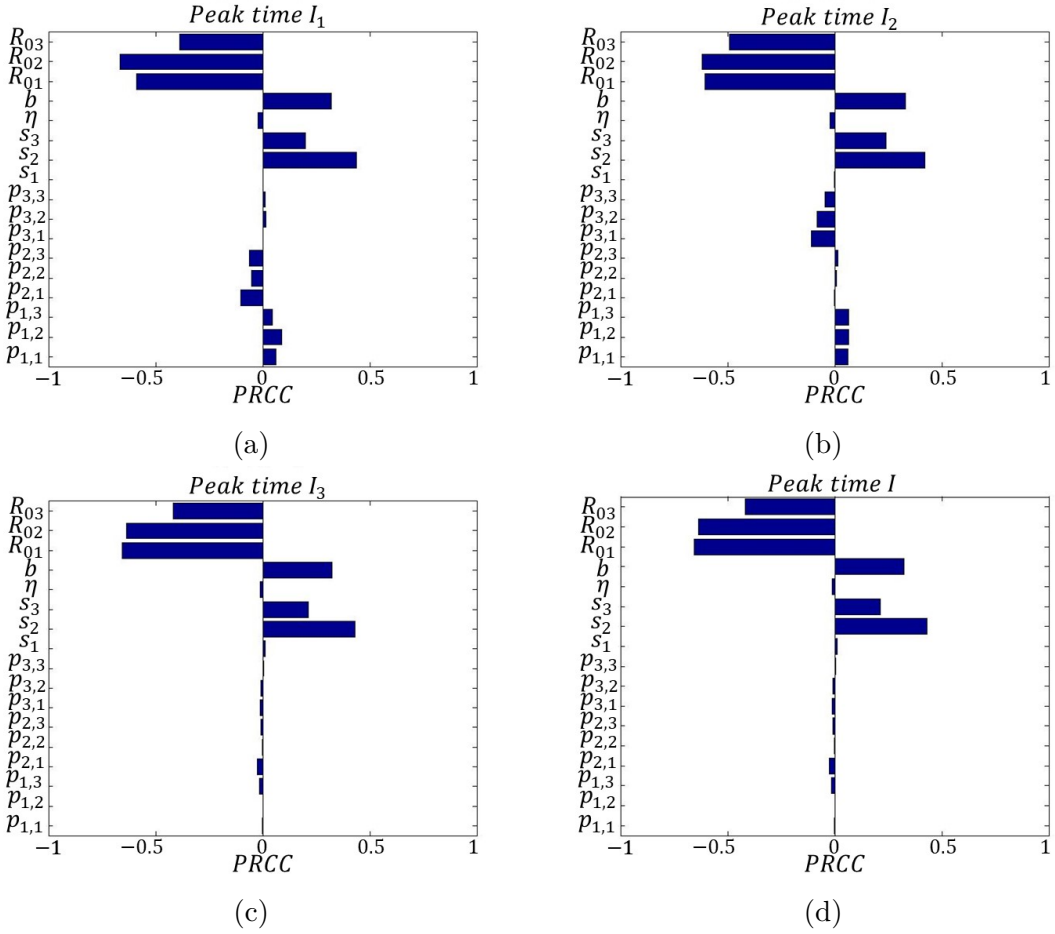

Figure F.5: Toronto-York-Peel (York infected): PRCC plots on the time at which the asymptomatic cases reach the peak when the infection is seeded in patch 2

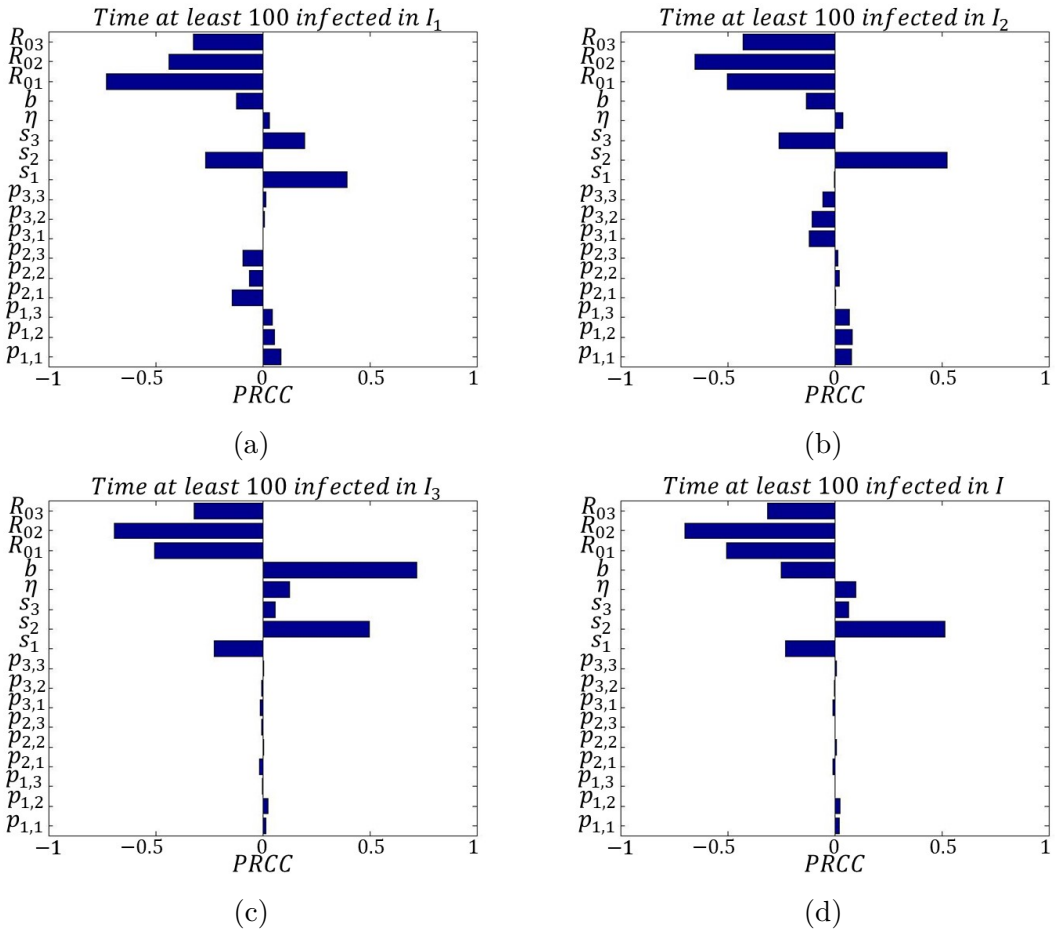

Figure F.6: Toronto-York-Peel (York infected): PRCC plots on the time at which the first 100 symptomatic cases occur when the infection is seeded in patch 2

Appendix G

Tables of Parameters for Model (4.8)

Figure G.1 shows the death rate in Canada ([121]) in 2016 by age groups as well as the population size of each group.

Age Group	Male	Female
<1 year	0.005	0.004
1-4 years	0	0
5-9 years	0	0
10-14 years	0	0
15-19 years	0	0
20-24 years	0.001	0
25-29 years	0.001	0
30-34 years	0.001	0
35-39 years	0.001	0.001
40-44 years	0.001	0.001
45-49 years	0.002	0.001
50-54 years	0.003	0.002
55-59 years	0.006	0.004
60-64 years	0.009	0.005
65-69 years	0.013	0.008
70-74 years	0.021	0.014
75-79 years	0.034	0.023
80-84 years	0.055	0.04
85+ years	0.145	0.125

(a)

Age Group	Male	Female
<1 year	100000	100000
1-4 years	99540.41	99603.57
5-9 years	99454.38	99533.69
10-14 years	99407.88	99495.4
15-19 years	99348.32	99440.2
20-24 years	99157.51	99319.2
25-29 years	98828.25	99167.42
30-34 years	98475.7	99005.24
35-39 years	98085.45	98795.23
40-44 years	97641.73	98536.42
45-49 years	96954.59	98111.1
50-54 years	95927.06	97425.9
55-59 years	94391.97	96342.83
60-64 years	91768.42	94559
65-69 years	87932.8	92126.93
70-74 years	82546.89	88331.55
75-79 years	74256	82425.45
80-84 years	62670.48	73482.63
85+ years	47550.56	60184.48

(b)

Figure G.1: Data used to estimate parameters (a) age specific death rate for Canada in 2016 (nMx) as given by WHO [121] (b) People left in the age group at the beginning of the time interval (lx)

Table G.1 represents the daily contacts among 15 different age groups in The Netherlands. This table is the results of a study conducted by Mossong et al. [69] in 2008 to study the infection dynamics among age groups.

	age group of participant														
age of contact	00-04	05-09	10-14	15-19	20-24	25-29	30-34	35-39	40-44	45-49	50-54	55-59	60-64	65-69	70+
00-04	3.50	1.71	0.25	0.19	0.33	0.57	1.00	0.92	3.00	0.00	0.00	0.23	0.39	0.12	0.22
05-09	2.47	11.88	1.56	0.19	0.00	0.50	1.25	1.62	1.14	0.71	0.31	0.08	0.28	0.24	0.29
10-14	0.32	1.06	10.97	2.50	0.08	0.00	1.50	1.00	0.71	0.93	0.08	0.31	0.22	0.06	0.2
15-19	0.15	0.24	1.44	9.19	0.83	0.29	1.25	0.08	0.57	0.79	0.46	0.46	0.39	0.00	0.24
20-24	0.24	0.18	0.16	1.25	2.42	0.57	0.75	0.85	2.29	0.71	2.23	0.85	0.5	0.29	0.29
25-29	0.21	0.88	0.13	0.44	1.58	1.86	2.25	0.62	0.86	1.21	1.85	0.38	0.56	0.41	0.32
30-34	1.26	0.71	0.25	0.44	2.67	1.00	3.75	1.00	1.71	0.86	0.85	0.92	0.94	0.18	0.49
35-39	1.15	1.53	0.78	0.75	1.58	0.86	3.00	3.92	1.29	1.79	1.23	0.69	1.17	0.59	0.71
40-44	0.53	1.76	1.56	0.69	0.67	1.07	2.13	3.08	1.86	2.50	0.38	1.54	0.78	0.65	0.71
45-49	0.24	0.47	0.94	1.38	0.92	0.50	1.63	1.69	1.29	2.21	1.23	1.00	0.61	0.35	1.24
50-54	0.47	0.47	0.56	0.69	0.83	1.21	0.88	1.62	1.14	1.5	1.31	1.34	1.17	0.24	0.51
55-59	0.38	0.24	0.19	0.31	0.25	0.57	0.25	0.46	0.00	0.93	0.69	2.38	1.67	0.71	0.51
60-64	0.35	0.41	0.03	0.06	0.08	0.29	0.5	0.92	0.14	0.43	0.38	1.15	1.61	1.12	0.46
65-69	0.29	0.29	0.13	0.13	0.00	0.14	0.13	0.69	0.14	0.00	0.31	0.69	0.72	0.82	0.46
70+	0.24	0.24	0.56	0.56	0.33	0.21	0.63	0.46	0.00	0.79	0.62	0.23	1.11	1.00	1.95

Table G.1: Contact rates per day between age groups as surveyed by Mossong et al. [69] in Netherlands

Table G.1 and Figure G.1 have been reproduced by Dr. Teslya.

Appendix H

Probability of Extinction and Outbreak for Model (4.1)

In this appendix we show the probability of extinction, 10 or 150 cases for the Model in system (4.1).

Case $k_1 = k_2 = 1/300$

In this section we consider the scenario with $k_1 = k_2 = 1/300$. We observe that when immunity is lifelong, for small reproduction numbers (Figures (H.1a)-(H.2a)), the probability of having an outbreak with 10 cumulative cases is very small. This probability decreases as the vaccination coverage and the proportion of individuals with boosted immunity increase. Moreover, when $G = 0$ (top-row panels) the chances to have 10 cases is smaller than the ones for $G = 1$. If we look at an outbreak with 150 cumulative cases, then we observe that the probability of reaching this high number of infected individuals is almost 0. On the other hand, for $\mathcal{R}_0 = 18$, the results are different (Figures (H.1b)-(H.2b)). In fact, although the probability of getting 10 or 150 cases decreases as the p increases, the chance of an outbreak is very high. Moreover, this probability is higher if the secondary cases are as infectious as the primary ones (i.e. $G = 1$).

Case $k_1 = k_2 = 1/30$

Here, the total immunity waning period is considered to be 60 years. Contrary to the life long immunity, we observe that an outbreak with 10 or 150 cumulative cases can occur with very high probability for both small (Figures (H.3a)-(H.4a)) and large (Figures (H.3b)-(H.4b)) reproduction number. As expected, when the secondary cases are able to transmit the infection with the same infection force of I, then the probability of having an outbreak increases

This pattern is visible for all the other cases with waning periods shorter than life span: $k_1 = 1/50, k_2 = 1/5$ (Figures (H.4-H.5b)), $k_1 = 1/5, k_2 = 1/50$ (Figures (H.7-H.8)), $k_1 = 1, k_2 = 1/25$ (Figures (H.9-H.10)).

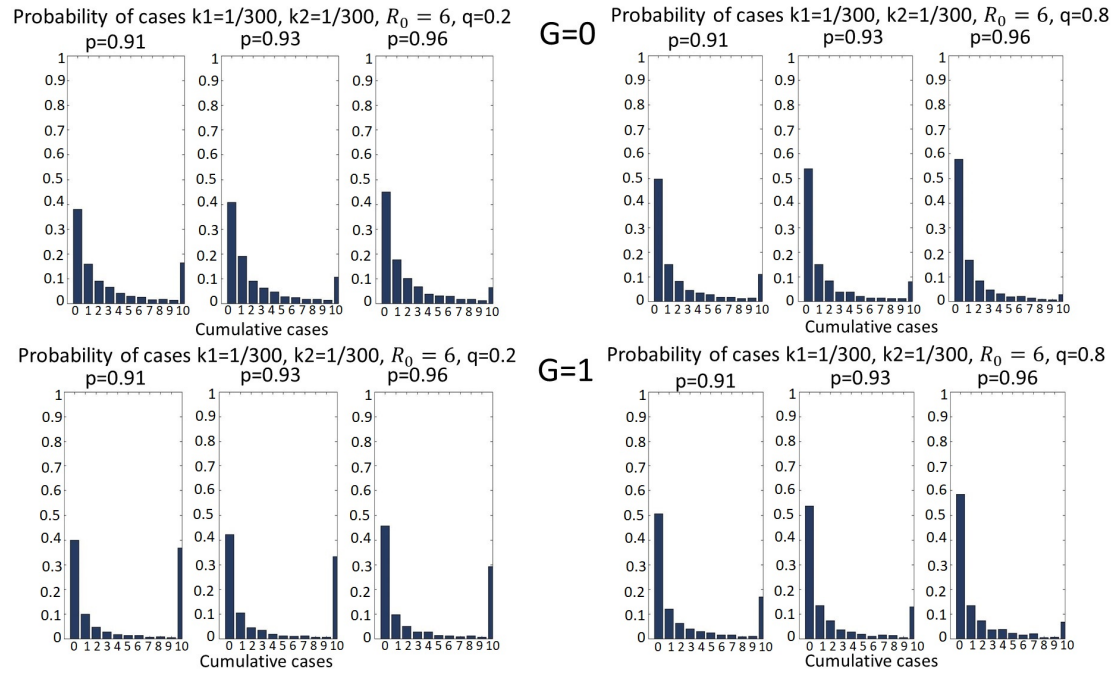

(a)

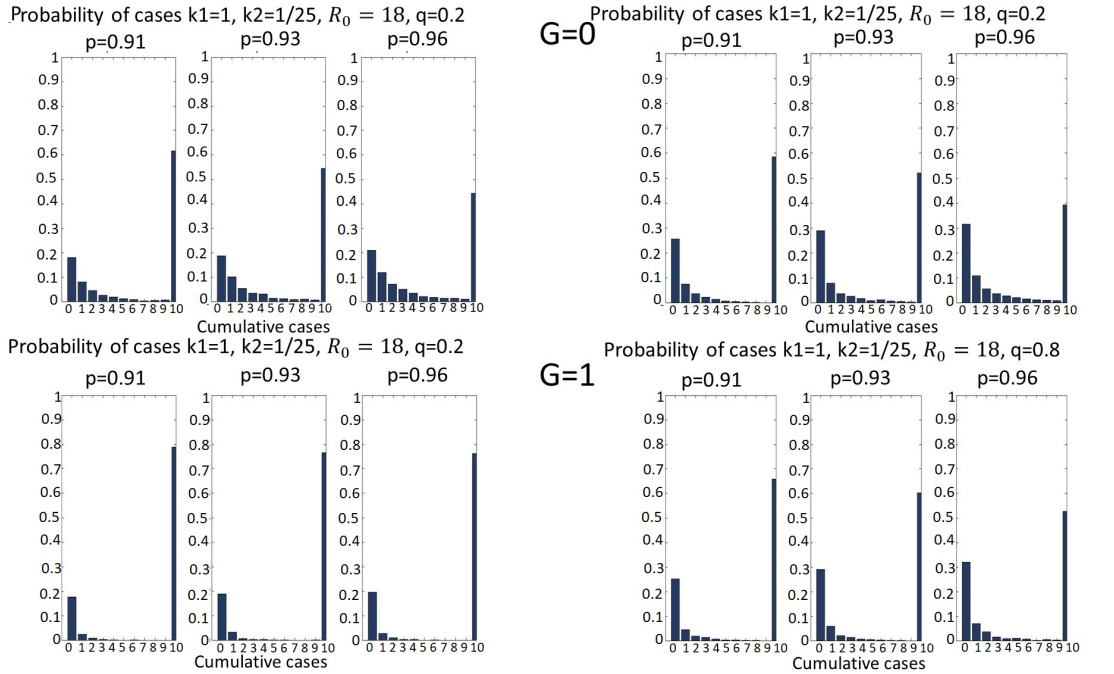

(b)

Figure H.1: Probability of having extinction, 10 cases when $G = 0$, 1 for $p = 0.91$, 0.93, 0.96, $q = 0.2$, 0.8, $k_1 = k_2 = 1/300$ and (a) $\mathcal{R}_0 = 6$ (b) $\mathcal{R}_0 = 18$

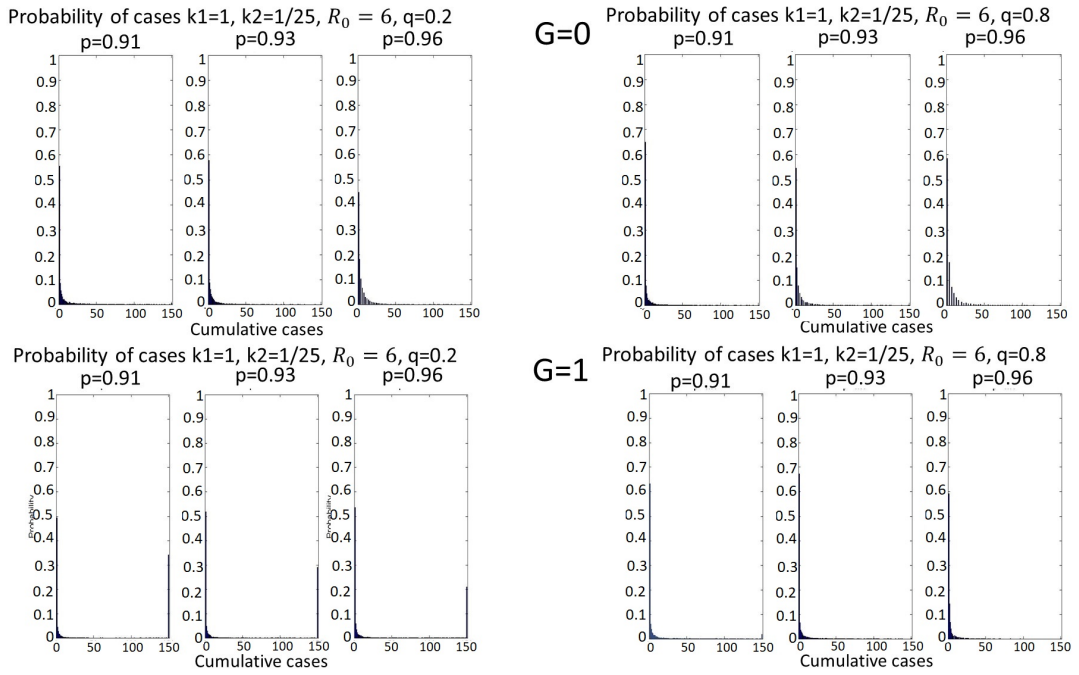

(a)

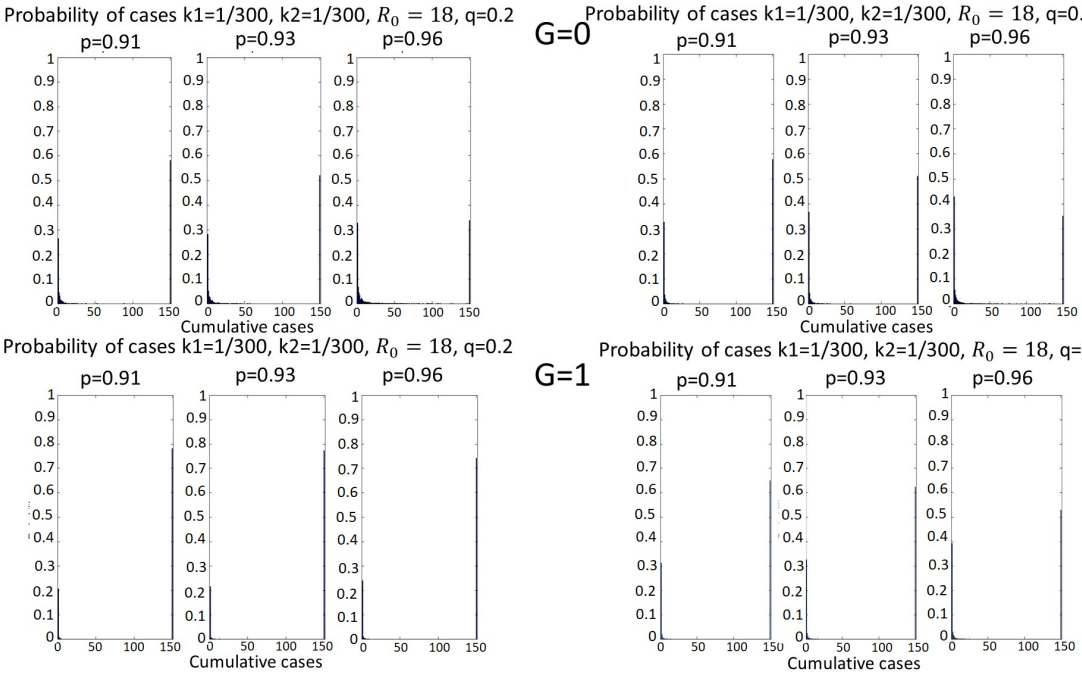

(b)

Figure H.2: Probability of having extinction, 150 cases when $G = 0$, 1 for $p = 0.91$, 0.93, 0.96, $q = 0.2$, 0.8, $k_1 = k_2 = 1/300$ and (a) $\mathcal{R}_0 = 6$ (b) $\mathcal{R}_0 = 18$

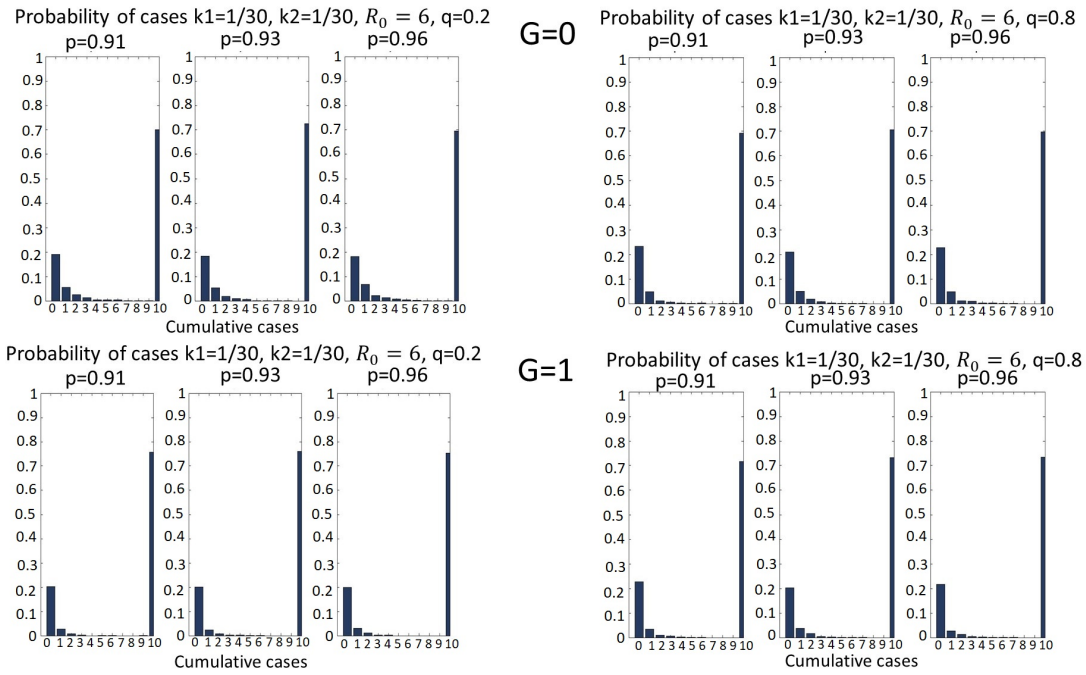

(a)

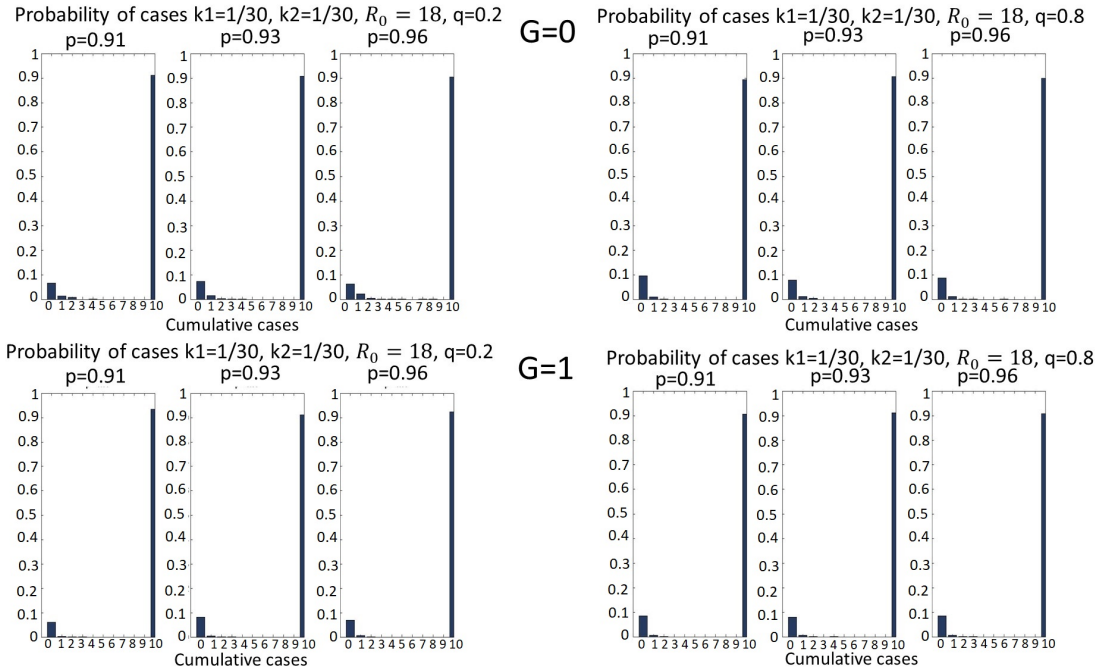

(b)

Figure H.3: Probability of having extinction, 10 cases $G = 0$, 1 for $p = 0.91$, 0.93, 0.96, $q = 0.2$, 0.8, $k_1 = k_2 = 1/30$ and (a) $\mathcal{R}_0 = 6$ (b) $\mathcal{R}_0 = 18$

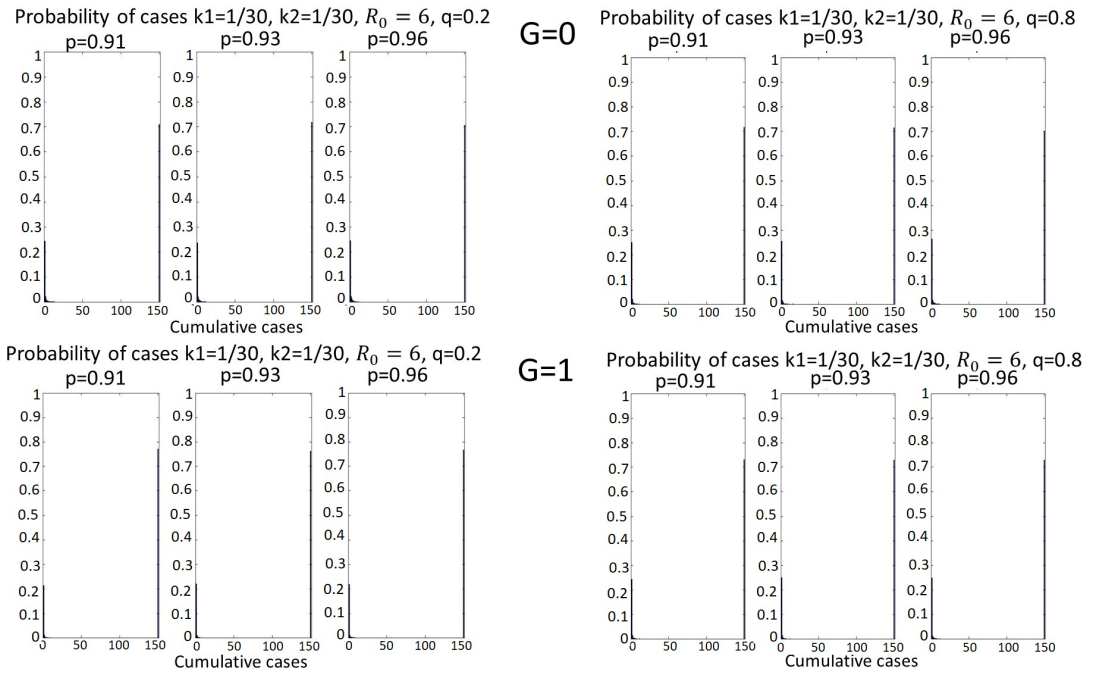

(a)

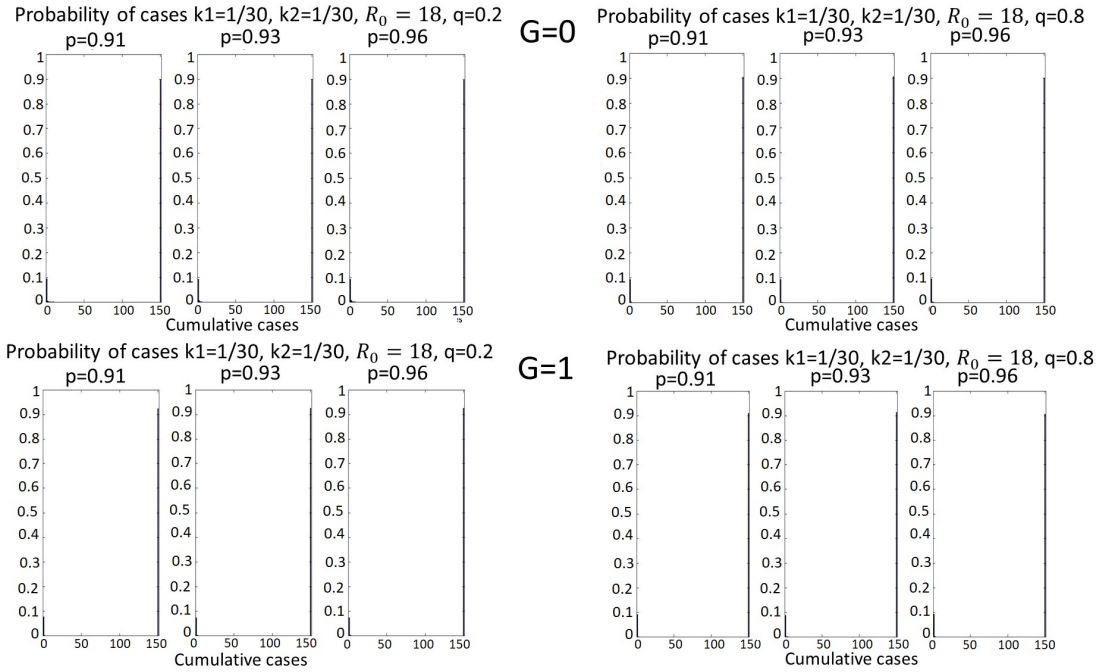

(b)

Figure H.4: Probability of having extinction, 150 cases when $G = 0$, 1 for $p = 0.91$, 0.93, 0.96, $q = 0.2$, 0.8, $k_1 = k_2 = 1/300$ and (a) $\mathcal{R}_0 = 6$ (b) $\mathcal{R}_0 = 18$

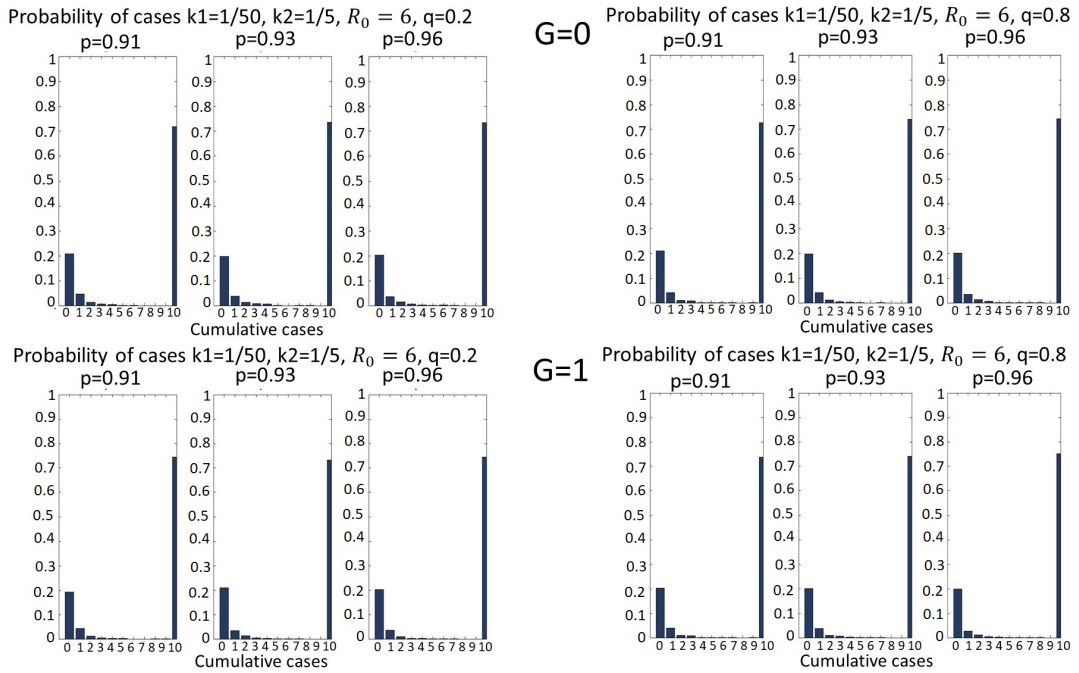

(a)

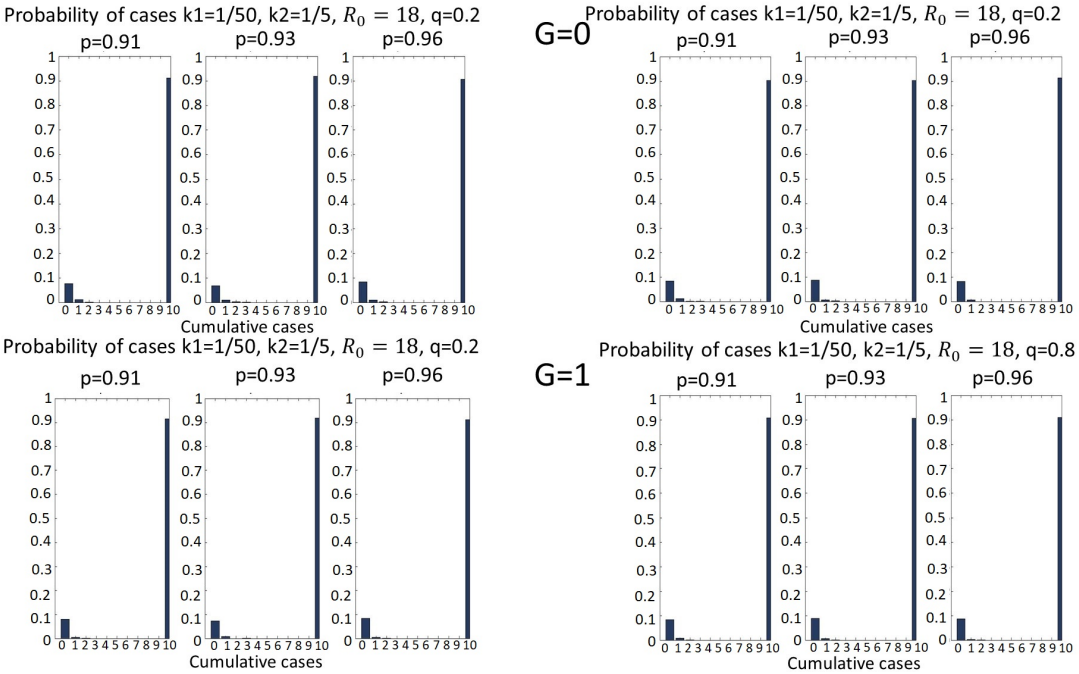

(b)

Figure H.5: Probability of having extinction, 10 cases when $G = 0$, 1 for $p = 0.91$, 0.93, 0.96, $q = 0.2$, 0.8, $k_1 = 1/50$, $k_2 = 1/5$ and (a) $\mathcal{R}_0 = 6$ (b) $\mathcal{R}_0 = 18$

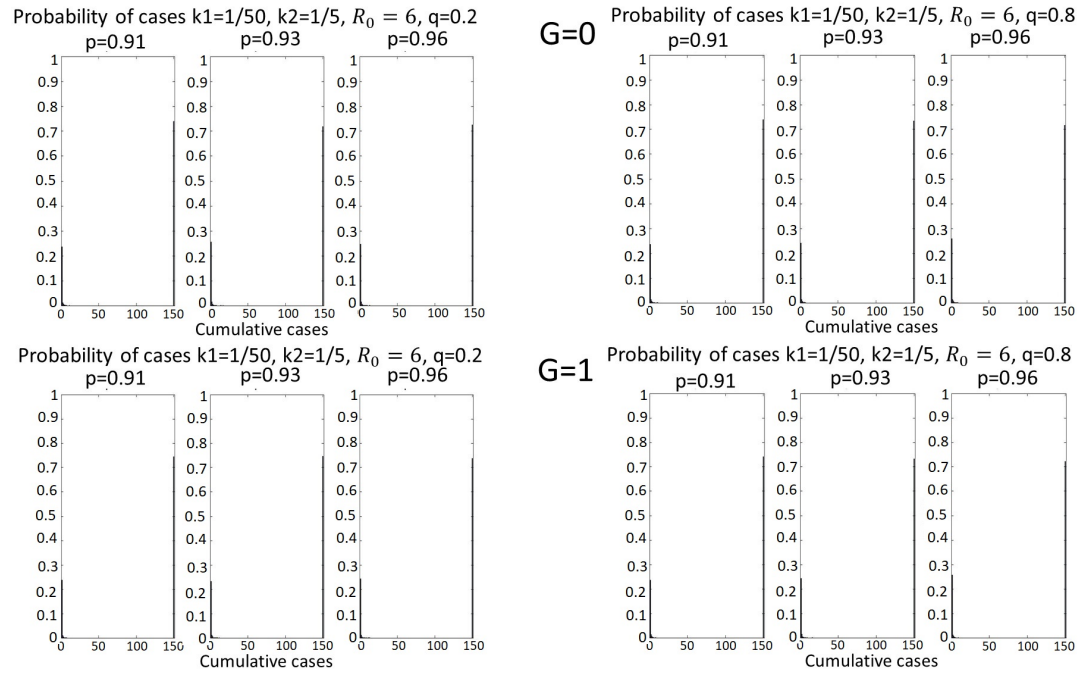

(a)

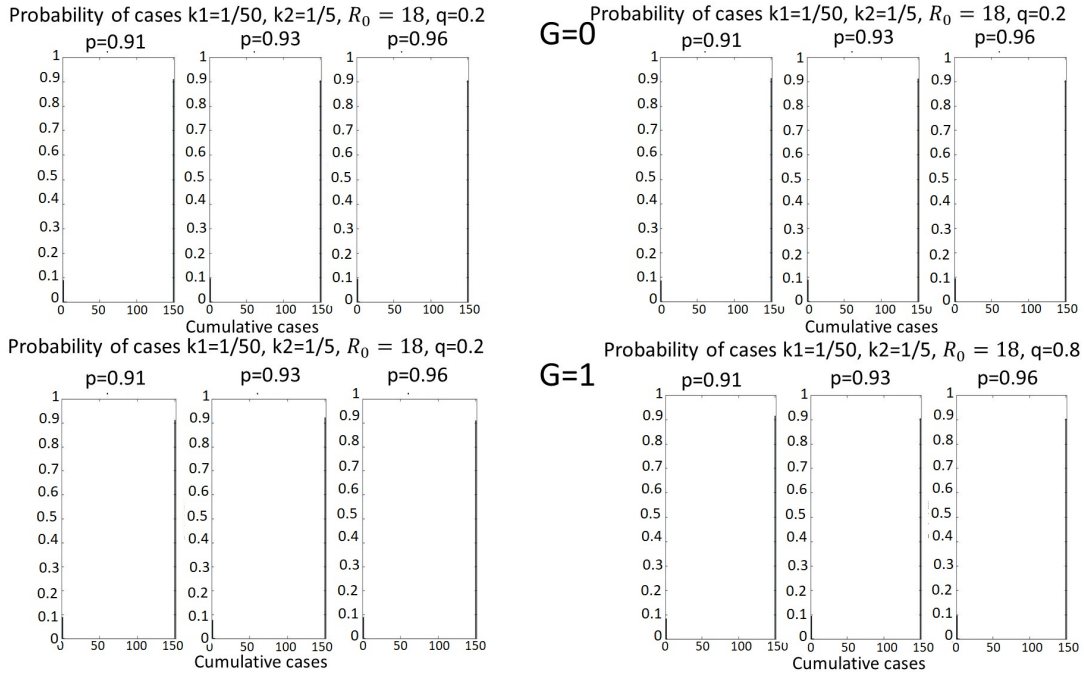

(b)

Figure H.6: Probability of having extinction, 150 cases when $G = 0$, 1 for $p = 0.91$, 0.93, 0.96, $q = 0.2$, 0.8, $k_1 = 1/50$, $k_2 = 1/5$ and (a) $\mathcal{R}_0 = 6$ (b) $\mathcal{R}_0 = 18$

Case $k_1 = 1/5, k_2 = 1/50$

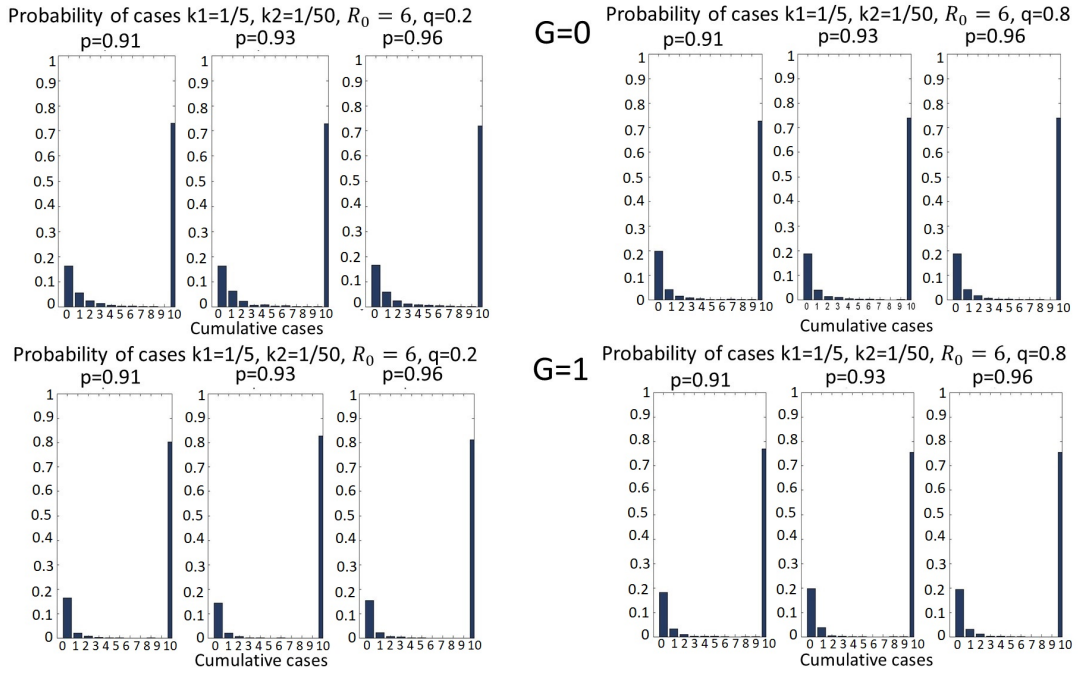

(a)

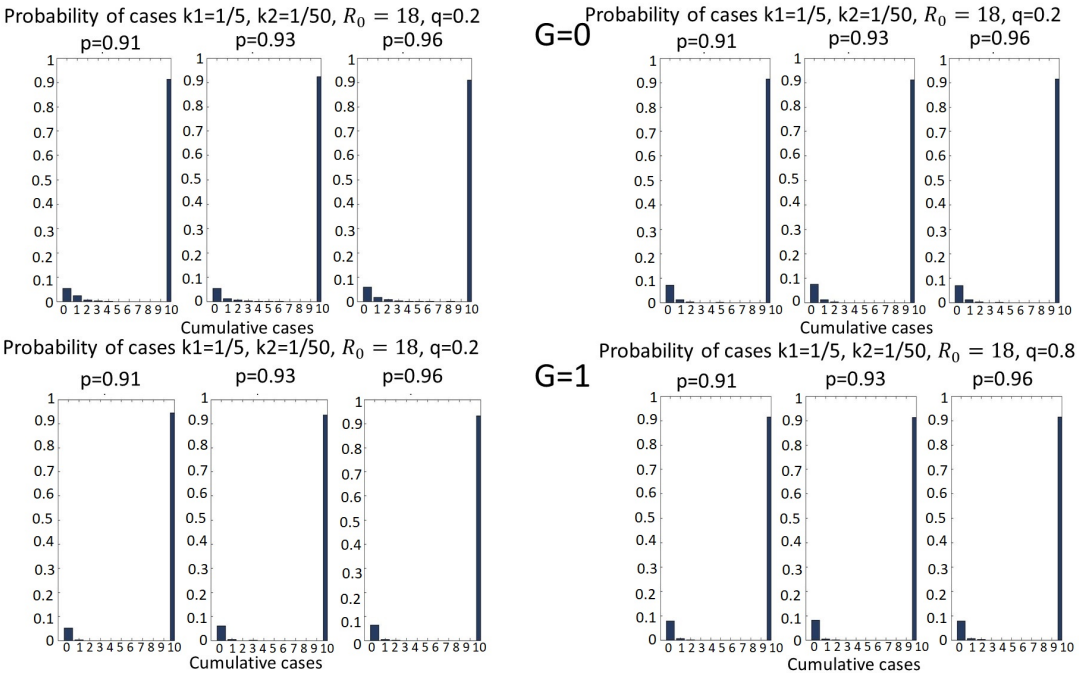

(b)

Figure H.7: Probability of having extinction, 10 cases when $G = 0$, 1 for $p = 0.91$, 0.93, 0.96, $q = 0.2$, 0.8, $k_1 = 1/5$, $k_2 = 1/50$ and (a) $\mathcal{R}_0 = 6$ (b) $\mathcal{R}_0 = 18$

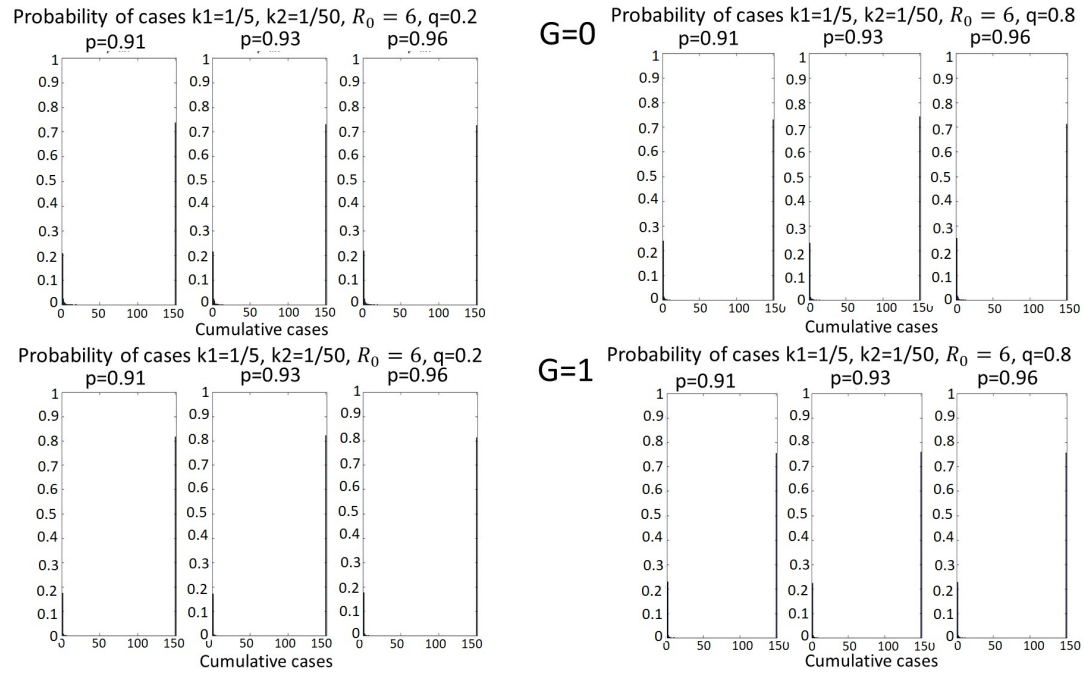

(a)

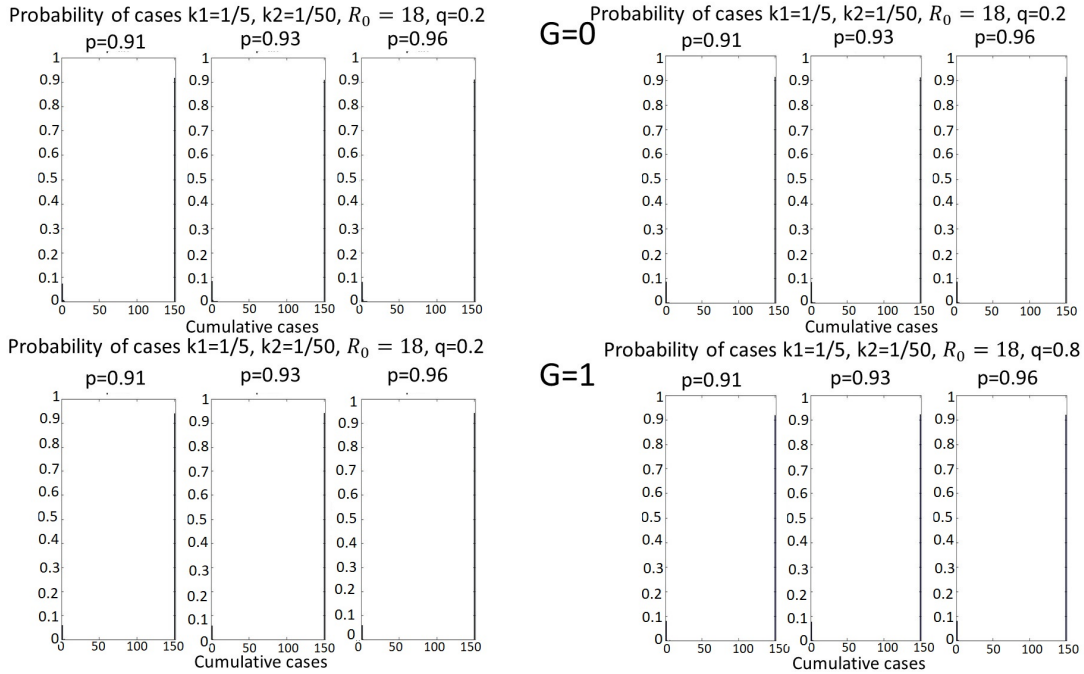

(b)

Figure H.8: Probability of having extinction, 150 cases when $G = 0$, 1 for $p = 0.91$, 0.93, 0.96, $q = 0.2$, 0.8, $k_1 = 1/5$, $k_2 = 1/50$ and (a) $\mathcal{R}_0 = 6$ (b) $\mathcal{R}_0 = 18$

Case $k_1 = 1, k_2 = 1/25$

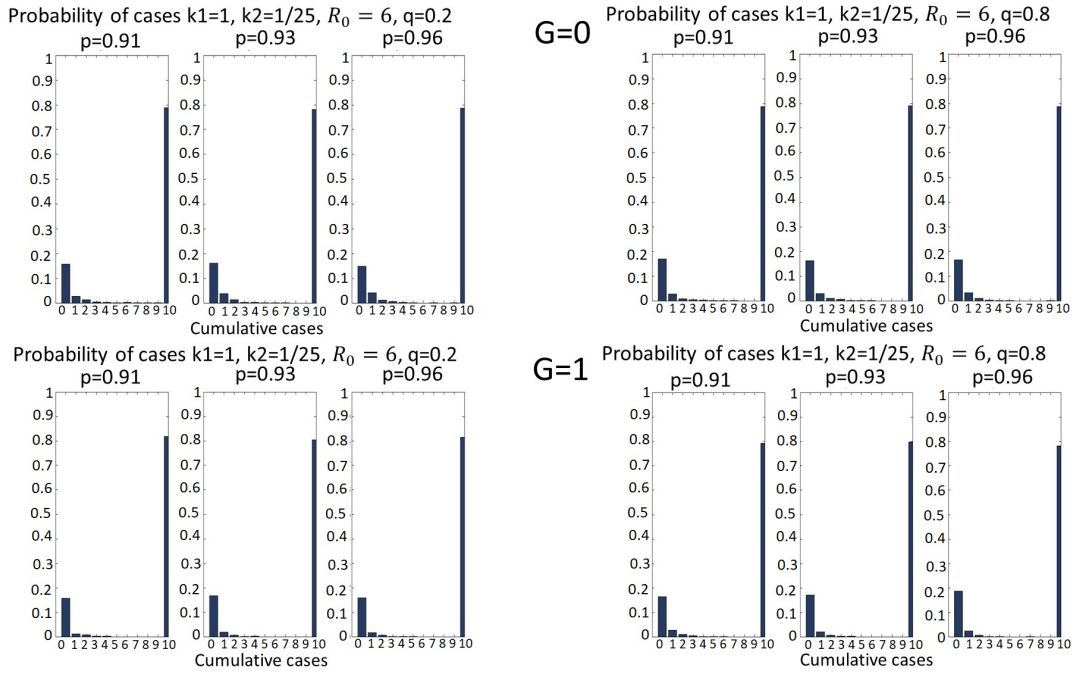

(a)

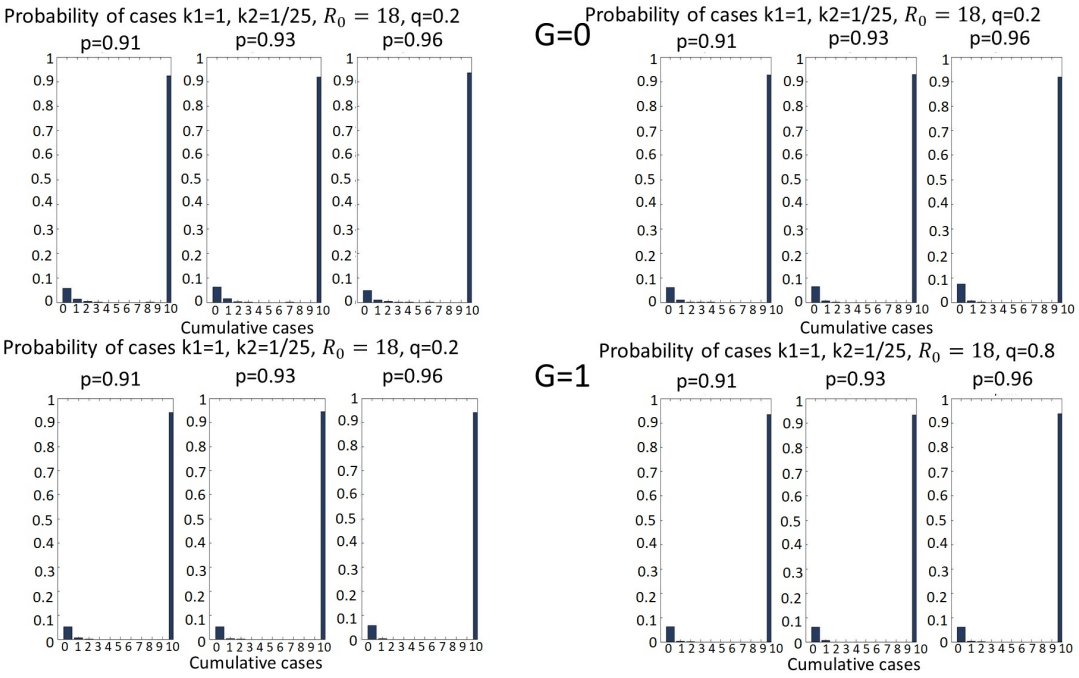

(b)

Figure H.9: Probability of having extinction, 10 cases when $G = 0$, 1 for $p = 0.91$, 0.93, 0.96, $q = 0.2$, 0.8, $k_1 = 1$, $k_2 = 1/25$ and (a) $\mathcal{R}_0 = 6$ (b) $\mathcal{R}_0 = 18$

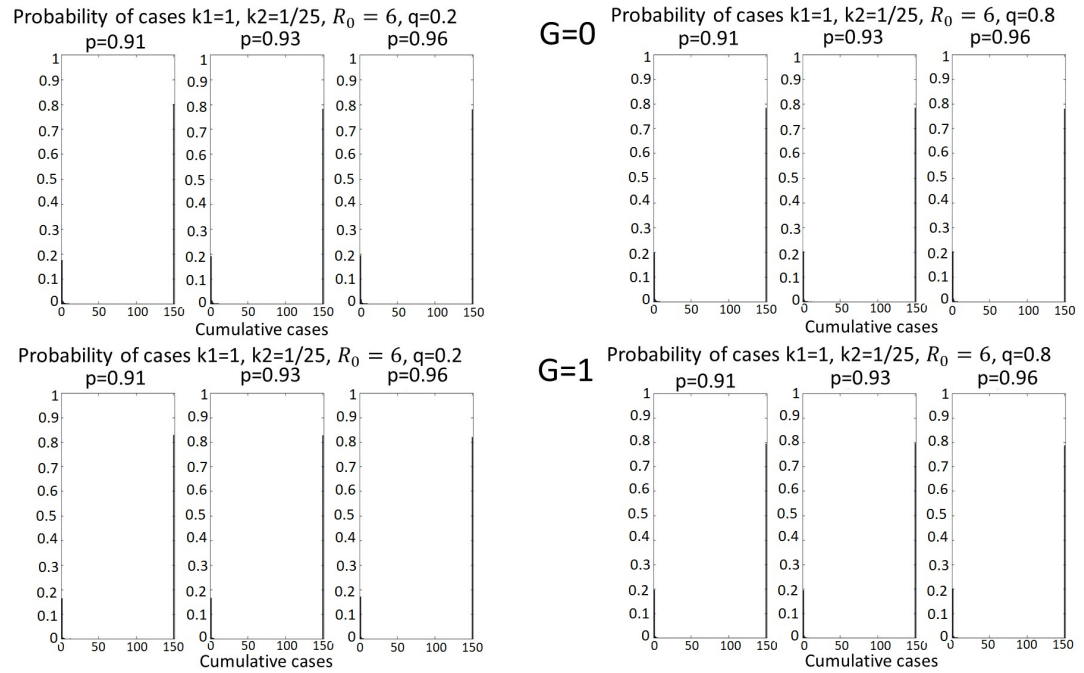

(a)

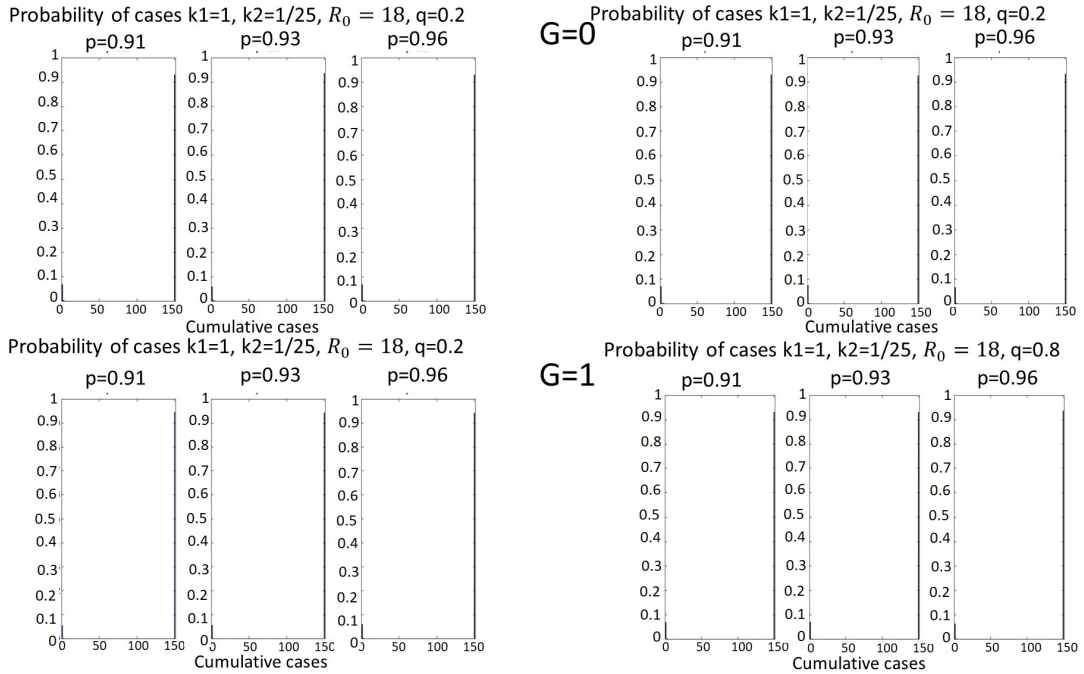

(b)

Figure H.10: Probability of having extinction, 150 cases when $G = 0$, 1 for $p = 0.91$, 0.93, 0.96, $q = 0.2$, 0.8, $k_1 = 1$, $k_2 = 1/25$ and (a) $\mathcal{R}_0 = 6$ (b) $\mathcal{R}_0 = 18$

Appendix I

Probability of Extinction and Outbreak for Model (4.8)

In this appendix we provide the plots for all the waning periods investigated.

Case $k_1 = k_2 = 1/300$

We start with the case assuming life long immunity (i.e., $k_1 = k_2 = 1/300$). We immediately observe that as the vaccination coverage increases, the probability of extinction increases for both $G = 0, 1$. However, for small reproduction numbers (Figures (I.1a)-(I.2a)), we observe that the probability of having an outbreak of at least 10 or 150 cumulative cases is extremely small or even 0. This probability slightly increases when the secondary cases are infectious (bottom-rows panels each figure) and less individuals are boosted to the V compartment after encountering the pathogen (left panels each figure). For large $\mathcal{R}_0$ (Figures (I.1b)-(I.2b)) the probability of an outbreak is high for $q = 0.2$ and $p \leq 0.93$. Our results also suggest that the probability to have an outbreak with at least 150 cases is lower than the one with 10.

Cases $k_1 = k_2 = 1/30$**,** $k_1 = 1/50, k_2 = 1/5$**,** $k_1 = 1/5, k_2 = 1/50$ **and** $k_1 = 1, k_2 = 1/25$

In this section, and the following, we consider immunity waning periods to be shorter than the life span. In all these scenarios (Figures (I.3-I.4)-(I.5-I.6)-(I.7-I.8)-(I.9-I.10)), the probability of having an outbreak with at least 10 or 150 cases is always possible and it is higher than the probability of extinction. These results are visible for both small and large reproduction numbers. The possibility of an outbreak increases if the number of secondary cases increases and they are considered to be infectious.

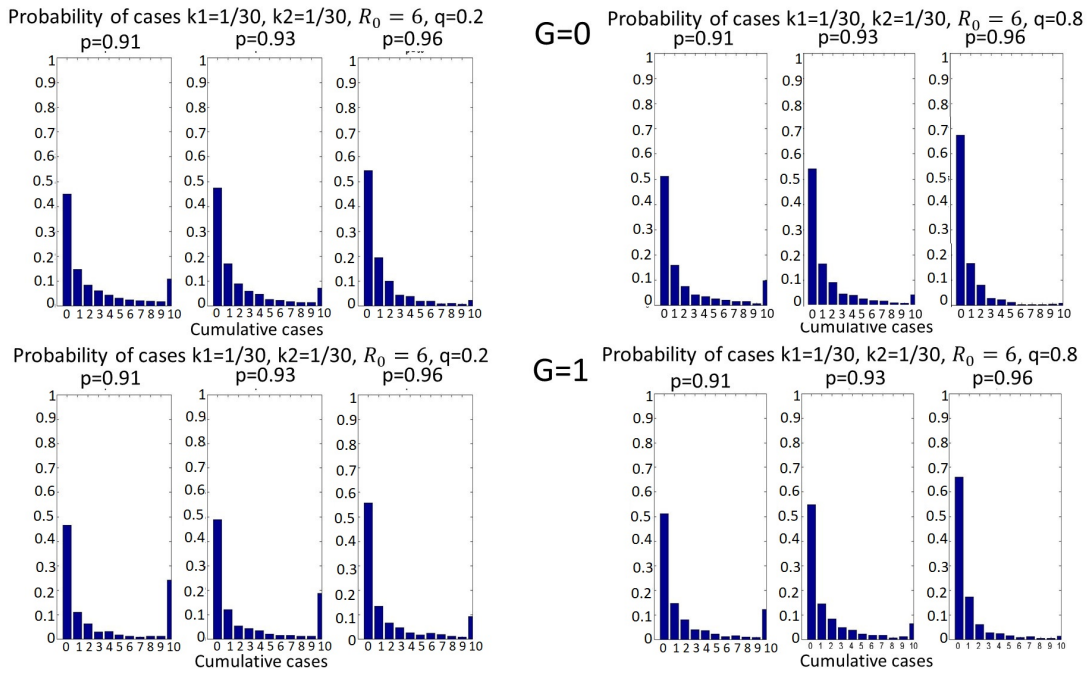

(a)

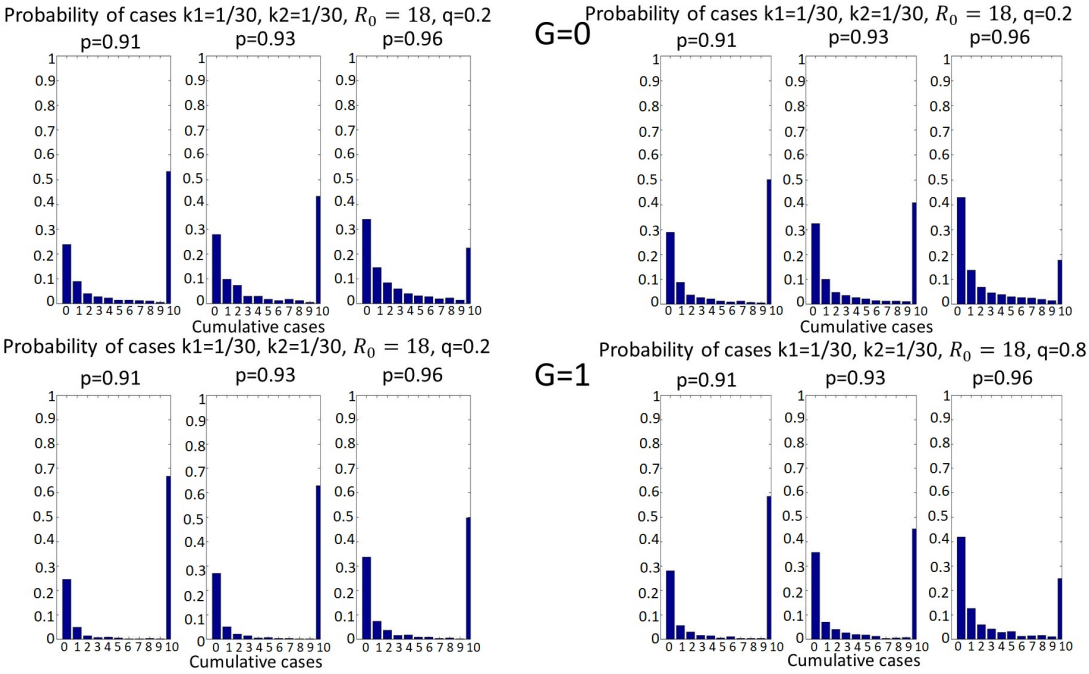

(b)

Figure I.1: Probability of having extinction, 10 cases when $G = 0$ (top-row plots describe the scenario) and $G = 1$ (bottom-row plots) for $p = 0.91$, 0.93, 0.96, $q = 0.2$, 0.8, $\mathcal{R}_0 = 6$, 18 (a-b) and (c-d), respectively, and $k_1 = k_2 = 1/300$

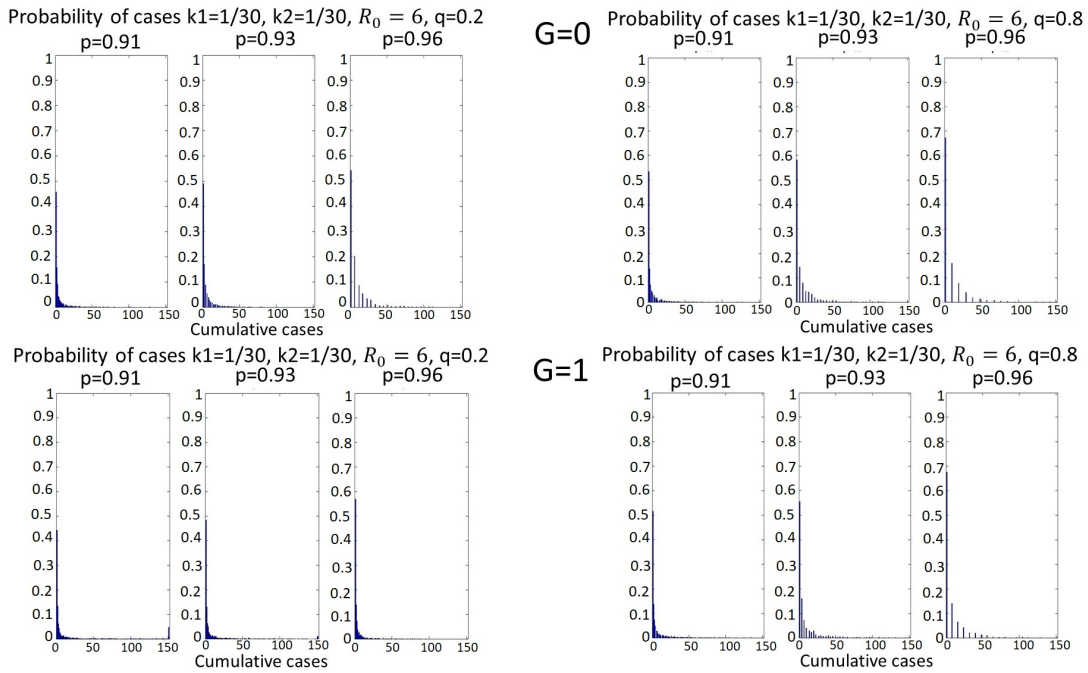

(a)

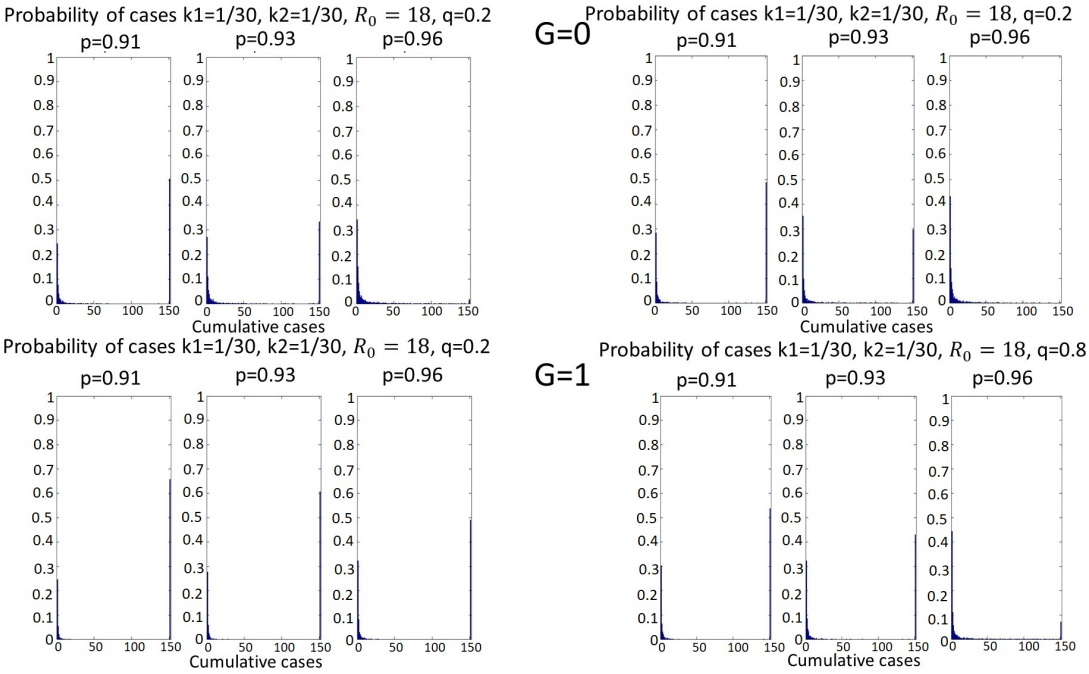

(b)

Figure I.2: Probability of having extinction, 150 cases when $G = 0$ (top-row plots describe the scenario) and $G = 1$ (bottom-row plots) for $p = 0.91$, 0.93, 0.96, $q = 0.2$, 0.8, $\mathcal{R}_0 = 6$, 18 (a-b) and (c-d), respectively, and $k_1 = k_2 = 1/300$

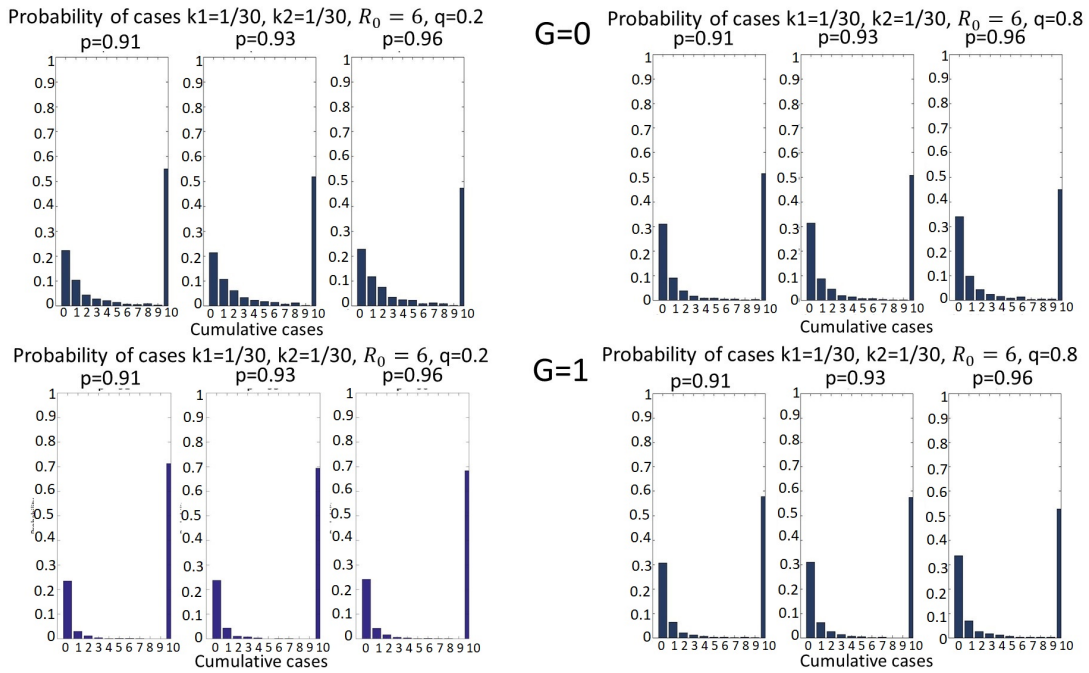

(a)

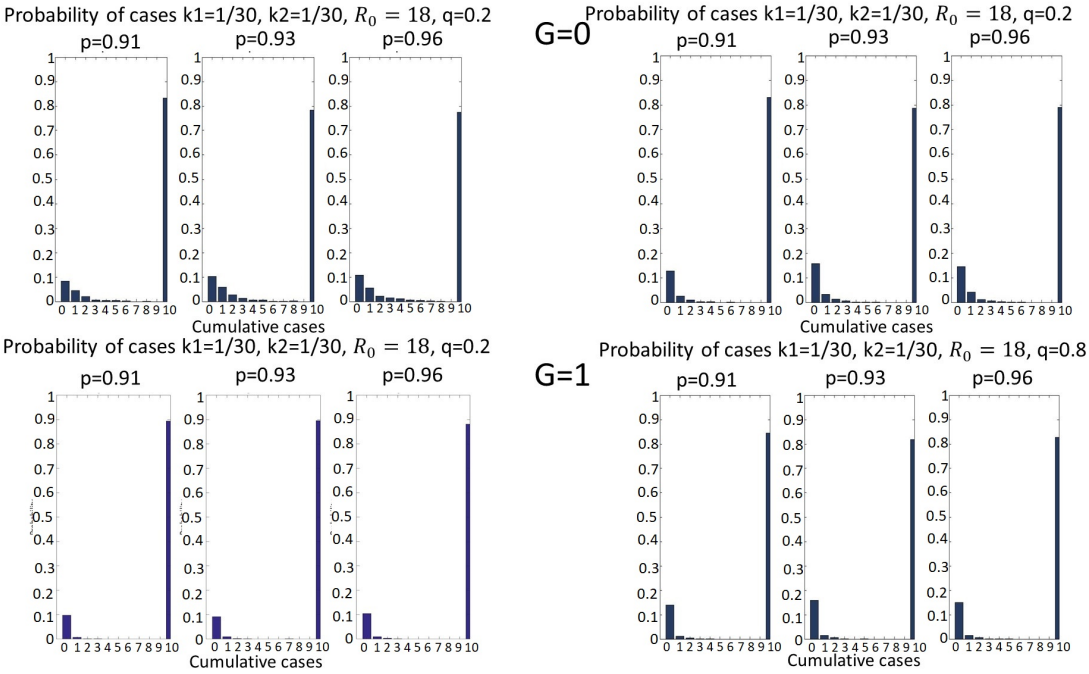

(b)

Figure I.3: Probability of having extinction, 10cases when $G = 0$ (top-row plots describe the scenario) and $G = 1$ (bottom-row plots) for $p = 0.91$, 0.93, 0.96, $q = 0.2$, 0.8 and $k_1 = k_2 = 1/30$

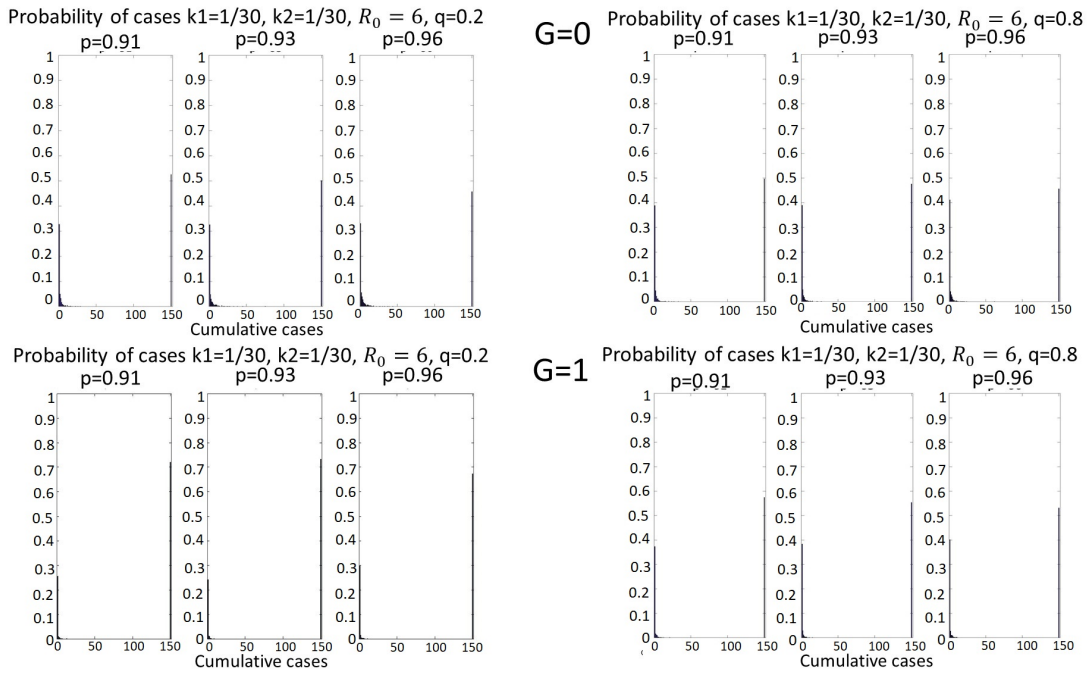

(a)

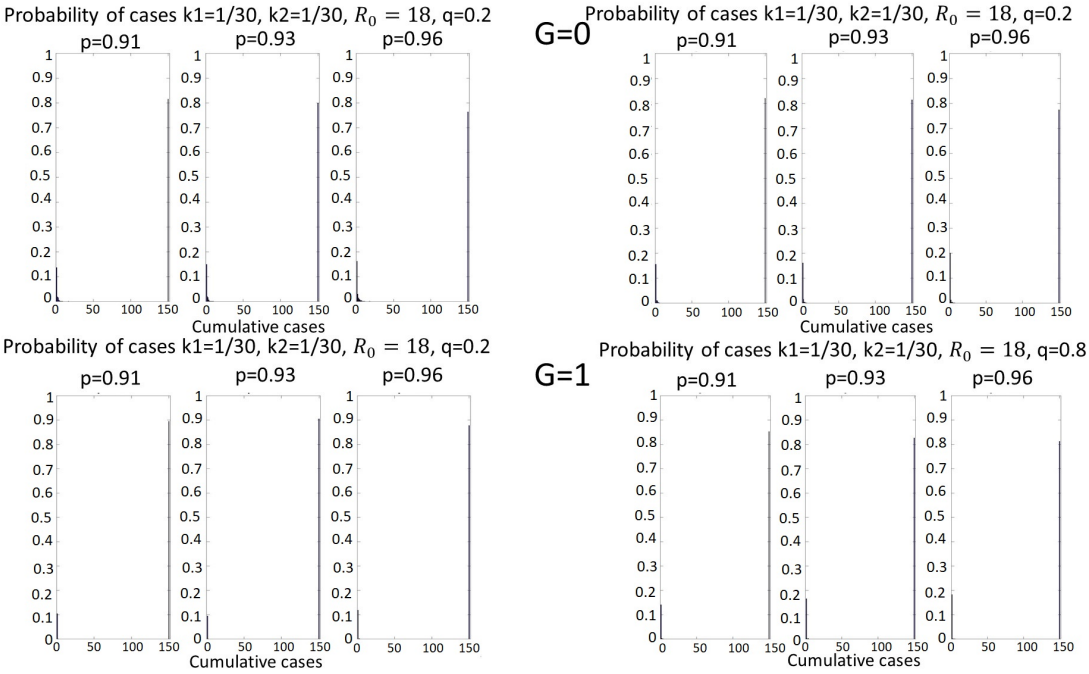

(b)

Figure I.4: Probability of having extinction, 150 cases when $G = 0$ (top-row plots describe the scenario) and $G = 1$ (bottom-row plots) for $p = 0.91$, 0.93, 0.96, $q = 0.2$, 0.8 and $k_1 = k_2 = 1/30$

Case $k_1 = 1/50, k_2 = 1/5$

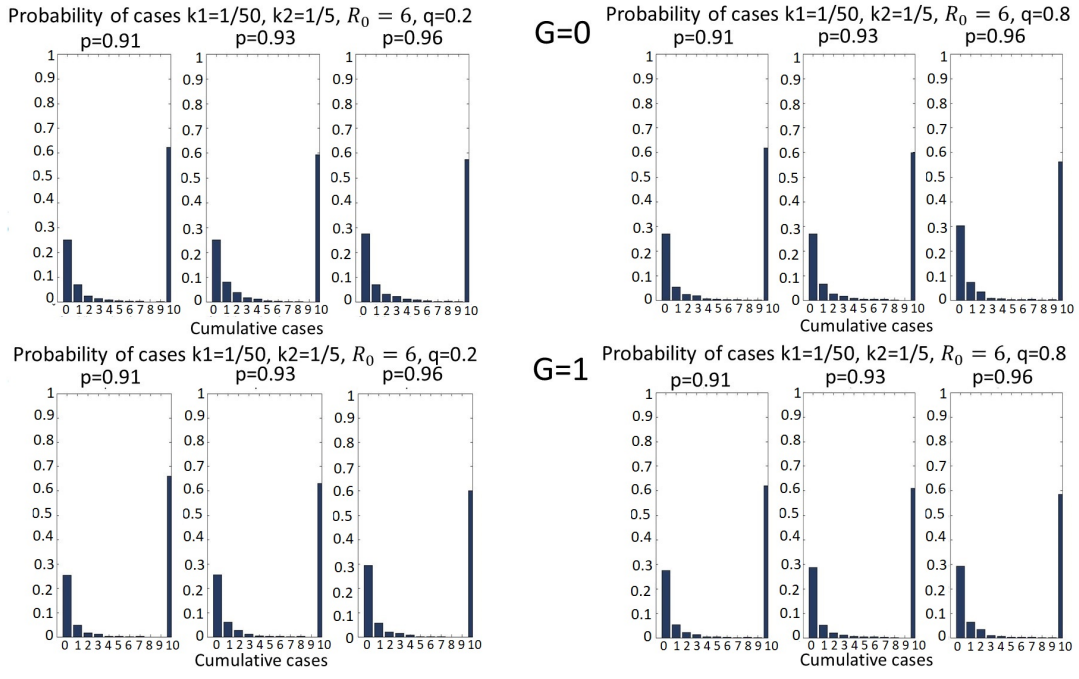

(a)

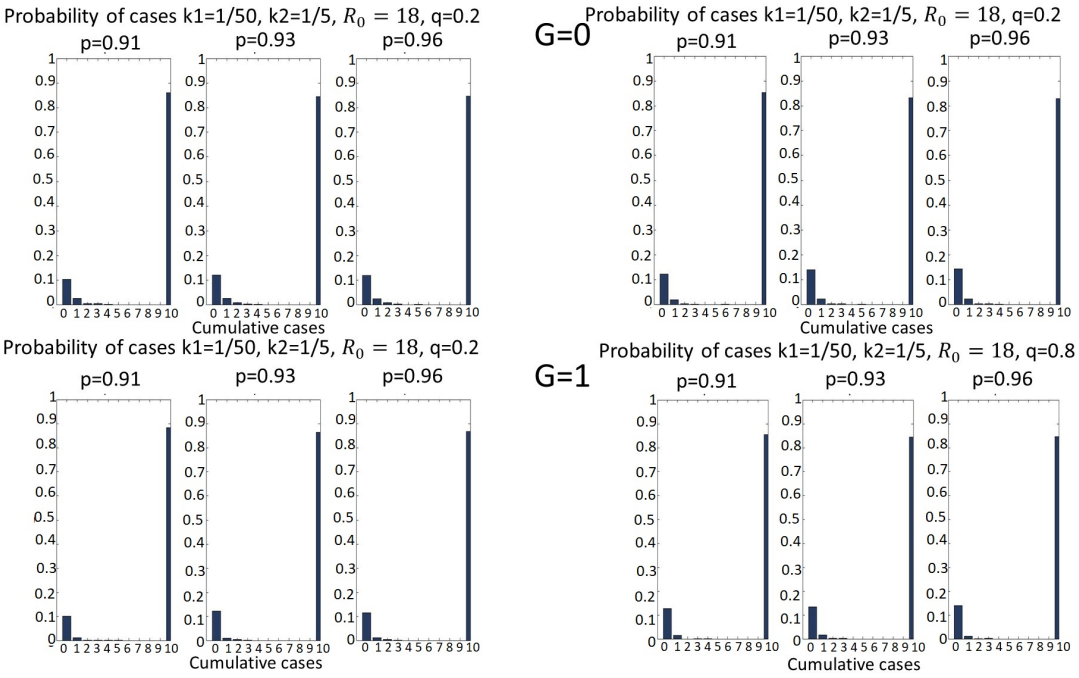

(b)

Figure I.5: Probability of having extinction, 10 cases when $G = 0$ (top-row plots describe the scenario) and $G = 1$ (bottom-row plots) for $p = 0.91$, 0.93, 0.96, $q = 0.2$, 0.8 and $k_1 = 1/50$, $k_2 = 1/5$

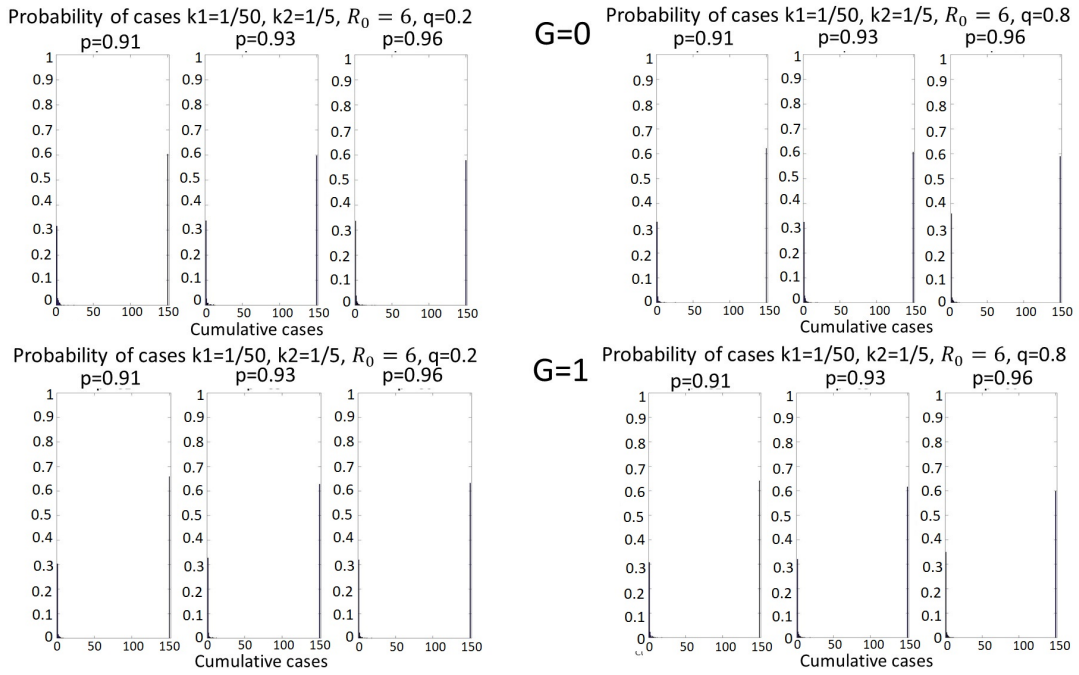

(a)

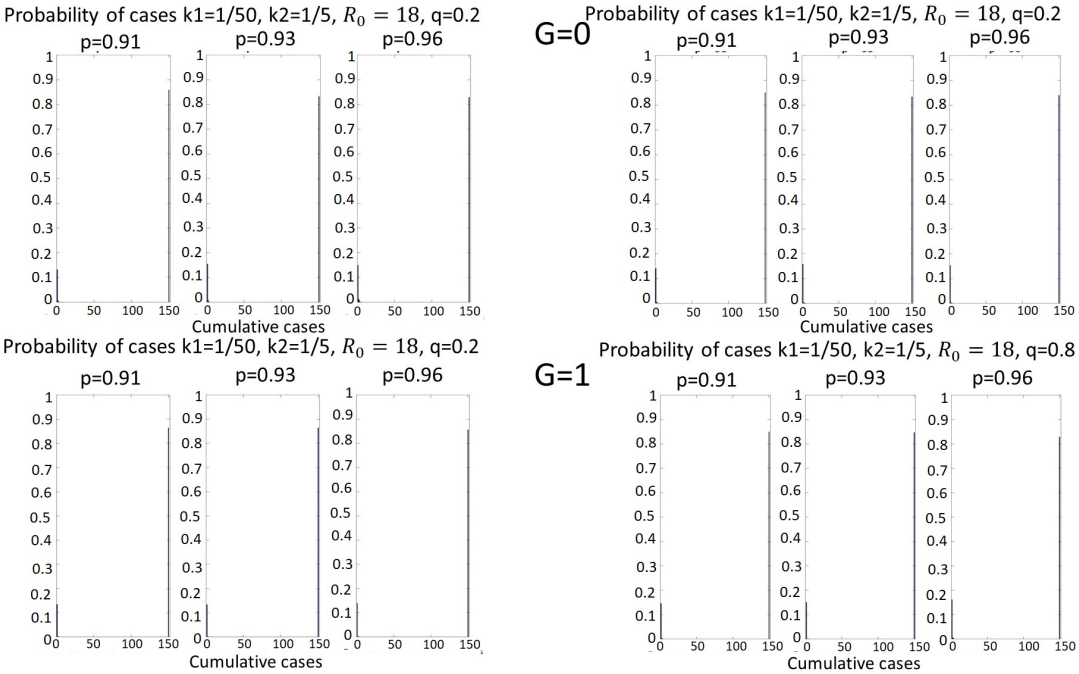

(b)

Figure I.6: Probability of having extinction, 150 cases when $G = 0$ (top-row plots describe the scenario) and $G = 1$ (bottom-row plots) for $p = 0.91$, 0.93, 0.96, $q = 0.2$, 0.8 and $k_1 = 1/50$, $k_2 = 1/5$

Case $k_1 = 1/5, k_2 = 1/50$

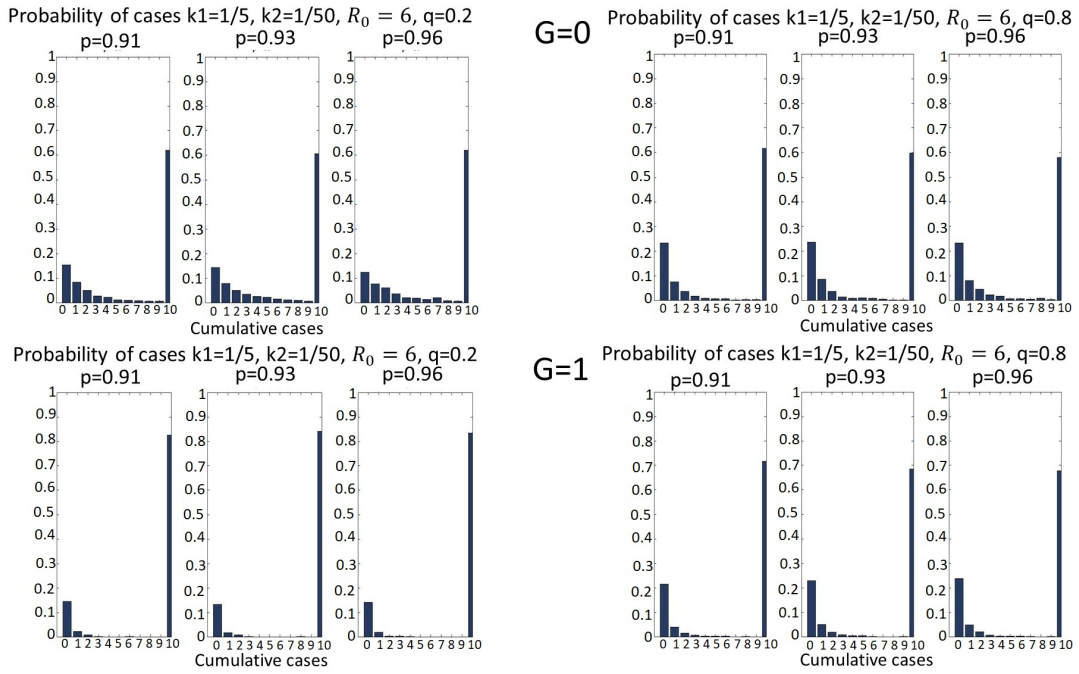

(a)

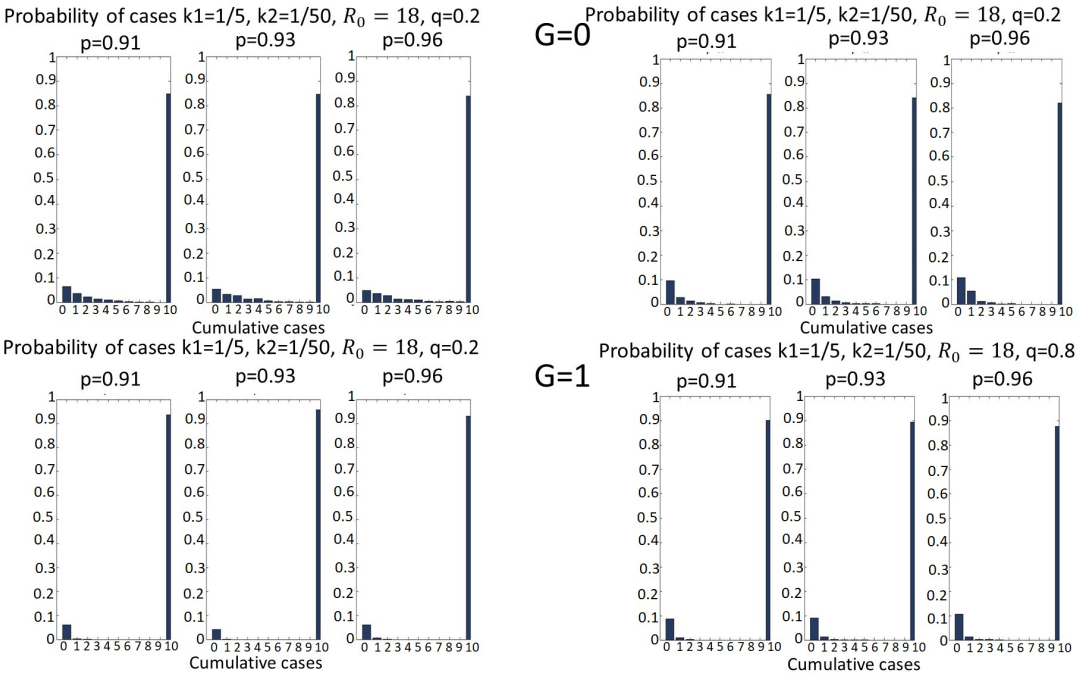

(b)

Figure I.7: Probability of having extinction, 10cases when $G = 0$ (top-row plots describe the scenario) and $G = 1$ (bottom-row plots) for $p = 0.91$, 0.93, 0.96, $q = 0.2$, 0.8 and $k_1 = 1/5$, $k_2 = 1/50$

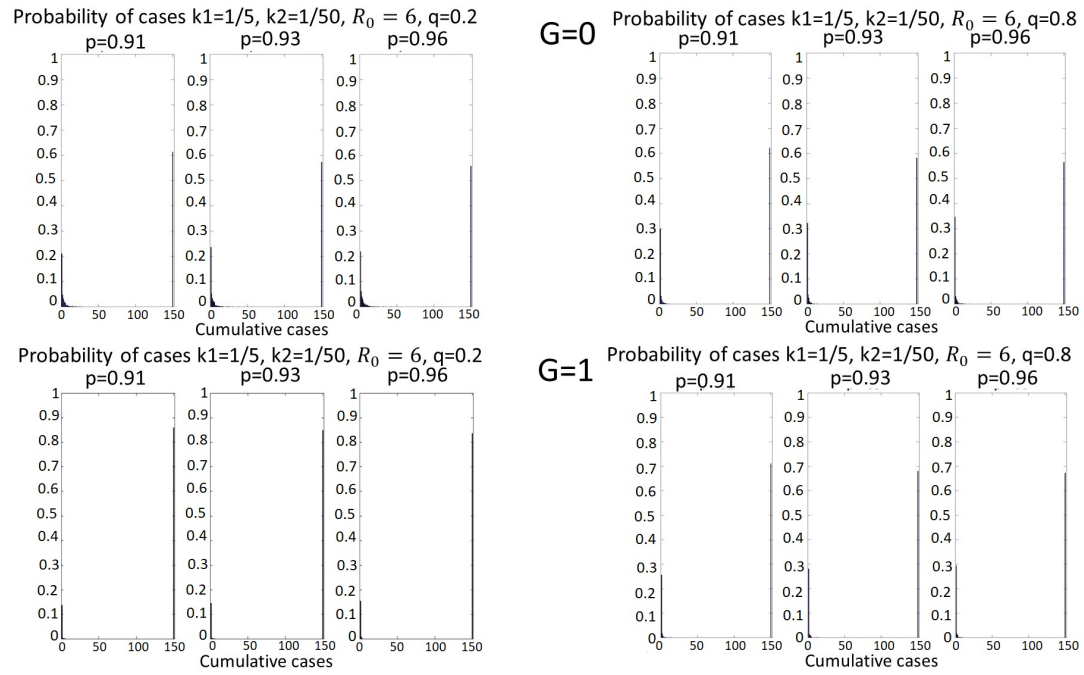

(a)

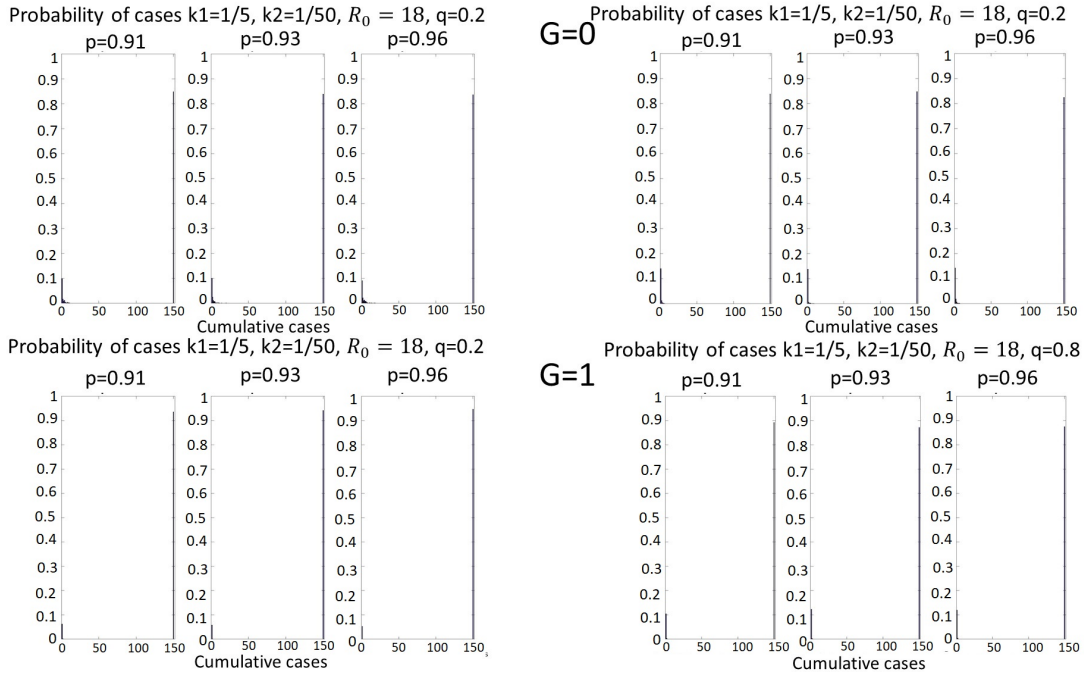

(b)

Figure I.8: Probability of having extinction, 150 cases when $G = 0$ (top-row plots describe the scenario) and $G = 1$ (bottom-row plots) for $p = 0.91$, 0.93, 0.96, $q = 0.2$, 0.8 and $k_1 = 1/5$, $k_2 = 1/50$

Case $k_1 = 1, k_2 = 1/25$

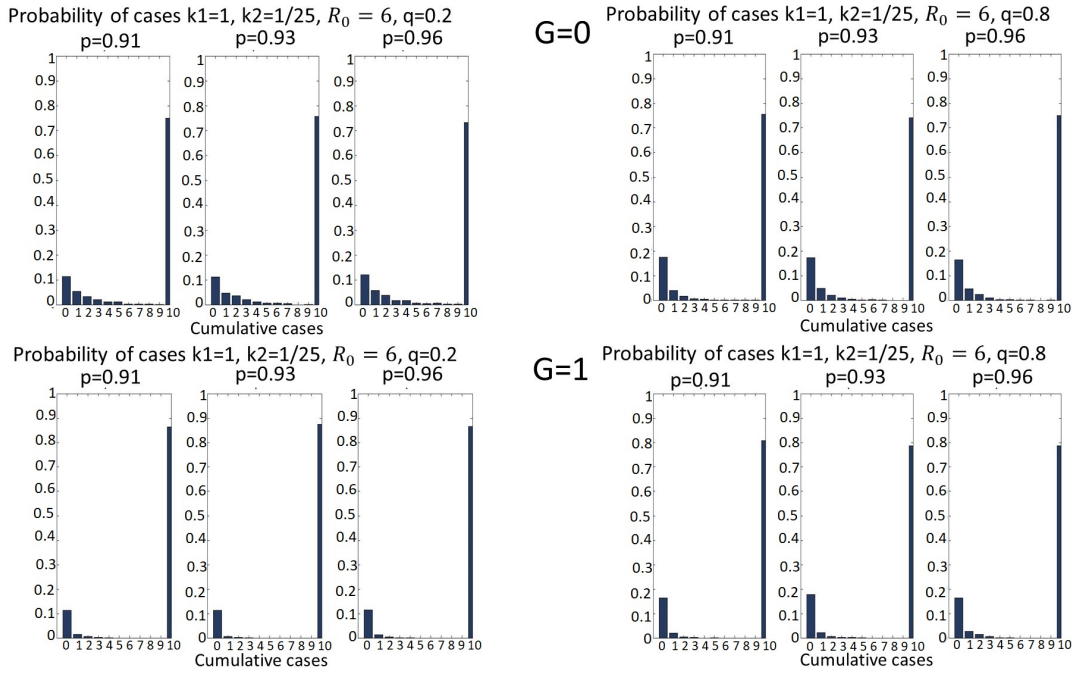

(a)

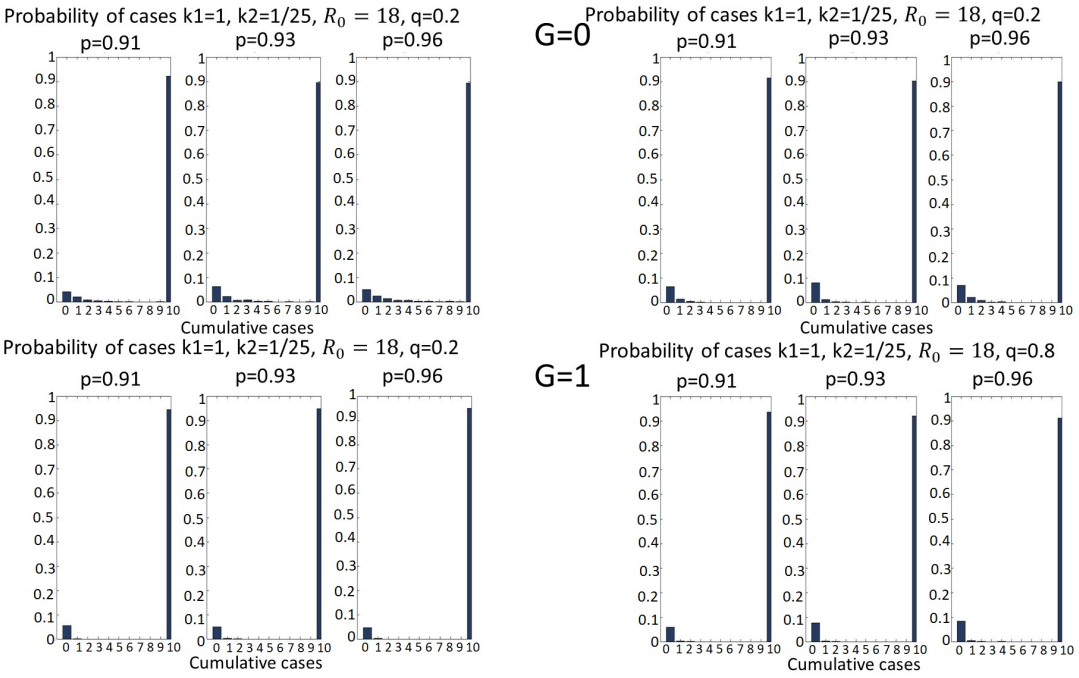

(b)

Figure I.9: Probability of having extinction, 10 cases when $G = 0$ (top-row plots describe the scenario) and $G = 1$ (bottom-row plots) for $p = 0.91$, 0.93, 0.96, $q = 0.2$, 0.8 and $k_1 = 1$, $k_2 = 1/25$

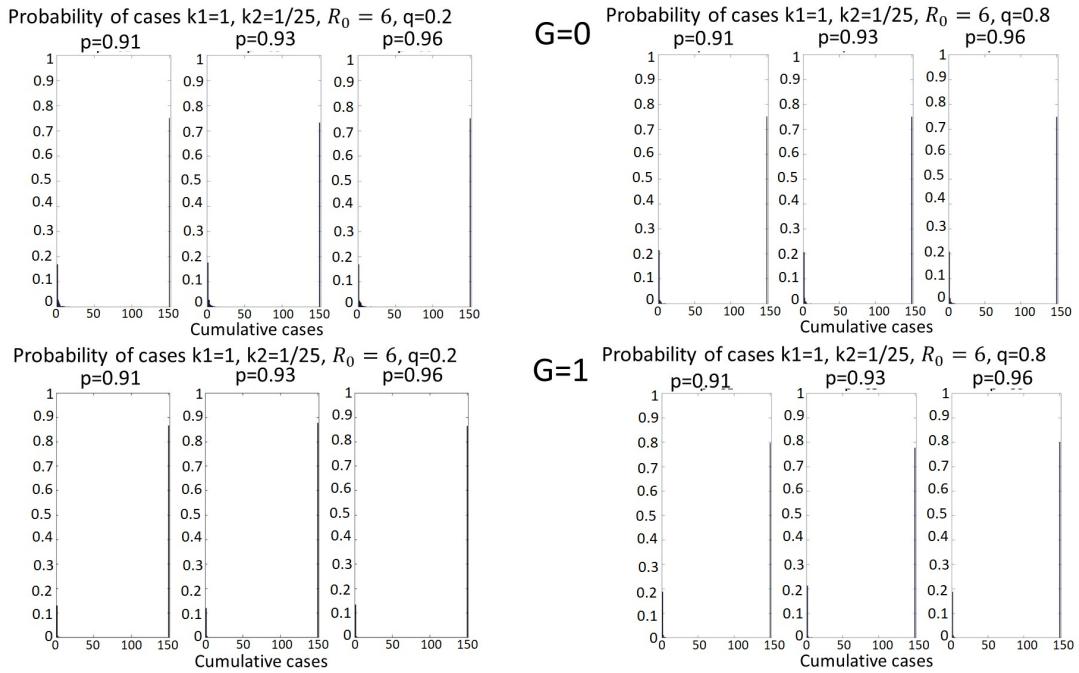

(a)

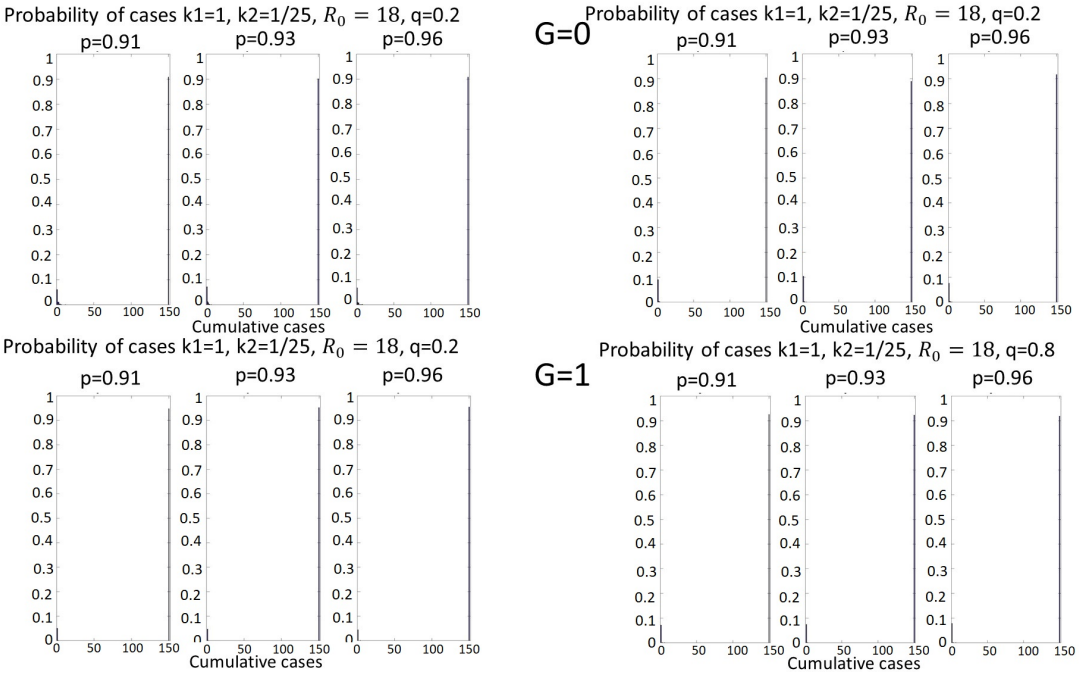

(b)

Figure I.10: Probability of having extinction, 150 cases when $G = 0$ (top-row plots describe the scenario) and $G = 1$ (bottom-row plots) for $p = 0.91$, 0.93, 0.96, $q = 0.2$, 0.8 and $k_1 = 1$, $k_2 = 1/25$